Spring 2024

Quasi-Static and Impact Load Response of BFRP-Reinforced Concrete Beams and Post-Terrorist-Attack Sub-Assemblages

José Luis Carrasquillo
Old Dominion University

QUASI-STATIC AND IMPACT LOAD RESPONSE OF BFRP-REINFORCED CONCRETE BEAMS AND POST-TERRORIST-ATTACK SUB-ASSEMBLAGES

by

José Luis Carrasquillo
B.S. Civil Engineering, July 1997, Polytechnic University of Puerto Rico
M.E. Civil Engineering, May 2006, University of Virginia

A Dissertation Submitted to the Faculty of
Old Dominion University
in Partial Fulfillment of the Requirement of the
Degree of

DOCTOR OF PHILOSOPHY

CIVIL ENGINEERING

OLD DOMINION UNIVERSITY
May 2024

Approved by:

Zia Razzaq (Director)

Mojtaba B. Sirjan (Member)

Shahin N. Amiri (Member)

Gene J. Hou (Member)

ABSTRACT

QUASI-STATIC AND IMPACT LOAD RESPONSE OF BFRP-REINFORCED CONCRETE BEAMS AND POST-TERRORIST-ATTACK SUB-ASSEMBLAGES

José Luis Carrasquillo
Old Dominion University, 2024
Director: Dr. Zia Razzaq

This dissertation presents the outcome of a theoretical and experimental study of Basalt Fiber Reinforced Polymer (BFRP) reinforced concrete beams and post-terrorist-attack sub-assemblages subjected to either quasi-static or impact load. Both BFRP reinforcement as well as BFRP fabric are used in this investigation. The sub-assemblage consists of an otherwise two-span beam converted to a fixed-end single-span one owing to the loss of a middle column blasted off during the terrorist attack. The simply supported beams are subjected to a midspan quasi-static or an impact load. However, each sub-assemblage is subjected to a quasi-static load up to collapse to simulate the residual strength after the terrorist attack. A materially nonlinear analysis based on a coupling of nonlinear moment-curvature relations with a finite-difference scheme was formulated and programmed to predict the quasi-static response of the beams up to collapse and the results were found to have a good agreement with those based on the experiments. A damped single-degree-of-freedom (SDOF) theoretical dynamic model is used to capture the post-impact free vibration of the simply supported beams. The study shows a significant enhancement of both the performance and the strength of the beams and sub-assemblages when BFRP material is used as a primary reinforcement or for retrofitting in practical applications including damage reduction associated with progressive collapse during a terrorist attack. Lastly, a twelve-fold increase in the beam impact collapse resistance is observed when the primary steel reinforcement is combined with a pair of externally bonded BFRP rebars.

This research is dedicated to my wife, Madeline A. Carrasquillo for all her support that she gave me during the times I was away from her, and the time spent in school to achieve my bachelor's, master's, and doctorate degrees. She is my biggest inspiration and supported me through the journey of achieving this research project.

ACKNOWLEDGMENTS

It is especially important to recognize all the people that helped me to complete this goal, because without their help I would not have achieved one of the biggest goals in my life.

First, my two kids; José Luis Jr. and Madeliza, my parents who helped me accomplish this goal, engineers Manuel Martínez and Armando Rodríguez who were my inspiration in my early civil engineering career.

I am immensely grateful to Dr. Pindera (Professor, Dept. of Civil Engineering, University of Virginia) for the motivation they provided during my master's degree and the way they pushed me every day to achieve the next level in my education.

I am grateful to Dr. Zia Razzaq (Professor and Advisor, Dept. of Civil Engineering, ODU) for all his motivation, the way he continuously inspired me in achieving this goal, and for providing me the necessary information throughout the process of completing the program.

I am immensely grateful to Ms. Laura Hash for all the support as a technical editor on this report. Without her support, this report would not have been possible.

I am extremely thankful to Professor Nestor Escobales's support in the material laboratory. Also, I would like to thank Herish Hussain PhD candidate, Graduate student Rutvik R. Patel and Ramani Ayakannu for all their help in the structural laboratory to set up my research.

I am grateful to the Engineering Model Shop at Old Dominion University for their help in preparing the test setups.

NOMENCLATURE

A	Area
Ac	Elastic area of the cross section
Ast	Area of the steel reinforcement
Abas	Area of the Basalt reinforcement
Afac	Area of the Basalt fabric
B	Beam width
Cc	Force of the concrete
c	Distance of the neutral axis
d	Distance from the top fiber to the centroid of the tension steel reinforcement
ds	Distance from the top fiber to the centroid of the tension steel reinforcement
dbas	Distance from the top fiber to the centroid of the tension Basalt reinforcement
E	Modulus of Elasticity
Es	Modulus of Elasticity for Steel
Ec	Modulus of Elasticity for concrete
Eb	Modulus of Elasticity for Basalt reinforcement
Ef	Modulus of Elasticity for Basalt fabric
fc	Computed concrete compression strength
f’c	Specified concrete compressive strength
ff	Basalt fabric tensile strength
fr	Modulus of rupture of concrete
Hc	Minimum height for a concrete beam with steel tensile reinforcement
Hb	Minimum height for a concrete beam with Basalt tensile reinforcement
L	Length of the concrete beam
F(t)	Force with respect to time
I	Moment of inertia
C.L.	Center line of the beam
ε	Normal strain
ε_o	Axial strain

$\dot{\varepsilon_o}$	Strain rate
$\dot{\varphi_x}$	Curvature rate
F_s	Stress in steel tension
ε_b	Basalt reinforcement strain
ε_f	Fabric strain
ε_s	Steel strain
ε_y	Strain at yield
f_y	Steel yield strength
ft	Feet
FRP	Fiber Reinforced Polymer
GFRP	Glass Fiber Reinforced Polymer
CFRP	Carbon Fiber Reinforced Polymer
AFRP	Aramid Fiber Reinforced Polymer
BFRP	Basalt Fiber Reinforced Polymer
psi	Pound per square inches
K	Kips
k	Neutral axis factor
ksi	Kips per square inches
M_{crack}	Crack moment
M_y	Moment at yield point
M_n	Nominal moment
M_u	Ultimate moment
mm	Millimeter
N_s	Modular ration between steel and concrete
N_f	Modular ration between fiber and concrete
in	inches
T_{steel}	Tension force of the steel reinforcement
T_{Basalt}	Tension force of the Basalt reinforcements
$\bar{Y}$	Centroid of the transformed area

Φ_{crack}	Curvature at crack moment
Φ_{y}	Curvature at yield moment
Φ_{ult}	Curvature at ultimate moment
Φ_{x}	Bending curvature about x-axis
$M_{\ddot{y}}$	Mass

TABLE OF CONTENTS

Page

LIST OF TABLES xiii

LIST OF FIGURES xiv

Chapter

CHAPTER 1 INTRODUCTION 1

1.1 Background 1

1.2 Literature Review 9

1.3 Problem Definition 17

1.4 Objectives and Scope 17

1.5 Assumptions and Conditions 19

CHAPTER 2 EXPERIMENTAL STUDY 21

2.1 Introduction 21

2.2 Material Properties 21

2.2.1 Concrete 21

2.2.2 Steel Reinforcement 24

2.2.3 Basalt Fiber Reinforced Polymer (BFRP) 26

2.2.4 Epoxy Materials 30

2.3 Test Setup and Testing Procedures 32

2.3.1 Test Specimen Preparation 32

2.3.2 Procedure to Mount Exterior BFRP Bars on the Reinforced Concrete Simply Supported Beam 51

2.3.3 Procedure to Install the Basalt Fabric to the Simply Supported 54

Page

2.3.4 Summary of the Simply Supported Beam Configurations 57

2.3.5 Simply Supported Beam Specimens 58

2.3.6 Test Procedures for Static and Impact Load for the Simply Supported Beams.... 59

2.3.7 Sub-assemblage Specimens 62

2.3.8 Test Procedures for Continue Two Span Sub-assemblage Specimen 62

2.3.9 Summary of the Two-Span Sub-assemblage Configurations 65

2.4 Test Results for Material Used on the Specimen during this Research 66

2.4.1 Concrete Compression Test 66

2.4.2 Steel and BFRP Tension Test Results……67

2.5 Test Result for a Simply Supported Beam…….78

2.5.1 Strain Gauges Location in the Simply Supported Beams…….78

2.5.2 Strain Gauge Results for the Simply Supported Beams……80

2.5.3 Quasi-static Load Test Results……...89

2.5.4 Deflection Results……..90

2.5.5 Beam Cracks Pattern Results 99

2.5.6 Impact Load Test……..109

2.5.7 Impact Load Results…….111

2.5.8 Impact Load Strain Gauge Results……...117

2.5.9 Impact Load Beam Acceleration Responses Results……139

2.6 Test Results for the Sub-assemblage Specimens……...159

Page

2.6.1 Strains Gauge Locations for the Sub-assemblage Tests 159

2.6.2 Strain Gauge Results for the Sub-assemblage Specimens.....160

2.6.3 Strain versus Displacement at the Failure Column..... 172

2.6.4 Strain Versus Rotation at The Fixed Supports..... 182

2.6.5 Sub-assemblage Deflection Results..... 190

2.6.6 Sub-assemblage Crack Results for All Tests 194

2.6.7 Beam Catenary Action..... 222

2.6.8 Plastic Hinge Formation 235

2.7 Observations and Discussions..... 251

CHAPTER 3 THEORETICAL ANALYSIS.....254

3.1 Introduction 254

3.2 Formulation of the Moment-Curvature Approach 254

3.3 Nonlinear Finite-Difference Analysis of a Simply Supported Beam..... 257

3.4 Theoretical Moment-Curvature of the Simply Supported Specimens 260

3.5 Theoretical Moment Curvature of the Sub-assemblage Beam..... 267

3.6 Damped Single-degree-of-freedom (SDOF) Theoretical Dynamic Analysis…….271

CHAPTER 4 COMPARISON OF RESULTS AND DISCUSSION 274

4.1 The Simply Supported Beams Under Quasi-Static Load..... 274

4.2 The Simply Supported Beam Under Impact Load 297

4.2.1 Acceleration Response for Each Simply Supported Beam..... 300

4.3 The Sub-assemblage Behavior Under Quasi-Static Load……..311

CHAPTER 5 CONCLUSION AND FUTURE RESEARCH 329

Page

5.1 Conclusions 329

5.2 Future Research 331

REFERENCES 332

APPENDICES 334

A. MatLab Program to Calculate the M-Phi Relation of Singly Reinforced Rectangular Beams by Layered Element Technique Unretroffited Beams 334

B. MatLab Program to Calculate the M-Phi Relation of Singly Reinforced Rectangular Beams by Layered Element Technique – Beam with Steal Reinforcement and Retroffitted in Tension Zone 338

C. MatLab Program to Calculate the M-Phi Relation of Singly Reinforced Rectangular Beams by Layered Element Technique Unretroffited Basalt Beams 343

D. MatLab Program to Calculate the M-Phi Relation of Singly Reinforced Rectangular Beams by Layered Element Technique Basalt Reinforcement and Retrofitted in Tension Zone 347

E. MatLab Program to Calculate Deflection at the Center of Reinforced Concrete Beam by Piecewise Linear Finite Difference Algorithm 351

F. MatLab Program to Calculate Deflection at the Center of Reinforced Concrete Beam by Piecewise Linear Finite Algorithm Beam with Basalt FRP Reinforcement 354

G. Code to Determine the Beam and Impactor Mass, Omega Impact Velocity of Each Test, Natural Frequency, and Natural Period 357

VITA 359

LIST OF TABLES

Table Page

1. Comparison between BFRP, Other FRP, and Steel Reinforcements 9

2. Concrete Mix Composition for Each Concrete Batch 22

3. Summary of the Configurations for the Simply Supported Specimens 58

4. Summary of the Configuration for the Sub-assemblage Specimens 66

5. Concrete Compression Test Summary 67

6. Steel Tension Test Summary 77

7. BFRP Tension Test Summary 78

8. Weights and Mass of Each Beam 272

9. Length, Weights, and Mass of Each Impactor 273

10. Comparison between Experimental and Theoretical Maximum Load at Mid-span of the Beam 274

11. Comparison between Experimental and Theoretical Maximum Moments at Mid-span of the Beam 275

12. Impact Force, Natural Frequency, Natural Period, and Impact Velocity at 10 inches Drop 298

13. Impact Force at 10 inches Drop 298

14. Impact Force at Collapse 299

15. Post-impact Natural Frequency at Collapse and Post-impact Natural Frequency at 10 inches drop 299

16. Impact Force at Collapse Normalized with Impact Force at 10 inches Drop 300

17. Comparison between Experimental and Theoretical Maximum Load 312

18. Comparison between Experimental and Theoretical Maximum Moments at Missing Column 312

LIST OF FIGURES

Figure Page

1. Alfred P. Murrah Building and World Trade Center after Collapse 1

2. The Process to Remove a Column during the Alternate Path Load Method (Source: UFC4-023-03 and GSA Progressive Collapse Guidelines) 4

3. Typical 2-D Concrete Building Frame under Terrorist Attack 5

4. Typical 2-D Concrete Building Frame with a Lost Column 6

5. Equivalent Boundary Conditions for Two-bay Sub-assemblage 6

6. Typical Layout of FRP Production (Picture Courtesy of Smarter Building Systems LLC in Newport, RI) 8

7. Concrete Stress-strain Relationships 23

8. Sample of Compression Concrete Cylinder Test 24

9. Stress-strain Relationship of # 3 Reinforcements 25

10. Stress-strain Relationship Theoretical Value of Steel 26

11. Stress-strain Relationship Theoretical Value of BFRP Reinforcement 28

12. Stress-strain Relationship for the BFRP 4mm, 8mm, and 10mm Bar 29

13. Stress-strain Relationship for the BFRP Fabric 30

14. Sikadur 30-Part A and Part B Product 31

15. Sikadur 330-Part A and Part B Product 32

16. Typical Cross Section for the Simply Supported Beam with Steel Tension Only 35

17. Typical Cross-section for the Simply Supported Beam with BFRP Tension Only 36

18. Stirrup Fabrication 37

19. Typical Steel Skeleton Fabrication 38

20. Typical Formwork for All Simply Supported Beams 39

21. Steel and BFRP Skeleton within the Formwork Ready to Pour Concrete 40

22. Typical Steel Skeleton for Regular Steel Beams 41

23. Typical BFRP Skeleton for the Beams with BFRP Reinforcement 42

24. Pre-grove Beams that Will Retrofit with External Reinforcement 43

25. Preparation of the Concrete Mix 44

26. Fours Beams with Steel Reinforcement (left) and Four Beams with BFRP Reinforcement (right) 45

27. Typical Cross-section for Two-span Sub-assemblage with Steel Reinforcement and Seismic Detail 46

28. Typical Cross-section for Two-span Sub-assemblage with BFRP Reinforcement 47

29. Typical Cross-section for Two-span Sub-assemblage with BFRP Reinforcement and Seismic Detail 48

30. Typical Form Work for Two Span Sub-assemblages 49

31. Steel and BFRP Skeleton of Two Span Sub-assemblage Beams 50

32. Two Span Sub-assemblage 51

33. Two Beams Ready for Epoxy Sikadur 30 and 2-4mm External BFRP Reinforcement 53

34. Two Simply Supported Beams Were Retrofitted with 2-4mm External BFRP Reinforcement 54

35. Beam Preparation for BFRP Fabric Installation 55

36. BFRP Fabric Installation on Simply Supported Beam 56

37. BFRP Fabric Installed on Simply Supported Beam 57

38. Illustration for the Simply Supported Beam Testing 61

39. Setup for the Simply Supported Beam Testing in the Laboratory 62

40. Illustration for the Two-span Sub-assemblages Testing in the Laboratory 64

41. Setup for the Two-span Sub-assemblages Testing in the Laboratory..... 65

42. Steel Reinforcement # 3 Tension Tests Setup in the Laboratory..... 68

43. Results of Steel Reinforcement # 3 Tension Tests in the Laboratory..... 69

44. BFRP Reinforcement 10mm Tension Test Setup in the Laboratory 70

45. Results of the BFRP 10mm Tension Test in the Laboratory 71

46. Failure of the BFRP 10mm Tension during a Test in the Laboratory 72

47. BFRP Reinforcement 4mm Tension Test Setup in the Laboratory 73

48. Results of the BFRP 4mm Tension Test in the Laboratory 74

49. Results of the BFRP 8mm Tension Test in the Laboratory 75

50. Results of the BFRP Fabric Tension Test in the Laboratory 76

51. Results of the # 2 Steel Reinforcement Tension Test in the Laboratory 77

52. Strain Gauge's Locations on Simply Supported Beams 79

53. Installation of the Strain Gauges on Simply Supported Beam 80

54. Experimental Load-strain Values for All Strain Gauges for Specimen S-1 81

55. Experimental Load-strain Values for All Strain Gauges for Specimen B-1..... 82

56. Experimental Load-strain Values for All Strain Gauges for Specimen S-B-1 83

57. Experimental Load-strain Values for All Strain Gauges for Specimen B-B-1..... 84

58. Experimental Load-strain Values for All Strain Gauges for Specimen S-F-1..... 85

59. Experimental Load-strain Values for All Strain Gauges for Specimen B-F-1 87

60. Experimental Load-Strain Values for All Strain Gauges for Specimen B-F-1 88

61. Experimental Load-strain Values for All Strain Gauges for Specimen B-1 (retrofitted)..... 89

62. Experimental Load Deflection for Specimen S-1 92

63. Experimental Load Deflection for Specimen B-1 93

64. Experimental Load Deflection for Specimen S-B-1 94

65. Experimental Load Deflection for Specimen B-B-1 95

66. Experimental Load Deflection for Specimen S-F-1 96

67. Experimental Load Deflection for Specimen B-F-1 97

68. Experimental Load Deflection for Damaged Specimen S-1 (retrofitted) 98

69. Experimental Load Deflection for Damaged Specimen S-1 (retrofitted) 99

70. Crack Pattern of Specimen S-1 101

71. Crack Pattern of Specimen B-1 102

72. Crack Pattern of Specimen S-B 103

73. Crack Pattern of Specimen B-B 104

74. Crack Pattern of Specimen S-F-1 105

75. Crack Pattern of Specimen B-F-1 106

76. Crack Pattern of Specimen S-1 (retrofitted) 107

77. Crack Pattern of Specimen B-1 (retrofitted) 108

78. Three Steel Solid Impactors Used for the Impact Load 110

79. Setup of the Dynamic Test Procedure in the Laboratory for Specimen S-2 111

80. The Final Failure Pattern of Specimen S-2 112

81. The Final Failure Pattern of Specimen S-B-2 113

82. The Final Failure Pattern of Specimen B-B-2 114

83. The Final Failure Pattern of Specimen B-F-2 116

84. The Final Failure Pattern of Specimen S-F-2 117

85. Experimental Strain-time Value for S-2 Test at 10 inches 119

86. Experimental Strain-time Value for S-2 Test at 10 inches 120

87. Experimental Strain-time Value for S-2 Test at 21 inches 122

88. Experimental Strain-time Value for S-2 Test at 21 inches 123

89. Experimental Strain-time Value for S-B-2 Test at 10 inches 124

90. Experimental Strain-time Value for S-B-2 Test at 10 inches 125

91. Experimental Strain-time Value for S-B-2 Test at 7 inches 126

92. Experimental Strain-time Value for S-F-2 Test at 10 inches..... 128

93. Experimental Strain-time Value for S-F-2 Test at 10 inches..... 129

94. Experimental Strain-time Value for S-F-2 Test at 21 inches..... 130

95. Experimental Strain-time Value for S-F-2 Test at 21 inches..... 131

96. Experimental Strain-time Value for B-B-2 Test at 10 inches..... 132

97. Experimental Strain-time Value for B-B-2 Test at 10 inches..... 133

98. Experimental Strain-time Value for B-B-2 Test at 25 inches..... 134

99. Experimental Strain-time Value for B-B-2 Test at 25 inches..... 135

100. Experimental Strain-time Value for B-F-2 Test at 10 inches 136

101. Experimental Strain-time Value for B-F-2 Test at 10 inches 137

102. Experimental Strain-time Value for B-F-2 Test at 17 inches 138

103. Experimental Strain-time Value for B-F-2 Test at 17 inches 139

104. Represents the Impactor Acceleration on Specimen S-2 at 10 inches..... 140

105. Beam Acceleration on Specimen S-2 at 10 inches 141

106. The Impactor Acceleration on Specimen S-2 at 21 inches..... 142

107. The Beam Acceleration on Specimen S-2 at 21 inches 143

108. The Impactor Acceleration on Specimen S-B at 10 inches 144

109. The Beam Acceleration on Specimen S-B at 10 inches 145
110. The Impactor Acceleration on Specimen S-B at 7 inches 146
111. The Beam Acceleration on Specimen S-B at 7 inches 147
112. The Impactor Acceleration on Specimen S-F at 10 inches 148
113. The Beam Acceleration on Specimen S-F at 10 inches 149
114. The Impactor Acceleration on Specimen S-F at 21 inches 150
115. The Beam Acceleration on Specimen S-F at 21 inches 151
116. The Impactor Acceleration on Specimen B-B at 10 inches 152
117. The Beam Acceleration on Specimen B-B at 10 inches 153
118. The Impactor Acceleration on Specimen B-B at 25 inches 154
119. The Beam Acceleration on Specimen B-B at 25 inches 155
120. The Impactor Acceleration on Specimen B-F at 10 inches 156
121. The Beam Acceleration on Specimen B-F at 10 inches 157
122. The Impactor Acceleration on Specimen B-F at 17 inches 158
123. The Beam Acceleration on Specimen B-F at 17 inches 159
124. Strain Gauge Locations on Sub-assemblage 160
125. Strain on Front Side for the Sub-assemblage S2-1 162
126. Strain on Rear Side for the Sub-assemblage S2-1 163
127. Strain on Front Side for the Sub-assemblage S2-2 165
128. Strain on Rear Side for the Sub-assemblage S2-2 166
129. Strain on Front Side for the Sub-assemblage B2-1 168
130. Strain on Rear Side for the Sub-assemblage B2-1 169
131. Strain on Front Side for the Sub-assemblage B2-2 171

132. Strain on Rear Side for the Sub-assemblage B2-2 172

133. Left Side of the Middle Joint Displacement for Sub-assemblage S2-1 173

134. Right Side of the Middle Joint Displacement for Sub-assemblage S2-1 175

135. Left Side of the Middle Joint Displacement for Sub-assemblage S2-2 176

136. Right Side of the Middle Joint Displacement for Sub-assemblage S2-2 177

137. Left Side of the Middle Joint Displacement for Sub-assemblage B2-1 179

138. Right Side of the Middle Joint Displacement for the Sub-assemblage B2-1 180

139. Left Side of the Middle Joint Displacement for Sub-assemblage B2-2 181

140. Right Side of the Middle Joint Displacement for Sub-assemblage B2-2 182

141. Left Support Rotation for Sub-assemblage S2-1 183

142. Right Support Rotation for Sub-assemblage S2-1 184

143. Left Support Rotation of Sub-assemblage S2-2 185

144. Right Support Rotation for Sub-assemblage S2-2 186

145. Left Support Rotation for Sub-assemblage B2-1 187

146. Right Support Rotation for Sub-assemblage B2-1 188

147. Left Support Rotation for Sub-assemblage B2-2 189

F148. Right Support Rotation for Sub-assemblage B2-2 190

149. Experimental Load Deflection for Sub-assemblage S2-1 191

150. Experimental Load Deflection for Sub-assemblage S2-2 192

151. Experimental Load Deflection for Sub-assemblage B2-1 193

152. Experimental Load Deflection for Sub-assemblage B2-2 194

153. Left Support Crack Pattern for Sub-assemblage S2-1 196

154. Right Support Crack Pattern for Sub-assemblage S2-1 197

155. Missing Column Crack Pattern at the Collapsed Load for Sub-assemblage S2-1..... 198

156. Crack Pattern at the Collapsed Load for Sub-assemblage S2-1 199

157. Underneath Crack Pattern in the Missing Column for Sub-assemblage S2-1..... 200

158. Crack Pattern on the Missing Column for Sub-assemblage S2-2..... 201

159. Crack Pattern on the Left Support for Sub-assemblage S2-2 202

160. Crack Pattern on the Right Support for Sub-assemblage S2-2..... 203

161. Missing Column Crack Pattern at the Collapsed Load for Sub-assemblage S2-2..... 204

162. Crack Pattern at the Collapsed Load for Sub-assemblage S2-2 205

163. Underneath Crack Pattern in the Missing Column for Sub-assemblage S2-2..... 206

164. Left Support Crack Pattern for Sub-assemblage B2-1..... 207

165. Right Support Crack pattern for Sub-assemblage B2-1..... 208

166. Missing Column Crack Pattern at the Collapsed Load for Specimen B2-1 209

167. Crack Pattern at the Collapsed Load for Specimen B2-1 210

168. Left Support Beam Fractured from Column at the Collapsed Load for Specimen B2-1 ... 211

169. Right Support Beam Fractured from Column at the Collapsed Load for Specimen B2-1 . 212

170. Right Support Concrete Crushed at Collapsed Load for Specimen B2-1..... 213

171. Underneath Crack Pattern in the Missing Column for Specimen B2-1..... 214

172. Left Support Crack Pattern for Specimen B2-2..... 215

173. Crack Pattern on the Missing Column for Specimen B2-2..... 216

174. Missing Column Crack Pattern at the Collapsed Load for Specimen B2-2 217

175. Crack Pattern at the Collapsed Load for Specimen B2-2 218

176. Left Support Beam Fractured from Column at the Collapsed Load for Specimen B2-2 ... 219

177. Right Support Beam Fractured from Column at the Collapsed Load for Specimen B22... 220

178. Missing Column Crack Pattern at the Collapsed Load for Specimen B2-2 221

179. Underneath Crack Pattern in the Missing Column for Specimen B2-2..... 222

180. Catenary Forces Provided through the Positive Moment Reinforcement [20]..... 223

181. Catenary Action on Specimen S2-1..... 224

182. Catenary Action from Side Strain-load Relationships of Sub-assemblage S2-1..... 225

183. Catenary Action Rear Side Strain-load Relastionships of Sub-assemblage S2-1..... 226

184. Catenary Action on Specimen S2-2..... 227

185. Catenary Action from Side Strain-load Relationships of Sub-assemblage S2-2..... 228

F186. Catenary Action Rear Side Strain-load Relationships of Sub-assemblage S2-2..... 229

187. Catenary Action on Specimen B2-1 230

188. Catenary Action Front Side Strain-load Relationships of Sub-assemblage B2-1..... 231

189. Catenary Action Rear Side Strain-load Relationships of Sub-assemblage B2-1..... 232

190. Catenary Action on Specimen B2-2 233

191. Catenary Action Front Side Strain-load Relationships of Sub-assemblage B2-2..... 234

192. Catenary Action Rear Side Strain-load Relationships of Sub-assemblage B2-2..... 235

193. Hinge System Theoretical Formation (Fadhil, 2012) 237

194. Hinge Formation on the Left Support for Specimen S-21..... 238

195. Hinge Formation on the Right Support for Specimen S-21..... 239

196. Hinge Formation on the Missing Column for Specimen S-21 240

197. Hinge Formation on the Left Support for Specimen S2-2..... 242

198. Hinge Formation on the Right Support for Specimen S2-2..... 243

199. Hinge Formation on the Missing Column for Specimen S2-2 244

200. Hinge Formation on the Left Support for Specimen B2-1 245

201. Hinge Formation on the Right Support for Specimen B2-1 246

202. Hinge Formation on the Missing Column for Specimen B2-1 247

203. Hinge Formation on the Left Support for Specimen B2-2 249

204. Hinge Formation on the Right Support for Specimen B2-2 250

205. Hinge Formation on the Missing Column Specimen B2-2 251

206. (A) Layered Rectangular Section (B) Strain Distribution (C) Stresses and Forces 255

207. Beam with Concentrated Point Load, Deflected Shape, and Bending Moment Diagram .. 258

208. Theoretical Moment-Curvature for Specimen S-1 260

209. Theoretical Moment-Curvature for Specimen B-1 261

210. Theoretical Moment-Curvature for Specimen S-B-1 262

211. Theoretical Moment-Curvature for Specimen B- B-1 263

212. Theoretical Moment-Curvature for Specimen S-F-1 264

213. Theoretical Moment-Curvature for Specimen B-F-1 265

214. Theoretical Moment-Curvature for Damaged Specimen S-F-1 (retrofitted) 266

215. Theoretical Moment-Curvature for Damaged Specimen B-F-1 (retrofitted) 267

216. Theoretical Moment-Curvature for Sub-assemblage S2-1 268

217. Theoretical Moment-Curvature for Sub-assemblage S2-2 269

218. Theoretical Moment-Curvature for Sub-assemblage B2-1 270

219. Theoretical Moment-Curvature for Sub-assemblage B2-2 271

220. The Comparison of the Theoretical and Experimental Load-deflection Curve for Specimen S-1 280

221. The Comparison of the Theoretical and Experimental Strain Moment-curvature for Specimen S-1 281

222. The Comparison of the Theoretical and Experimental Load-deflection Curve for Specimen B-1..... 282

223. The Comparison of the Theoretical and Experimental Strain Moment-curvature for Specimen B-1..... 283

224. The Comparison of the Theoretical and Experimental Load-deflection Curve for Specimen S-B-1..... 284

225. The Comparison of the Theoretical and Experimental Strain Moment-curvature for Specimen S-B-1..... 285

226. The Comparison of the Theoretical and Experimental Load-deflection Curve for Specimen B-B-1..... 286

227. The Comparison of the Theoretical and Experimental Load-deflection Curve for Dpecimen S-F-1..... 287

228. The Comparison of the Theoretical and Experimental Load-deflection Curve for Specimen B-F-1..... 288

229. The Comparison of the Theoretical and Experimental Strain Moment-curvature for Specimen B-F-1..... 289

230. The Comparison of the Theoretical and Experimental Load-deflection Curve for Specimen S-1 damaged (retrofitted)..... 290

231. The Comparison of the Theoretical and Experimental Strain Moment-curvature for Specimen S-1 damaged (retrofitted)..... 291

232. The Comparison of the Theoretical and Experimental Load-deflection Curve for Specimen B-1 damaged (retrofitted)..... 292

233. The Comparison of the Theoretical and Experimental Strain moment-curvature for Specimen B-1 damaged (retrofitted)..... 293

234. Experimental Comparison between Beams S-1, S-B, and S-F at Ultimate Strength..... 294

235. Experimental Comparison between Beams S-1, S-B, and S-F Deflection at Service Load of 5.0 kips 295

236. Experimental Comparation between Beams B-1, B-B, and B-F at Ultimate Strength..... 296

237. Experimental Comparation of Beam B-1, B-B, B-F, and B-1 D-R Deflection at Service Load of 5.0 kip-..... 297

238. Experimental Beam Acceleration versus Theoretical Value for Specimen S-2 with Impactor 2 at 10 inches 302

239. Experimental Beam Acceleration for Specimen S-2 with Impactor 2 at Collapsed Load.. 303

240. Experimental Beam Acceleration versus Theoretical Value for Specimen S-B with Impactor 2 at 10 inches 304

241. Experimental Beam Acceleration for Specimen S-B 2 with Impactor 2 at Collapsed Load 305

242. Experimental Beam Acceleration for Specimen S-F 2 with Impactor 2 at 10 inches 306

243. Experimental Beam Acceleration versus Theoretical Value for Specimen S-F h Impactor 2 at Collapsed Load 307

244. Experimental Beam Acceleration versus Theoretical Value for Specimen B-B with Impactor 2 at 10 inches 308

245. Experimental Beam Acceleration for Specimen B-B with Impactor 2 at Collapsed Load 309

246. Experimental Beam Acceleration Value for Specimen B-F with Impactor 2 athes 310

247. Experimental Beam Acceleration for Specimen B-F 2 with Impactor 3 at Collapsed Load 311

248. The Comparison of the Theoretical and Experimental Load-Deflection Curve for the Sub-assemblage S2-1..... 317

249. The Comparison of the Theoretical and Experimental Moment-Curvature for Sub-assemblage S2-1..... 318

250. The Comparison of the Theoretical and Experimental Load-deflection Curve for Sub-assemblage S2-2 319

251. The Comparison of the Theoretical and Experimental Moment- curvature for Sub-assemblage S2-2 320

252. The Comparison of the Theoretical and Experimental Load-deflection Curve for Sub-assemblage B2-1 321

253. The Comparison of the Theoretical and Experimental Moment- curvature for Sub-assemblage B2-1 322

254. The Comparison of the Theoretical and Experimental Load-deflection Curve for Sub-assemblage B2-2 323

255. The Comparison of the Theoretical and Experimental Moment-curvature for Sub-assemblage B2-2 324 256. Experimental Comparison between Sub-assemblages S2-1 and S2-2 at Ultimate Strength 325

257. Experimental Comparison between Sub-assemblages B2-1 and B2-2 at Ultimate Strength 326

258. Experimental Comparison between Sub-assemblages S2-1 and B2-1 at Ultimate Strength 327

259. Experimental Comparison between Sub-assemblages S2-2 and B2-2 at Ultimate Strength 328

CHAPTER 1 INTRODUCTION

1.1 Background

The subject matter of post-terrorist attack residual strength of buildings gained considerable importance after incidents such as the 1995 Alfred P. Murrah Federal Building, Oklahoma City disaster and the 9/11 events related to the destruction of the World Trade Center twin towers. Figure 1 represents the final conditions of both buildings after the terrorist attacks. This dissertation presents the outcome of research related to determining the effectiveness of Basalt Fiber Reinforced Polymer (BFRP) when used in concrete beams and building sub-assemblages for enhancing both the structural performance and strength. Specifically, a quasi-static and impact load response of BFRP reinforced concrete beams and a post-terrorist-attack sub-assemblage is investigated both theoretically and experimentally.

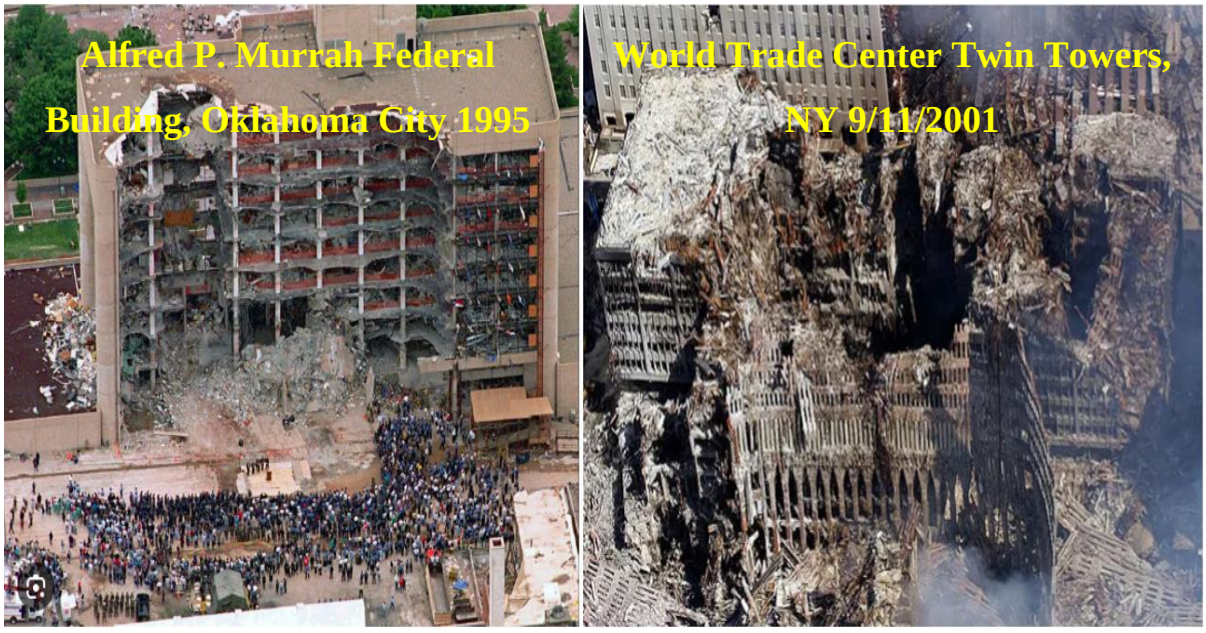

Figure 1. Alfred P. Murrah Building and World Trade Center after Collapse

Prior to SEI/ASCE 7-05, there were no general design guidelines in the United States to circumvent progressive collapse [1]. Typically, during the design phase of a commercial building, the analysis of progressive collapse is not performed due to the cost and time. Only the Department of Defense, General Services Administration, and Homeland Security have requirements to meet the progressive collapse criteria during the design stage. Each new building is designed according to the Federal agency's criteria.

In accordance with UFC 4-023-03, "DoD Progressive Collapse Guidelines", the use of fiber-reinforced polymer (FRP) to provide the tie forces is prohibited due to the limitation on the guideline of rotation limitation of 11.3 degree or 0.20-rad [2]. Due to the rotation limitation, controlling rotation using BFRP reinforcement became a big challenge in this project as this material has similar rigidized of regular steel reinforcement.

The use of the Alternate Path Method is very typical during this analysis. This concept consists of removing a column so the structure will be capable of bridging over the removed vertical element. For this research, an innovative Basalt fiber reinforced polymer (BFRP) retrofitting scheme for strengthening this sub-assembled section of the concrete building in order to reduce damage or prevent progressive collapse was used.

Analysis and design for progressive collapse in structures before the Alfred P. Murrah Building collapse in 1995 is not very clear because design codes did not have specific sections for a structural engineer to follow. ACI-318-05, "Building Code Requirements for Structural Concrete" [3] refers to use of Section 7.13, "Requirements for Structural Integrity" where it indicates some recommendations on what type of splice, location, and minimum reinforcement to utilize in the support area. Chapter 21, "Earthquake-Resistant Structures" was used to design the shear capacity of different types of structures, such as ordinary moment frames, intermediate moment frames, special moment frames, etc.

Progressive collapse analysis was never a priority until after the Oklahoma City bombing and the terrorist attacks on September 11, 2001, after which the Department of Defense (DoD, 2009) and General Services Administration (GSA, 2003) established guidelines on progressive collapse. These were developed by the Federal Government after the bombing of Alfred P. Murrah Federal Building with approximately 4,000 lbs. of a fertilizer-based explosive (ANFO) which

resulted in approximately 75 percent of the building in Oklahoma City to experience a dramatic collapse on April 19, 1995.

There are two ways to analyze and design a structure to resist progressive collapse: direct design and indirect design [2]. Direct design has two methods: Alternate Path Method and Specific Local Resistance Method. The Alternate Path Method allows local failure to occur but seeks to provide alternate load paths so that the damage is absorbed, and major collapse is averted. The Specific Local Resistance Method provides sufficient strength to resist failure from accidents or misuse.

For indirect design, implicit consideration of resistance to progressive collapse during the design process through the provision of minimum levels of strength, continuity, and ductility.

In private industry, there are not many buildings that are designed to resist progressive collapse. Only Federal Buildings built after 2001 meet some conditions, such as buildings more than three-stories tall that require analysis against progressive collapse.

The DoD and GSA use two different approaches. The DoD approach removes exterior and interior columns on each floor, while the GSA approach removes exterior columns only on the first floor. These analysis procedures are for both approaches [2]:

- Static linear–demand-capacity ratio
- Static nonlinear rotation / ductility
- Dynamic linear demand–capacity ratio
- Dynamic nonlinear rotation / ductility

The UFC 4-023-03 and GSA Progressive Collapse Guidelines Figure 2 explained the correct approach of how to remove a column during the progressive collapse analysis.

The outcome of the results presented in the dissertation has the potential for practical applications in reducing the progressive collapse of concrete structures.

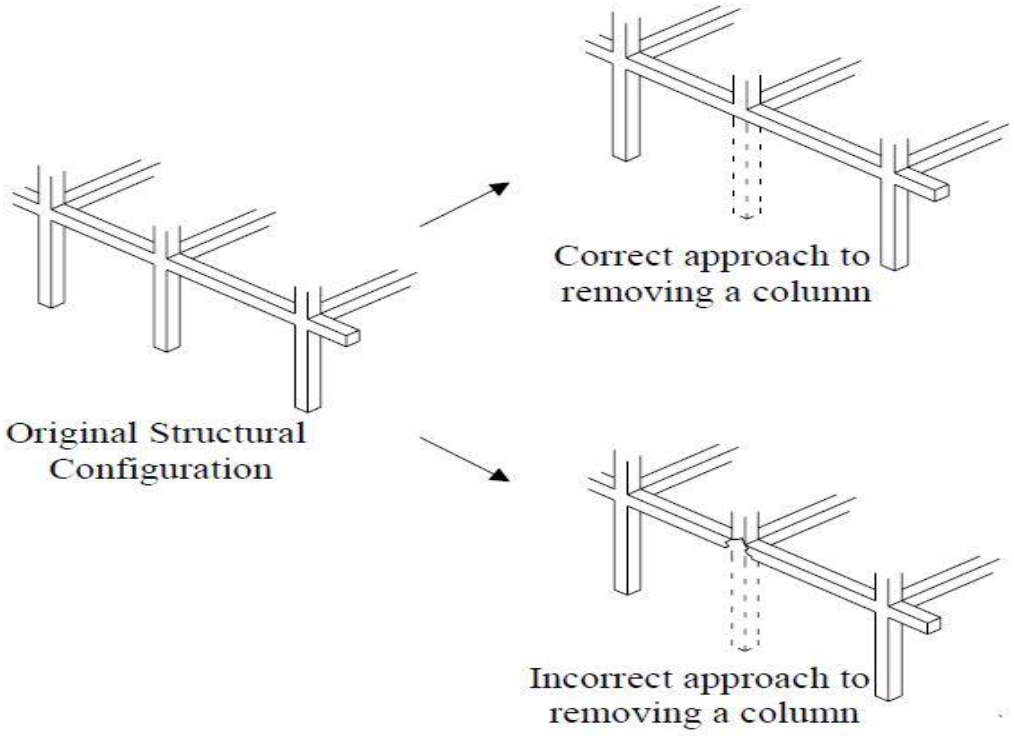

Figure 2. The Process to Remove a Column during the Alternate Path Load Method (Source: UFC4-023-03 and GSA Progressive Collapse Guidelines)

Figure 3 represents a concrete frame building with a car bomb in front of one column. Figure 4 represents a single column that failed during the explosion and the effect of the explosion on the structural members in the building. Figure 5 is the structural representation of the equivalent boundary conditions for two bay beams and column of interest during this research and the components, forces, and displacement analyzed during this research. The q load in the beam represents the distribution load in the floor area and P load applied in the column represents the total loads applied in the building per floor to the column. The sub-assemblage is assumed to have fixed-end boundary conditions. The theoretical prediction model should be applicable to a full-scale concrete building sub-assemblage.

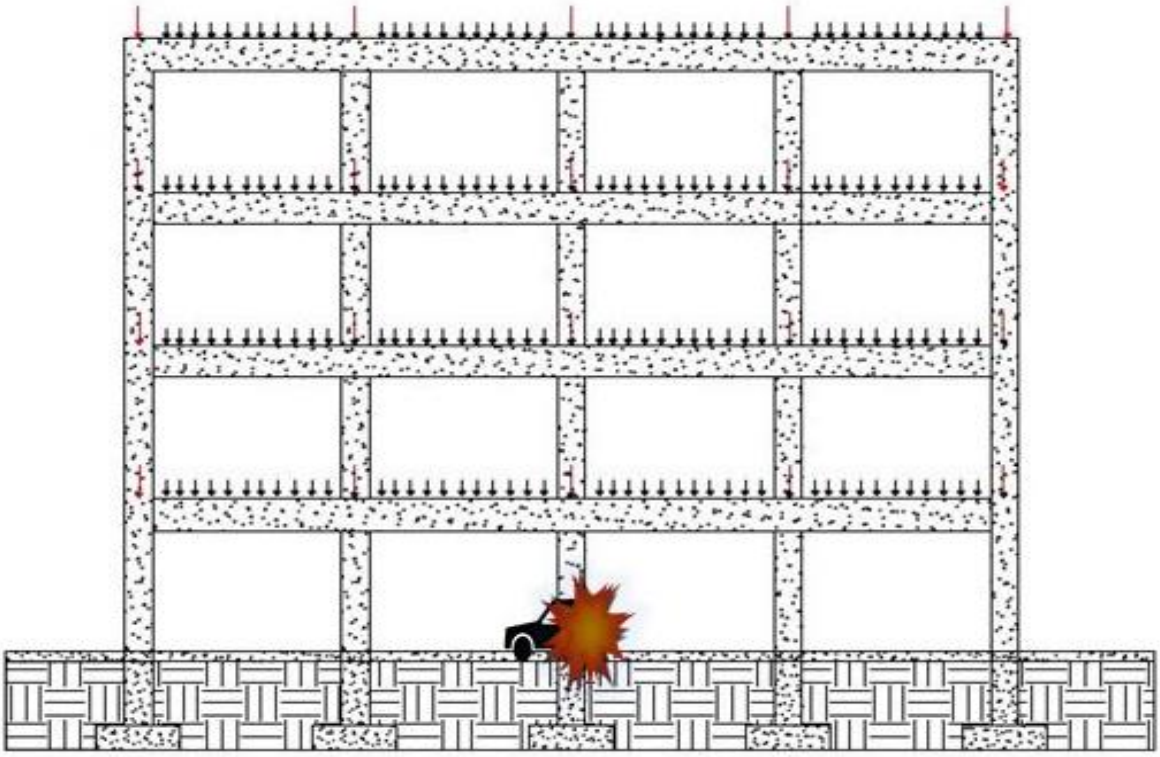

Figure 3. Typical 2-D Concrete Building Frame under Terrorist Attack

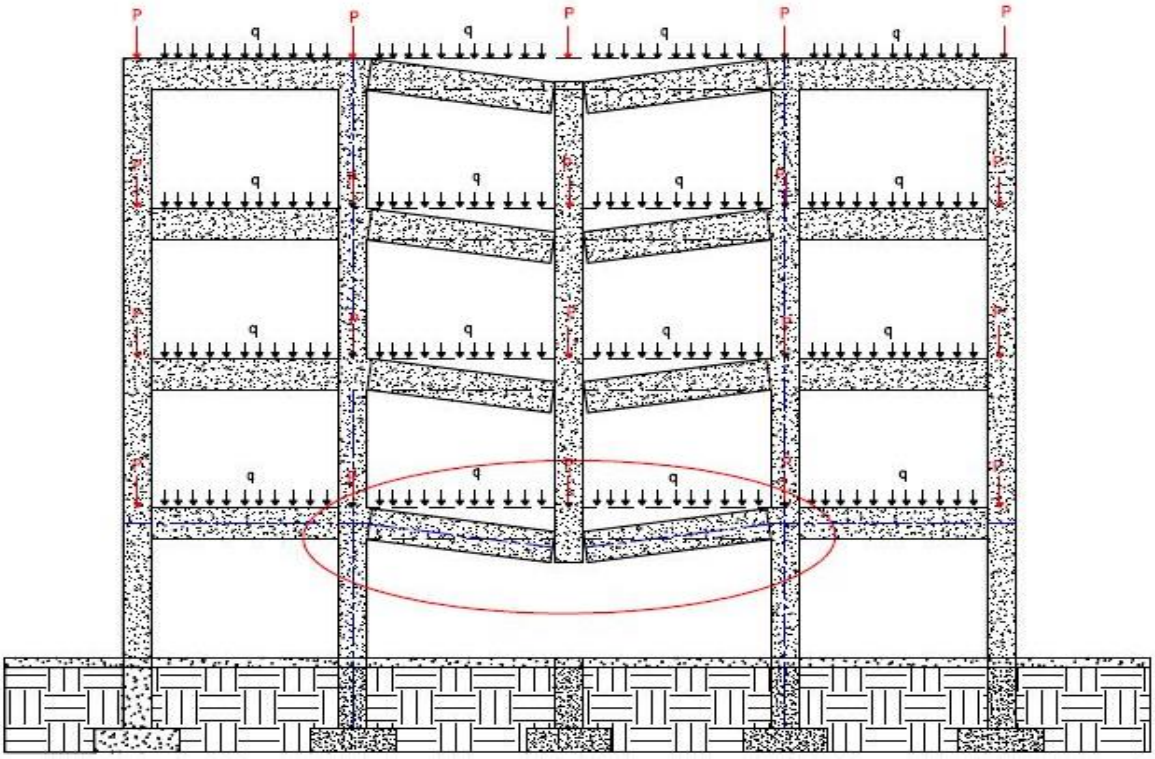

Figure 4. Typical 2-D Concrete Building Frame with a Lost Column

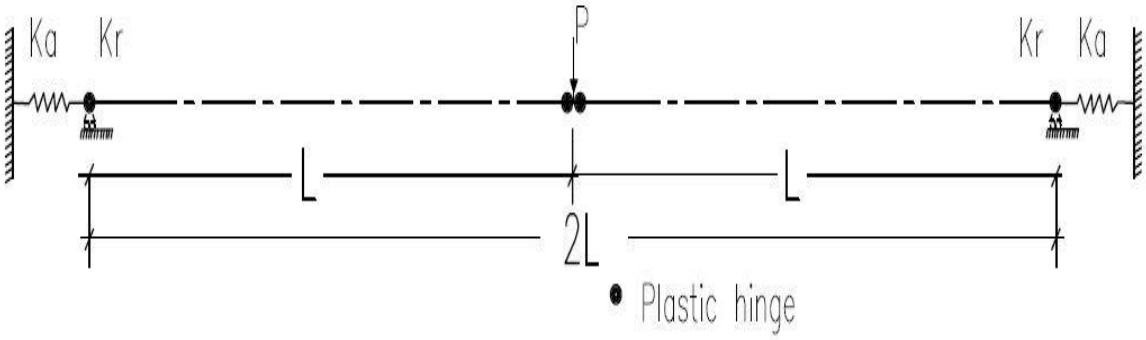

Figure 5. Equivalent Boundary Conditions for Two-bay Sub-assemblage

BFRP is a relatively new engineering material. ACI 440-1R-15 [4] and ACI-440-2R-08 [5] does not have all the coefficients as a regular FRP material that have been in the construction industry for long time, in particular environmental reduction factor, creep rupture, and typical tensile properties. The manufacturers are dependent upon providing the design values needed for your design. The fiber is made from volcanic rock melted in high heat temperature. It is approximately four times lighter than regular steel bars. BFRP strength is comparable with carbon fiber reinforced polymer (CFRP) strength and the modulus of elasticity is very similar to glass fibers reinforced polymer (GFRP). BFRP is more economical material than CFRP. The manufacturing process used to form composite reinforcement is known as Pultrusion. Figure 6 illustrates a typical layout of FRP production with all the production components. Table 1 illustrates the comparison of properties between BFRP, CFRP, GFRP, AFRP and regular steel reinforcement [4].

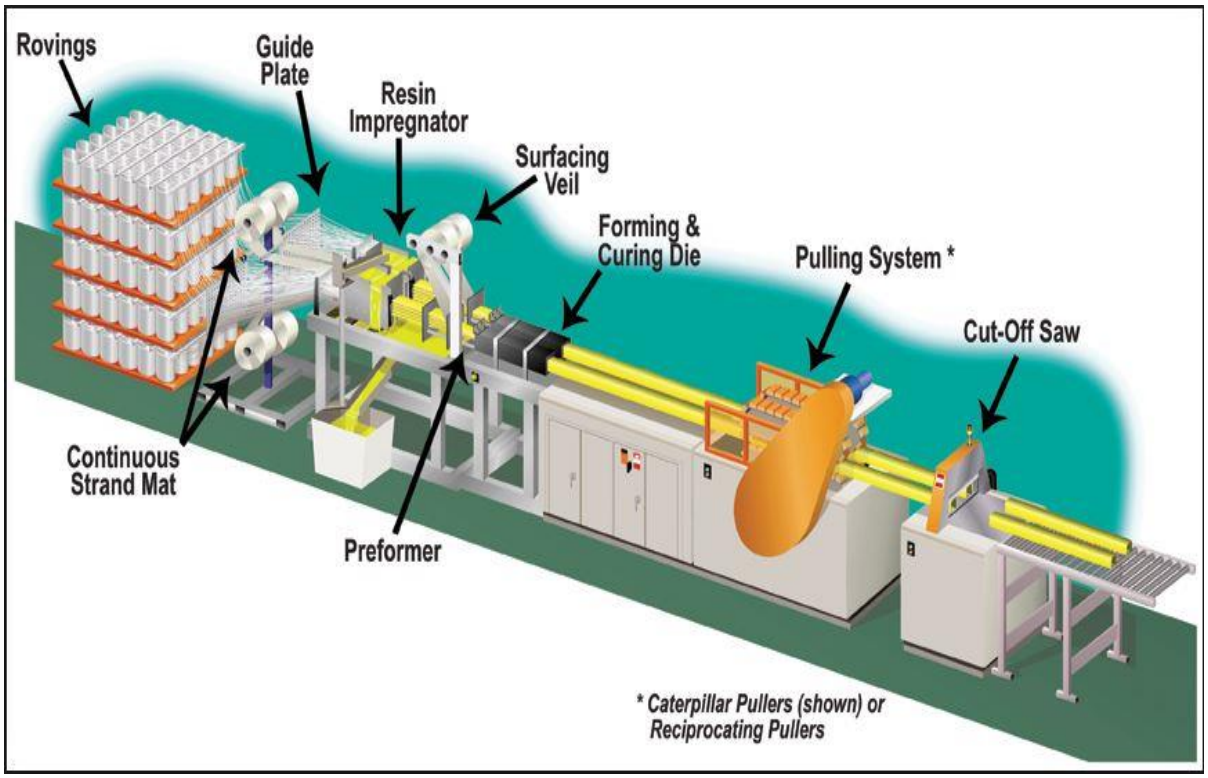

Figure 6. Typical Layout of FRP Production (Picture Courtesy of Smarter Building Systems LLC in Newport, RI)

Table **1**. Comparison between BFRP, Other FRP, and Steel Reinforcements

Items		Steel*	GFRP*	CFRP*	AFRP*	BFRP**
Nominal yield stress (ksi)		40 to 75	NA	NA	NA	NA
Tensile strength (ksi)		70 to 100	70 to 230	87 to 535	250 to 368	101.5 to 188.5
Elastic modulusx10^3 (ksi)		29	5.1 to 7.4	15.9 to 84.0	6.0 to 18.2	6.5 to 9.4
Yield strain, percent		0.14 to 0.25	NA	NA	NA	NA
Rupture strain, percent		6.0 to 12.0	1.2 to 3.1	0.5 to 1.7	1.9 to 4.4	Pending
Coefficient of thermalx10e-6 ºC	lengthwise	11.7	6.0 to 10.0	-1 to 0	-6 to -2	9.0 to 12.0
	transverse	11.7	21.0 to 23.0	22 to 50	60 to 80	21.0 to 22.0
* From ACI440-1R-15 ** information provided by vendors						

1.2 Literature Review

Unified Facilities Criteria 4-023-03 [2] were developed after 9/11 to protect DoD properties against progressive collapse, the criteria are divided by different construction materials, such as steel, concrete, masonry, cold-framed steel, and wood structures in addition to the analysis and general design section. The review of this material focused on Chapter 2, “Progressive Collapse Design Requirements”, Chapter 3, “Design Procedures”, and Chapter 4, “Reinforced Concrete Structures”. The most important element of the UFC is the design analysis and procedure to conduct progressive collapse analysis in DoD facilities. Explain the process of how you will remove the column during progressive collapse analysis. The UFC includes dynamic increase factor (DIF) for nonlinear static analysis in lieu of conducting dynamic analysis. The majority of the design values referred to in the UFC criteria are from the ASCE-41, which is the code for earthquake design and the evaluation of the existing structures.

Yu and Hai Tan [6] investigated the case of four reinforced concrete frame with non-seismic and seismic detailing where the quasi-statically testing was used to investigate the structural behavior of a concrete frame under the column removal scenario (CRS). The entire specimen was designed with different design details and different boundary conditions. The purpose of using this literature was to investigate the effects of different boundary conditions and different design details on the overall structural behavior and compare their results against the UFC-4-023-03, particularly how the longitudinal reinforcement can function as effective ties to develop the catenary action in the system. One of the findings was that the seismic shear detail in the sub-assemblages does not help to the progressive collapse. Another major finding was that top longitudinal reinforcement was broken at the joint and does not provide any additional tie force due to a major rotation in the joint and does not meet UFC-4-023-03 criteria for tie force rotation.

Wang, Zhang, Li, and Yan [7] compared three major building progressive collapses: the Ronan Point Tower in Canning Town, London in 1968; the Alfred P. Murrah Federal Building in Oklahoma City in 1995; and the World Trade Center in New York in 2001. The international design criteria and codes for buildings to prevent progressive collapse were created and edited after each of the cases presented in this paper. In the United States, it was not until the Oklahoma event that progressive collapse requirements were created, particularly for federal Buildings. They identified in this research that the deformations under progressive collapse are much bigger than the deformations under the seismic study completed.

Mosalam, Talaat, and Park [8] utilized existing information from structures tested at the University of California, Berkeley, and developed 3D scale (1/3 scale) structures with three bays and four columns. Two columns were designed using non-ductile details with widely spaced ties and the other two were designed following ACI-318-2002. The design used the weak-column strong beam mechanism. It was concluded that the algorithm used simulated the dynamic redistribution of forces in addition to providing a simplified model of the impact. The comparison between the computationally estimated and experimentally observed from previous

tests in the shaking table for the collapse modes and results revealed the validity of the developed computational approach of progressive collapse simulation using direct elements removal.

Starossek [9] focuses on different areas of progressive collapse and types of progressive collapse–in this area, the author explains each mechanism in detail and explains how it originated in each one. It also explains the brittle material behavior and how the brittle material can be particularly beneficial or when the material can be particularly harmful.
In the design procedures section, the author explains how the local check in term of stress and stability can affect the progressive collapse analysis of the final structural design. The majority of the design codes do not require that the designer verify the entire structure as a single structure against progressive collapse; not all structures behave the same way in the local failure and the possible code improvement to validate large deformation and displacement, structural elements separation and overturning components.

Design against progressive collapse is the difference between robustness and collapse resistance. Starossek defines robustness as the insensitivity to a local failure in terms of qualitative and quantitative and the collapse resistance as and insensitivity to accidental circumstances with a low probability of happening. It also explains the four design criteria steps with a flow diagram, these are: design requirements, design objectives, design methods and verification procedures. Design methods–this section the author used as an example the Alfred P. Murrah Federal Building in Oklahoma to explain exactly what happened in this building and how the building behaved after the explosion.

Starossek explained how to prevent local failure using the specific local resistance approached using the Oklahoma case. He explained that this meant that the lower-level columns can be designed against blast load to prevent local failure. On the alternative load paths, he explained that if the Oklahoma case during the original design the designer had eliminated the transfer girder on the second floor and transferred all the load in a direct column line to the foundation the alternative load paths can be prevent the progressive collapse of the building despite the building having local failure. In the isolation by segmentation area, he explains the process to avoid progressive collapse in particular multi-span bridges, in particular the big role that the

connection between spans plays. In the applications section, the author explained all the use and how to prevent progressive collapse in bridges, cable bridges and multistory buildings. The approach that they took during the theoretical analysis was focused on the progressive collapse resistance demand and the robustness assessment for the building structures. The author concluded with three main concerns: The majority of the experiments used static load and not dynamic load, progressive collapse is a dynamic phenome, if this effect is ignoring, the design may misunderstand the collapse mechanism of the building and its material properties. Second, the author introduced the numerical method in this research, however this method only applied to simple structures. Third, he identified that the nonlinear dynamic effect in regular simple structures is based on dynamic and energy theory and the nonlinear effect for complex structures is still needed.

Ovitigaka, Ibrahim, and Issa [10] used eight RC beams with the same cross section and same length. The design of the specimens followed the ACI 440-1R-06 guide for the design and construction of structural concrete reinforcement with fiber-reinforced polymer (FRP) bars and used the reduction factor of 0.65. It was observed that too large of a beam would create a deformation prior to failing due to the lack of ductility in the FRP and low modulus of elasticity. The eight RC beams were designed with different areas of Basalt FRP bars (10, 13, 16, and 25mm diameter bars), and compared with the reinforcement ratio and the balanced ratio, all eight beams are over-reinforced. This specimen was divided into three different groups based on reinforced ratio and deflection. The failure of the eight beams was a plan, that the concrete will crush the top center part of the beam and the beam fail. Some of the findings were the rate of change in moment capacity and deflection decrease with increases in the reinforcing ratio / reinforcement ratio at balance strain condition. ACI 440.1P-06 underestimated the ultimate moment capacity.

Elgabbas, Vincent, Ahmed, and Bermokrane [11] conducted research of the bar's flexural behavior at service and ultimate load and to evaluate the bond-dependent coefficient (kb) of the Basalt FRP. Three different bar diameters were used during this project (10, 12, and 16mm) as main tension beam reinforcement. The investigation consisted of six rectangular beams designed in accordance with the rectangular cross section and Ontario, Canada: Canadian Standard

Association 2012 (CAN CSA-S-806-12), and the design and construction of building structures with fiber reinforced polymer. Each beam was tested using four-point loads with a clear span between loads of 500 mm. All the beams had two 10mm bars in the compression zone and two or four bars in the main tension reinforcement. Each beam was provided steel for shear using regular 10mm steel bar to avoid shear failure and no stirrups was provided in the constant moment zone. The test was designed to fail by concrete crushing. The strain was measured using strain gauges 6 mm in length and the deflection was recorded using linear variable differential transduces (LVDTs). The six beams behaved very similarly until the first crack. In the conclusion they found that the cracking moments were lower than was predicted, the Basalt FRP RC-concrete beams showed typical bilinear behavior for strain and deflection until failure, beams with low reinforcement ratio showed sharp increase in strains and deflection at cracking, the axial stiffness of the flexural reinforcement significantly affected the general behavior of the Basalt RC beams and indicated that ACI (2006) underestimated the deflection at $0.30M_n$.

Maariappan and Singaravadivelan [12] conducted research on nine sub-assemblages with a cantilever beam being tested. All specimens had the same cross section and same length. Two different codes were utilized to develop this research: IS 456:2000 and IS 13920:1993. Only three specimens were provided with lateral ties in the column area. The test consisted of loading the specimen with axial load only up to 15 and 30 percent of the specimen load capacity and recorded load, cracks, and deflection. Lateral load was applied in intervals of 5KN. The first beam was identified as a control specimen, all the specimens were tested in this mode only. Three specimens designed using IS 456:2000 was retrofitted with Basalt fabric and tested. The beam with Basalt fabric took additional load before it developed the first crack in all cases. One of the results was that the specimens designed using IS 13290:1993 had better behavior than the specimens designed using IS 456:200. The second finding was the results for the specimen retrofitted with Basalt fabric had very good behavior in terms of less deflection from more load before developing cracks than the beam designed using IS 456:2000 and IS 13290:1993.

Ghrobarah and Said [13] conducted research consisting of four sub-assemblage joints that were designed to represent existing structures before 1970’s design and construction. The specimens

were tested using two different types of loads: constant axial load and reversing quasi-static cycle load. The load was applied very slowly to prevent the dynamic effect in the specimen. Two specimens were tested with only 10 and 20 percent load capacity and were identified as control beams. The rehabilitation schemes were with GFRP bi-directional glass fiber woven at +/- 45 degree, wrapping the specimen as U shape, one layer, two layers and three layers of fabric was used during the rehabilitation of the specimens. Only the beam with two layers of fiber performed well, the other three specimens had different types of problems such as: deboned, unanchored layer of the GFRO around the joint.

Sigavadivelant [14] conducted research in four simply supported beams with the same cross section and same length, one beam was used as a control beam and the other three were retrofitted with Basalt fabric. The second beam installed one layer, the third beam installed two layers and the last beam installed three layers of fabric, this material was installed using Araldite LY 556 and Hardener HY 951 these are Indian products. At the end of the investigation was it found that the beam with one layer increased the load capability by 60 percent compared with the control beam, the beam with two layers increased the capability by 62 percent and the beam with three layers increased the load capability by 70 percent compared with the control beam.

Hall, Woodson, Baulot, Hayes, and Shon [15] conducted research with the intention to develop a progressive collapse analysis and damage assessment methodology using previous progressive collapse research and high-performance computer simulations. They divided the methodology into three stages. Phase I was a progressive collapse analysis methodology where they identified 6 steps to follow: identify the problem; theory review and procedure definition; numerical approaches and computer code review; modify and/or develop numerical code; validation; and parametric study. Phase II used call system identification and was developed using 6 steps: identify behavioral characteristics; theory review and procedure definition; review computer codes; develop or modify numerical codes; validation; and parametric study. Phase III’s physical tests included 5 stages: structural model; structural prototypes; test; system identification; and test data analysis. As a result of this study, they developed a methodology that any designer can follow to provide safety structures subjected to abnormal loads and provided some tools for an

engineer to predict the type and range of possible progressive collapse at the design stage or after any incidents.

Baldridge and Humay [16] investigated a five-story building with typical floor to floor height of 12 feet with the exception of the first floor, which as was 15 feet, five bays of 24 feet in the longitudinal direction, and three 24 feet bays in the transverse direction. The building was designed to meet the 1997 UBC. The analysis for this building under progressive collapse was conducted using U.S. General Services Administration (GSA) Progressive Collapse Analysis and Design Guidelines for New Federal Buildings and Major modernization Projects. They conducted structural analysis under Seismic Zone 4 and 2B. This guideline used the load factor of 1 for dead load and 0.25 for live load and multiplied by two to account for the dynamic factor that will occur during progressive collapse in the structures. They also evaluated the results of the linear elastic analysis using FEMA 273 and 274 where the definition of the demand-capacity ratio (DCR) for shear and flexure should be below 1.0 to prevent progressive collapse if this value exceeds 1.0. The failure of an element is imminent if the DCR value for shear is called a brittle failure mode. The concept of the DCR identified the magnitude and distribution of potential areas of the inelastic demand. For each seismic zone they developed two cases; in one case they removed one column in the middle of the longitudinal side, and in the other case a corner column was removed. Due to the design pattern in which all columns were designed equally in the long and short direction, the transversal bays did not control the design for progressive collapse. Their finding was that the maximum beam DCR in flexure was 1.02, which is acceptable for flexure, and the beam had enough reserve capacity to redistribute moments to other portions of the structure. On the DRC, the shear maximum value obtained was 0.69 for the same case 1 zone 2B and progressive collapse was not obtained. Their recommendation was that the moment resistant frame was adequate for Zone 2B and Zone 4. The reinforced concrete moment-resisting frames provided adequate structure continuity, redundancy, and ductility, and selecting the lateral load resisting systems will provide, simultaneously, the lateral load and the progressive collapse requirements.

Zhou, Li, Wang, and Zhao [17] conducted research on a one story, two bays in each direction reinforced concrete frame. The dimension of the frame was 3.6m x 2.6m and 1.75m in height,

following the Code for Design of Concrete Structures (GB50010-2010) and Building Seismic Design Code (JGJ101-96) from China. The approach used in this investigation was a quasi-static loading method, where the load was applied to the column in the corner. The loading procedure was force-displacement hybrid control. The force was used to control the load in increments of 1kn until part of the component yield. At that point, the displacement controlled the load. Using this approach, the displacement was increased in multiples of 5mm and delayed for 10 minutes until the data collection instrumentation was stable, and then the strain gauges in the beams were read. At each of the load stages, strains and crack widths were recorded with a crack microscope. These measurements were taken until the structure failed. A relationship was established between resistance and vertical displacement and was divided into three areas: elastic state, plastic state, and failure state. In the elastic state, the load and displacement were increased; the first crack was observed at 5kn in the upper part of the beam away from the corner column. This crack finished the elastic stage. In the plastic stage, a plastic hinge was formatted. At 25mm vertical displacement and load of 16.4kn, the member reached maximum bearing capacity. After this displacement and load, the beam connection started to fail, and the angle of failure in the column was gradually formed. The concrete strain curve, strain of steel, and development of plastic hinge was plotted. The conclusion of this research was that when the corner column failed, the frame beam in the failure region resisted the external load by bending and provided resistance to continuous collapse. It was also found that the plastic limit load of the frame was calculated by plasticity theory and was smaller than the experimental value; however, the percentage of difference between the two values was not indicated in the paper.

Minimum Design Loads and associated criteria for building and other structures (ASCE7-16) [18] in Section 2.5 included a load combination for extraordinary events where it defines the applicability of this load combination during fires, explosions, and vehicular impact without disproportionate collapse. The Code provided a load combination to check again the structure or structural element to withstand the effect of an extraordinary event. It also provided residual capacity equation to check the structure or elements after the event and provided stability requirements for the entire structure or elements.

Jun, Tan, and Hai [19] investigated two RC sub-assemblages following ACI 318-05, one specimen was designed without seismic criteria and the second specimen was designed with seismic design criteria, under middle column removal scenarios. Part of the investigation was to determine the flexural action and the compressive arch action followed by the catenary action when the middle column was removed, and the beam developed a significant deformation at mid-span. They concluded that the compressive arch action and the catenary action provided a much higher resistance than the flexural action. The specimens' designs according to ACI-318-05 have sufficient integrity of reinforcement and the catenary action can be mobilized successfully. Also, they did not find any significant differences in structural performance due to different detailing rules.

1.3 Problem Definition

The problem addressed in this dissertation deals with quasi-static and impact load response of concrete beams and building post-terrorist-attack sub-assemblages when reinforced or retrofitted with Basalt Fiber Reinforced Polymer (BFRP) reinforcement and wraps in order to mitigate structural damage. A materially nonlinear quasi-static analysis is formulated and verified by laboratory tests. The post-impact response of the sub-assemblages is studied using a simplified dynamic analysis model with practical damping. The principal problem is to quantify the degree of the effectiveness of BFRP reinforcement and wraps in increasing the ultimate strength and the overall performance of both the beams and a typical sub-assemblage in reinforced concrete buildings subjected to a terrorist attack.

1.4 Objectives and Scope

The main objective in this research is to present the outcome of experimental and theoretical investigation on progressive collapse behavior on continued fixed end supported concrete sub-assemblages. The principal part of this research is to understand the behavior and ductility of building concrete joints during progressive collapse. A second objective is to determine the effectiveness of the BFRP reinforcement in the original beams and the retrofitting of the beams, and how the beams with Basalt material will behave, particularly in the degree of rotation.

This dissertation deals with the behavior of continued fixed end supported concrete sub-assemblage during progressive collapse. This dissertation is divided into two sections. The first part consisted of the analysis and behavior of thirteen simply supported concrete beams with regular steel and BFRP reinforcement. Nine of these thirteen beams were retrofitted using BFRP fabric or external BFRP reinforcement prior to load, and two were retrofitted after loaded and some damage was generated. A total of thirteen simply supported beams were evaluated using regular reinforcement steel and BFRP under quasi-static and impact load. Based on the failures of the beams during this research, retrofitting schemes will be developed to analyze their effectiveness and compare them with requirements in UFC-4-023-03 [2]; particularly, the rotation issues and compliances. The results obtained from this research will provide a better understanding of the behavior of sub-assemblages under progressive collapse.

This dissertation includes a series of tests investigating of the particular sub-assemblage connection line, using the strain gage in all the adjacent elements is our main point of interest in order to determine the behavior of all elements around the critical point (the joint between the beam and column) where the impact load is applied. The impact load was used because it represents a blast load from a terrorist attack and that dynamic load can be used as blast load where one exterior column will fail during any stream load such as: blast explosion or impact load during a terrorist attack.

For the first part of this research, a total of thirteen simply supported beams were prepared for testing. The cross section is 4.5 inches x 5.5 inches and length of 60 inches, with a clear distance between supports of 55 inches. The height of 5.5 inches was selected between the minimum height of the beam with steel reinforced from the ACI 318 Table 9.2 [3] using Equation 1 and ACI 440.1R-15 Table 7.3.2.1 [4] using Equation 2, after calculating both equations. The equation from ACI-440.1R governed the design selection for this experiment.

$$Hc = L/16 \quad [3] \tag{1}$$

$$Hb = L/10 \quad [4] \tag{2}$$

With these equations, the smaller height section was selected for a simply supported beam or continuous beam without calculating deflection as a control for the design. Both the steel and the BFRP reinforcement are identical with two bars on the tension section, spacing between stirrups of 4.5 inches, and two reinforcements # 3 in the compression section to hold in place the stirrups.

The second part of this research consisted in determining the best combination reinforcement from the first part of this experiment to develop four sub-assemblages that are the main point of interest in this research: two without seismic shear design and two with seismic shear design were loaded in the intermediate column until failure as simulation of the progressive collapse due to a column failure.

The second part of this experiment used sub-assemblage specimens to evaluate two span beams with the most efficient steel / BFRP reinforcement configuration from the first part of this research. The cross section for this part of the experiment was 4 inches x 5 inches x 32 inches clear span between support and total length from outside of column to outside column of 76 inches.

1.5 Assumptions and Conditions

A. Concrete has no tensile strength.
B. The stress-strain relationship for concrete in compression is nonlinear.
C. The stress-strain relationship for steel is elastic perfectly plastic on both tension and compression.
D. The effects of creep and shrinkage of the concrete are disregarded; however, a stirrup will be provided to prevent early shear failure.
E. Plane sections remain plane before and after bending, implying no warping deformation.
F. Small deflection theory
G. Weak-beam, strong-column. Beam failure is generally preferable to column failure. Beam failure typically only affects the structure in close proximity; column failure could lead to progressive collapse.

H. Maximum strain at the extreme compression fiber of the concrete is assumed to be 0.003 in/in.
I. Reinforcing bars are recommended to be ASTM A706.
J. Straight reinforcing bars should be used to avoid reduced ductility at bends.
K. Transverse reinforcement continued through joint.
L. No splice reinforcement within 2d of the joint.
M. No splice at the hinge zone.

CHAPTER 2 EXPERIMENTAL STUDY

2.1 Introduction

This chapter presents the experimental part of this research study. This experimental study included three stages. In the first stage of the experiments, the mechanical properties of the constituent materials are determined and compare the theoretical values with the experimental values. These materials consist of concrete, steel reinforcing reinforcement, and Basalt reinforcement and Basalt fabric. In the second stage, rectangular beam members were tested under various combinations of reinforced tension and retrofitting. In the third stage, four two-span sub-assemblage specimens having fixed supported at the end are tested.

2.2 Material Properties

It is required to conduct an experimental test for all the material and components that were used during this research in order to determine the final stress or shear value and compare it with the nominal stress value to obtain the most precise results from the laboratory. During this experimental study, four different types of material were used: concrete, steel reinforcement, BFRP reinforcement, and BFRP fabric.

2.2.1 Concrete

The compressive strength of concrete used for the design is 4.00 ksi. The final concrete strength was obtained after a series of concrete cylinders tests. The concrete strength averages a 28 days was 4.21 ksi at an ultimate strain of 0.0032 in/in and elastic modulus of 3,699.74 ksi. Due to the reinforcement congestion on the sub-assemblage specimens the coarse aggregate was selected as ½ inches and addition of water was required to have better workability during the concrete pour stage, this reduced the concrete strength to 3.08 ksi. at an ultimate strain of 0.0031 in/in and elastic modulus of 3,163.4 ksi. Figure 7 indicates the stress-strain plot using the non-linear equation 3 to determine the stress-strain relationship of the concrete. Figure 8 shows a concrete cylinder (4”x8”) test.

$$f_c = f_c' \left[\frac{2\epsilon}{\epsilon_0} - \left(\frac{\epsilon}{\epsilon_0} \right)^2 \right] \quad (3)$$

2.2.1.1 Concrete mix tabulation for the four batches for construction of all specimens

Table 2 represents the four concrete batch mixes used during this research. It indicates the weight of each material and the quantity of water used in each concrete mix.

Table 2. Concrete Mix Composition for Each Concrete Batch

Concrete mix/Cylinder #	Cylinder length (in)	Cylinder area (in^2)	Load Applied (Kips)	Concrete Strength (ksi)
M1 / 1	8	12.57	55.53	4.42
M1 / 2	8	12.57	53.42	4.25
M1 / 3	8	12.57	55.48	4.41
M2 / 1	8	12.57	48.95	3.89
M2 / 2	8	12.57	55.42	4.41
M2 / 3	8	12.57	55.53	4.42
M3 / 1	8	12.57	55.47	4.41
M3 / 2	8	12.57	53.42	4.25
M3 / 3	8	12.57	48.75	3.88
M4 / 1	8	12.57	38.72	3.08
M4 / 2	8	12.57	37.46	3.06
M4 / 3	8	12.57	38.97	3.10

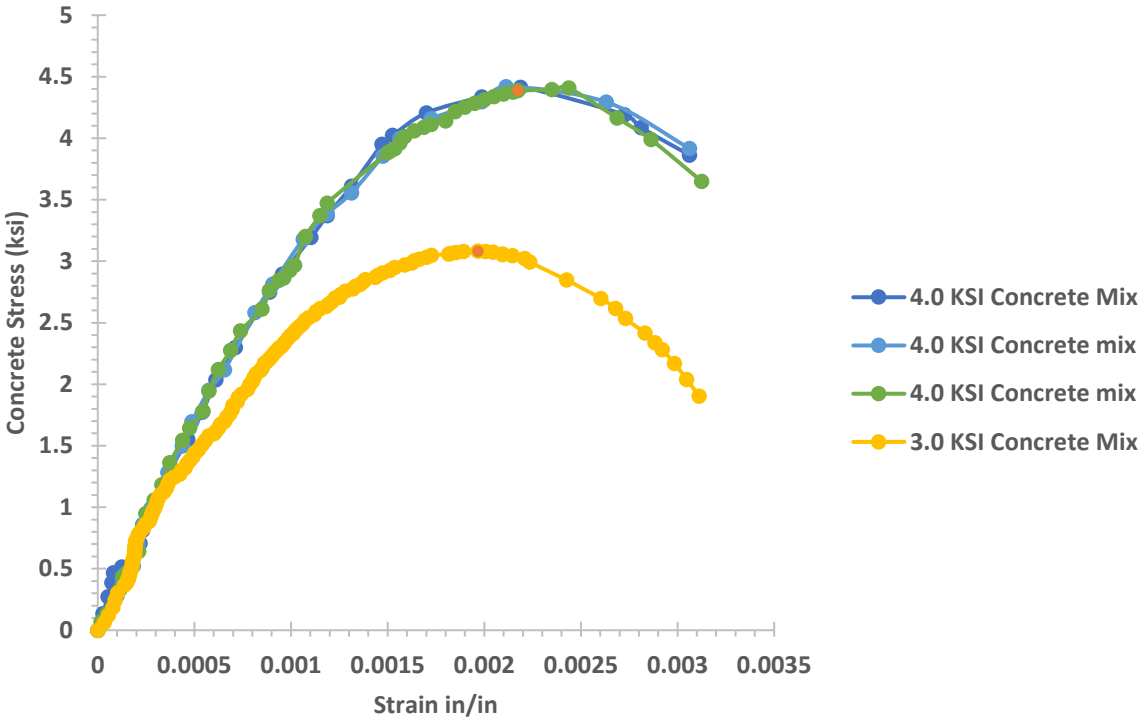

Figure 7. Concrete Stress-strain Relationships

Figure 8. Sample of Compression Concrete Cylinder Test

2.2.2 Steel Reinforcement

During this experimental study, two different types of steel reinforcement were used: bar # 3 (3/8 inch) for all bending reinforcement and ¼ inches for the stirrups. All specimens were steel grade (60 ksi). Tensile test results of these reinforcements were presented in Figure 9 and 10, respectively.

The steel yield used in the design phase of this research was steel grade 60 (60 ksi). A series of experimental tests were conducted to determine the final yield stress of the material used in this research. Final yield stress for # 3 reinforcement was obtained after a series of tests using the elongation to calculate the strain and to determine the average final yield stress of 68.2 ksi at an ultimate strain of 0.0023 in/in and modulus of elasticity of 29,380.0 ksi. Final yield stress for # 2

reinforcement was obtained after a series of tension tests and the final yield stress was 89.82 ksi at an ultimate strain of 0.0295 in/in.

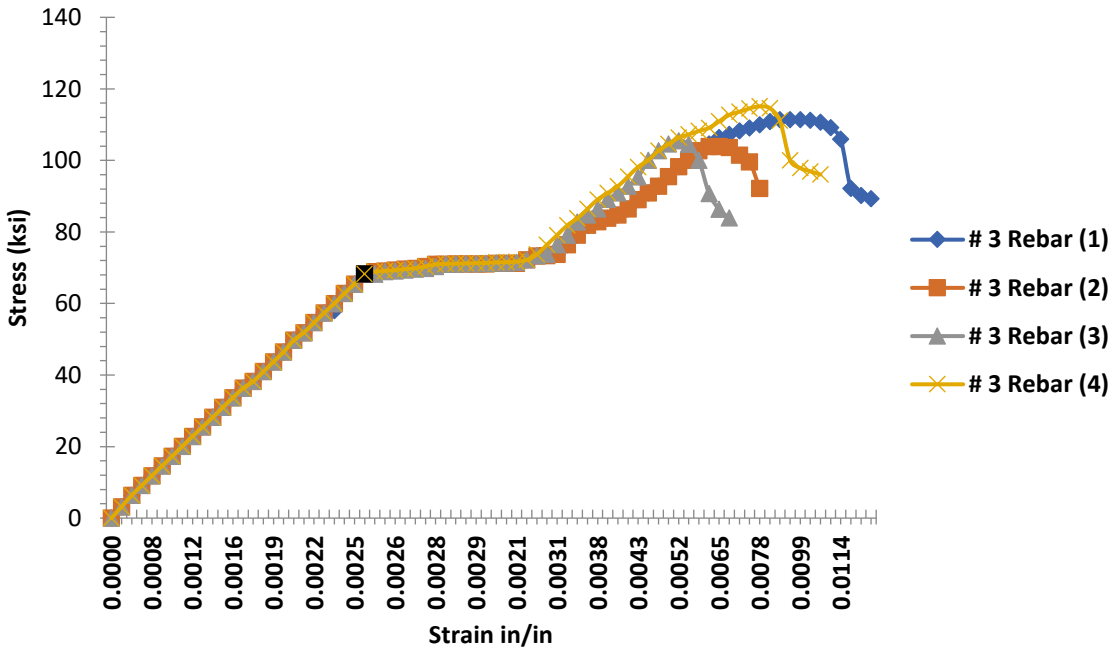

Figure 9. Stress-strain Relationship of # 3 Reinforcements

The bilinear approximation of the stress-strain relationship is represented mathematically as shown below in Equations # 4 and # 5.

$$f_s = E\varepsilon_s \qquad when \quad |\varepsilon_s| \leq \varepsilon_y \tag{4}$$

$$f_s = f_y \qquad when \quad |\varepsilon_s| > \varepsilon_y \tag{5}$$

The stress strain relationship is represented graphically in Figure 10:

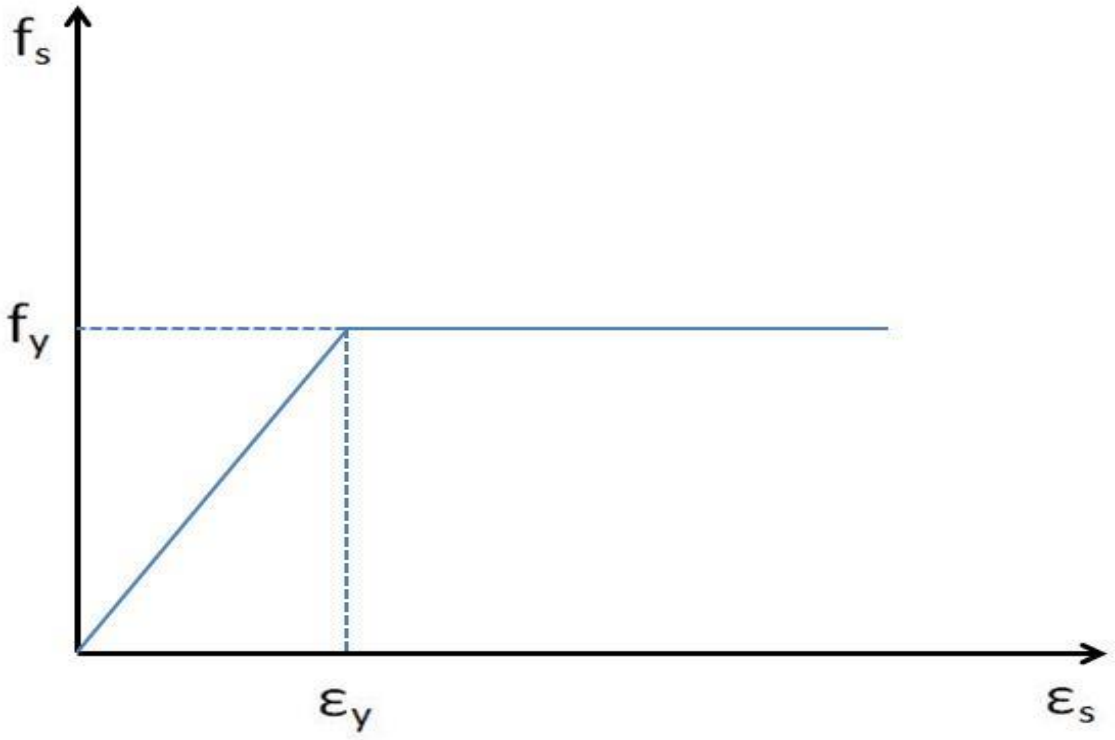

Figure 10. Stress-strain Relationship Theoretical Value of Steel

2.2.3 Basalt Fiber Reinforced Polymer (BFRP)

Two different types of BFRP reinforcement were used during this research; one type of basalt reinforcement for main longitudinal reinforcement (10mm for the simply supported beam and 8mm for the beam column beam) and one smaller cross section (4mm) for the exterior retrofitted reinforcement. BFRP mesh was installed in four beams as a retrofitted provision; however, after more detailed analysis, it was found that the location of the mesh does not provide an additional retrofitted system. BFRP fabrics were installed in four beams as a retrofitted mechanism to increase the beams strength, load capability, and reduction deflection.

2.2.3.1 BFRP Bars 4mm

The tensile yield strength of the BFRP is 217.556 ksi and elastic modulus of 7,125.886 ksi. BFRP has the commercial name “BRB-4 Basalt Reinforcement FRP” sold by Smarter Building Systems LLC in Newport, RI. This material will be used for substitution of the regular steel reinforcement. The bar is 4mm diameter with a cross sectional area of 12.57 mm^2 or 0.019 in^2. These bars will be tested for tensile properties using ASTM D7205/D7205M-06. Final tensile strength (rupture point) obtained after a series of tensile tests using the elongation to calculate the strain due to the small cross section made it impossible to install the strain gauge to determine the final tensile strength of 138.85 ksi at an ultimate strain of 0.02229 in/in and modulus of elasticity of 6,228.80 ksi. Figures 11 and 12 represent the stress-strain relationship theoretical and experimental value of BFRP bar.

2.2.3.2 BFRP Bars 8mm

The tensile strength of the Basalt FRP is 80.65 ksi and elastic modulus of 6,950.38 ksi. BFRP with commercial name “BRB-8 Basalt Reinforcement FRP” sold by Smarter Building Systems LLC in Newport, RI. This material will be used for substitution of the regular steel reinforcement.

The bar was 8mm diameter with a cross sectional area of 50.28 mm^2 or 0.0779 in^2. These bars were tested for tensile properties using ASTM D7205/D7205M-06. Final tensile strength (rupture point) obtained after a series of tensile test using the elongation to calculate the strain and to determine the final tensile strength of 69.15 ksi at an ultimate strain of 0.0100 in/in and modulus of elasticity of 6,854.92 ksi. Figures 11 and 12 represent the stress-strain relationship theoretical and experimental value of BFRP bar.

2.2.3.3 BFRP Bars 10mm

The tensile strength of the Basalt FRP is 145.00 psi and elastic modulus of 6,700.0 ksi. BFRP with commercial name “BRB-10 Basalt Reinforcement FRP” sold by Smarter Building Systems LLC in Newport, RI. This material was used for substitution of the regular steel reinforcement.

The bar was 10mm diameter with a cross sectional area of 78.57 mm^2 or 0.12 in^2. These bars were tested for tensile properties using ASTM D7205/D7205M-06. Final tensile yield obtained after a series of tensile tests with strain gages on each side to determine the final tensile strength (rupture point) of 71.56 ksi at an ultimate strain of 0.0124 in/in and elastic modulus of 5,777.65 ksi. Figures 11 and 12 graphically represents the stress-strain relationships for the BFRP reinforcement.

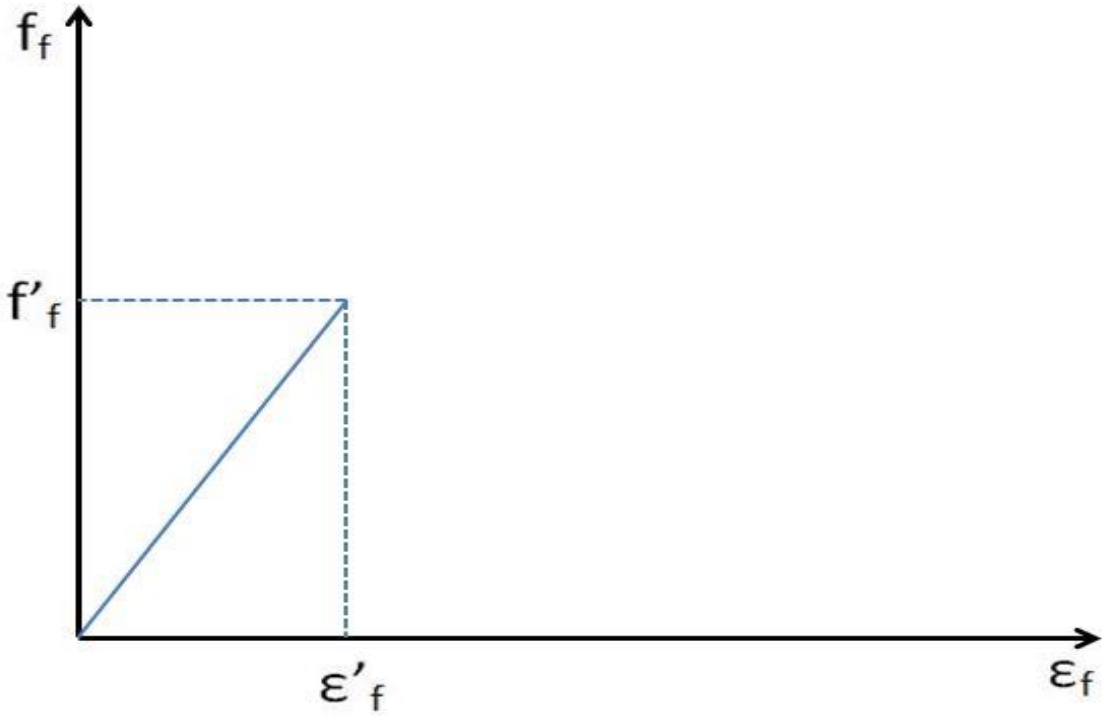

Figure 11. Stress-strain Relationship Theoretical Value of BFRP Reinforcement

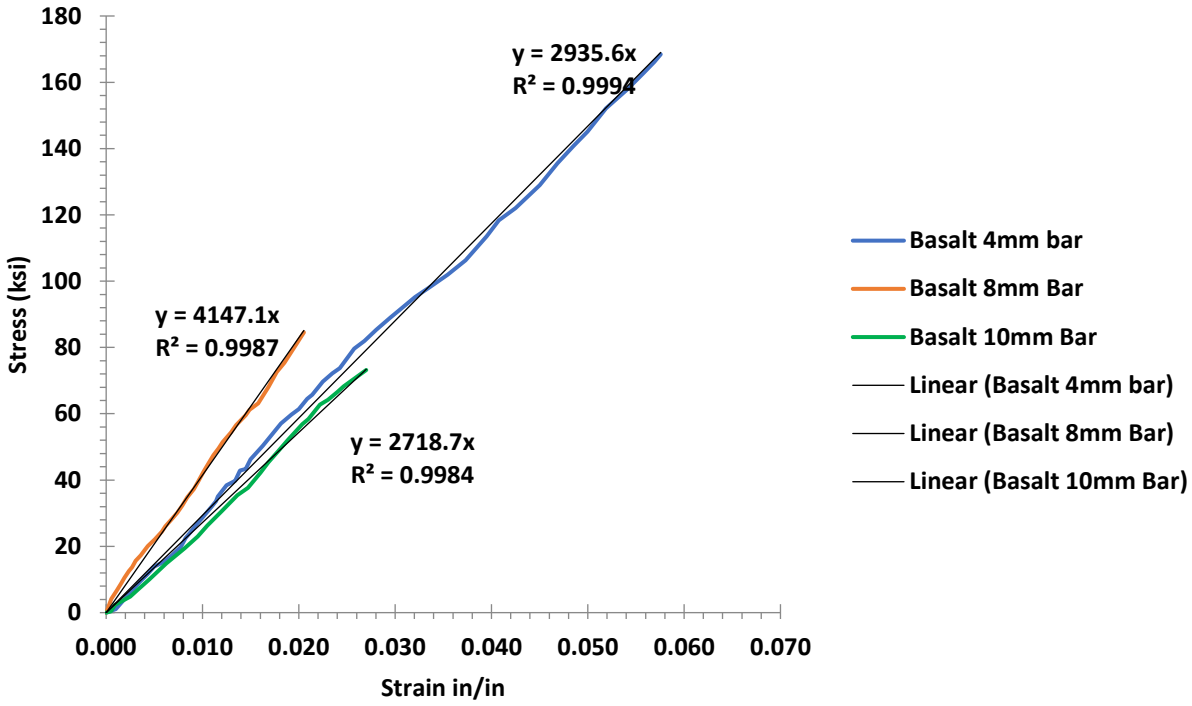

Figure 12. Stress-strain Relationship for the BFRP 4mm, 8mm, and 10mm Bar

2.2.3.4 BFRP Fabric

The multi-directional Basalt fabric with commercial name BA-450-13 +/-0.45-0.45-127 with width of 50 inches sold by Smarter Building Systems LLC in Newport, RI has the following properties: density (g/cm^3) of 2.8, elastic modulus of 12,908.359 ksi, tensile strength of 406.11 ksi, and elongation to fracture of 3.15 percent. This material was used to retrofit some specimens during this experiment. The final tensile yield was obtained using Sikadur 330 and BFRP fabric after a series of tensile tests to determine the final tensile strength (rupture point) of 35.32 ksi at an ultimate strain of 0.0325 in/in and elastic modulus of 1,017.27 ksi. Figure 13 graphically represents the stress-strain relationship of the Basalt fabric.

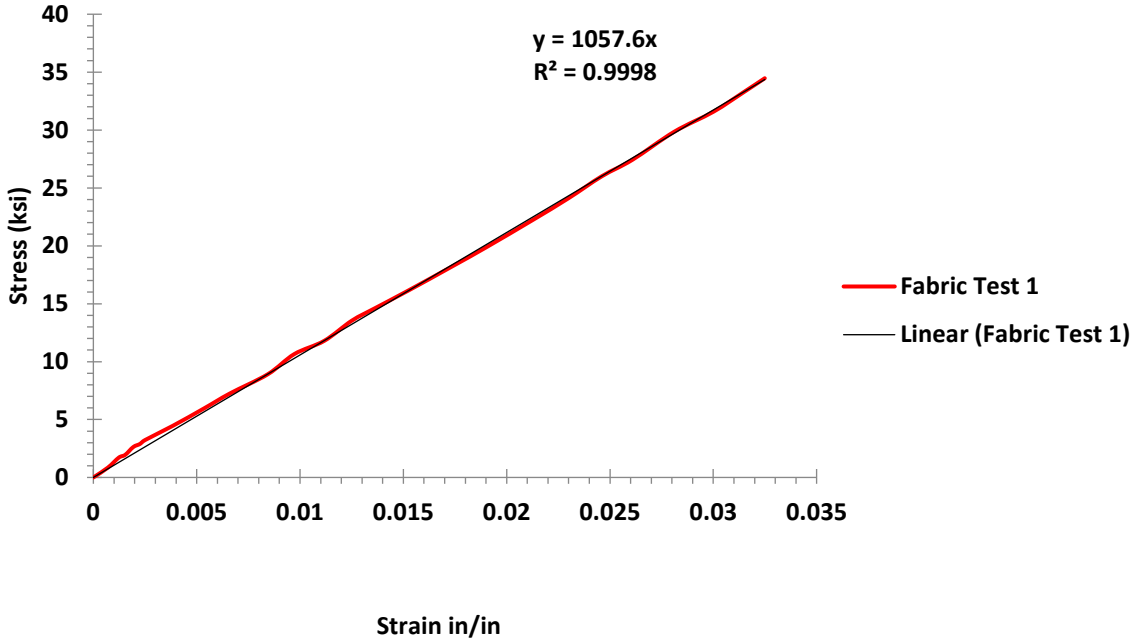

Figure 13. Stress-strain Relationship for the BFRP Fabric

2.2.4 Epoxy Materials

Two different types of epoxies were used during this research; one solid mix to install the exterior Basalt reinforcement as a retrofitted and a liquid epoxy mix to install the Basalt fabric.

2.2.4.1 Sikadur 30

Figure 14 illustrates the Sikadur 30 material as a two-component mix. It is a 100 percent solid with high modulus and strength and is a structural epoxy paste adhesive. This epoxy paste was used to bond the Basalt 4mm in the tension side of the beams with regular steel. The installation followed the manufacturer's recommendation. Material required a seven-day curing process after installed. The Basalt reinforcement was installed 28 days after the beams were pored. The

application requires a minimum temperature of 40^{o} F. This product is in compliance with the current ASTM-C-881 Type I, IV Grade 3, Class C and AASHTO M-235.

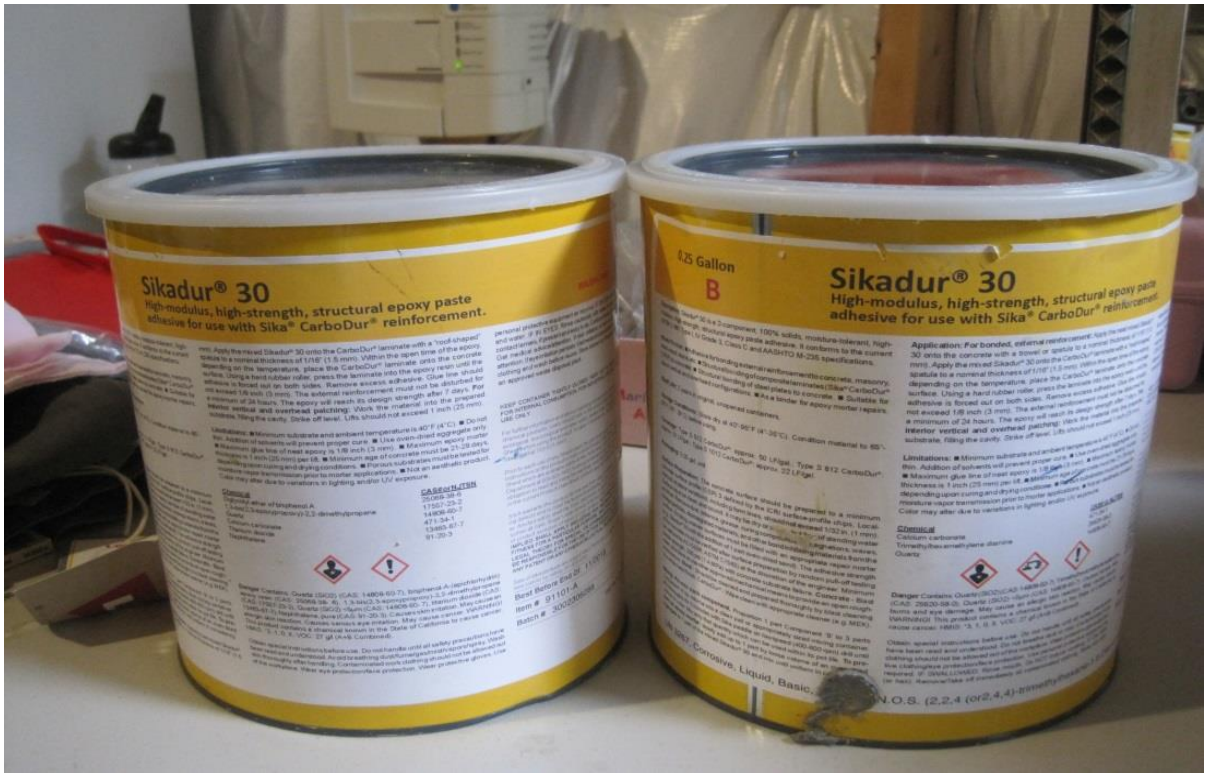

Figure 14. Sikadur 30-Part A and Part B Product

2.2.4.2 Sikadur 330

Figure 15 illustrates the Sikadur 330. This material as a two-component mix. It is solvent-free, moisture-tolerant, high modulus and strength, and is structural epoxy adhesive. This epoxy was used to bond the Basalt fabric on three sides of the beams with regular steel and Basalt reinforcement. The installation followed the manufacturer's recommendations. Material required a seven-day curing process after installed. The Basalt fabric was installed 28 days after the beams were pored. The application requires a minimum temperature of 40^{o} F. This product is in

compliance with the current ASTM-D-695 for compressive and ASTM D-638 for tensile strength.

Figure 15. Sikadur 330-Part A and Part B Product

2.3 Test Setup and Testing Procedures

The test setup, specimen preparation, data recorded, testing arrangement and procedure are discussed in the subsequent sections.

2.3.1 Test Specimen Preparation

The first part of this research as conducting analysis and lab tests of a simply supported concrete beam specimens to establish preliminary design parameters such as concrete strength, steel yield,

some dynamic results, and design efficiency in terms of steel/Basalt configuration prior to design and constructed the two span sub-assemblage specimens.

The second part of this research conducted analysis in continuous two span fixed end supported concrete sub-assemblage. During the analysis, the area cross section and quasi-static loads applicable to the specimen were defined. Four sub-assemblage specimens were tested. The first step was preparing the reinforcement skeleton with tension and compression reinforcement with stirrup to prevent early shear failure. This steel skeleton was set inside of a wood form work to be ready for pouring concrete, letting the beams cure for at least 28 days before start of the testing procedures.

Figure 16 illustrates the retrofit steel reinforcements, shear reinforcement, the BFRP 4mm reinforcement used as external retrofitted method, and the location of the BFRP fabric that was used as a second method of retrofit. Figure 17 illustrates the longitudinal BFRP reinforcements, shear reinforcement, the BFRP 4mm reinforcement used as the external retrofitted method, and the location of the BFRP fabric that was used as a second method of retrofit. Figure 18 illustrates the fabrication of the stirrups used ¼ inches diameter reinforcement and with exterior dimensions of 4 inches x 3 inches; these dimensions provided ¾ inches clear space around the entire beam. Figure 19 illustrates the fabrication of the reinforcement skeleton for all beams. Figure 20 illustrates five formworks for the simply supported beams. Figure 21 illustrates the reinforcement skeleton of the beam located inside of the formwork and ready to pour concrete. Figures 22 and 23 illustrate how the reinforcement was cut at the center points, and that no stirrup was provided 5 inches at both sides of the center line to obtain pure flexural moment zone in the center of the beam for the beam reinforced with steel reinforcement and for the beam reinforced with BFRP reinforcement.

Two beams with regular steel reinforcement in the tension side were constructed as a control specimen and were tested as a static and impact load. One beam with BFRP reinforcement in the tension side was constructed as a control specimen and was tested as a quasi-static load. Four beams with BFRP reinforcement were retrofitted: two with external BFRP reinforcement (2-

4mm) using Sikadur 30 as structural epoxy paste adhesive. Figure 24 illustrates the pre-grooved of the two beams that were retrofitted with basalt 4mm. Figures 25 and 26 illustrates the concrete mix preparation, concrete pour, and the eight beams after concrete was poured. From this first part, the most efficient beam construction will be obtained to develop the second part of this research.

Figure 27 represents the typical cross section for the two-span sub-assemblage with steel reinforcement: (A-A) typical beam cross section, (B-B) typical column cross section. Figure 28 represents the typical cross section for the two-span sub-assemblages with steel reinforcement and seismic detail: (A-A) typical beam cross section, (B-B) typical column cross section. Figure 29 represents the typical cross section for the two-span sub-assemblage with BFRP reinforcement: (A-A) typical beam cross section, (B-B) typical column cross section. Figure 30 represents the typical cross section for the two-span sub-assemblages with Basalt reinforcement and seismic detail: (A-A) typical beam cross section, (B-B) typical column cross section. Figure 31 represents the typical form work for two continuous span beams. Figure 32 represents regular steel reinforcement, regular steel reinforcement with seismic detail, BFRP reinforcement and BFRP reinforcement with seismic detail skeletons within the formwork ready to pour concrete of two-span sub-assemblage.

Experiments included non-retrofitted specimens and nonlinear theoretical analysis of the systems of two beams and three columns as framed. Figure 33 illustrates a two span sub-assemblage without retrofit.

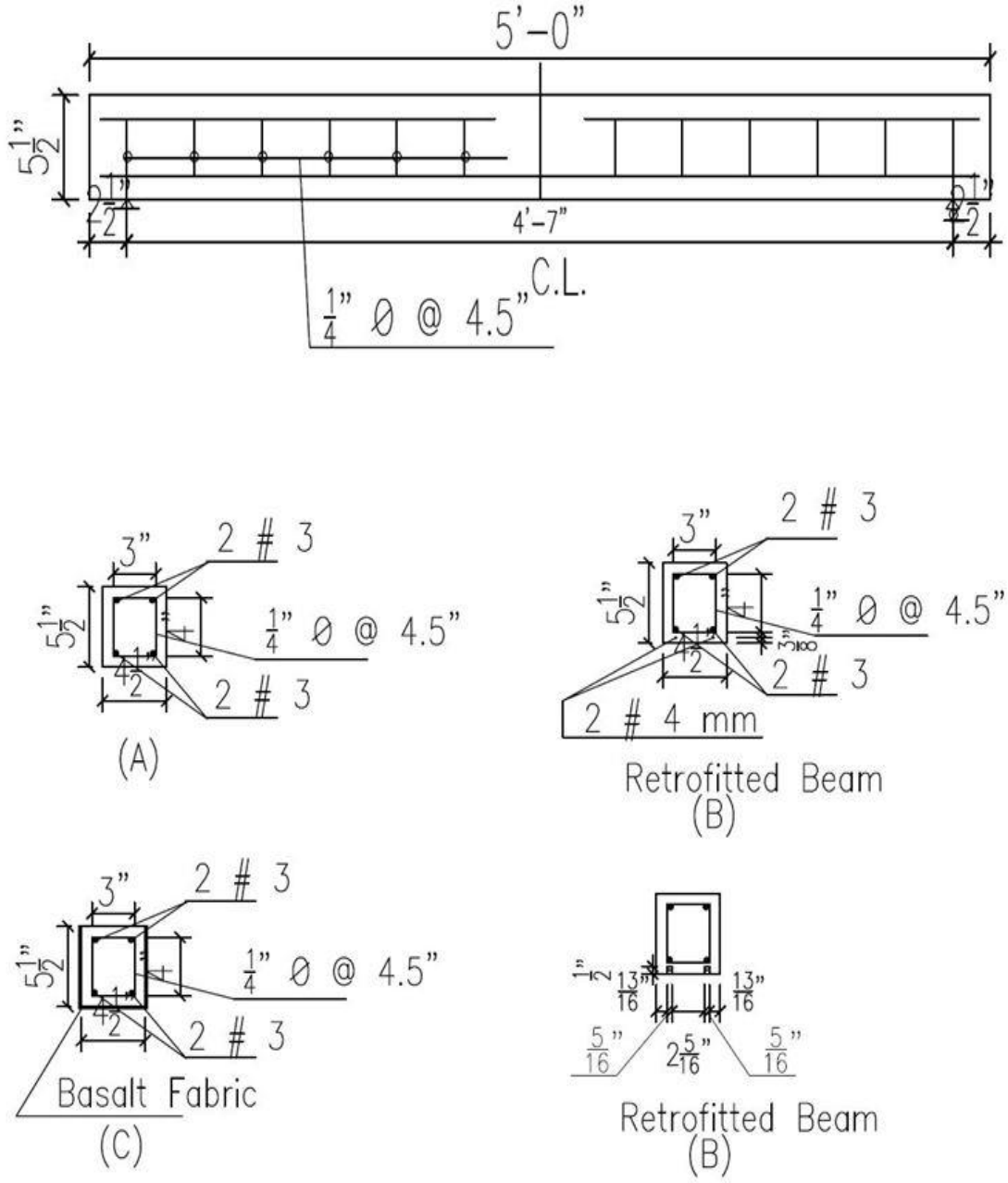

Figure 16. Typical Cross Section for the Simply Supported Beam with Steel Tension Only

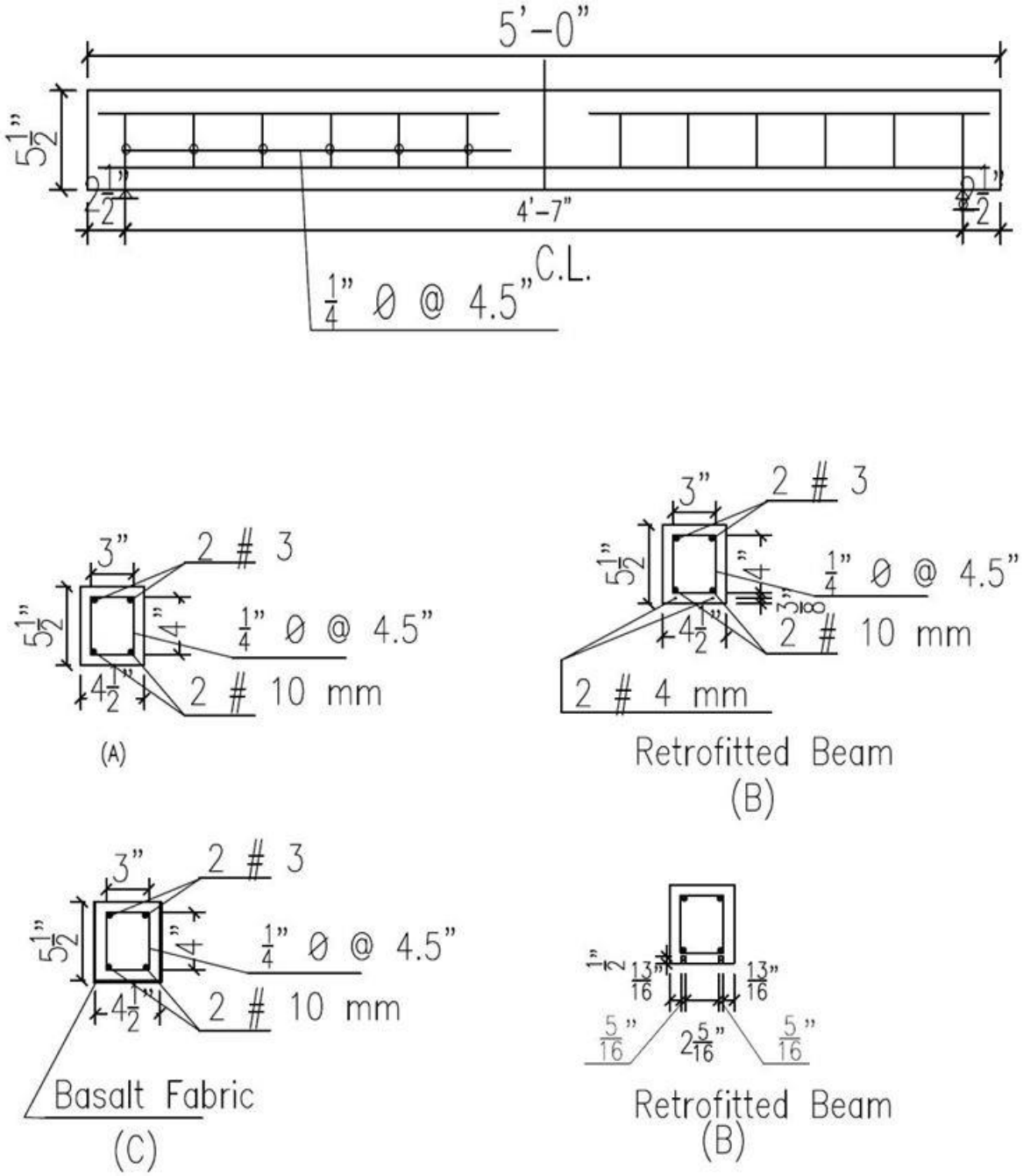

Figure 17. Typical Cross-section for the Simply Supported Beam with BFRP Tension Only

Figure 18. Stirrup Fabrication

Figure 19. Typical Steel Skeleton Fabrication

Figure 20. Typical Formwork for All Simply Supported Beams

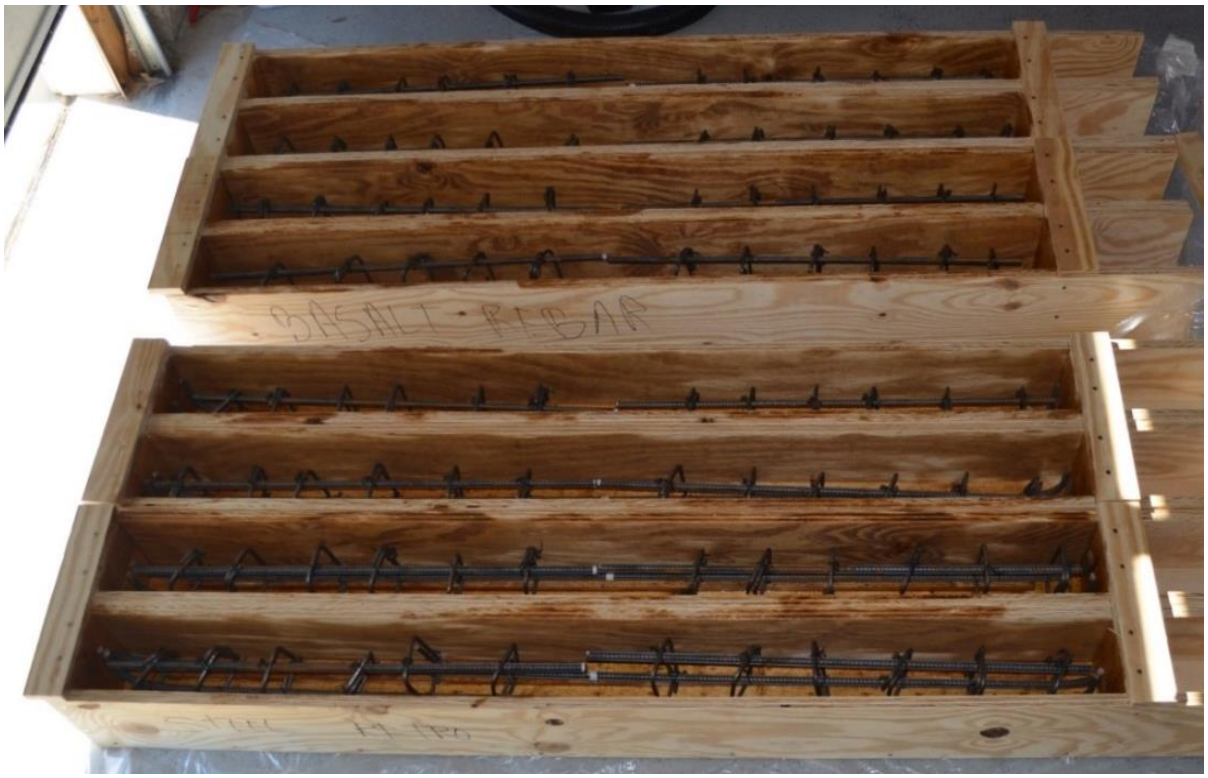

Figure 21. Steel and BFRP Skeleton within the Formwork Ready to Pour Concrete

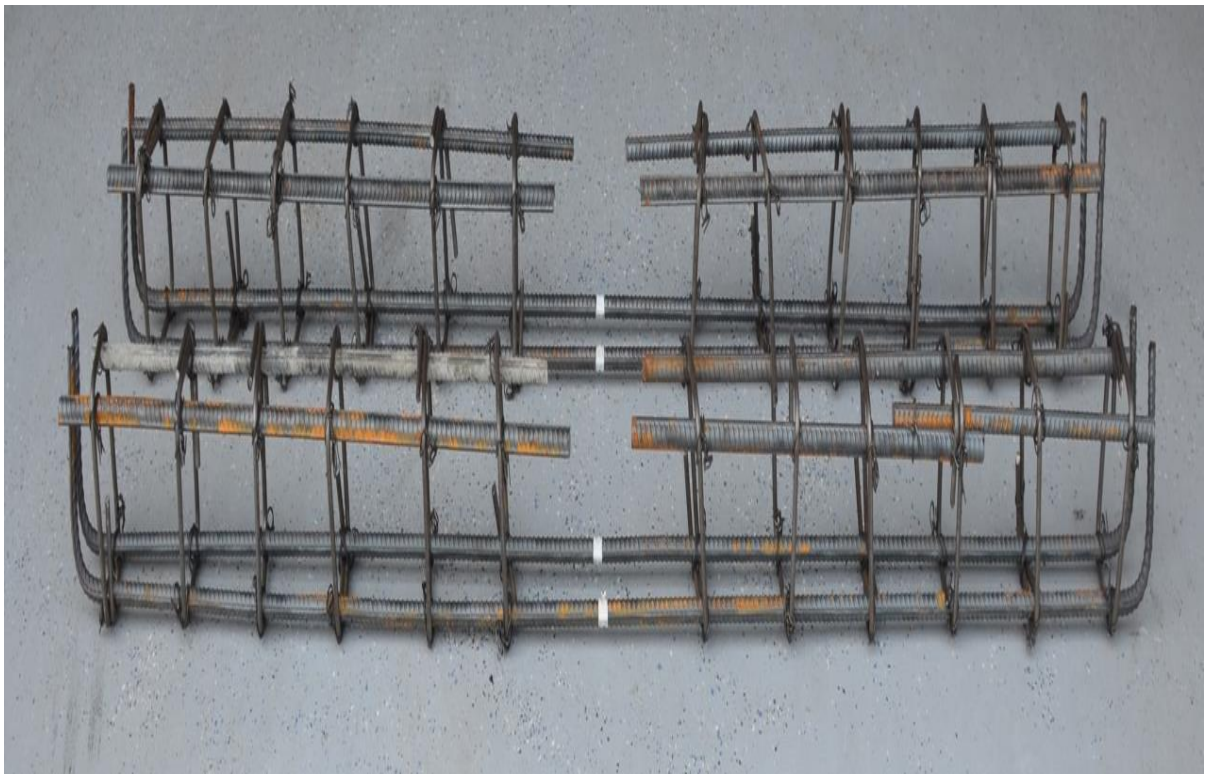

Figure 22. Typical Steel Skeleton for Regular Steel Beams

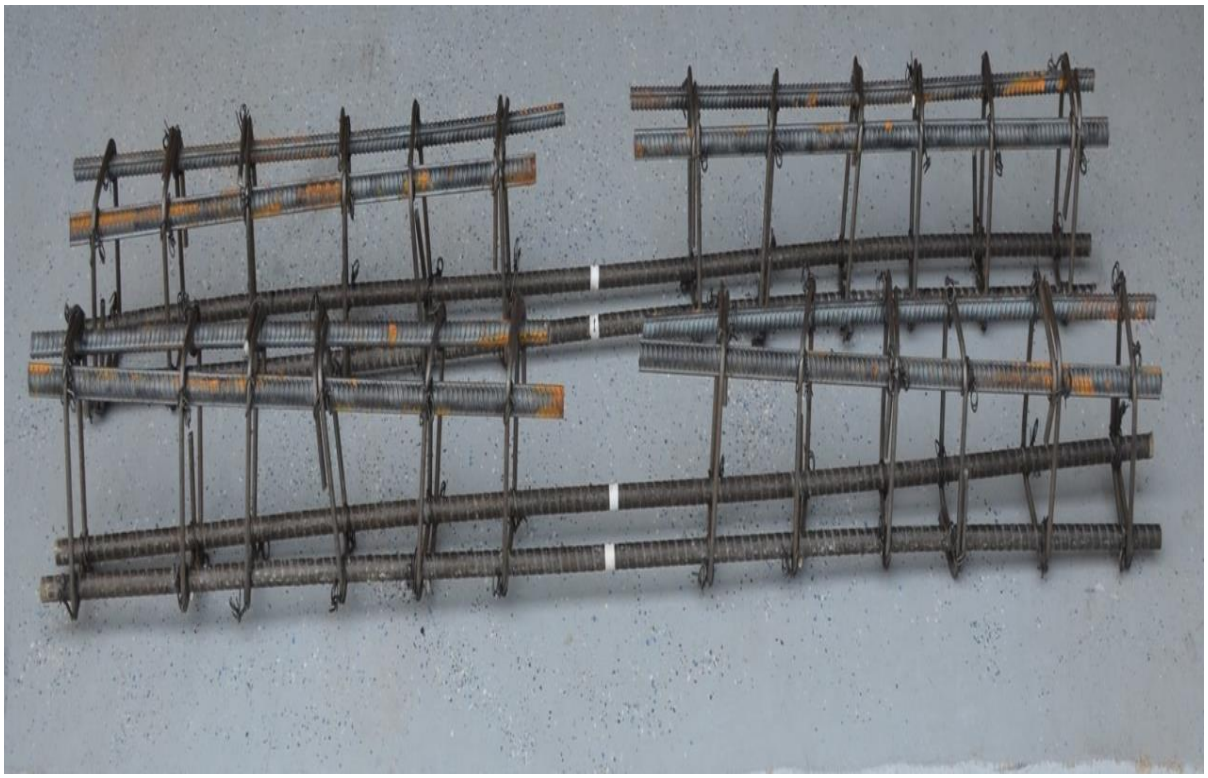

Figure 23. Typical BFRP Skeleton for the Beams with BFRP Reinforcement

Figure 24. Pre-grove Beams that Will Retrofit with External Reinforcement

Figure 25. Preparation of the Concrete Mix

Figure 26. Fours Beams with Steel Reinforcement (left) and Four Beams with BFRP Reinforcement (right)

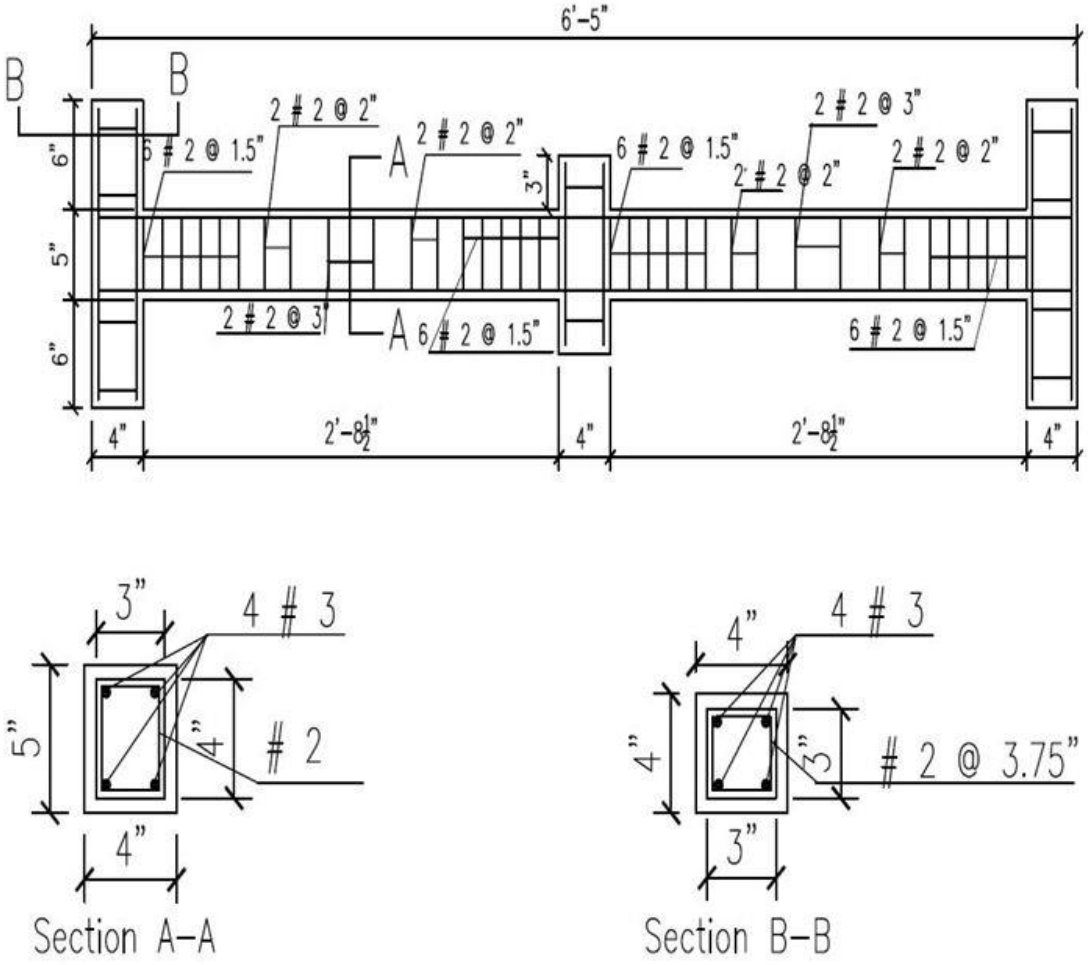

Figure 27. Typical Cross-section for Two-span Sub-assemblage with Steel Reinforcement and Seismic Detail

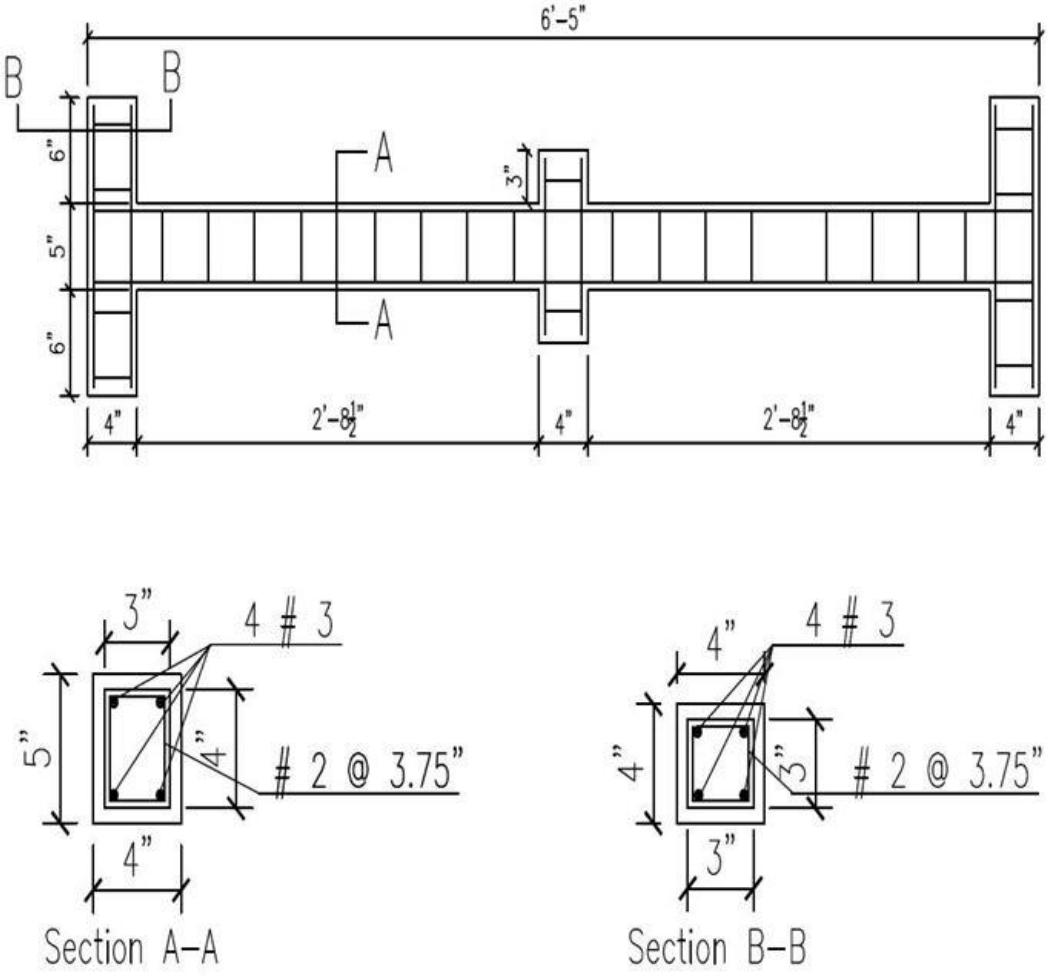

Figure 28. Typical Cross-section for Two-span Sub-assemblage with BFRP Reinforcement

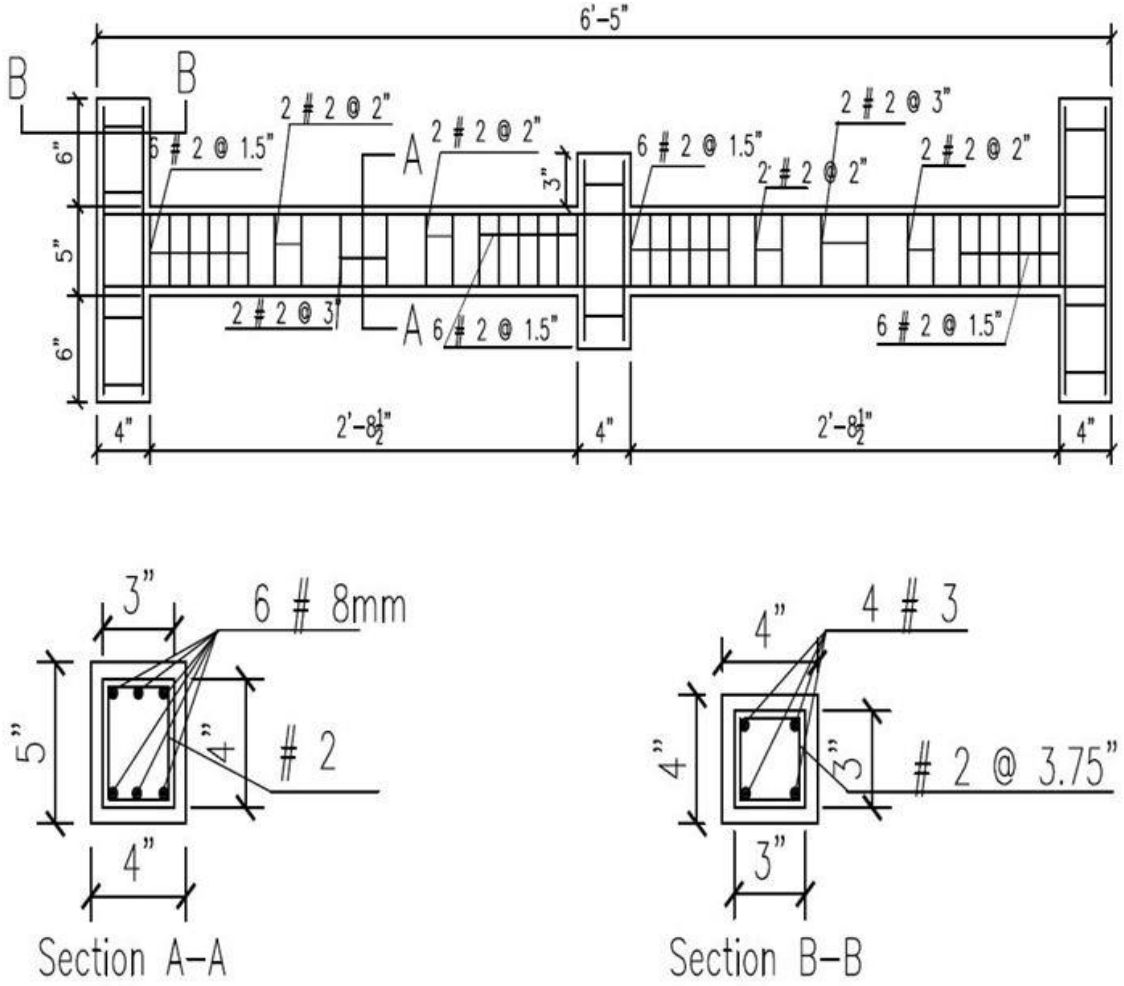

Figure 29. Typical Cross-section for Two-span Sub-assemblage with BFRP Reinforcement and Seismic Detail

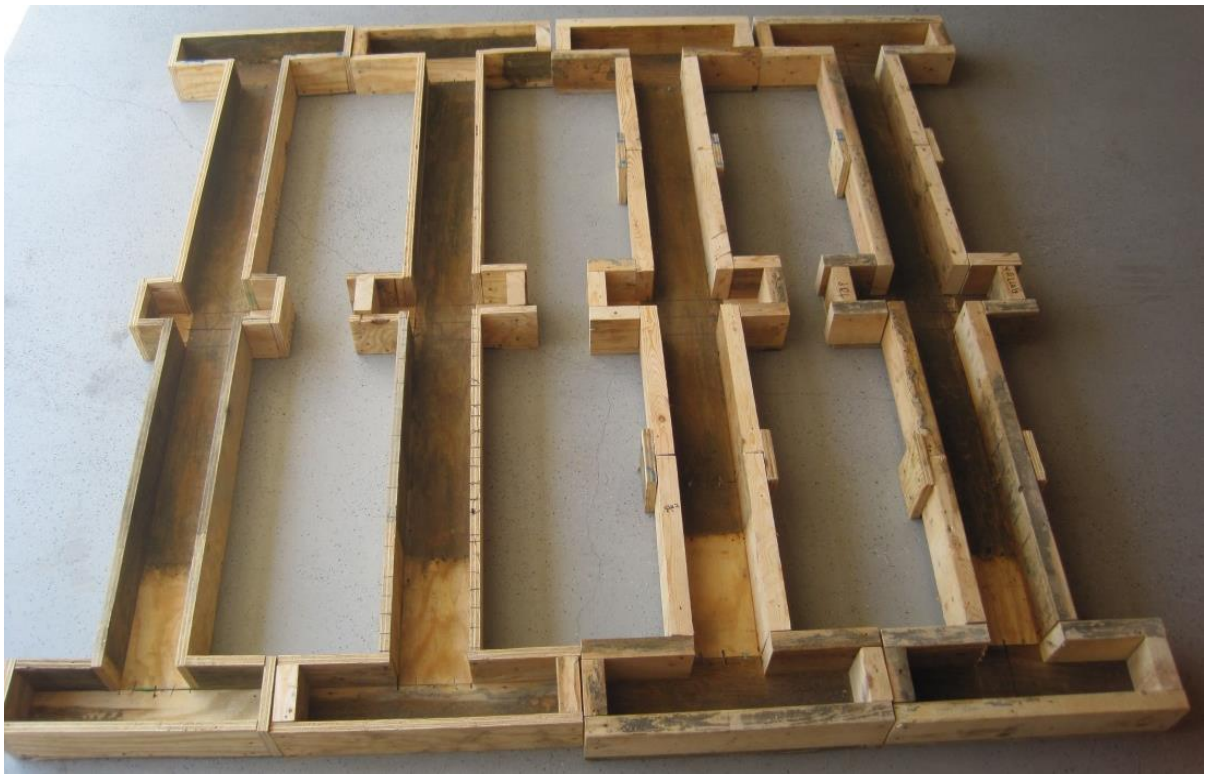

Figure 30. Typical Form Work for Two Span Sub-assemblages

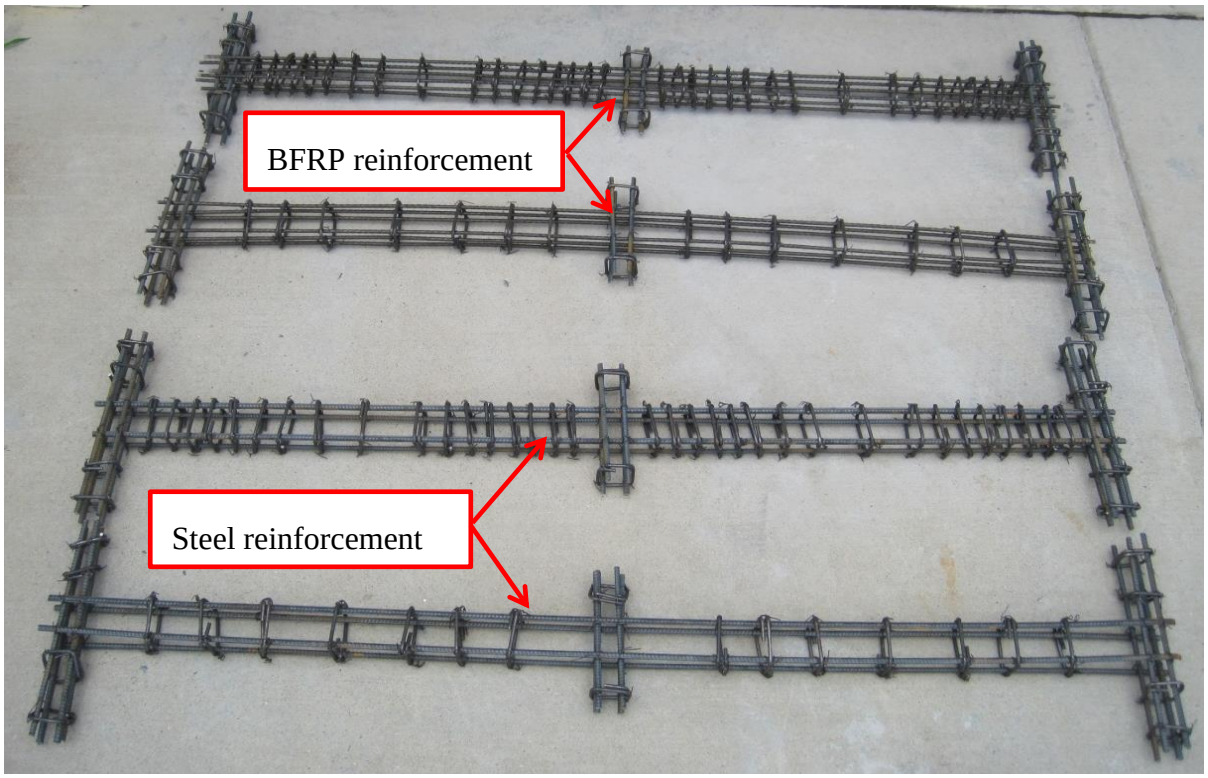

Figure 31. Steel and BFRP Skeleton of Two Span Sub-assemblage Beams

Figure 32. Two Span Sub-assemblage

2.3.2 Procedure to Mount Exterior BFRP Bars on the Reinforced Concrete Simply Supported Beam

Figure 34 illustrates the beam preparation and the BFRP reinforcement of 0.157 inch (4mm) used to retrofit the reinforced concrete beam with regular steel reinforcement. Figure 35 illustrates the two beams with external BFRP fabric using Sikadur 330 as structural epoxy adhesive. Four beams with regular steel reinforcement were retrofitted; two with external BFRP reinforcement (2-4mm) using Sikadur 30 as structural epoxy paste adhesive and two with external BFRP fabric using Sikadur 330 as structural epoxy adhesive.

The procedure was as follows:

1. A pre-groove of 5/16-inch-wide x ½ inch deep was used using wood Figure 24. The groove can also be made using a diamond blade saw or a grinder after the beam is constructed.
2. The groove was cleaned with a vacuum or with air to remove any dust or concrete particulate.
3. Masking tape was used next to the groove to prevent excessive adhesive.
4. The slot was filled with Sikadur 30 epoxy up to half of the depth to prevent entrapped air voids.
5. The Basalt reinforcement 4mm was inserted into the groove and maintaining a 4mm distance from the bottom of the concrete surface.
6. The groove was completely filled with Sikadur 30.
7. The masking tape was removed and the area around the grooves were grooved.

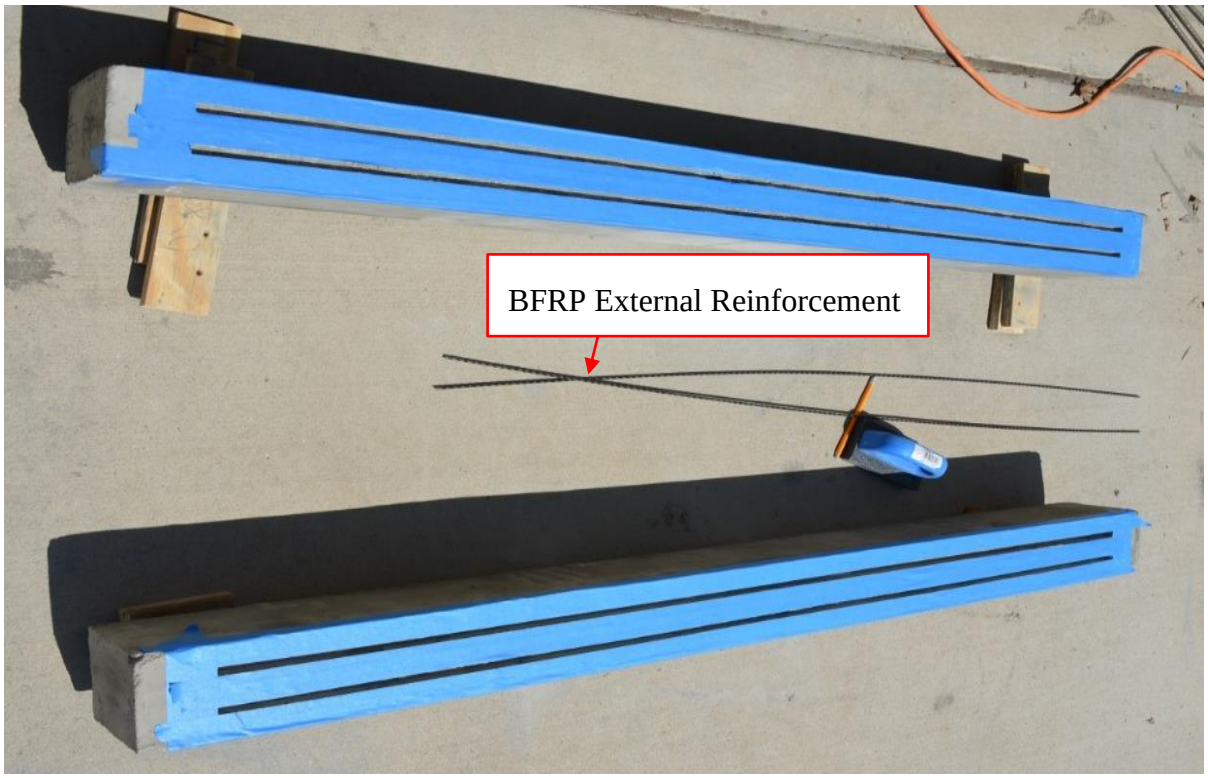

Figure 33. Two Beams Ready for Epoxy Sikadur 30 and 2-4mm External BFRP Reinforcement

Figure 34. Two Simply Supported Beams Were Retrofitted with 2-4mm External BFRP Reinforcement

2.3.3 Procedure to Install the Basalt Fabric to the Simply Supported

Figures 36 to 38 illustrate the BFRP fabric installed on three sides of the beam; two vertical sides and the bottom of the beam with a single layer of BFRP fabric to test and determine the increase of load capacity using Basalt fabric.

The procedure was as follows:

1. Cleaned the beam of any dust, oil, and corrected any damage in the beam.
2. Prepared the Sikadur 330 liquid mix epoxy according with manufacturer recommendations.
3. Cut the fabric to the size needed for each specimen.

4. Applied the liquid mix with a carpet adhesive trowel 1/8-inch x1/8-inch x1/16 inch.

5. Laid down the fabric and removed any air bubbles in the fabric with a spatula.

6. Saturated the fabric with the liquid mix epoxy using a small spatula and let dry for at least 7 days.

Figure 35. Beam Preparation for BFRP Fabric Installation

Figure 36. BFRP Fabric Installation on Simply Supported Beam

Figure 37. BFRP Fabric Installed on Simply Supported Beam

2.3.4 Summary of the Simply Supported Beam Configurations

Table 3 represents all the simply supported beams tested in the laboratory under quasi-static load and impact load. It defines the reinforcement configuration and if the beam was retrofitted prior to loading or after loading and re-tested.

Table 3. Summary of the Configurations for the Simply Supported Specimens

Beam name:	Steel Bars	No of BFRP bars or Fabric	Retest after repair	Load scheme
S-1	2 # 3	0	Yes	Quasi-Static
S-2	2 # 3	0	No	Impact
B-1	0	2 # 10 mm	Yes	Quasi-Static
S-B 1	2 # 3	2 # 4 mm	No	Quasi-Static
S-B 2	2 # 3	2 # 4 mm	No	Impact
B-B 1	0	2# 10 mm	No	Quasi-Static
B-B 2	0	2 # 10 mm	No	Impact
S-F 1	2 # 3	Basalt Fabric	No	Quasi-Static
S-F 2	2 # 3	Basalt Fabric	No	Impact
B-F 1	2 # 10 mm Basalt	Basalt Fabric	No	Quasi-Static
B-F 2	2 # 10 mm Basalt	Basalt Fabric	No	Impact
S-1 (Retro)	2 # 3	Basalt Fabric	No	Quasi-Static
B-1 (Retro)	2 # 10 mm Basalt	Basalt Fabric	No	Quasi-Static

2.3.5 Simply Supported Beam Specimens

Thirteen rectangular cross section beams were tested under static and impact load. Based on the test setup, space available, and transportation method available for this testing, 60 inches long beams were used with a clear span of 55 inches and cross section of 4.5 inches x 5.5 inches. All horizontal specimens had the same amounts of longitudinal and shear reinforcement.

2.3.6 Test Procedures for Static and Impact Load for the Simply Supported Beams

Below is a step-by-step procedure for the static load test.

Figures 39 and 40 illustrate the beam set-up in the laboratory prior to starting the test. A static point load on a small increment of load was applied at the center of the simply supported beam. During each increment, deflection was measured using dial gages to plot load deflection as part of the results.

The procedures of the static load analysis were the following:

1. Set the Vishay Micro-Measurement 7000 multichannel.
2. Connected all the strain gauges into the multichannel machine.
3. Set the 7000 multichannel with type of test that was performed and included the strain gauge factor which in this case was 2.14.
4. Set the load cell to zero.
5. Recorded the information in the 7000 multichannel.
6. Applied load in intervals of 0.10 kips using a manual hydraulic jack.
7. Waited two minutes to read dial gauges.
8. Stopped recording.
9. Observed numbers of cracks and length and recorded.
10. Repeated steps 6 and 9 for every load interval.

Below is a step-by-step procedure for the impact load test.

An impact loading was applied in smaller increments to this research. A pre-defined steel impactor weight with a 5.5 inches diameter section and three different lengths was used and drop free from a pre-calculated height at the midpoint of the simply supported beam to simulate a dynamic or stream load created by blast or earthquake or progressive collapse.

The procedures of the impact load analysis were as follows:

A: For collecting strain gauge information:

1. Set the Vishay Micro-Measurement 7000 multichannel.
2. Connected all the strain gauges into the multichannel machine.
3. Set the 7000 multichannel with type of test that was performed and included the strain gauge factor which in this case was 2.14.
4. Set the pre-defined steel cylinder with 5.5 inches diameter and specified length and weight and a selected elevation.
5. Cylinders were dropped at different elevations each time.
6. Recorded the information in the 7000 multichannel.
7. Dropped the steel impactor at different heights.
8. Stopped recording.
9. Observed numbers of cracks and length and recorded.
10. Tests were continued until the specimens exceed the deflection or collapse.
11. Repeated steps 4 and 9 for every load interval.

B: For collect acceleration information:

1. Set the computer with the NI signal Express 2014 software.
2. Connected all the accelerometers in the interface adapter with the computer.
3. Added a step to acquire the signal and select DAQMA acquire.
4. Selected analog input from DAQMA.
5. Selected the channel of each accelerometer.
6. Configured each accelerometer with a specific specification of each accelerometer and added signal.
7. Selected the recording option.
8. Selected loads save signal and selected analog signal.
9. Save the information in an ASCII/LVM file.
10. Exported file in generic ASCII file.
11. Created a file to save your output on each test.
12. Selected relative time.

13. Selected run and conduct your test. After each test was finished, selected the stop, and recorded the data. The output was recorded automatically in the select file as a txt file.
14. Tests were continued until the specimens failed and collapsed.
15. Repeated steps 13 and14 for every load interval.

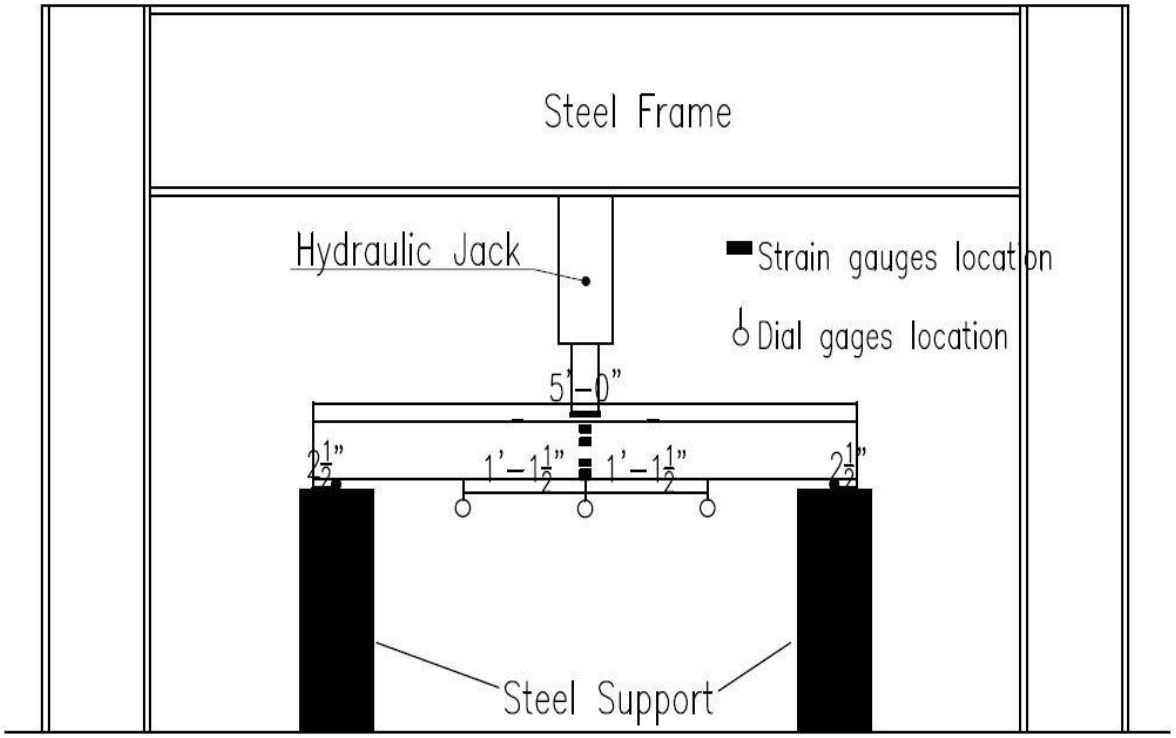

Figure 38. Illustration for the Simply Supported Beam Testing

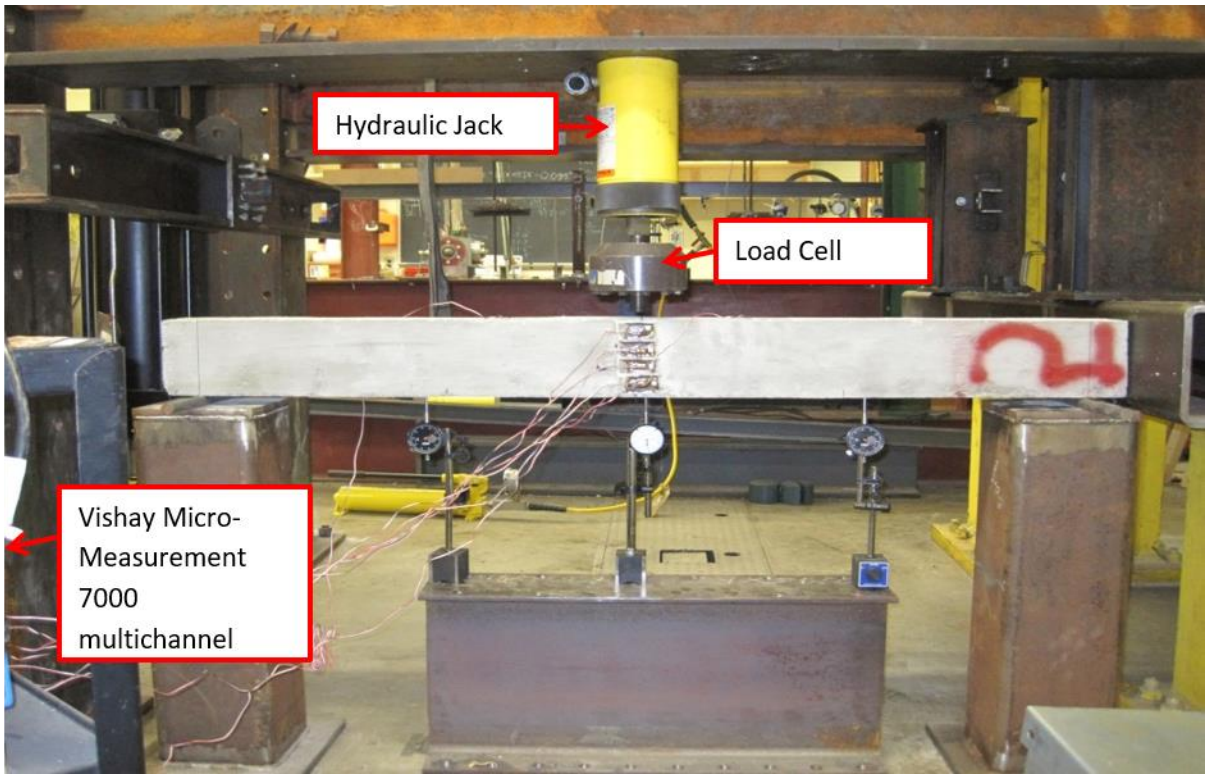

Figure 39. Setup for the Simply Supported Beam Testing in the Laboratory

2.3.7 Sub-assemblage Specimens

Four rectangular cross section sub-assemblages were tested under quasi-static load. Based on the test setup, space available, and transportation method available for this testing, 76 inches long continuous beams with a 4 inches x 5 inches cross section with a column of 17 inches long with 4 inches x 4 inches cross section were tested. All horizontal specimens had the same amounts of longitudinal and shear reinforcement.

2.3.8 Test Procedures for Continue Two Span Sub-assemblage Specimen

Figures 41 and 42 illustrate the beam set-up in the laboratory prior to the start of the test. A static point load on a small increment of load was applied at the mid center column of the continue beams using a manual hydraulic jack at frequent intervals until the specimen fails. During each

increment, deflection was measured using dial gages to plot load deflection as part of the results, strain was recorded using multichannel 7000 system, and length and numbers of cracks were observed and recorded.

The procedures of the static load analysis were the following:

1. Set the Vishay Micro-Measurement 7000 multichannel.
2. Connected all the strain gauges into the multichannel machine.
3. Set the 7000 multichannel with type of test that was performed and included the strain gauge factor which in this case was 2.14.
4. Set the load cell to zero.
5. Recorded the information in the 7000 multichannel.
6. Applied load in interval of 0.100 kips using a manual hydraulic jack.
7. Waited two minutes to read dial gauges.
8. Stopped recording.
9. Observed numbers of cracks and length and recorded.
10. Repeated steps 6 and 9 for every load interval.

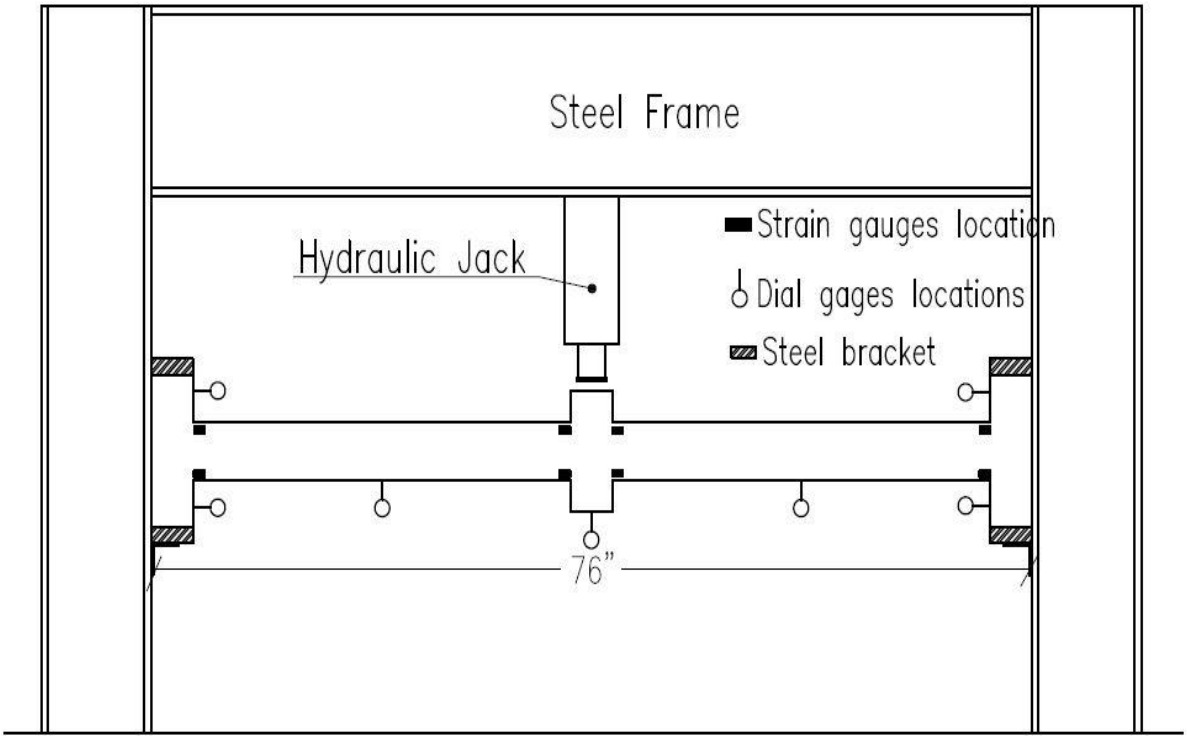

Figure 40. Illustration for the Two-span Sub-assemblages Testing in the Laboratory

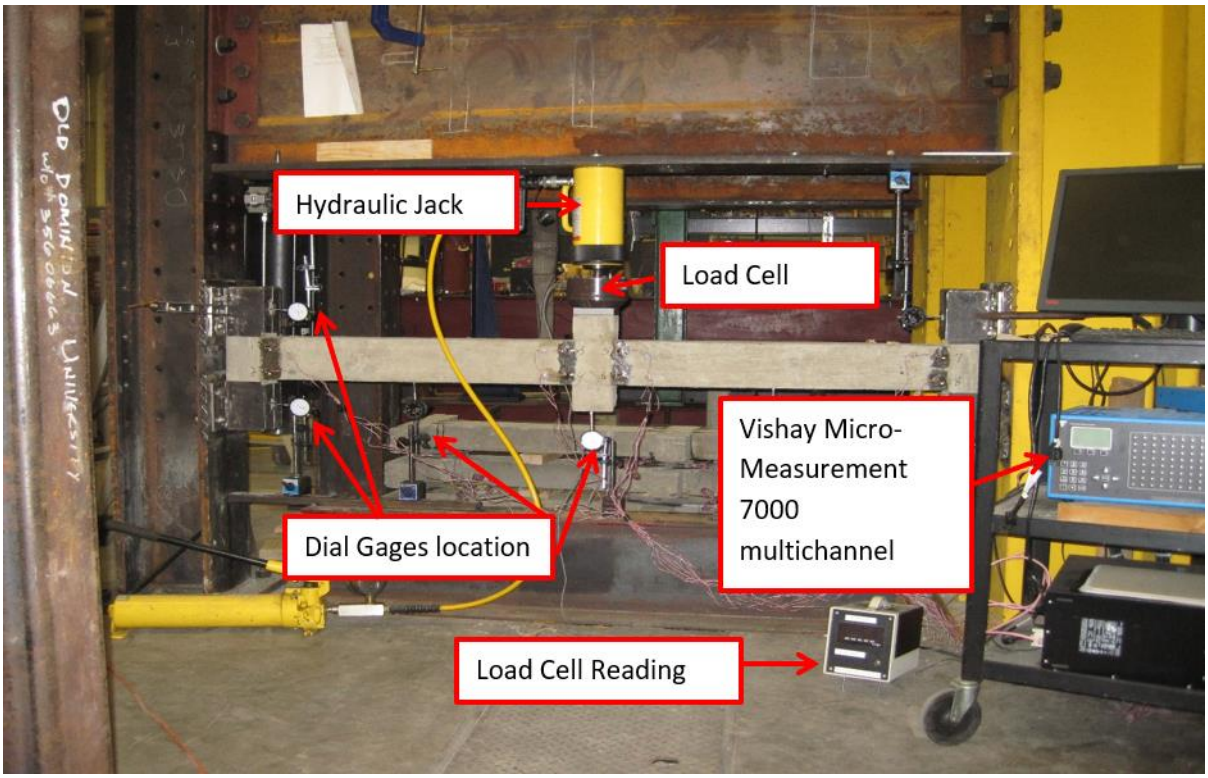

Figure 41. Setup for the Two-span Sub-assemblages Testing in the Laboratory

2.3.9 Summary of the Two-Span Sub-assemblage Configurations

Table 4 represents the configurations of the four specimens tested under the sub-assemblage configurations tested.

Table 4. Summary of the Configuration for the Sub-assemblage Specimens

Beam name:	Steel Bars	No of BFRP bars or Fabric	Retest after repair	No of beam	Load scheme
S2-1	4 # 3	------	No	1	NS
S2-2	4 # 3	------	No	1	SD
B2-1	------	6 # 8 mm	No	1	NS
B2-2	------	6 # 8 mm	No	1	SD

NS = Non seismic detail SD = Seismic Detail

2.4 Test Results for Material Used on the Specimen during this Research

In this section, all the material results used during this research are presented, including the concrete compression strength, tension test for the steel reinforcement, and BFRP reinforcement.

2.4.1 Concrete Compression Test

A custom concrete mix was provided for this research. Twelve cylinders that were 4 inches diameter x 8 inches long were tested in the compression machine in the laboratory. Two cylinders of each mix for a total of 6 cylinders were tested for compression prior to testing the concrete specimen. One cylinder of each mix was kept breaking at the time of the specimen testing to validate the concrete strength of the specimen. A full compression test on Table 5 is provided in this section.

Table 5. Concrete Compression Test Summary

Concrete mix/ Cylinder #	Cylinder length (in)	Cylinder area (in^2)	Load Applied (Kips)	Concrete Strength (ksi)
M1 / 1	8	12.57	55.53	4.42
M1 / 2	8	12.57	53.42	4.25
M1 / 3	8	12.57	55.48	4.41
M2 / 1	8	12.57	48.95	3.89
M2 / 2	8	12.57	55.42	4.41
M2 / 3	8	12.57	55.53	4.42
M3 / 1	8	12.57	55.47	4.41
M3 / 2	8	12.57	53.42	4.25
M3 / 3	8	12.57	48.75	3.88
M4 / 1	8	12.57	38.72	3.08
M4 / 2	8	12.57	37.46	3.06
M4 / 3	8	12.57	38.97	3.10

2.4.2 Steel and BFRP Tension Test Results

A total of four steel reinforcement #3 were tested for tension. Two BFRP reinforcement 10mm, two BFRP reinforcement 4mm, one BFRP 8mm, one BFRP fabric, and one steel bar #2 were tested for tension. Figure 43 illustrates the set-up for steel reinforcement #3. Figure 44 illustrates the result and failed mode of one of the # 3 steel. Figure 45 illustrates the setup for the BFRP 10mm reinforcement prior to testing. Figure 46 illustrates the result and failed mode of one of the 10mm BFRP reinforcements. Figure 47 illustrates the failed mode from the anchor of one 10mm BFRP reinforcement during the test procedure. Figure 48 illustrates the setup for the BFRP 4mm reinforcement prior to test. Figure 49 illustrates the result and failed mode of one of the 4mm BFRP reinforcements. Figure 50 represents the result and failed mode of one of the

8mm BFRP reinforcement. Figure 51 illustrates the result and failed mode of one of BFRP Fabric test. Figure 52 illustrates the failed mode of the #2 steel reinforcement.

Figure 42. Steel Reinforcement # 3 Tension Tests Setup in the Laboratory

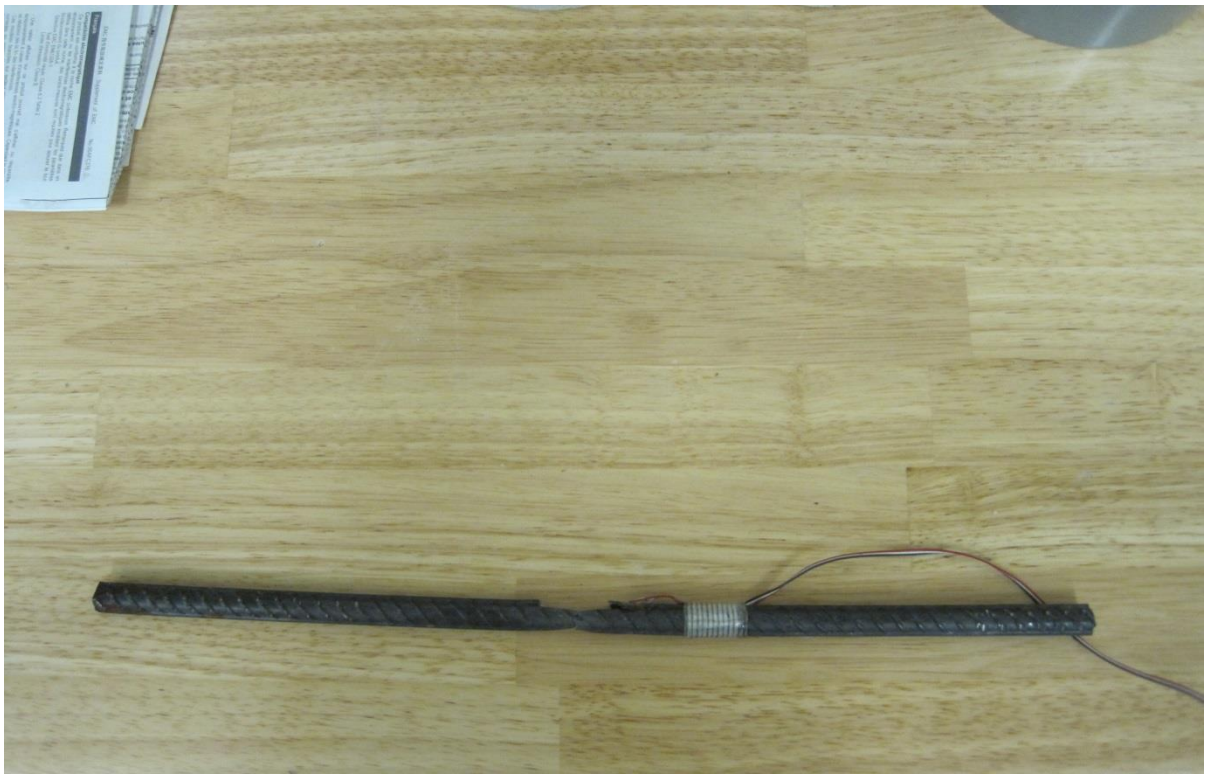

Figure 43. Results of Steel Reinforcement # 3 Tension Tests in the Laboratory

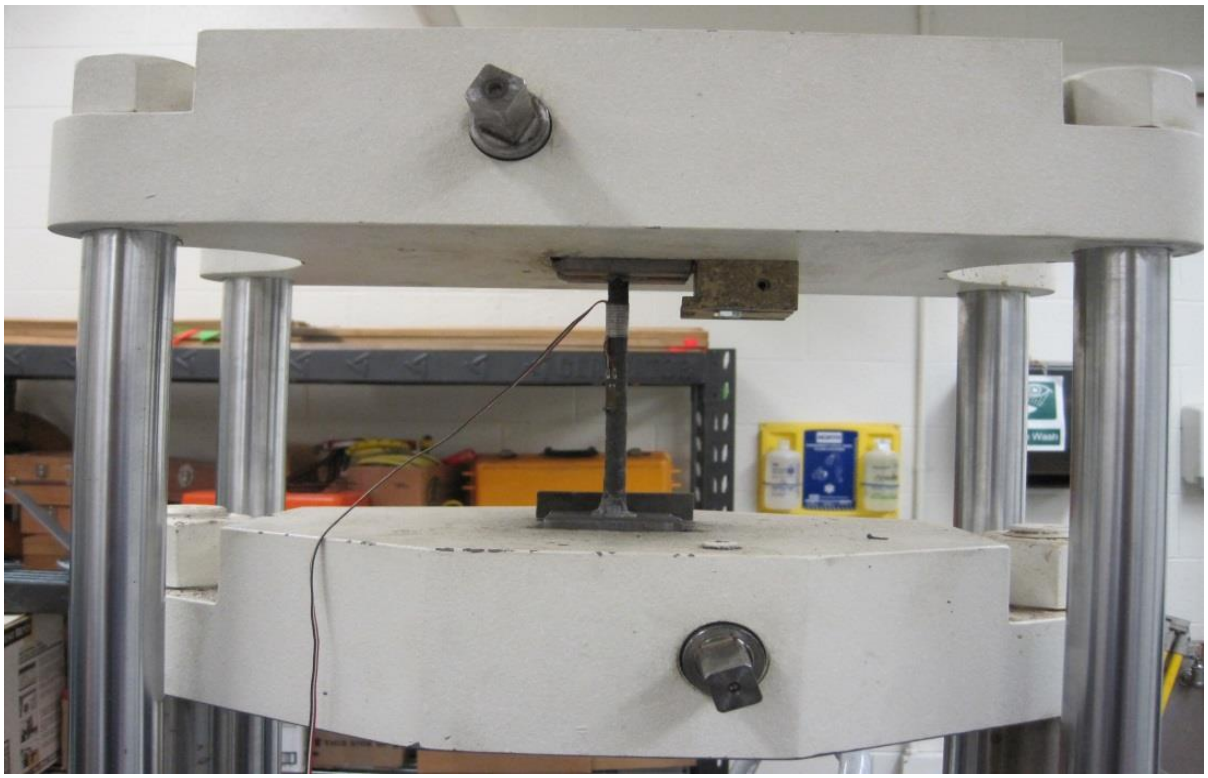

Figure 44. BFRP Reinforcement 10mm Tension Test Setup in the Laboratory

Figure 45. Results of the BFRP 10mm Tension Test in the Laboratory

Figure 46. Failure of the BFRP 10mm Tension during a Test in the Laboratory

Figure 47. BFRP Reinforcement 4mm Tension Test Setup in the Laboratory

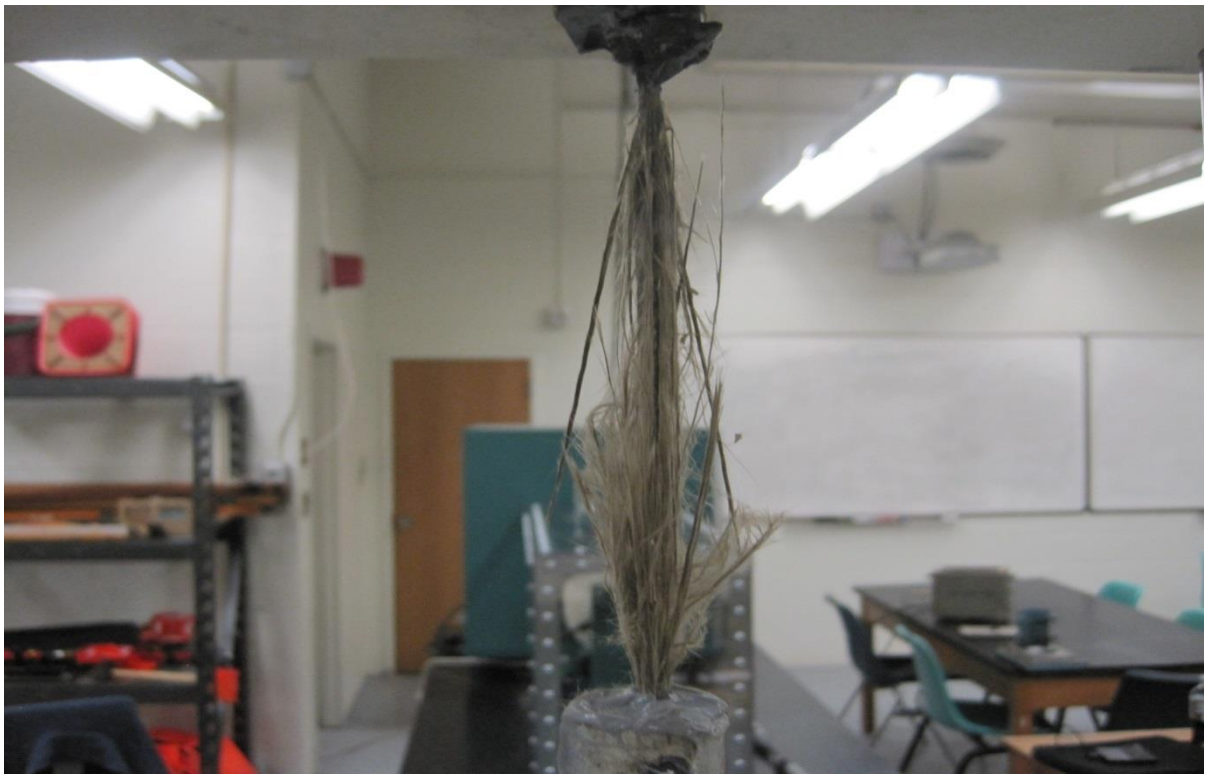

Figure 48. Results of the BFRP 4mm Tension Test in the Laboratory

Figure 49. Results of the BFRP 8mm Tension Test in the Laboratory

Figure 50. Results of the BFRP Fabric Tension Test in the Laboratory

Figure 51. Results of the # 2 Steel Reinforcement Tension Test in the Laboratory

Table 6 and 7 represent all the tension test results for the steel and BFRP reinforcements tested during this research.

Table 6. Steel Tension Test Summary

Specimen	Specimen area (in^2)	Load Applied (Kips)	Yield Strength (ksi)
1 - # 2	0.049	4.40	89.82
1 - # 3	0.11	7.50	68.22
1 - # 3	0.11	7.50	68.22
1 - # 3	0.11	7.50	68.22
1 - # 3	0.11	7.50	68.22

Table 7. BFRP Tension Test Summary

Specimen	Specimen area (in^2)	Load Applied (kips)	Rupture Point (ksi)
B – 10mm	0.12	8.59	71.56
B – 8mm	0.08	5.53	69.15
B – 4mm	0.02	2.64	138.85

2.5 Test Result for a Simply Supported Beam

In this section, the strain gauge location, strain gauges readings, load-deflection results, beams cracks, and impact test results are presented.

2.5.1 Strain Gauge Location in the Simply Supported Beams

A total of seven strain gauges were mounted on each beam to measure the strains in three different areas of the beam as shown in Figure 53. Two were set-up at the top of the beam at 7 inches from the center point of the beam and 2.25 inches from the edge on the beam. Four strain gauges were installed on the side of the beam at 1 inch from the top of the compression concrete fiber, the second was installed at 2.25 inches from the top of the compression concrete fiber, the third was installed at 3.25 inches from the top of the compression concrete fiber, and the fourth was installed at 4.25 inches from the top of the compression concrete fiber of the beams. The last strain gauge was installed in the center of the bottom side of the beam. Strain readings were recorded for each load increment applied to the beam. Figure 54 represents the installation for strain gauges in the beam.

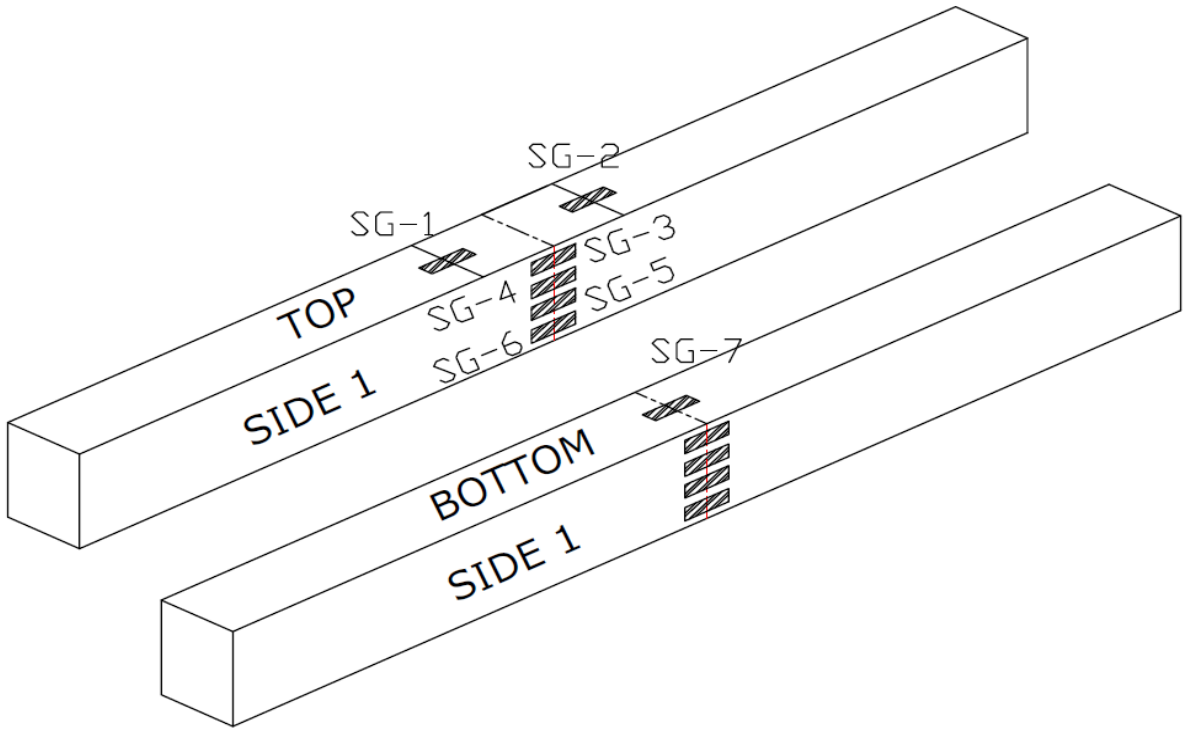

Figure 52. Strain Gauge's Locations on Simply Supported Beams

Figure 53. Installation of the Strain Gauges on Simply Supported Beam

2.5.2 Strain Gauge Results for The Simply Supported Beams

Figure 55 represents all strain gauges plotted for the control Specimen S-1under quasi-static load. All strain gauges recorded data during this test with the exception of Strain Gauge 7, which stopped recording data after the 3.25 kips load applied. The maximum strain recorded for strain gauge 1 was -0.0007 in/in when a load of 5.00 kips was applied. The maximum strain recorded for Strain Gauge 2 was -0.0010 in/in when a load of 5.00 kips was applied. The maximum strain recorded for Strain Gauge 3 was -0.0005 in/in when a load of 5.00 kips was applied. The maximum strain recorded for Strain Gauge 4 was 0.0000 in/in when a load of 2.92 kips. was applied. The maximum strain recorded for Strain Gauge 5 was -0.0000 in/in when a load of 5.00 kips was applied. The maximum strain recorded for Strain Gauge 6 was -0.0001 in/in when a load of 5.00 kips. was applied. The maximum strain recorded for Strain Gauge 7 was 0.0000 in/in when a load of 3.25 kips was applied. This beam was not loaded up to the collapse load.

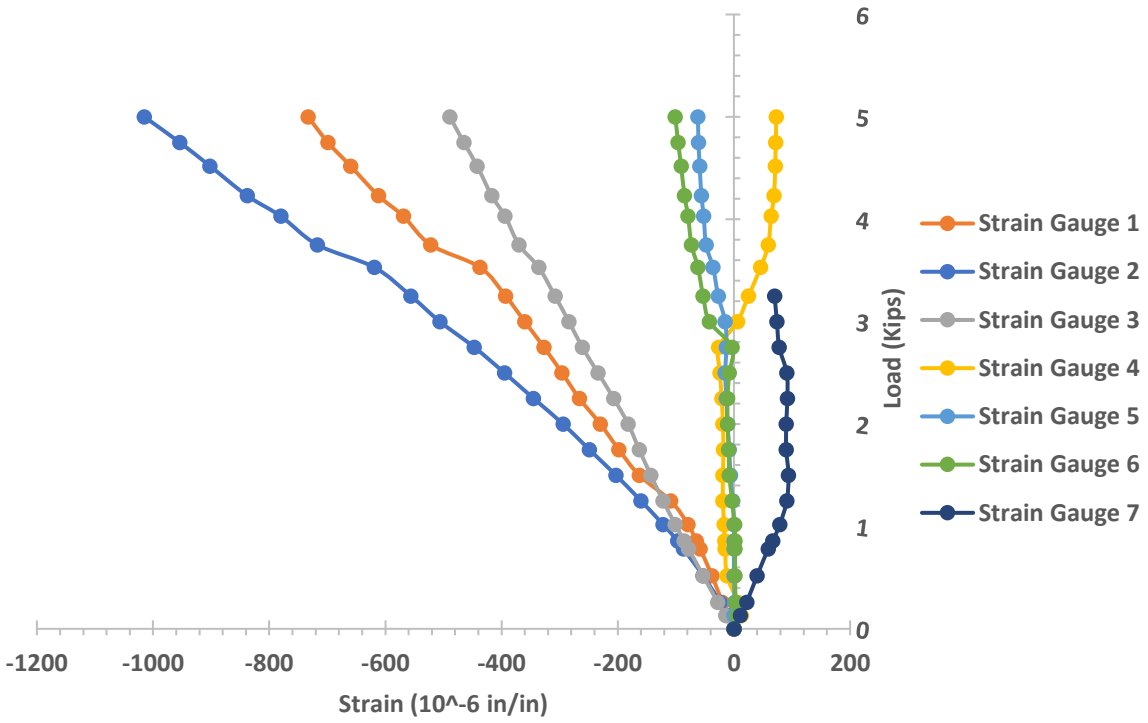

Figure 54. Experimental Load-strain Values for All Strain Gauges for Specimen S-1

Figure 54 represents all strain gauges plotted for the control Specimen B-1under quasi-static load. All strain gauges recorded data during this test with the exception of Strain Gauge 3, which stopped recording data after the 3.32 kips load applied. The maximum strain recorded for Strain Gauge 1 was -0.0016 in/in when a load of 5.57 kips was applied. The maximum strain recorded for Strain Gauge 2 was -0.0019 in/in when a load of 5.57 kips was applied. The maximum strain recorded for Strain Gauge 3 was 0.0011 in/in when a load of 3.32 kips was applied. The maximum strain recorded for Strain Gauge 4 was 0.0001 in/in when a load of 5.57 kips was applied. The maximum strain recorded for Strain Gauge 5 was -0.0000 in/in when a load of 5.57

kips was applied. The maximum strain recorded for Strain Gauge 6 was -0.0004 in/in when a load of 5.57 kips was applied. The maximum strain recorded for Strain Gauge 7 was -0.0001 in/in when a load of 5.57 kips was applied. This beam was not loaded at collapse load.

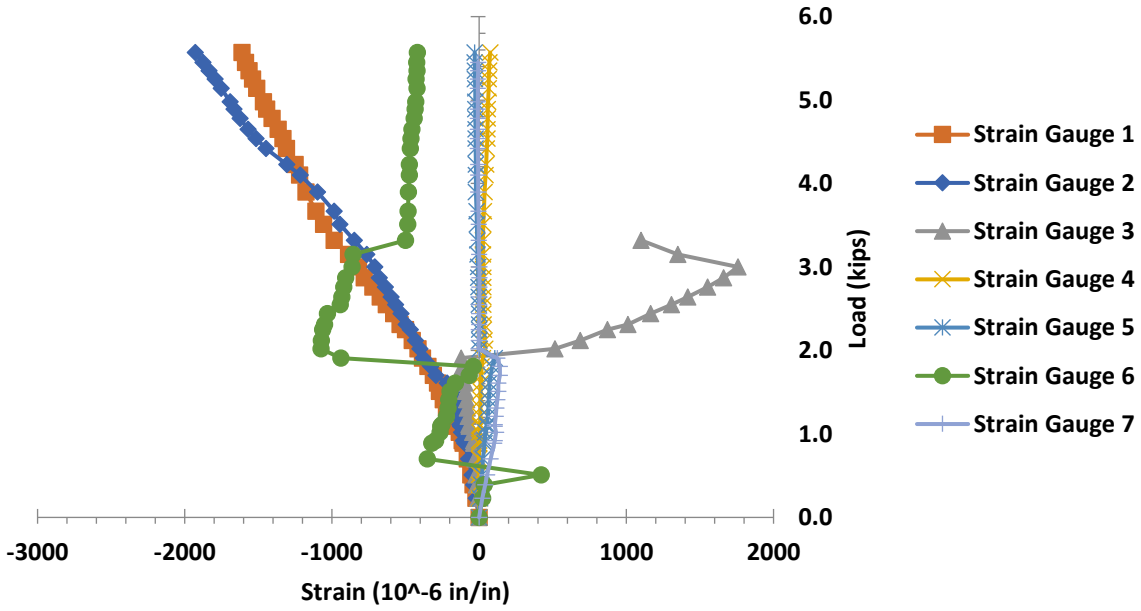

Figure 55. Experimental Load-strain Values for All Strain Gauges for Specimen B-1

Figure 55 represents all strain gauges plotted for Specimen S-B 1 under quasi-static load. All strain gauges recorded data during this test with the exception of Strain Gauges 4, 5, and 6, which stopped recording data after the 2.92 kips load applied. The maximum strain recorded for Strain Gauge 1 was -0.0010 in/in when a load of 5.94 kips was applied. The maximum strain recorded for Strain Gauge 2 was -0.0012 in/in when a load of 6.04 kips was applied. The maximum strain recorded for Strain Gauge 3 was -0.0003 in/in when a load of 6.04 kips was

applied. The maximum strain recorded for Strain Gauge 4 was 0.0030 in/in when a load of 2.92 kips was applied. The maximum strain recorded for Strain Gauge 5 was 0.0035 in/in when a load of 2.92 kips was applied; the strain exceeded the concrete strain of 0.0031 in/in and the yield strain of 0.0023 in/in for steel. The maximum strain recorded for Strain Gauge 6 was 0.0071 in/in when a load of 2.92 kips was applied. This strain value exceeded the concrete strain of 0.0031 in/in and the yield strain of 0.0023 in/in for steel. The maximum strain recorded for Strain Gauge 7 was 0.0126 in/in when a load of 5.00 kips was applied. This strain value exceeded the concrete strain of 0.0031 in/in and the yield strain of 0.0023 in/in for steel. The collapse load was 6.14 kips.

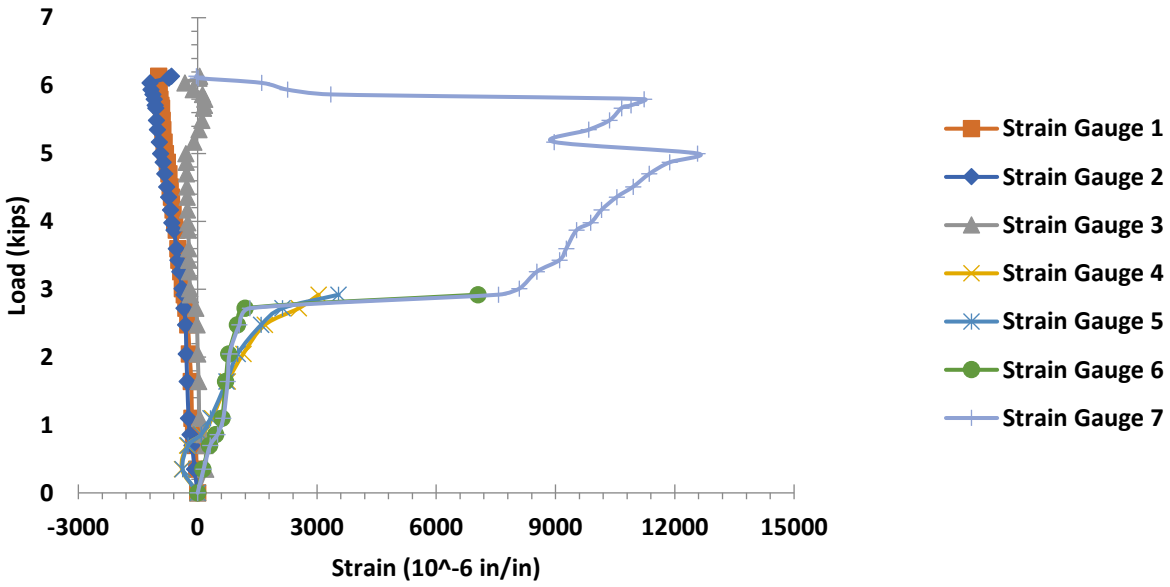

Figure 56. Experimental Load-strain Values for All Strain Gauges for Specimen S-B-1

Figure 56 represents all strain gauges plotted for Specimen B-B 1 under quasi-static load. All strain gauges recorded data during this test. The maximum strain recorded for Strain Gauge 1

was -0.0021 in/in when a load of 6.32 kips was applied. The maximum strain recorded for Strain Gauge 2 was -0.0018 in/in when a load of 6.41 kips was applied. The maximum strain recorded for Strain Gauge 3 was -0.0011 in/in when a load of 6.41 kips was applied. The maximum strain recorded for Strain Gauge 4 was -0.0002 in/in when a load of 2.10 kips was applied. The maximum strain recorded for Strain Gauge 5 was 0.0002 in/in when a load of 1.30 kips was applied. The maximum strain recorded for Strain Gauge 6 was -0.0002 in/in when a load of 6.41 kips was applied. The maximum strain recorded for Strain Gauge 7 was 0.0007 in/in when a load of 2.10 kips was applied. The collapse load was 6.14kips.

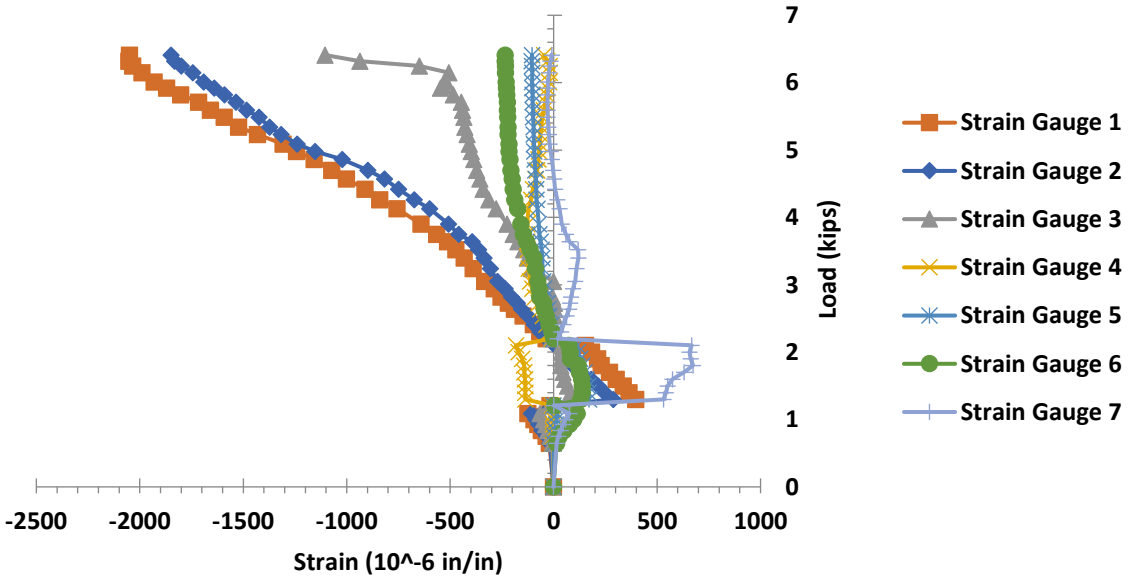

Figure 57. Experimental Load-strain Values for All Strain Gauges for Specimen B-B-1

Figure 58 represents all strain gauges plotted for Specimen S-F 1 under quasi-static load. All strain gauges recorded data during this test. The maximum strain recorded for Strain Gauge 1

was -0.0016 in/in when a load of 7.04 kips was applied. The maximum strain recorded for Strain Gauge 2 was -0.0014 in/in when a load of 7.04 kips was applied. The maximum strain recorded for Strain Gauge 3 was -0.0005 in/in when a load of 5.95 kips was applied. The maximum strain recorded for Strain Gauge 4 was 0.0004 in/in when a load of 6.00 kips was applied. The maximum strain recorded for Strain Gauge 5 was 0.0008 in/in when a load of 6.20 kips was applied. The maximum strain recorded for Strain Gauge 6 was 0.0034 in/in when a load of 6.00 kips was applied; the strain exceeded the concrete strain of 0.0031 in/in and the yield strain of 0.0023 in/in for steel. The maximum strain recorded for Strain Gauge 7 was 0.0016 in/in when a load of 7.04 kips was applied. The collapse load was 7.04 kips.

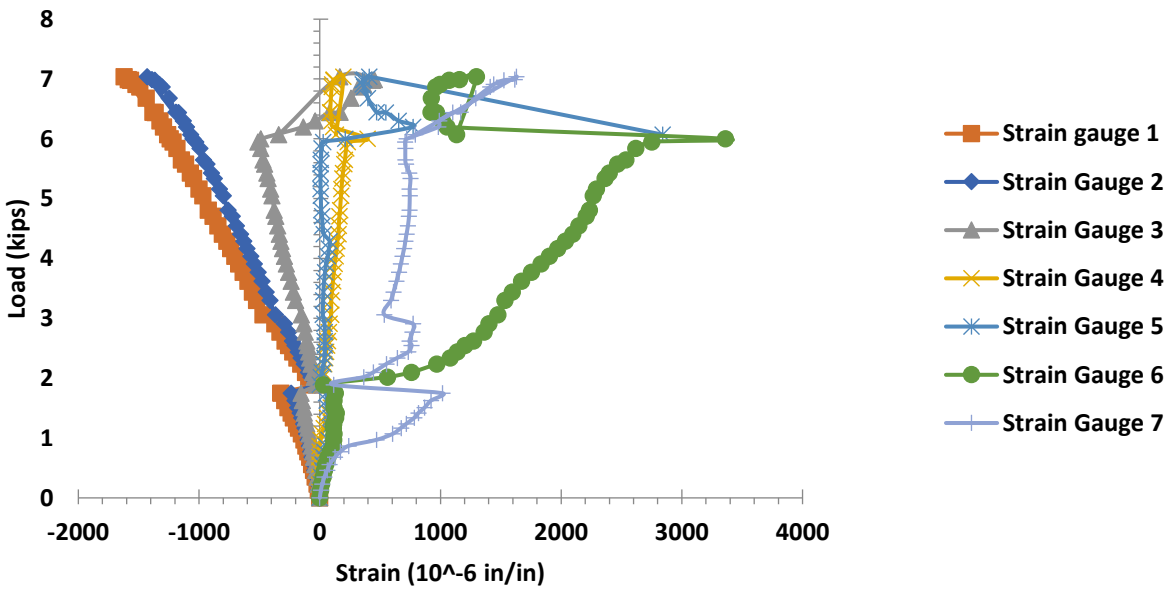

Figure 58. Experimental Load-strain Values for All Strain Gauges for Specimen S-F-1

Figure 59 represents all strain gauges plotted for Specimen B-F 1 under quasi-static load. All strain gauges recorded data during this test. The maximum strain recorded for Strain Gauge 1 was -0.0045 in/in when a load of 8.45 kips was applied; the strain exceeded the concrete strain of

0.0031 in/in and the yield strain of 0.0023 in/in for steel. The maximum strain recorded for Strain Gauge 2 was -0.0028 in/in when a load of 8.45 kips was applied; the strain exceeded the yield strain of 0.0023 in/in for steel. The maximum strain recorded for Strain Gauge 3 was 0.0009 in/in when a load of 7.14 kips was applied. The maximum strain recorded for Strain Gauge 4 was 0.0039 in/in when a load of 7.71 kips was applied; the strain exceeded the concrete strain of 0.0031 in/in and the yield strain of the steel of 0.0023 in/in. The maximum strain recorded for Strain Gauge 5 was 0.0033in/in when a load of 7.71 kips was applied; the strain exceeded the concrete strain of 0.0031 in/in and the yield strain of 0.0023 in/in for steel. The maximum strain recorded for Strain Gauge 6 was 0.0048 in/in when a load of 7.49 kips was applied; the strain exceeded the concrete strain of 0.0031 in/in and the yield strain of 0.0023 in/in for steel. The maximum strain recorded for Strain Gauge 7 was 0.0016 in/in when a load of 7.49 kips was applied. The collapse load was 8.45 kips.

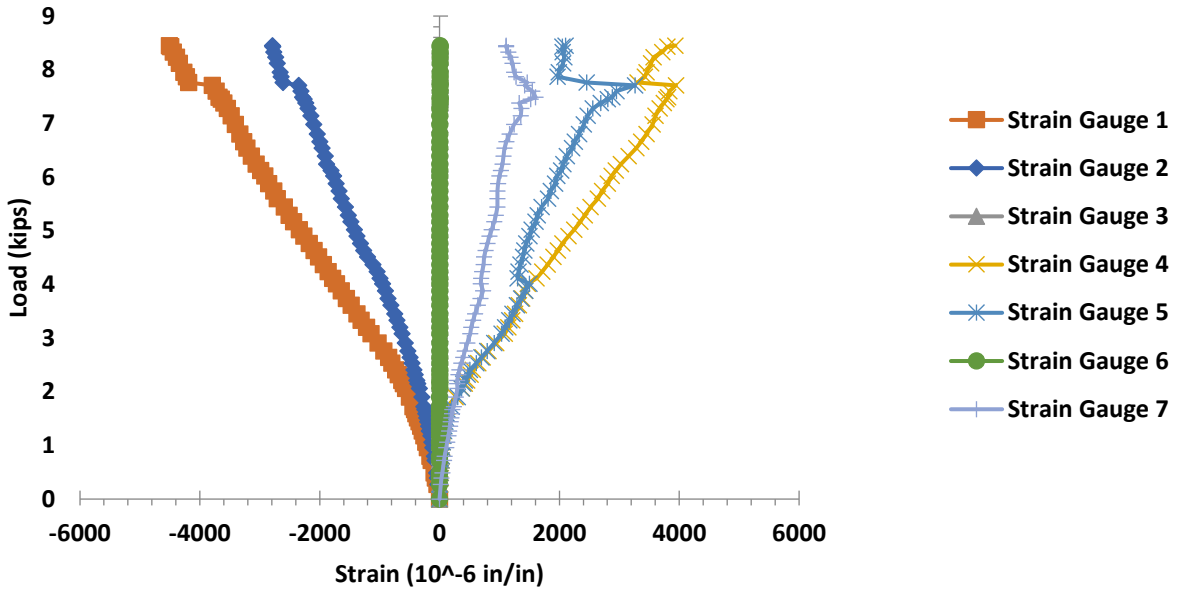

Figure 59. Experimental Load-strain Values for All Strain Gauges for Specimen B-F-1

Figure 60 represents all strain gauges plotted for Specimen S-1 (retrofitted) under quasi-static load. All strain gauges recorded data during this test. The maximum strain recorded for Strain Gauge 1 was -0.0019 in/in when a load of 7.82 kips was applied. The maximum strain recorded for Strain Gauge 2 was -0.0027 in/in when a load of 7.82 kips was applied; the strain exceeded the yield strain of 0.0023 in/in for steel. The maximum strain recorded for Strain Gauge 3 was -0.0012 in/in when a load of 7.82 kips was applied. The maximum strain recorded for Strain Gauge 4 was -0.0001 in/in when a load of 7.82 kips was applied. The maximum strain recorded for Strain Gauge 5 was -0.0002 in/in when a load of 7.71 kips was applied. The maximum strain recorded for Strain Gauge 6 was -0.0002 in/in when a load of 7.82 kips was applied. The maximum strain recorded for Strain Gauge 7 was 0.0120 in/in when a load of 7.82 kips was applied; the strain exceeded the concrete strain of 0.0031 in/in and the yield strain of 0.0023 in/in for steel. The collapse load was 7.82 kips.

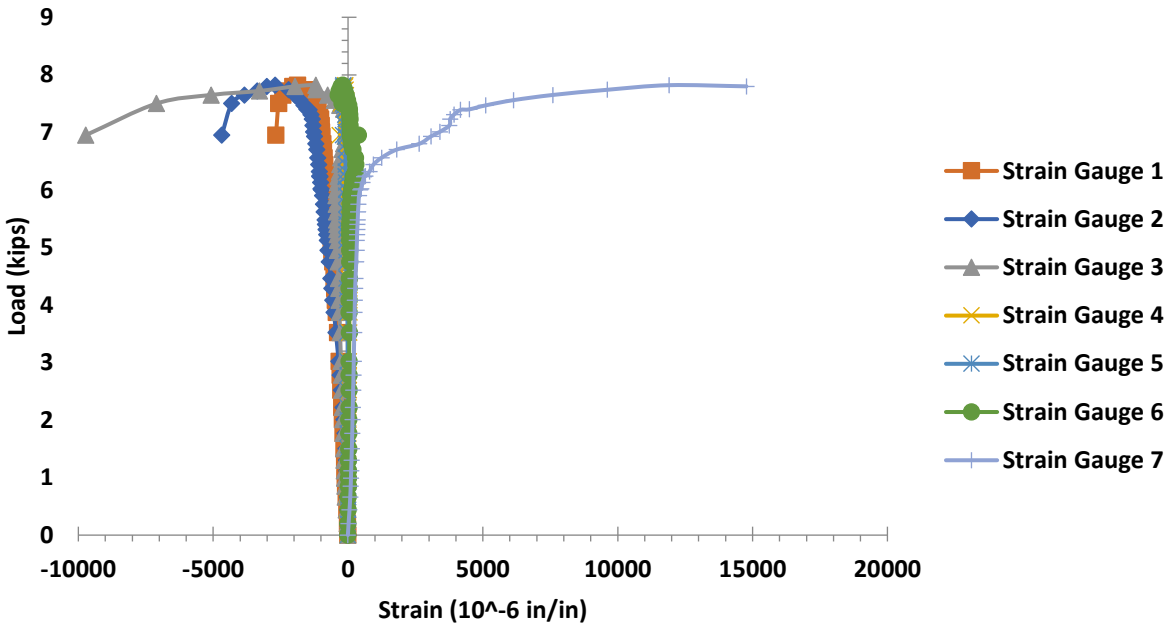

Figure 60. Experimental Load-Strain Values for All Strain Gauges for Specimen B-F-1

Figure 61 represents all strain gauges plotted for Specimen B-1 (retrofitted) under quasi-static load. All strain gauges recorded data during this test with the exception of Strain Gauge 3. Strain gauges 4 and 5 stopped recording data after a load of 7.44 kips was applied and strain gauges 6 and 7 stopped recording data after 7.15 kips was applied. The maximum strain recorded for Strain Gauge 1 was -0.0017 in/in when a load of 7.30 kips was applied. The maximum strain recorded for Strain Gauge 2 was -0.0023 in/in when a load of 7.30 kips was applied. The maximum strain recorded for Strain Gauge 4 was 0.0005 in/in when a load of 5.99 kips was applied. The maximum strain recorded for Strain Gauge 5 was 0.0007 in/in when a load of 6.60 kips was applied. The maximum strain recorded for Strain Gauge 6 was 0.0123 in/in when a load of 6.74 kips was applied; this strain value exceeded the concrete strain of 0.0031 in/in and the yield strain of 0.0023 in/in for steel. The maximum strain recorded for Strain Gauge 7 was 0.0044 in/in when a load of 7.15 kips was applied; this strain value exceeded the concrete strain of 0.0031 in/in and the yield strain of 0.0023 in/in for steel. The collapse load was 7.44 kips.

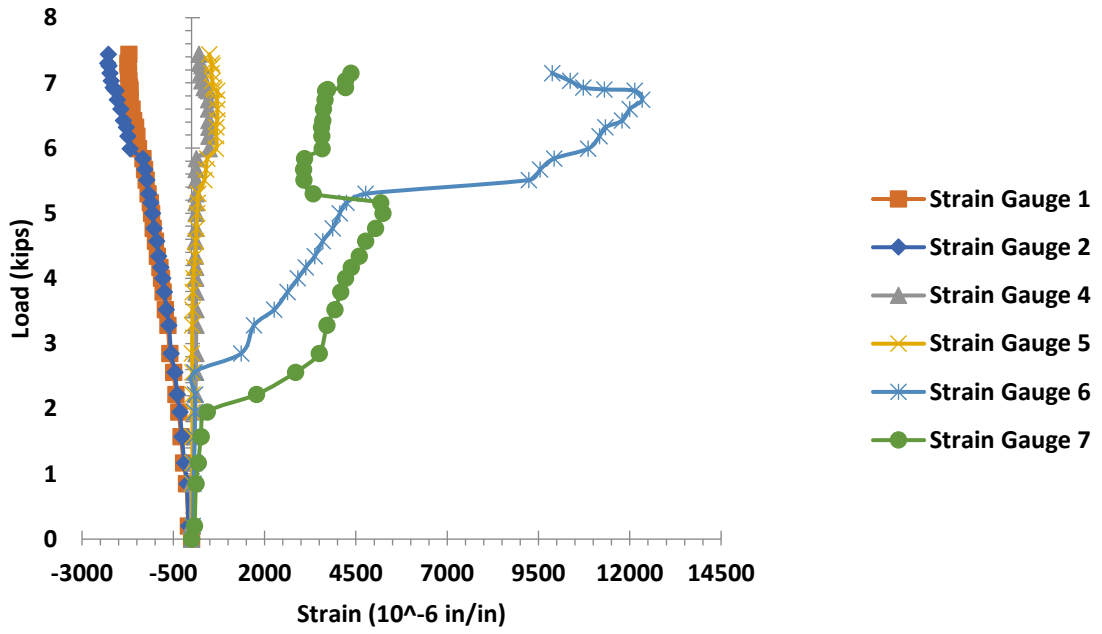

Figure 61. Experimental Load-strain Values for All Strain Gauges for Specimen B-1 (retrofitted)

2.5.3 Quasi-static Load Test Results

All the results were obtained from the 7000 multichannel machine record and converted to Excel format. This information was analyzed and plotted using Excel spreadsheets.

During the quasi-static test, the following data was collected; load increments, deflections, cracks pattern, and strain reading for each quasi-static for each quasi-static test. This information was analyzed and plotted to determine the observations and conclusion described later in this dissertation.

The first two beams analyzed were the beam with regular steel reinforcement in the tension area and Basalt reinforcement in the tension area. These beams were not loaded until the collapse stage and were used as two control beams for the entire research.

2.5.4 Deflection Results

Deflection on the simply supported beams were recorded using three dial gauges at 13.75 inches from supports and one at mid-span of the beam.

Figure 62 represents the deflection of the control steel beam (S-1) for the entire research. The maximum deflection of the first steel beam without retrofit was recorded at the midpoint of the beam. The maximum deflection was recorded at 0.26 inch and the load applied at this time was 5.00 kips.

Figure 63 represents the deflection of the control Basalt beam B-1 for the entire research. The maximum deflection of the Basalt beam without retrofit was recorded at the midpoint of the beam. The maximum deflection was recorded at 0.99 inch and the load applied at this time was 5.57 kips.

Figure 64 represents the deflection for the Specimen S-B 1 external retrofit. The maximum deflection of specimen was recorded at the midpoint of the beam. The maximum deflection was recorded at 0.59 inch and the load applied at this time was 6.14 kips.

Figure 65 represents the deflection for Specimen B-B 1 external retrofit. The maximum deflection of specimen was recorded at the midpoint of the beam. The maximum deflection was recorded at 1.20 inches and the load applied at this time was 6.46 kips.

Figure 66 represents the deflection for Specimen S-F 1. The maximum deflection of specimen was recorded at the midpoint of the beam. The maximum deflection was recorded at 0.95 inch and the load applied at this time was 7.04 kips.

Figure 67 represents the deflection for Specimen B-F 1. The maximum deflection of specimen was recorded at the midpoint of the beam. The maximum deflection was recorded at 1.22 inches and the load applied at this time was 8.45 kips.

Figure 68 represents the deflection for Specimen S-1 (retrofitted with Basalt fabric). The maximum deflection of specimen was recorded at the midpoint of the beam. This specimen

developed a deflection of 0.26 inch during the first specimen test when the specimen was loaded up to 5.00 kips. After retrofitting the specimen and re-loading again, the maximum deflection was recorded at 0.66 inch and the load applied at this time was 7.82 kips.

Figure 69 represents the deflection for Specimen B-1 (retrofitted with Basalt fabric). The maximum deflection of specimen was recorded at the midpoint of the beam. The specimen developed a deflection of 1.37 inches during the first test prior retrofitted and was loaded with 5.57 kips after retrofitted and re-loaded again the maximum deflection was recorded at 1.08 inches and the load applied at the time was 7.44 kips.

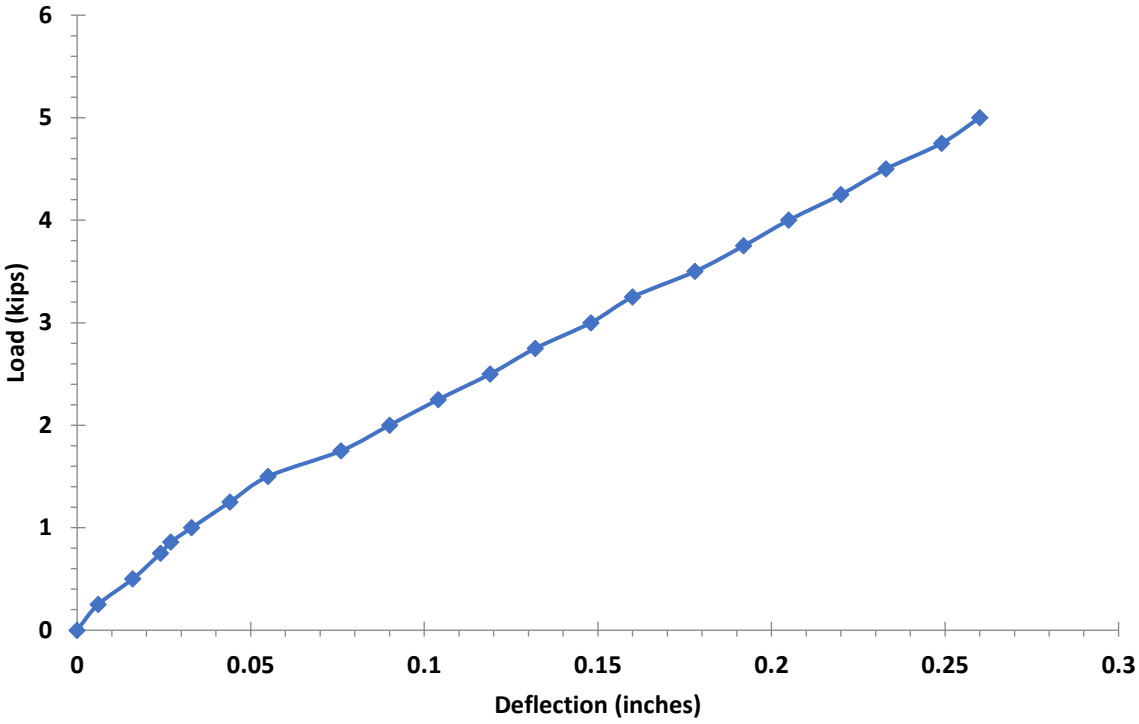

Figure 62. Experimental Load Deflection for Specimen S-1

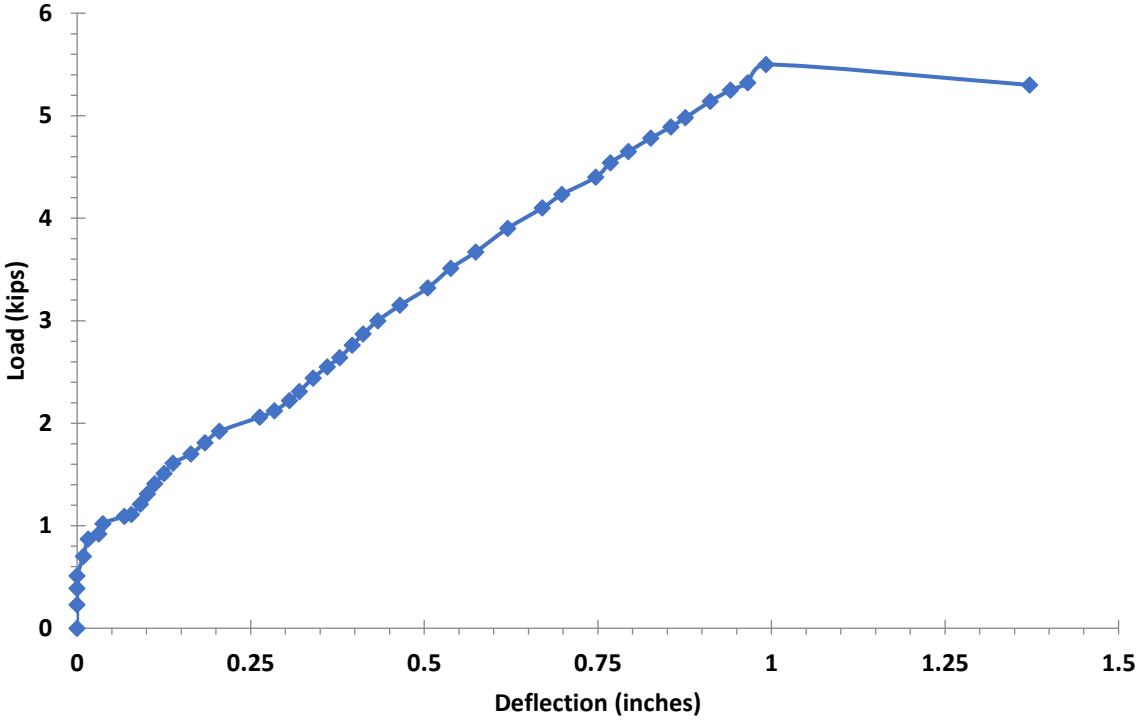

Figure 63. Experimental Load Deflection for Specimen B-1

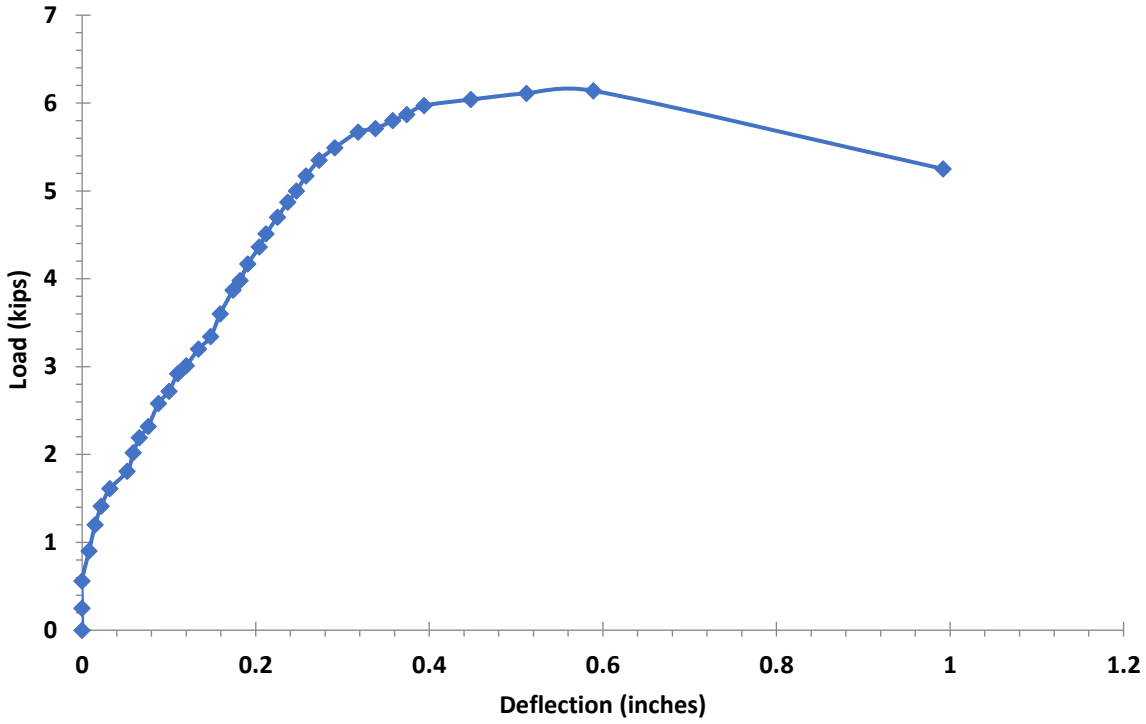

Figure 64. Experimental Load Deflection for Specimen S-B-1

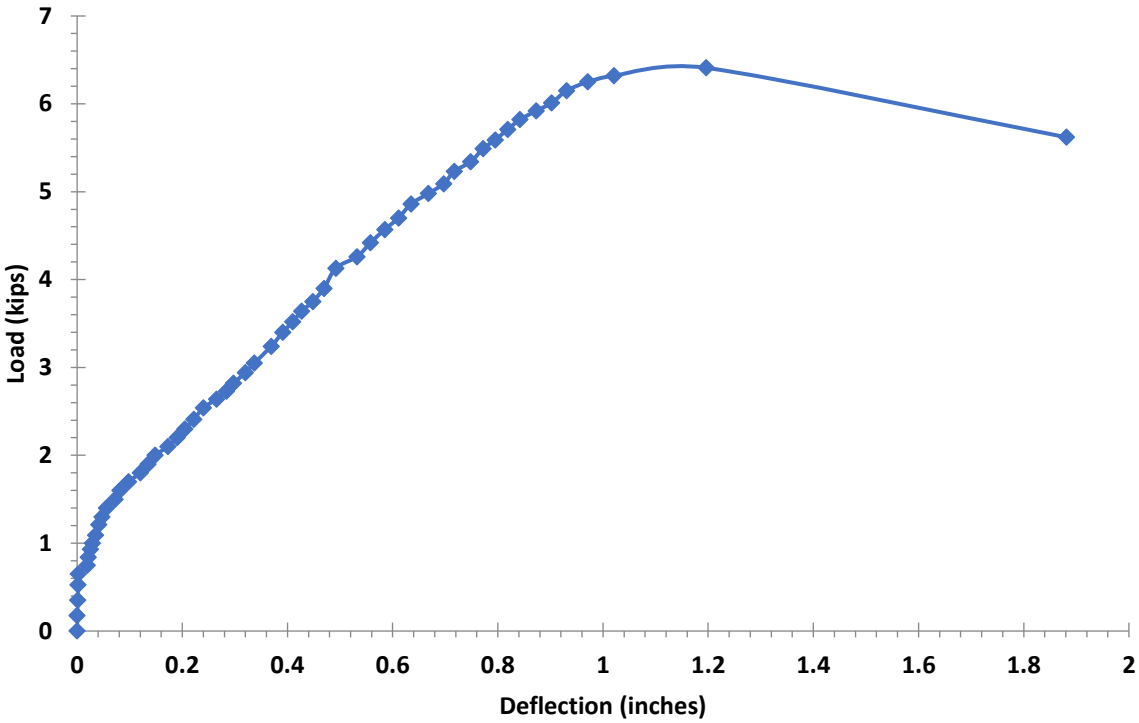

Figure 65. Experimental Load Deflection for Specimen B-B-1

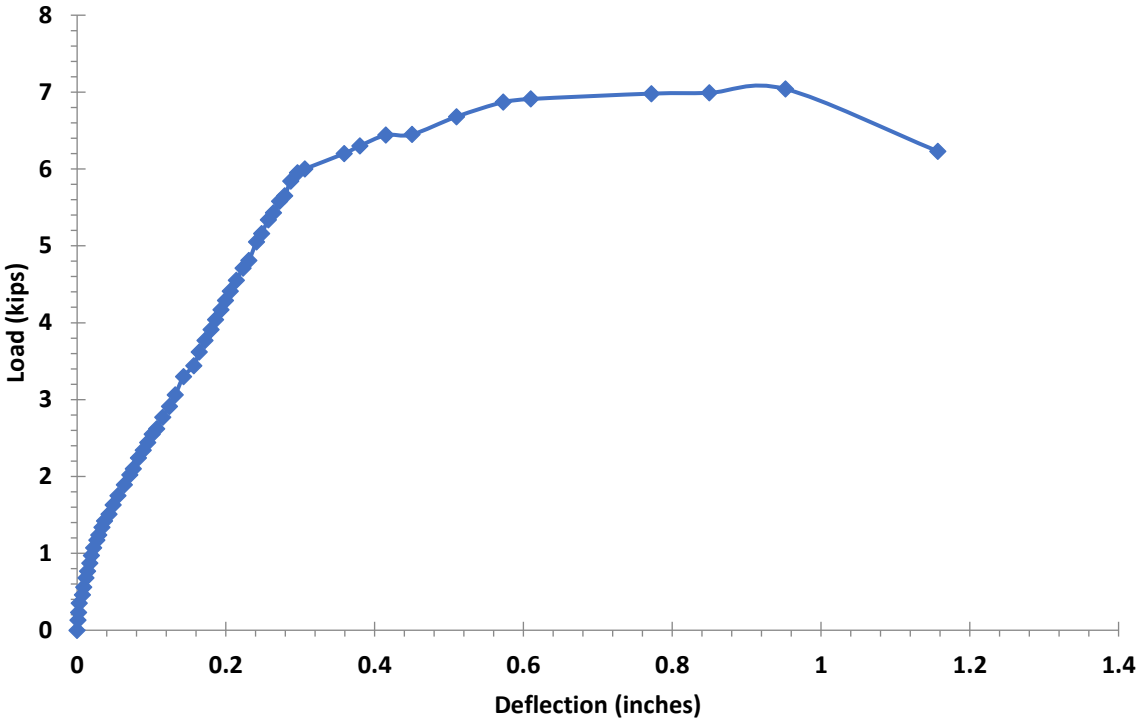

Figure 66. Experimental Load Deflection for Specimen S-F-1

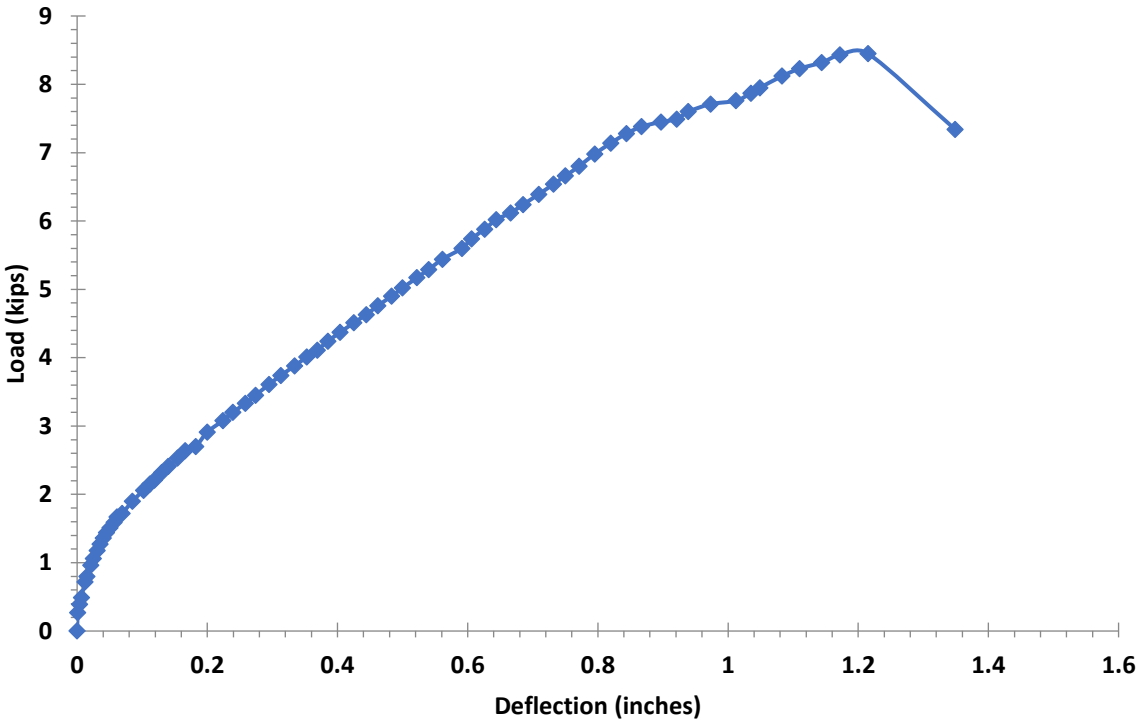

Figure 67. Experimental Load Deflection for Specimen B-F-1

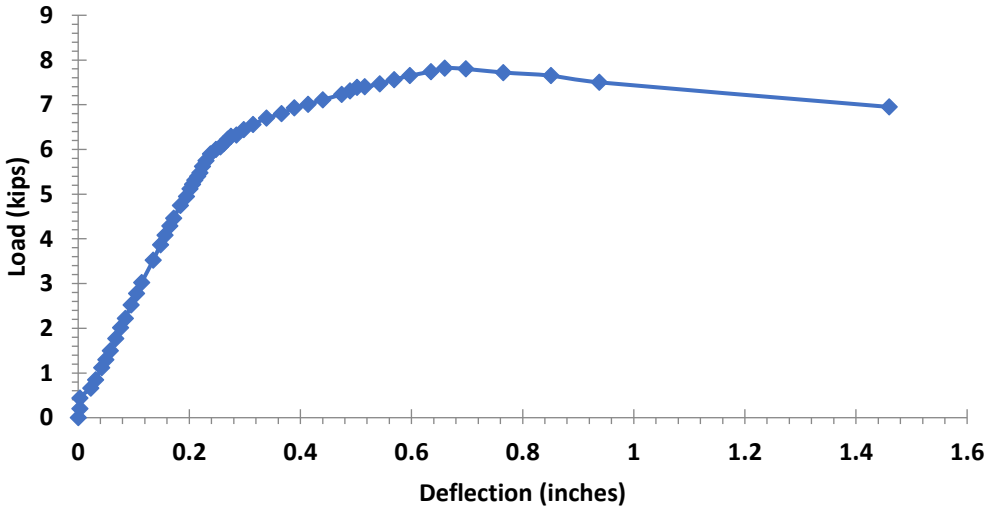

Figure 68. Experimental Load Deflection for Damaged Specimen S-1 (retrofitted)

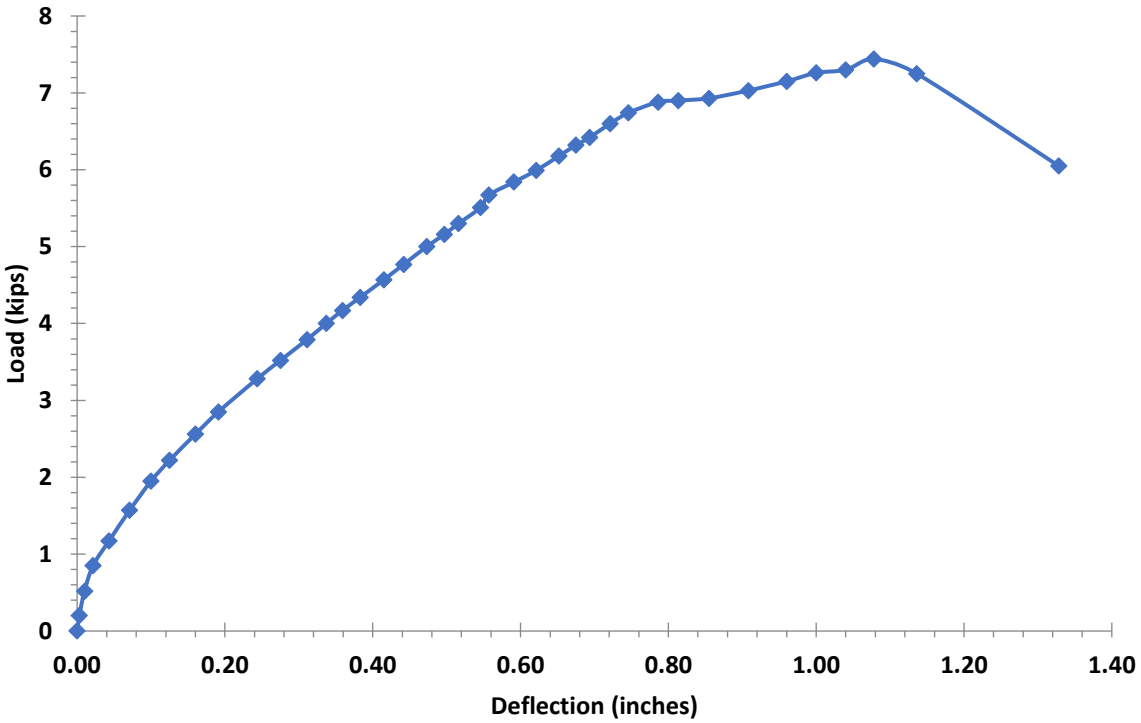

Figure 69. Experimental Load Deflection for Damaged Specimen S-1 (retrofitted)

2.5.5 Beam Cracks Pattern Results

Cracks were observed during each specimen test and the location and the load that created each crack in each beam was recorded. There were no cracks or failures due to shear failure during any of the simply supported tests.

Figure 70 represents all ten cracks observed during this test on Specimen S-1. The first crack in the specimen was developed at mid-point of the specimen when load of 0.86 kips was applied. The total load applied to this specimen was 5.00 kips.

Figure 71 represents all nine cracks observed during this test on Specimen B-1. The first crack in the specimen was developed at mid-point of the specimen when load of 0.92 kips was applied. The total load applied to this specimen was 5.57 kips.

Figure 72 represents all twelve cracks observed during this test on Specimen S-B 1. Also, the top fiber of the concrete started to crunch at 6.04 kips applied load. The first crack in the specimen was developed at mid-point of the specimen when load of 0.90 kips was applied. The total load applied to this specimen was 6.14 kips.

Figure 73 represents all eleven cracks observed during this test on Specimen B-B 1. Also, the top fiber of the concrete started to crunch at 6.32 kips applied load. The first crack in the specimen was developed at mid-point of the specimen when load of 1.06 kips was applied. The total load applied to this specimen was 6.48 kips.

Figure 74 represents the beam wrapping with the Basalt fabric, it was impossible to observe the cracks on Specimen S-F 1. The first crack was heard and recorded at 2.55 kips. Due to the fabric wrapping, it was impossible to observe all the cracks generated in this test. BFRP fabric was not broken at the time of the collapse load for the beam. Also, the top fiber of the concrete started to crunch at 7.00 kips applied load. The total load applied to this specimen was 7.01 kips.

Figure 75 represents the beam wrapping with the Basalt fabric, it was impossible to observe the cracks on Specimen B-F 1. The first crack noise was recorded at 2.06 kips. The fabric was not broken at the time of the collapse load for the beam. Also, the top fiber of the concrete started to crunch at 7.71 kips applied load. The total load applied to this specimen was 8.45 kips.

Figure 76 represents the steel reinforced beam which had ten cracks from the original test and was retrofitted and loaded for a second test on Specimen S-1 (retrofitted with BFRP fabric). Due to the fabric wrapping, it was impossible to observe any new cracks generated in this test. The BFRP fabric started to crack and was damaged at around 7.30 kips of applied load. A total of three areas of damage in the fabric were observed during this test on the beam with steel reinforcement and basalt fabric retrofitted. The specimen failed at 7.82 kips.

Figure 77 represents the Basalt reinforced beam which had nine cracks from the original test and was retrofitted and loaded for a second test on Specimen B-1 (retrofitted with Basalt fabric). Due to the fabric wrapping, it was impossible to observe any new cracks generated in this test. The top fiber of the concrete started to crunch when a load of 7.10 kips was applied. The Basalt fabric started to crack and was damaged at around 7.30 kips of applied load. A total of three areas of damage in the fabric were observed during this test on the beam with BFRP reinforcement and BFRP fabric retrofit. The specimen failed at 7.44 kips.

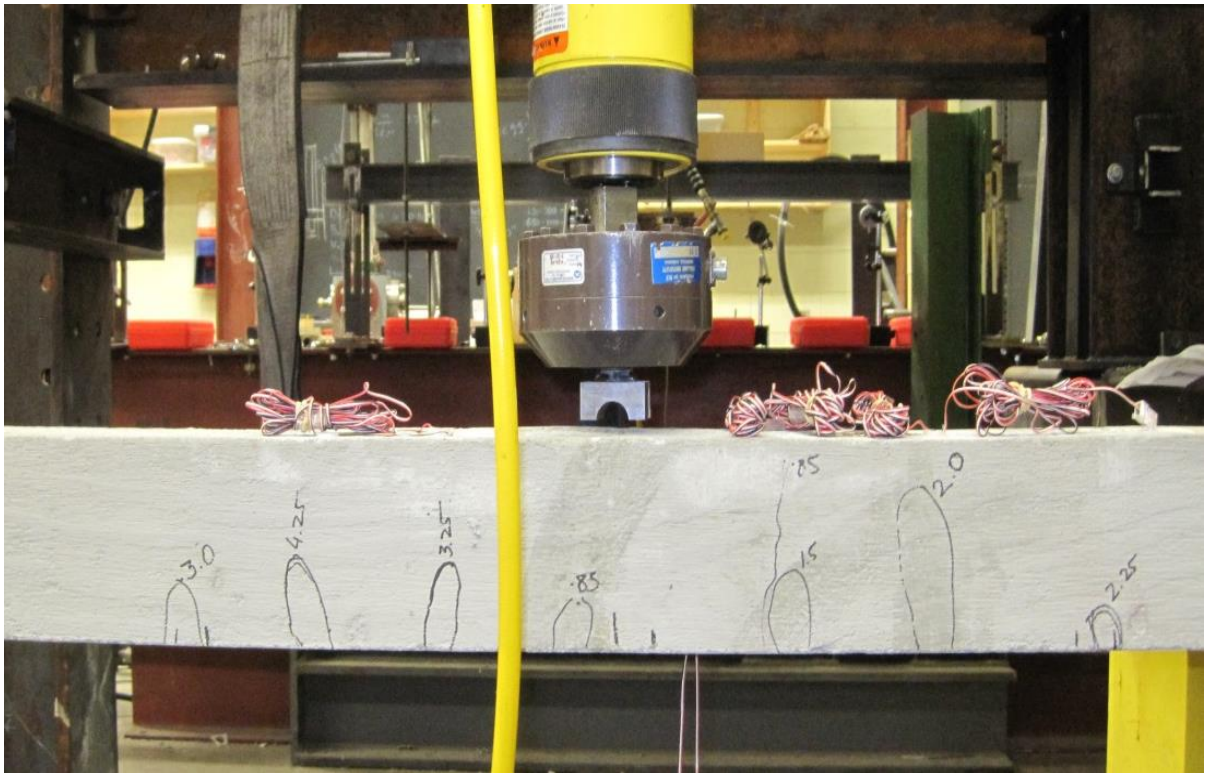

Figure 70. Crack Pattern of Specimen S-1

Figure 71. Crack Pattern of Specimen B-1

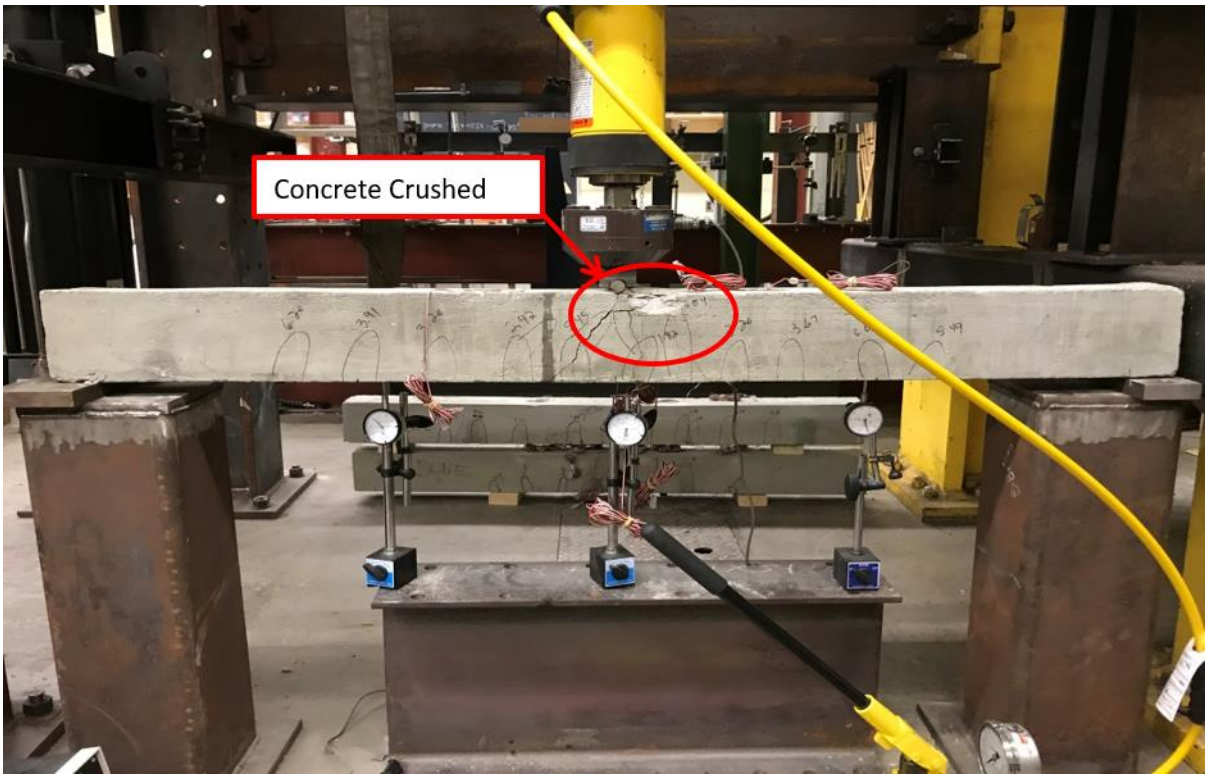

Figure 72. Crack Pattern of Specimen S-B

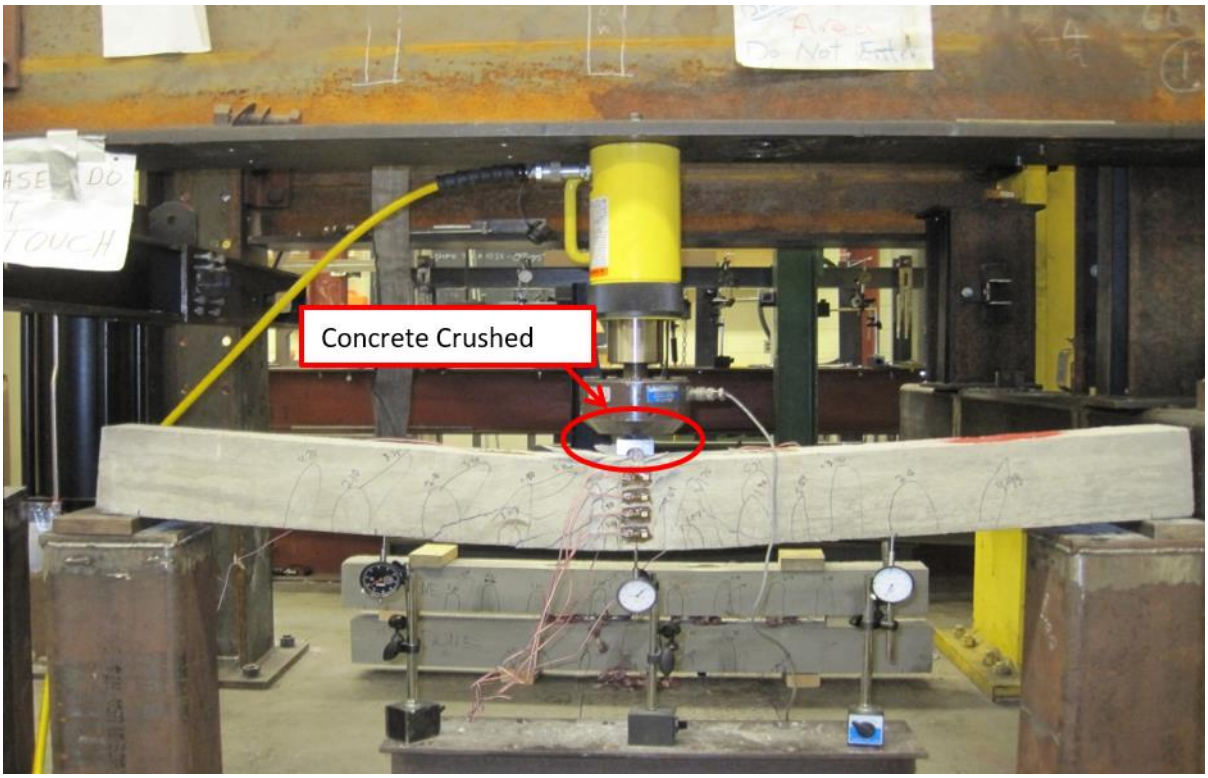

Figure 73. Crack Pattern of Specimen B-B

Figure 74. Crack Pattern of Specimen S-F-1

Figure 75. Crack Pattern of Specimen B-F-1

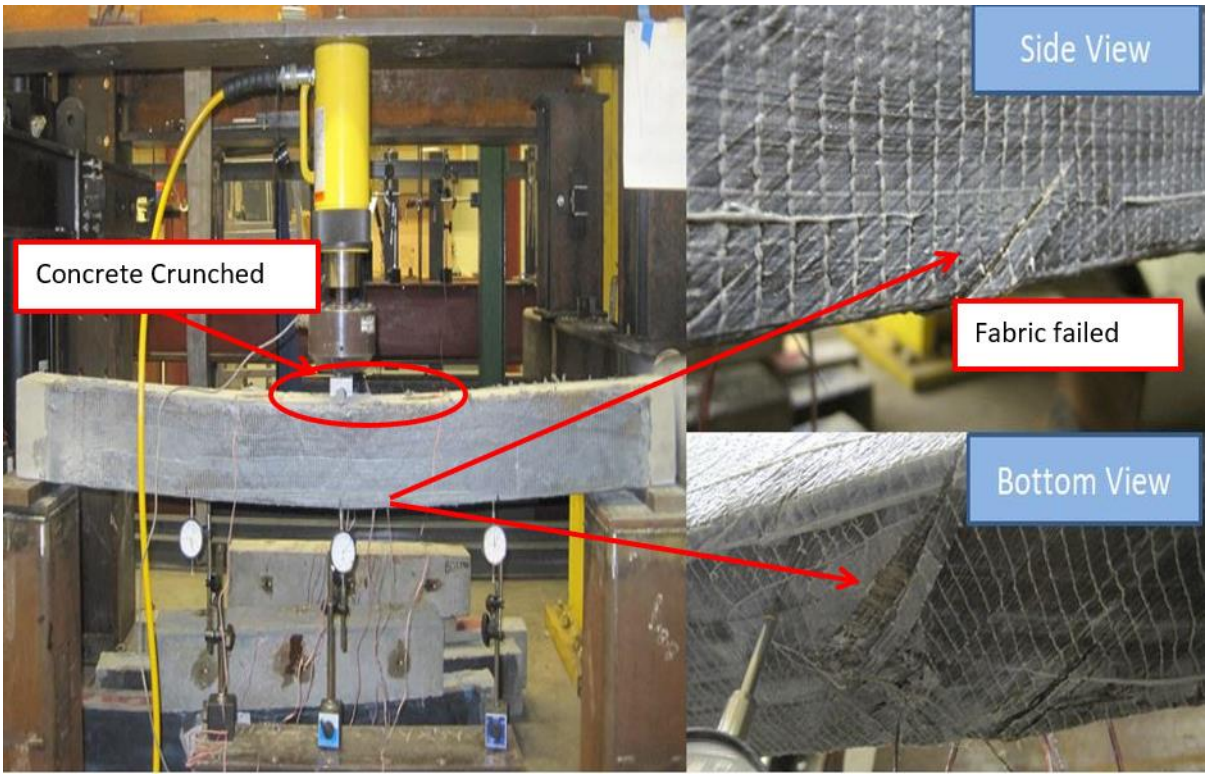

Figure 76. Crack Pattern of Specimen S-1 (retrofitted)

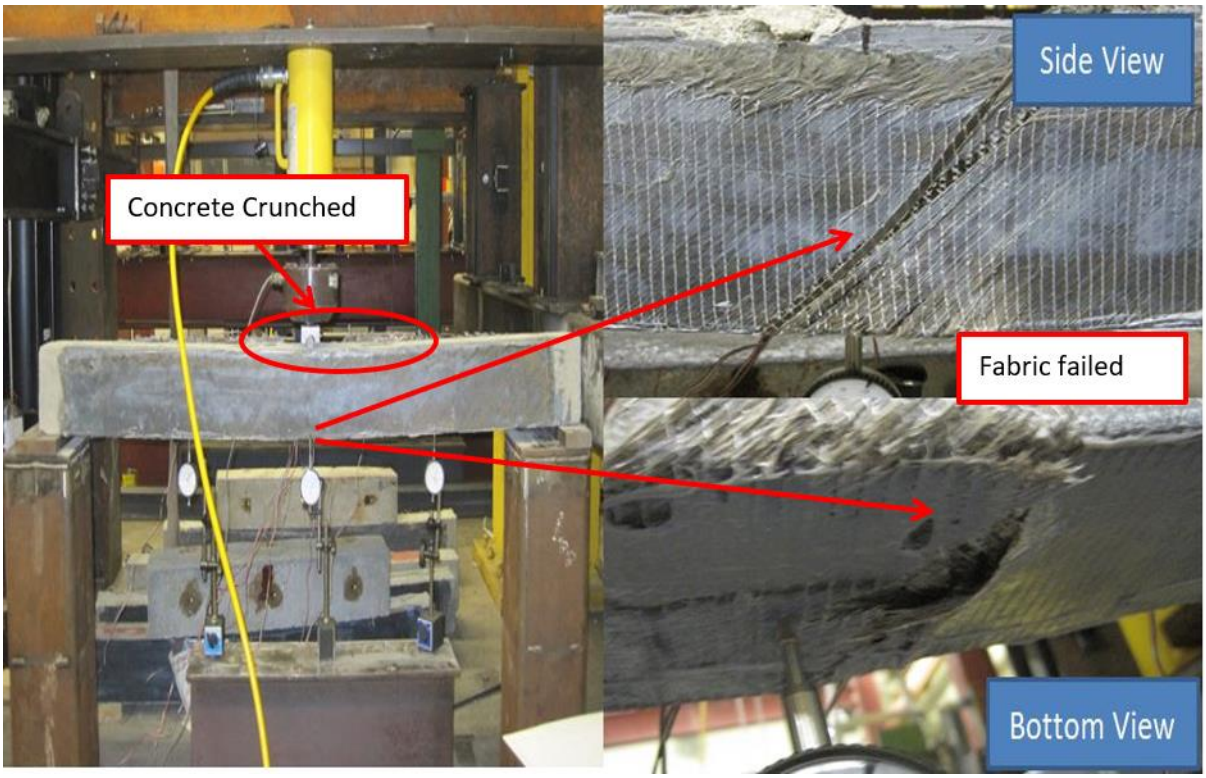

Figure 77. Crack Pattern of Specimen B-1 (retrofitted)

2.5.6 Impact Load Tests

Not all reinforced concrete structures are designed for an impact load. The ones that are designed for impact loads are designed for heavy objects and a small velocity that are typical occur in a warehouse accidents. The behavior of the concrete structures can be defined in two phases: 1) the local response due to the stress waves that occur at the impact point in the structures during a very short of period after the impact and 2) the overall response including the free vibration effect due to the elastic-plastic deformation that occur over a long period in the whole structure's member after the impact [22]. It is important to estimate both its flexural capacity and its maximum deformation response as an important damages index.

The test was conducted using three different impactors that were dropped at different heights.

The primary objective of the impact load test was to capture the primary impact in the beam; however, the operating mechanism, secondary, and tertiary impact on the specimen could not be avoided. Figure 79 represents the three impactors and weights; a 500 g accelerometer was installed inside the steel housing facing the hitting point of the impactor. The small impactors (0.06 kips) were dropped at 1, 2, 3, 5, 7, and 10 inches; the medium impactor (0.14 kips) was dropped at 1, 2, 3, 5, 7, 10, 12, 14, 16, 17, 18, 19, 21, 23, and 25 inches; and the large impactor (0.40 kips) was dropped at 2, 5, 7, 9, 11, 13, 15, 17, 19, 21, 23, and 25 inches until the beam fully collapsed. The only results provided were using the impactor of 0.14 kips at 10-inch drops for all specimens and the collapsed results of each specimen. The 10 inches were selected as a representation of structures failure after the loss of one column during a blast incident or terrorist attack.

A series of impact tests were conducted on reinforced simply supported concrete beams. The final test set-up prior to starting the test is illustrated in Figure 80. The concrete beams were made using regular steel reinforcement, Basalt reinforcement and retrofitted with external basalt reinforcement, and external BFRP fabric. The typical cross section was 4.5 inches x 5.5 inches and 60 inches long with a clear distance between supports of 55 inches. The impact load was applied at mid-distance of the specimen. During this test the mass for the impactor was lifted after the second impact, the beam mass and impactor mass was in contact no more than 0.05 to 0.07second during the first impact.

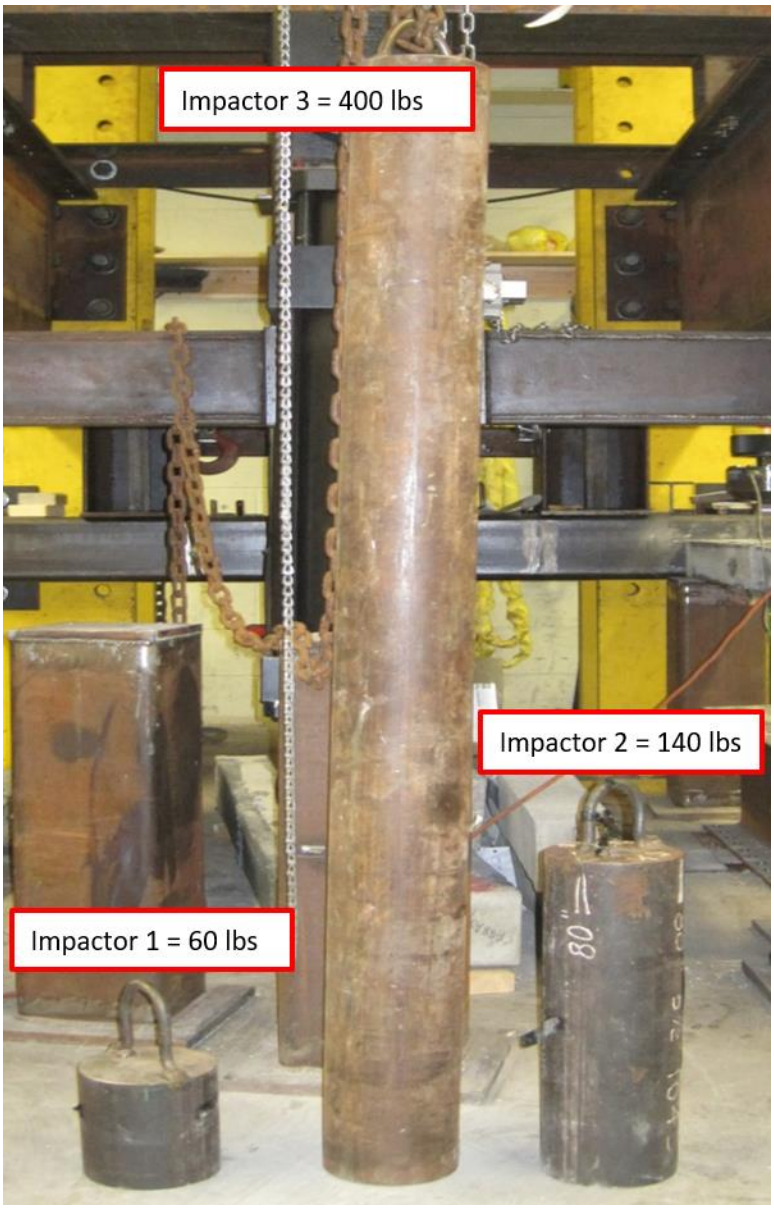

Figure 78. Three Steel Solid Impactors Used for the Impact Load

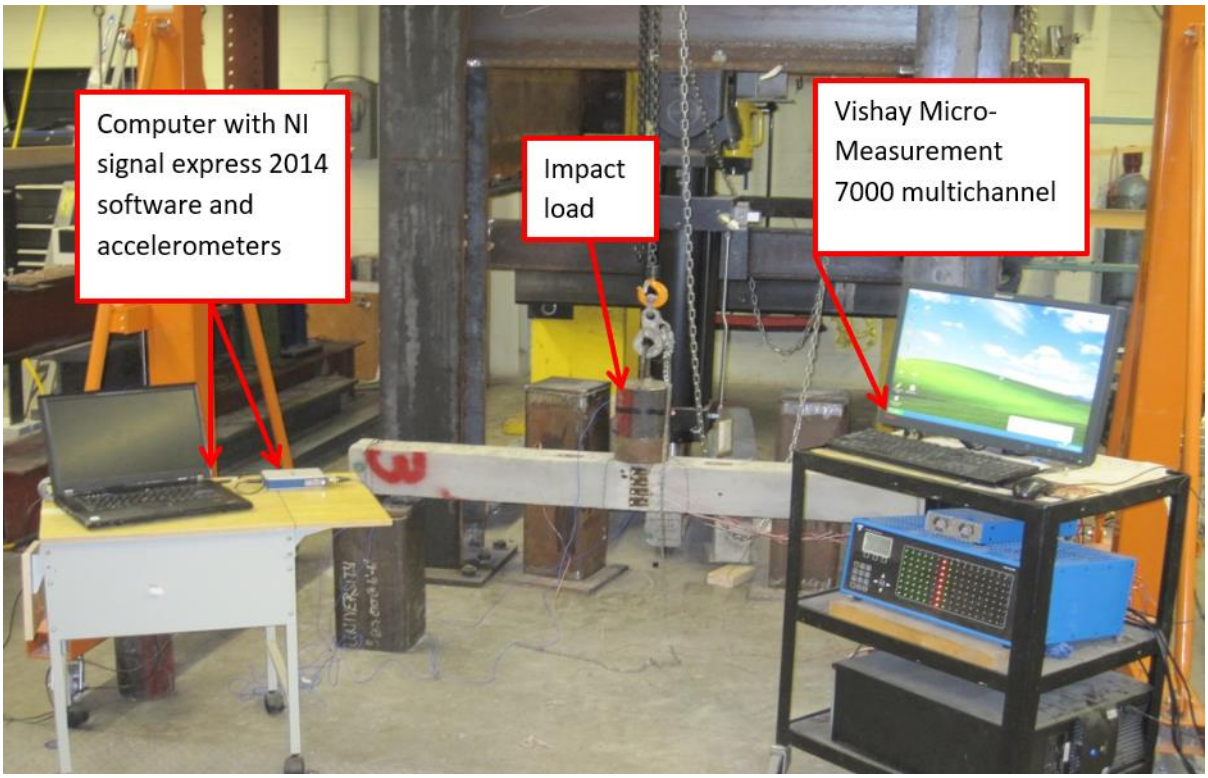

Figure 79. Setup of the Dynamic Test Procedure in the Laboratory for Specimen S-2

2.5.7 Impact Load Results

In this section, the final condition of each of the fifth specimen test under impact load is presented. Figures 80 to 84 represent the final beam condition of the five beams tested under impact load. Each beam was collapsed by different impactors and at different heights.

Figure 80 illustrates Specimen S-2 collapsed using 0.14 impactor and dropped at 21 inches. This specimen had two #3 steel reinforcements. During the first set of the impact test using 0.06 kips there was no record of any visible cracks. A total of eleven cracks were recorded. The first crack was observed during the 0.14 kips impactor and dropped height of 12 inches in one location of the specimen. Three additional cracks were observed at the 14 inches drop. At this impact load, the concrete started to crunch in the top mid-point of the specimen. The concrete continued to crunch at any additional impact load until the test was completed at 25 inches height drop with

the 0.14 kips impactor. Permanent deflection of 0.25 inches was recorded at the impact of a 21-inch drop. Final permanent deflection was recorded at the impact of a 25-inch drop of 0.75 inch.

Figure 80. The Final Failure Pattern of Specimen S-2

Figure 81 illustrates the collapse of Specimen S-B 2 using 0.40 kips impactor and dropped at 7 inches. This specimen had # 3 reinforcement and was retrofitted with 2-4mm external Basalt reinforcement.

This specimen had two #3 steel reinforcements and was retrofitted with 2-4mm external Basalt reinforcements. During the first set of the impact test using the 0.06 kips impactor did not record any visible cracks. A total of ten cracks were recorded. Seven cracks were observed during the

0.14 kips impactor and dropped height of 7 inches. Two additional cracks were developed at the 10 inches height impact. An additional five cracks were developed at the 12-inch drop. At 16 inches dropped, the concrete started to crunch in the top mid-point of the specimen. The concrete continued to crunch at any additional impact load above 19 inches in impact height until the test was completed at 15 inches height drop with the 0.40 kips impactor. Permanent deflection of 0.5 inch was recorded at the impact of the 7 inches drop with the 0.40 kips impactor. Final permanent deflection was recorded at the impact of the 25-inch drop of 1.00 inches.

Figure 81. The Final Failure Pattern of Specimen S-B 2

Figure 82 illustrates Specimen B-B 2 collapsed using 0.14 kips impactor and dropped at 25 inches. This specimen had two-10 mm Basalt reinforcements and was retrofitted with 2-4mm external Basalt reinforcements. During the first set of the impact test using the 0.06 kips impactor did not record any visible cracks. A total of twelve cracks were recorded. The first crack was observed during the 0.14 kips impactor and dropped height of 7 inches. One additional crack was observed in the top of the specimen from front to back at the 16 inches height impact. Cracks continued to develop at this point until the specimen failed. At the impact of 0.14 kips and the impact height of 25 inches, the beam had a permanent deflection of 0.63 inch. At the 3 inches drop with the impactor of 0.40 kips, the concrete started to crunch in the top mid-point of the specimen. The concrete continued to crunch at any additional impact load above 9 inches height until the test was completed at 15 inches height drop with the 0.40 kips impactor. Final permanent deflection was recorded at the impact of the 15 inches drop of 1.88 inches.

Figure 82. The Final Failure Pattern of Specimen B-B 2

Figure 83 illustrates Specimen B-F 2 collapsed using 0.40 kips impactor and dropped at 17 inches. This specimen had two-10 mm Basalt reinforcements and was retrofitted with one layer of BA-450-13 +/-0.45-0.45-127 Basalt fabric. Due to the fabric wrapping it was impossible to observe cracks in the top of the specimen. The first top crack was observed at a drop of 14 inches with the 0.14 kips impactor. At the impact of 0.14 kips and the impact height of 21 inches, the beam had a permanent deflection of 0.5 inch. At the 23 inches drop with the impactor of 0.14 kips the concrete starts to crunch in the top mid-point of the specimen. The concrete continued to crunch at any additional impact load above 23 inches height until the test was completed at the 23 inches height drop with the 0.40 kips impactor. Permanent deflection was recorded at the impact of the 11 inches drop with the 0.40 kips impactor of 1.0 inch. Final permanent deflection was recorded at the impact of the 23 inches drop with the 0.40 kips impactor of 3.5 inches. The basalt fabric was broken at the mid-point of the specimen in the top and bottom part due to the stress and the concrete crunching.

Figure 83. The Final Failure Pattern of Specimen B-F 2

Figure 84 illustrates the Specimen S-F 2 collapse using 0.14 kips impactor and dropped at 21 inches. This specimen had two #3 steel reinforcements and was retrofitted with one layer of BA-450-13 +/-0.45-0.45-127 BFRP fabric. Due to the fabric wrapping it was impossible to observe any crack that happened in the top of the specimen. The first top crack was observed at the drop of 12 inches with the 0.14 kips impactor. At an impact of 0.14 kips and the impact height of 21 inches, the beam had a permanent deflection of 0.25 inch. At the 23 inches drop with the impactor of 0.14 kips, the concrete started to crunch in the top mid-point of the specimen. The concrete continued to crunch at any additional impact load above 23 inches height until the test was completed at the 17 inches height drop with the 0.40 kips impactor. Permanent deflection was recorded at the impact of the 11 inches drop with the 0.40 kips impactor of 1.25 inches. Final permanent deflection was recorded at the impact of the 17 inches drop with the 0.40 kips

impactor of 2.63 inches. The Basalt fabric was broken at the mid-point of the specimen in the top and bottom part due to the stress, and the concrete crunched.

Figure 84. The Final Failure Pattern of Specimen S-F 2

2.5.8 Impact Load Strain Gauge Results

This section presents the strain gauge values for the specimens tested under impact load. The purpose of this section is to illustrate the continuation of strain values of each strain gauge from one test to the next test. Three strain values are reported; the first is the strain value of each of the strain gauges at the beginning of the recorded data. The second strain value reported in this

section is the maximum strain value of each strain gauge after the specimen was impacted. The last strain value reported in this section is the final strain value of each strain gauge after the specimen returned to rest position. I also identified the time of the impact on the beam (ti), time of rebound for the second impact (td) and time of the second impact on the beam (tsi). Some strain gauges that are not illustrated in the graphics of each beam mean the strain gauge was damaged during the test or not recorded. The analysis for the small impactors yielded 0.60 kips that were dropped at 1, 2, 3, 5, 7, and 10 inches; the medium impactor 0.14 kips was dropped at 1, 2, 3, 5, 7, 10, 12, 14, 16, 17, 18, 19, 21, 23, and 25 inches; and the large impactor 0.40kips was dropped at 2, 5, 7, 9, 11, 13, 15, 17, 19, 21, 23, and 25 inches. These were conducted until the beam fully collapsed. The only results provided in this section were using the impactor of 0.14 kips at 10-inch drops for all specimens in representation of a real building collapsed and the drop for each beam at failure. Figures 86 to 104 represent the strain-time relationship of each gauge reading for each impact load test on each specimen.

Figures 85 and 86 represent the record of all strain gauges for the Specimen S-2 using the impactor 0.14 dropped at 10 inches height. Strain Gauge 1 had a reading of -0.0001 in/in from the previous test. During the impact a reading of -0.0002 in/in was recorded. The final reading of Strain Gauge 1 was -0.0001 in/in after the beam returned to rest. Strain Gauge 2 had a reading of 0.0000 in/in from the previous test. During the impact a reading of -0.0001 in/in was recorded. The final reading of Strain Gauge 2 was -0.0000 in/in after the beam returned to rest. Strain Gauge 3 had a reading of -0.0001 in/in from the previous test. During the impact a reading of -0.0003 in/in was recorded. The final reading of Strain Gauge 3 was -0.0002 in/in after the beam returned to rest. Strain Gauge 4 had a reading of -0.0000 in/in from the previous test. During the impact a reading of -0.0000 in/in was recorded. The final reading of strain Gauge 4 was -0.0000 in/in after the beam returned to rest. Strain Gauge 5 had a reading of 0.0001 in/in from the previous test. During the impact a reading of 0.0001 in/in was recorded. The final reading of strain Gauge 5 was 0.0001 in/in after the beam returned to rest. Strain Gauge 6 had a reading of -0.0082 in/in from the previous test. During the impact a reading of -0.0083 in/in was recorded. The final reading of Strain Gauge 6 was -0.0083 in/in after the beam returned to rest; this strain value exceeded the yield point of 0.0023 in/in for the steel reinforcement at this location. Strain Gauge 7 had a reading of -0.0000 in/in from the previous test. During the impact a reading of -

0.0001 in/in was recorded. The final reading of Strain Gauge 7 was -0.0000 in/in after the beam returned to rest. This This test was recorded for 0.20 seconds and the impact occurred at 0.022 seconds.

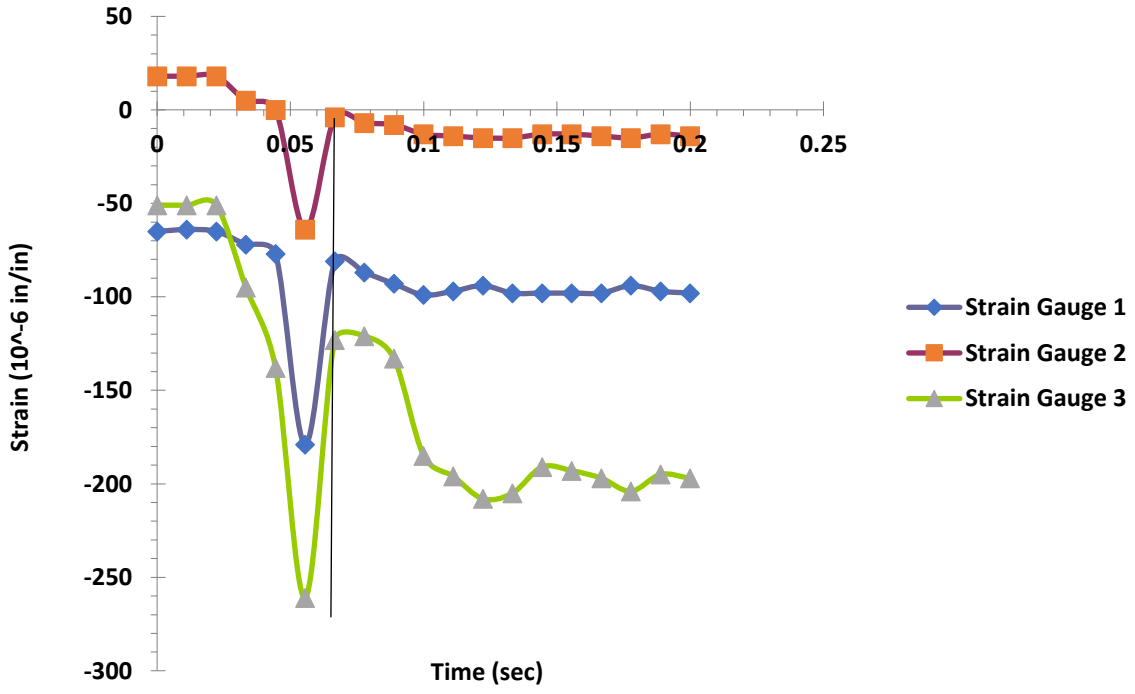

Figure 85. Experimental Strain-time Value for S-2 Test at 10 inches

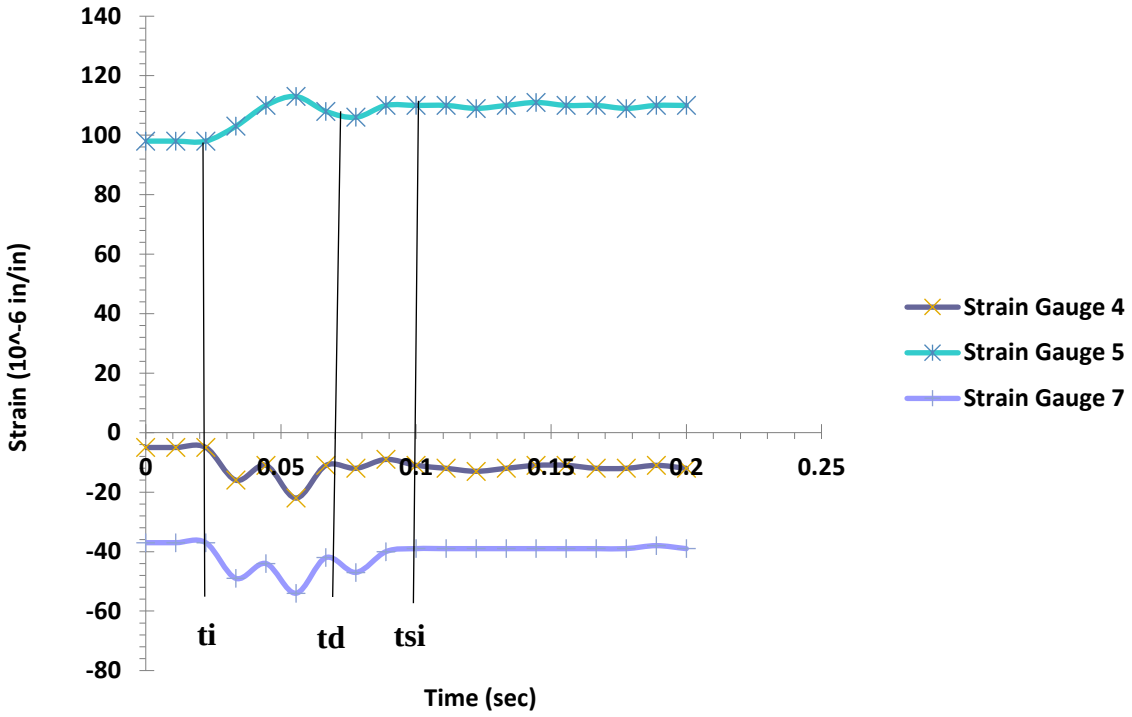

Figure 86. Experimental Strain-time Value for S-2 Test at 10 inches

Figures 87 and 88 represent the record of all strain gauges for the Specimen S-2 using the impactor #2 (0.14 kips) dropped at 21 inches height. During this test the beam developed two additional cracks. During this test the concrete in the top part of the beam continued to crunch. Strain Gauge 1 had a reading of -0.0002 in/in from the previous test. During the impact a reading of -0.0003 in/in was recorded. The final reading of Strain Gauge 1 was -0.0002 in/in after the beam returned to rest. Strain Gauge 2 had a reading of 0.0001 in/in from the previous test. During the impact a reading of -0.0152 in/in was recorded. This strain value exceeded the yield point for the concrete of 0.0031 in/in and the yield point of 0.0023 in/in for the steel reinforcement at this location. The final reading of Strain Gauge 2 was -0.0002 in/in after the beam returned to rest. Strain Gauge 3 had a reading of 0.0000 in/in from the previous test. During the impact strain gauge does not record any reading. This train gauge did not record any

reading at the end of this test. Strain Gauge 4 had a reading of -0.0000 in/in from the previous test. During the impact a reading of -0.0000 in/in was recorded. The final reading of Strain Gauge 4 was -0.0000 in/in after the beam returned to rest. Strain Gauge 5 had a reading of 0.0001 in/in from the previous test. During the impact a reading of 0.0002 in/in was recorded. The final reading of Strain Gauge 5 was 0.0001 in/in after the beam returned to rest. Strain Gauge 6 had a reading of -0.0084 in/in from the previous test. During the impact a reading of -0.0084 in/in was recorded. The final reading of Strain Gauge 6 was -0.0083 in/in after the beam returned to rest. This strain value exceeded the yield point of 0.0023 in/in for the steel reinforcement and the concrete strain of 0.0031 in/in at this location. Strain Gauge 7 had a reading of -0.0001 in/in from the previous test. During the impact a reading of -0.0004 in/in was recorded. The final reading of Strain Gauge 7 was -0.0002 in/in after the beam returned to rest. This This test was recorded for 0.20 seconds and the impact occurred at 0.03 second. Beam failure occurred at 21 inches Strain Gauge 2 past the yield strain point of the concrete and Strain Gauge 6 past the yield strain point of the steel.

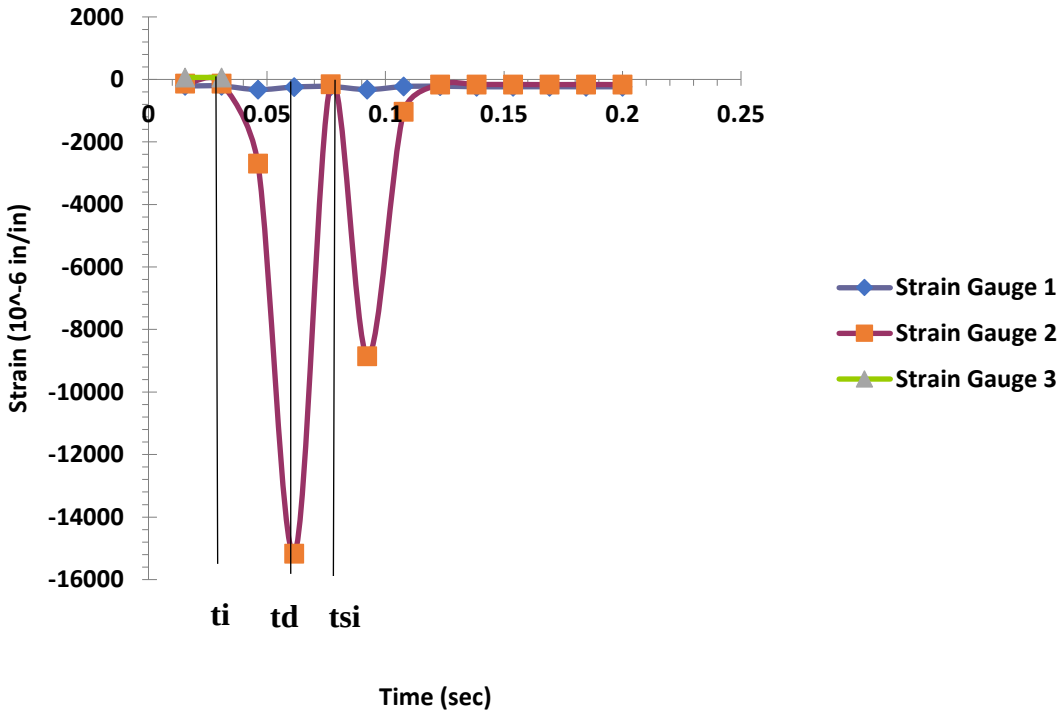

Figure 87. Experimental Strain-time Value for S-2 Test at 21 inches

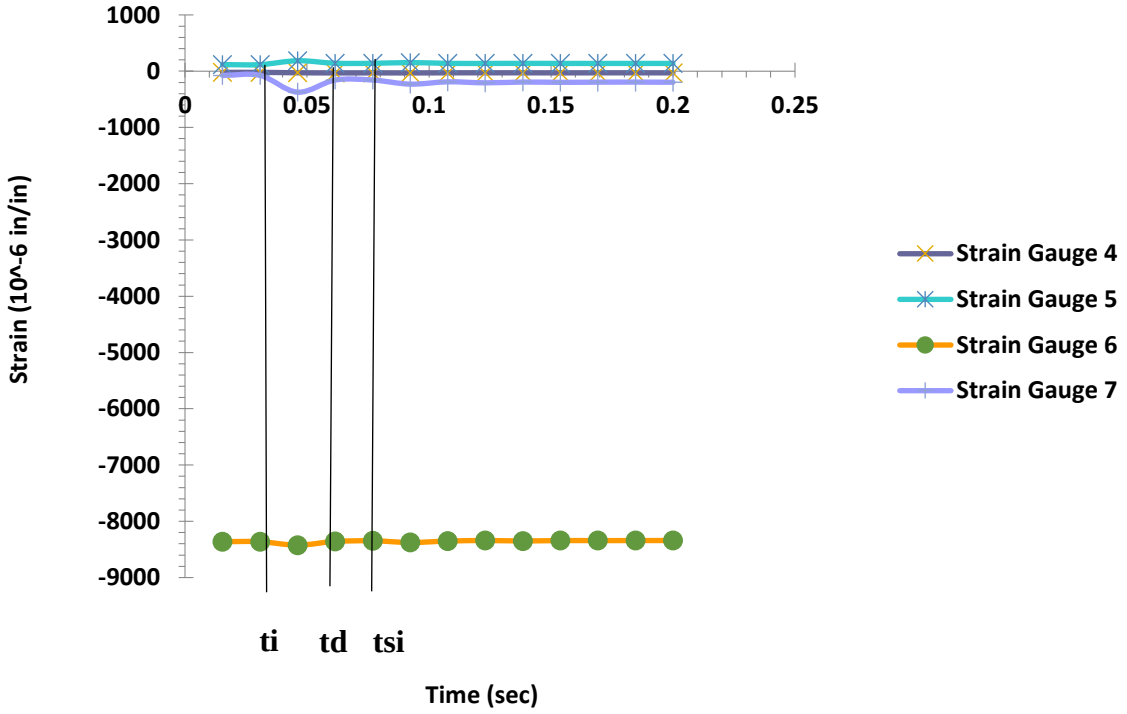

Figure 88. Experimental Strain-time Value for S-2 Test at 21 inches

Figures 89 and 90 represent the record of all strain gauges for the Specimen S-B 2 using the impactor 0.14 kips dropped at 10 inches height. During this test the beam developed two additional cracks. Strain Gauge 1 had a reading of -0.0003 in/in from the previous test. During the impact a reading of -0.0003 in/in was recorded. The final reading of Strain Gauge 1 was -0.0003 in/in after the beam returned to rest. Strain Gauge 2 had a reading of -0.0001 in/in from the previous test. During the impact a reading of -0.0001 in/in was recorded. The final reading of Strain Gauge 2 was -0.0001 in/in after the beam returned to rest. Strain Gauge 3 had a reading of -0.0002 in/in from the previous test. During the impact a reading of -0.0002 in/in was recorded. The final reading of Strain Gauge 3 was -0.0002 in/in after the beam returned to rest. Strain Gauge 4 had a reading of 0.0005 in/in from the previous test. During the impact a reading of 0.0006 in/in was recorded. The final reading of Strain Gauge 4 was 0.0005 in/in after the beam returned to rest. Strain Gauge 5 had a reading of -0.0001 in/in from the previous test. During the

impact a reading of -0.0001 in/in was recorded. The final reading of Strain Gauge 5 was -0.0001 in/in after the beam returned to rest. Strain Gauge 6 was damaged and did not record any data. Strain Gauge 7 had a reading of -0.0001 in/in from the previous test. During the impact a reading of -0.0001 in/in was recorded. The final reading of Strain Gauge 7was -0.0001 in/in after the beam returned to rest. This This test was recorded for 0.20 seconds and the impact occurred at 0.027 second.

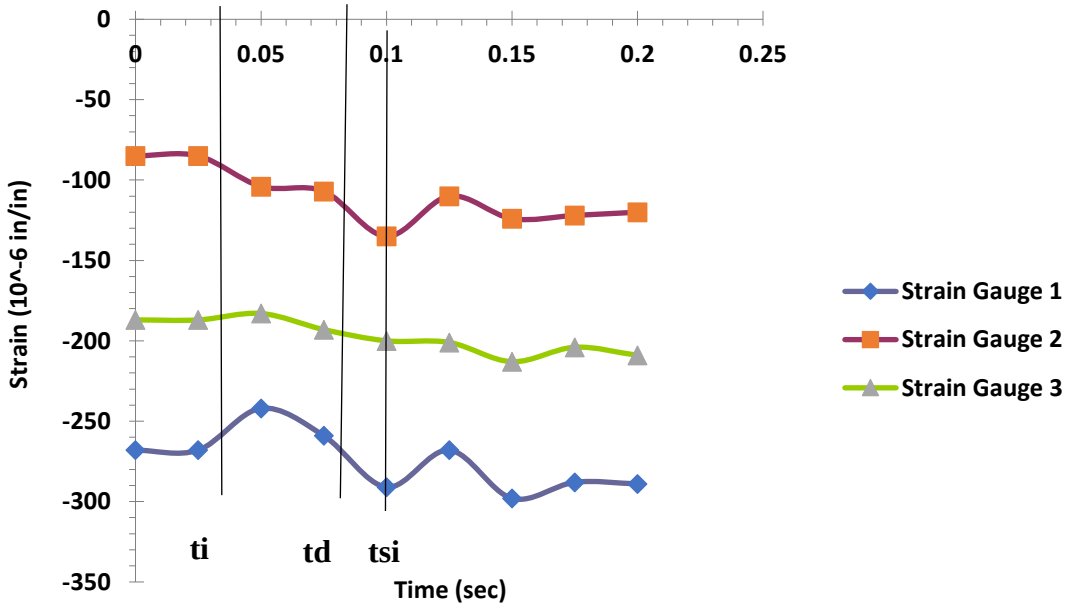

Figure 89. Experimental Strain-time Value for S-B 2 Test at 10 inches

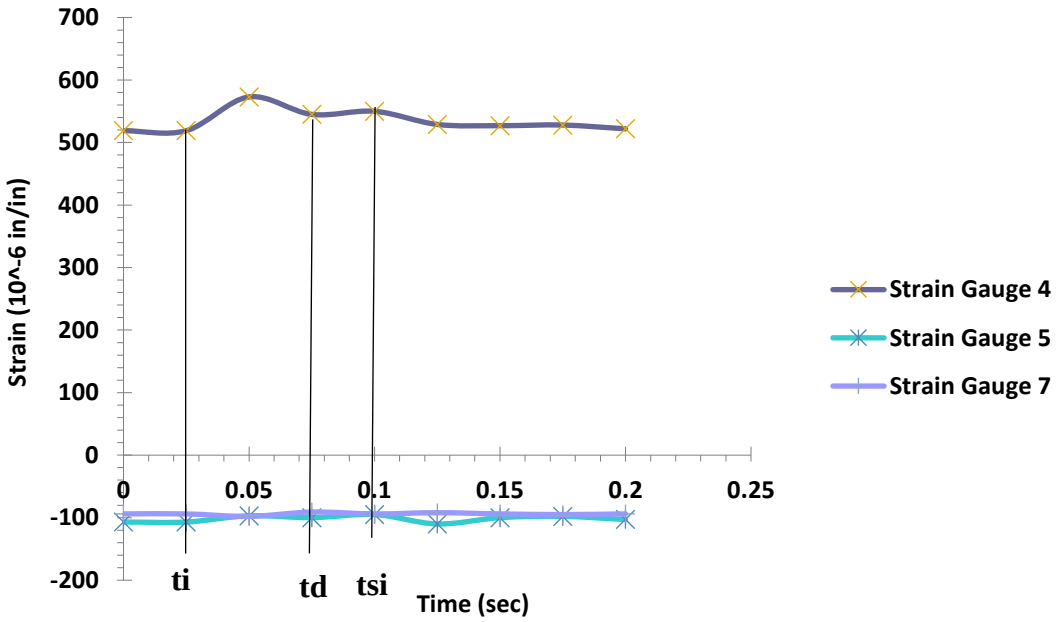

Figure 90. Experimental Strain-time Value for S-B 2 Test at 10 inches

Figure 91 represents the record of all strain gauges for the Specimen S-B 2 using the impactor 0.40 kips dropped at 7 inches height. Strain Gauge 2 was damaged in a previous test and does not record any additional data. Strain Gauge 2 had a reading of -0.0002 in/in from the previous test. During the impact a reading of -0.0005 in/in was recorded. The final reading of Strain Gauge 2 was -0.0003 in/in after the beam returned to rest. Strain Gauge 3 had a reading of -0.0009 in/in from previous test. During the impact a reading of -0.0009 in/in was recorded. The final reading of Strain Gauge 3 was -0.0009 in/in after the beam returned to rest. Strain Gauges four, five and six were damaged and do not record any data. Strain Gauge 7 had a reading of -0.0004 in/in from the previous test. During the impact a reading of 0.0048 in/in was recorded. This strain value exceeded the concrete strain of 0.0031 in/in also exceeded the steel reinforcement strain of

0.0232 at this location. After the impact the strain gauge does not record any additional data. This This test was recorded for 0.20 seconds and the impact occurred at 0.036 second. Beam failure occurred at 7 inches Strain Gauge 7 past the yield strain point of the concrete and past the yield strain point of the steel.

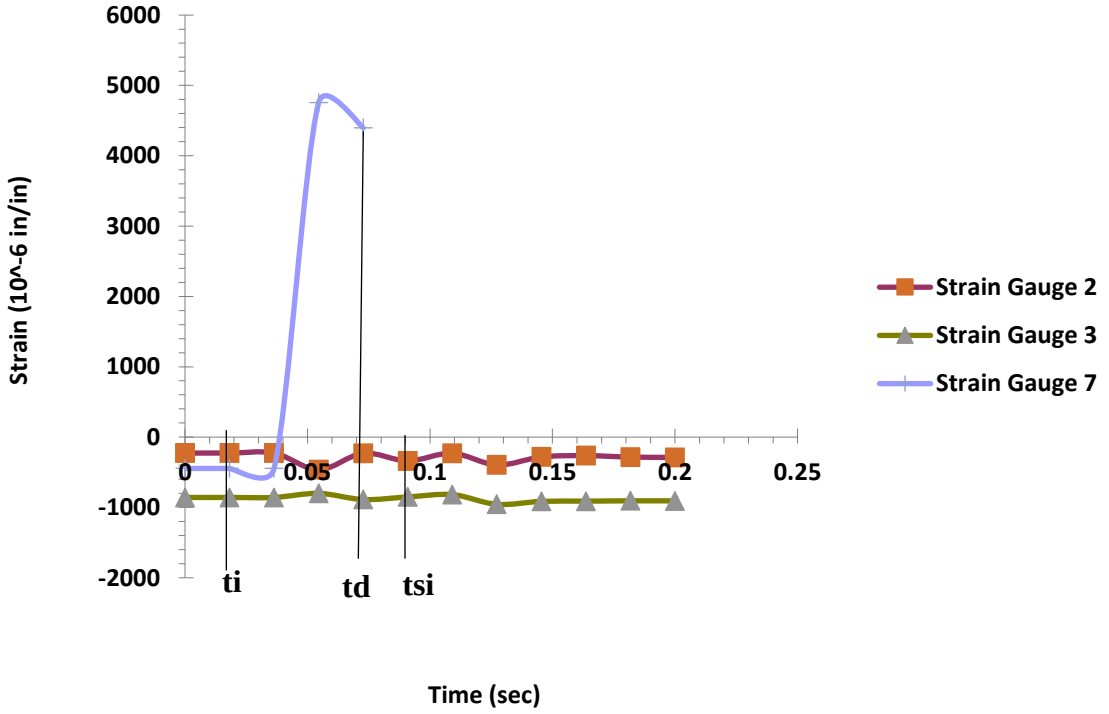

Figure 91. Experimental Strain-time Value for S-B 2 Test at 7 inches

Figures 92 and 93 represent the record of all strain gauges for the Specimen S-F 2 using the impactor #2 (0.14 kips) dropped at 10 inches height. Strain Gauge 1 had a reading of -0.0001 in/in from the previous test. During the impact a reading of -0.0005 in/in was recorded. The final reading of Strain Gauge 1 was -0.0002 in/in after the beam returned to rest. Strain Gauge 2 had a

reading of -0.0001 in/in from the previous test. During the impact a reading of -0.0002 in/in was recorded. The final reading of Strain Gauge 2 was -0.0001 in/in after the beam returned to rest. Strain Gauge 3 had a reading of -0.0000 in/in from the previous test. During the impact a reading of -0.0003 in/in was recorded. The final reading of Strain Gauge 3 was -0.00008 in/in after the beam returned to rest. Strain Gauge 4 had a reading of -0.0000 in/in from the previous test. During the impact a reading of -0.0000 in/in was recorded. The final reading of Strain Gauge 4 was -0.0000 in/in after the beam returned to rest. Strain Gauge 5 had a reading of -0.0000 in/in from the previous test. During the impact a reading of -0.0001 in/in was recorded. The final reading of Strain Gauge 5 was -0.0000 in/in after the beam returned to rest. Strain Gauge 6 had a reading of 0.0000 in/in from the previous test. During the impact a reading of 0.0000 in/in was recorded. The final reading of Strain Gauge 6 was 0.0000 in/in after the beam returned to rest. Strain Gauge 7 had a reading of 0.0001 in/in from the previous test. During the impact a reading of -0.0000 in/in was recorded. The final reading of Strain Gauge 7 was 0.0001 in/in after the beam returned to rest. This test was recorded for 0.20 seconds and the impact occurred at 0.019 second.

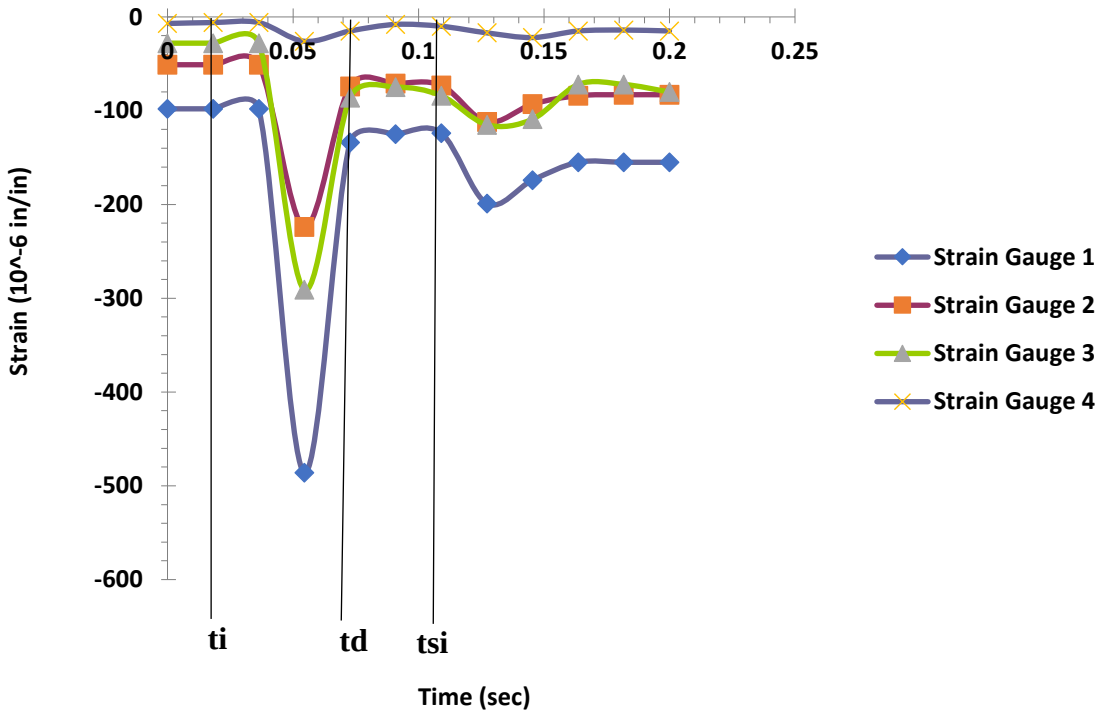

Figure 92. Experimental Strain-time Value for S-F 2 Test at 10 inches

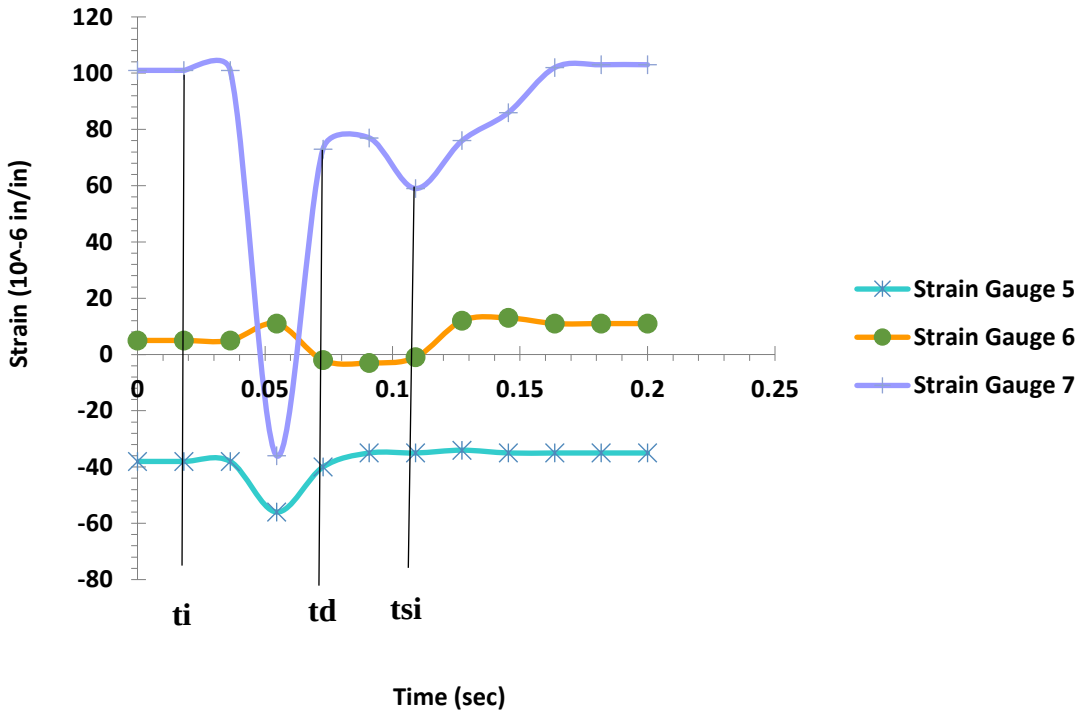

Figure 93. Experimental Strain-time Value for S-F 2 Test at 10 inches

Figures 94 and 95 represent the record of all strain gauges for the Specimen S-F 2 using the impactor #2 (0.14 kips) dropped at 21 inches height. A ¼ inch permanent deflection was recorded during this test this permanent deflection exceeded the L/360. Strain Gauge 1 had a reading of -0.0003 in/in from the previous test. During the impact a reading of -0.0008 in/in was recorded. The final reading of Strain Gauge 1 was -0.0003 in/in after the beam returned to rest. Strain Gauge 2 had a reading of -0.0001 in/in from the previous test. During the impact a reading of -0.0004 in/in was recorded. The final reading of Strain Gauge 2 was -0.0002 in/in after the beam returned to rest. Strain Gauge 3 had a reading of -0.0003 in/in from the previous test. During the impact a reading of -0.0007 in/in was recorded. The final reading of Strain Gauge 3 was -0.0003 in/in after the beam returned to rest. Strain Gauge 4 had a reading of -0.0000 in/in from the previous test. During the impact a reading of 0.0000 in/in was recorded. The final

reading of Strain Gauge 4 was 0.0000 in/in after the beam returned to rest. Strain Gauge 5 had a reading of 0.0000 in/in from the previous test. During the impact a reading of 0.0000 in/in was recorded. The final reading of Strain Gauge 5 was 0.0000 in/in after the beam returned to rest. Strain Gauge 6 had a reading of 0.0000 in/in from the previous test. During the impact a reading of 0.0000 in/in was recorded. The final reading of Strain Gauge 6 was 0.0000 in/in after the beam returned to rest. Strain Gauge 7 had a reading of -0.0001 in/in from the previous test. During the impact a reading of -0.0001 in/in was recorded. The final reading of Strain Gauge 7 was -0.0001 in/in after the beam returned to rest. This test was recorded for 0.20 seconds and the impact occurred at 0.017 seconds.

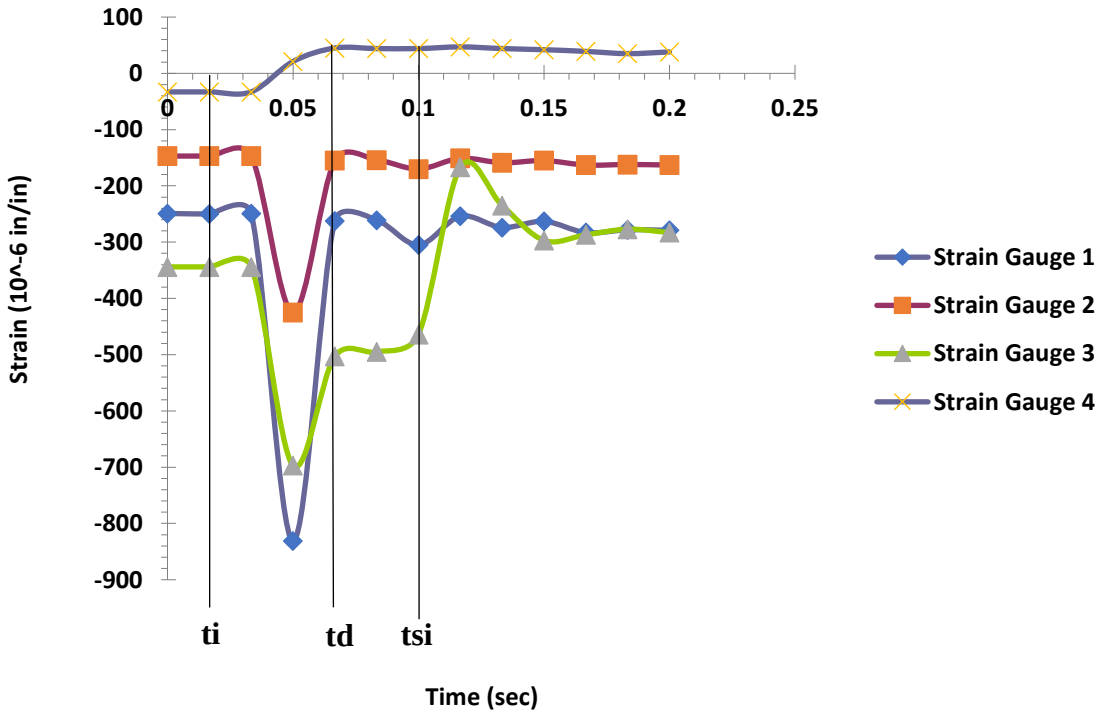

Figure 94. Experimental Strain-time Value for S-F 2 Test at 21 inches

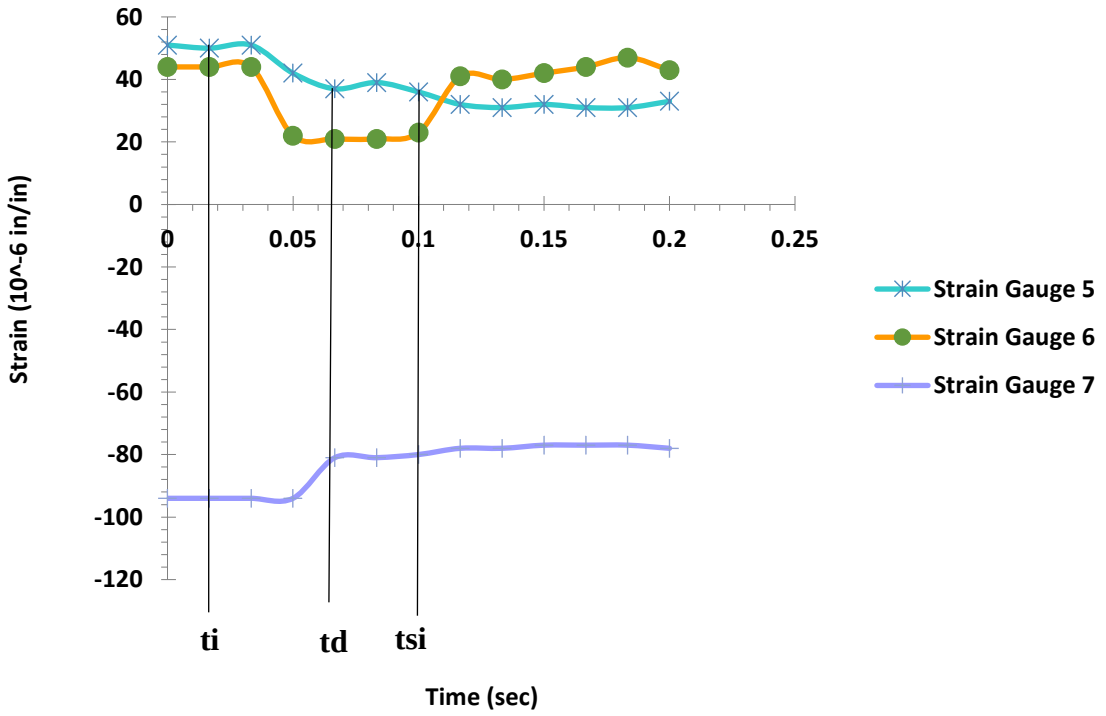

Figure 95. Experimental Strain-time Value for S-F 2 Test at 21 inches

Figures 95 and 96 represent the record of all strain gauges for Specimen B-B 2 using the impactor #2 (0.14 kips) dropped at 10 inches height. Strain Gauge 1 had a reading of -0.0001 in/in from the previous test. During the impact a reading of -0.0002 in/in was recorded. The final reading of Strain Gauge 1 was -0.0002 in/in after the beam returned to rest. Strain Gauge 2 had a reading of -0.0002 in/in from the previous test. During the impact a reading of -0.0002 in/in was recorded. The final reading of Strain Gauge 2 was -0.0002 in/in after the beam returned to rest. Strain Gauge 3 had a reading of 0.0001 in/in from the previous test. During the impact a reading of 0.0003 in/in was recorded. The final reading of Strain Gauge 3 was 0.0002 in/in after the beam returned to rest. Strain Gauge 4 was damaged in the previous test and does not record any data in this test. Strain Gauge 5e was damaged in the previous test and did not record any data in this test. Strain Gauge 6 had a reading of 0.0001 in/in from the previous test. During the impact a

reading of -0.0001 in/in was recorded. The final reading of Strain Gauge 6 was -0.0001 in/in after the beam returned to rest. Strain Gauge 7 had a reading of -0.0001 in/in from the previous test. During the impact a reading of -0.0001 in/in was recorded. The final reading of Strain Gauge 7 was -0.0001 in/in after the beam returned to rest. This test was recorded for 0.20 seconds and the impact occurred at 0.029 seconds.

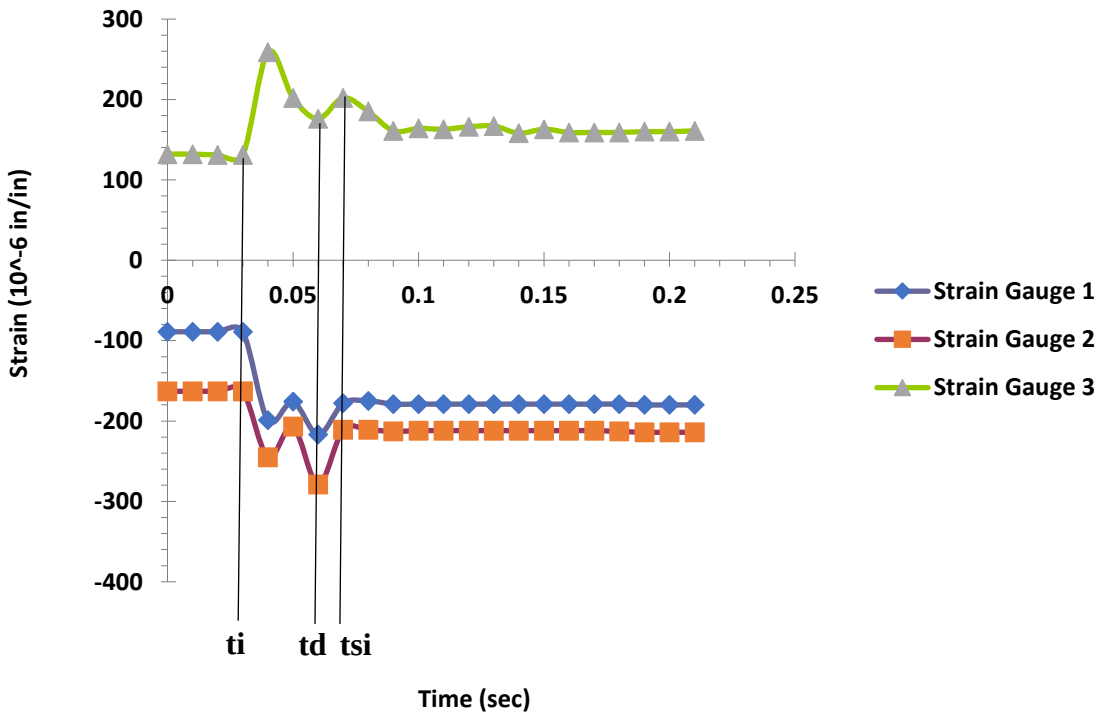

Figure 96. Experimental Strain-time Value for B-B 2 Test at 10 inches

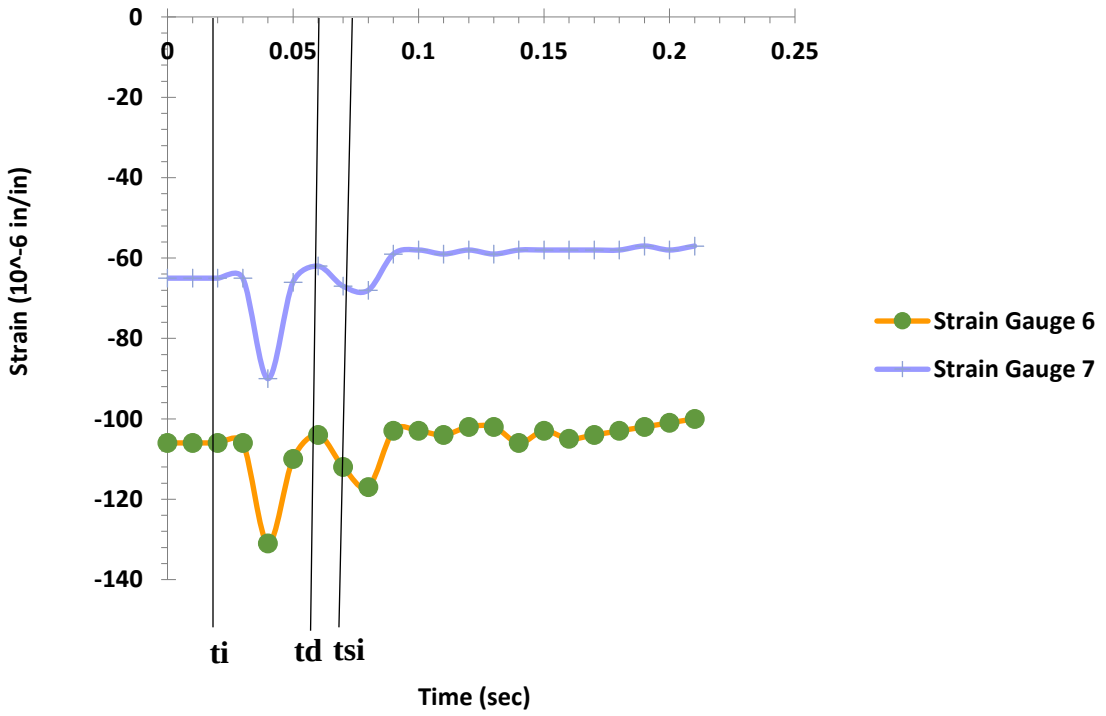

Figure 97. Experimental Strain-time Value for B-B 2 Test at 10 inches

Figures 98 and 99 represent the record of all strain gauges for Specimen B-B 2 using the impactor 0.14 kips dropped at 25 inches height. A ¼ inch permanent deflection was recorded during this test this permanent deflection exceeded the L/360. Strain Gauge 1 had a reading of -0.0004 in/in from the previous test. During the impact a reading of -0.0005 in/in was recorded. The final reading of Strain Gauge 1 was -0.0004 in/in after the beam returned to rest. Strain Gauge 2 had a reading of -0.0005 in/in from the previous test. During the impact a reading of -0.0006 in/in was recorded. The final reading of Strain Gauge 2 was -0.0005 in/in after the beam returned to rest. Strain Gauge 3 had a reading of 0.0004 in/in from the previous test. During the impact a reading of -0.0004 in/in was recorded. The final reading of Strain Gauge 3 was -0.0006 in/in after the beam returned to rest. Strain Gauge 4 was damaged in the previous test and did not record any data in this test. Strain Gauge 5 was damaged in the previous test and did not record

any data in this test. Strain Gauge 6 had a reading of 0.0001 in/in from the previous test. During the impact a reading of -0.0001 in/in was recorded. The final reading of Strain Gauge 6 was -0.0001 in/in after the beam returned to rest. Strain Gauge 7 had a reading of 0.0002 in/in from the previous test. During the impact a reading of -0.0002 in/in was recorded. The final reading of Strain Gauge 7 was -0.0002 in/in after the beam returned to rest. This test was recorded for 0.20 seconds and the impact occurred at 0.015 seconds.

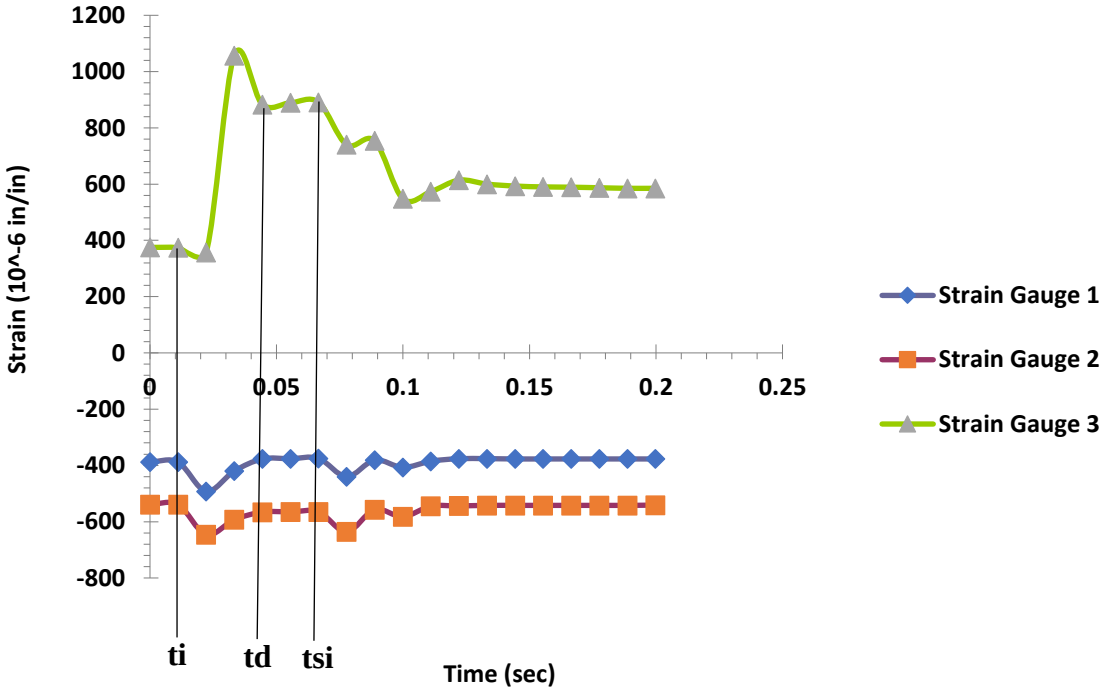

Figure 98. Experimental Strain-time Value for B-B 2 Test at 25 inches

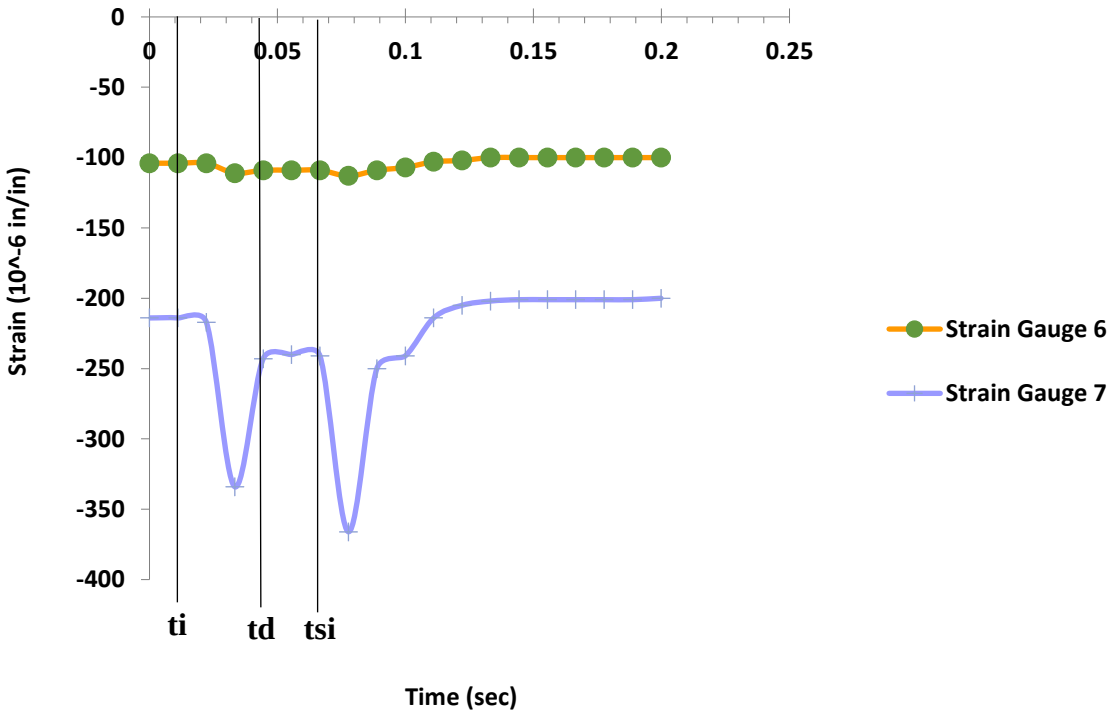

Figure 99. Experimental Strain-time Value for B-B 2 Test at 25 inches

Figures 100 and 101 represent the record of all strain gauges for the Specimen B-F 2 using the impactor #2 (0.14 kips) dropped at 10 inches height. Strain Gauge 2 had an original reading of -0.0011 in/in. During the impact a reading of -0.0011 in/in was recorded. The final reading of Strain Gauge 2 was -0.0011 in/in after the beam returned to rest. Strain Gauge 2 had an original reading of -0.0007 in/in. During the impact a reading of -0.0008 in/in was recorded. The final reading of Strain Gauge 2 was -0.0008 in/in after the beam returned to rest. Strain Gauge 3 had an original reading of -0.0009 in/in. During the impact a reading of -0.0008 in/in was recorded. The final reading of Strain Gauge 3 was -0.0009 in/in after the beam returned to rest. Strain Gauge 4 had an original reading of -0.0007 in/in. During the impact a reading of -0.0007 in/in was recorded. The final reading of Strain Gauge 4 was -0.0007 in/in after the beam returned to rest. Strain Gauge 5 had an original reading of -0.0027 in/in. This strain value exceeded the steel

reinforcement strain of 0.0232 in/in in this location. During the impact a reading of -0.0028 in/in was recorded. This strain value exceeded the steel reinforcement strain of 0.0232 in/in in this location. The final reading of Strain Gauge 5 was -0.0028 in/in after the beam returned to rest. This strain value exceeded the steel reinforcement strain of 0.0232 in/in in this location. Strain Gauge 6 had an original reading of -0.0008 in/in. During the impact a reading of -0.0008 in/in was recorded. The final reading of Strain Gauge 6 was -0.0008 in/in after the beam returned to rest Strain Gauge 7 had original reading of -0.0015 in/in. During the impact a reading of -0.0015 in/in was recorded. The final reading of Strain Gauge 7 was -0.00150 in/in after the beam returned to rest. This test was recorded for 0.20 seconds and the impact occurred at 0.015 seconds.

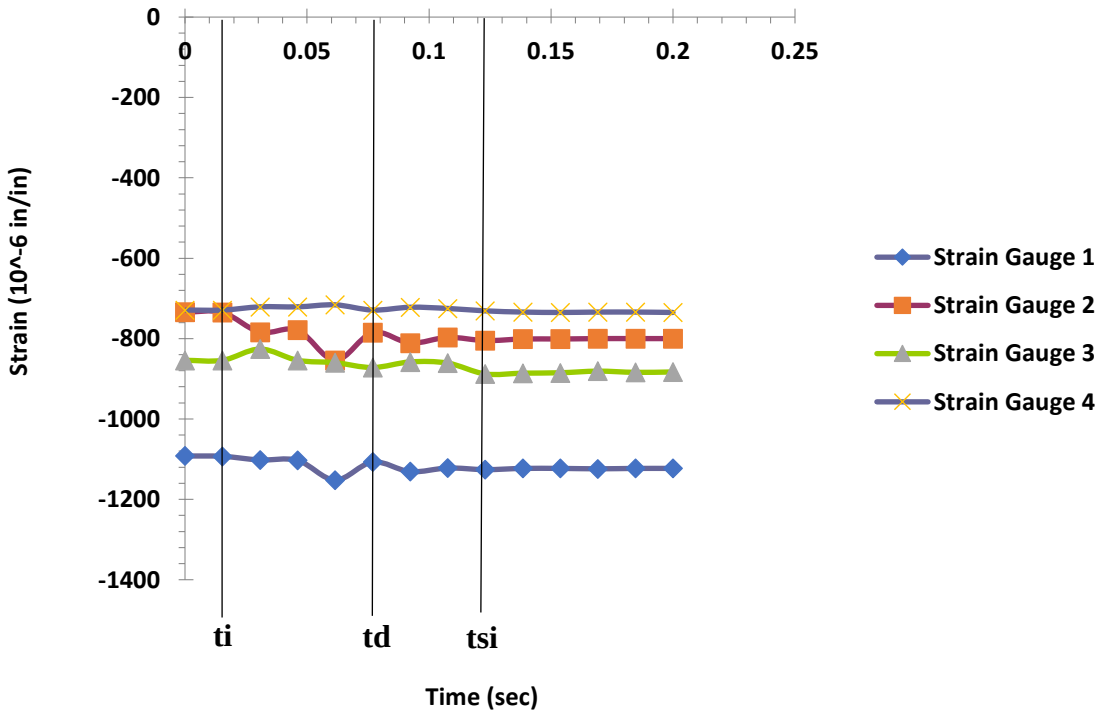

Figure 100. Experimental Strain-time Value for B-F 2 Test at 10 inches

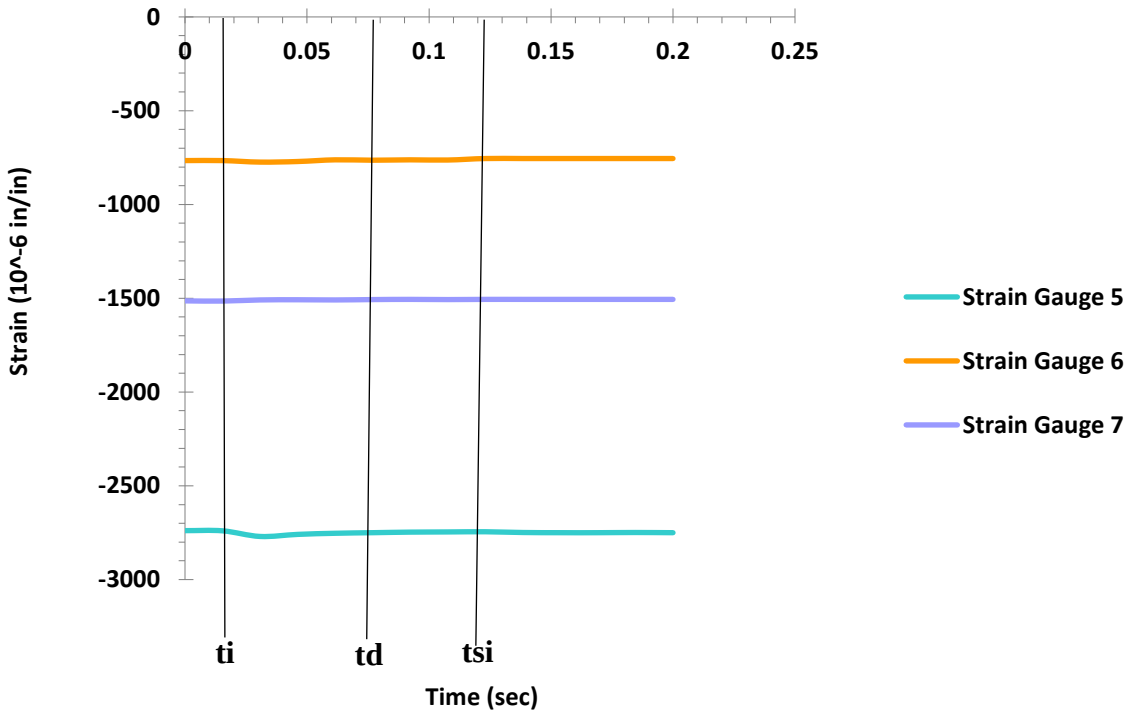

Figure 101. Experimental Strain-time Value for B-F 2 Test at 10 inches

Figures 102 and 103 represent the record of all strain gauges for Specimen B-F 2 using the impactor #3 (0.40 kips) dropped at 17 inches height. A ¼ inch permanent deflection was recorded during this test this permanent deflection exceeded the L/360. The concrete on the top part of the beam continued to crunch. Strain Gauge 1 had an original reading of -0.0008 in/in. During the impact a reading of -0.0015 in/in was recorded. The final reading of Strain Gauge 1 was -0.0007 in/in after the beam returned to rest. Strain Gauge 2 had an original reading of -0.0016 in/in. During the impact a reading of -0.0026 in/in was recorded. The final reading of Strain Gauge 2 was -0.0011 in/in after the beam returned to rest. Strain Gauge 4 had an original reading of -0.0008 in/in. During the impact a reading of -0.0011 in/in was recorded. The final reading of Strain Gauge 4 was -0.0010 in/in after the beam returned to rest. Strain Gauge 5 had an original reading of -0.0033 in/in. This strain value exceeded the concrete strain of 0.0031 in/in and the steel of 0.0021 in/in in this location. During the impact a reading of -0.0033 in/in was

recorded. This strain value exceeded the concrete strain of 0.0031 in/in and the steel of 0.0021 in/in in this location. The final reading of Strain Gauge 5 was -0.0033 in/in after the beam returned to rest. This strain value exceeded the concrete strain of 0.0031 in/in and the steel of 0.0021 in/in in this location. This test was recorded for 0.20 seconds and the impact occurred at 0.012 seconds.

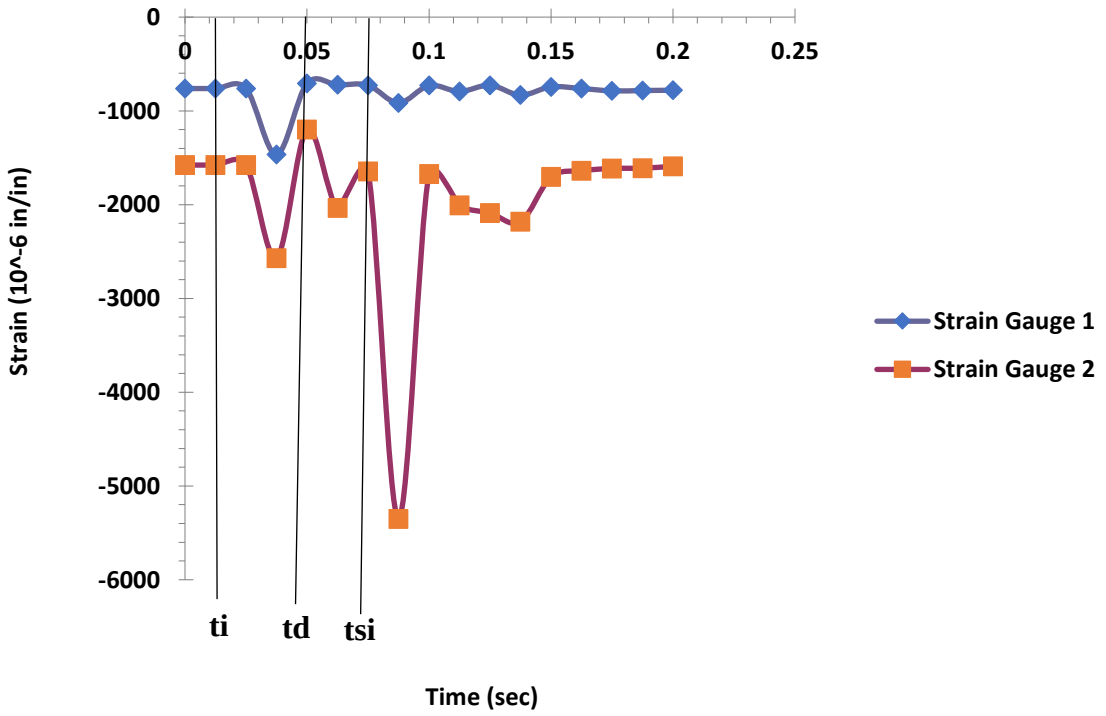

Figure 102. Experimental Strain-time Value for B-F 2 Test at 17 inches

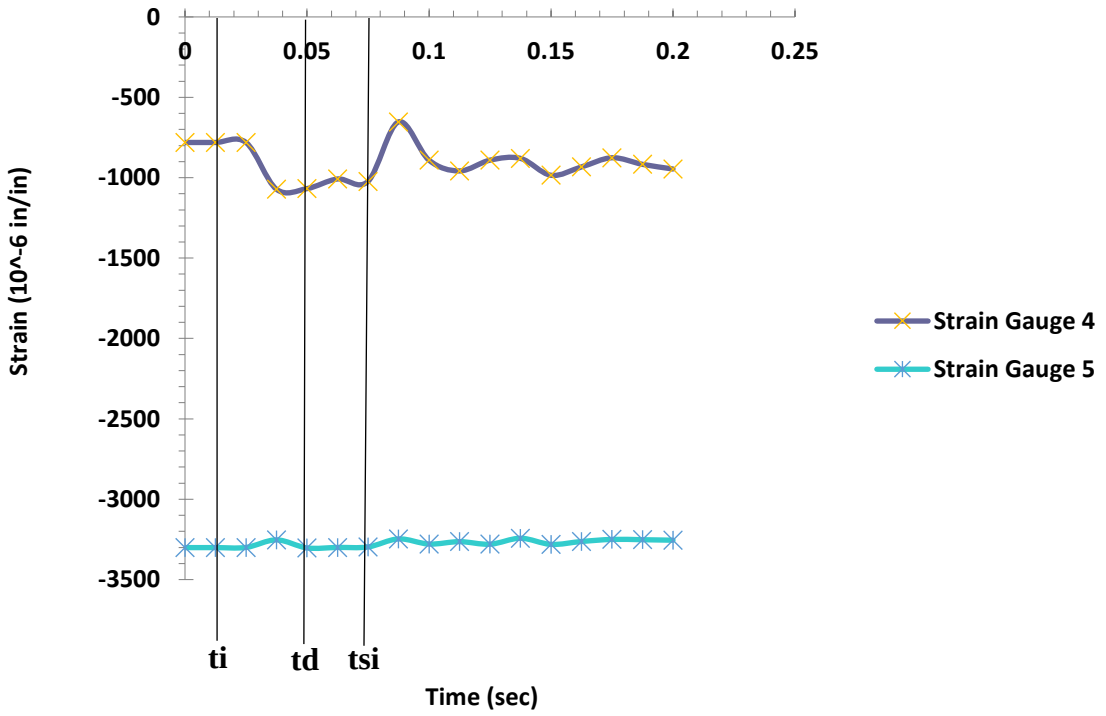

Figure 103. Experimental Strain-time Value for B-F 2 Test at 17 inches

2.5.9 Impact Load Beam Acceleration Responses Results

Acceleration of each beam was recorded at each drop the acceleration of the impactor and the beam was recorded at each test. The only results provided in this section were using the impactor of 0.14 kips at 10-inch drops for all specimens in representation of a real building collapsing and the drop for each beam at failure.

Figure 104 represents the maximum and minimum acceleration recorded for Specimen S-2 at the impact load of 0.14 kips at 10 inches height. The maximum positive acceleration recorded for the impactor was 0.27 g's at 0.02 second and the maximum negative acceleration was 0.31 g's at 0.0022 second. Figure 106 represents the maximum positive acceleration for the beam was 0.16

g's at 0.0043 seconds and the maximum negative acceleration was 0.14 g's at 0.0195 seconds. The beam acceleration at the maximum impactor acceleration was 0.02 g's at 0.0022 seconds. The time t_i was 0.001 seconds, t_d was 0.007 seconds, and t_{si} was 0.193 seconds.

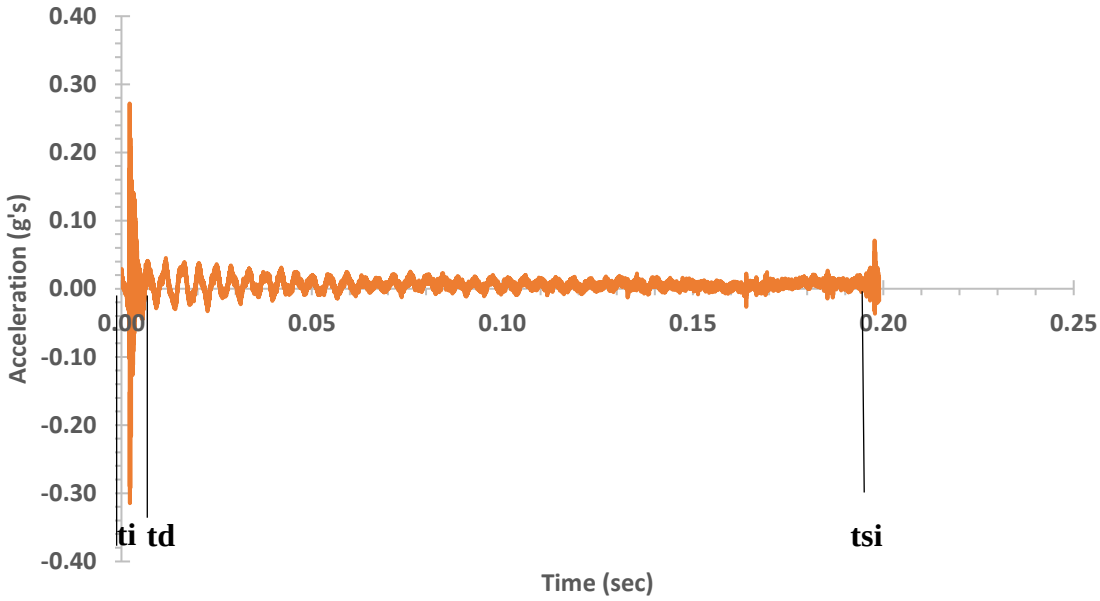

Figure 104. Represents the Impactor Acceleration on Specimen S-2 at 10 inches

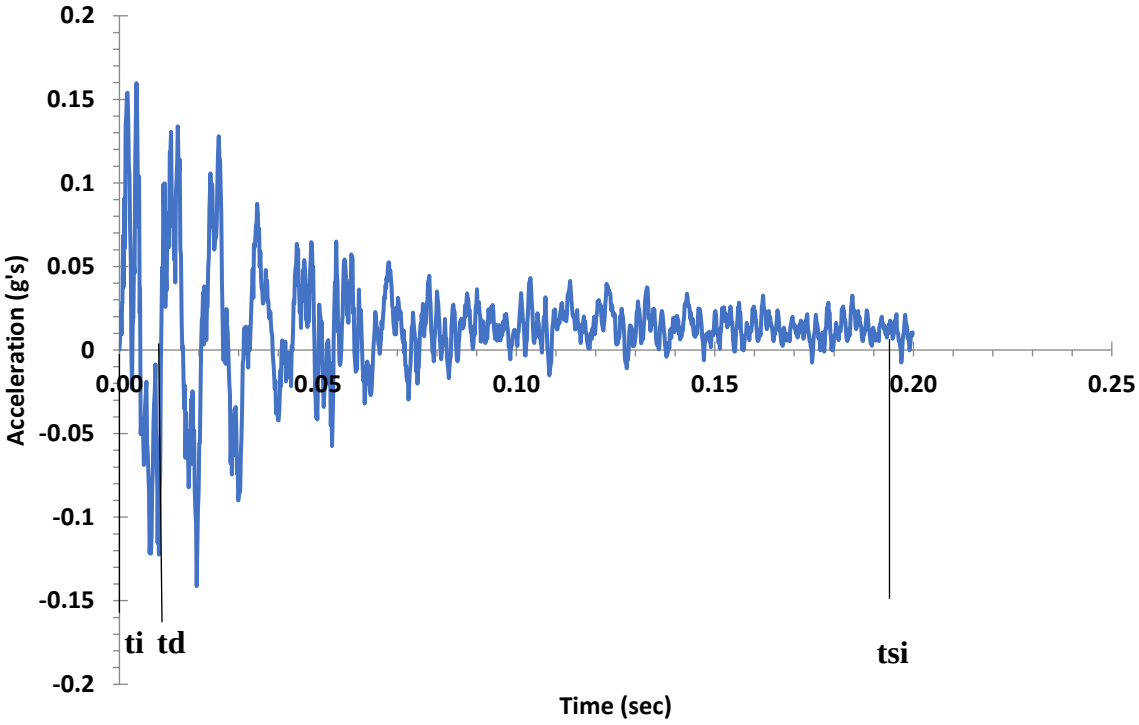

Figure 105. Beam Acceleration on Specimen S-2 at 10 inches

Figure 106 represents the maximum and minimum acceleration recorded for Specimen S-2 at the impact load of 0.14 kips at 21 inches height. The maximum positive acceleration recorded for the impactor was 1.37 g's at 0.0020 second and the maximum negative acceleration was 0.27 g's at 0.0048 seconds. Figure 108 represents the maximum positive acceleration for the beam was 1.5 g's at 0.0594 second and the maximum negative acceleration was 0.38 g's at 0.0738 seconds. The beam acceleration at the maximum impactor acceleration was negative 0.12 g's at 0.0020 seconds. The time t_i was 0.0013 seconds, t_d was 0.0143 second, and t_{si} was 0.1985 seconds.

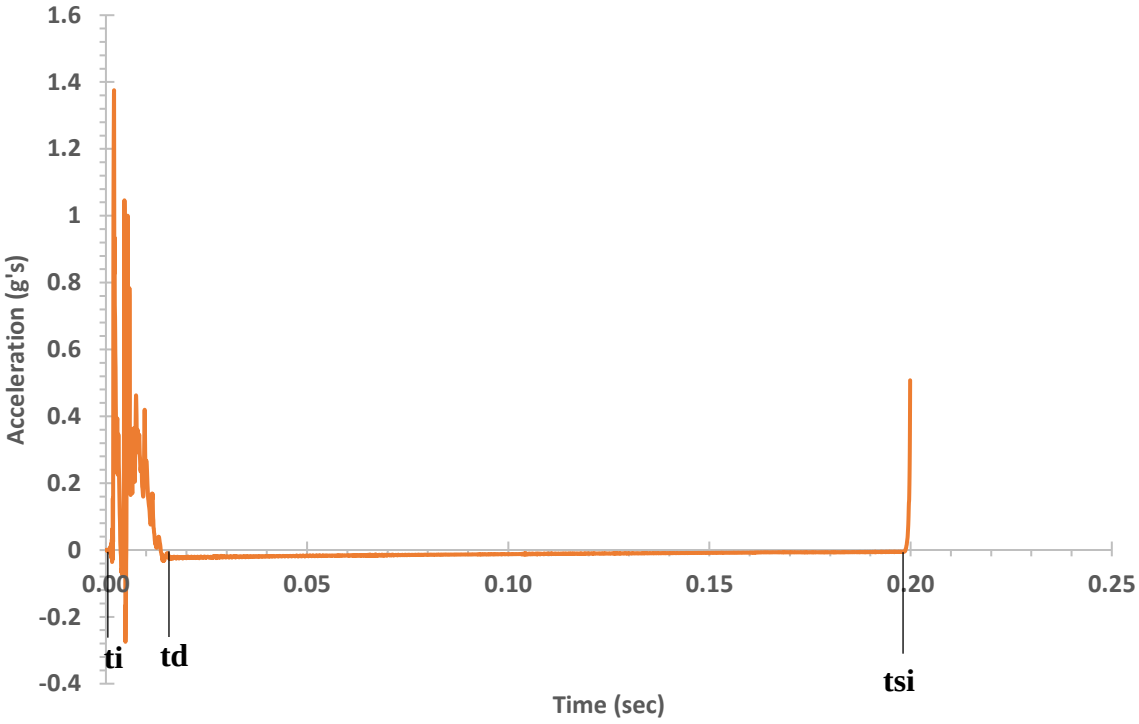

Figure 106. The Impactor Acceleration on Specimen S-2 at 21 inches

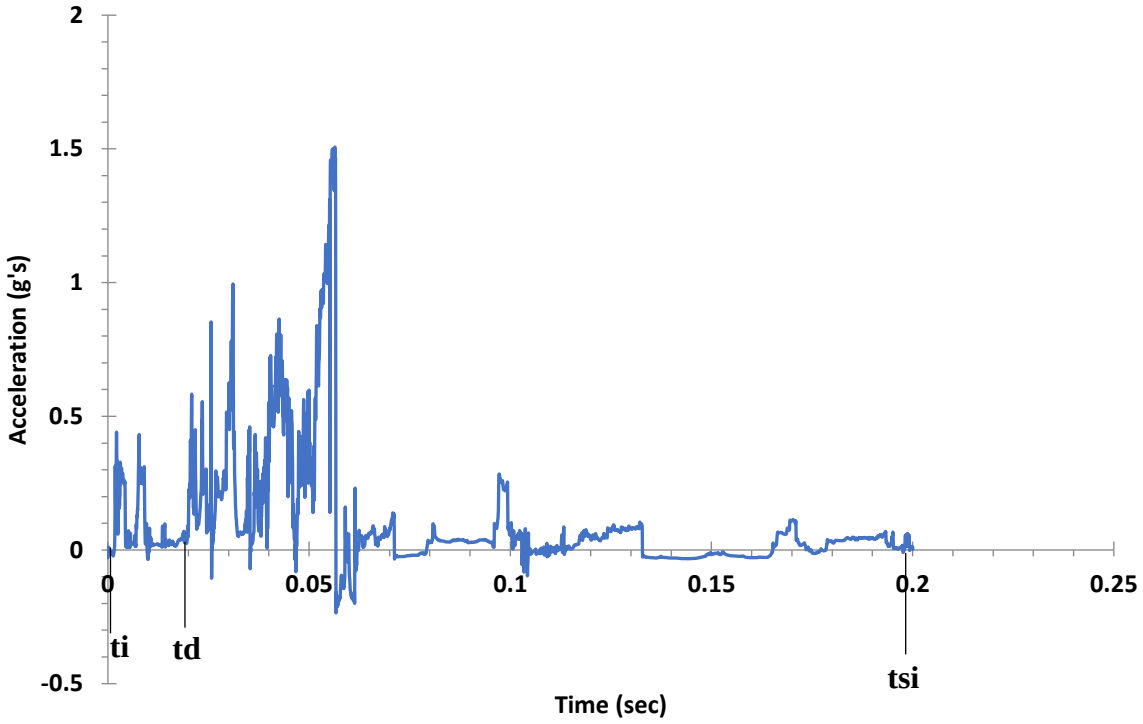

Figure 107. The Beam Acceleration on Specimen S-2 at 21 inches

Figure 108 represents the maximum and minimum acceleration recorded for Specimen S-B at the impact load of 0.14 kips at 10 inches height. The maximum positive acceleration recorded for the impactor was 1.17 g's at 0.0018 seconds and the maximum negative acceleration was the 0.06 g's at 0.0032 seconds. Figure 109 represents the maximum positive acceleration for the beam was 0.27 g's at 0.0287 seconds and the maximum negative acceleration was 0.35 g's at 0.0152 seconds. The beam acceleration at the maximum impactor acceleration was 0.00 g's at 0.0018 seconds. The time t_i was 0.0001 seconds, t_d was 0.0121 seconds, and t_{si} was 0.1928 seconds.

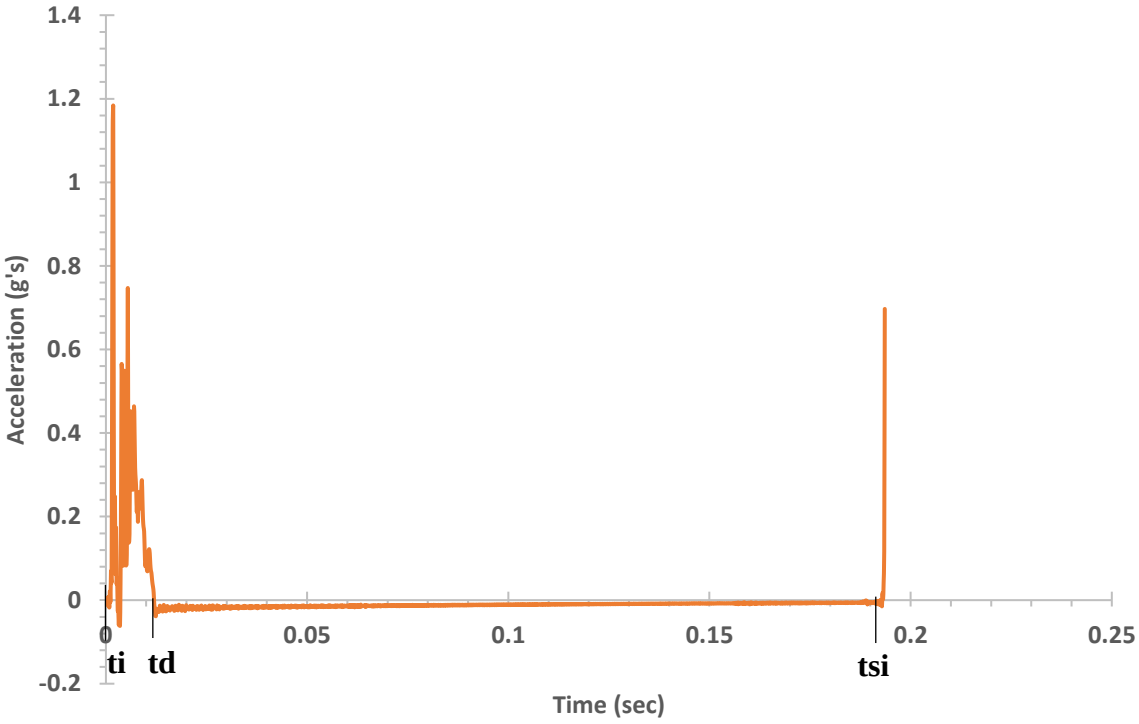

Figure 108. The Impactor Acceleration on Specimen S-B at 10 inches

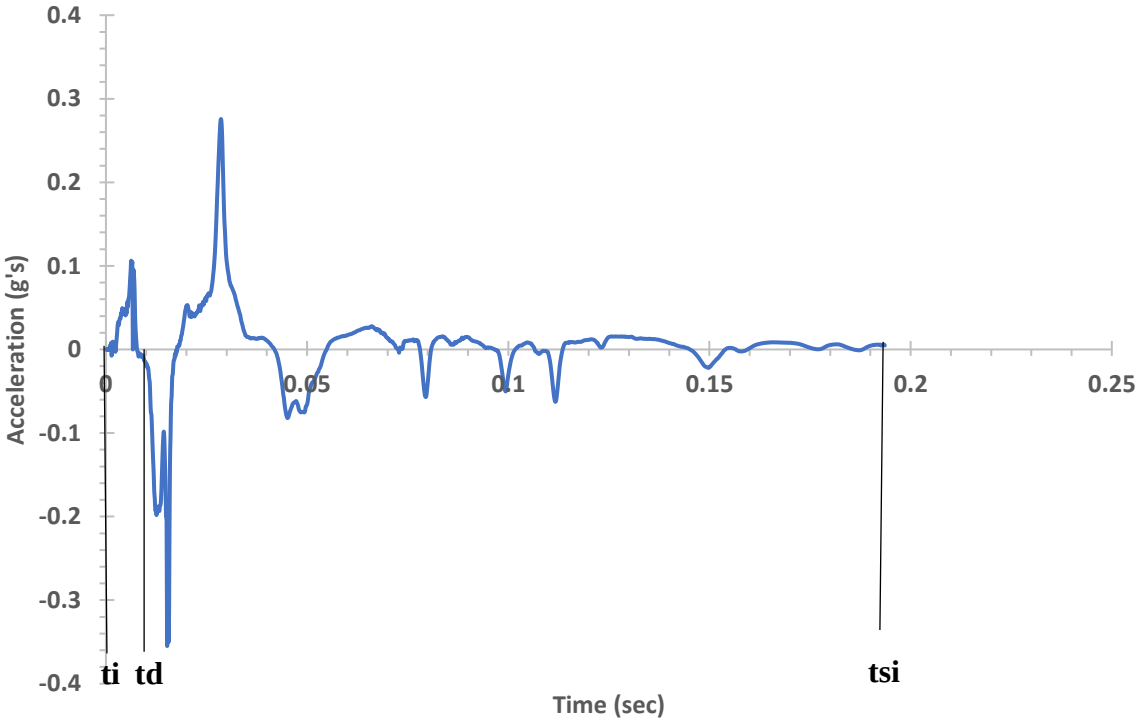

Figure 109. The Beam Acceleration on Specimen S-B at 10 inches

Figure 110 represents the maximum and minimum acceleration recorded for Specimen S-B at the impact load of 0.40 kips at 7 inches height. The maximum positive acceleration recorded for the impactor was 3.79 g's at 0.0138 seconds and the maximum negative acceleration was the 3.23 g's at 0.0134 seconds. Figure 112 represents the maximum positive acceleration for the beam was 4.2 g's at 0.0117 seconds and the maximum negative acceleration was 4.5 g's at 0.0231 seconds. The beam acceleration at the maximum impactor acceleration was 1.2 g's at 0.0138 seconds. The time t_i was 0.001 seconds, t_d was 0.04 seconds, and t_{si} was 0.198 seconds.

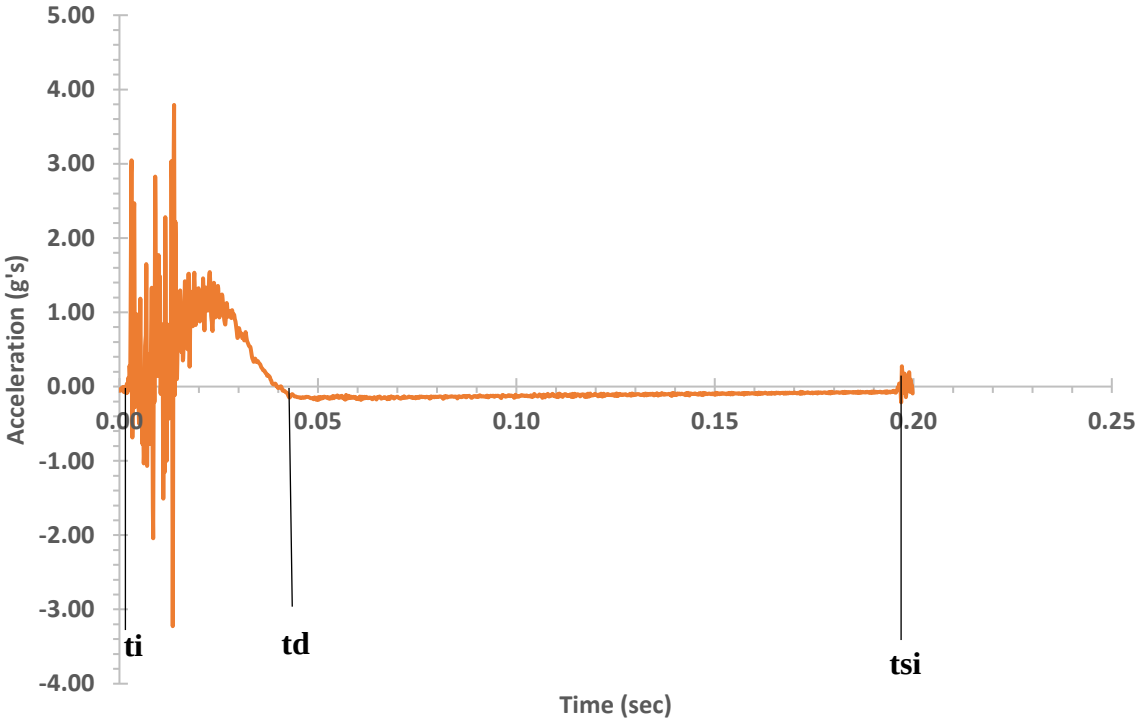

Figure 110. The Impactor Acceleration on Specimen S-B at 7 inches

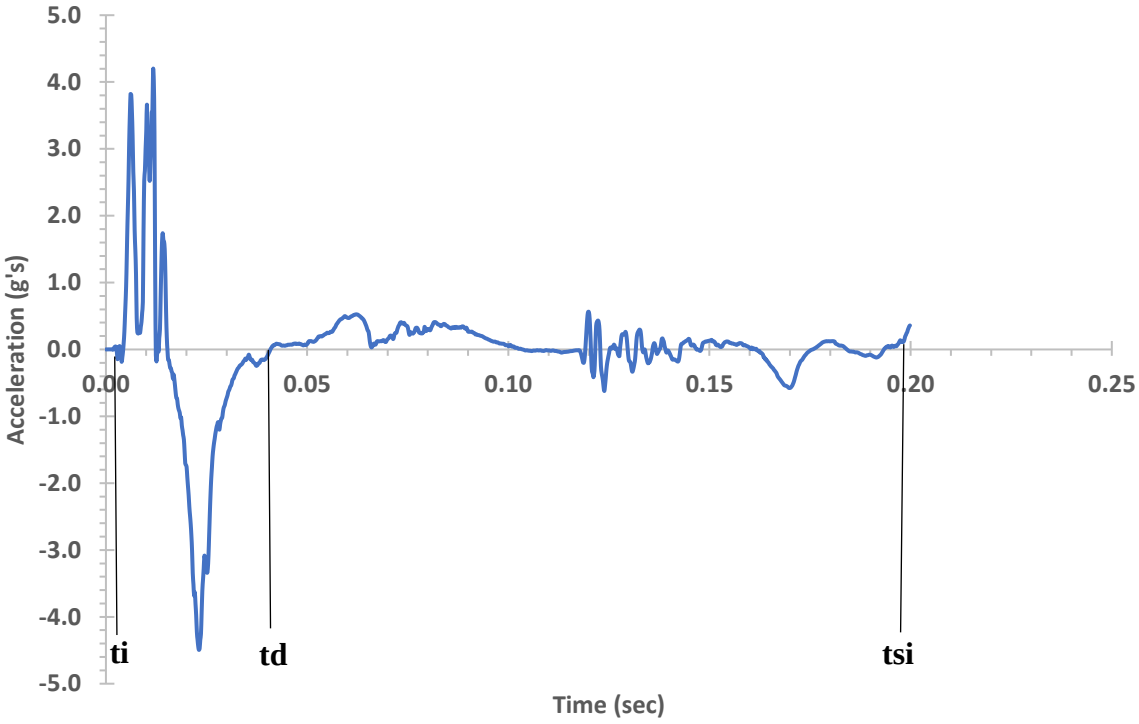

Figure 111. The Beam Acceleration on Specimen S-B at 7 inches

Figure 112 represents the maximum and minimum acceleration recorded for Specimen S-F at the impact load of 0.14 kips at 10 inches height. The maximum positive acceleration recorded for the impactor was 1.62 g's at 0.0073 seconds and the maximum negative acceleration was the 0.43 g's at 0.0030 seconds. Figure 113 represents the maximum positive acceleration for the beam was 0.12 g's at 0.0078 seconds and the maximum negative acceleration was 0.01 g's at 0.088 second. The beam acceleration at the maximum impactor acceleration was 0.01 g's at 0.0073 second. The time t_i was 0.0001 second, t_d was 0.0149 seconds, and t_{si} was 0.1935 seconds.

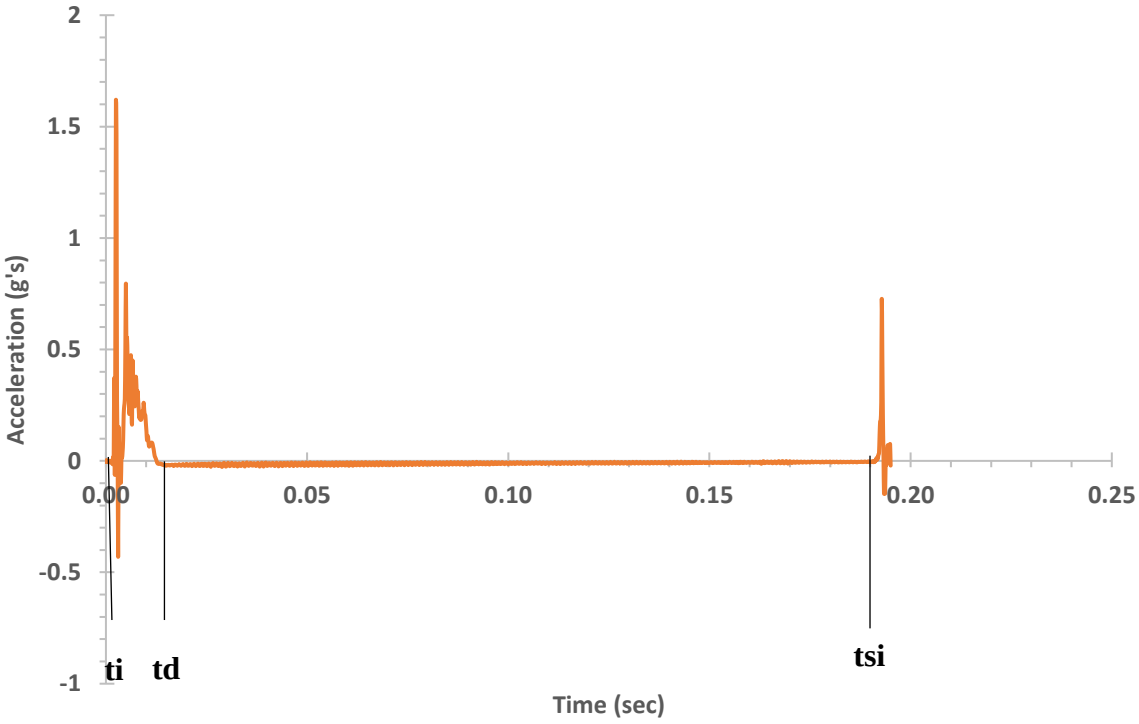

Figure 112. The Impactor Acceleration on Specimen S-F at 10 inches

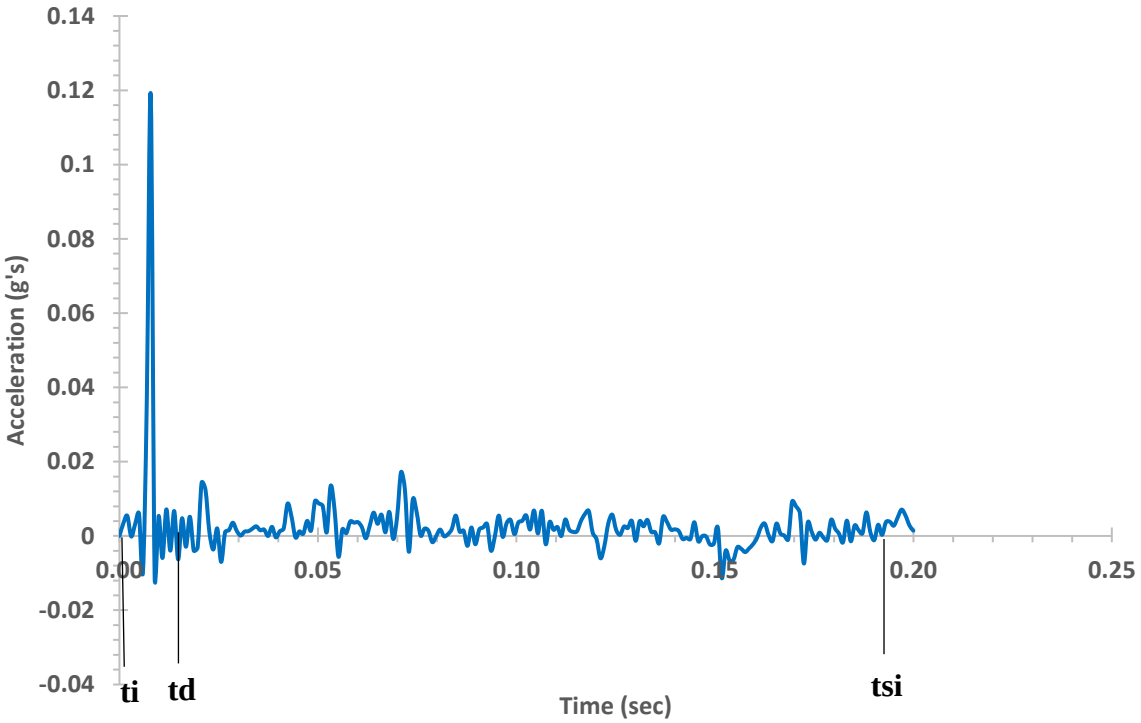

Figure 113. The Beam Acceleration on Specimen S-F at 10 inches

Figure 114 represents the maximum and minimum acceleration recorded for Specimen S-F at the impact load of 0.14 kips at 21 inches height. The maximum positive acceleration recorded for the impactor was 50.34 g's at 0.0215 seconds and the maximum negative acceleration was the 1.71 g's at 0.02945 seconds. Figure 116 represents the maximum positive acceleration for the beam was 9.72 g's at 0.0395 seconds and the maximum negative acceleration was 10.39 g's at 0.08192 seconds. The beam acceleration at the maximum impactor acceleration was 0.83 g's at 0.0215 seconds. The time t_i was 0.0167 seconds, t_d was 0.0829 second, and t_{si} was 0.1012 seconds.

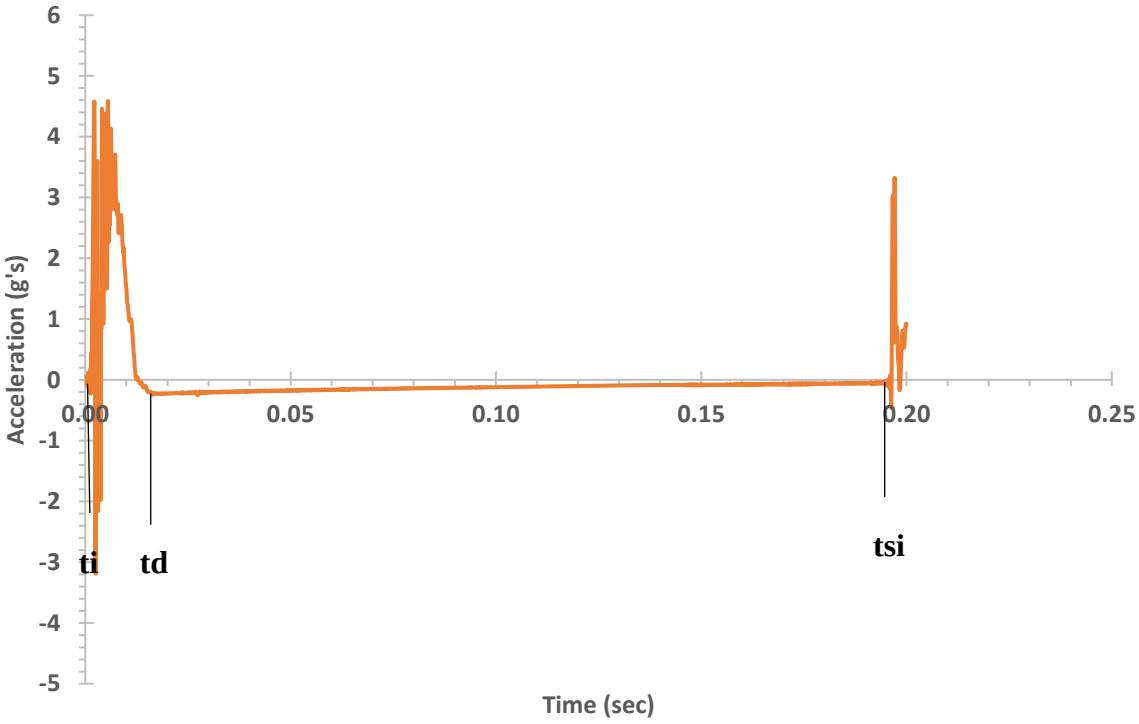

Figure 114. The Impactor Acceleration on Specimen S-F at 21 inches

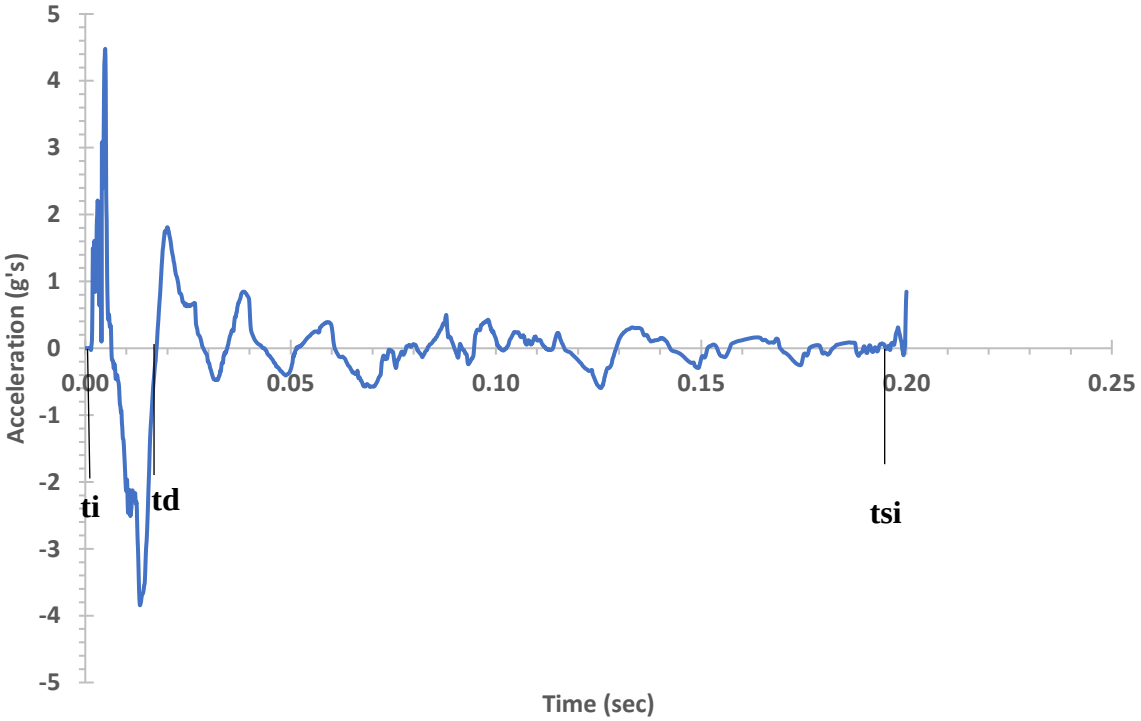

Figure 115. The Beam Acceleration on Specimen S-F at 21 inches

Figure 116 represents the maximum and minimum acceleration recorded for Specimen B-B at the impact load of 0.14 kips at 10 inches height. The maximum positive acceleration recorded for the impactor was 1.31 g's at 0.0031 seconds and the maximum negative acceleration was the 0.19 g's at 0.0069 seconds. Figure 118 represents the maximum positive acceleration for the beam was 0.17 g's at 0.0015 seconds and the maximum negative acceleration was 0.15 g's at 0.0109 seconds. The beam acceleration at the maximum impactor acceleration was 0.00 g's at 0.0031 seconds. The time t_i was 0.0021 second, t_d was 0.0215 seconds, and t_{si} was 0.1938 seconds.

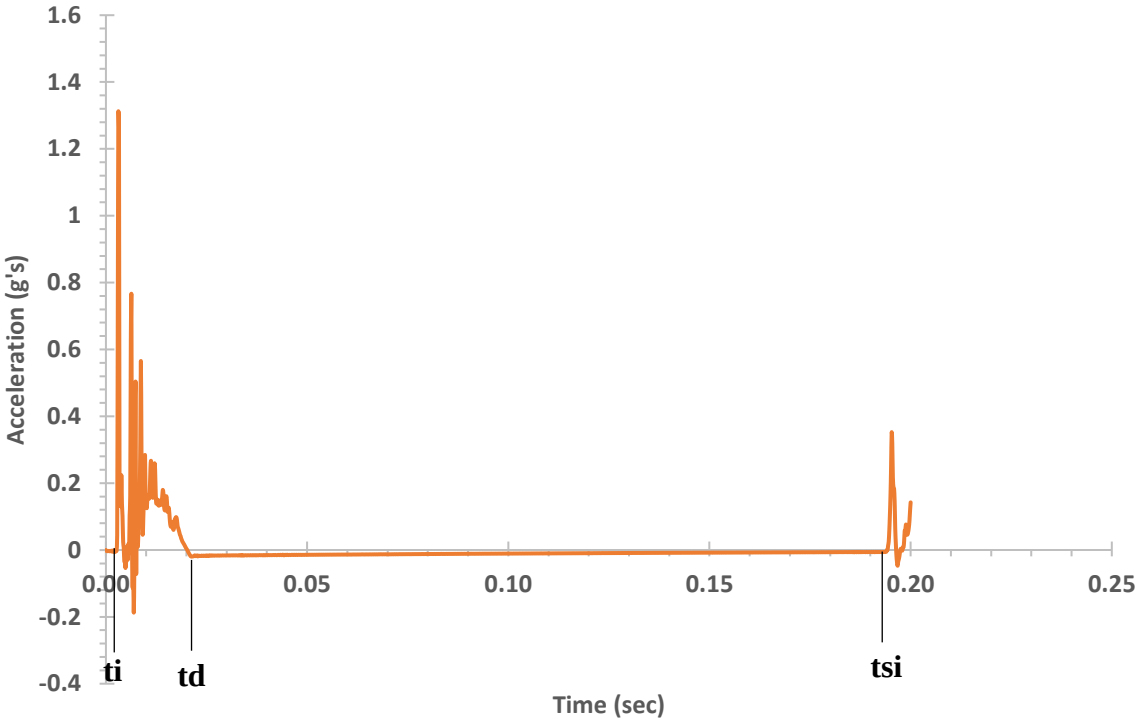

Figure 116. The Impactor Acceleration on Specimen B-B at 10 inches

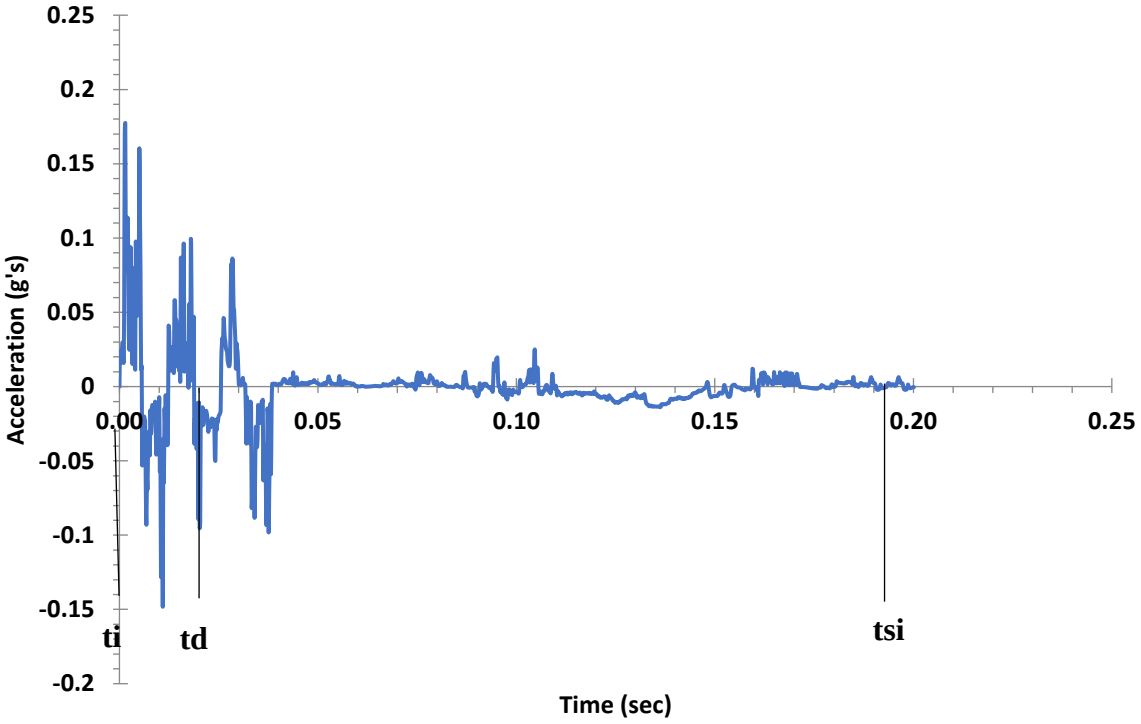

Figure 117. The Beam Acceleration on Specimen B-B at 10 inches

Figure 118 represents the maximum and minimum acceleration recorded for Specimen B-B at the impact load of 0.14 kips at 25 inches height. The maximum positive acceleration recorded for the impactor was 3.26 g's at 0.0026 second and the maximum negative acceleration was the 0.95 g's at 0.0033 seconds. Figure 120 shows the maximum positive acceleration for the beam was 0.38 g's at 0.0028 seconds and the maximum negative acceleration was 0.03 g's at 0.0032 seconds. The beam acceleration at the maximum impactor acceleration was 0.0014 g's at 0.0026 seconds. The time t_i was 0.0015 seconds, t_d was 0.0157 seconds, and t_{si} was 0.1963 seconds.

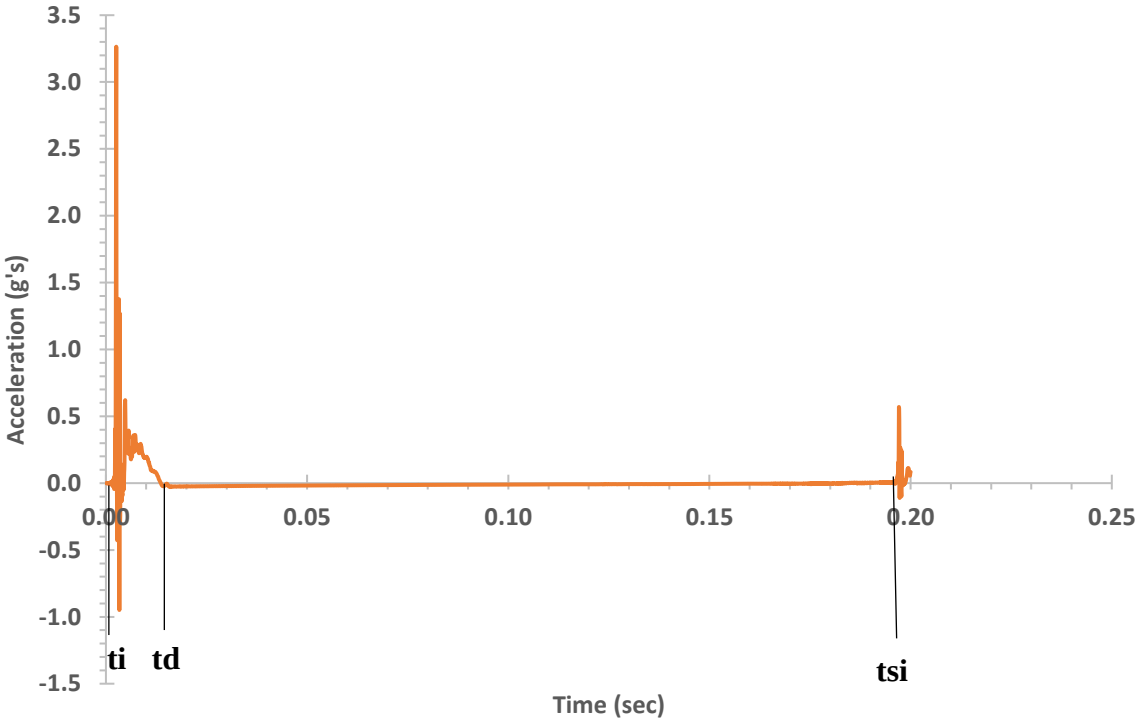

Figure 118. The Impactor Acceleration on Specimen B-B at 25 inches

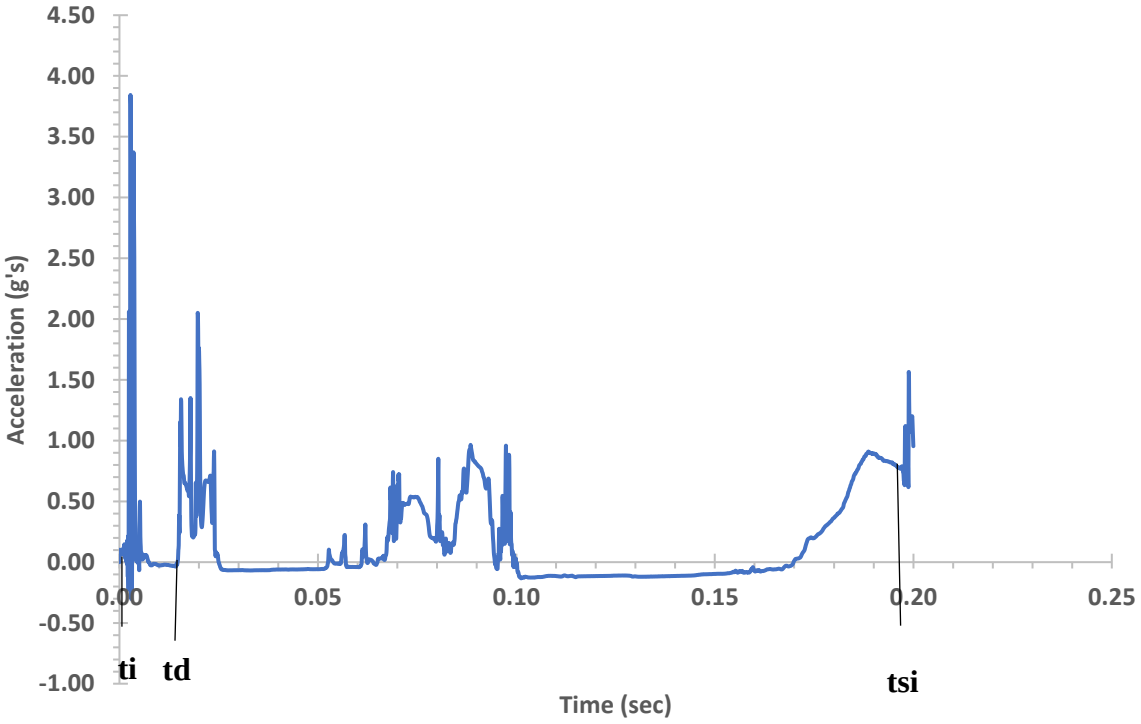

Figure 119. The Beam Acceleration on Specimen B-B at 25 inches

Figure 120 represents the maximum and minimum acceleration recorded for Specimen B-F at the impact load of 0.14 kips at 10 inches height. The maximum positive acceleration recorded for the impactor was 1.50 g's at 0.0064 second and the maximum negative acceleration was the 0.28 g's at 0.0011 seconds. Figure 122 represents the maximum positive acceleration for the beam was 0.26 g's at 0.1613 seconds and the maximum negative acceleration was 0.60 g's at 0.0903 seconds. The beam acceleration at the maximum impactor acceleration was 0.02 g's at 0.0064 seconds. The time t_i was 0.0032 seconds, t_d was 0.0910 seconds, and t_{si} was 0.20 seconds.

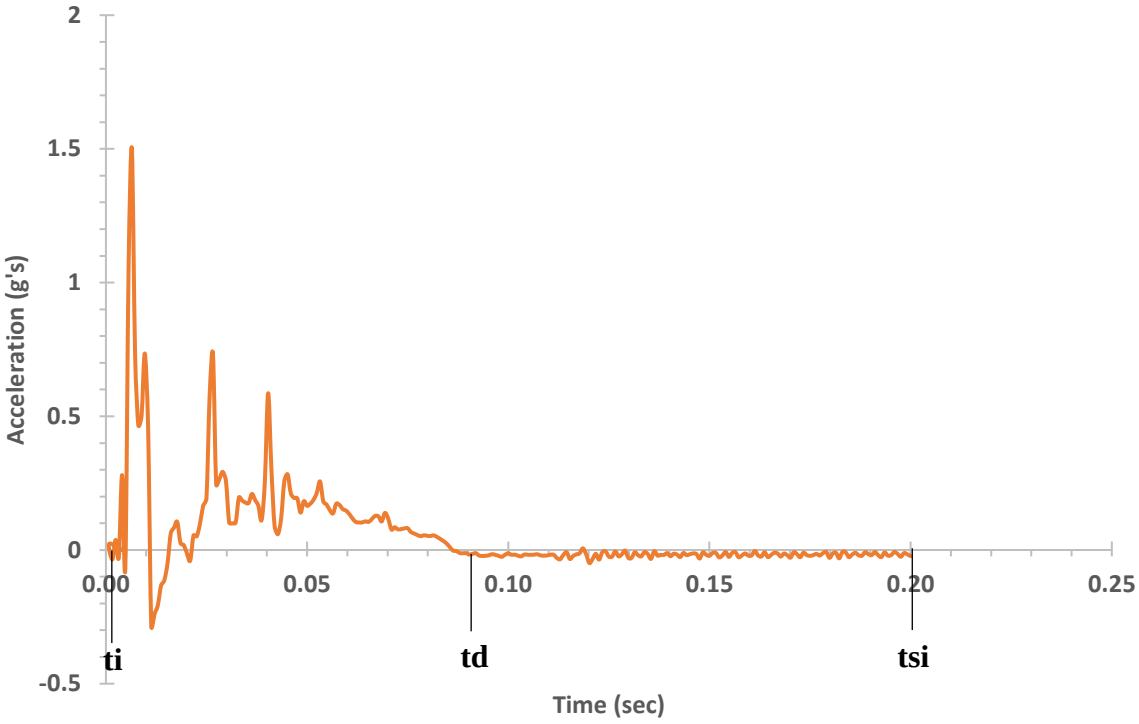

Figure 120. The Impactor Acceleration on Specimen B-F at 10 inches

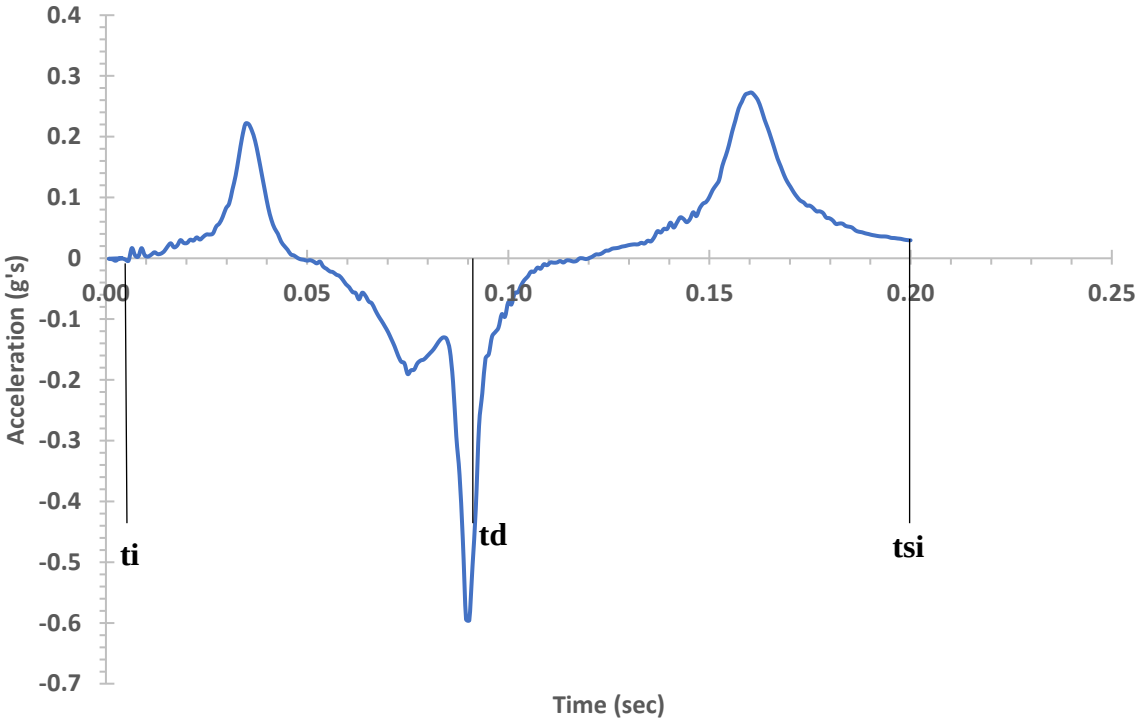

Figure 121. The Beam Acceleration on Specimen B-F at 10 inches

Figure 122 represents the maximum and minimum acceleration recorded for Specimen B-F at the impact load of 0.40 kips at 17 inches height. The maximum positive acceleration recorded for the impactor was 10.32 g's at 0.0010 seconds and the maximum negative acceleration was the 7.72 g's at 0.0030 seconds. Figure 124 represents the maximum positive acceleration for the beam was 8.36 g's at 0.0012 seconds and the maximum negative acceleration was 5.77 g's at 0.0115 seconds. The beam acceleration at the maximum impactor acceleration was 0.66 g's at 0.0002 seconds. The time t_i was 0.0004 seconds, t_d was 0.0443 seconds, and t_{si} was 0.1982 seconds.

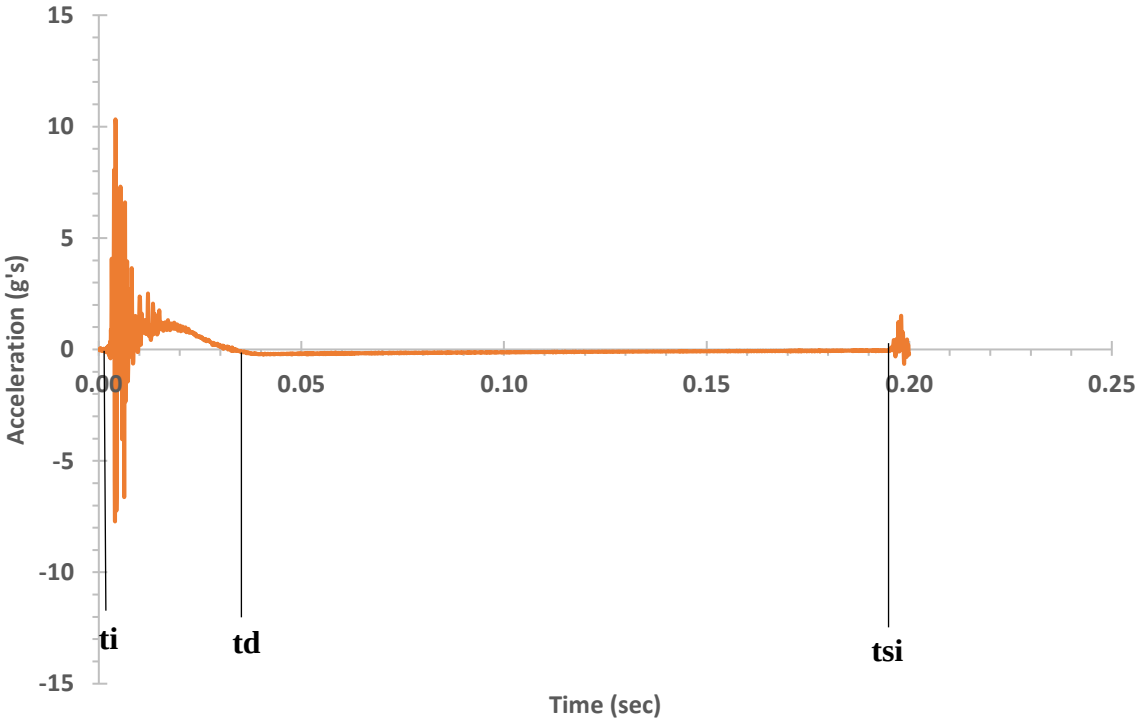

Figure 122. The Impactor Acceleration on Specimen B-F at 17 inches

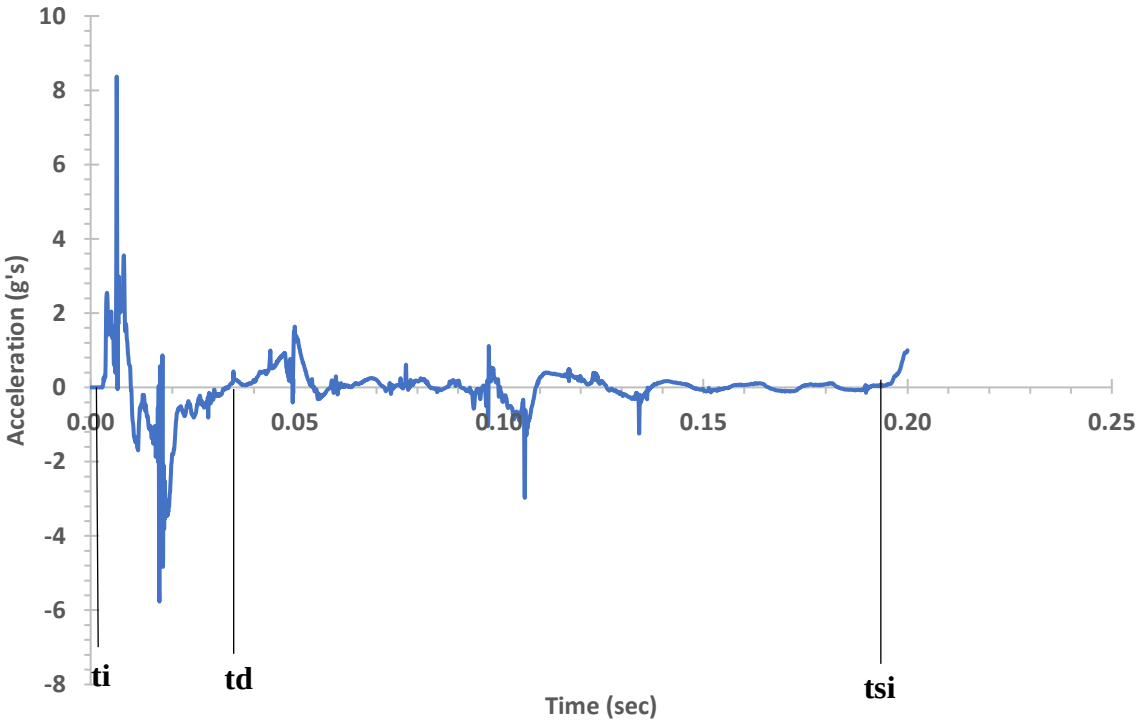

Figure 123. The Beam Acceleration on Specimen B-F at 17 inches

2.6 Test Results for the Sub-assemblage Specimens

A total of four sub-assemblage specimens were tested under quasi-static load until the specimen failed: two with regular steel as a main reinforcement (4-# 3 reinforcement) and two with BFRP reinforcement as a main reinforcement (6-8mm reinforcement). During the sub-assemblage testing the deflection information, load increments, maximum load at collapse, and rotation on both fixed support at each increment load was recorded.

2.6.1 Strains Gauge Locations for the Sub-assemblage Tests

A total of sixteen strain gauges were mounted on the specimen to measure the strains in four different areas of the beam as shown in Figure 124. Four were set up at the edges of the beam

and column line on each beam and the same distribution was set up in the real side of the beams. The strain gauges were located a 1-1/8 inches from the top and bottom of the beam and ½ inches from the column line inside of the beam. This measure is the center of the reinforcement in the top and bottom of the beam. Strain readings were recorded for each load increment applied to the beam.

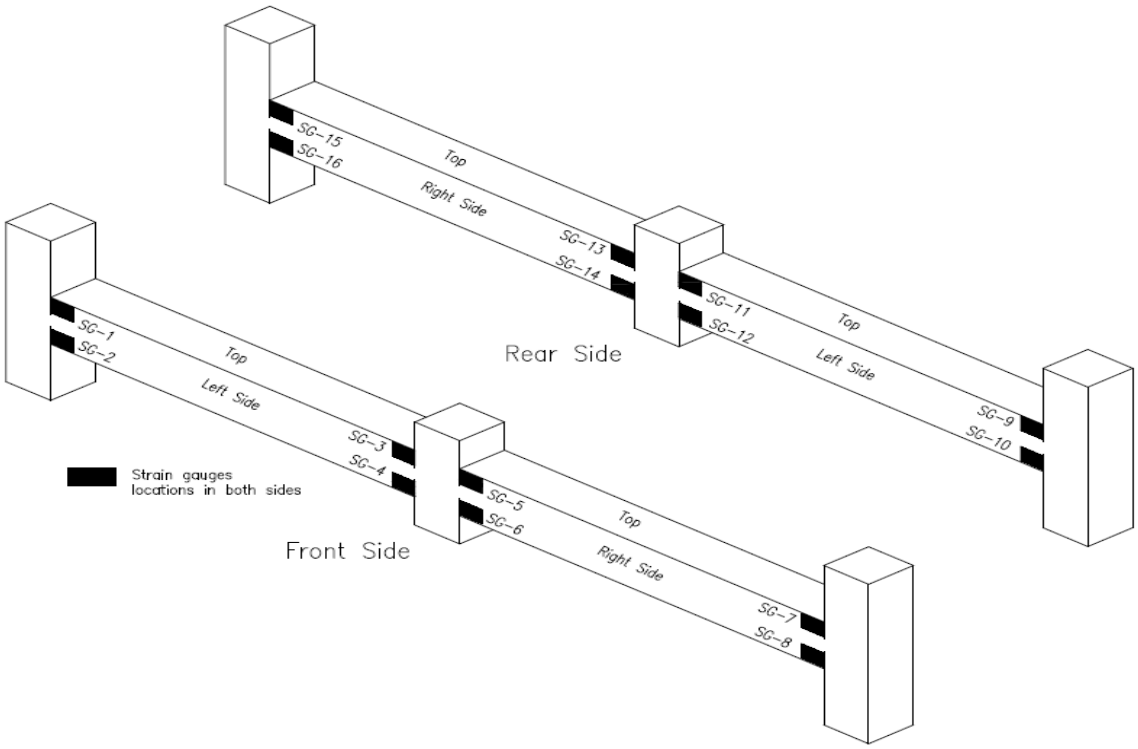

Figure 124. Strain Gauge Locations on Sub-assemblage

2.6.2 Strain Gauge Results for the Sub-assemblage Specimens

Figures 125 and 126 represent the sixteen strain gauges installed in Specimen S2-1 and data recorded during the entire test. The maximum strain recorded for Strain Gauge 1 was -0.0003 in/in when a load of 5.80 kips was applied. The maximum strain recorded for Strain Gauge 2 was

-0.0015 in/in when a load of 5.63 kips was applied. The maximum strain recorded for Strain Gauge 3 was -0.0025 in/in when a load of 5.80 kips was applied; this strain exceeded the steel yield point of 0.0023 in/in. The maximum strain recorded for Strain Gauge 4 was -0.0044 in/in when a load of 0.36 kips was applied; this strain exceeded the concrete strain of 0.0031 in/in and the steel yield point of 0.0023 in/in, this strain gauge was deleted from the graphic, it is as if the strain gauge after the crack moment load stopped recording and came in a vertical line. It is possible that the gauge was damaged or separated from the beam. The maximum strain recorded for Strain Gauge 5 was -0.0006 in/in when a load of 4.04 kips was applied. The maximum strain recorded for Strain Gauge 6 was -0.0006 in/in when a load of 5.60 kips was applied. The maximum strain recorded for Strain Gauge 7 was -0.0008 in/in when a load of 5.80 kips was applied. The maximum strain recorded for Strain Gauge 8 was -0.0014 in/in when a load of 5.80 kips was applied. The maximum strain recorded for Strain Gauge 9 was 0.0000 in/in when a load of 5.80 kips was applied. The maximum strain recorded for Strain Gauge 10 was 0.0007 in/in when a load of 0.36 kips was applied. The maximum strain recorded for Strain Gauge 11 was -0.0015 in/in when a load of 5.80 kips was applied. The maximum strain recorded for Strain Gauge 12 was -0.0053 in/in when a load of 0.75 kips was applied; this strain exceeded the concrete strain of 0.003 in/in and the steel yield point of 0.0023 in/in, this strain gauge was deleted from the graphic, it is as if the strain gauge after the crack moment load stopped recording and came in a vertical line. It is possible that the gauge was damaged or separated from the beam. The maximum strain recorded for Strain Gauge 13 was -0.0036 in/in when a load of 5.66 kips was applied; this strain exceeds the concrete strain of 0.0031 in/in and the steel yield point of 0.0023 in/in. The maximum strain recorded for Strain Gauge 14 was 0.0004 in/in when a load of 0.55 kips was applied. The maximum strain recorded for Strain Gauge 15 was -0.0005 in/in when a load of 0.36 kips was applied. The maximum strain recorded for Strain Gauge 16 was -0.0019 in/in when a load of 5.66 kips was applied. The collapse load was 5.80 kips.

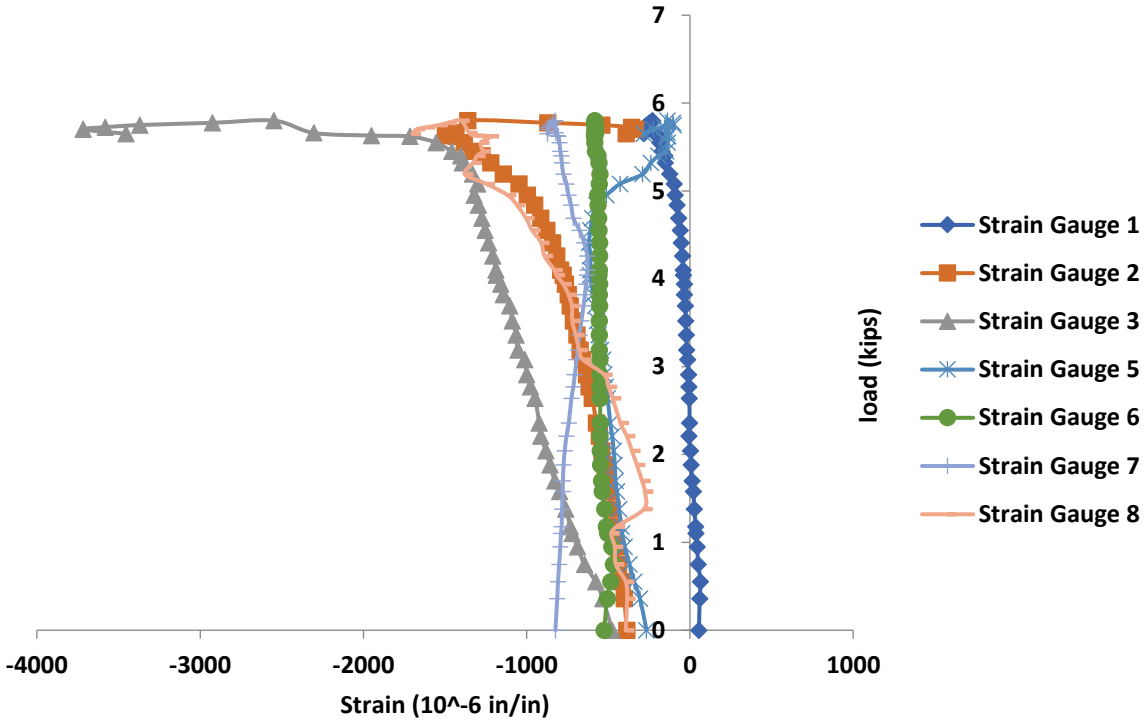

Figure 125. Strain on Front Side for the Sub-assemblage S2-1

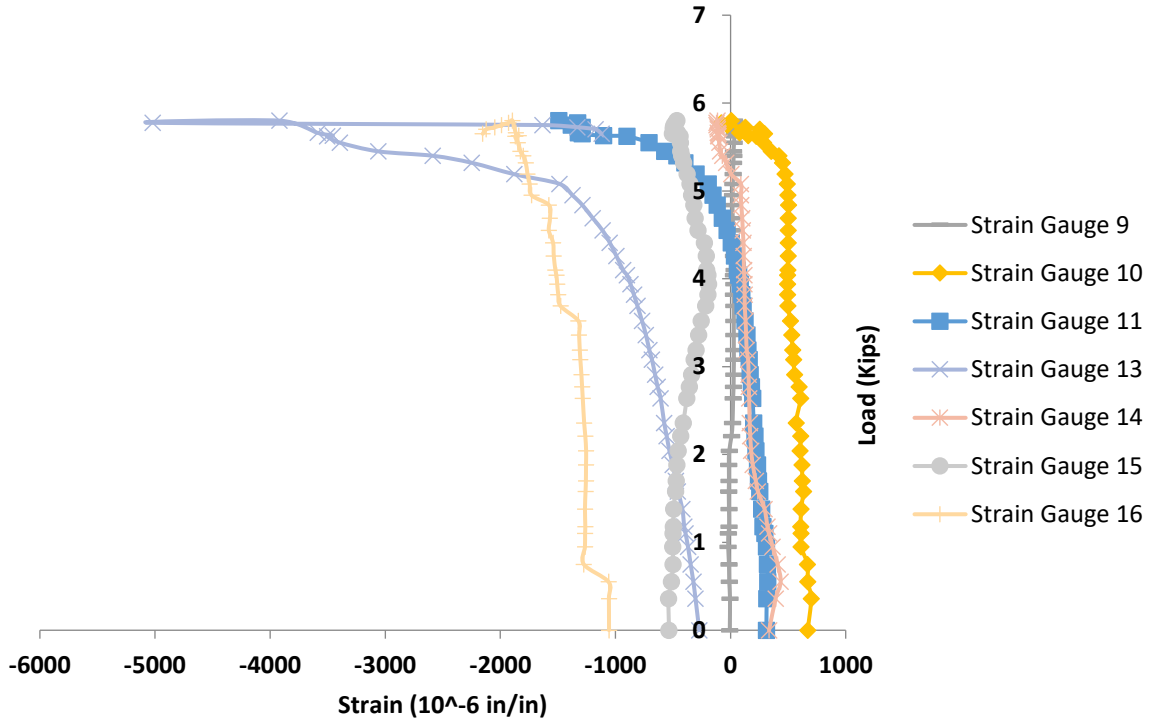

Figure 126. Strain on Rear Side for the Sub-assemblage S2-1

Figures 127 and 128 represent the sixteen strain gauges installed in Specimen S2-2 and data recorded during the entire test with the exception of Strain Gauge 4 which did not record any data after 2.15 kips load was applied. The maximum strain recorded for Strain Gauge 1 was -0.0006 in/in when a load of 5.35 kips was applied. The maximum strain recorded for Strain Gauge 2 was -0.0009 in/in when a load of 5.35 kips was applied. The maximum strain recorded for Strain Gauge 3 was -0.0064 in/in when a load of 5.35 kips was applied; the strain exceeded the concrete strain of 0.0031 in/in and the steel yield point of 0.0023 in/in. The maximum strain recorded for Strain Gauge 4 was -0.0002 in/in when a load of 0.00 kips was applied. The maximum strain recorded for Strain Gauge 5 was -0.0039 in/in when a load of 5.35 kips was applied; the strain exceeded the concrete strain of 0.0030 in/in and the steel yield point of 0.0023 in/in. The maximum strain recorded for Strain Gauge 6 was -0.0007 in/in when a load of 5.35

kips was applied. The maximum strain recorded for Strain Gauge 7 was -0.0009 in/in when a load of 5.35 kips was applied. The maximum strain recorded for Strain Gauge 8 was -0.0026 in/in when a load of 5.35 kips was applied; the strain exceeded the 0.0023 in/in steel yield point. The maximum strain recorded for Strain Gauge 9 was 0.0001 in/in when a load of 4.24 kips was applied. The maximum strain recorded for Strain Gauge 10 was -0.0023 in/in when a load of 5.35 kips was applied; the strain exceeded the 0.0023 in/in steel yield point. The maximum strain recorded for Strain Gauge 11 was -0.0014 in/in when a load of 1.08 kips was applied. The maximum strain recorded for Strain Gauge 12 was -0.0024 in/in when a load of 3.46 kips was applied; the strain exceeded the 0.0023 in/in steel yield point. The maximum strain recorded for Strain Gauge 13 was -0.0043 in/in, when a load of 5.37 kips was applied this strain exceeds the concrete strain of 0.0030 in/in and the steel yield point of 0.0023 in/in. The maximum strain recorded for Strain Gauge 14 was -0.0014 in/in when a load of 5.35 kips was applied. The maximum strain recorded for Strain Gauge 15 was -0.0007 in/in when a load of 5.35 kips was applied. The maximum strain recorded for Strain Gauge 16 was -0.0004 in/in when a load of 5.35 kips was applied. The collapse load was 5.35 kips.

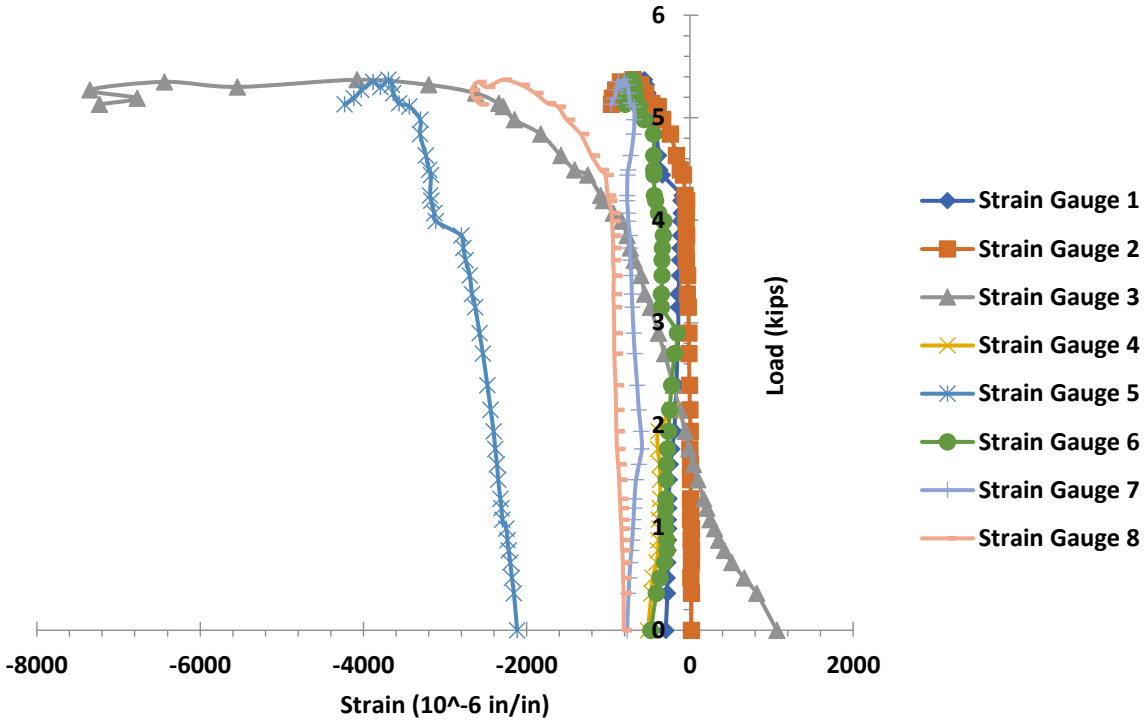

Figure 127. Strain on Front Side for the Sub-assemblage S2-2

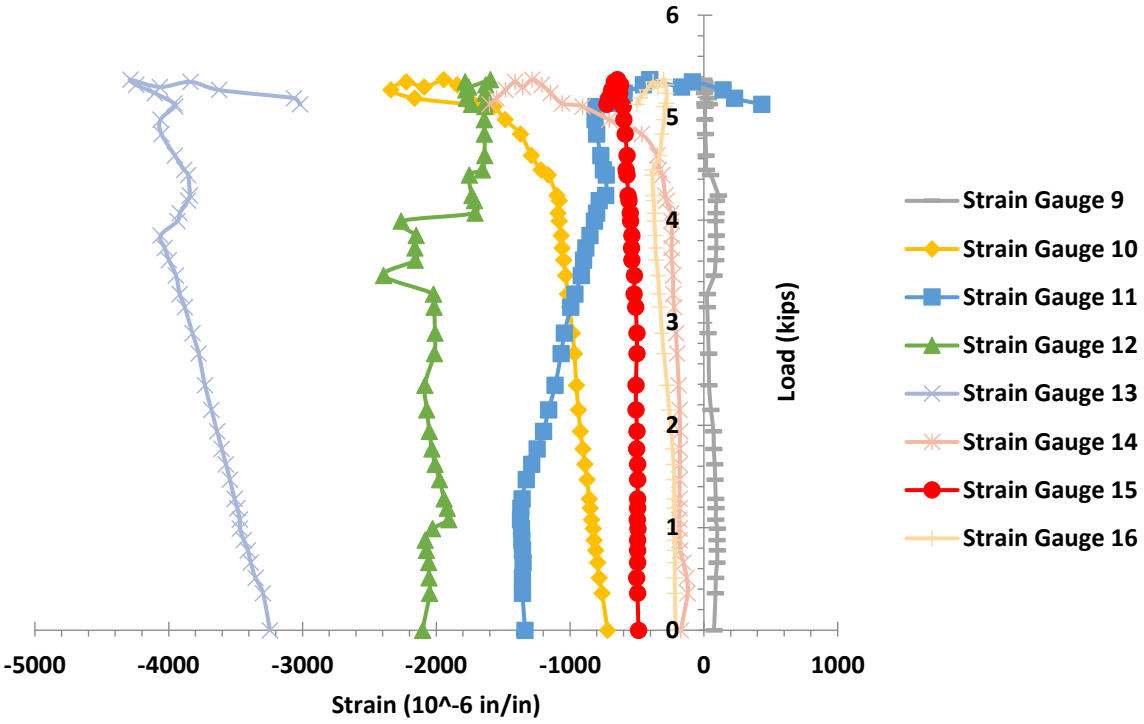

Figure 128. Strain on Rear Side for the Sub-assemblage S2-2

Figures 129 and 130 represent the sixteen strain gauges installed in Specimen B2-1 and data recorded during the entire test. The maximum strain recorded for Strain Gauge 1 was -0.0001 in/in when a load of 4.85 kips was applied. The maximum strain recorded for Strain Gauge 2 was -0.0012 in/in when a load of 4.85 kips was applied. The maximum strain recorded for Strain Gauge 3 was -0.0034 in/in when a load of 4.85 kips was applied; the strain exceeded the concrete strain of 0.0031 in/in and the steel yield point of 0.0023 in/in. The maximum strain recorded for Strain Gauge 4 was 0.0005 in/in when a load of 0.55 kips was applied. The maximum strain recorded for Strain Gauge 5 was -0.0022 in/in when a load of 4.85 kips was applied. The maximum strain recorded for Strain Gauge 6 was -0.0010 in/in. When a load of 0.55 kips was applied this strain exceeded the concrete strain of 0.0031 in/in. The maximum strain recorded for Strain Gauge 7 was -0.0018 in/in when a load of 4.52 kips was applied. The maximum strain recorded for Strain Gauge 8 was -0.0051 in/in when a load of 2.38 kips was applied; the strain

exceeded the concrete strain of 0.0031 in/in and the steel yield point of 0.0023 in/in. The maximum strain recorded for Strain Gauge 9 was 0.0019 in/in when a load of 0.72 kips was applied. The maximum strain recorded for Strain Gauge 10 was 0.0003 in/in when a load of 4.34 kips was applied. The maximum strain recorded for Strain Gauge 11 was 0.0029 in/in when a load of 4.72 kips was applied; this strain exceeded the steel yield point of 0.0023 in/in. The maximum strain recorded for Strain Gauge 12 was -0.0010 in/in when a load of 1.90 kips was applied. The maximum strain recorded for Strain Gauge 13 was -0.0042 in/in, when a load of 4.85 kips was applied this strain exceeds the concrete strain of 0.0031 in/in and the steel yield point of 0.0023 in/in. The maximum strain recorded for Strain Gauge 14 was -0.0083 in/in when a load of 4.64 kips was applied; this strain exceeds the concrete strain of 0.0031 in/in and the steel yield point of 0.0023 in/in. The maximum strain recorded for Strain Gauge 15 was -0.0011 in/in when a load of 4.78 kips was applied. The maximum strain recorded for Strain Gauge 16 was -0.0035 in/in when a load of 4.64 kips was applied, this strain exceeds the concrete strain of 0.0031 in/in and the steel yield point of 0.0023 in/in. The collapse load was 4.85 kips.

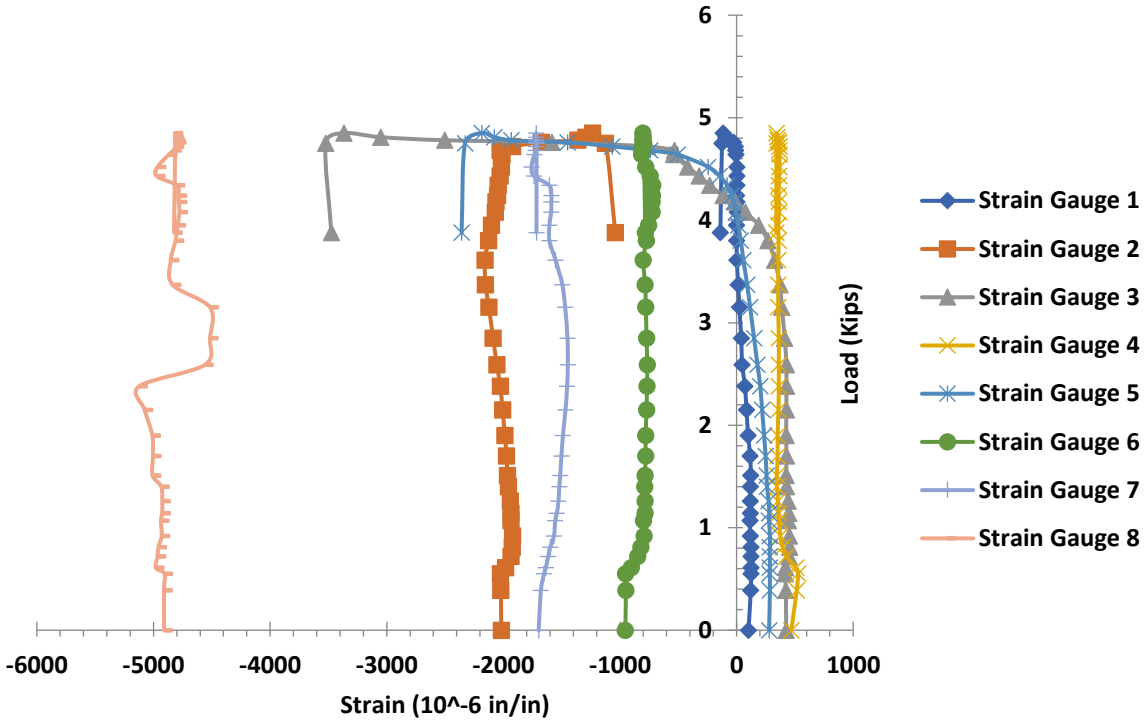

Figure 129. Strain on Front Side for the Sub-assemblage B2-1

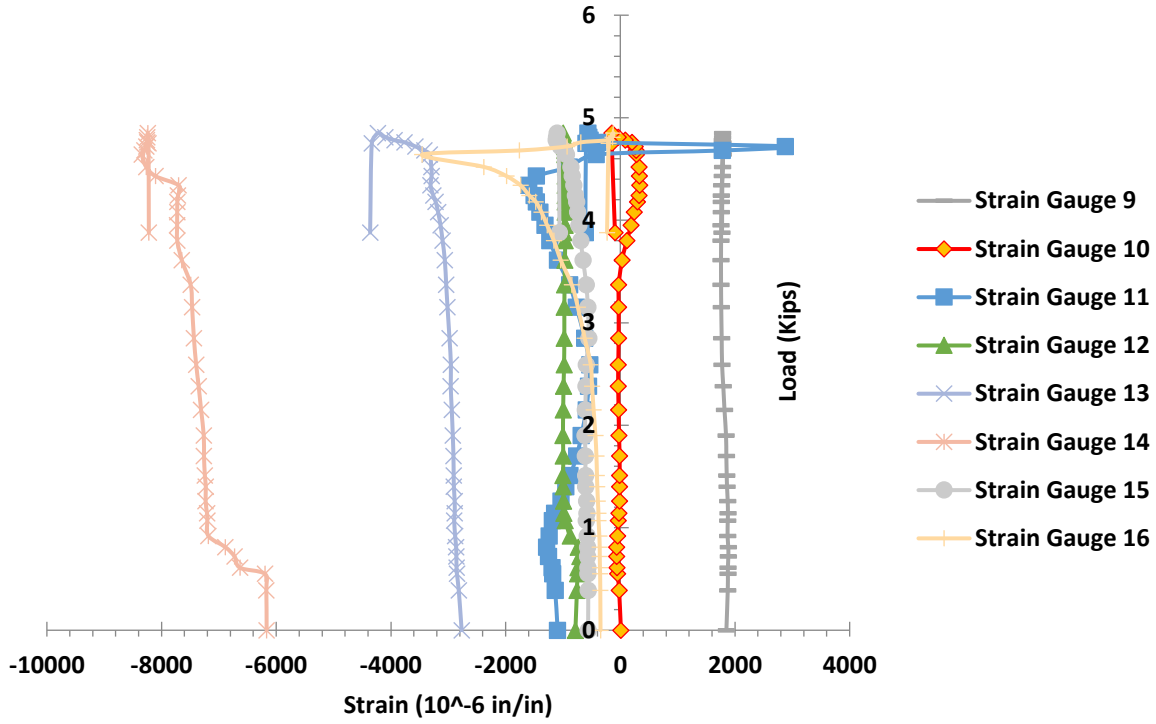

Figure 130. Strain on Rear Side for the Sub-assemblage B2-1

Figures 131 and 132 represent the sixteen strain gauges installed in Specimen B2-2 and data recorded during the entire test with the exception of Strain Gauges 5, 8, and 9. Strain gauge # 5 did not record any data after 5.04 kips load was applied. Strain gauge 8 did not record any data after 4.49 kips load was applied. Strain Gauge 9 does not record any data after 2.16 kips load was applied. The maximum strain recorded for Strain Gauge 1 was -0.0004 in/in when a load of 5.20 kips was applied. The maximum strain recorded for Strain Gauge 2 was 0.0007 in/in when a load of 5.20 kips was applied. The maximum strain recorded for Strain Gauge 3 was -0.0027 in/in when a load of 5.20 kips was applied. The maximum strain recorded for Strain Gauge 4 was -0.0005 in/in when a load of 3.68 kips was applied. The maximum strain recorded for Strain Gauge 5 was -0.0018 in/in when a load of 5.04 kips was applied. The maximum strain recorded for Strain Gauge 6 was -0.0007 in/in when a load of 0.00 kips was applied. The maximum strain recorded for Strain Gauge 7 was -0.0005 in/in when a load of 4.80 kips was applied. The

maximum strain recorded for Strain Gauge 8 was 0.0026 in/in when a load of 4.49 kips was applied; this strain exceeds the steel yield point of 0.0023 in/in. The maximum strain recorded for Strain Gauge 9 was -0.0034 in/in when a load of 0.58 kips was applied; the strain exceeded the concrete strain of 0.0031 in/in and the steel yield point of 0.0023 in/in. The maximum strain recorded for Strain Gauge 10 was -0.0013 in/in when a load of 5.20 kips was applied. The maximum strain recorded for Strain Gauge 11 was -0.0031 in/in when a load of 2.92 kips was applied; the strain exceeded the concrete strain of 0.0031 in/in and the steel yield point of 0.0023 in/in. The maximum strain recorded for Strain Gauge 12 was -0.0004 in/in when a load of 5.04 kips was applied. The maximum strain recorded for Strain Gauge 13 was -0.0045 in/in when a load of 5.12 kips was applied this strain exceeded the concrete strain of 0.0031 in/in and the steel yield point of 0.0023 in/in. The maximum strain recorded for Strain Gauge 14 was -0.0007 in/in when a load of 5.20 kips was applied. The maximum strain recorded for Strain Gauge 15 was -0.0005 in/in when a load of 5.20 kips was applied. The maximum strain recorded for Strain Gauge 16 was 0.0008 in/in when a load of 2.36 kips was applied. The collapse load was 5.20 kips.

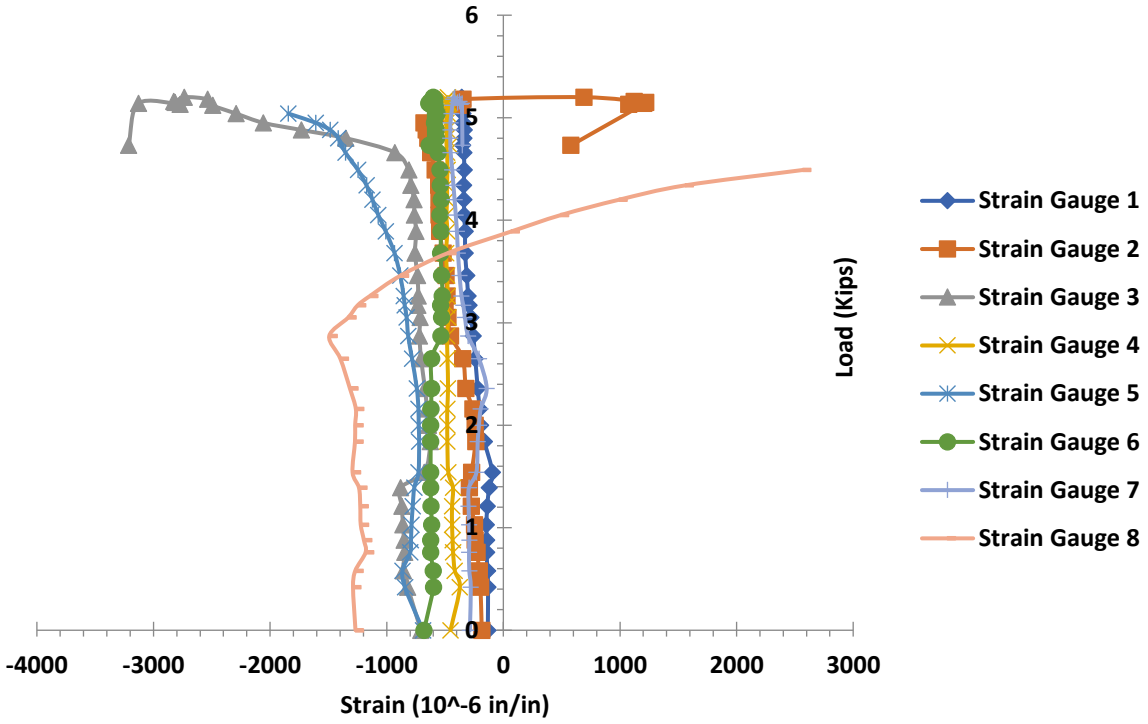

Figure 131. Strain on Front Side for the Sub-assemblage B2-2

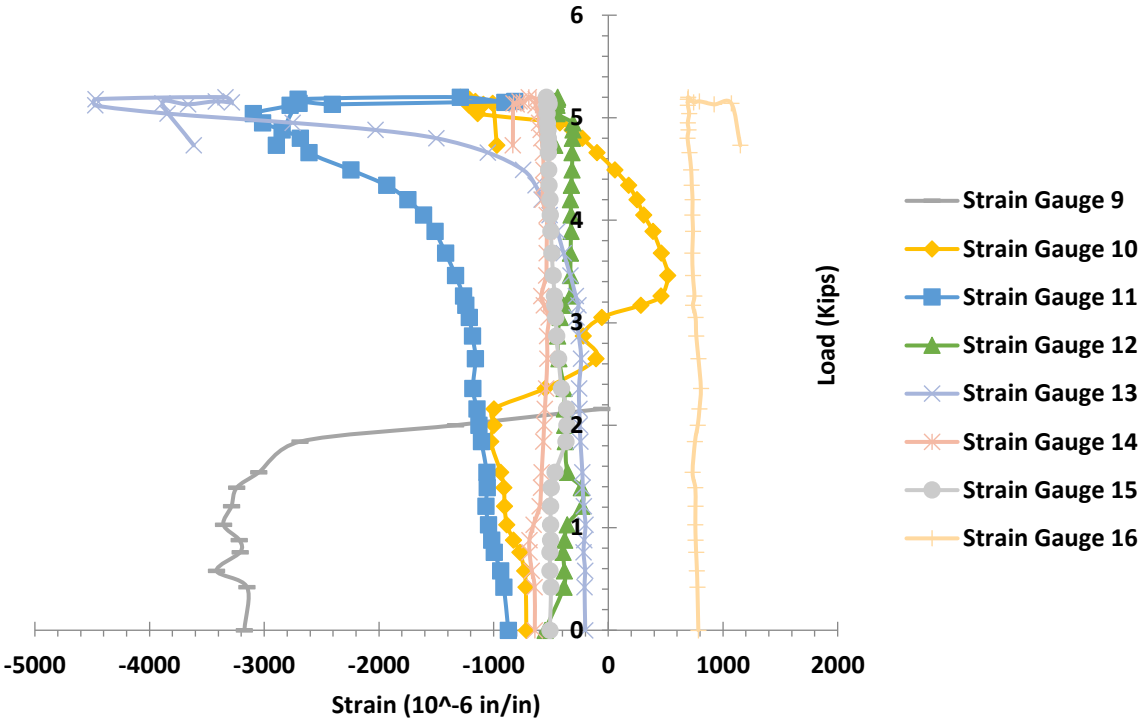

Figure 132. Strain on Rear Side for the Sub-assemblage B2-2

2.6.3 Strain versus Displacement at the Failure Column

This section illustrates the strain-displacement of the reinforcement in the joint of failure column. In the area next to the joint on the left and right side four strain gauges were installed in the front face of the specimen and four strain gauges in the back face of the specimen. Load, strain, and displacement was recorded to illustrate the strain-displacement graphic of the four specimens tested in this section.

Figure 133 represents the four strain gauges located on the left side of the failure column. Specimen S2-1 failure occurred with an applied load of 5.80 kips and developed a maximum displacement of 1.11 inches at the failure column. Strain Gauges 3 and 4 were located in the front face of the specimen and Strain Gauges 11 and 12 were located in the back face of the

specimen. Strain Gauge 3 recorded in compression during the entire test. Strain Gauge 3 reached the reinforcement yield point at the applied load of 5.66 kips and developed a displacement of 1.00 inches. Strain Gauge 4 recorded in compression during the entire test and greater strain than the steel yield point of 0.0023 in/in. Strain Guage 11 recorded data in tension and changed to compression at the applied load of 4.41 kips and developed a displacement of 0.46 inches. After this point the strain gauge continued recording data in compression. Strain Gauge 12 recorded data in compression during the entire test and greater strain than the steel yield point of 0.0023 in/in. The yielding of the tensile reinforcement indicated the formation of the plastic hinges. Due to the changes in the bending moment at the joint of the column failure and the lack of reinforcement in the bottom side of the beam in the joint area, the bottom reinforcement yielded at very small joint displacement and very low load.

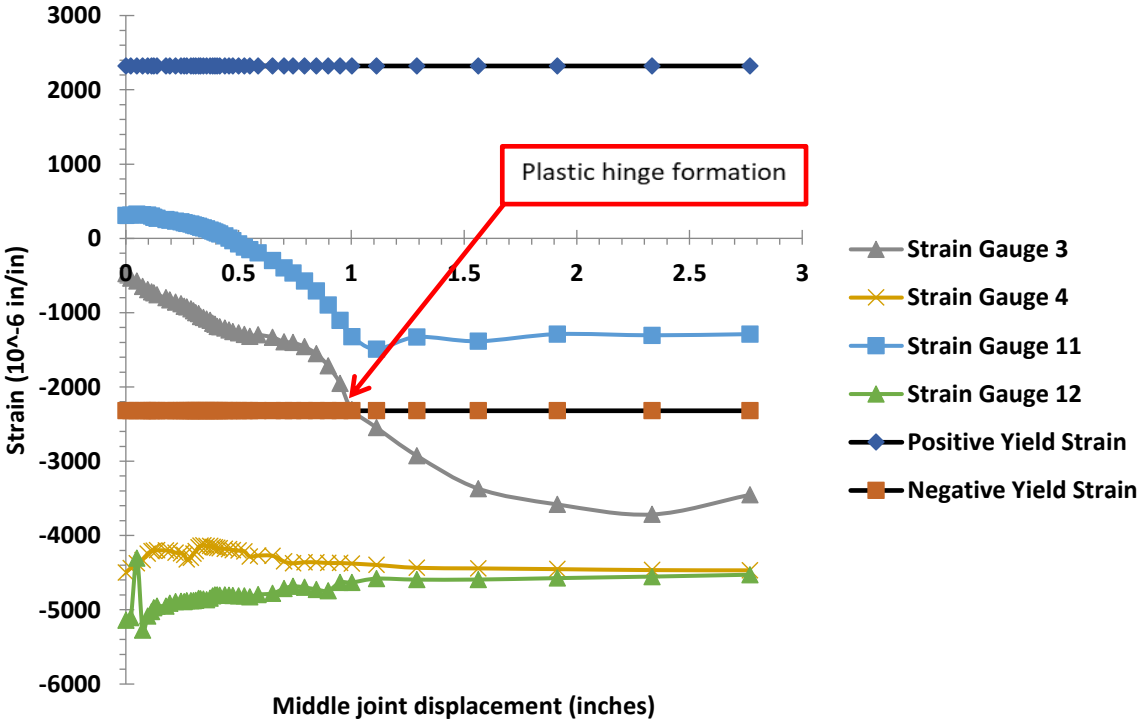

Figure 133. Left Side of the Middle Joint Displacement for Sub-assemblage S2-1

Figure 134 represents the four strain gauges located on the right side of the failure column. Specimen S2-1 failure occurred with an applied load of 5.80 kips and developed a maximum displacement of 1.11 inches at the failure column. Strain Gauges 5 and 6 were located in the front face of the specimen and Strain Gauges 13 and 14 were located in the back face of the specimen. Strain Gauge 5 recorded data in compression during the entire test. Strain gauge 6 recorded data in compression during the entire test. Strain Gauge 13 recorded data in compression. Strain Gauge 13 reached the yield point at the applied load of 5.40 kips and developed a displacement of 0.74 inches. Strain Gauge 14 recorded data in tension and changes to recorded compression data an applied load of 5.32 kips and displacement of 0.70 inch. The yielding of the tensile reinforcement indicated the formation of the plastic hinges. Due to the changes in the bending moment at the joint of the column failure and the lack of reinforcement in the bottom side of the beam in the joint area, the bottom reinforcement yielded at very small joint displacement and very low load.

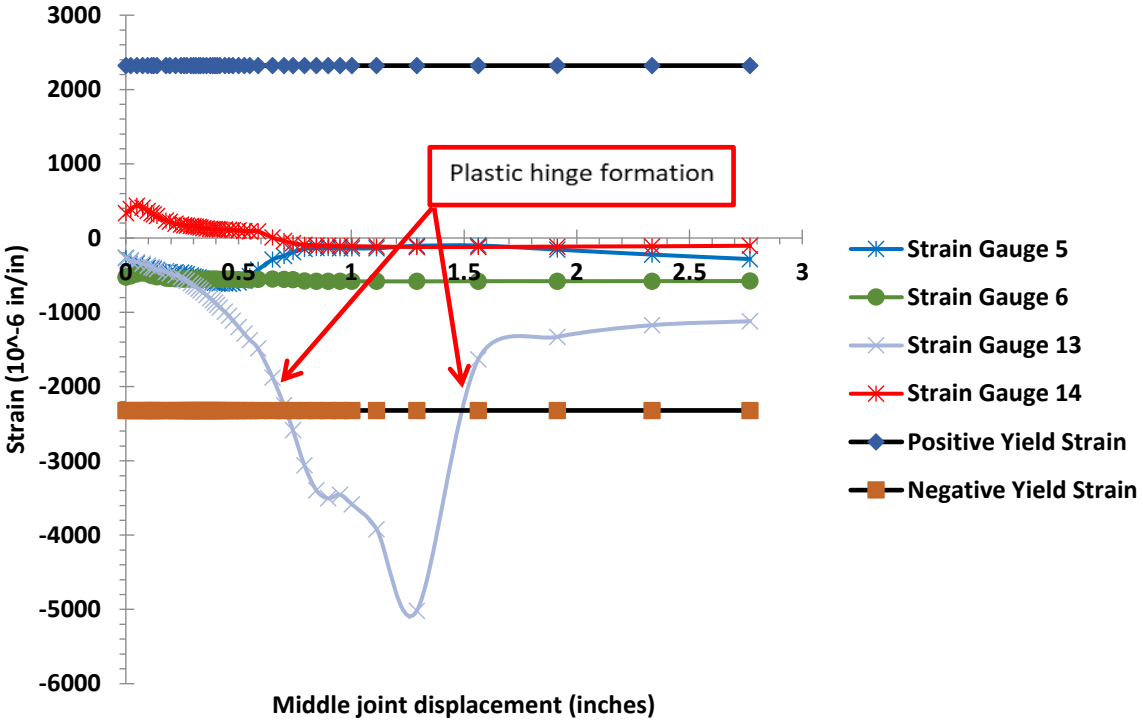

Figure 134. Right Side of the Middle Joint Displacement for Sub-assemblage S2-1

Figure 135 represents the four strain gauges located on the left side of the failure column. Specimen S2-2 failure occurred with an applied load of 5.35 kips and developed a maximum displacement of 1.68 inches at the failure column. Strain Gauges 3 and 4 were located in the front face of the specimen and Strain Gauges 11 and 12 were located in the back face of the specimen. Strain Gauge 3 recorded data in tension up to the applied load of 1.77 kips and displacement of 0.18 inch, at this point the strain gauge continued recording data in compression for the remaining duration of the test. Strain Gauge 3 reached the reinforcement yield point at the applied load of 5.14 kips and developed a displacement of 1.15 inches. The yielding of the tensile reinforcement indicated the formation of the plastic hinges. Strain Gauge 4 recorded data in compression up to the applied load of 2.15 kips and developed a displacement of 0.23 inch, after that applied load the strain gauge does not record any other data. Strain Gauge 11 recorded in compression and change to tension at the applied load of 5.27 kips was applied and

displacement of 1.80 inches was developed. After this point the strain gauge continued recording data in tension for the remaining duration of the test. Strain Gauge 12 recorded in compression during the entire test. At the applied load of 3.46 kips and developed a displacement of 0.40 inch the reinforcement reached the steel yield point of 0.0023 in/in. The yielding of the tensile reinforcement indicated the formation of the plastic hinges. Due to the changes in the bending moment at the joint of the column failure and the lack of reinforcement in the bottom side of the beam in the joint area, the bottom reinforcement yielded at very small joint displacement and very low load.

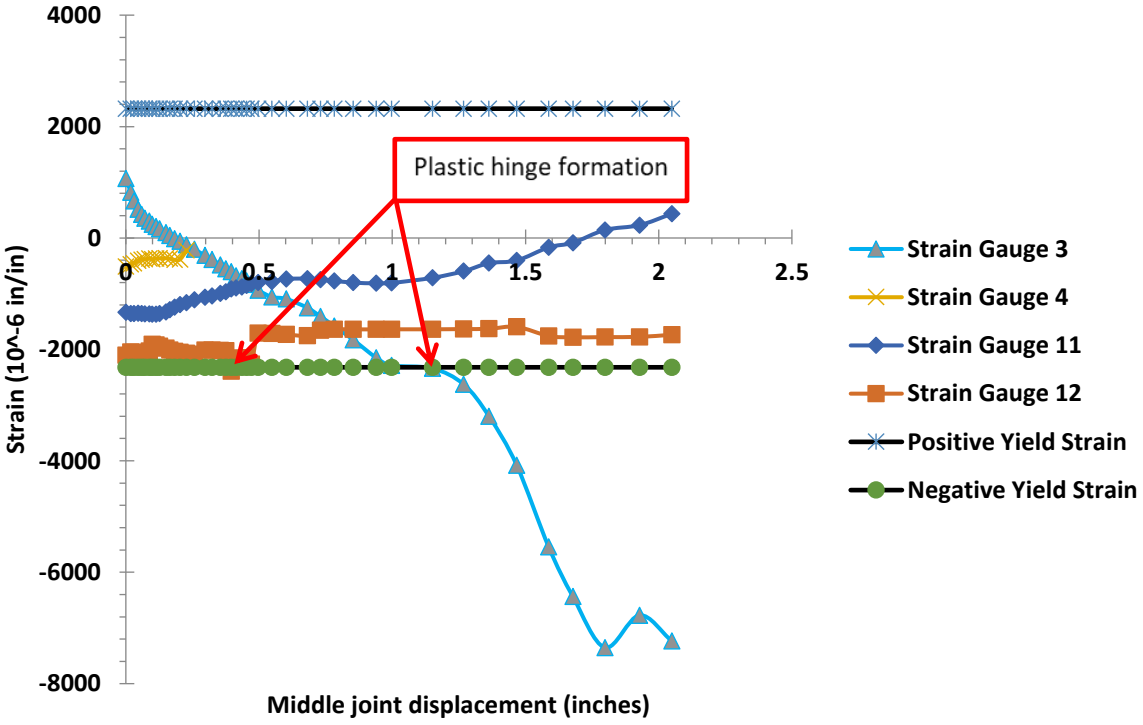

Figure 135. Left Side of the Middle Joint Displacement for Sub-assemblage S2-2

Figure 136 represents the four strain gauges located on the right side of the failure column. Specimen S2-2 failure occurred with an applied load of 5.35 kips and developed a maximum displacement of 1.68 inches at the failure column. Strain Gauges 5 and 6 were located in the front face of the specimen and Strain Gauges 13 and 14 were located in the back face of the specimen. Strain gauge 5 recorded in compression during the entire test. Strain Gauge 5 reached the reinforcement yield point at the applied load of 1.28 kips and developed a displacement of 0.13 inch. The yielding of the tensile reinforcement indicated the formation of the plastic hinges Strain gauge 6 recorded in compression during the entire test. Strain Gauge 13 recorded in compression and greater strain than the steel yield point of 0.0023 in/in. Strain Gauge 14 recorded in compression during the entire test. Due to the changes in the bending moment at the joint of the column failure and the lack of reinforcement in the bottom side of the beam in the joint area, the bottom reinforcement yielded at very small joint displacement and very low load.

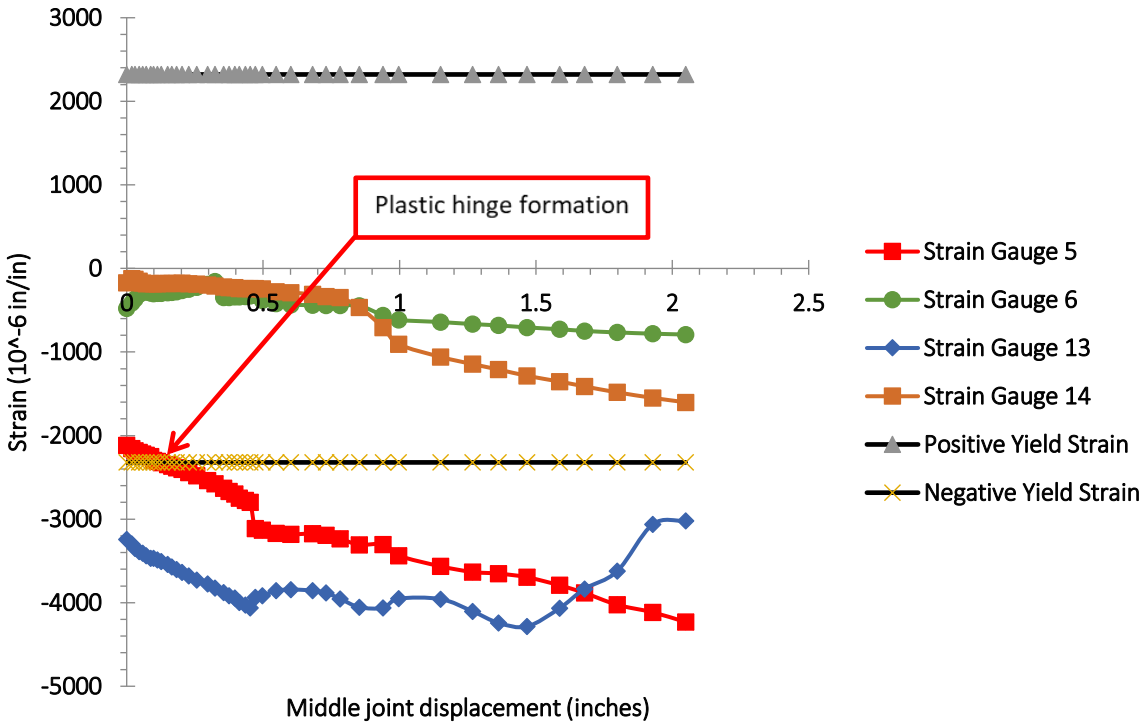

Figure 136. Right Side of the Middle Joint Displacement for Sub-assemblage S2-2

Figure 137 represents the four strain gauges located on the left side of the failure column. Specimen B2-1 failure occurred with an applied load of 4.85 kips and developed a maximum displacement of 4.10 inches at the failure column. Strain Gauges 3 and 4 were located in the front face of the specimen and Strain Gauges 11 and 12 were located in the back face of the specimen. Strain Gauge 3 recorded tension until an applied load of 4.08 kips and developed a displacement of 0.88 inches, then changed to record data in compression for the remainder of the test. Strain gauge 4 recorded tension for the entire test. Strain Gauge 11 recorded in compression until applied load of 4.64 kips and developed a displacement of 1.18 inches, then changed to record data in tension until a load applied of 4.72 kips and developed a displacement of 1.60 inches then changed to record data in compression until the remainder of the test. Strain Gauge 12 recorded in compression for the entire test. Due to the changes in the bending moment at the joint of the column failure and the lack of reinforcement in the bottom side of the beam in the joint area, the bottom reinforcement yielded at very small joint displacement and very low load.

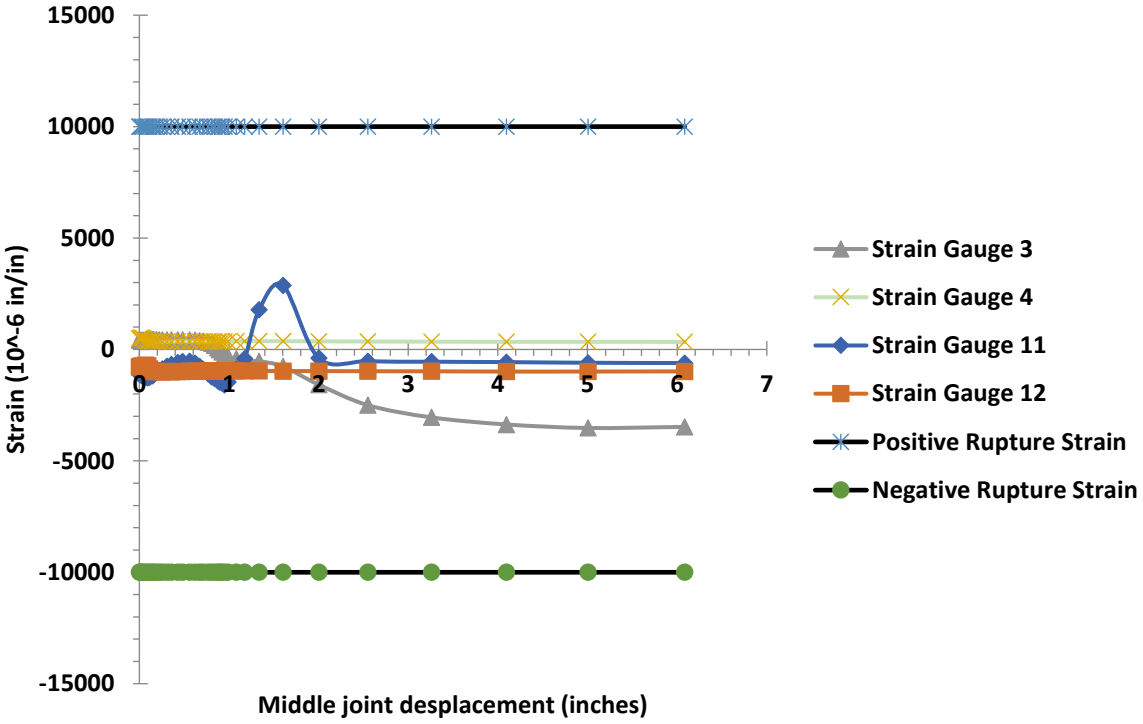

Figure 137. Left Side of the Middle Joint Displacement for Sub-assemblage B2-1

Figure 138 represents the four strain gauges located on the right side of the failure column. Specimen B2-1 failure occurred with an applied load of 4.85 kips and developed a maximum displacement of 4.10 inches at the failure column. Strain Gauges 5 and 6 were located in the front face of the specimen and Strain Gauges 13 and 14 were located in the back face of the specimen. Strain Gauge 5 recorded tension until an applied load of 3.95 kips and developed a displacement of 0.84 inches, then changed to record data in compression for the remainder of the test. Strain Gauge 6 recorded in compression for the entire test. Strain Gauge 13 recorded in compression for the entire test. Strain Gauge 14 recorded in compression for the entire test. Due to the changes in the bending moment at the joint of the column failure and the lack of reinforcement in the bottom side of the beam in the joint area, the bottom reinforcement yielded at very small joint displacement and very low load.

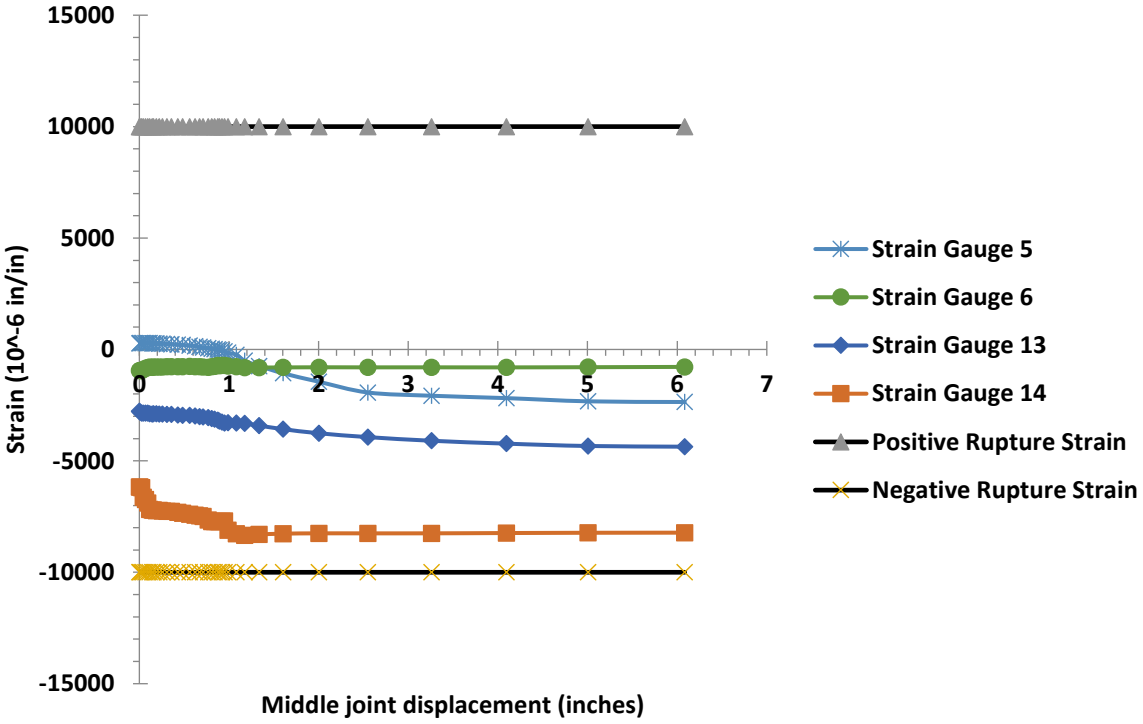

Figure 138. Right Side of the Middle Joint Displacement for the Sub-assemblage B2-1

Figure 139 represents the four strain gauges located on the left side of the failure column. Specimen B2-2 failure occurred with an applied load of 5.20 kips and developed a maximum displacement of 1.98 inches at the failure column. Strain Gauges 3 and 4 were located in the front face of the specimen and Strain Gauges 11 and 12 were located in the back face of the specimen. Strain Gauge 3 recorded in compression during the entire test. Strain Gauge 4 was recorded in compression for the entire test. Strain Gauge 11 was recorded in compression for the entire test. Strain Gauge 12 recorded in compression for the entire test. Due to the changes in the bending moment at the joint of the column failure and the lack of reinforcement in the bottom side of the beam in the joint area, the bottom reinforcement yielded at very small joint displacement and very low load.

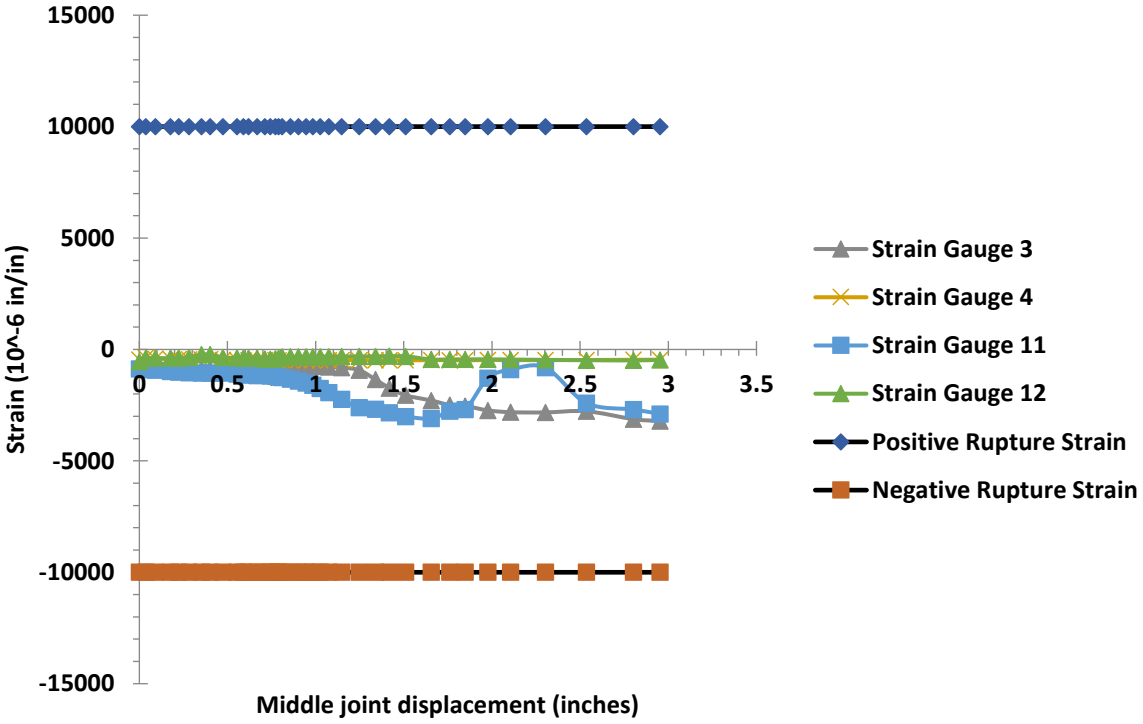

Figure 139. Left Side of the Middle Joint Displacement for Sub-assemblage B2-2

Figure 140 represents the four strain gauges located on the left side of the failure column. Specimen B2-2 failure occurred with an applied load of 5.20 kips and developed a maximum displacement of 1.98 inches at the failure column. Strain Gauges 5 and 6 were located in the front face of the specimen and Strain Gauges 13 and 14 were located in the back face of the specimen. Strain Gauge 5 recorded tension until an applied load of 5.04 kips and developed a displacement of 1.66 inches. After this load the strain gauge did not record any additional data. Strain Gauge 6 recorded in compression for the entire test. Strain Gauge 13 recorded in compression for the entire test. Strain Gauge 14 recorded in compression for the entire test. Due to the changes in the bending moment at the joint of the column failure and the lack of reinforcement in the bottom side of the beam in the joint area, the bottom reinforcement yielded at very small joint displacement and very low load.

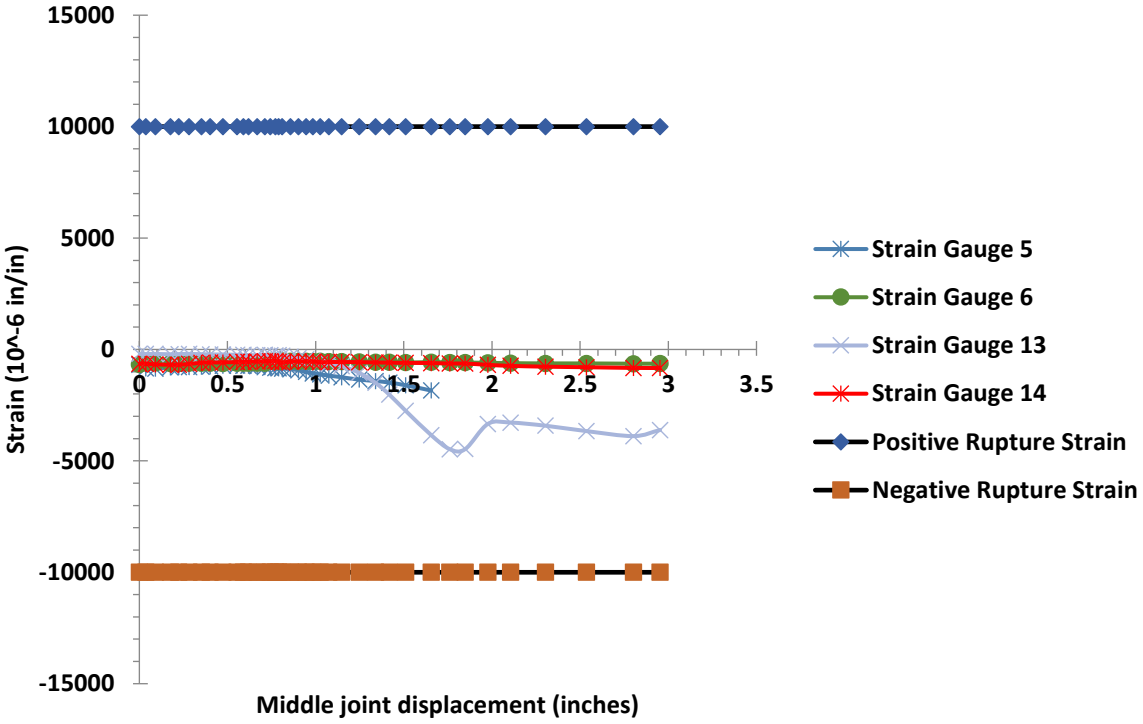

Figure 140. Right Side of the Middle Joint Displacement for Sub-assemblage B2-2

2.6.4 Strain Versus Rotation at The Fixed Supports

Support rotation was measured and recorded at each fixed support. This measurement was recorded using two dial gauges on each support, one above the beam and one below the beam.

Figures 141 and 142 represent the strain-rotation for sub-assemblage S2-1. This specimen collapsed at 5.80 kips and generated the following rotations: left fixed-end support developed a rotation of 0.36° (0.006 rad) and right fixed-end support developed a rotation of 1.07° (0.019 rad). The first crack load was 0.95 kips, and the left support developed a rotation of 0.034° (0.001 rad) and the right support developed a rotation of 0.172° (0.003 rad). The first crack near to the missing column was at 1.58 kips and the left support developed a rotation of0.103° (0.002 rad) and the right support developed a rotation of 0.367° (0.006 rad). The first crack in the

missing column area was developed at 2.04 kips and the left support developed a rotation of 0.132° (0.002 rad) and the right support developed a rotation of 0.493° (0.009 rad).

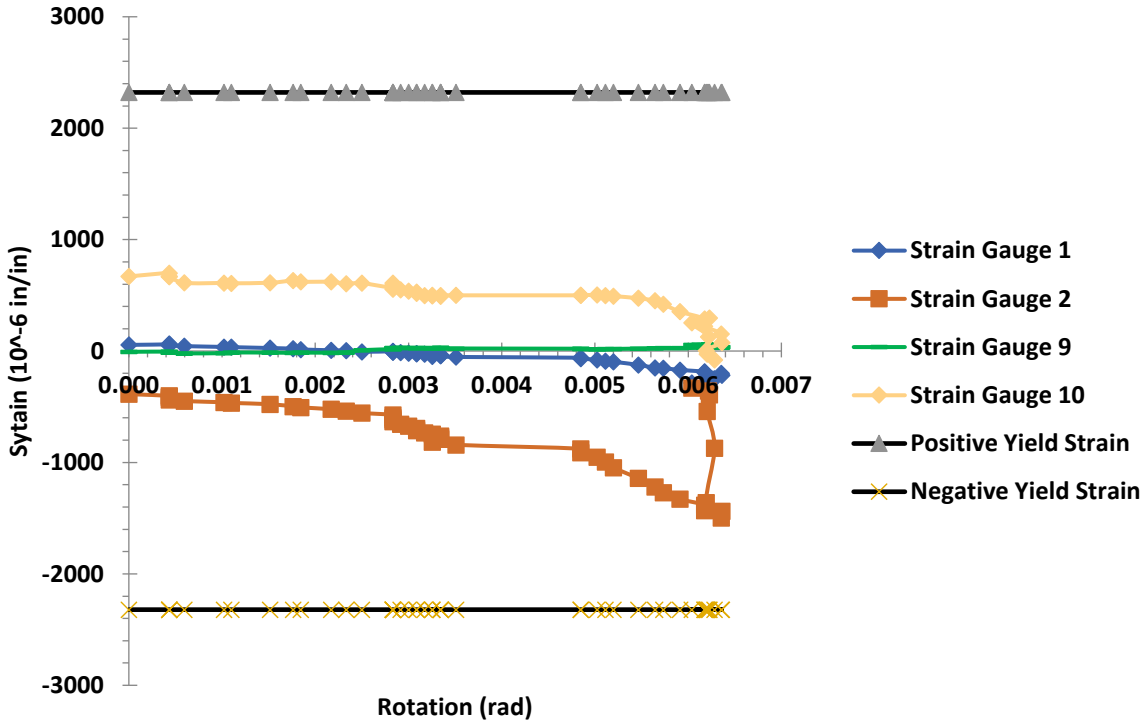

Figure 141. Left Support Rotation for Sub-assemblage S2-1

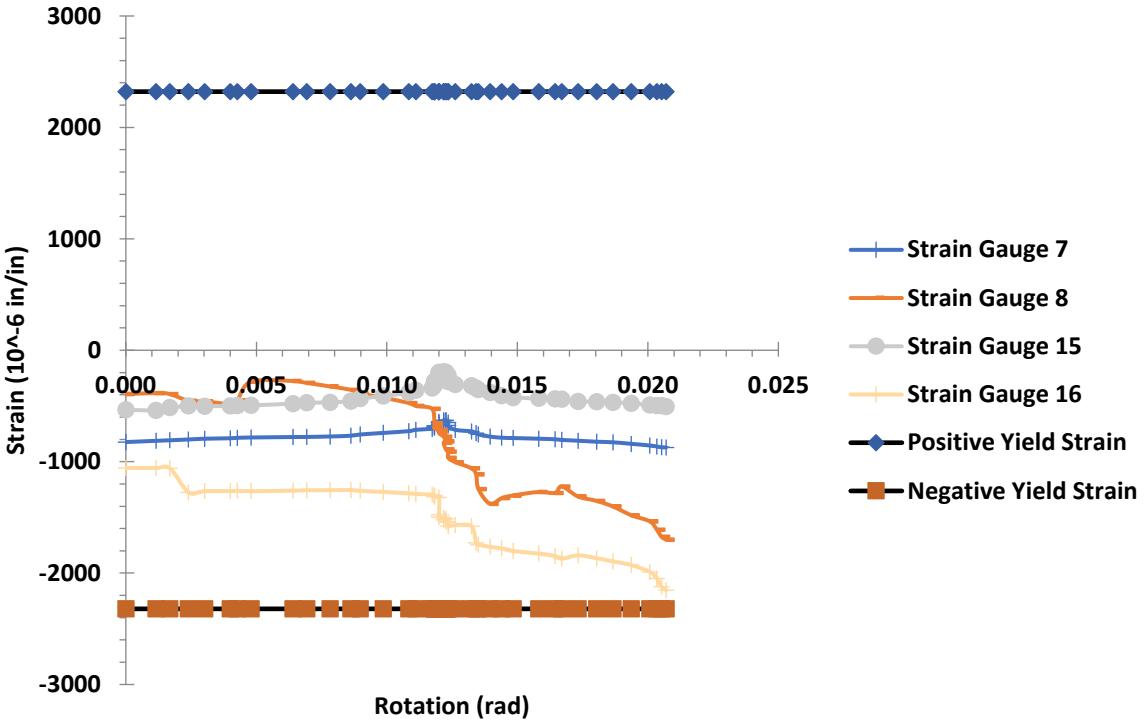

Figure 142. Right Support Rotation for Sub-assemblage S2-1

Figures 143 and 144 represent the strain-rotation for Specimen S2-2. This specimen collapsed at 5.37 kips and generated the following rotations: left fixed-end support developed a rotation of 1.06° (0.019 rad) and right fixed-end support developed a rotation of 1.12° (0.020 rad). The first crack load was of 0.99 kips and the missing column, and the left support developed a rotation of 0.14° (0.003 rad) and the right support developed a rotation of 0.10° (0.002 rad). The concrete crunched at the support when a load of 3.28 kips was applied, and the left support developed a rotation of 0.48° (0.008 rad) and the right support developed a rotation of 0.48° (0.008 rad). Strain Gauge 8 at collapse load recorded strain value of -0.020 in/in. Strain Gauge 10 at collapse load recorded strain value of -0.020 in/in.

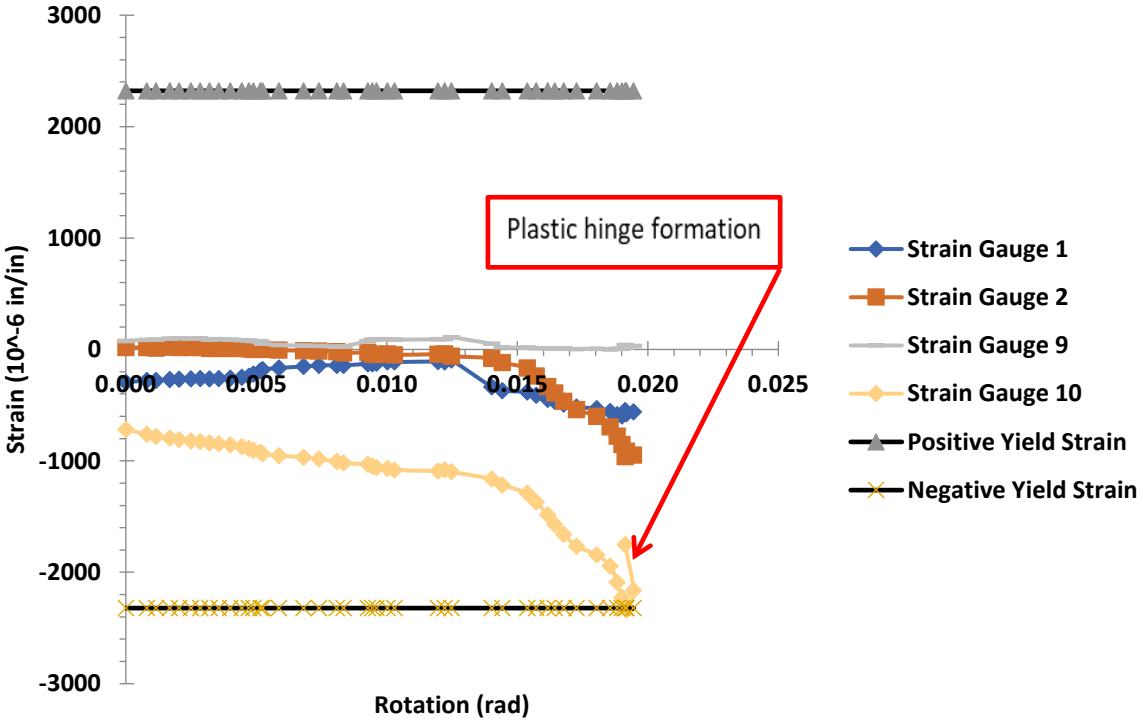

Figure 143. Left Support Rotation of Sub-assemblage S2-2

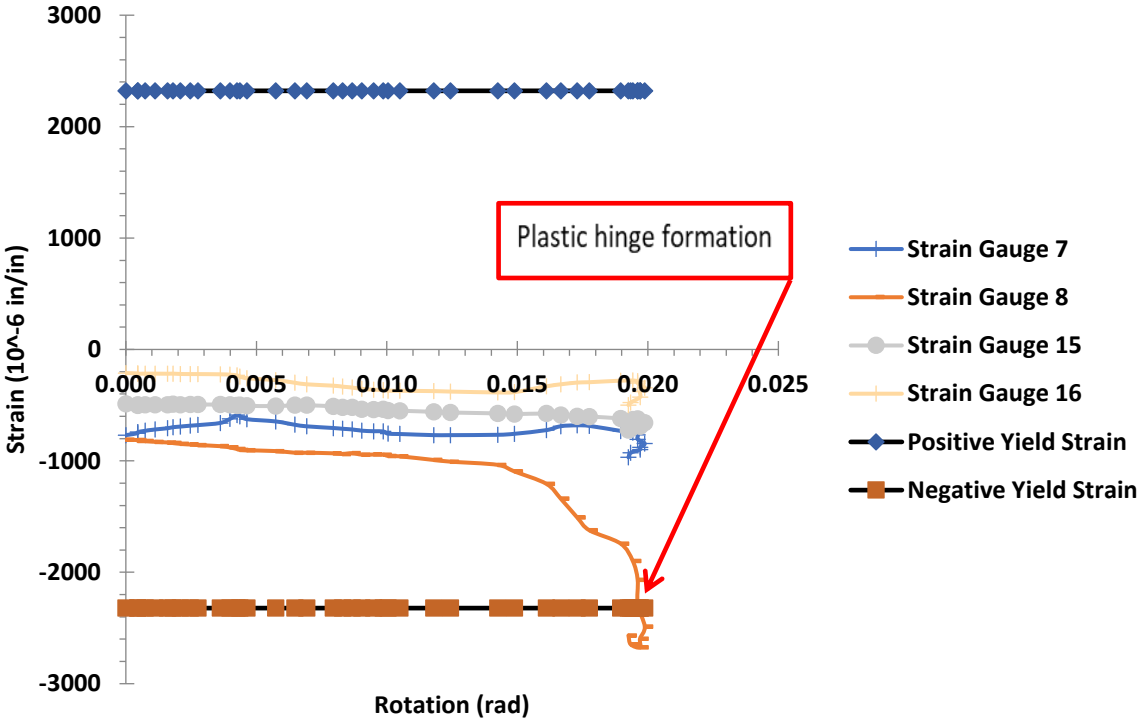

Figure 144. Right Support Rotation for Sub-assemblage S2-2

Figures 145 and 146 represent the strain-rotation for Specimen B2-1. This specimen collapsed at 4.85 kips and generated the following rotations: left fixed-end support developed a rotation of 0.56° (0.010 rad) and right fixed-end support developed a rotation of 1.75° (0.031 rad). The first crack load was at both supports when applied load of 0.81 kips and the left support developed a rotation of 0.13° (0.002 rad) and the right support developed a rotation of 0.07° (0.001 rad). The concrete crunched at the support when a load of 4.80 kips was applied, and the left support developed a rotation of 0.56° (0.010 rad) and the right support developed a rotation of 1.75° (0.031 rad).

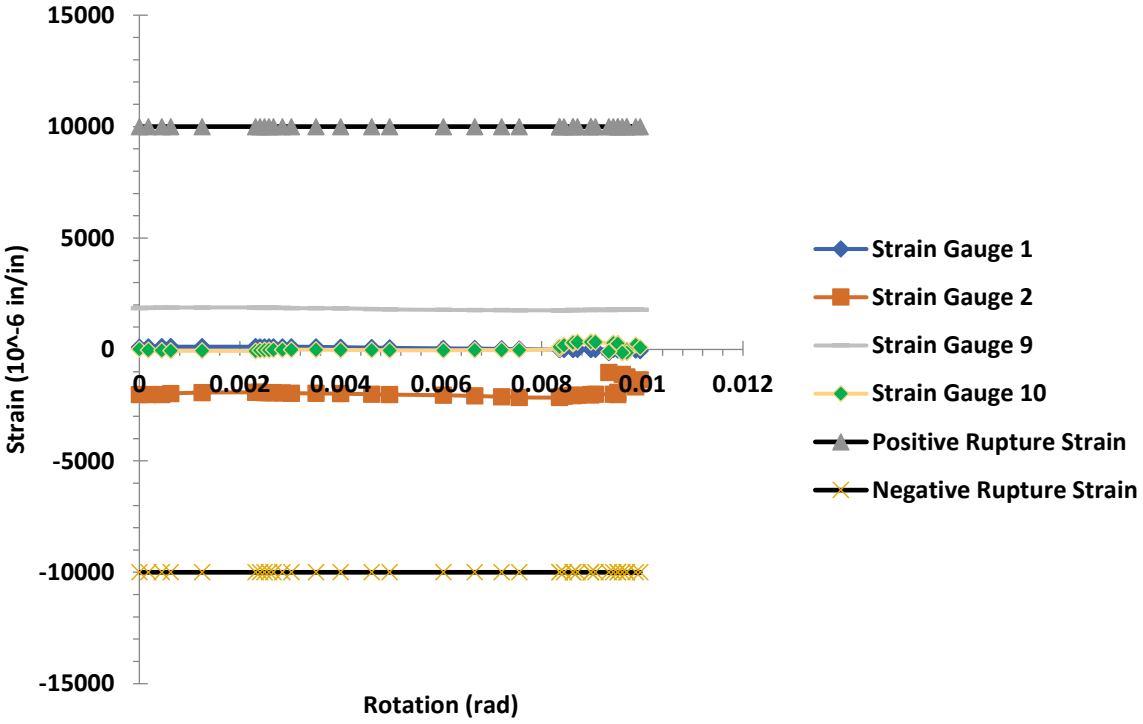

Figure 145. Left Support Rotation for Sub-assemblage B2-1

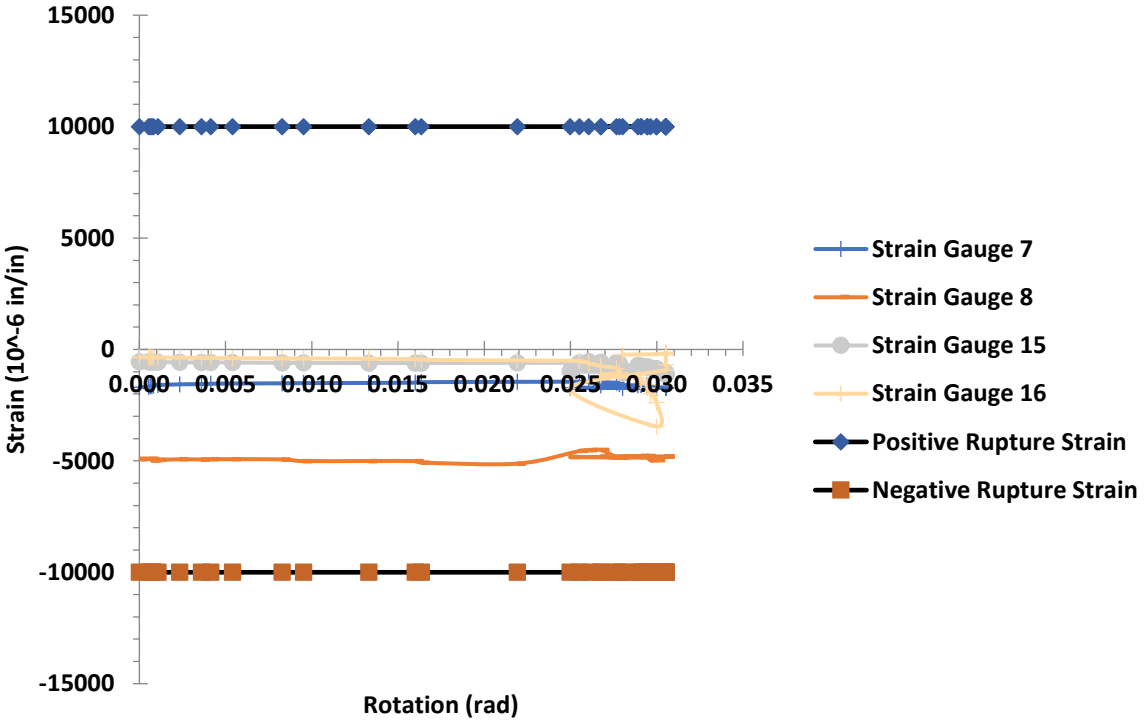

Figure 146. Right Support Rotation for Sub-assemblage B2-1

Figures 147 and 148 represent the strain-rotation for Specimen B2-2. This specimen collapsed at 5.20 kips and generated the following rotations: left fixed-end support developed a rotation of 1.19° (0.021 rad) and right fixed-end support developed a rotation of 1.29° (0.023 rad). The first crack load was at both supports when applied load of 0.88 kips and the left support developed a rotation of 0.35° (0.006 rad) and the right support developed a rotation of 0.39° (0.007 rad). The first crack at the missing column area was when a load of 1.84 kips was applied and the left support developed a rotation of 0.9419° (0.016 rad) and the right support developed a rotation of 0.98° (0.017 rad). The concrete crunched at the support when a load of 4.80 kips was applied, and the left support developed a rotation of 1.13° (0.020 rad) and the right support developed a rotation of 1.20° (0.021 rad).

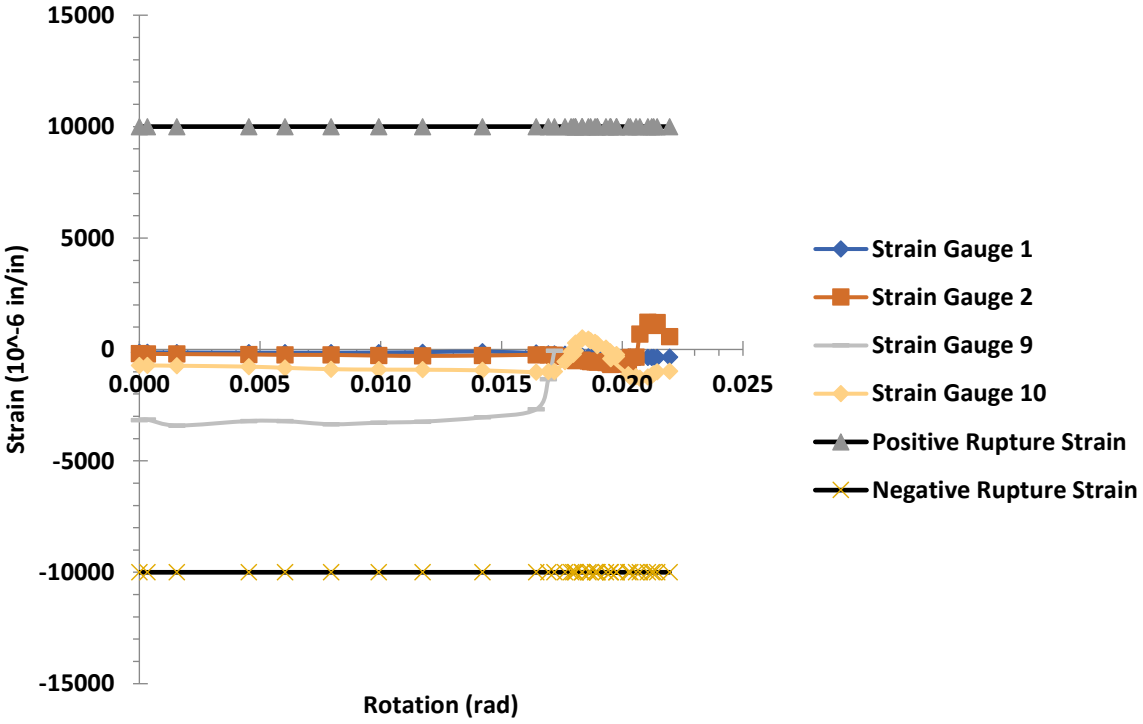

Figure 147. Left Support Rotation for Sub-assemblage B2-2

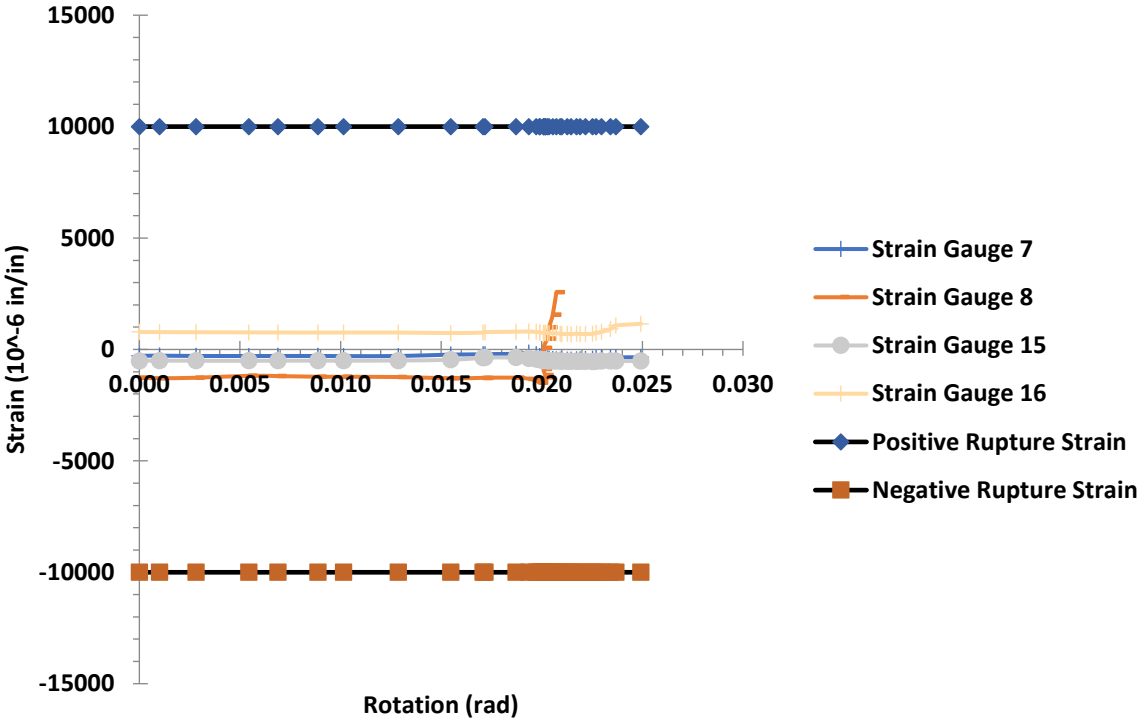

Figure 148. Right Support Rotation for Sub-assemblage B2-2

2.6.5 Sub-assemblage Deflection Results

Beam deflection was measured on three different locations in the specimen. The first location is the center point of the failure column (38 inches from the outside column), the second location was 18 inches from the center of the missing column to the left side of the first sub-assemblage specimen, and the last location was 18 inches from the center of the missing column to the right side of the second sub-assemblage specimen.

Specimen S2-1 collapsed at 5.80 kips and generated a deflection of 1.11 inches. At the collapse load the specimen developed the following rotation left fixed-end support developed a rotation of 0.35° (0.006 rad) and right fixed-end support developed a rotation of 1.07° (0.019 rad). After load removed the specimen had a 0.75-inch permanent deflection. The deflection at the crack

load was 0.01 inch. Maximum deflection at the mid span beam on the left side of the missing column was recorded at 0.59 inch and the maximum deflection at the mid span beam in the right side of the missing column was recorded at 0.60 inch. This beam developed a total of 11 cracks. Figure 150 represents the graphic of load deflection with the experimental information.

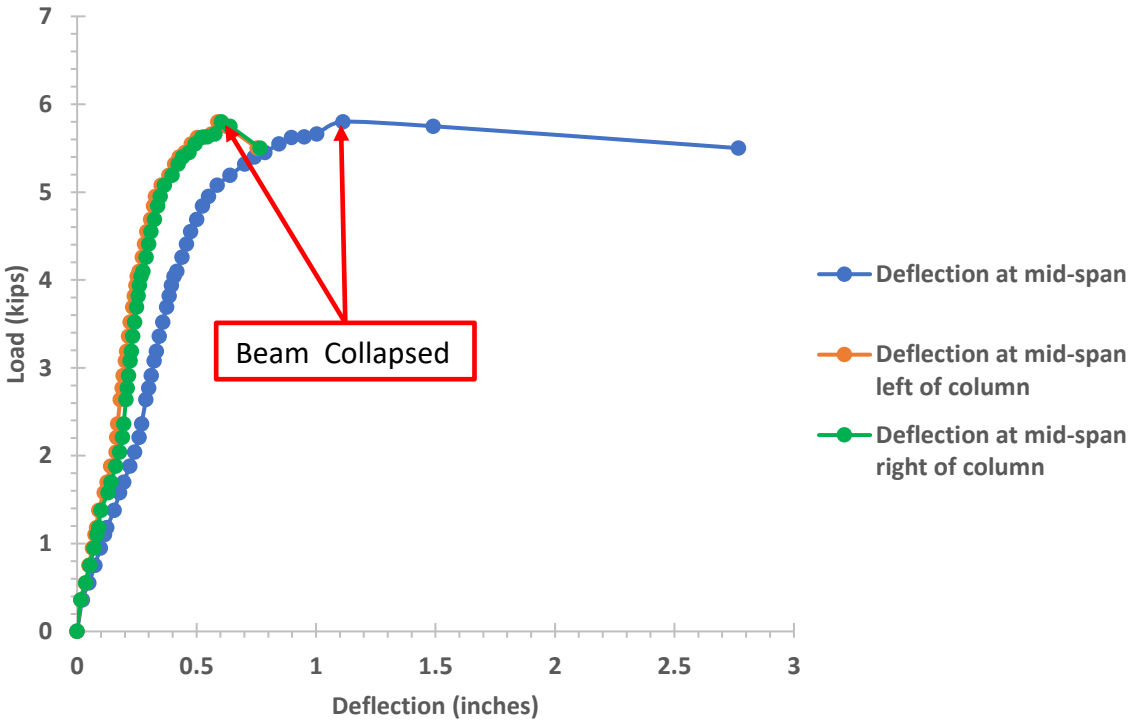

Figure 149. Experimental Load Deflection for Sub-assemblage S2-1

Specimen S2-2 collapsed at 5.37 kips and generated a deflection of 1.8 inches. At the collapse load the specimen developed the following rotation left fixed-end support developed a rotation of 1.06° (0.019 rad) and right fixed-end support developed a rotation of 1.12° (0.020 rad). After

load removed the specimen had a 0.63-inch permanent deflection. The deflection at the crack load was 0.09 inch. Maximum deflection at the mid span beam in the left side of the missing column was recorded a 0.78 inch and the maximum deflection at the mid span beam in the right side of the missing column was recorded 0.78 inch. This beam developed a total of 21 cracks. Figure 150 represents the graphic of load deflection with the experimental information.

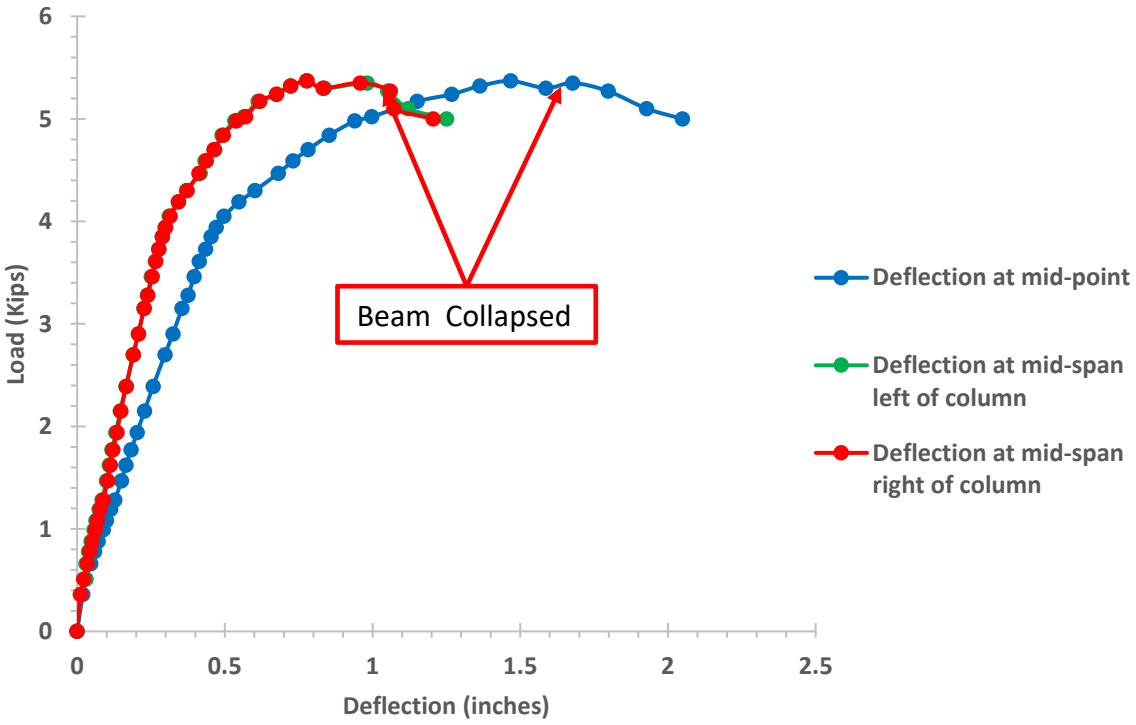

Figure 150. Experimental Load Deflection for Sub-assemblage S2-2

Specimen B2-1 collapsed at 4.85 kips and generated a deflection of 4.10 inches. At the collapse load the specimen developed the following rotation left fixed-end support developed a rotation of 0.56° (0.010 rad) and right fixed-end support developed a rotation of 1.75° (0.031 rad). After load removed the specimen had a 1.53 inches permanent deflection. The deflection at the crack load was 0.09 inch. Maximum deflection at the mid span beam in the left side of the missing

column was recorded a 0.28 inch and the maximum deflection at the mid span beam in the right side of the missing column was recorded a 0.30 inch. This beam developed a total of 16 cracks. Figure 151 represents the graphic of load deflection with the experimental information.

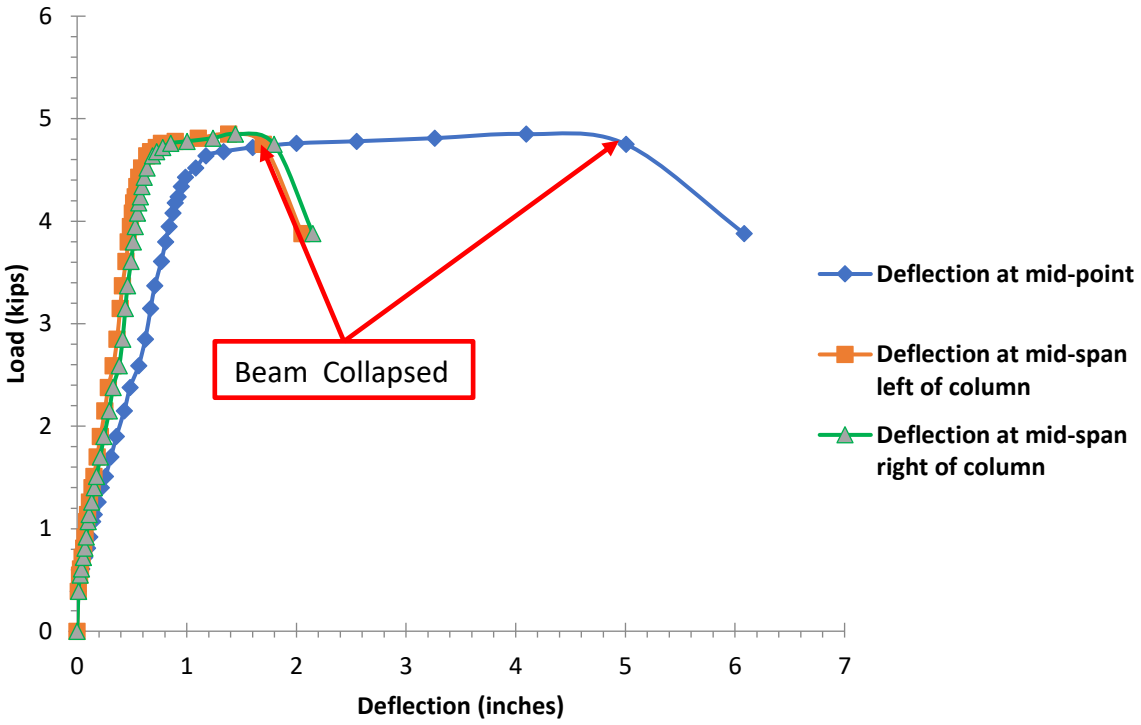

Figure 151. Experimental Load Deflection for Sub-assemblage B2-1

Specimen B2-2 collapsed at 5.20 kips and generated a deflection of 1.98 inch. At the collapse load the specimen developed the following rotation left fixed-end support developed a rotation of 1.19° (0.021 rad) and right fixed-end support developed a rotation of 1.29° (0.023 rad). After load removed the specimen had a 0.89-inch permanent deflection. The deflection at the crack load was 0.09 inch. Maximum deflection at the mid span beam in the left side of the missing

column was recorded at 0.86 inch and the maximum deflection at the mid span beam in the right side of the missing column was recorded 1.26 inches. This beam developed a total of 29 cracks. Figure 152 represents the graphic of load deflection with the experimental information.

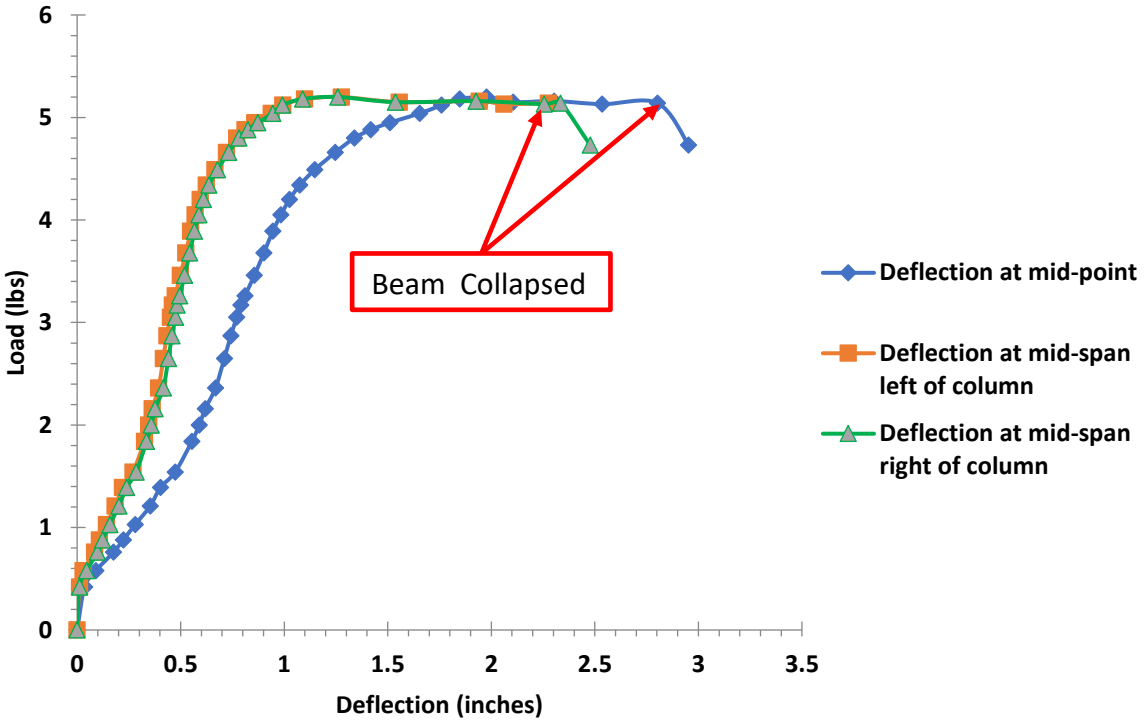

Figure 152. Experimental Load Deflection for Sub-assemblage B2-2

2.6.6 Sub-assemblage Crack Results for All Tests

Cracks were observed during each sub-assemblage test and the location and the load that created each crack in each sub-assemblage was recorded. There were no cracks or failures due to shear failure during any of the sub-assemblage tests.

Specimen S2-1 developed the first crack in the top corner of both fixed-end supports when the load of 0.95 kips was applied, during this load the left fixed-end support developed a rotation of

0.03° (0.000 rad) and the right fixed-end support developed a rotation of 0.18° (0.003 rad). Strain gauges 1and 9 located in the left fixed-end supported recorded strain of (0.0000 and 0.0000 in/in) Strain Gauges 7 and 15 located in the right fixed-end support recorded strain of (-0.0008 and -0.0005 in/in). The first crack in the missing column occurs when load of 2.04 kips was applied, during this load the left fixed-end support developed a rotation of 0.1337° (0.002 rad) and the right fixed-end support developed a rotation of 0.51° (0.008 rad). Strain Gauges 4 and 6 located in the front of the specimen in the missing column area recorded strain of (-0.0042 and -0.0005 in/in). Strain Gauges 12 and 14 located in the back of the specimen in the missing column area recorded strain of (-0.0049 and 0.0002 in/in) Figures 153 and 154 illustrated both cracks at fixed- end supports. The first crack near to the missing column was when a load of 1.58 kips was applied, during this load the left fixed-end support developed a rotation of 0.10° (0.002 rad) and the right fixed-end support developed a rotation of 0.38° (0.007 rad). Figure 155 represents all the cracks around the column that were removed. Figure 156 represents all the cracks recorded during this specimen test. Figure 157 represents the cracks on the bottom sides of the specimen, in the missing column area at the collapsed load. Strain Gauges 3, 4, 5, 6, 11, 12, 13, and 14 located in the missing column area of the specimen recorded a strain of (-0.0025, -0.0044, -0.0001, -0.0006, -0.0015, -0.0046, 0.0039, and -0.0001 in/in) at collapsed load. The specimen developed a total of 11 cracks during this testing process.

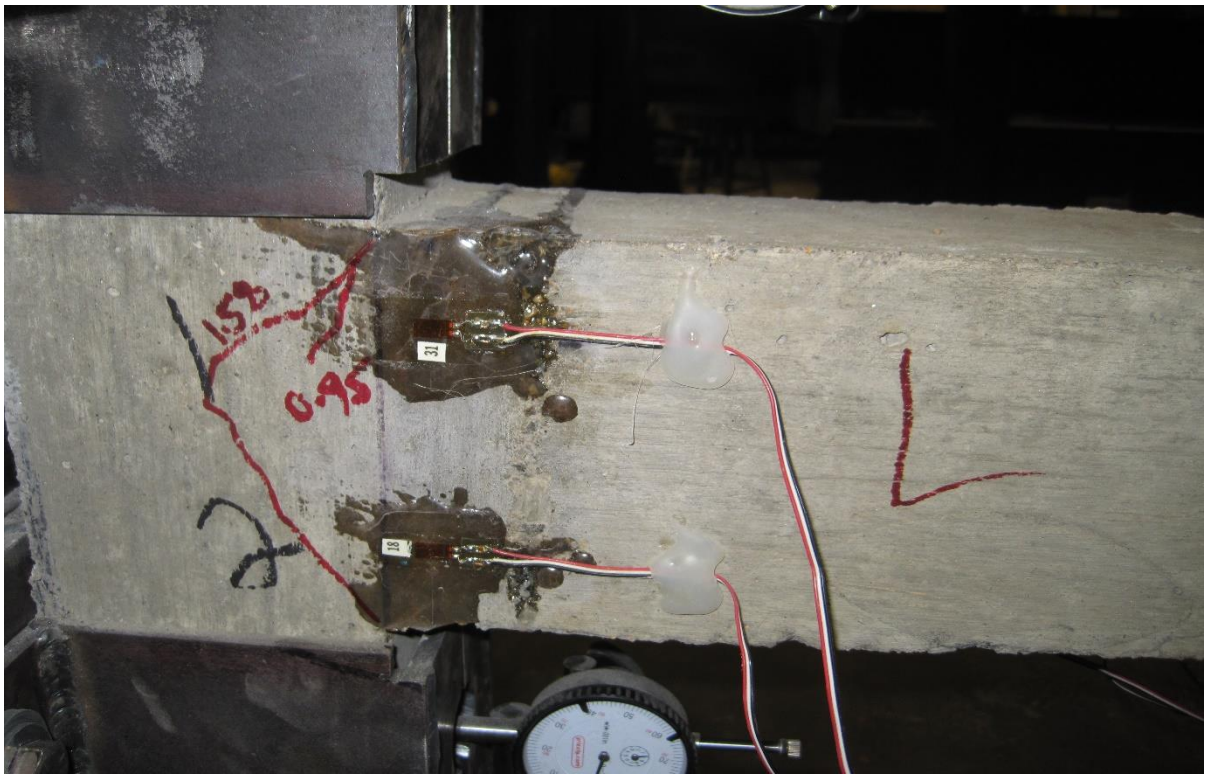

Figure 153. Left Support Crack Pattern for Sub-assemblage S2-1

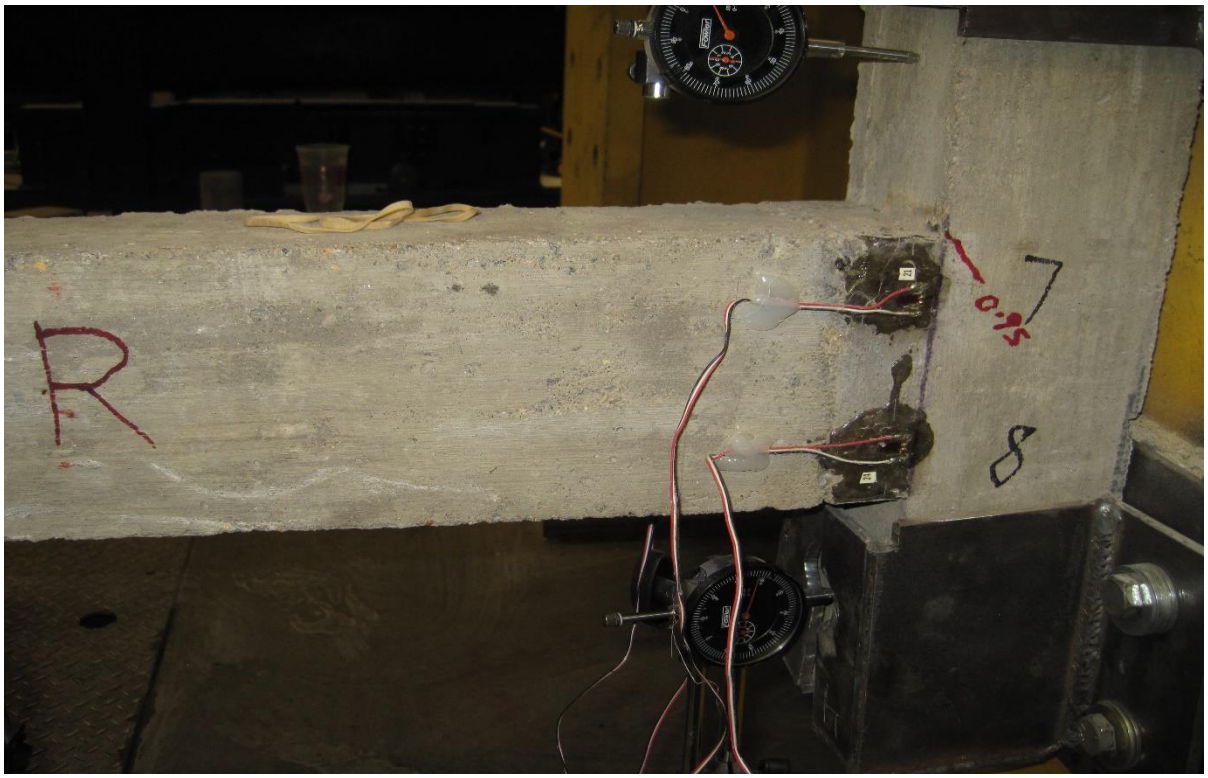

Figure 154. Right Support Crack Pattern for Sub-assemblage S2-1

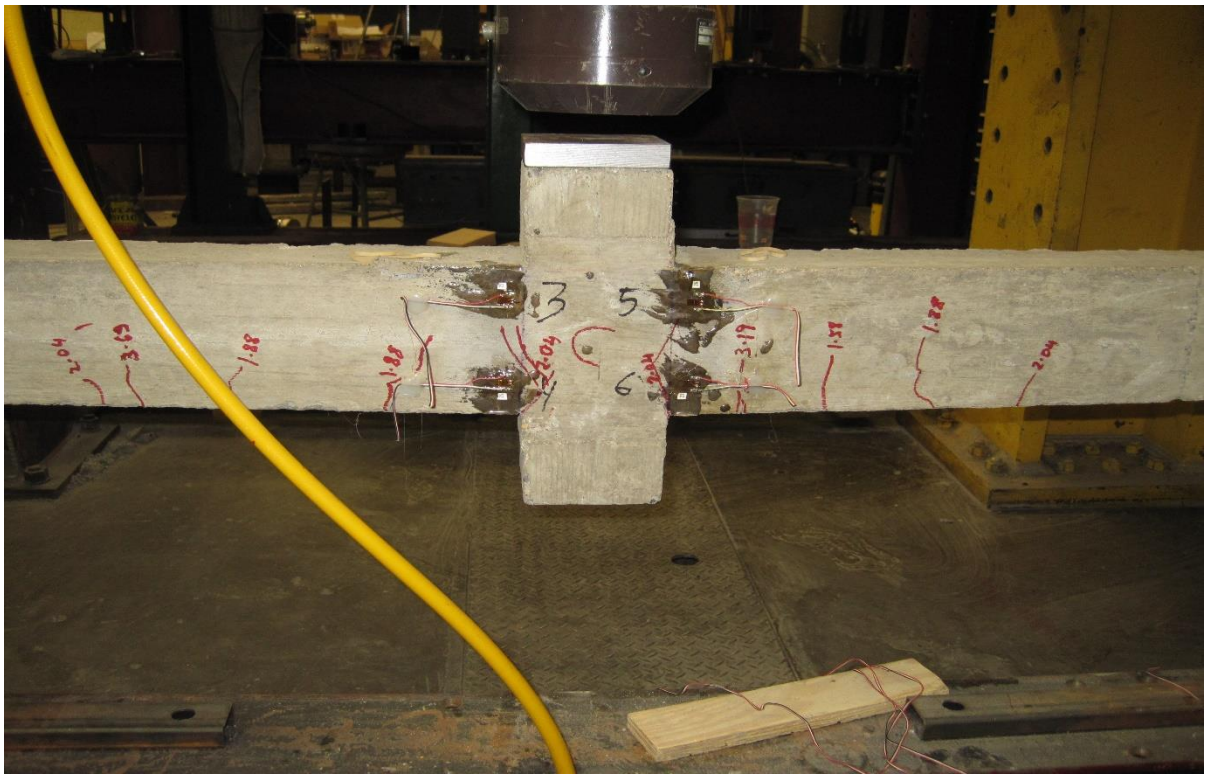

Figure 155. Missing Column Crack Pattern at the Collapsed Load for Sub-assemblage S2-1

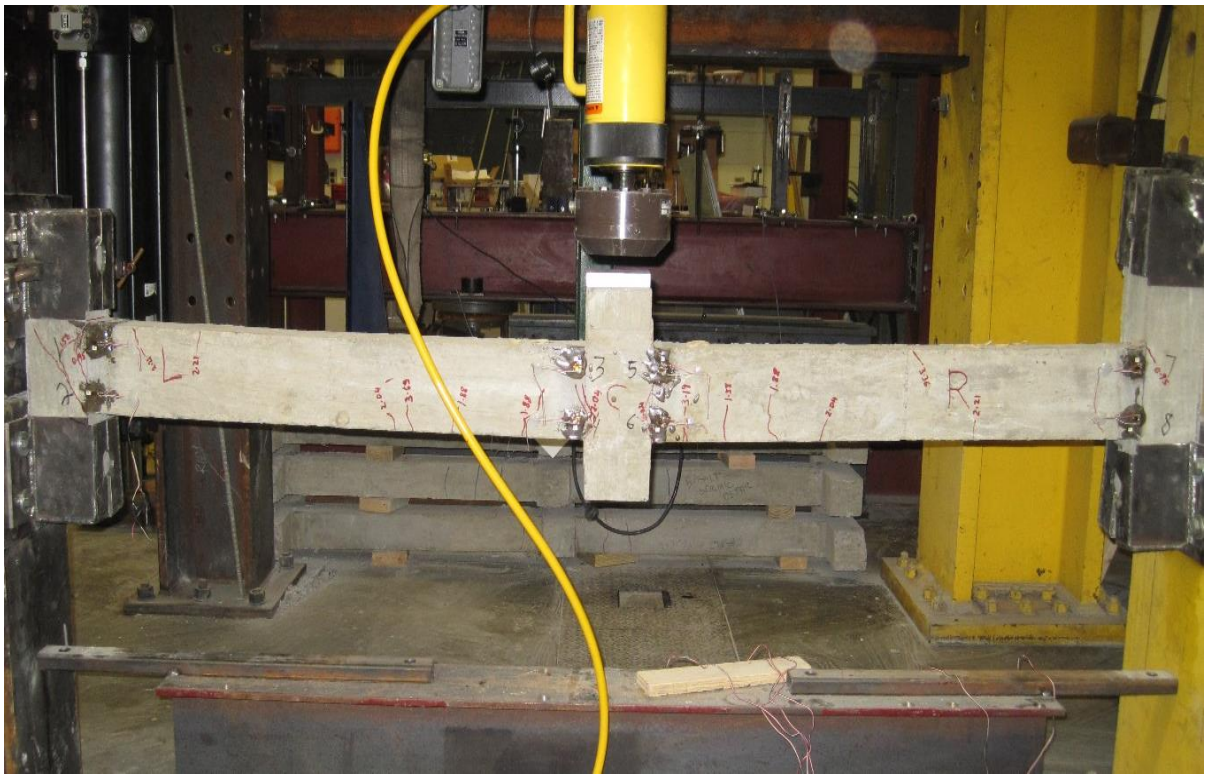

Figure 156. Crack Pattern at the Collapsed Load for Sub-assemblage S2-1

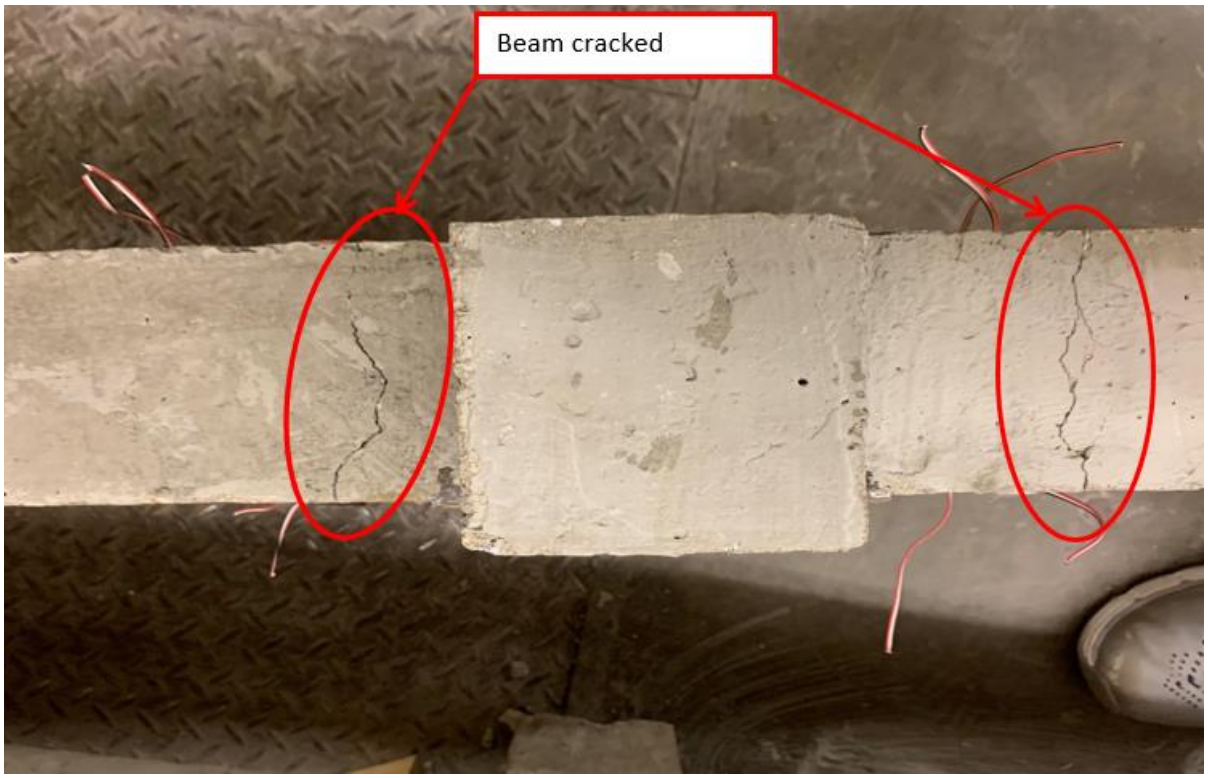

Figure 157. Underneath Crack Pattern in the Missing Column for Sub-assemblage S2-1

Specimen S2-2 developed the first crack in the center area around the removed column when load of 0.99 kips was applied, during this load the left fixed-end support developed a rotation of 0.16° (0.003 rad) and the right fixed-end support developed a rotation of 0.10° (0.002 rad). Strain gauges 4 and 6 are located in the missing column of the specimen recorded with a strain of (-0.0030 and -0.00029 in/in). Figure 158 illustrates a crack at the removed column area. The first cracks in each fixed-end support were when a load of 3.28 kips was applied, during this load the left fixed-end support developed a rotation of 0.48° (0.009 rad) and the right fixed-end support developed a rotation of 0.47° (0.008 rad). Strain Gauges 1 and 9 are located in the left fixed-end support of the specimen recorded a strain of -0.0001 and 0.0000 in/in. Strain gauges 7 and 15 are located in the right fixed-end support of the specimen recorded a strain of -0.0007 and -0.0005 in/in. Figures 159 and 160 represent the first crack developed at each fixed-end support when load of 3.28 kips was applied. Figure 161 illustrates all the cracks that were developed around

the column that was removed. Figure 162 illustrates all the cracks developed by this specimen during this test. Figure 163 represents the cracks on the bottom sides of the specimen, in the missing column area at the collapsed load. Strain Gauges 3, 4, 5, 6, 11, 12, 13, and 14 located in the missing column area of the specimen recorded a strain of -0.0408, 0.0, -0.0037, -0.0007, -0.0004, -0.0016, -0.0043, and -0.0013 in/in at collapsed load. The specimen developed a total of 21 cracks during this testing process.

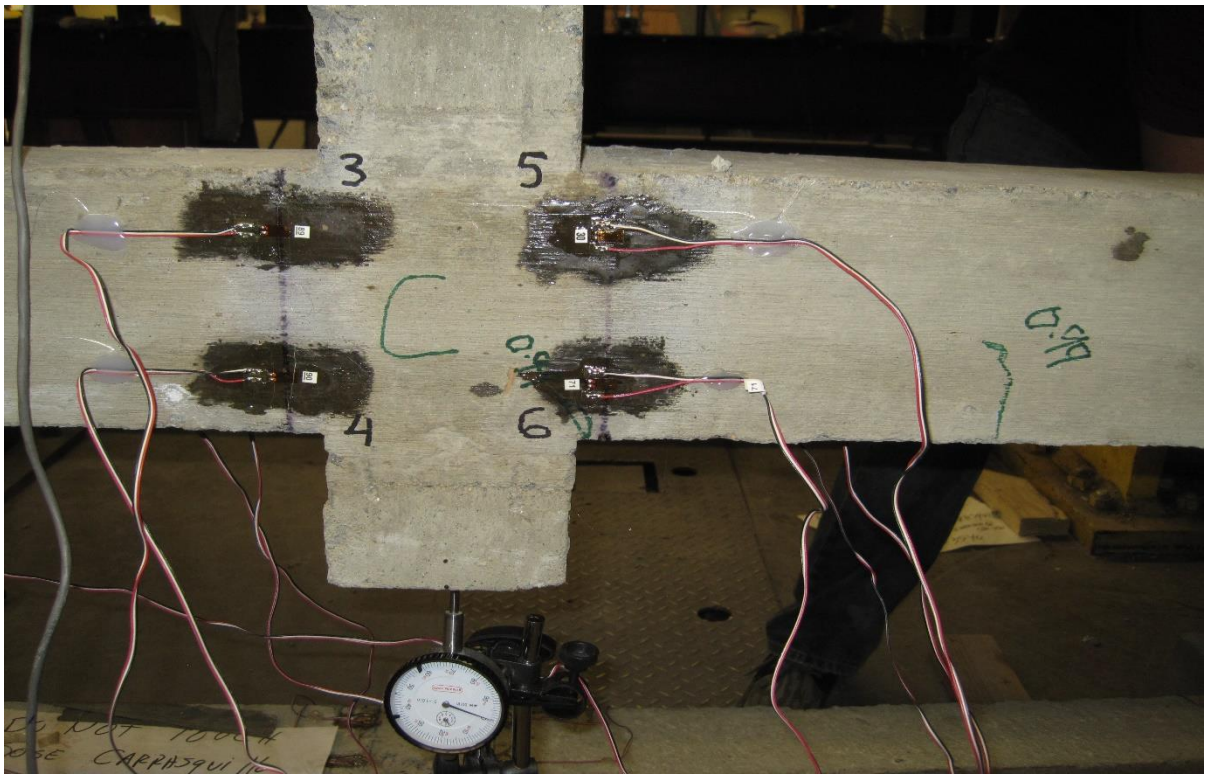

Figure 158. Crack Pattern on the Missing Column for Sub-assemblage S2-2

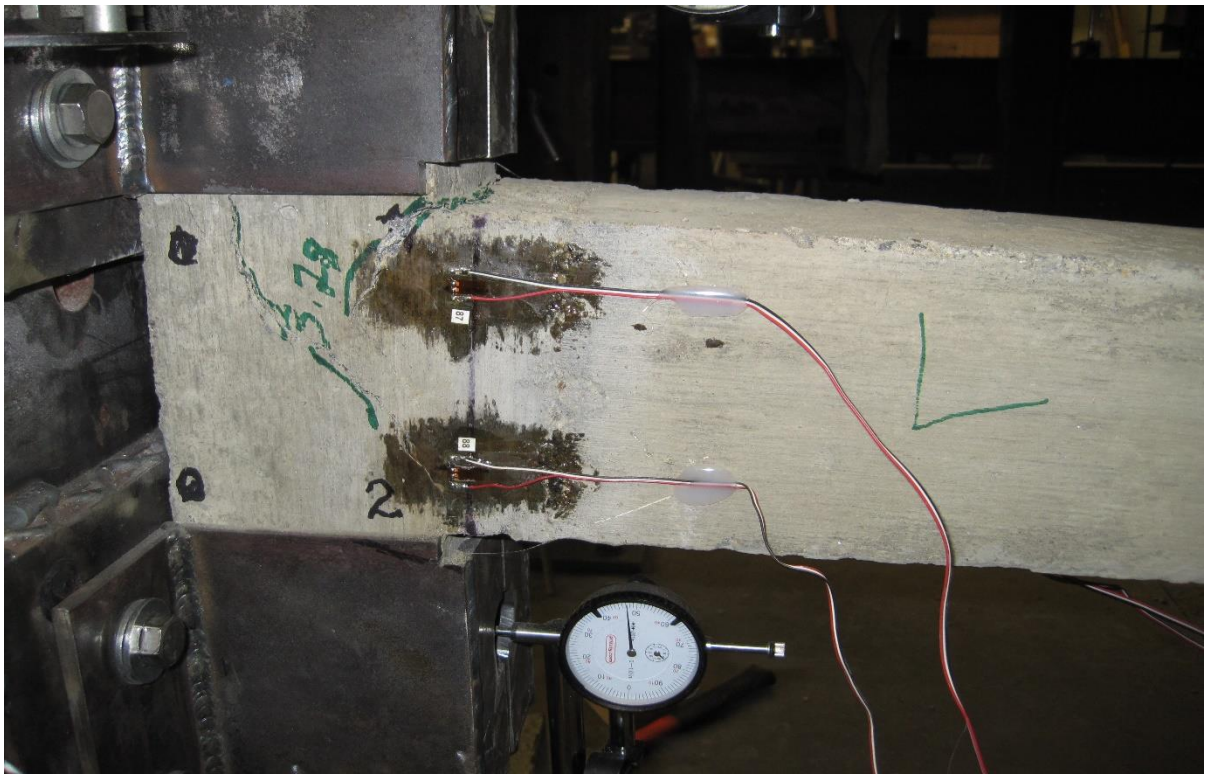

Figure 159. Crack Pattern on the Left Support for Sub-assemblage S2-2

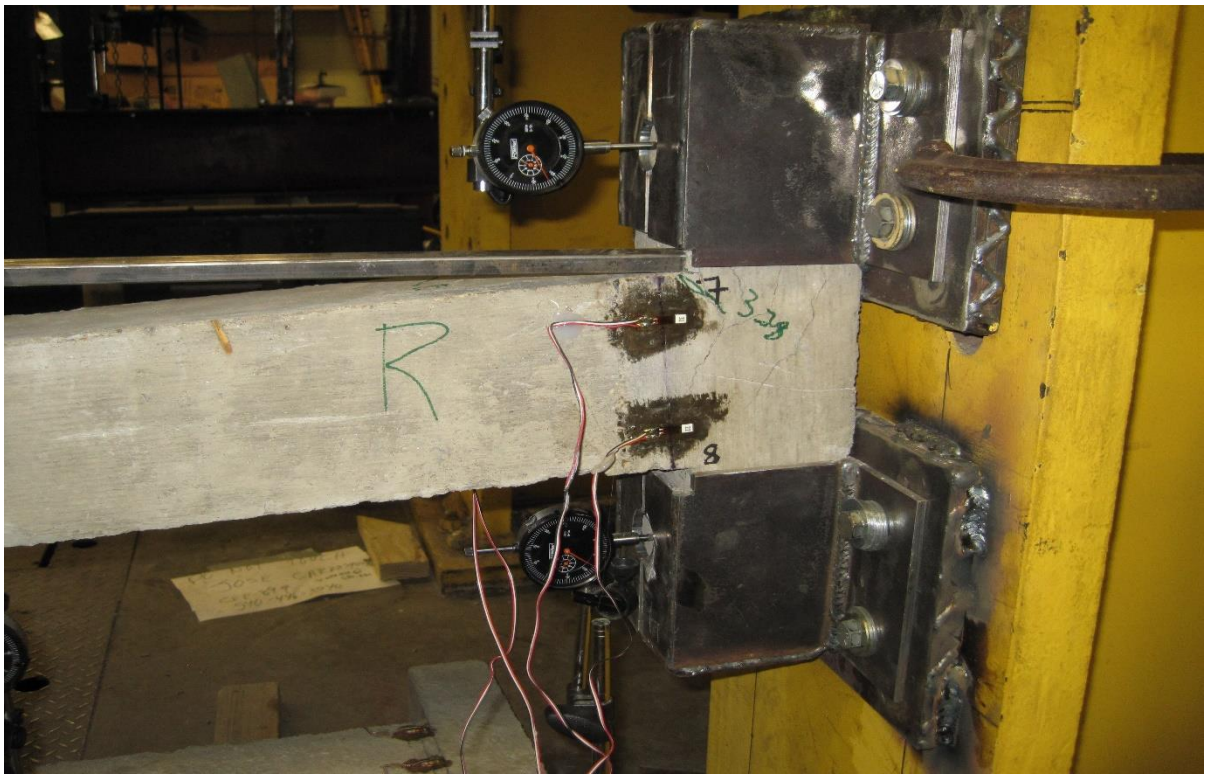

Figure 160. Crack Pattern on the Right Support for Sub-assemblage S2-2

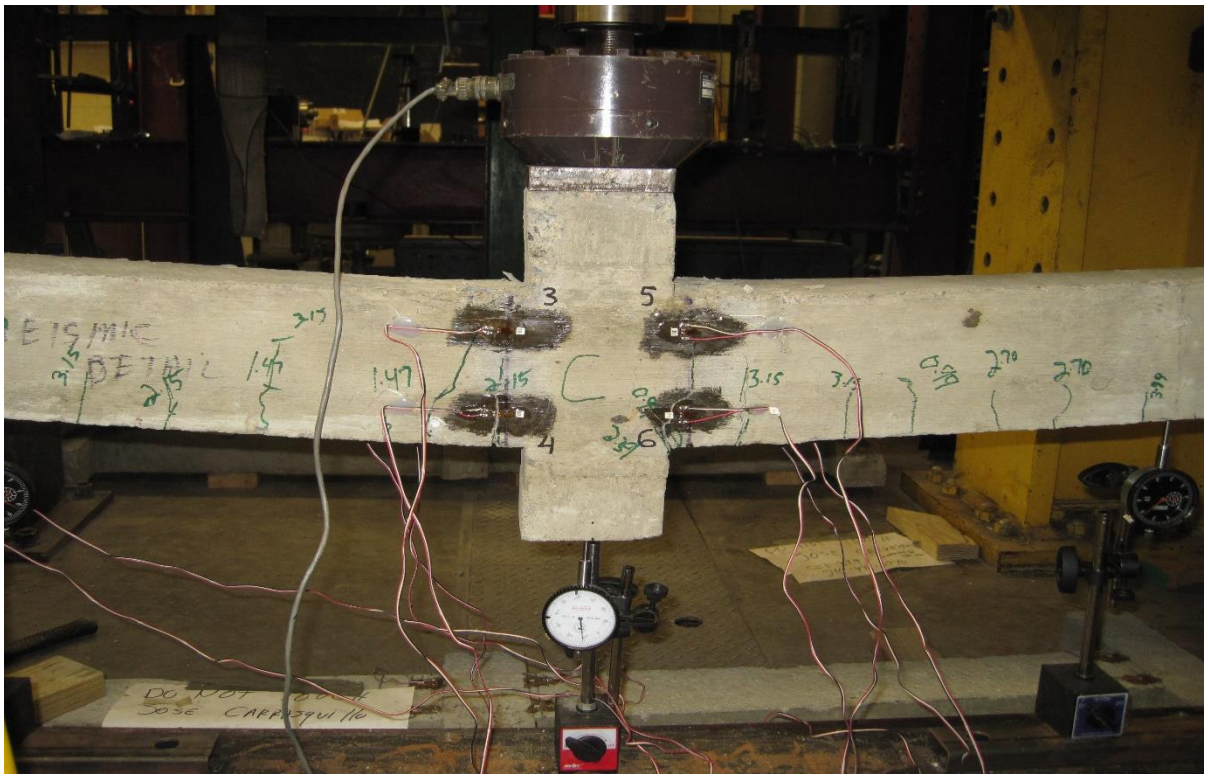

Figure 161. Missing Column Crack Pattern at the Collapsed Load for Sub-assemblage S2-2

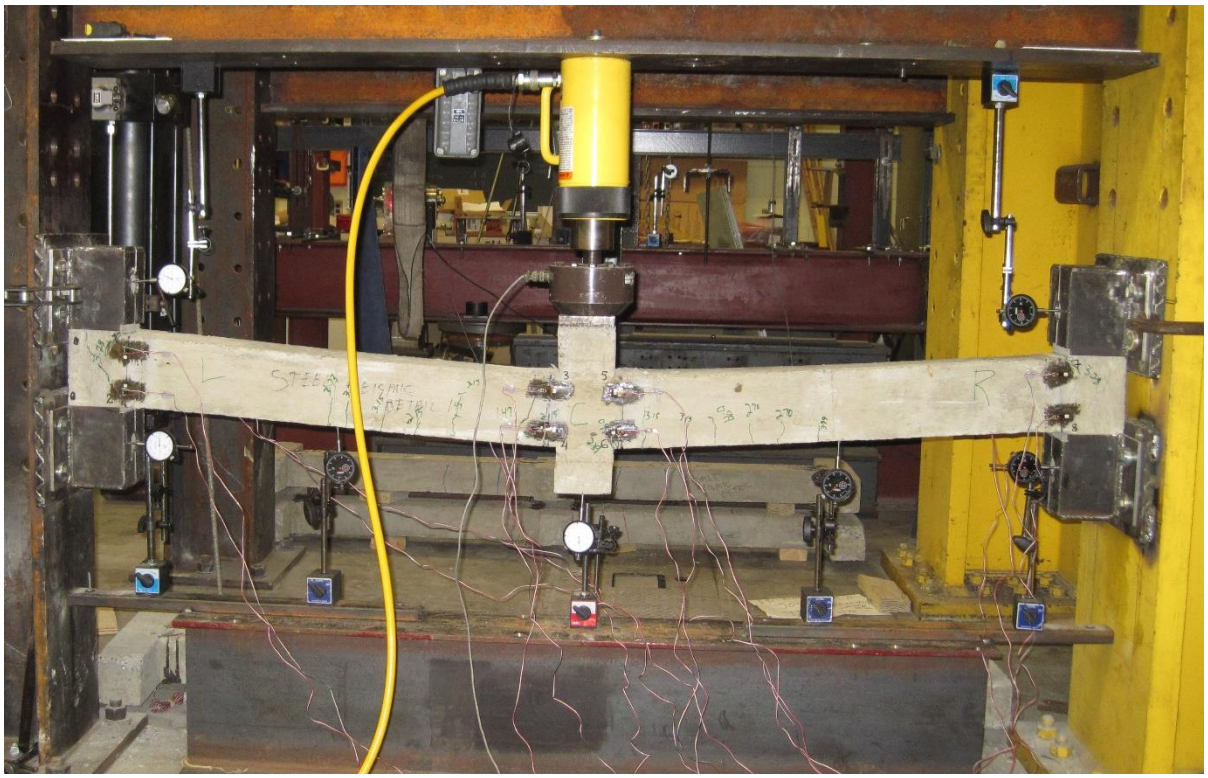

Figure 162. Crack Pattern at the Collapsed Load for Sub-assemblage S2-2

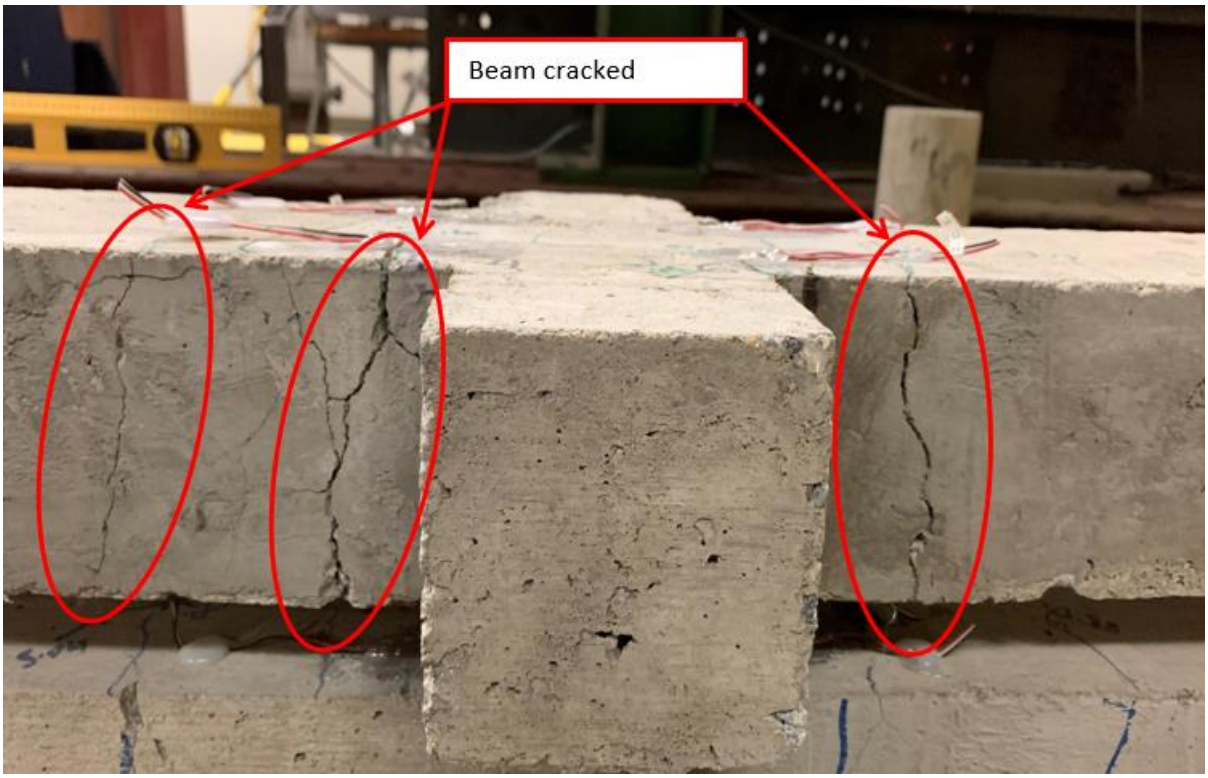

Figure 163. Underneath Crack Pattern in the Missing Column for Sub-assemblage S2-2

Specimen B2-1 developed five cracks at the same load in both fixed-end supports and in the missing column when load of 0.81 kips was applied, during this load the left fixed-end support developed a rotation of 0.13° (0.002 rad) and the right fixed-end support developed a rotation of 0.31° (0.006 rad). Strain gauges 1 and 9 are located in the left fixed-end support of the specimen recorded a strain of (0.0001 and 0.0019 in/in). Strain gauges 7, 15, 8, and 16 are located in the right fixed-end support of the specimen recorded a strain of (-0.0016, -0.0006, -0.0050, and -0.0004 in/in). Strain Gauges 4, 6, 12, and 14 located in the missing column area of the specimen recorded a strain of (0.0004, -0.0008, -0.0007, and -0.0069 in/in). Figure 164 illustrates the left support crack and Figure 165 illustrates the crack in the right support. Figure 166 illustrates cracks and concrete crushed at the removed column area. Figure 167 illustrates all cracks in the entire beam. Figure 168 illustrates that beam was separated from the column in the left semi-rigid support. Figure 169 illustrates that the beam was separated from the column in the semi-

rigid right support. Figure 170 illustrates the concrete crushed in the top side of the beam next to the column that was removed when load of 4.80 kips was applied, during this load the left fixed-end support developed a rotation of 0.51° (0.009 rad) and the right fixed-end support developed a rotation of 0.92° (0.016 rad). Figure 171 represents the cracks on the bottom sides of the specimen, in the missing column area at the collapsed load. Strain Gauges 3, 4, 5, 6, 11, 12, 13, and 14 located in the missing column area of the specimen recorded a strain of (-0.0034, 0.0003, -0.0022, -0.0008, -0.0006, -0.0010, -0.0042, and -0.0082 in/in) at collapsed. The specimen developed a total of 16 cracks during this testing process.

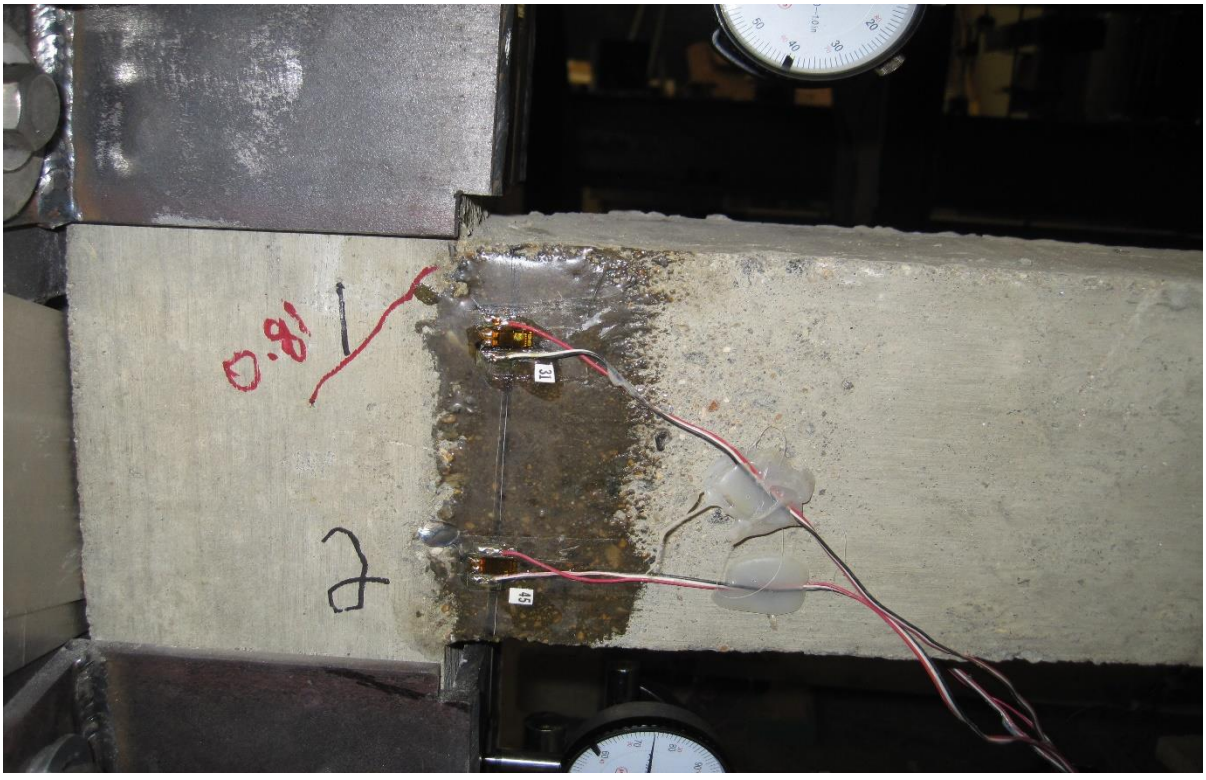

Figure 164. Left Support Crack Pattern for Sub-assemblage B2-1

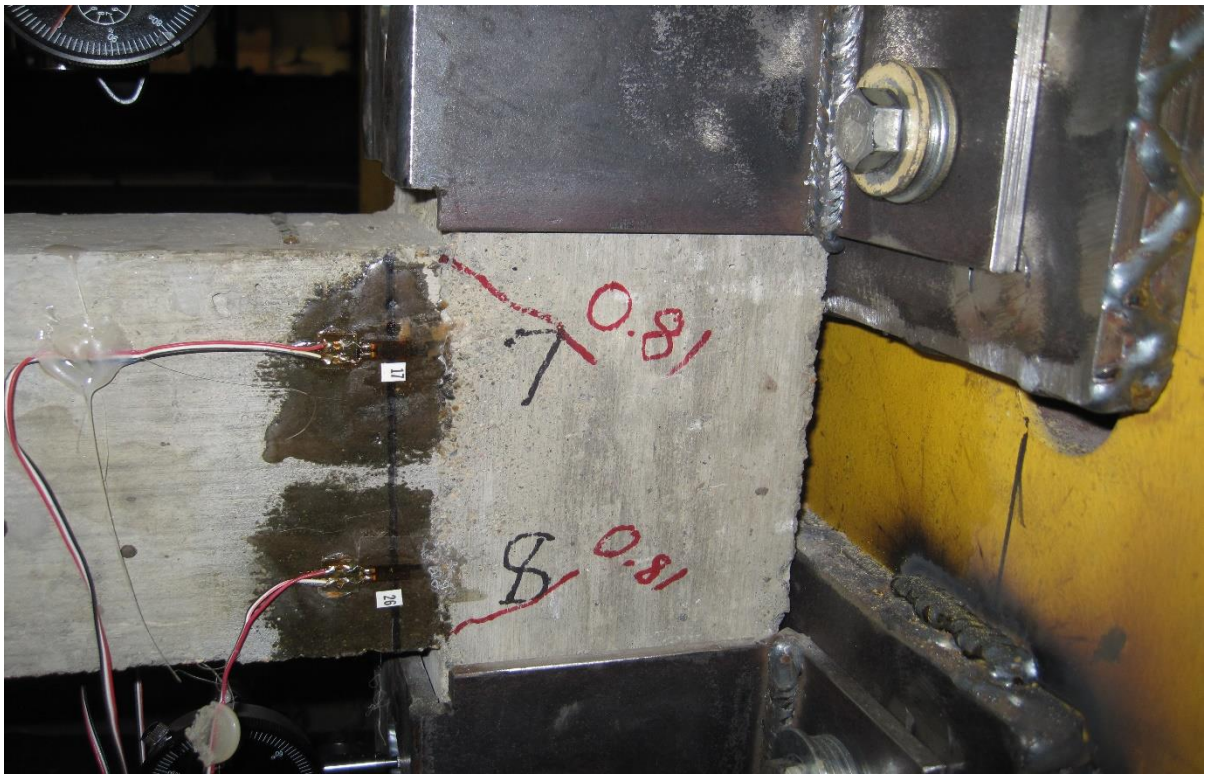

Figure 165. Right Support Crack pattern for Sub-assemblage B2-1

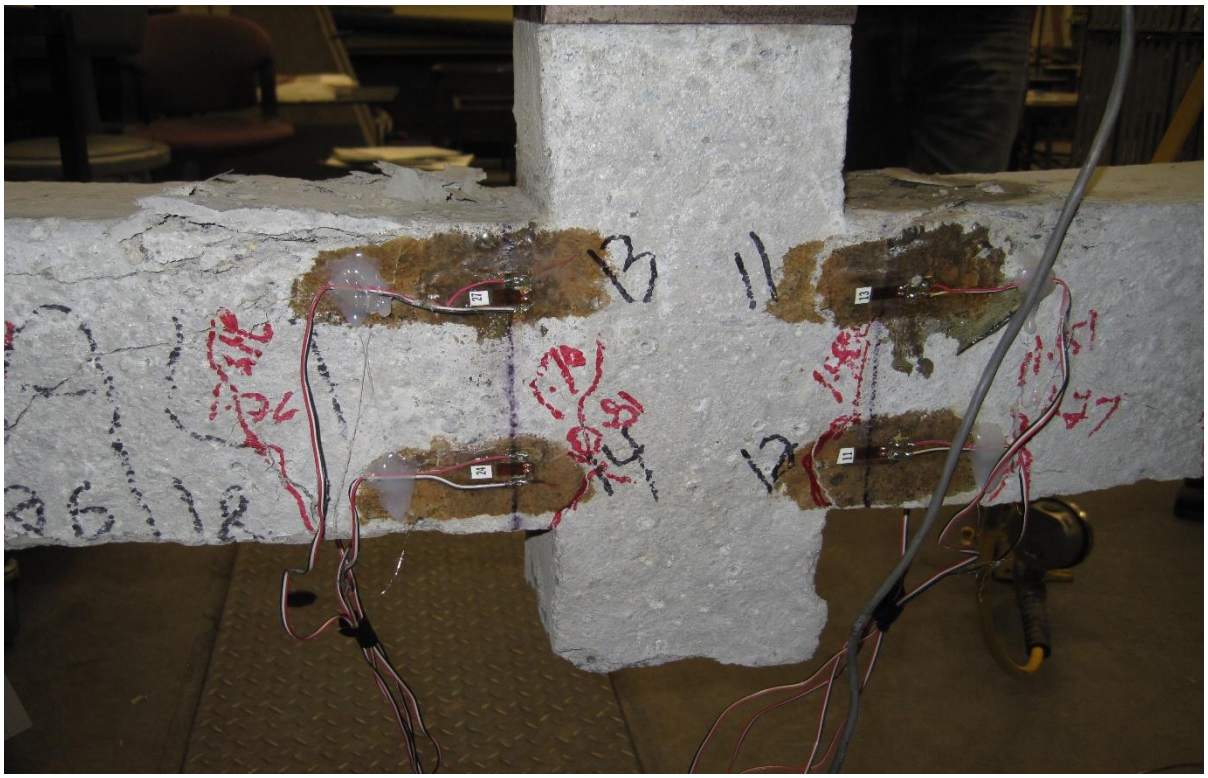

Figure 166. Missing Column Crack Pattern at the Collapsed Load for Specimen B2-1

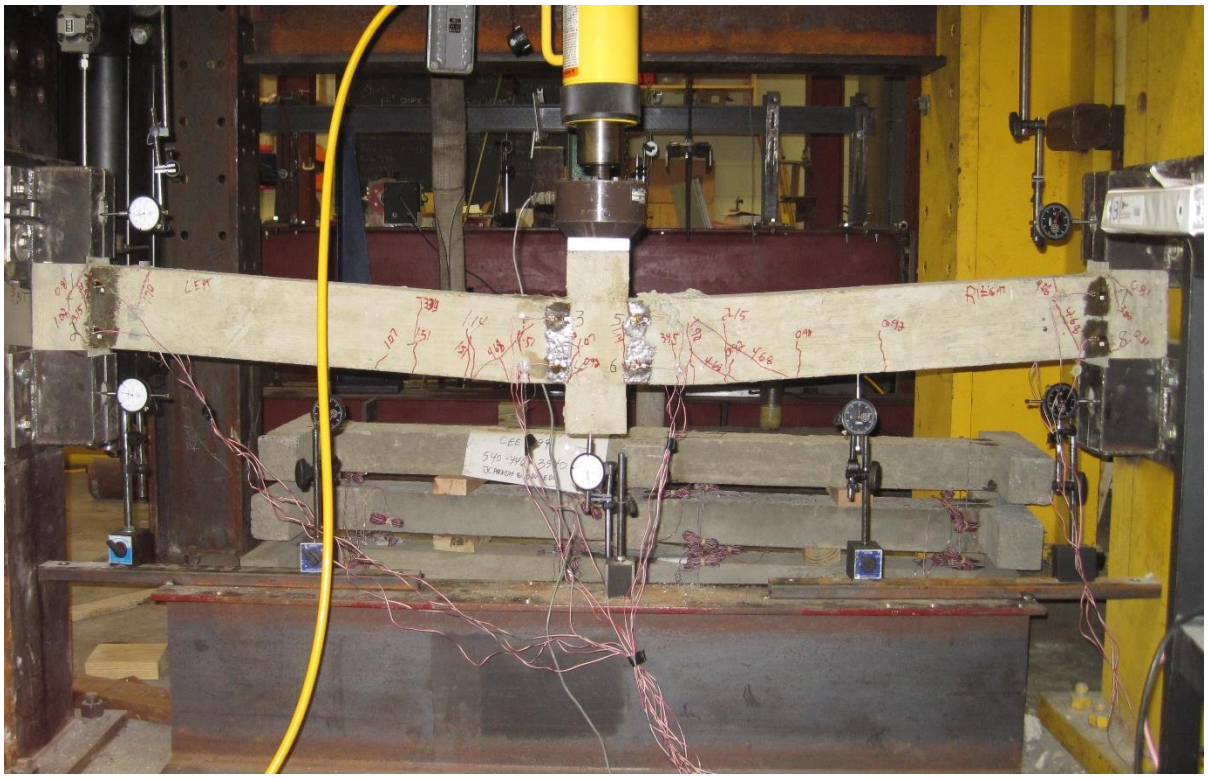

Figure 167. Crack Pattern at the Collapsed Load for Specimen B2-1

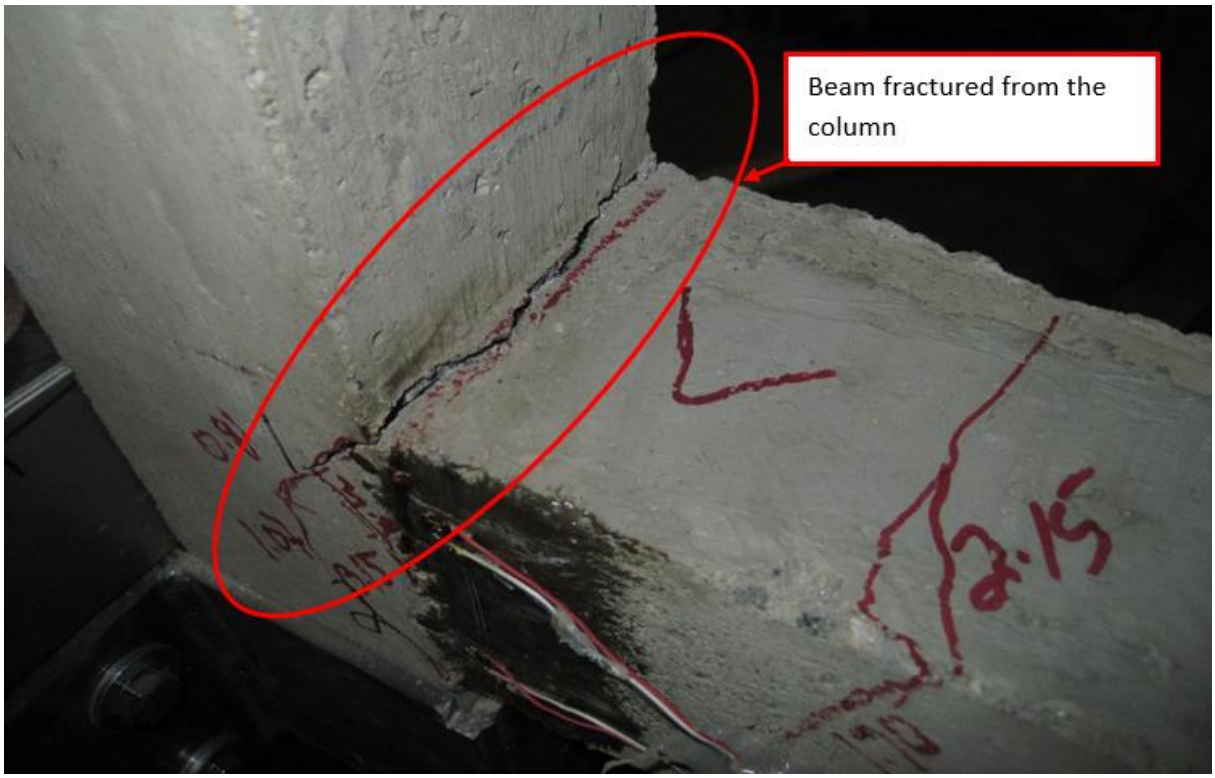

Figure 168. Left Support Beam Fractured from Column at the Collapsed Load for Specimen B2-1

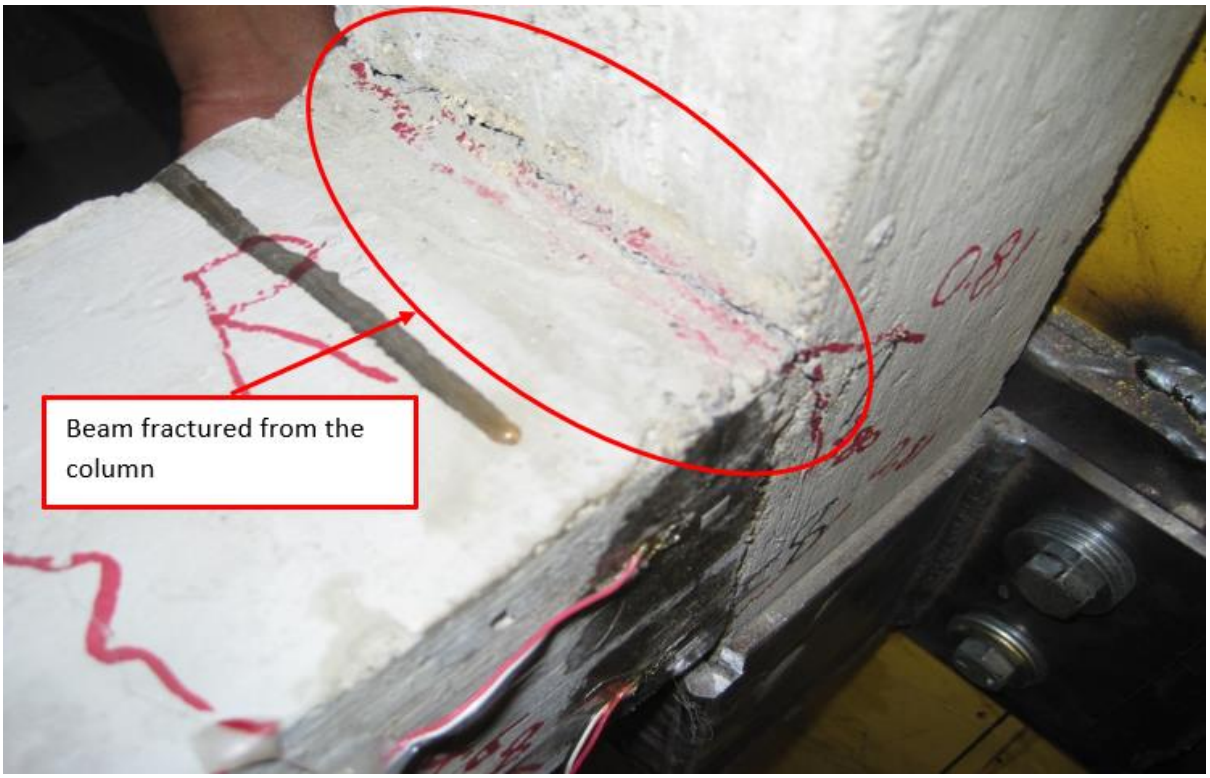

Figure 169. Right Support Beam Fractured from Column at the Collapsed Load for Specimen B2-1

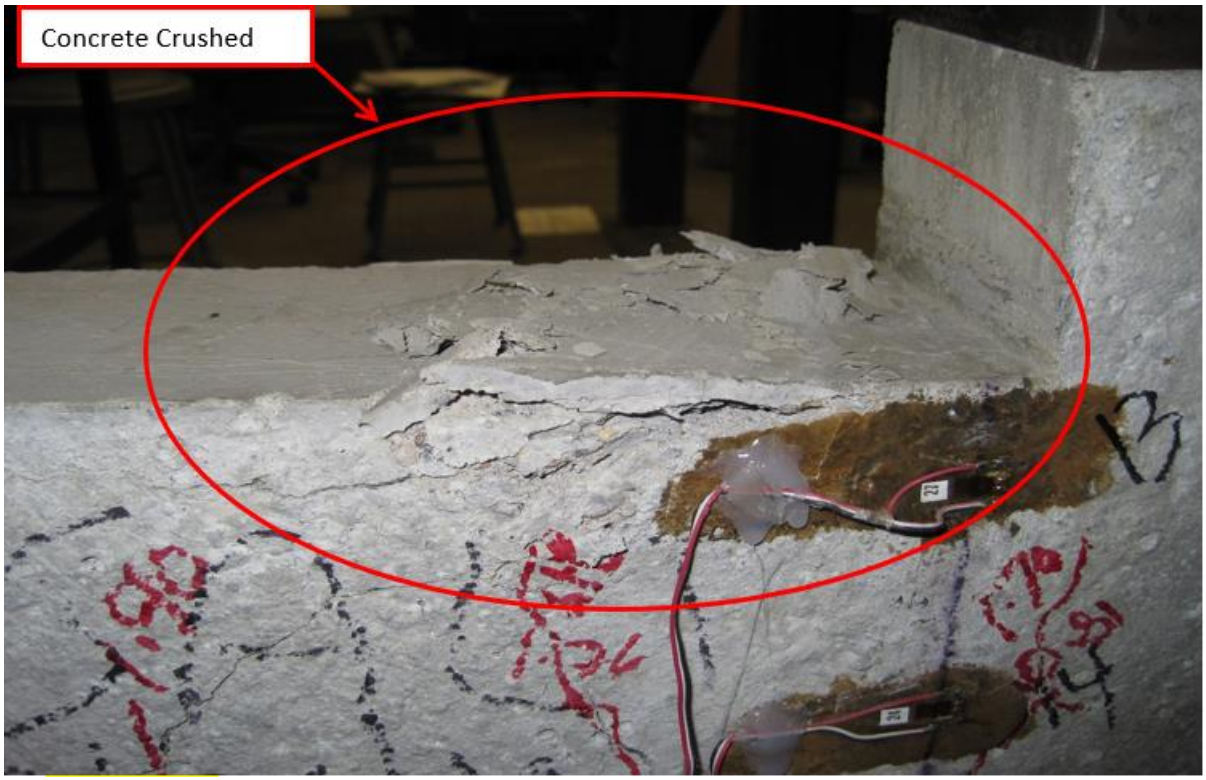

Figure 170. Right Support Concrete Crushed at Collapsed Load for Specimen B2-1

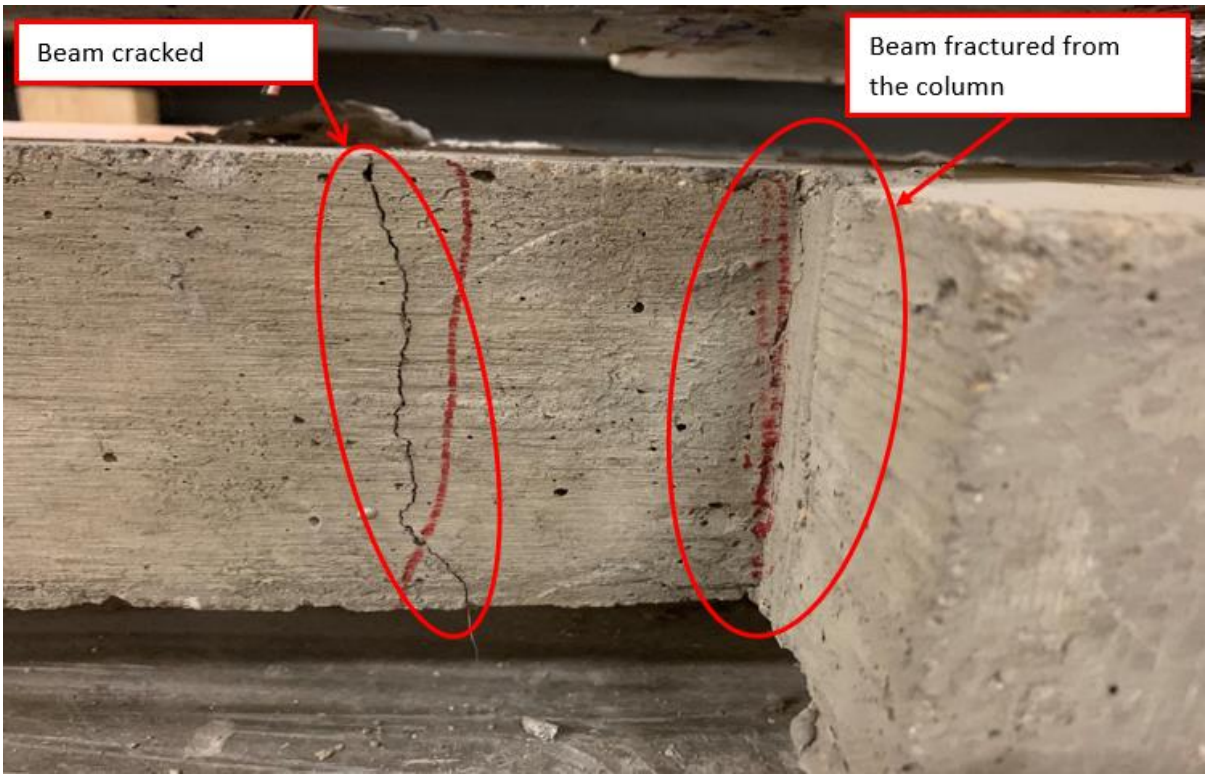

Figure 171. Underneath Crack Pattern in the Missing Column for Specimen B2-1

Specimen B2-2 developed the first crack in both fixed-end supports when load of 0.88 kips was applied, during this load the left fixed-end support developed a rotation of 0.35° (0.006 rad) and the right fixed-end support developed a rotation of 0.39° (0.007 rad). Strain Gauges 1 and 9 are located in the left fixed-end support of the specimen recorded a strain of (-0.0001 and -0.0032 in/in). Strain Gauges 7 and 15 are located in the right fixed-end support of the specimen recorded a strain of (-0.0003 and -0.0005 in/in). The first crack in the missing column occurred when a load of 1.84 kips was applied, during this load the left fixed-end support developed a rotation of 0.94° (0.0164 rad) and the right fixed-end support developed a rotation of 0.98° (0.017 rad). Strain gauges 4 and 6 located in the front of the specimen in the missing column area recorded strain of (-0.0005 and -0.0006 in/in). Strain Gauges 12 and 14 located in the back of the specimen in the missing column area recorded strain of (-0.0004 and -0.0006 in/in). Figure 172 illustrates the left fixed-end support crack and Figure 173 illustrates the crack in the area of the column that was removed. Figure 174 illustrates cracks in the removed column area. Figure 175

illustrates all cracks in the entire beam. Figure 176 illustrates that beam was separated from the column in the left support. Figure 177 illustrates that the beam was separated from the column in the right support. Figure 178 illustrates the concrete crunched in the top side of the beam next to the column that was removed when load of 4.80 kips was applied, during this load the left fixed-end support developed a rotation of 1.13° (0.020rad) and the right fixed-end support developed a rotation of 1.16° (0.020 rad). Figure 179 represents the cracks on the bottom sides of the specimen, in the missing column area at the collapsed load. Strain Gauges 3, 4, 5, 6, 11, 12, 13, and 14 located in the missing column area of the specimen recorded a strain of (-0.0027, -0.0005, -0.00, -0.0006, -0.0013, -0.0004, -0.0033, and -0.0007 in/in) at collapsed load. The specimen developed a total of 29 cracks during this testing process.

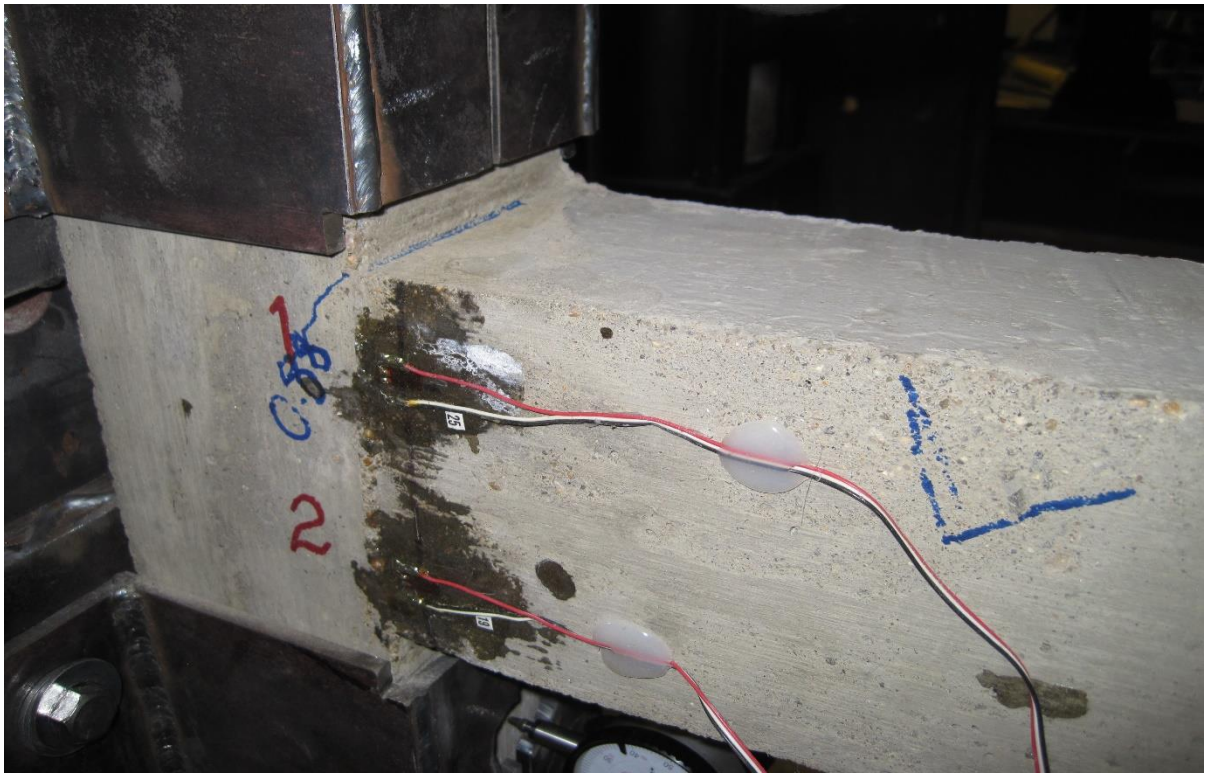

Figure 172. Left Support Crack Pattern for Specimen B2-2

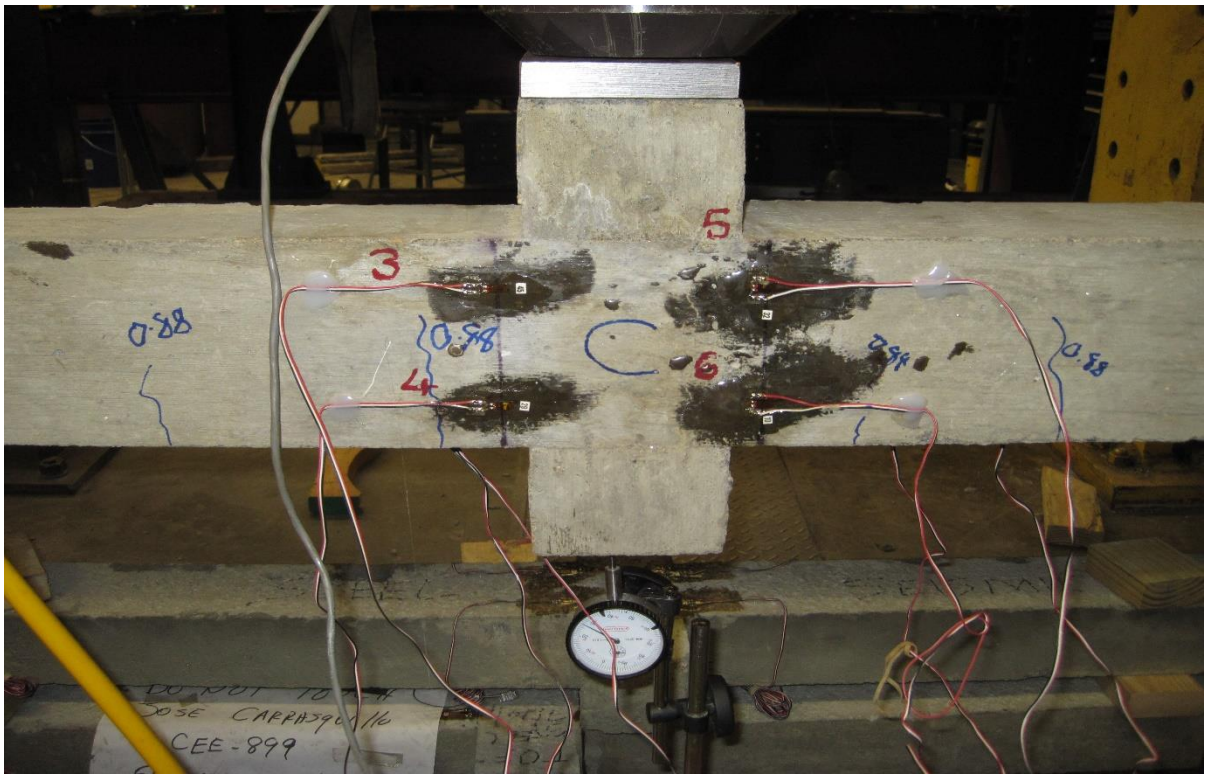

Figure 173. Crack Pattern on the Missing Column for Specimen B2-2

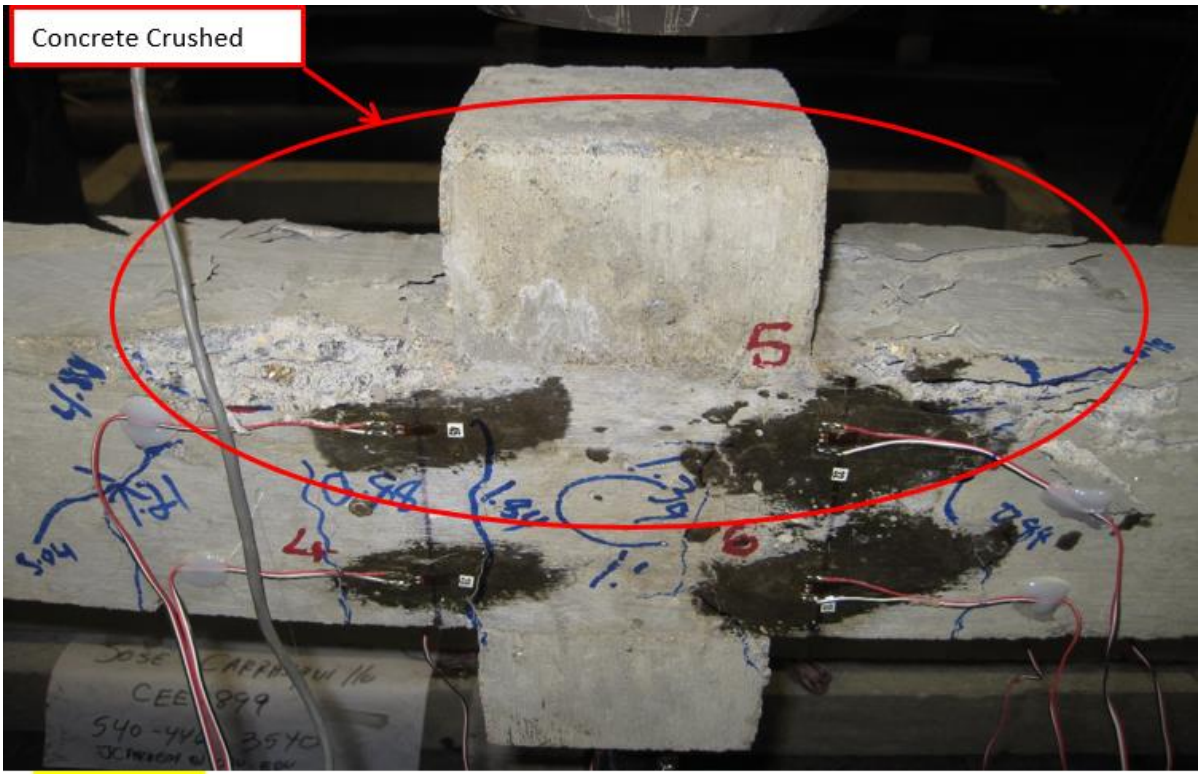

Figure 174. Missing Column Crack Pattern at the Collapsed Load for Specimen B2-2

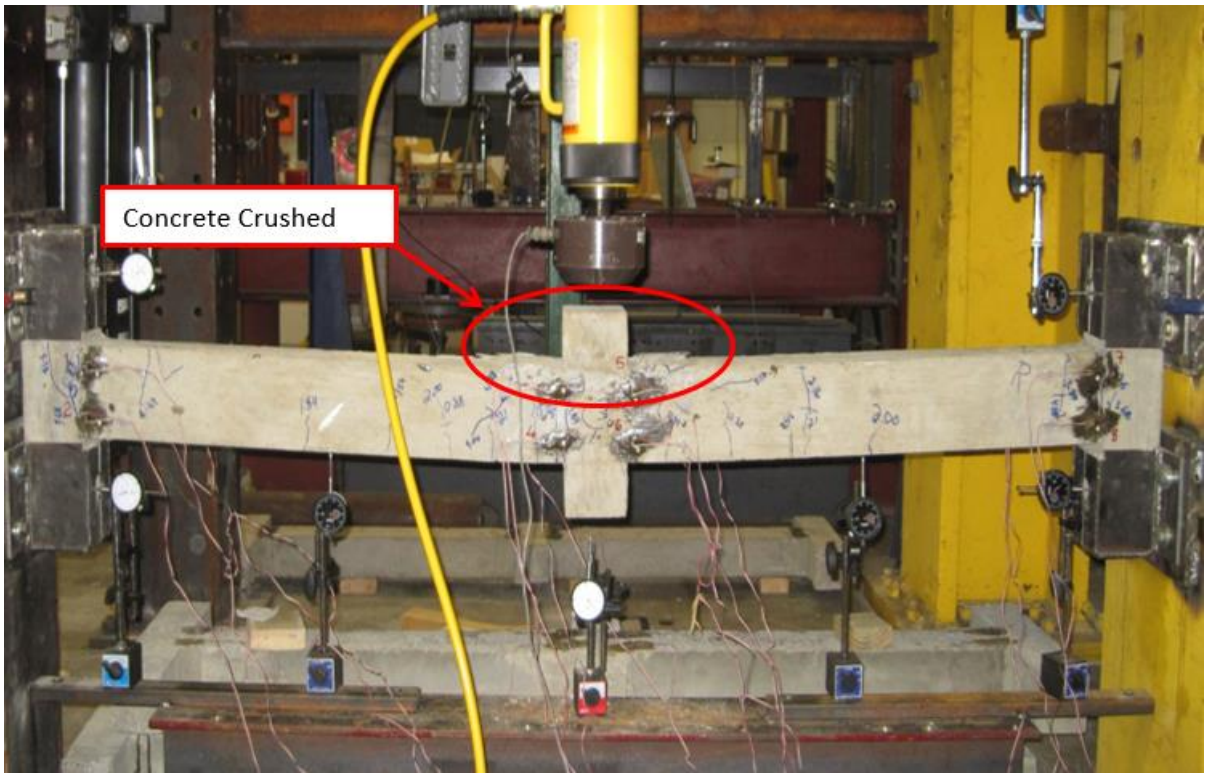

Figure 175. Crack Pattern at the Collapsed Load for Specimen B2-2

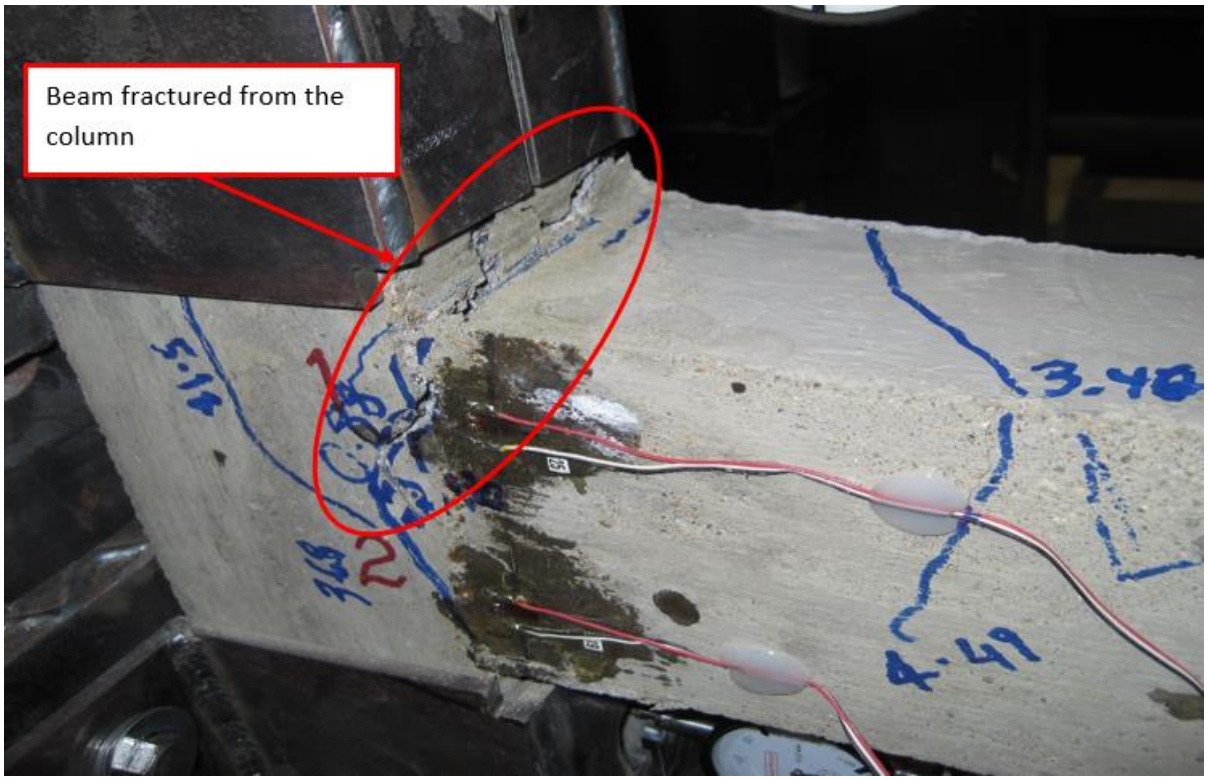

Figure 176. Left Support Beam Fractured from Column at the Collapsed Load for Specimen B2-2

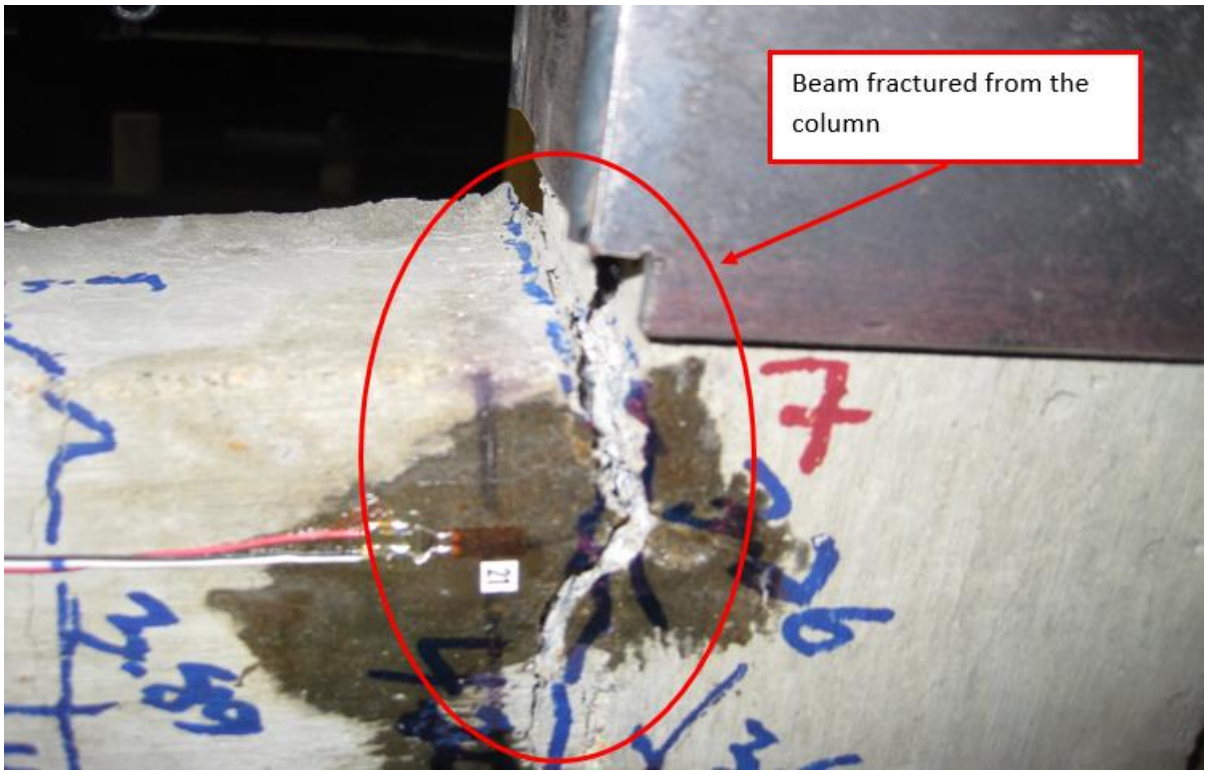

Figure 177. Right Support Beam Fractured from Column at the Collapsed Load for Specimen B2-2

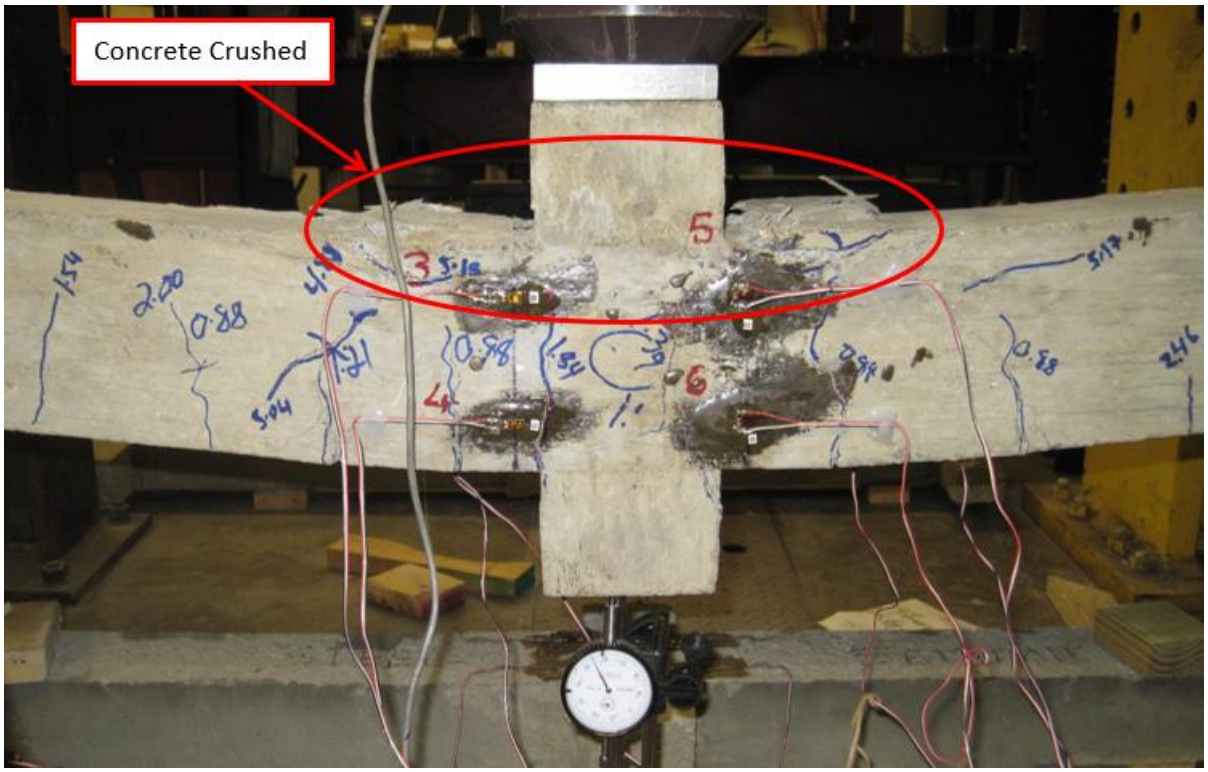

Figure 178. Missing Column Crack Pattern at the Collapsed Load for Specimen B2-2

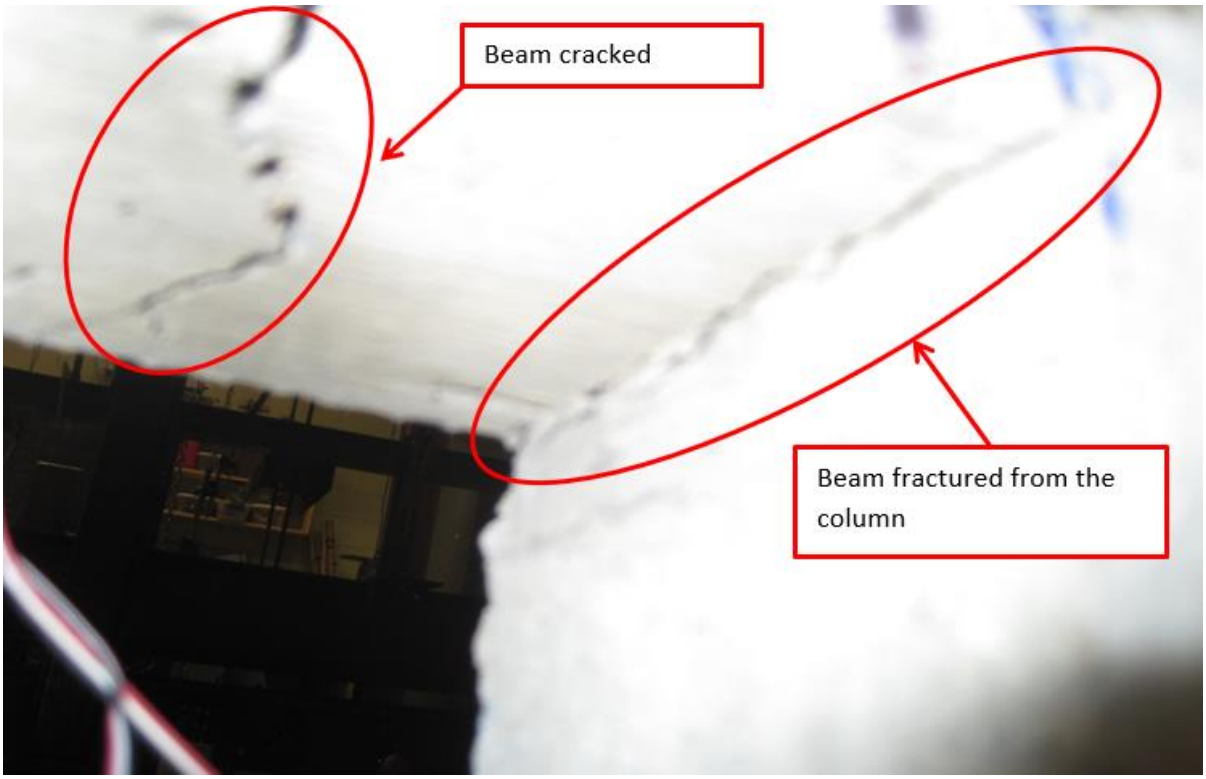

Figure 179. Underneath Crack Pattern in the Missing Column for Specimen B2-2

2.6.7 Beam Catenary Action

Under progressive collapse, the beam developed axial tension due to the large displacement in a double-span condition and the beam started to behave as a catenary system. It was found from previous research that the catenary action on the RC beam depends on beam geometry, length/height beam ratio (l/h), material properties, reinforcement detailing, axial restraint provided by surrounding structures, and axial extension in the sub-assemblage elements. The catenary action starts at the moment when the applied load decreases and increases again. Another way to determine the catenary action is at the moment that the beam axial force changes from compression to tension. The catenary action occurred when the catenary forces were transferred through the stirrups from the negative moment reinforcement to the positive moment reinforcement or vice-versa. Sarah Orton [20] found that the catenary effect does not occur until after the beam has reached its maximum extension, or until the deflection is equal to the height

of the beam. Due to all specimens tested during this research, negative and positive reinforcement was provided as continual reinforcement, the effect of the catenary action happened, but the catenary forces were not transferred using the stirrups between the negative and positive moment reinforcement. The catenary force was transferred using the positive moment reinforcement. Figure 180 graphically depicts the catenary action on the four specimens.

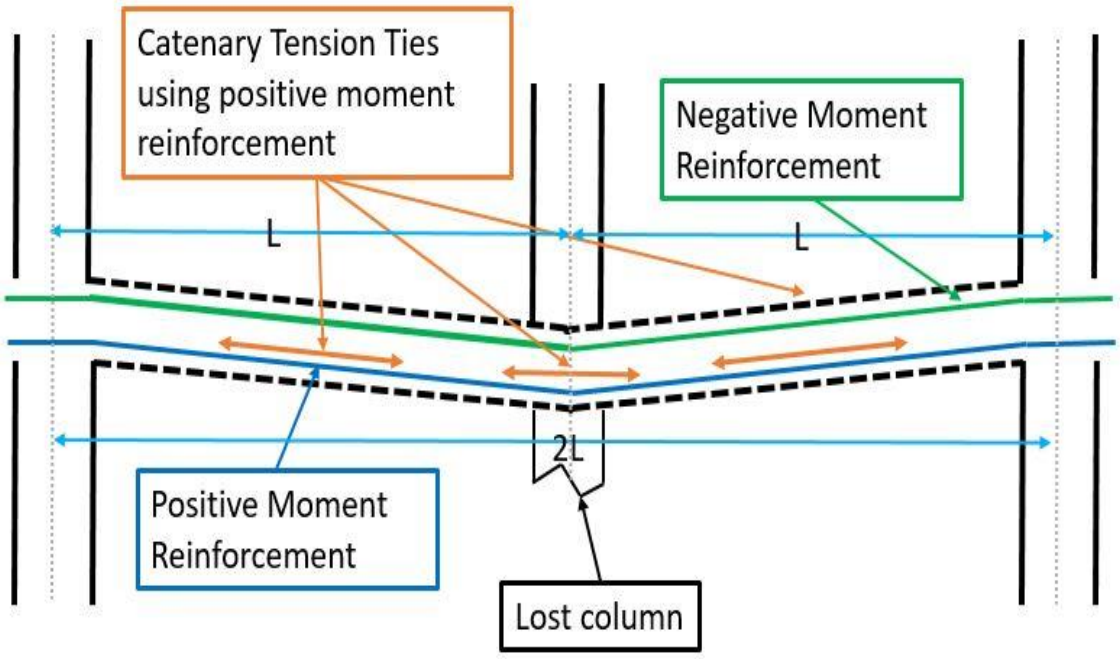

Figure 180. Catenary Forces Provided through the Positive Moment Reinforcement [20]

Figure 181 represents the small catenary action observed from the deflection graphic for the sub-assemblage S2-1. At an applied load of 5.63 kips the deflection drops to 0.95 inch, at applied load of 5.66 kips the deflection was 1.003 inches and at the applied load of 5.8 kips the

deflection recorded was 1.11 inches. This information was validated with the load-strain recorded during the experiment test. Figure 182 illustrates Strain Gauge 11 changed from tension to compression at applied load of 2.21 kips. Figure 183 illustrates Strain Gauge 10 changes from tension to compression at applied load of 5.75 kips. Strain Gauge 11 changed from compression to tension at applied load of 4.55 kips.

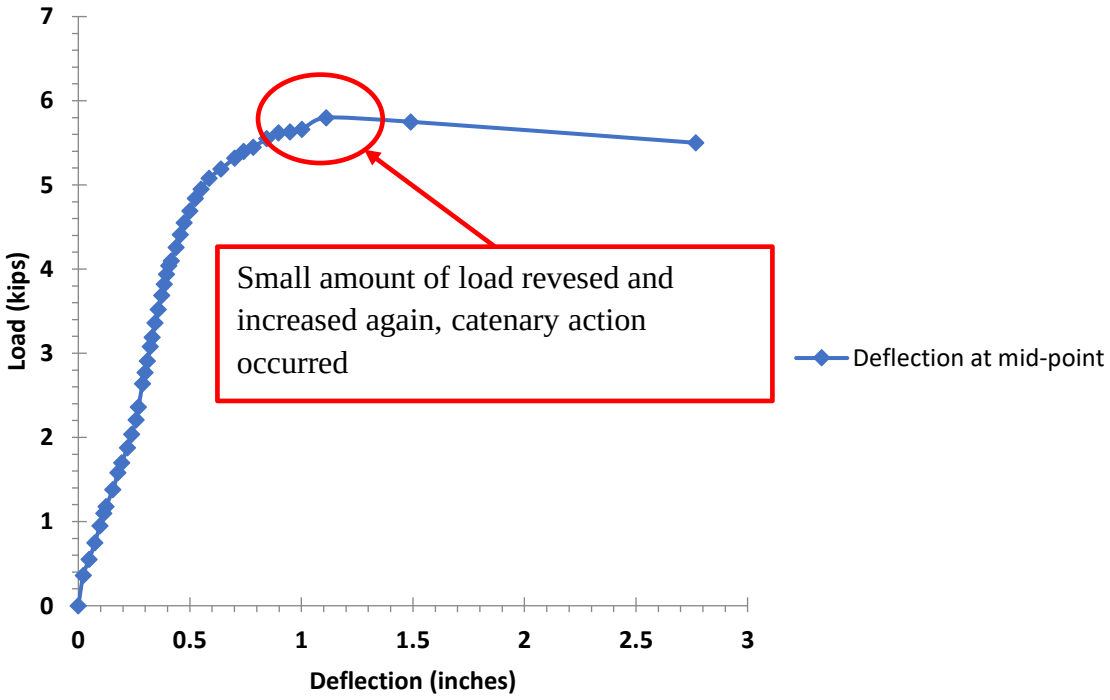

Figure 181. Catenary Action on Specimen S2-1

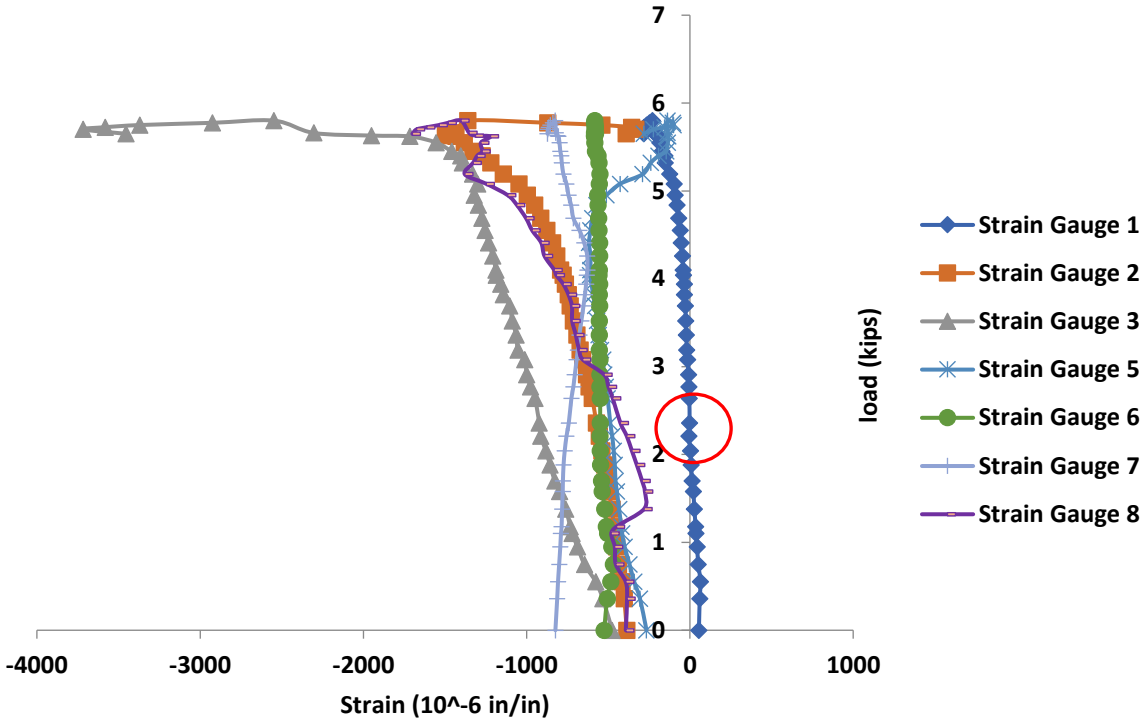

Figure 182. Catenary Action from Side Strain-load Relationships of Sub-assemblage S2-1

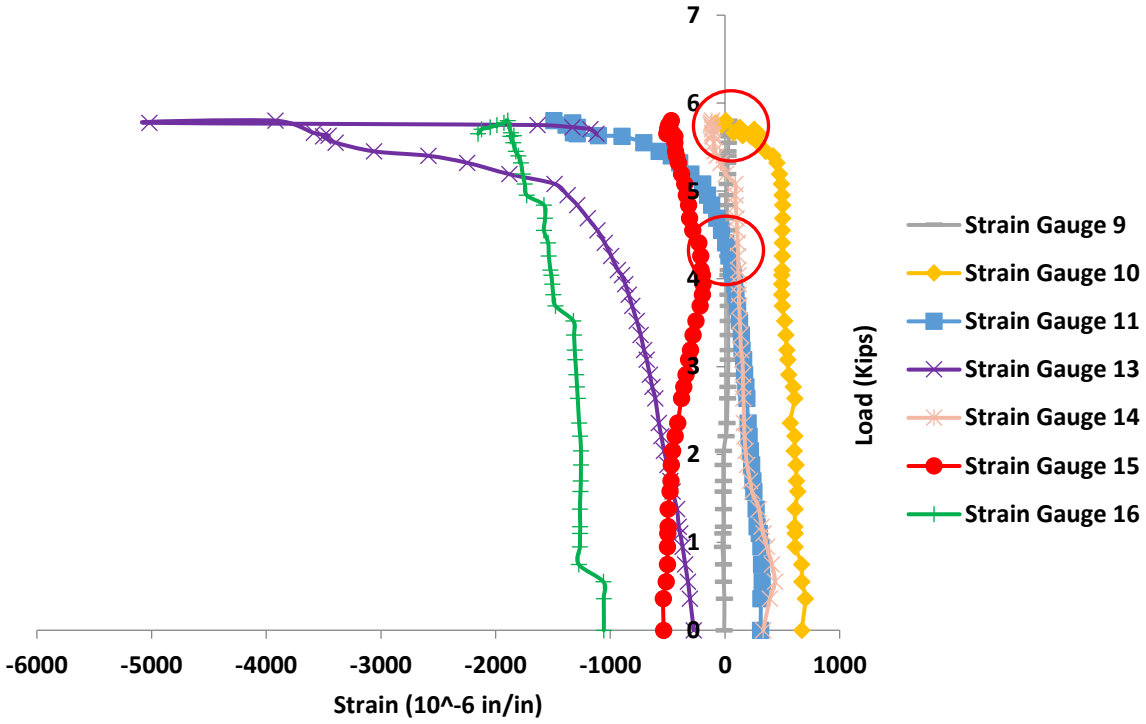

Figure 183. Catenary Action Rear Side Strain-load Relationships of Sub-assemblage S2-1

Figure 184 represents the small catenary action observed from the deflection graphic for the sub-assemblage S2-2. At an applied load of 5.37 kips the deflection drops to 1.47 inch, at applied load of 5.30 kips the deflection was 1.59 inches and at the applied load of 5.35 kips the deflection recorded was 1.68 inches. This information was validated with the load-strain recorded during the experiment test. Figure 185 illustrates Strain Gauge 2 changed from tension to compression at applied load of 2.39 kips. Strain Gauge 3 changed from tension to compression at applied load of 1.77 kips. Figure 186 illustrated Strain Gauge 11 changes from compression to tension at applied load of 5.27 kips.

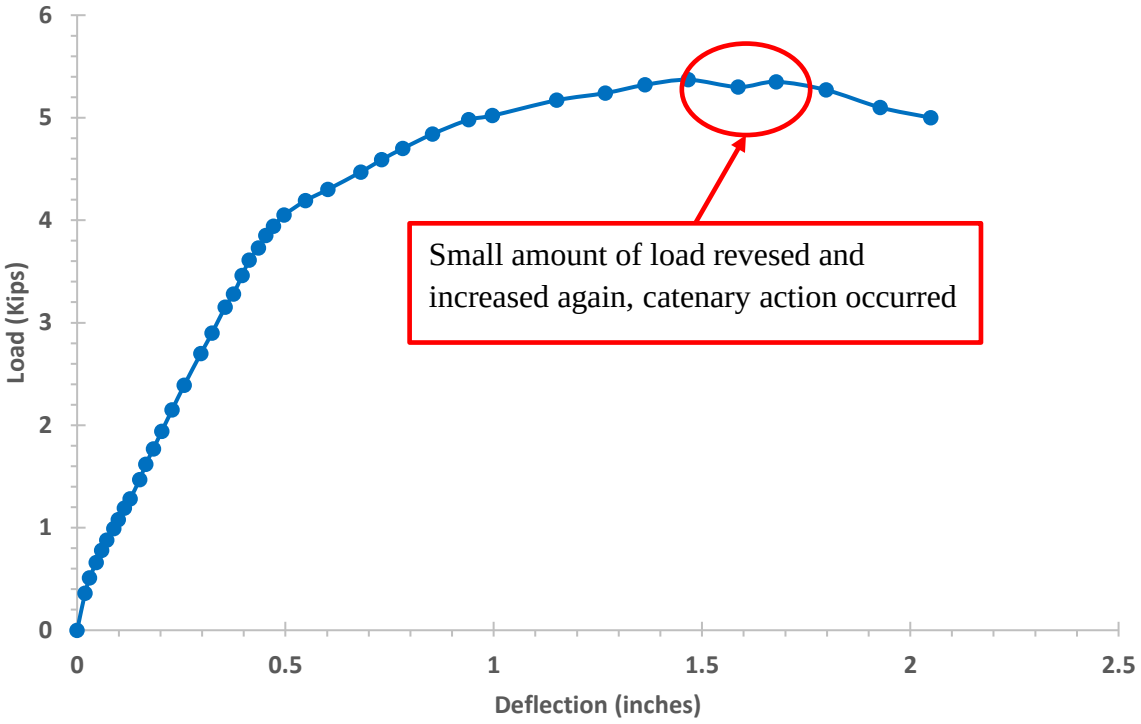

Figure 184. Catenary Action on Specimen S2-2

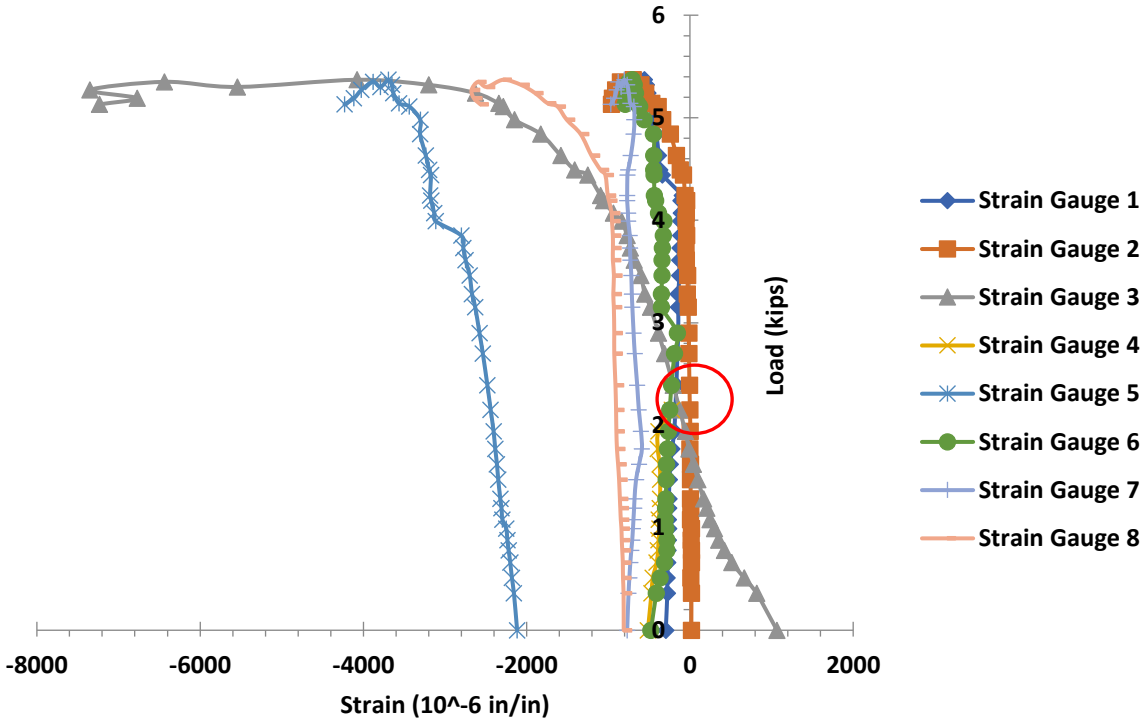

Figure 185. Catenary Action from Side Strain-load Relationships of Sub-assemblage S2-2

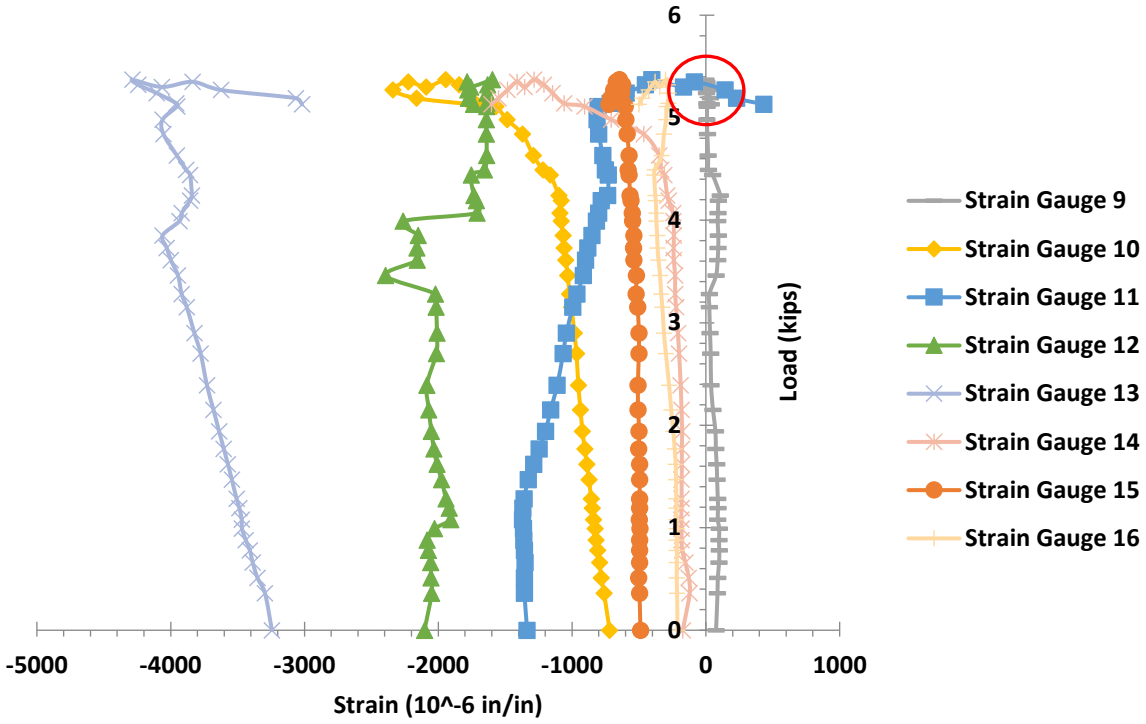

Figure 186. Catenary Action Rear Side Strain-load Relationships of Sub-assemblage S2-2

Figure 187 represents non-catenary action observed from the deflection graphic for the sub-assemblage B2-1. This information was validated with the load-strain recorded during the experiment test. Figure 188 illustrates Strain Gauge 1 changed from tension to compression at applied load of 4.64 kips. Strain Gauge 3 changed from tension to compression at applied load of 3.18 kips. Strain gauge 5 changed from tension to compression at an applied load of 4.08 kips. Figure 189 illustrates Strain Gauge 10 changes from tension to compression at applied load of 0.39 kips, also changed from compression to tension again at the applied load of 3.37 kips. Strain Gauge 11 changed from compression to tension at an applied load of 4.68 kips.

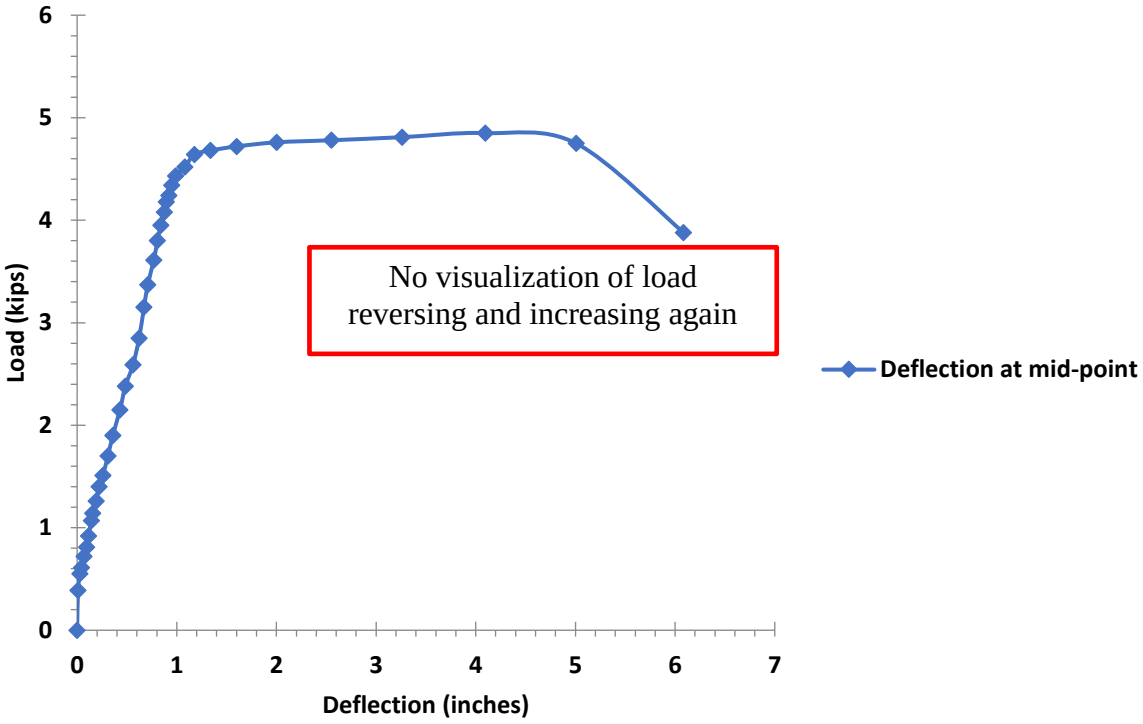

Figure 187. Catenary Action on Specimen B2-1

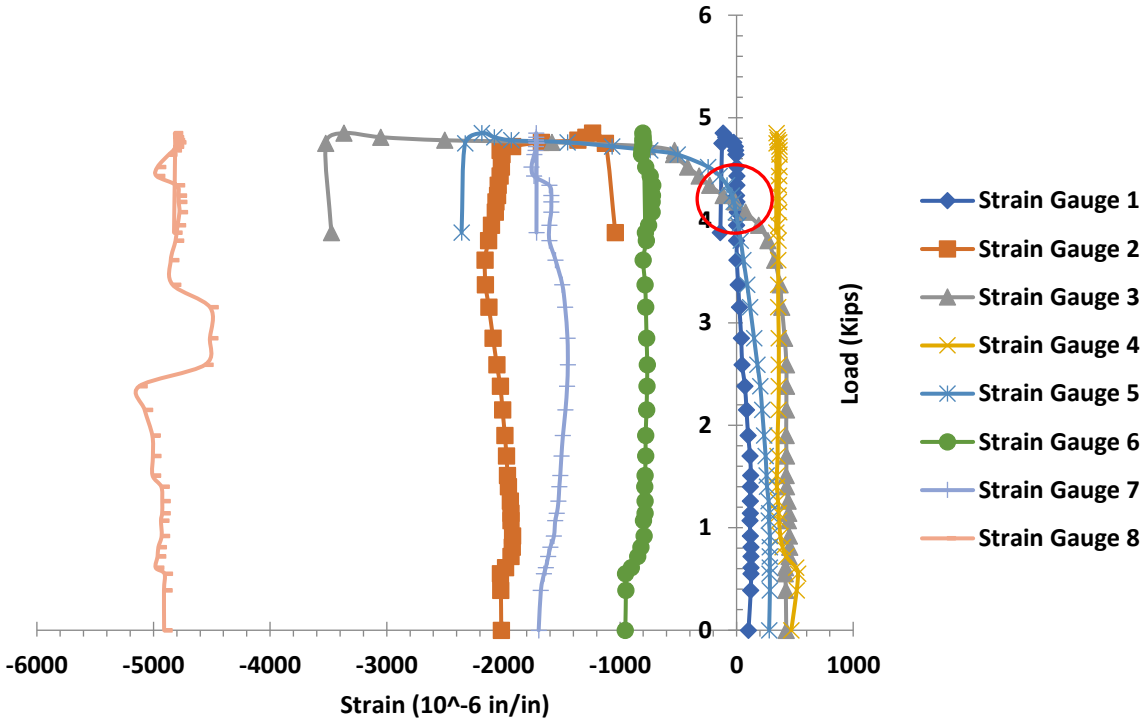

Figure 188. Catenary Action Front Side Strain-load Relationships of Sub-assemblage B2-1

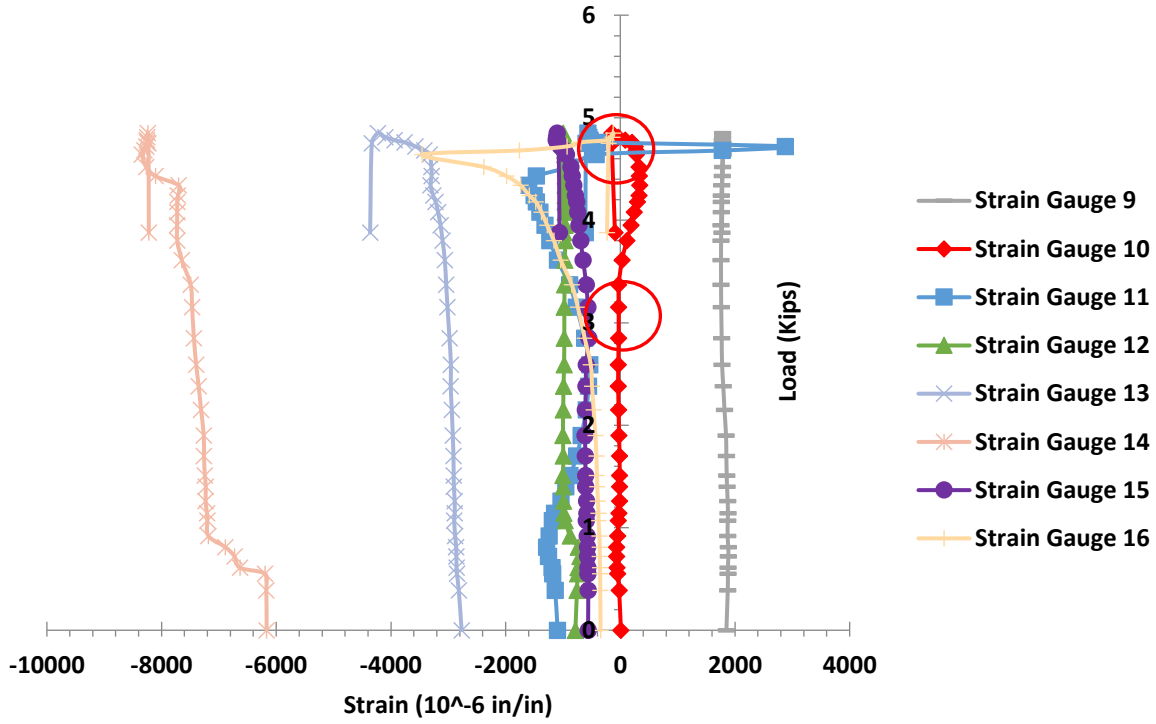

Figure 189. Catenary Action Rear Side Strain-load Relationships of Sub-assemblage B2-1

Figure 190 represents the small catenary action observed from the deflection graphic for the sub-assemblage B2-2. At an applied load of 5.20 kips the deflection drops to 1.98 inch, at applied load of 5.15 kips the deflection was 2.11 inches, at the applied load of 5.16 kips the deflection recorded was 2.30 inches, at the applied load of 5.13 kips the deflection recorded was 2.54 inches, and the applied load of 5.14 kips the deflection recorded was 2.80 inches. This information was validated with the load-strain recorded during the experiment test. Figure 191 illustrates Strain Gauge 2 changed from compression to tension at applied load of 5.20 kips. Strain gauge 8 changed from compression to tension at applied load of 3.89 kips. Figure 192 illustrates Strain Gauge 10 changes from compression to tension at applied load of 3.17 kips, also changed again from tension to compression at applied load of 4.66 kips.

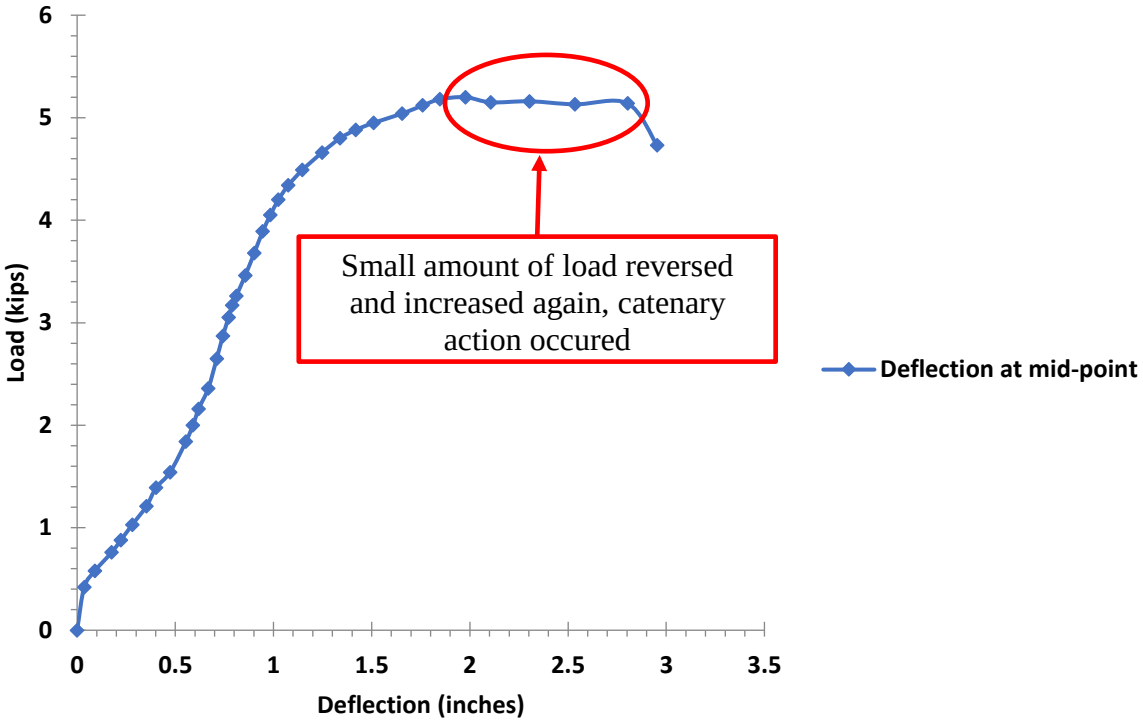

Figure 190. Catenary Action on Specimen B2-2

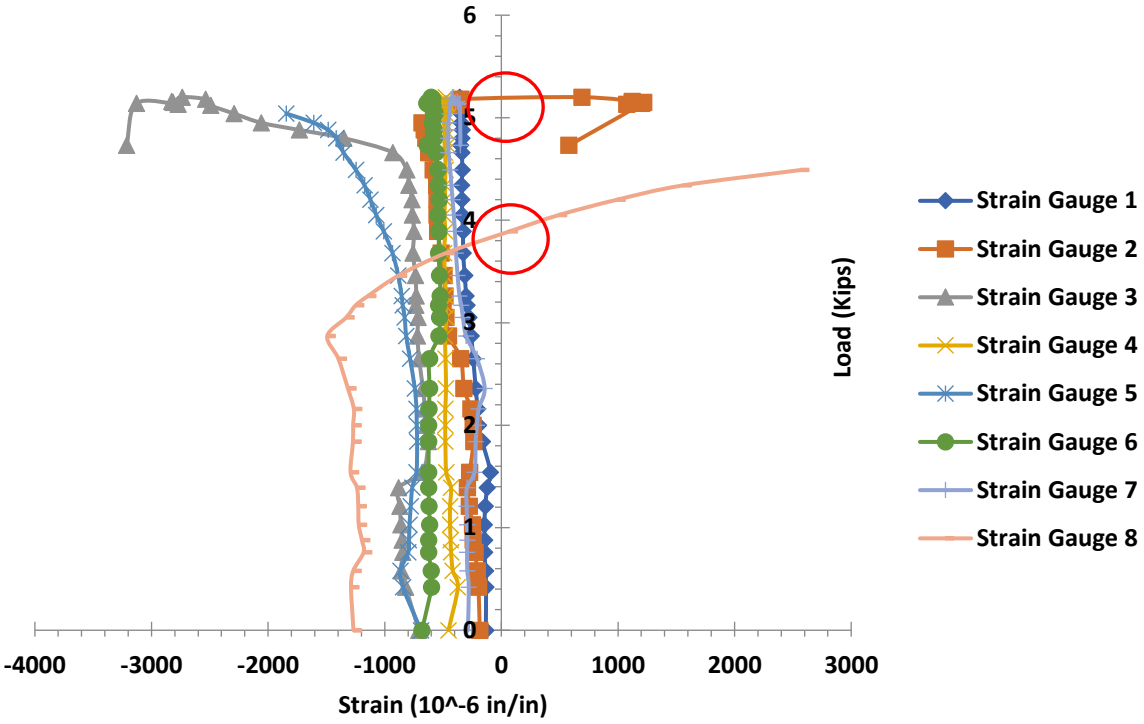

Figure 191. Catenary Action Front Side Strain-load Relationships of Sub-assemblage B2-2

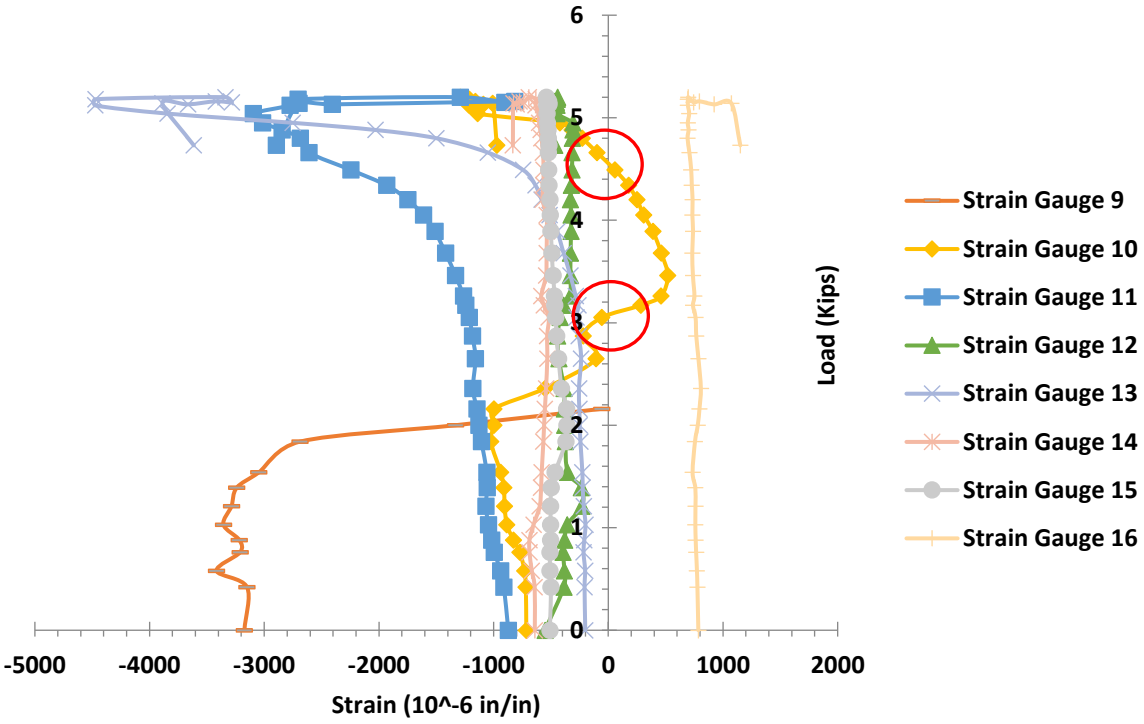

Figure 192. Catenary Action Rear Side Strain-load Relationships of Sub-assemblage B2-2

2.7.8 Plastic Hinge Formation

Figure 193 graphically depicts the location of the theoretical plastic hinge formation in the system due to the continue reinforcement in the negative and positives moments.

Figure 194 illustrates the formation of the hinges in the left support of Specimen S2-1. This hinge formation was not developed due to the excessive rotation in this support and sub-assemblages separated from the column. This information was confirmed through reading the strain gauges recorded during this test. Strain Gauges 1, 2, 9, and 10 located in the left support of the specimen recorded a strain of (-0.0002, -0.0014, 0.0000, and 0.0000 in/in). At the collapsed load, all of the strain gauges in the left support recorded a value under the yield point

of the steel of 0.0023, 0.0003 in/in, from this calculation it was determined that no plastic hinge was developed in this support.

Figure 195 illustrates the formation of the hinges in the right support of Specimen S2-1. This hinge formation was not developed due to the excessive rotation in this support and sub-assemblages separated from the column. This information was confirmed through reading the strain gauges during this test. Strain Gauges 7, 8, 15, and 16 located in the right support of the specimen recorded a strain of (-0.0008, -0.0014, -0.0005, and -0.0019 in/in). At collapsed load, all of the strain gauges in the right support recorded a value under the yield point of the steel of 0.0023 in/in, from this calculation it was determined that no plastic hinge was developed in this support.

Figure 196 illustrates the formation of the hinges in the missing column of Specimen S2-1. This hinge formation was developed on both sides of the missing column. These hinges were not straight line as supposed; however, are in the location of the predicted location from the theoretical plastic hinge formation on Figure 193. This information was confirmed through reading the strain gauges recorded during this test. Strain Gauges 3, 4, 5, 6, 11, 12, 13, and 14 are located in the missing column area of the specimen recorded a strain of (-0.0025, -0.0044, 0.0001, -0.0006, -0.0015, -0.004181, -0.00391, 0.0009, and -0.0001 in/in). At the collapsed load, four of the eight strain gauges installed in the missing column area recorded a value exceeding 0.0023 in/in that is the yield point of the steel and the specimen developed plastic hinges on both side of the missing column.

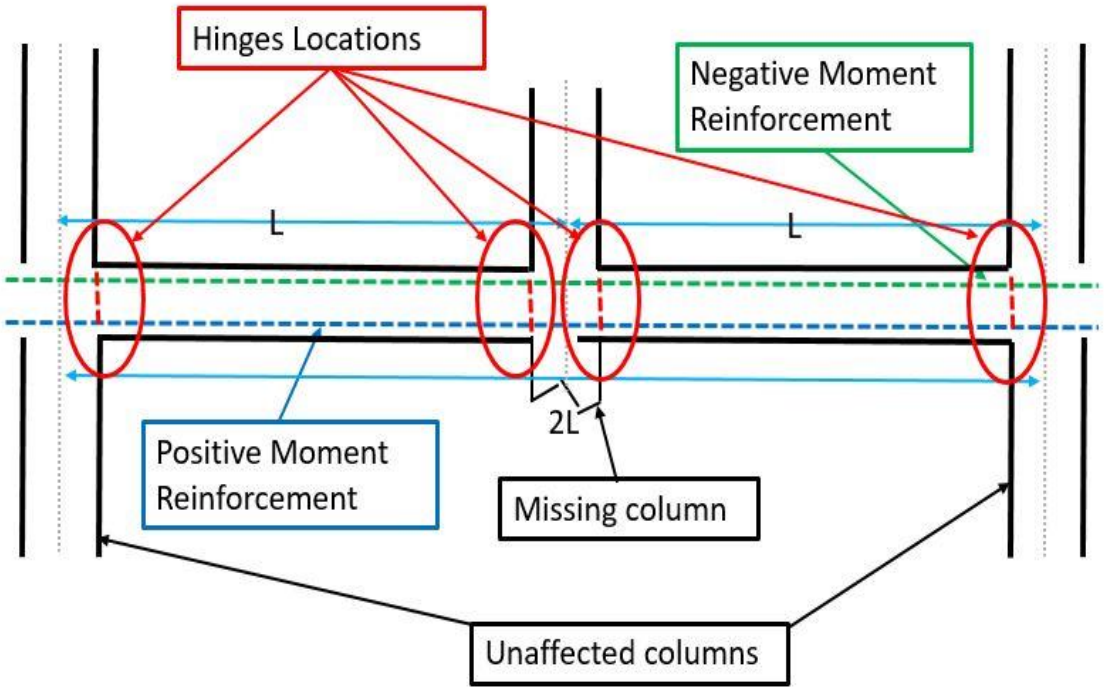

Figure 193. Hinge System Theoretical Formation (Fadhil, 2012)

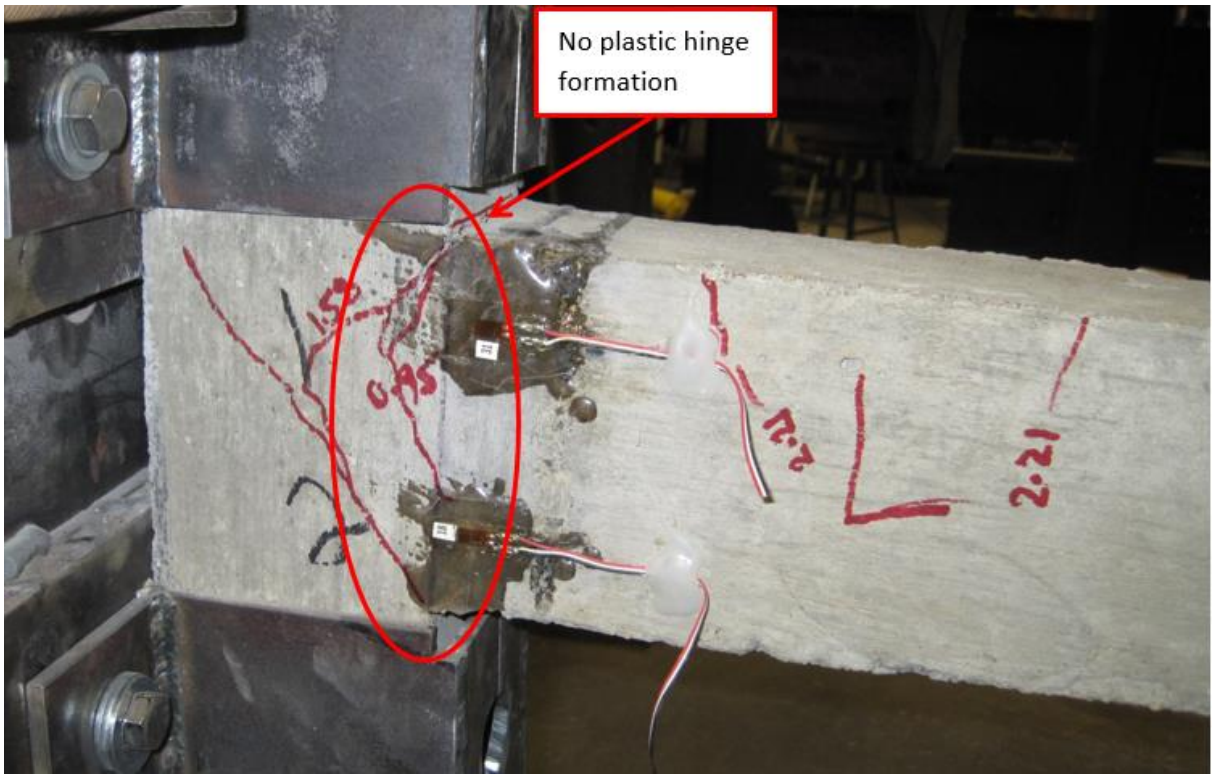

Figure 194. Hinge Formation on the Left Support for Specimen S-21

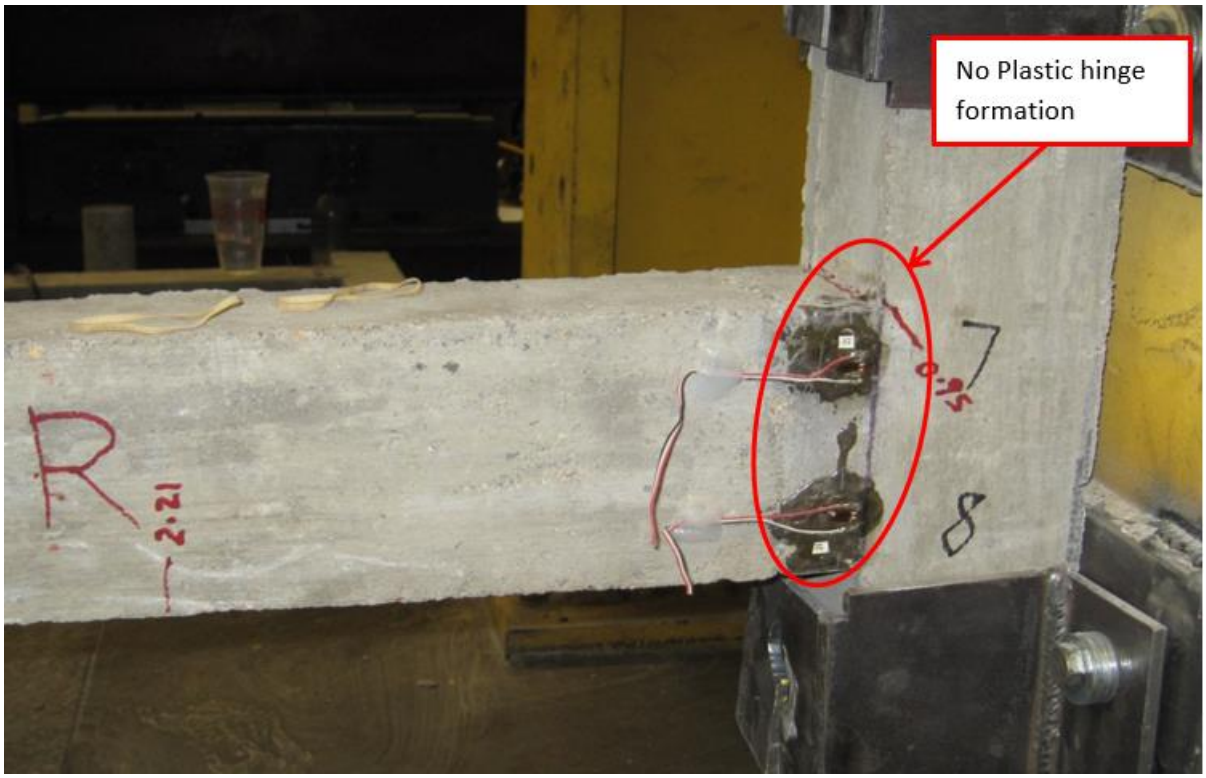

Figure 195. Hinge Formation on the Right Support for Specimen S-21

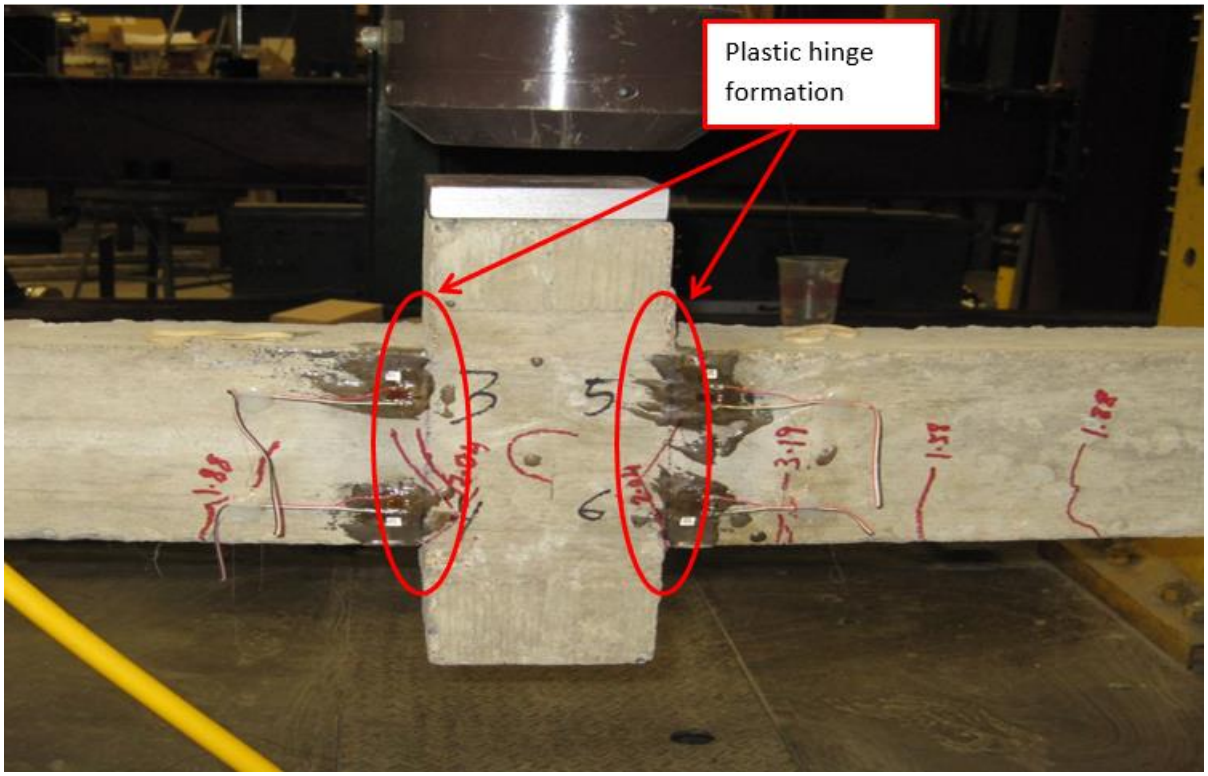

Figure 196. Hinge Formation on the Missing Column for Specimen S-21

Figure 197 illustrates the formation of the hinge in the left support of Specimen S2-2. This hinge formation was not developed due to the excessive rotation in this support and sub-assemblages separated from the column. This information was confirmed by reading the strain gauges recorded during this test. Strain Gauges 1, 2, 9, and 10 located in the left support of the specimen recorded a strain of (-0.0006, -0.0007, 0.0, and -0.0019 in/in at collapsed load, all of the strain gauges in the left support recorded a value under the yield point of the steel of 0.0023 in/in, from this calculation it was determined that no plastic hinge was developed in this support.

Figure 198 illustrates the formation on the hinge in the right support of Specimen S2-2. This hinge formation was not developed due to the excessive rotation in this support and sub-assemblages separated from the column. This information was confirmed by reading the strain

gauges recorded during this test. Strain Gauges 7, 8, 15, and 16 located in the right support of the specimen recorded a strain of (-0.0008, -0.0023, -0.0006, and -0.0003 in/in). At collapsed load, all of the strain gauges in the right support recorded a value under the yield point of the steel of 0.0023 in/in, from this calculation it was determined that no plastic hinge was developed in this support.

Figure 199 illustrates the formation of the hinges in the missing column of Specimen S2-2. These hinge formations were fully developed approximately 1.5 inches from the missing column and were in line with the theoretical locations of these hinges on Figure 194. This information was confirmed by reading the strain gauges recorded during this test. Strain Gauges 3, 4, 5, 6, 11, 12, 13, and 14 are located in the missing column area of the specimen recorded a strain of (-0.0041, -0.0, -0.0037, -0.0007, -0.0004, -0.0016, -0.0043, and -0.0013 in/in). At the collapsed load, three of the eight strain gauges installed in the missing column area recorded a value exceeding 0.0023 in/in that is the yield point of the steel and the specimen developed plastic hinges on both side of the missing column.

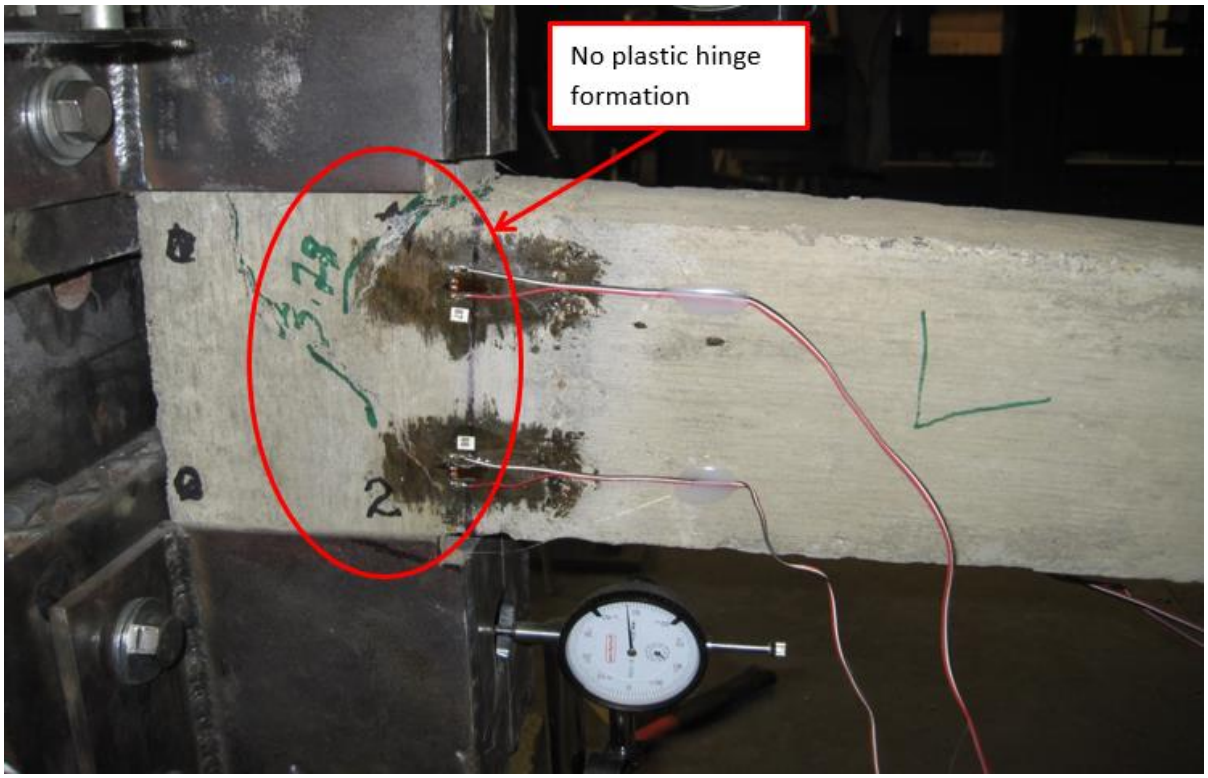

Figure 197. Hinge Formation on the Left Support for Specimen S2-2

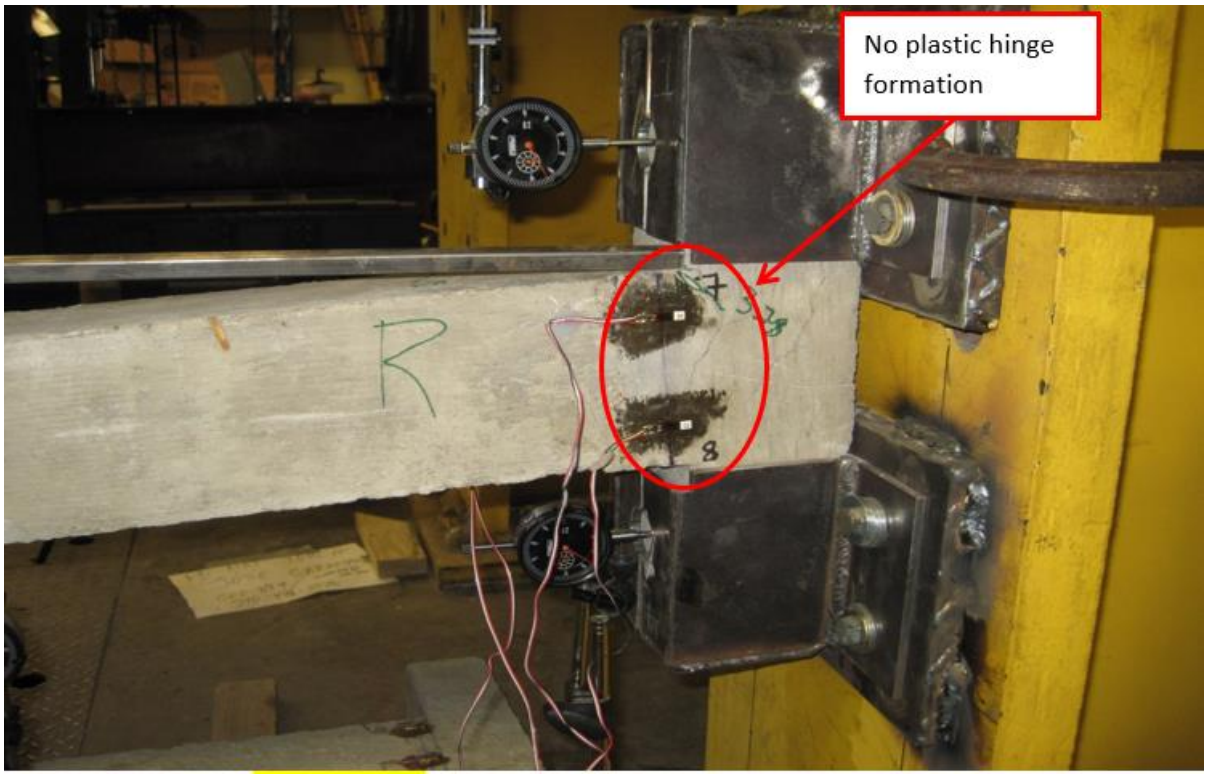

Figure 198. Hinge Formation on the Right Support for Specimen S2-2

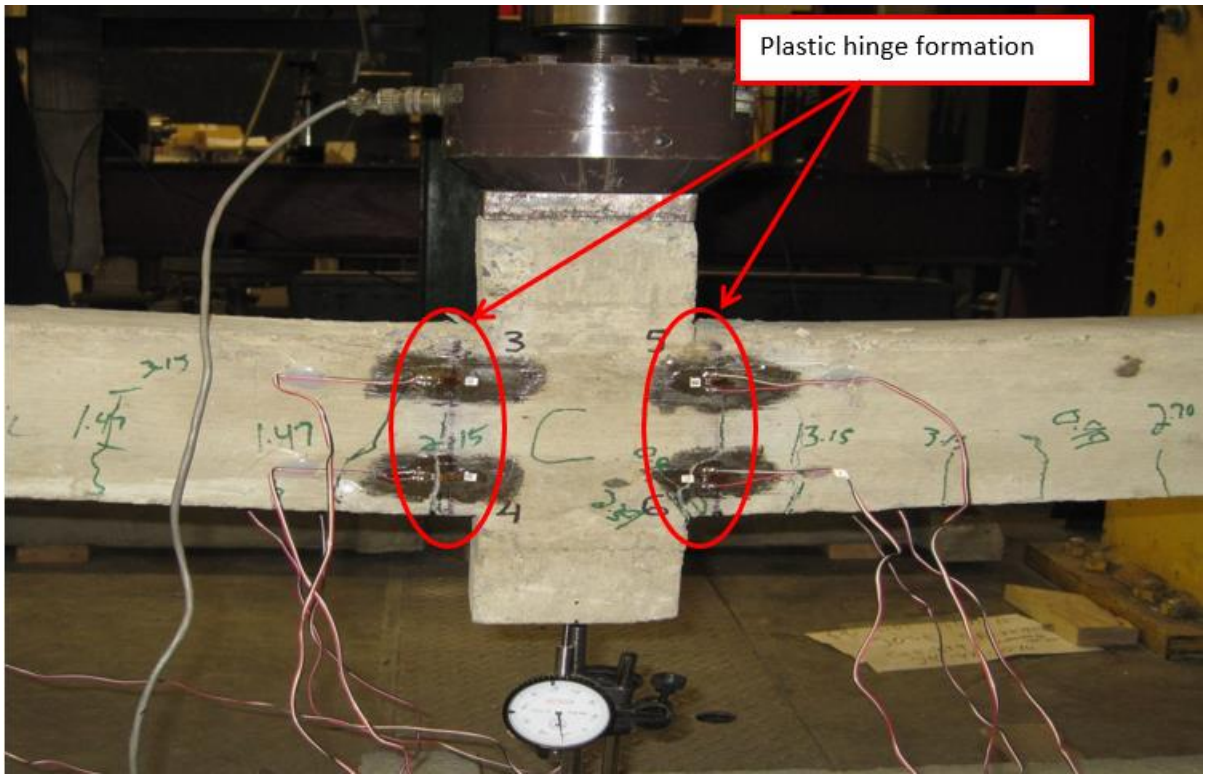

Figure 199. Hinge Formation on the Missing Column for Specimen S2-2

Figure 200 illustrates the formation on the hinge in the left support of Specimen B2-1. This hinge formation was not developed in this support; however, a full crack developed at the hinge location. This information was confirmed by reading the strain gauges recorded during this test. Strain Gauges 1, 2, 9, and 10 located in the left support of the specimen recorded a strain of (-0.0001, -0.0012, 0.0018, and -0.0001 in/in). At collapsed load, all of the strain gauges in the left support recorded a value under the rupture point for the Basalt FRP of 0.0100 in/in, from this calculation it was determined that no plastic hinge was developed in this support.

Figure 201 illustrates the formation on the hinge in the right support of Specimen B2-1. This hinge formation was not developed in this support; however, a full crack developed at the hinge location. This information was confirmed by reading the strain gauges recorded during this test. Strain Gauges 7, 8, 15, and 16 are located in the right support of the specimen recorded a strain

of (-0.0017, -0.0048, -0.0011, and -0.0001 in/in). At collapsed load, all of the strain gauges in the left support recorded a value under the rupture point for the Basalt FRP of 0.0100 in/in, from this calculation it was determined that no plastic hinge was developed in this support.

Figure 202 illustrates the formation of the hinges in the missing column of Specimen B2-1. This hinge formation was not developed in missing column; however, a full crack was developed at the hinge location. This information was confirmed by reading the strain gauges recorded during this test. Strain Gauges 3, 4, 5, 6, 11, 12, 13, and 14 located in the missing column area of the specimen recorded a strain of (-0.0034, 0.0003, -0.0022, -0.0008, -0.0006, -0.0010, -0.0042, and -0.0082 in/in). At collapsed load, all of the strain gauges in the left support recorded a value under the rupture point for the Basalt FRP of 0.0100 in/in, from this calculation it was determined that no plastic hinge was developed in this support.

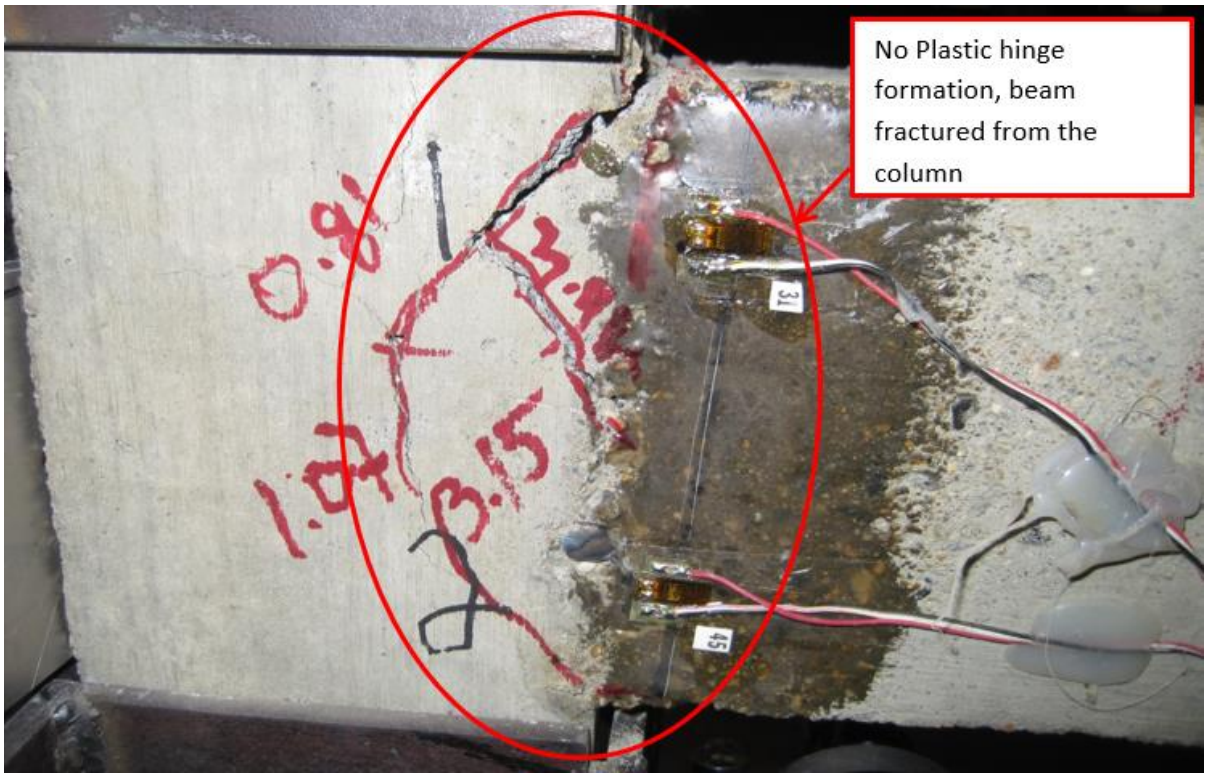

Figure 200. Hinge Formation on the Left Support for Specimen B2-1

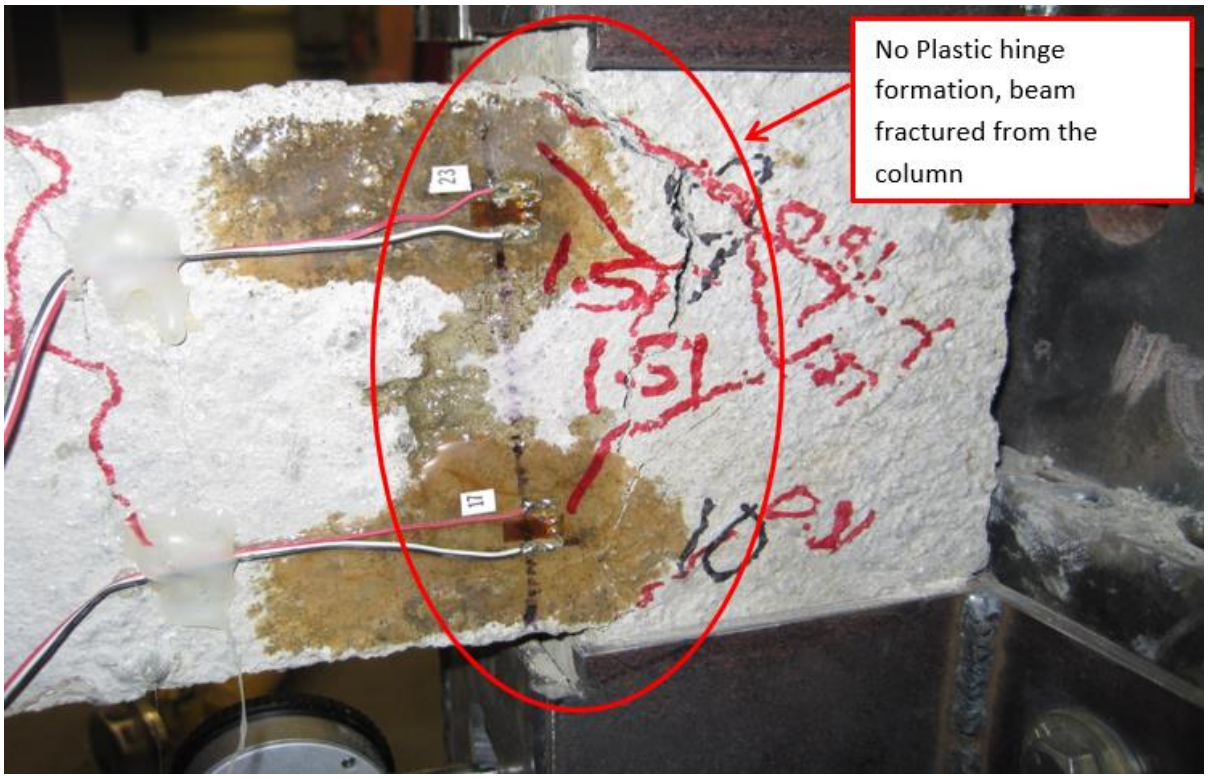

Figure 201. Hinge Formation on the Right Support for Specimen B2-1

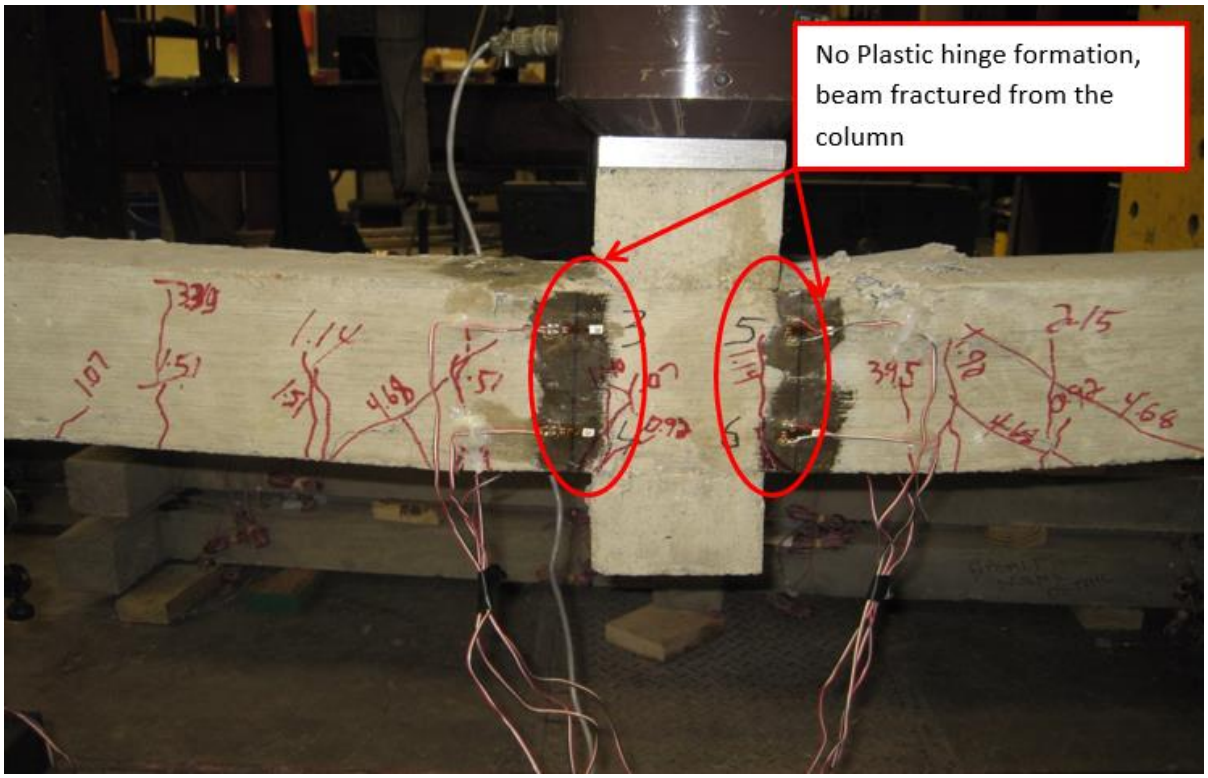

Figure 202. Hinge Formation on the Missing Column for Specimen B2-1

Figure 203 illustrates the formation of the hinge in the left support of Specimen B2-2. This hinge formation was not developed in this support; however, a full crack was developed at the hinge location. This information was confirmed by reading the strain gauges recorded during this test. Strain Gauges 1, 2, 9, and 10 are located in the left support of the specimen recorded a strain of (-0.0004, 0.0007, 0, and -0.0013 in/in). At collapsed load, all of the strain gauges in the left support recorded a value under the rupture point for the Basalt FRP of 0.0100 in/in, from this calculation it was determined that no plastic hinge was developed in this support.

Figure 204 illustrates the formation on the hinge in the right support of Specimen B2-2. This hinge formation was not developed in this support; however, a full crack was developed at the hinge location. This information was confirmed by reading the strain gauges recorded during this test. Strain Gauges 7, 8, 15, and 16 located in the right support of the specimen recorded a

strain of (-0.0004, 0, -0.0005, and 0.0007 in/in). At collapsed load, all of the strain gauges in the left support recorded a value under the rupture point for the Basalt FRP of 0.0100 in/in, from this calculation it was determined that no plastic hinge was developed in this support.

Figure 205 illustrates the formation of the hinges in the missing column of Specimen B2-2. This hinge formation was not developed in missing column; however, a full crack was developed at the hinge location. This information was confirmed by reading the strain gauges recorded during this test. Strain Gauges 3, 4, 5, 6, 11, 12, 13, and 14 located in the missing column area of the specimen recorded a strain of (-0.0027, -0.0005, 0, -0.0006, -0.0013, -0.0004, -0.0033, and -0.0007 in/in). At the collapsed load, all of the strain gauges in the missing column support recorded a value under the rupture point for the Basalt FRP of 0.0100 in/in, from this calculation it was determined that no plastic hinge was developed in this support.

Figure 203. Hinge Formation on the Left Support for Specimen B2-2

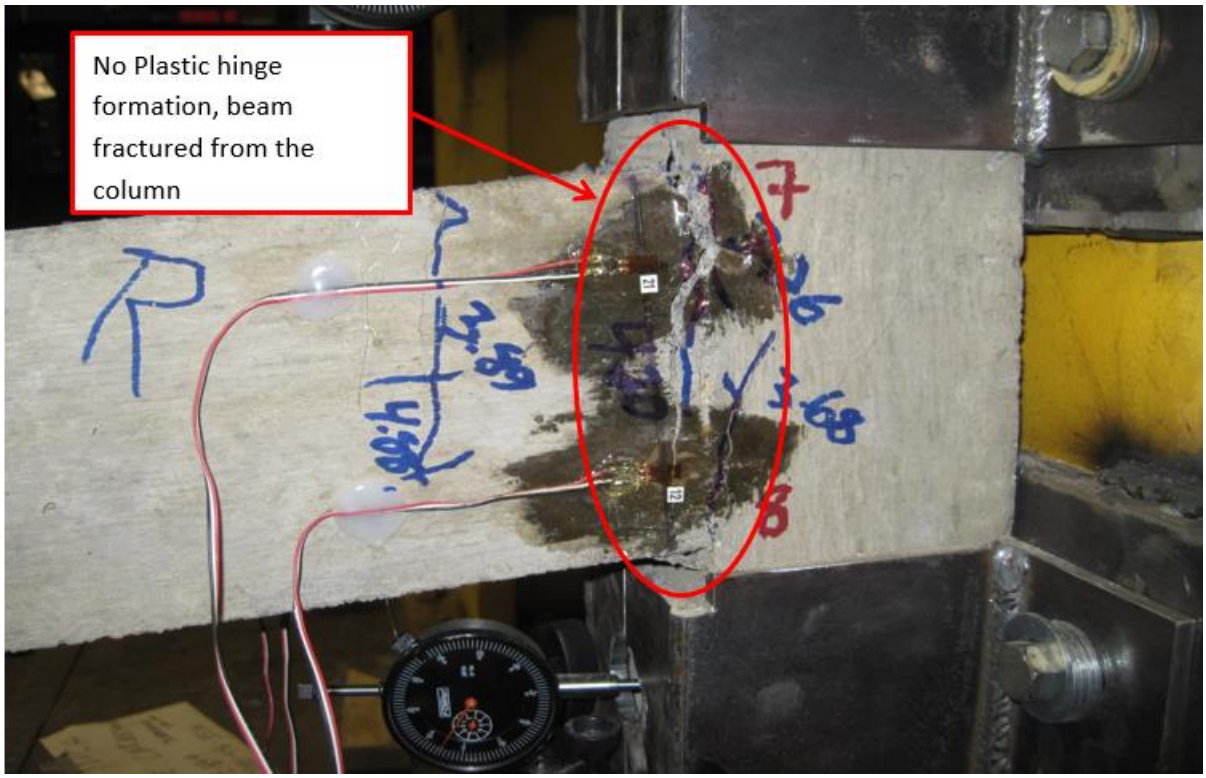

Figure 204. Hinge Formation on the Right Support for Specimen B2-2

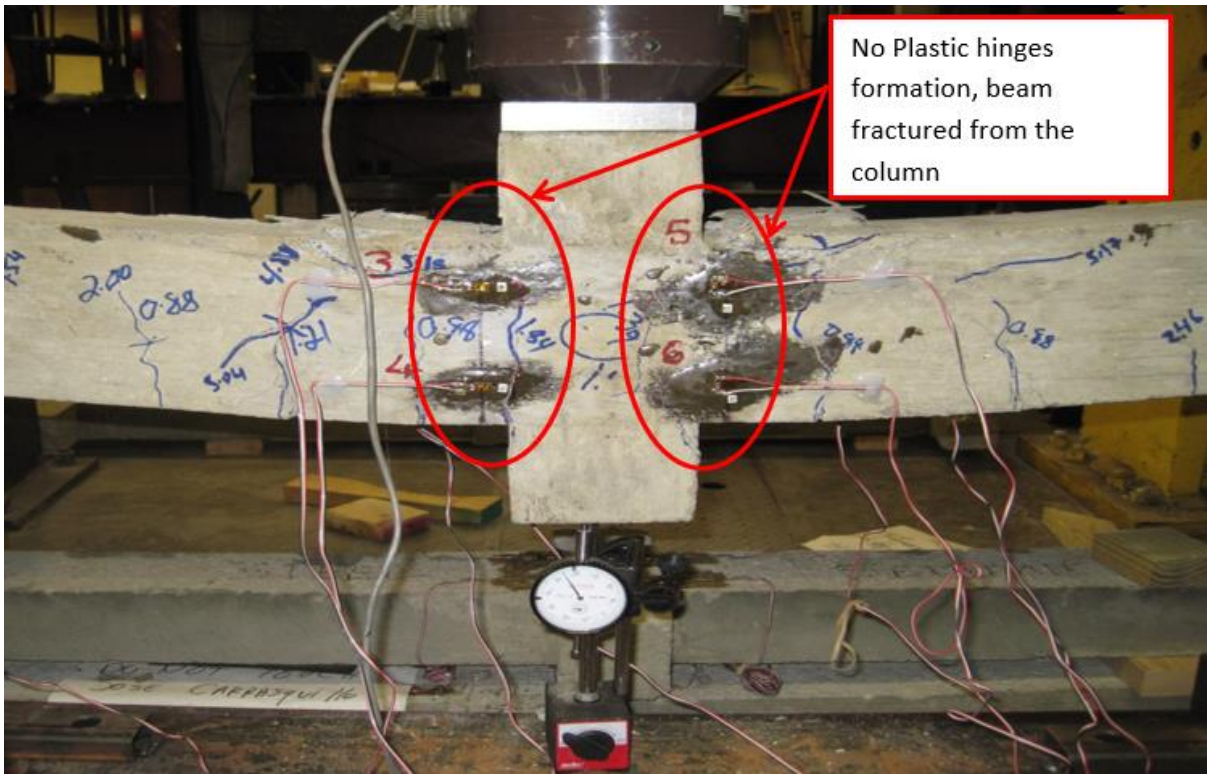

Figure 205. Hinge Formation on the Missing Column Specimen B2-2

2.7 Observations and Discussions

1. The basalt reinforcement created a problem during the tension test due to a deboning from the anchors because the smooth surface does not allow any type of grips with the epoxy.
2. During the experimental phase of the two control specimens, S-1 and B-1, it was observed that the Basalt reinforcement beam deflected 0.88 inch: 70 percent more than the steel reinforced beam at the same applied load (5.00 kips).
3. When comparing the two specimens, S-B 1 and B-B-1 with 4mm Basalt external retrofit, it was observed that the beam with Basalt reinforcement and Basalt external

retrofit increased the load capacity at collapsed point by 0.34 kips; 2.25 percent more compared with the beam with steel reinforcement and Basalt 4mm external retrofit.

4. The deflection at the collapsed load between the steel reinforced and Basalt external retrofitted specimens, S-B 1 and B-B 1, was 0.59 inch at 6.14 kips applied, and the Basalt reinforcement and Basalt external retrofitted beam was 1.20 inches at 6.48 kips applied. The deflection increases by 50.83 percent in the beam with Basalt reinforcement and Basalt external retrofitted compared with the beam used steel reinforcement and Basalt external retrofitted beam.
5. The beam with BFRP bars developed a large deflection before failure compared with the beam with steel bars due to the lack of ductility and low modulus of elasticity.
6. The adding of two 4mm BFRP reinforcement in the tension side of the simply supported beam as a retrofitting only increased beam load capacity by 5.25 percent.
7. Compared specimen with the steel S-1 control beam with the specimen with steel and BFRP fabric beam S-F 1 at 5.00 kips, the deflection was dropped from 0.26 inches to 0.24 inch. The fabric reduced the deflection by 7.69 percent at the same applied load.
8. Compared with the BFRP control beam with the BFRP fabric beam at 5.57 kips, the deflection was dropped from 1.37 inches to 0.59 inch. The fabric reduced the deflection by 56 percent at the same applied load.
9. Specimen S-1 was identified as a control beam after the first test. The beam was retrofitted and loaded at a collapse load of 7.82 kips with this load developed at 0.66-inch deflection. The comparison between the damaged beam and non-damaged beam with the same reinforcement and retrofitted type at 7.04 kips of applied load is the following: the damaged beam develops a deflection of 0.44 inch and the non-damaged beam develops a deflection of 0.95 inch; on the damaged beam, the deflection was reduced by 0.51 inch or 53.68 percent; and at the collapse load capacity, the damaged beam increased by 0.78 kips or 9.97 percent.
10. Specimen B-1 was identified as the control beam after the first test. The beam was retrofitted and loaded at collapse load of 7.44 kips; with this load, it developed at 1.08 inches deflection. The comparison between the damaged and non-damaged beam with the same reinforcement and retrofitted type at 7.44 kips of applied load is the

following: the damaged beam developed a deflection of 1.08 inches and the non-damaged beam developed a deflection of 0.90 inch. On the damaged beam, the deflection was reduced by 0.18 inch or 16.66 percent and the load capacity was reduced also by 1.01 kips or 11.95 percent. At the collapse load capacity, the non-damaged beam increased the load 1.01 kips or 11.95 percent.

11. Compared specimen first crack developed during the impact test the specimens B-B 2, B-F-2 S-B-2 developed the first crack at 7 inches with a 0.14 kips weight drop impactor and Specimens S-2 and S-F-2 developed the first crack at 12 inches with a 0.14 kips weight drop impactor.
12. Compared specimen at collapsed load during the impact test the specimen S-2 collapsed at 21 inches height drop and 0.14 kips weight drop impactor.
13. Used seismic detail in the sub-assemblage S2-2 minimized the shear failure in the sub-assemblage.
14. Used seismic detail in sub-assemblage B2-2 minimized the shear failure in the sub-assemblage.
15. Sub-assemblages without seismic detail developed less flexure cracks during this research compared with the sub-assemblages with seismic details.
16. Sub-assemblages failed due to the shear and bending cracks that developed during the different tests.

CHAPTER 3 THEORETICAL ANALYSIS

3.1 Introduction

Analytical modeling has two major roles: a) provide the preliminary measure of the expected response and results of the test that will be conducted and b) provide results and behavior of the specimen tested to compare with the analytical results.

The analytical analysis for this research was divided into two parts.

For the simply supported beams, the moment-curvature relationships and nonlinear finite-difference analysis were used to determine beam deflections. The moment curvature approached was developed by forcing the equilibrium and compatibility conditions. The approach divided the cross section into a number of layers. Steel and BFRP reinforcement were included in the program as an internal resistance force.

3.2 Formulation of the Moment-Curvature Approach

Used the rectangular reinforced concrete cross section as shown in Figure 206 to determine the moment-curvature for each beam.

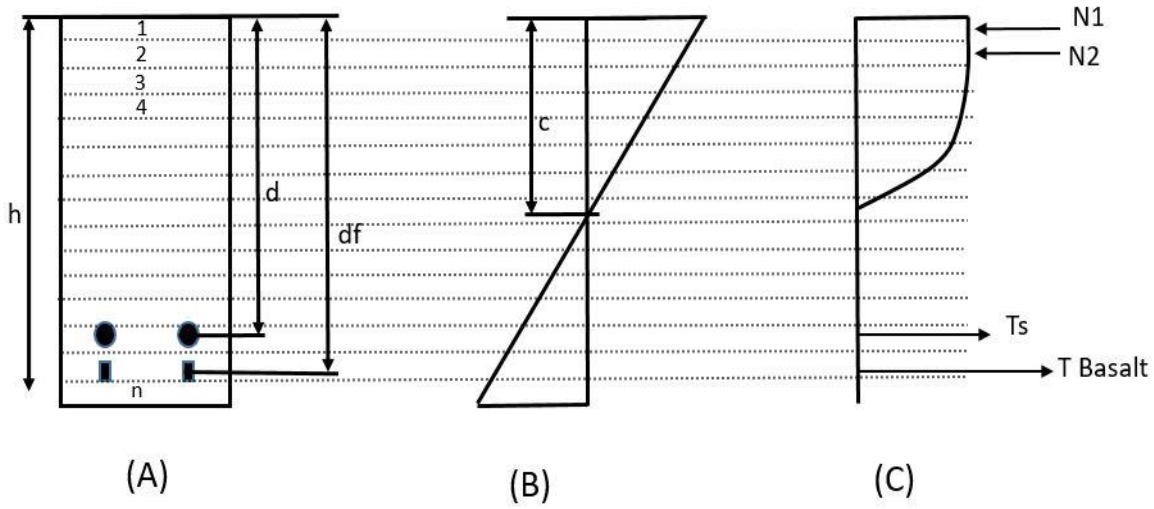

Figure 206. (A) Layered Rectangular Section (B) Strain Distribution (C) Stresses and Forces

This algorithm was developed and step by step process was indicated to determine the moment curvature of a simply supported beam with tension reinforcement only [21] and was modified to meet the requirements of this research. The same process was used for the beams without external retrofit and steps 7 and 8 were not needed. With the external retrofit the process was added. Divided into a multiple number of rectangular layers n with the same cross section and the depth of each layer was *h/n*.

1. Used a value less than 0.0031 for the top layer concrete strain.
2. Used a value less than *h* for the depth of the compression zone and preliminary neutral axis c.
3. For each layer shown in Figure 207, and having *n* number layer identified from the top of the cross section with depth of *h/n* determine the averages strain in each layer *i*.

$$\varepsilon_i = [\varepsilon_t \times (c - (h/n \times (i-0.5))] / c$$

4. Using the concrete stress-strain relationship illustrated in Figure 7 determine the concrete stress in each layer corresponding to the concrete strain average in the same layer corresponding to the strain value on step 3.

5. Determine the strain on the steel reinforcement using the following relation.

$$\varepsilon_s = [(c - d) \times \varepsilon_t] / c$$

6. Using the steel stress-strain relationship illustrated in Figure 9, determine the stress in steel corresponding to the strain value on step 5.
7. For the strain value in the BFRP reinforcement on each layer used the following relation.

$$\varepsilon_b = [(c + 0.5 - h) \times \varepsilon_t] / c$$

8. Using the BFRP reinforcement stress-strain relationship illustrated in Figure 12, determine the stress in BFRP bar corresponding to the strain value on step 7.
9. Determine the concrete compressive force for each layer N_{ci} above the assumed neutral axis selected on step 2.
10. Determine the total net compressive force in all concrete layer found on step 9 and add together using the following relation.

$$C = \sum_{i=1}^{n} Nci$$

11. Determine the tensile force in each concrete layer N_{ci} below the assumed neutral axis in step 2 up to the last un-cracked layer.
12. Determine the tensile force in steel and BFRP reinforcement.
13. Determine the total net tensile force by adding the forces found in step 11 and 12 using the following relation.

$$T = \sum_{i=1}^{n} Nci + Ts + Tbasalt$$

14. Determine the equilibrium of the internal force to validate that C = T, if not then take the following actions.
    a. If the force in the concrete C < the force in the steel T, then increase the value of the original arbitrary neutral axis *c*.
    b. If the force in the steel T > the force in the concrete C, then decrease the value of the original arbitrary neutral axis *c*.

15. To determine that C = T it was necessary to repeat steps 3 to 14 to obtain different values of *c* as soon as C = T or the difference between both values are within an acceptable range, equilibrium of the section was achieved.
16. The value of c and the strain at the top of the concrete was used to determine the corresponding curvature and moment using the following relation.

$$\text{Curvature} = \Phi_i = \varepsilon_t / c$$

17. The final moment M_i, is the summation of the product of each layer forced by their distances from the neutral axis to the center of each layer *i*.
18. To determine points in the moment-curvature graphic increase in small increments the value of ε_t until reach $\varepsilon_t = .0031$ and repeat steps 2 to 16 for every point in the moment curvature curve.

3.3 Nonlinear Finite-Difference Analysis of a Simply Supported Beam

The finite difference technique was used to obtain moment-curvature plots obtained in the cross-sectional analyses to obtain the load-deflection plots for the beam member. This algorithm was developed and step by step process was indicated to determine the moment curvature of a simply supported beam with tension reinforcement only [21] and was modified to meet the requirements of this research. The step-by-step procedure of this technique is summarized below with reference to Figure 207.

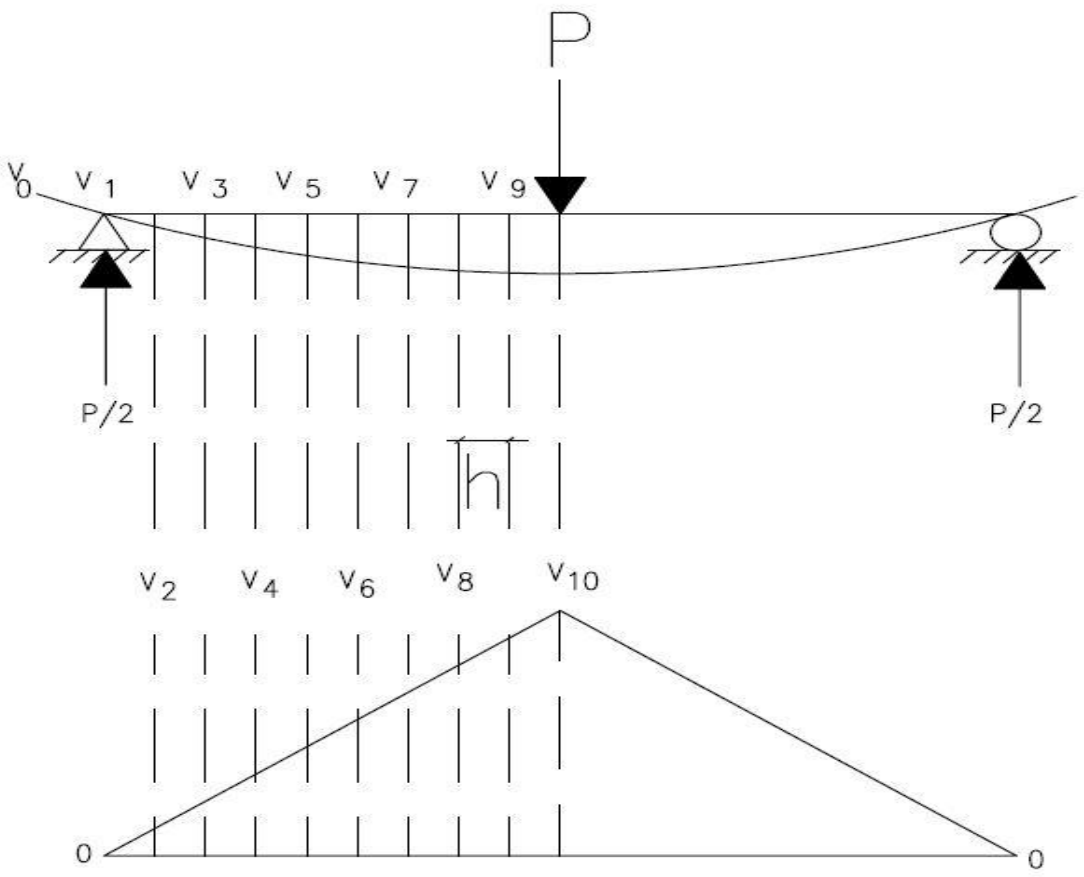

Figure 207. Beam with Concentrated Point Load, Deflected Shape, and Bending Moment Diagram

1. Utilize only half length of the clear beam span for this analysis.
2. Apply increments of load P at the center of the beam to obtain the corresponding moment.
3. With the corresponding moment from step 2 at each distance h with respect to the applied load at the center of the beam, generate the corresponding curvatures ϕi.
4. Select the curvature values from moment-curvature plots corresponding to the bending moments at each location from the procedure in step 3.

5. Determine the deflection at each υ location.
6. Calculate the total deflection.
7. Repeat steps 2 to 6 for the next increment of load.
8. These curvatures are related to the deflections of the beam in the y directions for this particular project, as derived in the following section.

$$\phi_{yi} = -\left(\frac{d^2 v}{dz^2}\right)_i = -\left[\frac{v_{i-1} - 2v_i + v_{i+1}}{(h)^2}\right] \qquad (6)$$

Substituting i = to 10 in the above equation we obtain the following expression:

Expanding these relations and then writing those in matrix form give the following relation:

$$\begin{pmatrix} 1 & 1 & 0 & 0 & 0 & 0 & 0 & 0 & 0 \\ 0 & -2 & 1 & 0 & 0 & 0 & 0 & 0 & 0 \\ 0 & 1 & -2 & 1 & 0 & 0 & 0 & 0 & 0 \\ 0 & 0 & 1 & -2 & 1 & 0 & 0 & 0 & 0 \\ 0 & 0 & 0 & 1 & -2 & 1 & 0 & 0 & 0 \\ 0 & 0 & 0 & 0 & 1 & -2 & 1 & 0 & 0 \\ 0 & 0 & 0 & 0 & 0 & 1 & -2 & 1 & 0 \\ 0 & 0 & 0 & 0 & 0 & 0 & 1 & -2 & 1 \\ 0 & 0 & 0 & 0 & 0 & 0 & 0 & 2 & -2 \end{pmatrix} \cdot \begin{pmatrix} \upsilon_0 \\ \upsilon_2 \\ \upsilon_3 \\ \upsilon_4 \\ \upsilon_5 \\ \upsilon_6 \\ \upsilon_7 \\ \upsilon_8 \\ \upsilon_9 \end{pmatrix} = h^2 \cdot \begin{pmatrix} \Phi_{oy} \\ \Phi_{2y} \\ \Phi_{3y} \\ \Phi_{4y} \\ \Phi_{5y} \\ \Phi_{6y} \\ \Phi_{7y} \\ \Phi_{8y} \\ \Phi_{9y} \end{pmatrix}$$

The size of the matrix depends on the number of sections of the member. The curvatures can be found through the moment curvature algorithm developed as part of this research by measuring the strains at appropriate locations.

For the sub-assemblage's specimen, the finite difference technique was used to obtain moment-curvature plots obtained in the cross-sectional analyses to obtain the load-deflection plots.

3.4 Theoretical Moment-Curvature of the Simply Supported Specimens

Figures 208 to 215 illustrate the theoretical value of the moment-curvature using a non-linear approach for each simply supported beam tested during this research.

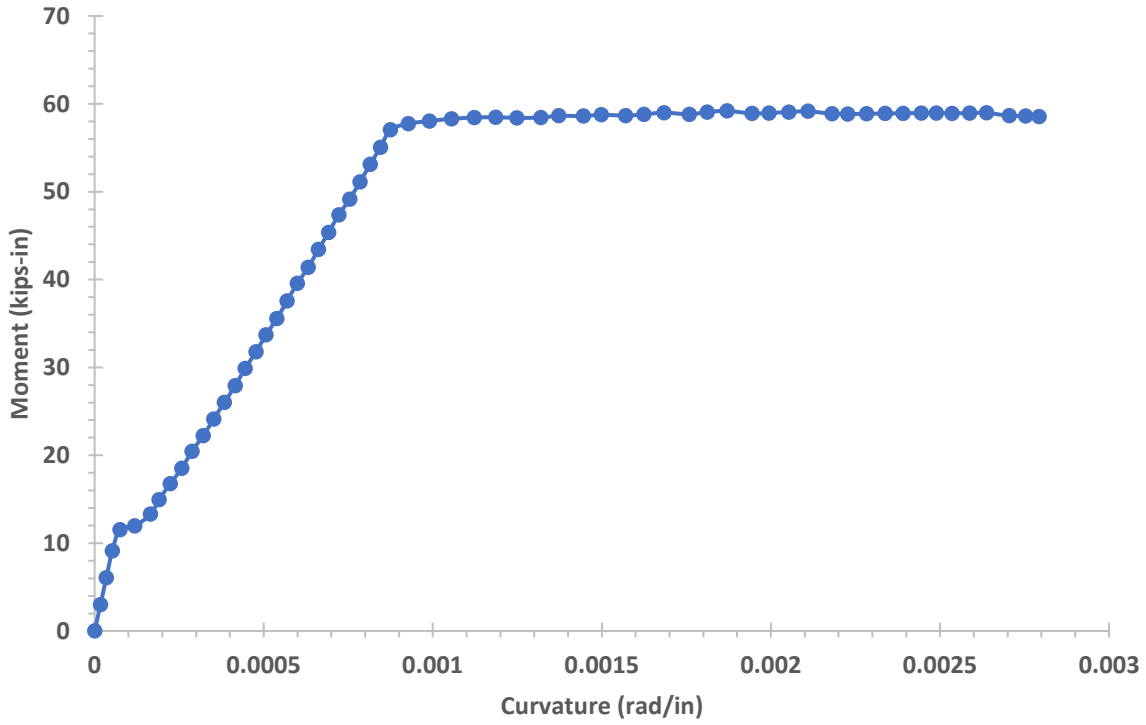

.

Figure 208. Theoretical Moment-Curvature for Specimen S-1

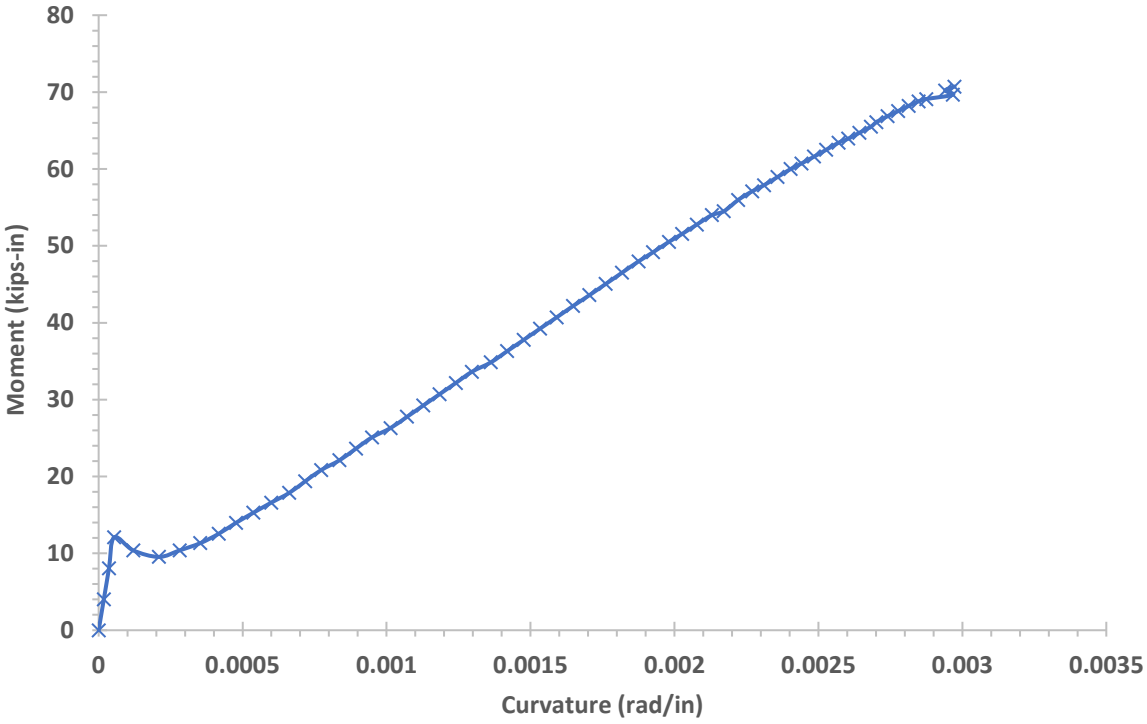

Figure 209. Theoretical Moment-Curvature for Specimen B-1

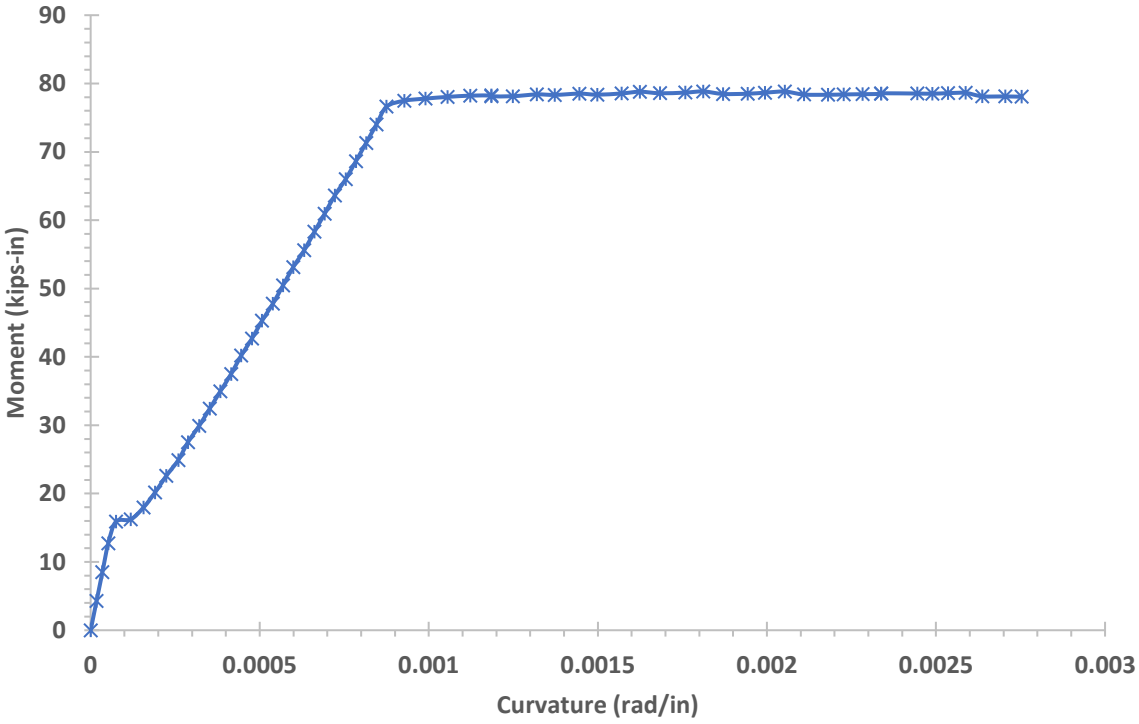

Figure 210. Theoretical Moment-Curvature for Specimen S-B-1

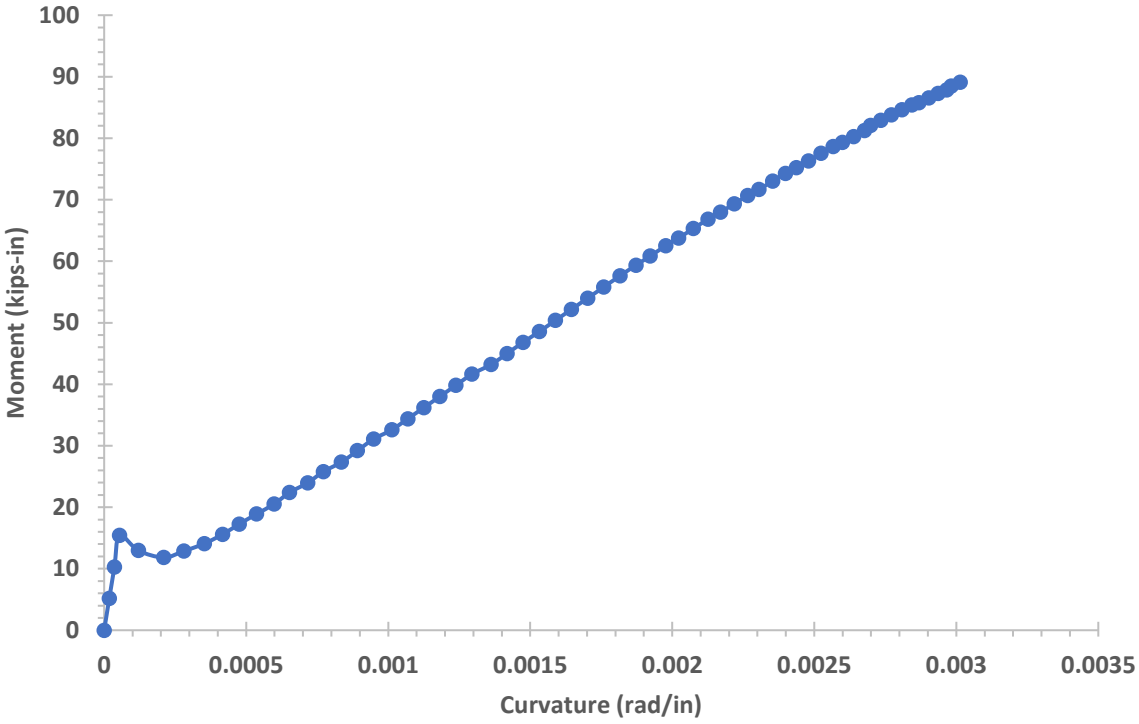

Figure 211. Theoretical Moment-Curvature for Specimen B- B 1

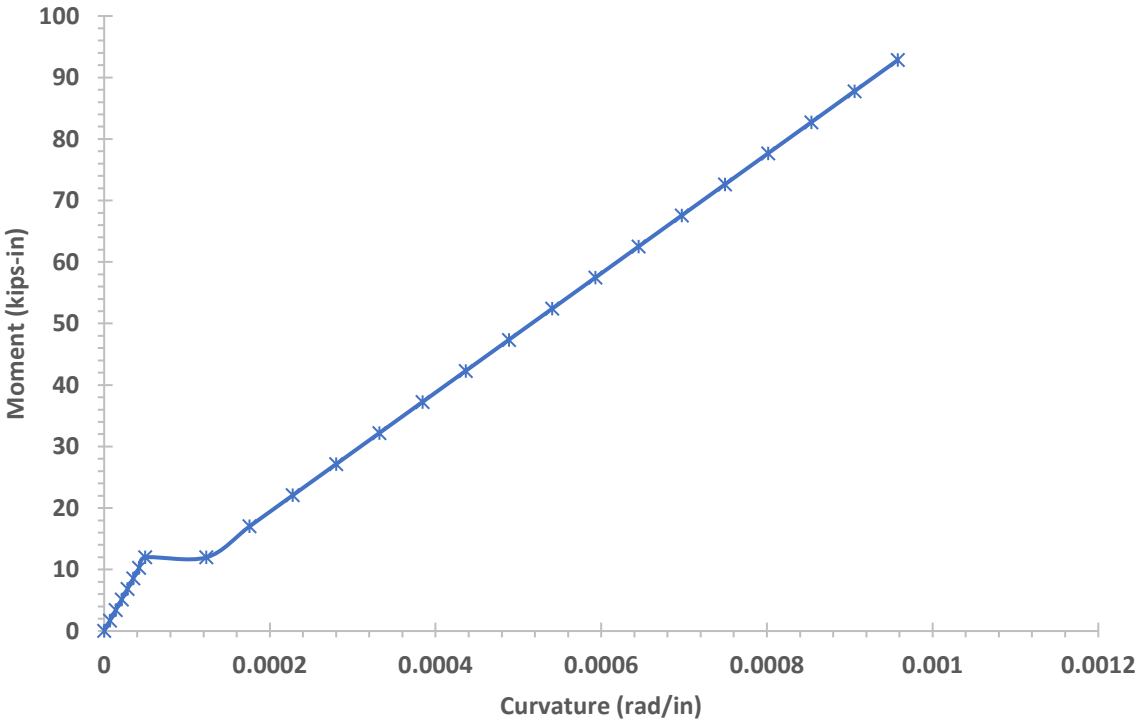

Figure 212. Theoretical Moment-Curvature for Specimen S-F-1

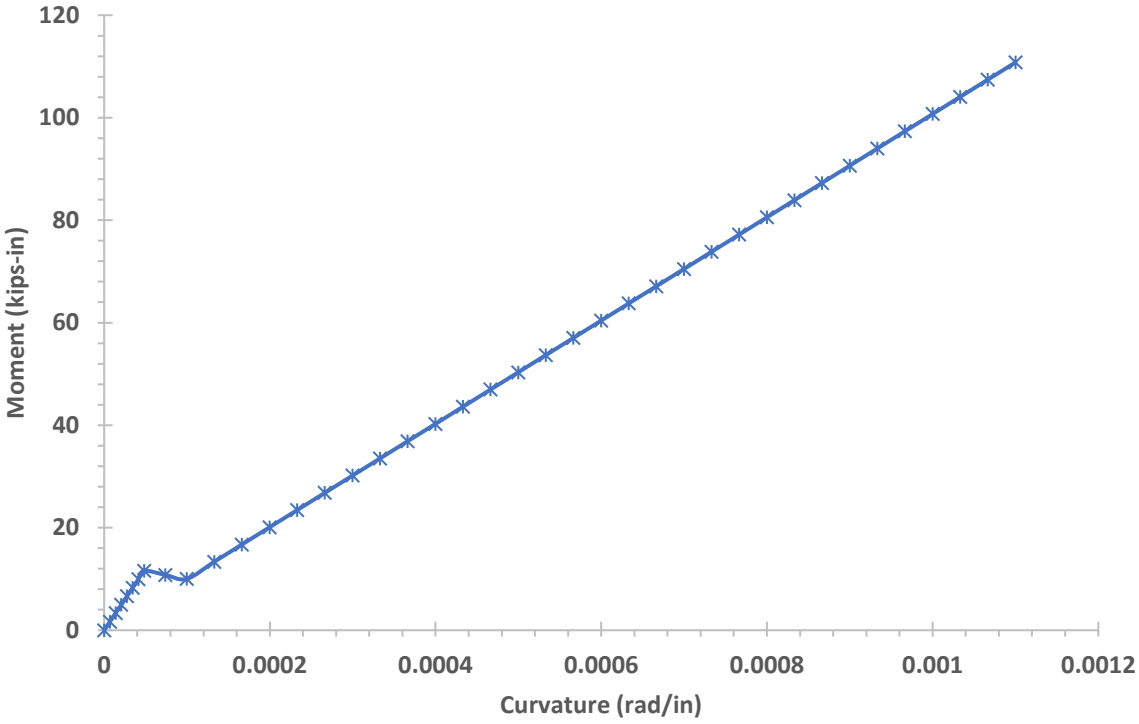

Figure 213. Theoretical Moment-Curvature for Specimen B-F-1

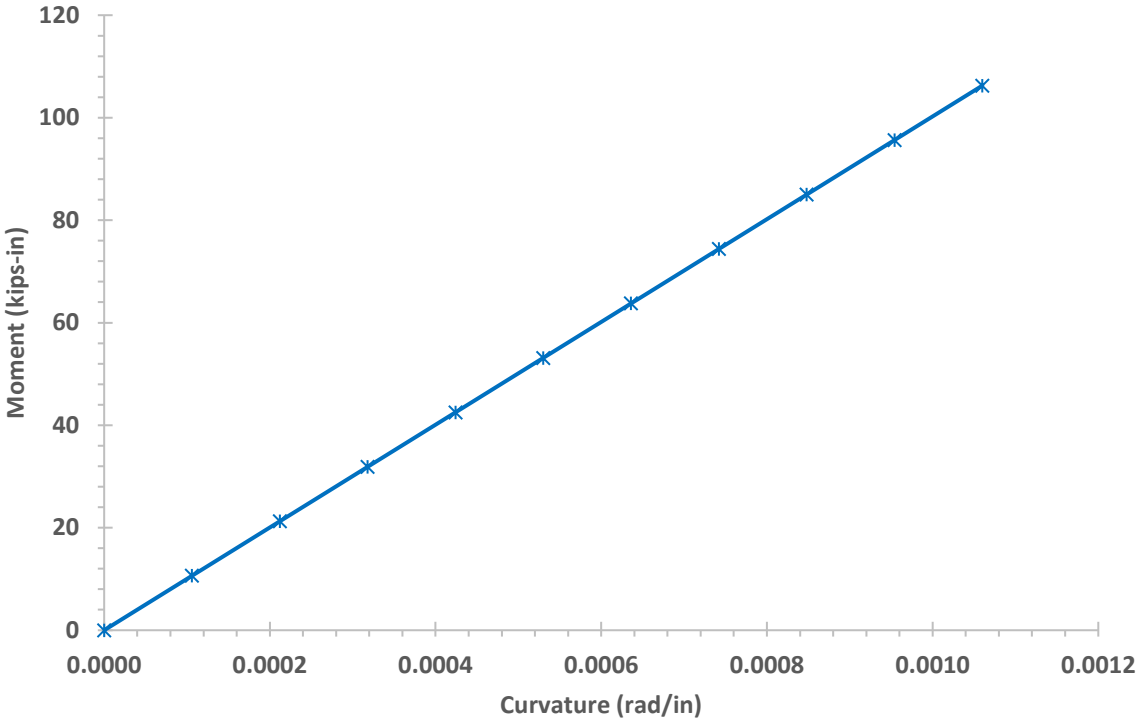

Figure 214. Theoretical Moment-Curvature for Damaged Specimen S-F-1 (retrofitted)

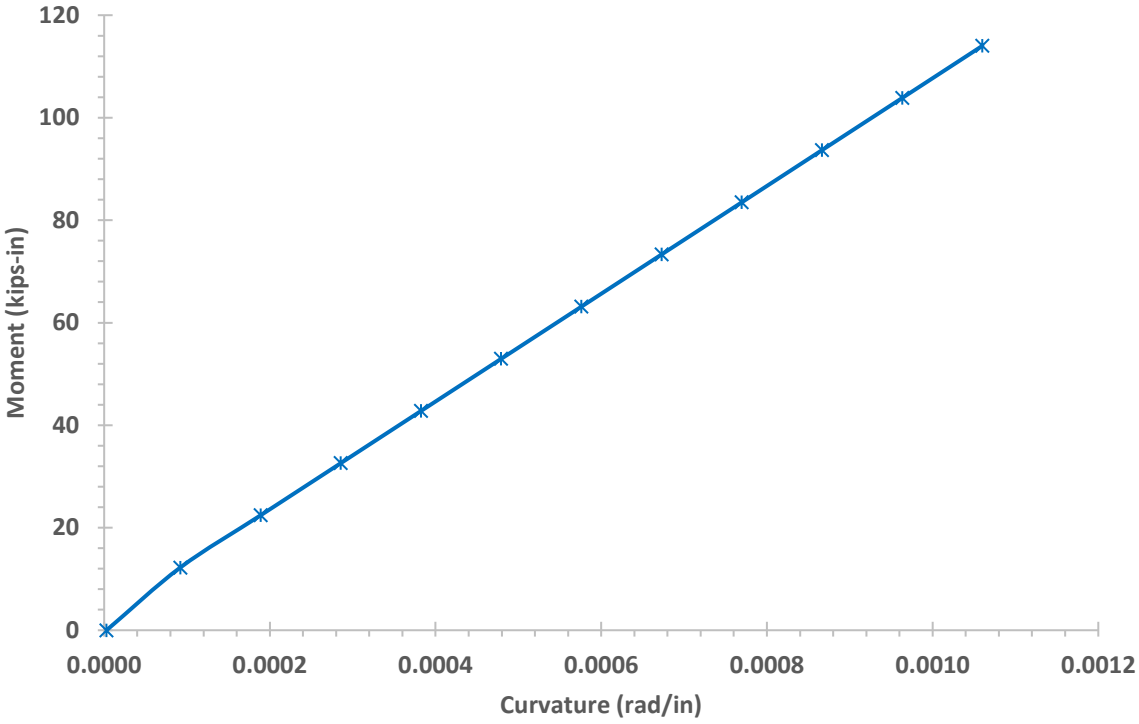

Figure 215. Theoretical Moment-Curvature for Damaged Specimen B-F-1 (retrofitted)

3.5 Theoretical Moment Curvature of the Sub-assemblage Beam

Figures 216 to 219 illustrate the theoretical value of the moment curvature using non-linear approaches for each simply supported beam tested during this research.

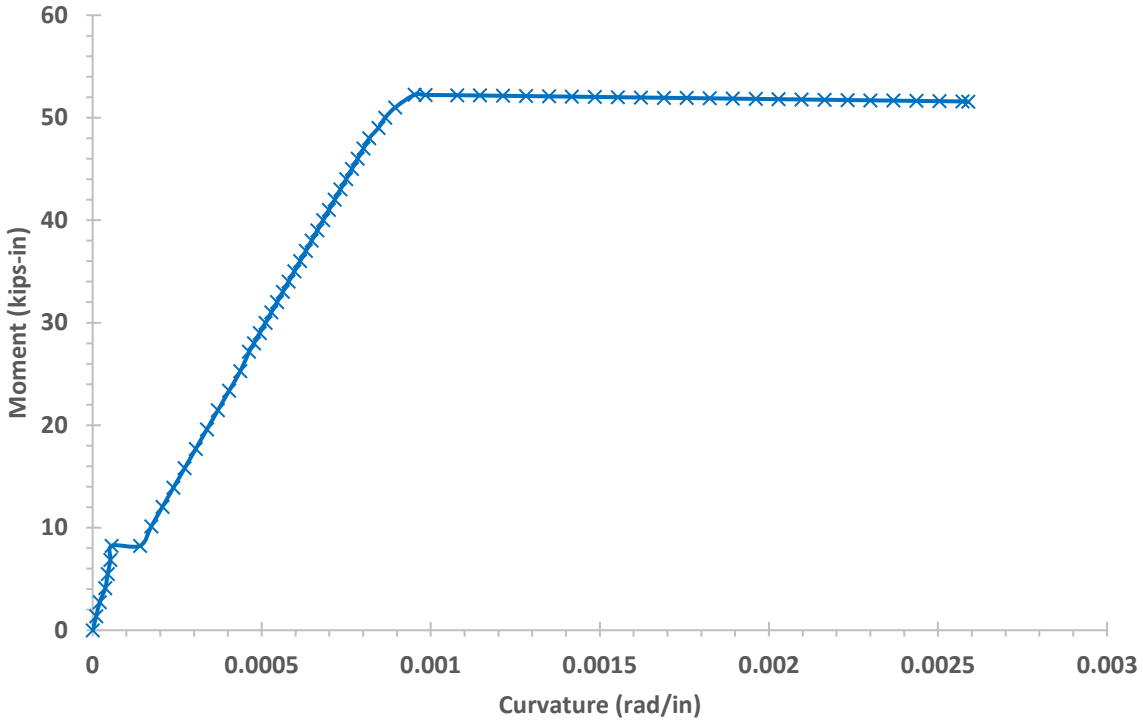

Figure 216. Theoretical Moment-Curvature for Sub-assemblage S2-1

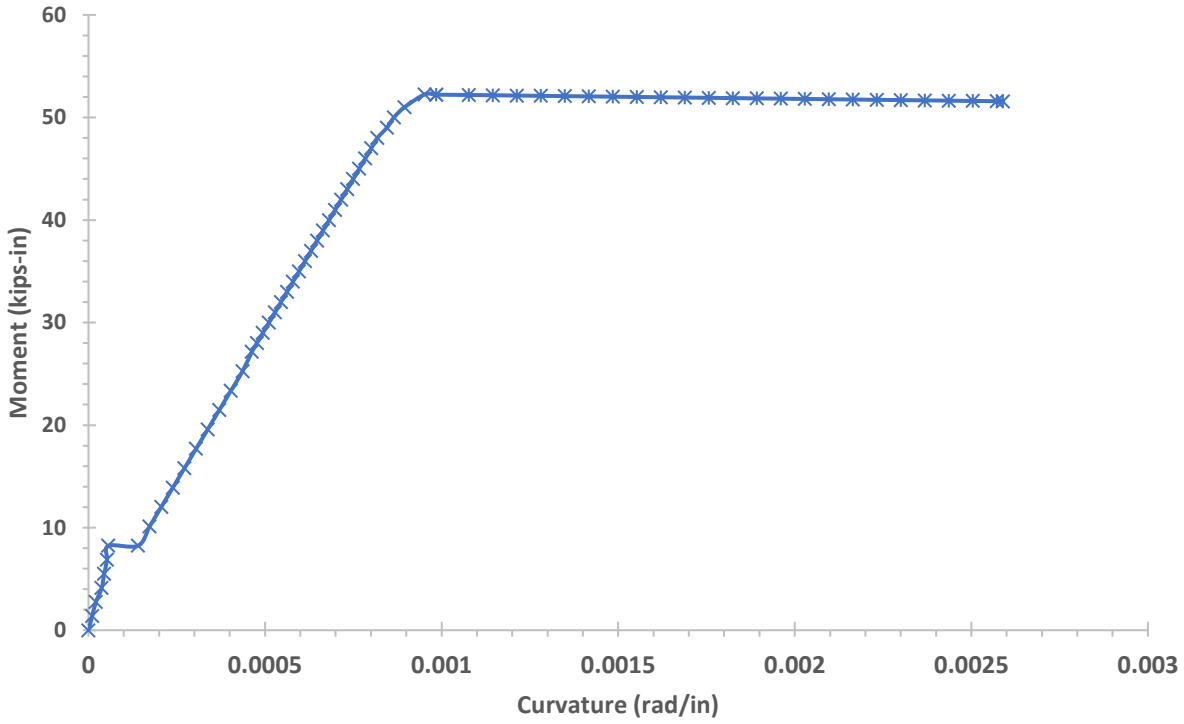

Figure 217. Theoretical Moment-Curvature for Sub-assemblage S2-2

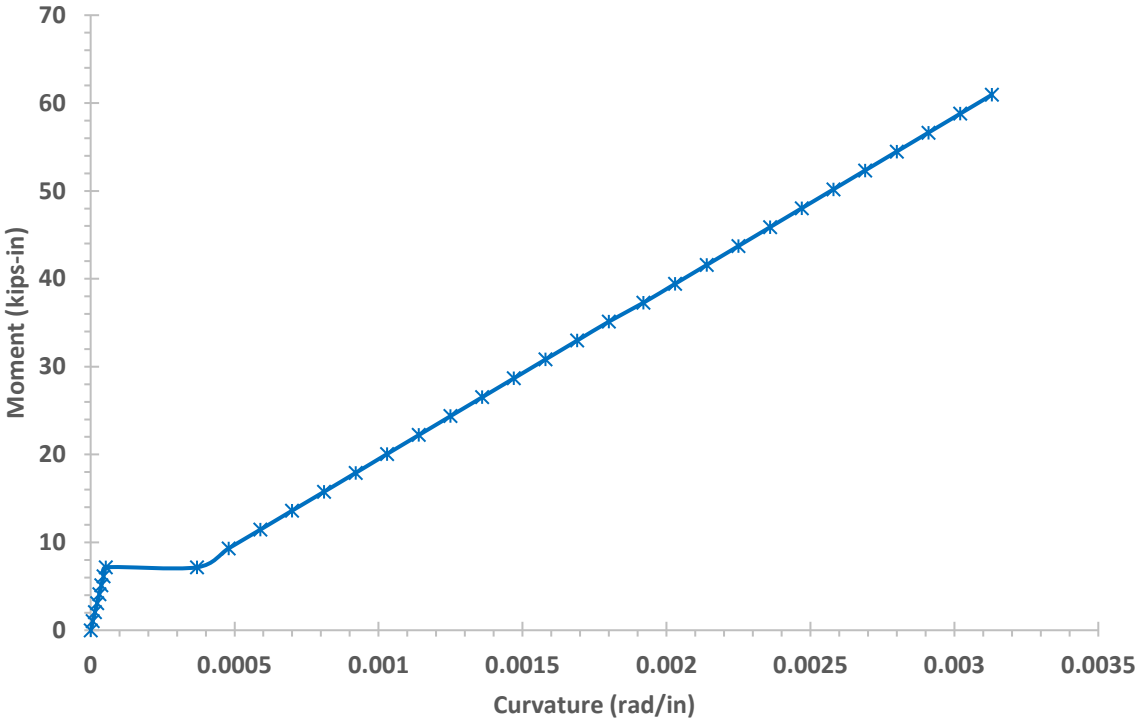

Figure 218. Theoretical Moment-Curvature for Sub-assemblage B2-1

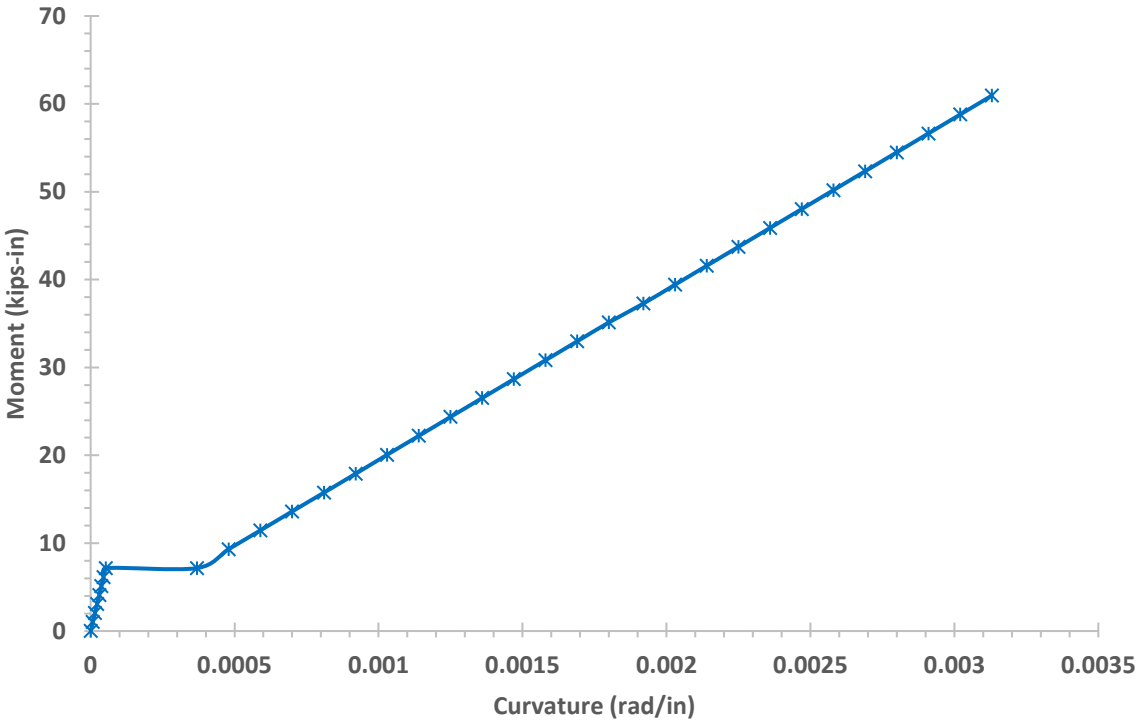

Figure 219. Theoretical Moment-Curvature for Sub-assemblage B2-2

3.6 Damped Single-degree-of-freedom (SDOF) Theoretical Dynamic Analysis

A damped single-degree-of-freedom (SDOF) theoretical dynamic model is used to capture the post-impact free vibration of the simply supported beams. Using Equation 7 in excel program was used to calculate the theoretical acceleration for each test and determine the correct damping.

$$a := \frac{\mathrm{d}}{\mathrm{d}t} v(t) \xrightarrow{simplify} e^{-(\omega \cdot X \cdot t)} \cdot \left(\omega^2 \cdot X^2 \cdot \sin(\phi + \omega_D \cdot t) - {\omega_D}^2 \cdot \sin(\phi + \omega_D \cdot t) + 2 \cdot \omega \cdot X \cdot \omega_D \cdot \left(2 \cdot \sin\left(\frac{\phi}{2} + \frac{\omega_D \cdot t}{2} \right)^2 - 1 \right) \right) \quad (7)$$

A total of five simply supported beams were tested during the impact load analysis. On each beam, an accelerometer was installed halfway on the beam. Another accelerometer was installed

on the impactor. Data from both accelerometers was recorded. The theoretical acceleration for each beam was calculated and compared with the experimental acceleration of the beam.

Finally, natural frequency for each beam was calculated to determine with material combination produces the best natural frequency in a whole building to produce less damages during extreme load events such blast, impact damages from a terrorist attack. Part of this analysis was determined if the scheme of BFRP reinforcement as a retrofitting used in the structures will be a problem in the natural frequency in the original structure. The lowers natural frequency will be an indication of a lot of displacement and damages in the structures in the other hand the higher natural frequency will turn the structure to ridged that will not provide any indication of structural problem until failed. Both cases are a real problem for the structure. Table 8 represents the weight and mass of each beam used during the theoretical calculation of the natural frequency. Table 9 represents the weight and mass of each impactor.

Table 8. Weights and Mass of Each Beam

Beam	Weight of Beam (kips)	Mass of each beam (kips-sec^2/in)
S-2	0.143	0.000371
S-B	0.144	0.000373
S-F	0.146	0.000378
B-B	0.140	0.000362
B-F	0.141	0.000364

Table 9. Length, Weights, and Mass of Each Impactor

Impactor	Length of impactor (in.)	Weight of Impactor (kips)	Mass of each beam (kips-sec^2/in)
1	6	0.06	0.000155
2	18	0.14	0.000362
3	60	0.40	0.001035

CHAPTER 4 COMPARISON OF RESULTS AND DISCUSSION

In this chapter, I will present a comparison between the experimental and the theoretical results of this research. The theory and analysis presented in chapter 3 is within a reasonable range with the results of the experimental results of this research.

4.1 The Simply Supported Beams Under Quasi-Static Load

Table 10 shows a comparison between the experimental maximum load and the theoretical maximum load for the eight simply supported beams tested during this research. It was tested using a non-linear analysis to determine the moment-curvature and the finite difference techniques to obtain the load deflection for each of the beams. Table 11 indicates the experimental maximum moment and the theoretical maximum moment for each test during this research.

Table 10. Comparison between Experimental and Theoretical Maximum Load at Mid-span of the Beam

Specimen	Experimental Load (kips)	Theoretical Load (kips)	Experimental / Theoretical
S-1	5.00	4.34	1.15
B-1	5.57	5.14	1.08
S-B -1	6.14	5.73	1.07
B-B-1	6.41	6.47	0.99
S-F-1	7.01	6.83	1.02
B-F-1	8.45	8.17	1.03
S-1 D-R	7.82	7.72	1.01
B-1 D-R	7.44	8.29	0.90

Table 11. Comparison between Experimental and Theoretical Maximum Moments at Mid-span of the Beam

Test	Experimental	Theoretical	Experimental / Theoretical
	Max. Moment at Mid-point (kips-in)	Max. Moment at Mid-point (kips-in)	
S-1	68.75	57.94	1.15
B-1	76.59	70.72	1.08
S-B-1	84.43	83.19	1.01
B-B-1	88.14	89.01	0.99
S-F-1	96.80	93.97	1.03
B-F-1	116.19	112.39	1.03
S-1 D-R	107.53	106.26	1.01
B-1 D-R	102.30	114.02	0.90

For Specimen, S-1, the experimental load applied was 5.00 kips. This beam was never loaded up to collapse load and the theoretical maximum load was 4.34 kips. The experimental load was 5.00 kips. The load capability of this beam was increased by 13.16 percent in comparison with the maximum theoretical load for the specimen. This percentage is considered as a reasonable number for this research. The experimental moment in this specimen was 68.75 kips-in, and the theoretical moment was 59.70 kips-in. This beam increased the moment capability by 13.16 percent in comparison with the maximum theoretical moment capacity for the specimen. This percentage is considered a reasonable number for this research. This beam was loaded 13.16 percent above the theoretical value to create significant damages and cracks, but it did not collapse, then was removed from the test setting, retrofitted with BFRP fabric, and re-tested again under Specimen S-1 D-R (damages and retrofitted). Strain gauge 7 received some type of damages that after 3.25 kips load applied and does not record any other data. Figure 220 represents the comparison of the theoretical and experimental load-deflection curve. Figure 221 represents the comparison of the theoretical and experimental strains of moment curvature.

For Specimen B-1, the experimental load applied was 5.57 kips. This beam was never loaded up to collapse load and the theoretical maximum load was 5.14 kips. The experimental load was 5.57 kips. The load capability of this beam was increased by 7.67 percent in comparison with the maximum theoretical load for the specimen. This percentage is considered as a reasonable number for this research. The experimental moment in this specimen was 76.59 kips-in, and the theoretical moment was 70.72 kips-in. This beam increased the moment capability by 7.67 percent in comparison with the maximum theoretical moment capacity for the specimen. This percentage is considered a reasonable number for this research. This beam was loaded 7.67 percent above the theoretical value to create significant damages and cracks, but it did not collapse, then it was removed from the test setting, retrofitted with BFRP fabric, and re-tested again under Specimen B-1 D-R (damages and retrofitted). Strain Gauge 3 received some type of damage that after 3.32 kips load applied and did not record any other data. Figure 222 represents the comparison of the theoretical and experimental load-deflection curve. Figure 223 represents the comparison of the theoretical and experimental strains moment curvature.

For Specimen S-B 1, the experimental load applied was 6.14 kips. This beam was loaded up to collapse load and the theoretical maximum load was 6.05 kips. The experimental load was 6.14 kips. The load capability of this beam was increased by 1.46 percent in comparison with the maximum theoretical load for the specimen. This percentage is considered reasonable for this research. The experimental moment in this specimen was 84.43 kips-in, and the theoretical moment was 83.19 kips-in. The moment capability of the beam was increased by 1.46 percent in comparison with the maximum theoretical moment capacity for the specimen. This percentage is considered reasonable for this research. Strain gauges 4, 5, and 6 received some type of damage after 2.92 kips load applied, and no other data was recorded. The comparison of the theoretical moment capacity between the S-1 and the S-B-1 was 59.70 kips-in without retrofit, and after retrofitted was 83.19 kips-in with an increased capacity of 28.24 percent. The comparison of the experimental moment capacity between the S-1 and the S-B-1 was 68.75 kips-in without retrofit, and after retrofitted was 84.43 kips-in with an increased capacity of 18.56 percent. The comparison of the theoretical moment capacity between the S-1 and the S-F-1 was 59.70 kips-in without retrofit, and after retrofitted was 94.02 kips-in with an increased capacity of 36.50 percent. The comparison of the experimental moment capacity between the S-1 and the S-B-1

was 68.75 kips-in without retrofit, and after retrofitted was 84.43 kips-in with an increased capacity of 18.57 percent. A single wrapping of Basalt fabric provided an increased load capacity of 36.50 percent. Figure 224 represents the comparison of the theoretical and experimental load-deflection curve. Figure 225 represents the comparison of the theoretical and experimental strains moment curvature.

For Specimen, B-B-1, the experimental load applied was 6.41 kips. This beam was loaded up to collapse load and the theoretical maximum load was 6.47 kips. The experimental load was 6.49 kips. The load capability of this beam was decreased by 0.99 percent in comparison with the maximum theoretical load for the specimen. This percentage is considered as a reasonable number for this research. The experimental moment in this specimen was 88.14 kips-in, and the theoretical moment was 89.01 kips-in. This beam decreased the moment capability by 0.99 percent in comparison with the maximum theoretical moment capacity for the specimen. This percentage is considered a reasonable number for this research. All strain gauges were recorded during the entire test. Figure 226 represents the comparison of the theoretical and experimental load-deflection curve.

The Specimen S-F-1, the experimental load applied was 7.01 kips. This beam was loaded up to collapse load and the theoretical maximum load was 6.83 kips. The experimental load was 7.01 kips. This beam increased the load capability by 2.51 percent in comparison with the maximum theoretical load for the specimen. This percentage is considered reasonable for this research. The experimental moment in this specimen was 96.80 kips-in, and the theoretical moment was 93.96 kips-in. This beam increased the moment capability by 2.51 percent in comparison with the maximum theoretical moment capacity for the specimen. This percentage is considered reasonable for this research. All strain gauges recorded data during the entire test. The comparison of the theoretical moment capacity between the S-1 and the S-F-1 was 59.46 kips-in without retrofit and after retrofitted was 94.02 kips-in with an increase capacity of 36.76 percent. The comparison of the experimental moment capacity between the S-1 and the S-B-1 was 68.75 kips-in without retrofitted and after retrofitted was 96.80 kips-in with an increase capacity of 28.98 percent. Figure 227 represents the comparison of the theoretical and experimental load-deflection curve.

For Specimen B-F-1, the experimental load applied was 8.45 kips. This beam was loaded up to collapse load and the theoretical maximum load was 8.17 kips. The experimental load was 8.45 kips. This beam increased the load capability by 3.27 percent in comparison with the maximum theoretical load for the specimen. This percentage is considered reasonable for this research. The experimental moment in this specimen was 116.19 kips-in, and the theoretical moment was 112.39 kips-in. This beam increased the moment capability by 3.27 percent in comparison with the maximum theoretical moment capacity for the specimen. This percentage is considered reasonable for this research. All strain gauges recorded data during the entire test. The comparison of the theoretical moment capacity between the B-1 and the B-F-1 was 76.59 kips-in without retrofit and after retrofitted was 116.19 kips-in with an increase capacity of 34.08 percent. The comparison of the experimental moment capacity between the B-1 and the B-B-1 was 76.59 kips-in without retrofit and after retrofitted was 89.10 kips-in with an increase capacity of 14.04 percent. A single wrapping of Basalt fabric provided an increase load capacity of 34.08 percent. Figure 228 represents the comparison of the theoretical and experimental load-deflection curve. Figure 229 represents the comparison of the theoretical and experimental strains moment curvature.

For Specimen S-1 D-R (damages and retrofitted), the experimental maximum load was 7.82 kips, and the theoretical maximum load was 7.72 kips. The experimental load was 7.82 kips; this beam increased the load capacity by 1.3 percent in comparison with the maximum theoretical load for the specimen. This percentage is considered reasonable for this research. The experimental moment in this specimen was 107.53 kips-in, and the theoretical moment was 106.26 kips-in. This beam increased the moment capability by 1.18 percent in comparison with the maximum theoretical moment capacity for the specimen. This percentage is considered reasonable for this research as the specimen was loaded in the previous test above the theoretical load but not at collapse. Strain Gauge 7 received some type of damage and after 7.80 kips load applied, did not record any other data. Figure 230 represents the comparison of the theoretical and experimental load-deflection curve. Figure 231 represents the comparison of the theoretical and experimental strains moment curvature.

For Specimen B-1 D-R (damages and retrofitted), the experimental maximum load was 7.44 kips, and the theoretical maximum load was 8.29 kips. The experimental load was 7.44 kips, this beam decreased the load capacity by 10.25 percent in comparison with the maximum theoretical load for the specimen. This percentage is considered reasonable for this research. The experimental moment in this specimen was 102.30 kips-in, and the theoretical moment was 114.02 kips-in. This beam decreased the moment capability by 10.25 percent in comparison with the maximum theoretical moment capacity for the specimen. This percentage is considered reasonable for this research as the specimen was loaded in the previous test above the theoretical load but not at collapse. Strain Gauge 3 was damaged in the original beam test at 3.32 kips applied load for this reason this strain gauge does not record any data for this entire test, gauges 4 and 5 received some type of damage and after 7.44 kips load applied, did not record any other data and Strain Gauges 6 and 7 received some type of damage and after 7.15 kips load applied did not record any other data. Figure 232 represents the comparison of the theoretical and experimental load-deflection curve. Figure 233 represents the comparison of the theoretical and experimental strains moment curvature.

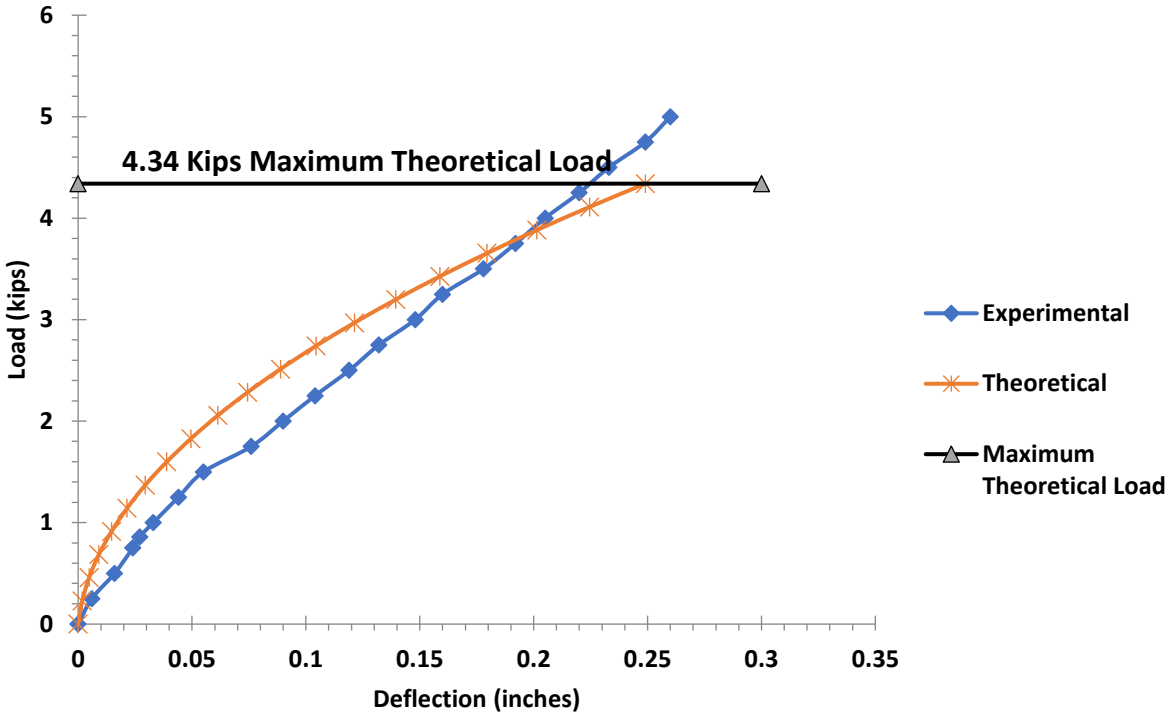

Figure 220. The Comparison of the Theoretical and Experimental Load-deflection Curve for Specimen S-1

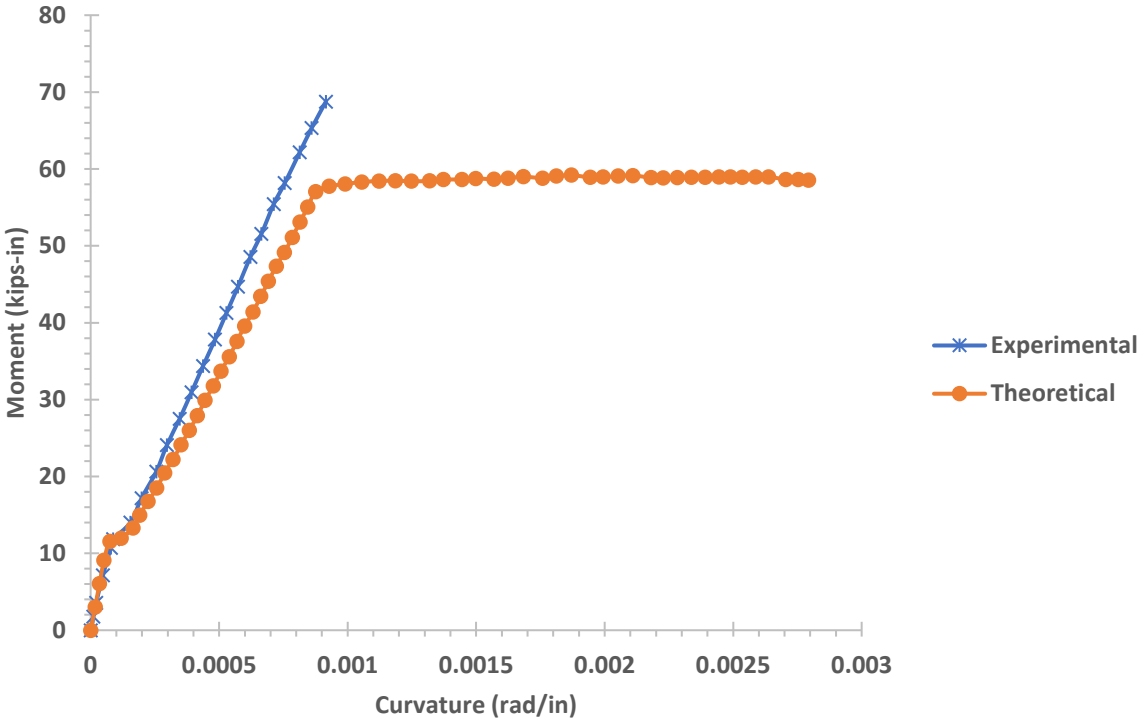

Figure 221. The Comparison of the Theoretical and Experimental Strain Moment-curvature for Specimen S-1

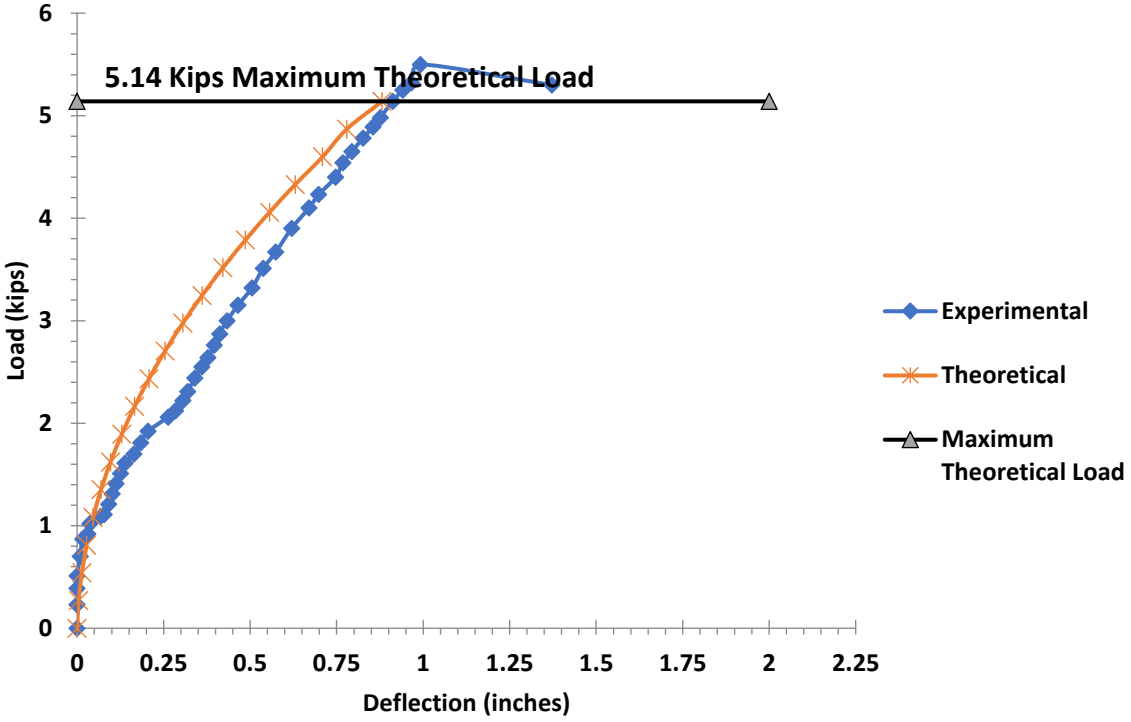

Figure 222. The Comparison of the Theoretical and Experimental Load-deflection Curve for Specimen B-1

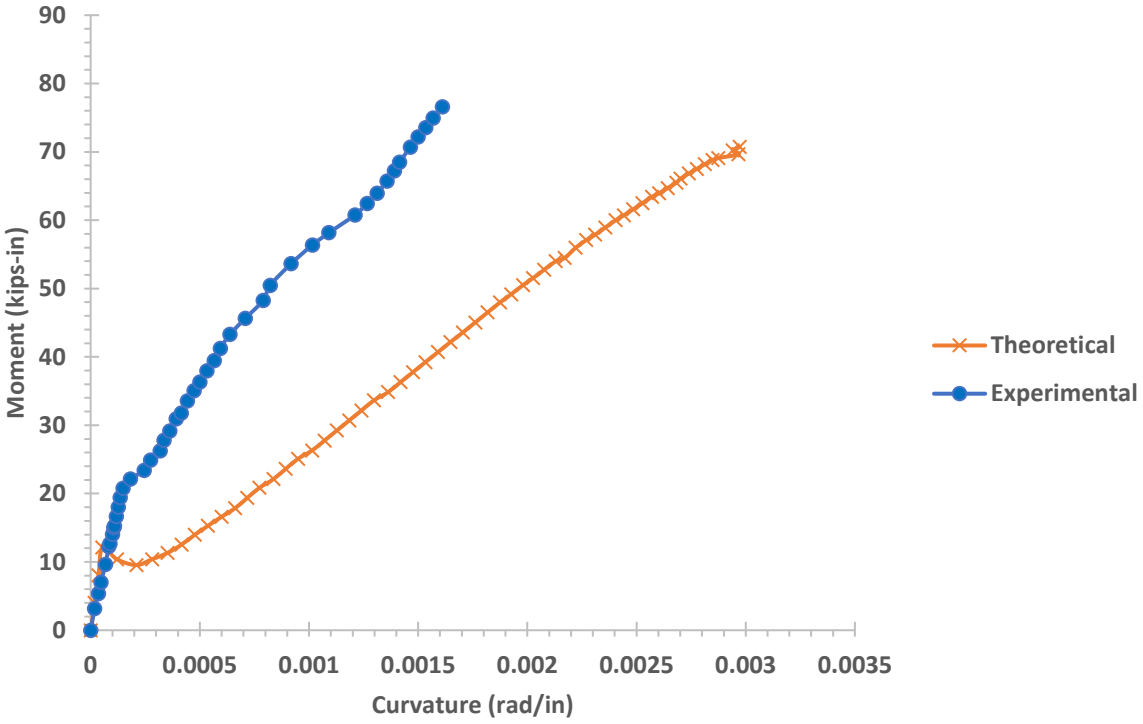

Figure 223. The Comparison of the Theoretical and Experimental Strain Moment-curvature for Specimen B-1

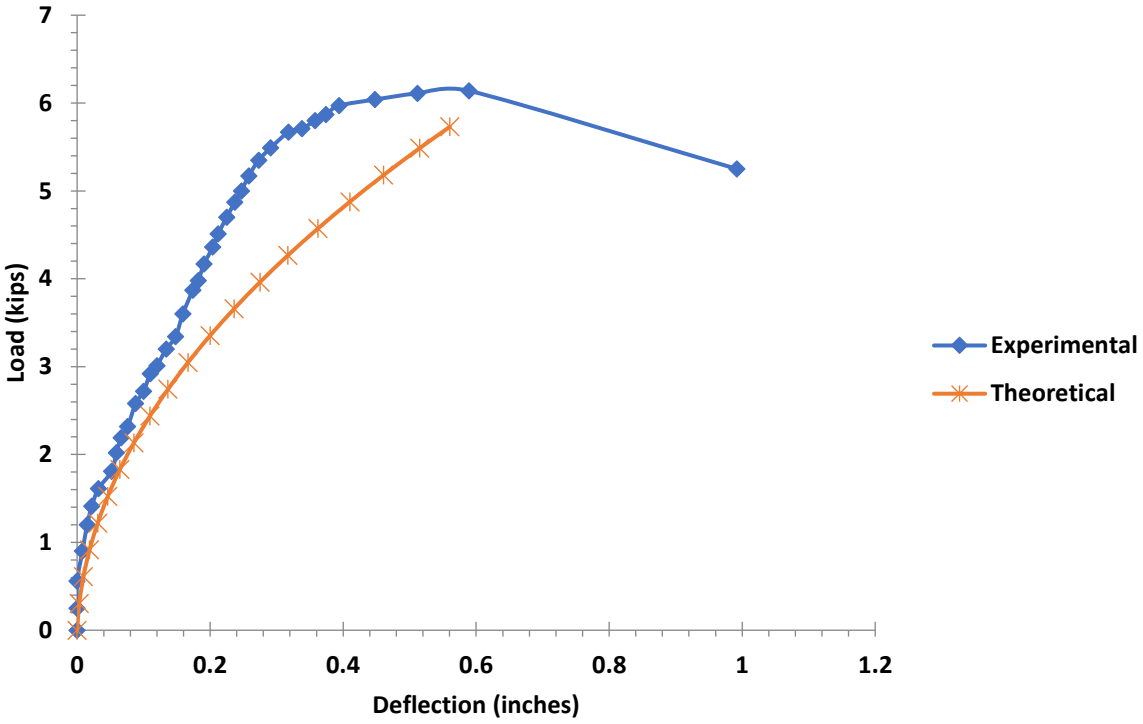

Figure 224. The Comparison of the Theoretical and Experimental Load-deflection Curve for Specimen S-B-1

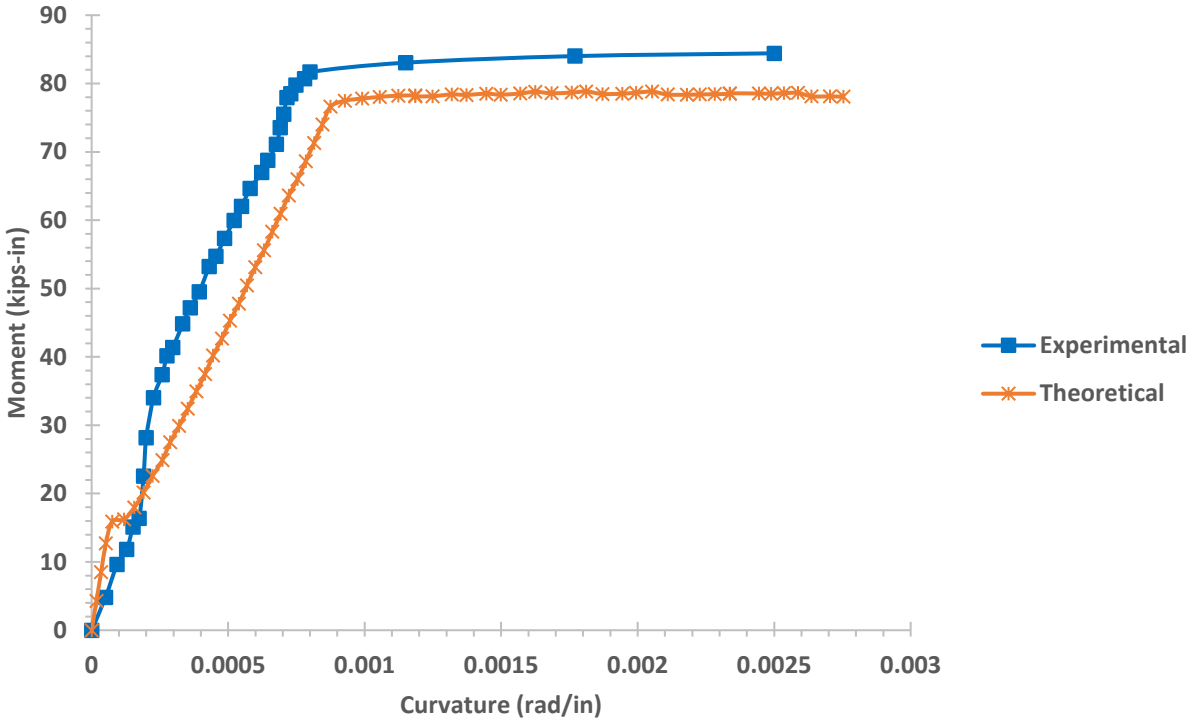

Figure 225. The Comparison of the Theoretical and Experimental Strain Moment-curvature for Specimen S-B-1

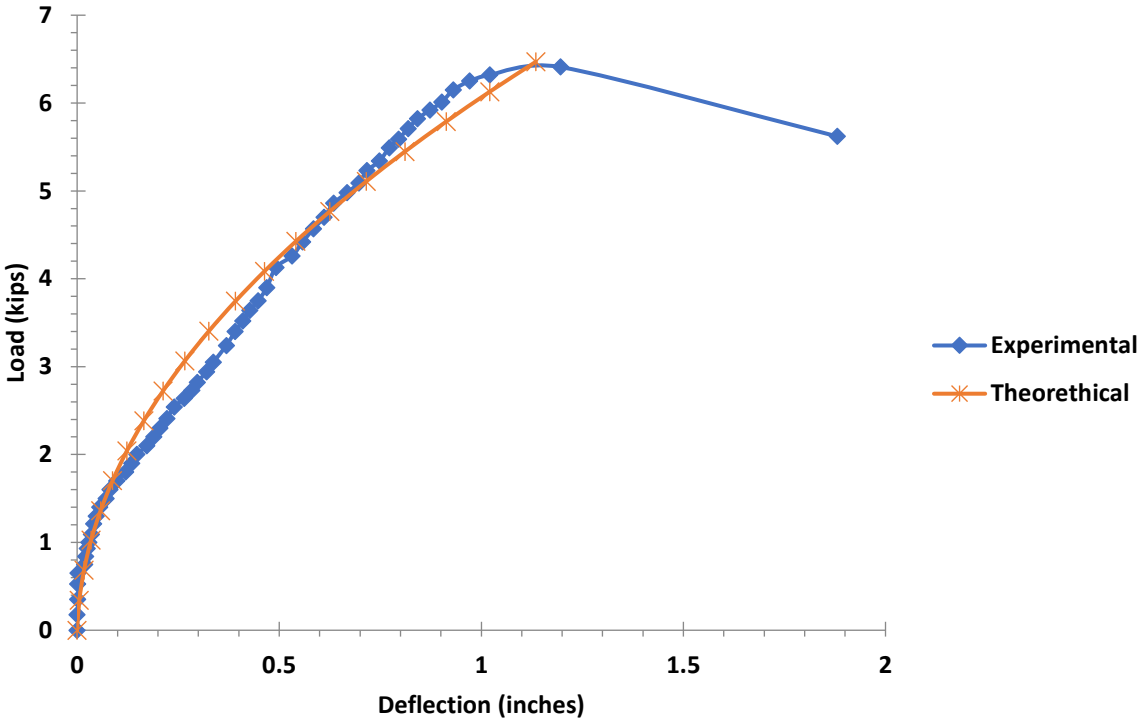

Figure 226. The Comparison of the Theoretical and Experimental Load-deflection Curve for Specimen B-B-1

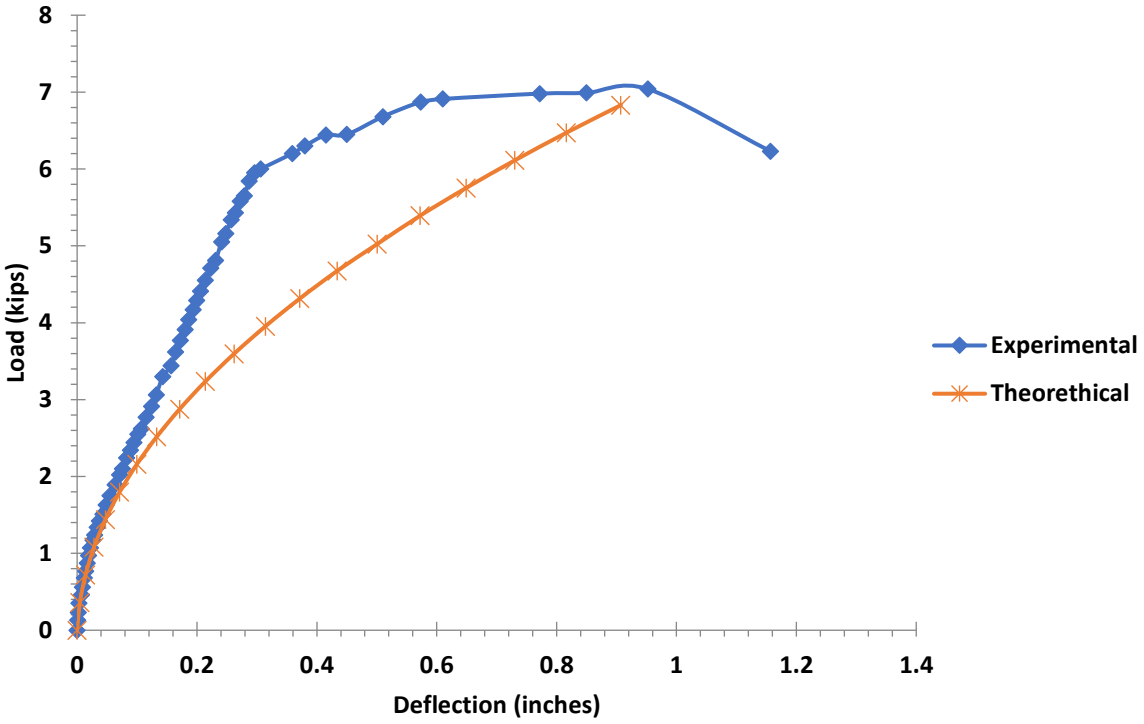

Figure 227. The Comparison of the Theoretical and Experimental Load-deflection Curve for Specimen S-F-1

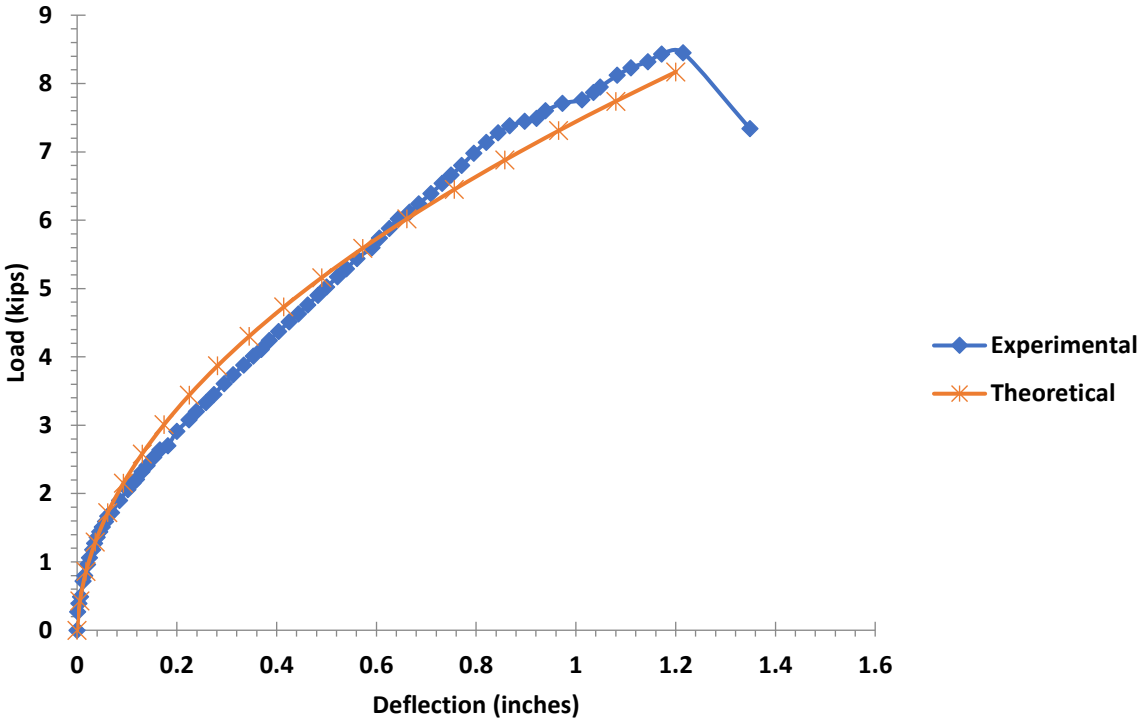

Figure 228. The Comparison of the Theoretical and Experimental Load-deflection Curve for Specimen B-F-1

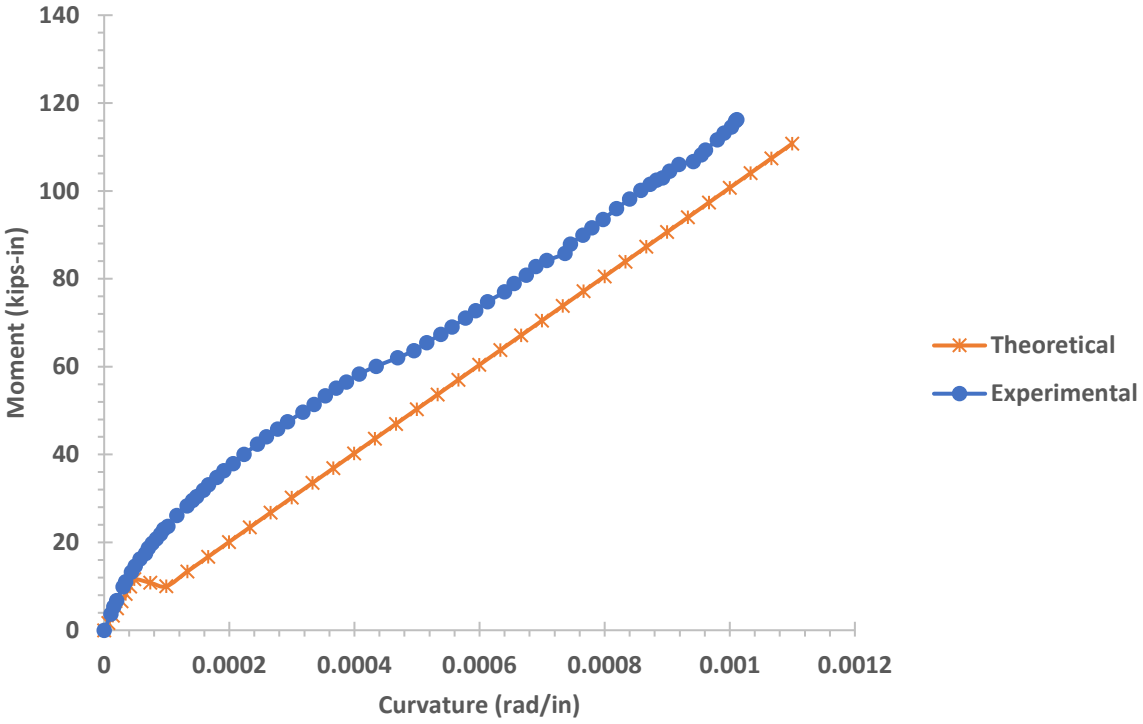

Figure 229. The Comparison of the Theoretical and Experimental Strain Moment-curvature for Specimen B-F-1

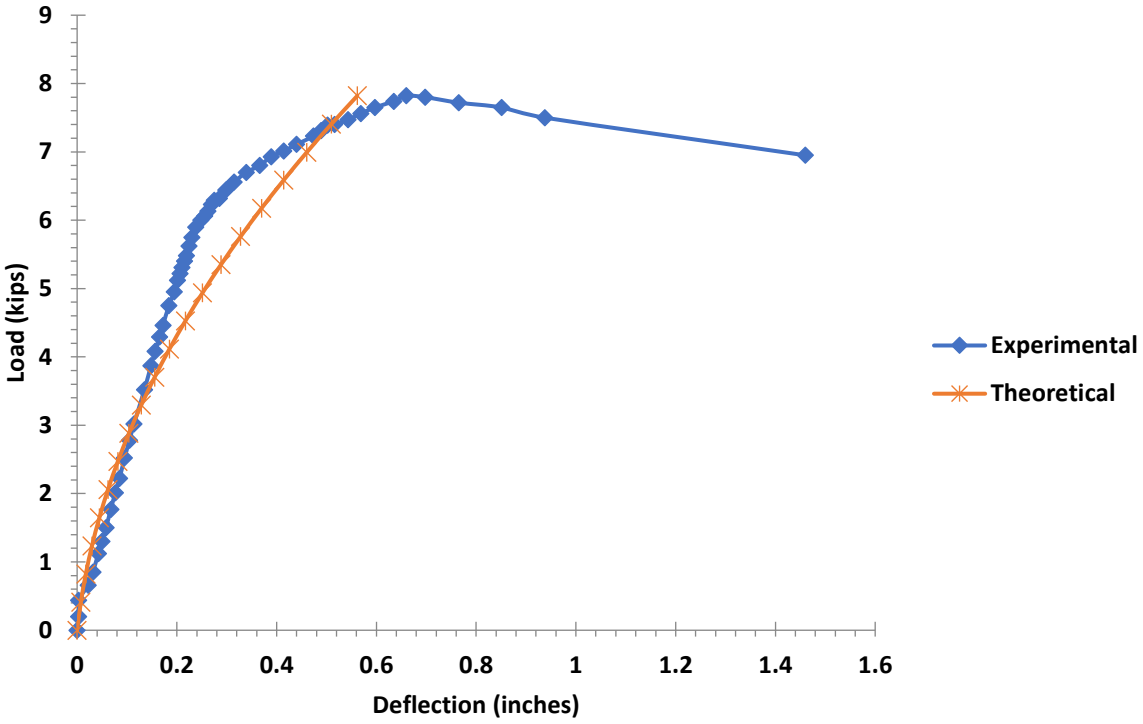

Figure 230. The Comparison of the Theoretical and Experimental Load-deflection Curve for Specimen S-1 damaged (retrofitted)

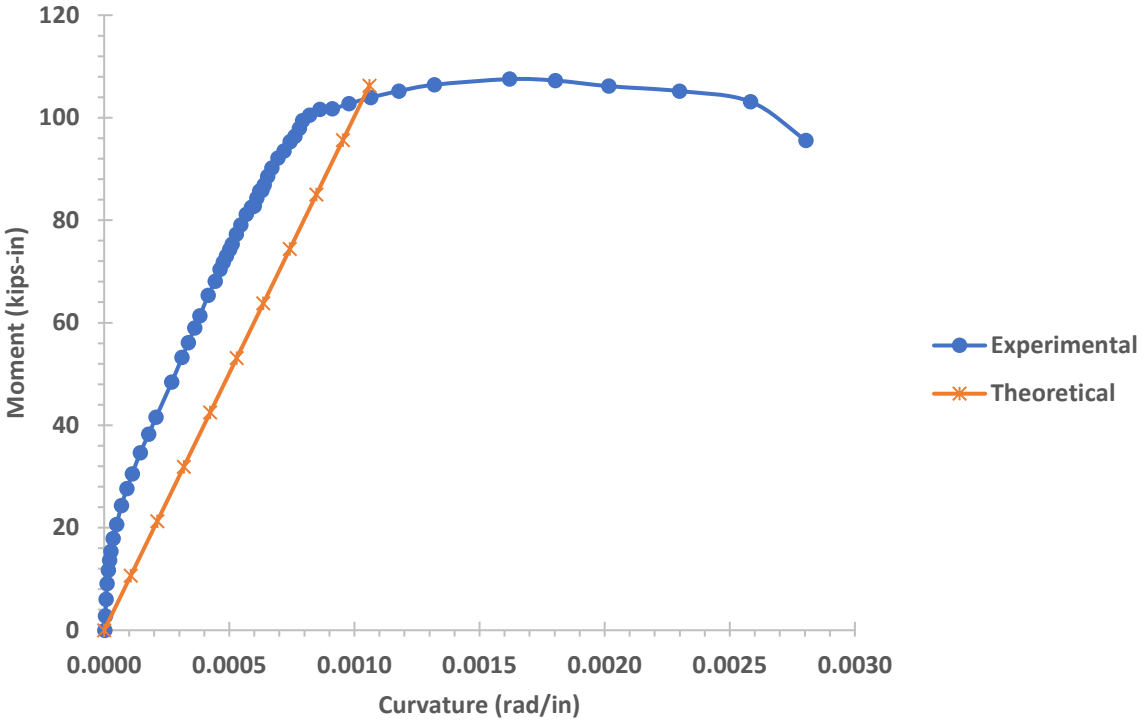

Figure 231. The Comparison of the Theoretical and Experimental Strain Moment-curvature for Specimen S-1 damaged (retrofitted)

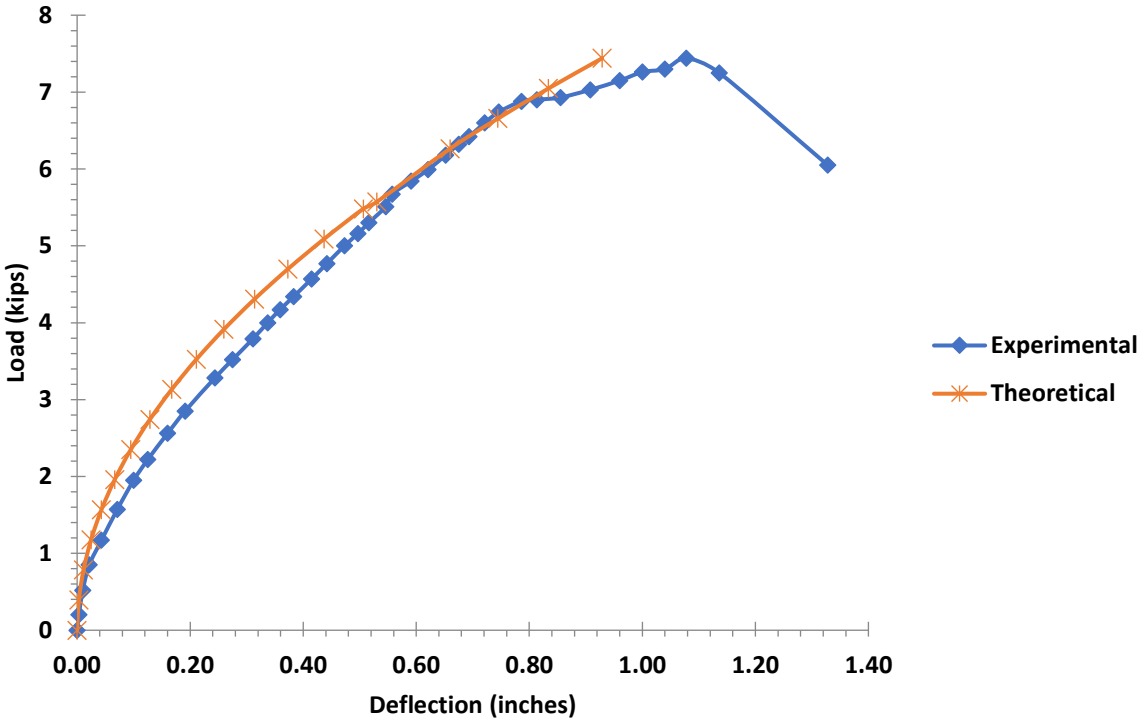

Figure 232. The Comparison of the Theoretical and Experimental Load-deflection Curve for Specimen B-1 damaged (retrofitted)

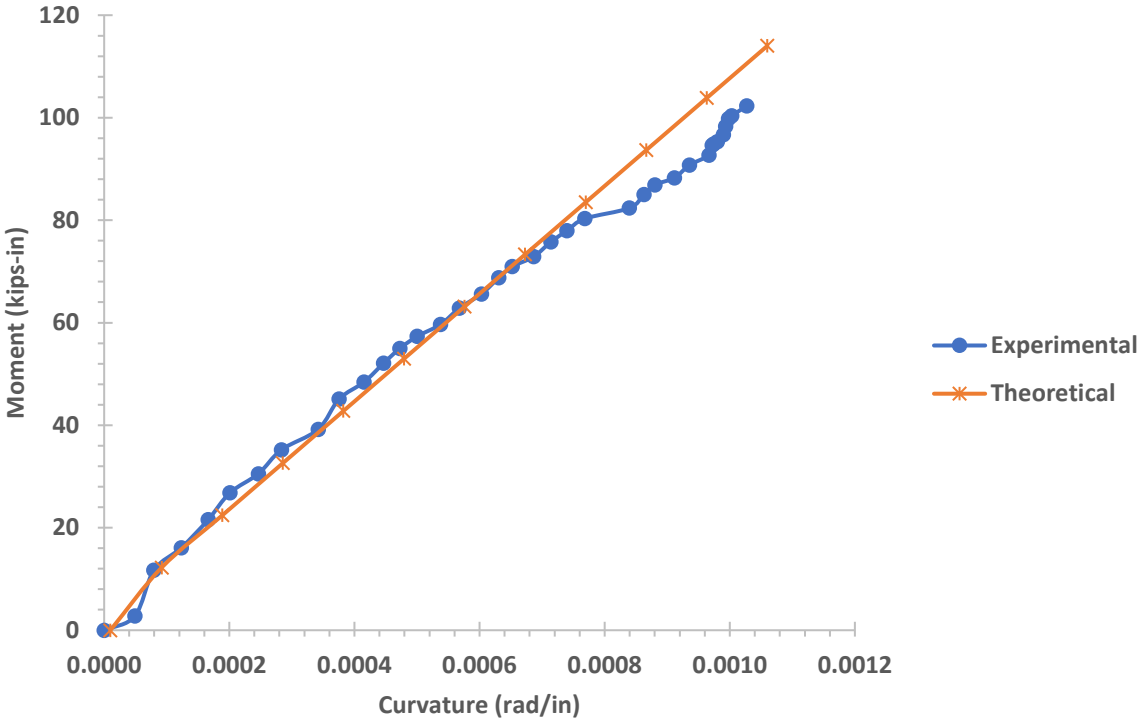

Figure 233. The Comparison of the Theoretical and Experimental Strain moment-curvature for Specimen B-1 damaged (retrofitted)

Figure 234 illustrates an experimental comparison of beam S-1, S-B, and S-F at the ultimate strength for each beam. Beam S-1 the ultimate load was 5.0 kips. Beam S-B the ultimate strength was 6.14 kips and Beam S-F the ultimate strength was 7.01 kips.

Figure 235 illustrates an experimental comparison of beams deflection at the service load of 5.0 kips for beams S-1, S-B, S-F, and S-1 D-R for each beam. Beam S-1 deflected 0.26 inch. Beam S-B deflected 0.24 inch. Beam S-F deflected 0.23 inch, and Beam S-1D-R deflected 0.19 inch.

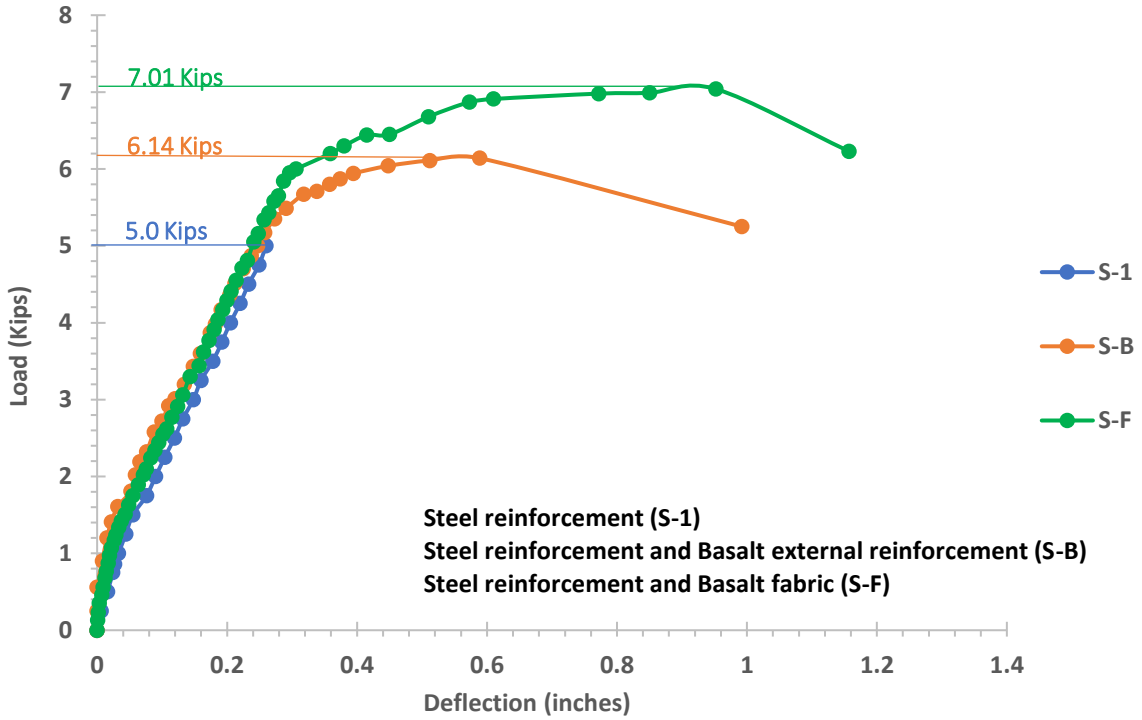

Figure 234. Experimental Comparison between Beams S-1, S-B, and S-F at Ultimate Strength

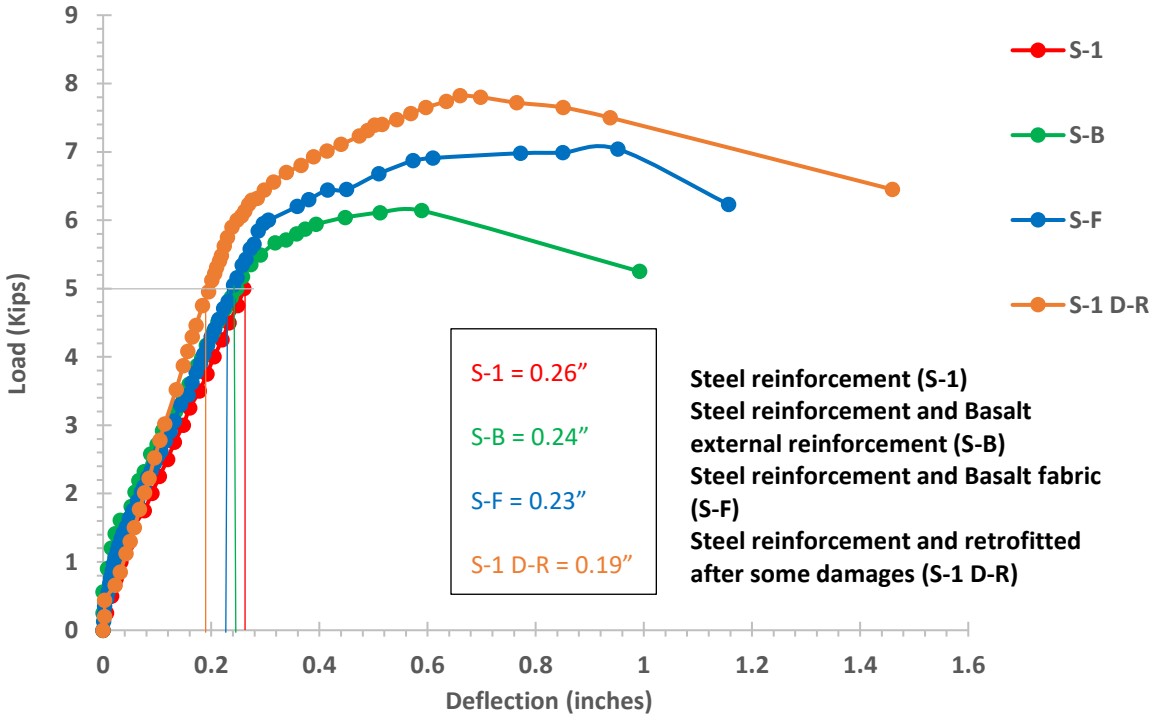

Figure 235. Experimental Comparison between Beams S-1, S-B, and S-F Deflection at Service Load of 5.0 kips

Figure 236 illustrates an experimental comparison of beams B-1, B-B, and B-F at the ultimate strength for each beam. Beam B-1 the ultimate load was 5.57 kips. Beam B-B the ultimate strength was 6.48 kips and Beam B-F the ultimate strength was 8.45 kips.

Figure 237 illustrates an experimental comparison of beams deflection at service load of 5.0 kips for beams B-1, B-B, B-F, and B-1 D-R for each beam. Beam B-1 deflected 0.89 inch. Beam B-B deflected 0.68 inch. Beam B-F deflected 0.47 inch, and Beam B-1D-R deflected 0.50 inch.

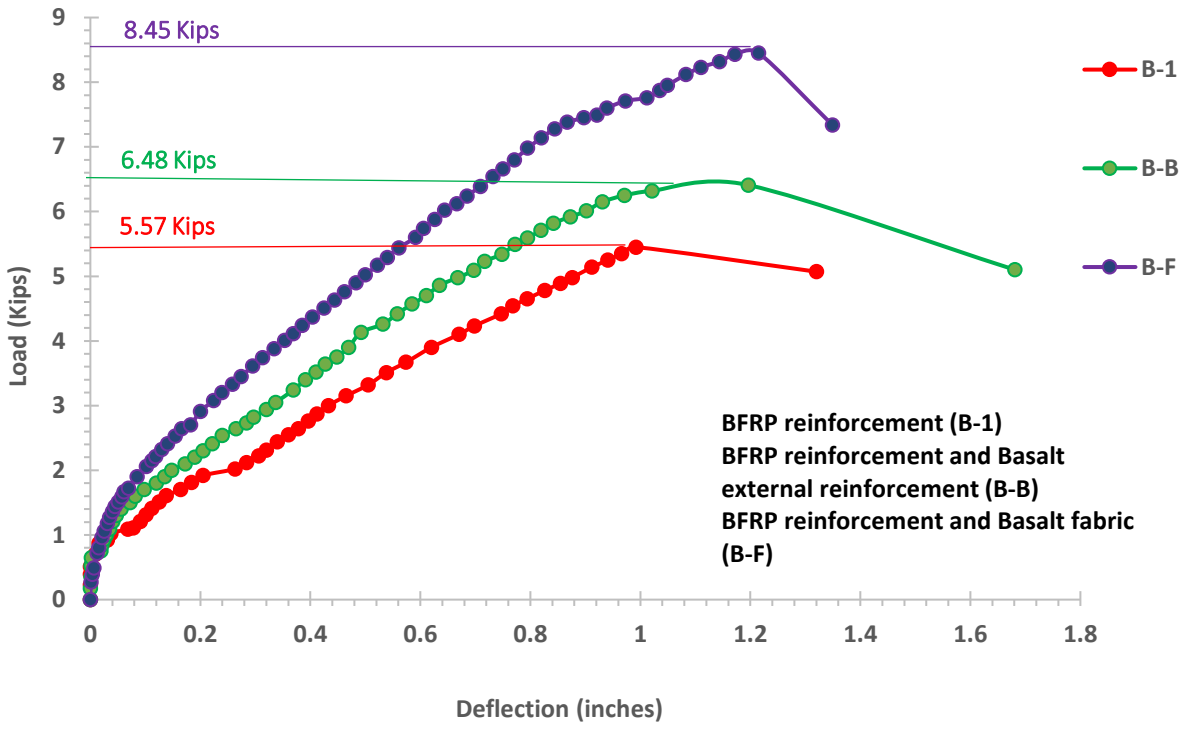

Figure 236. Experimental Comparation between Beams B-1, B-B, and B-F at Ultimate Strength

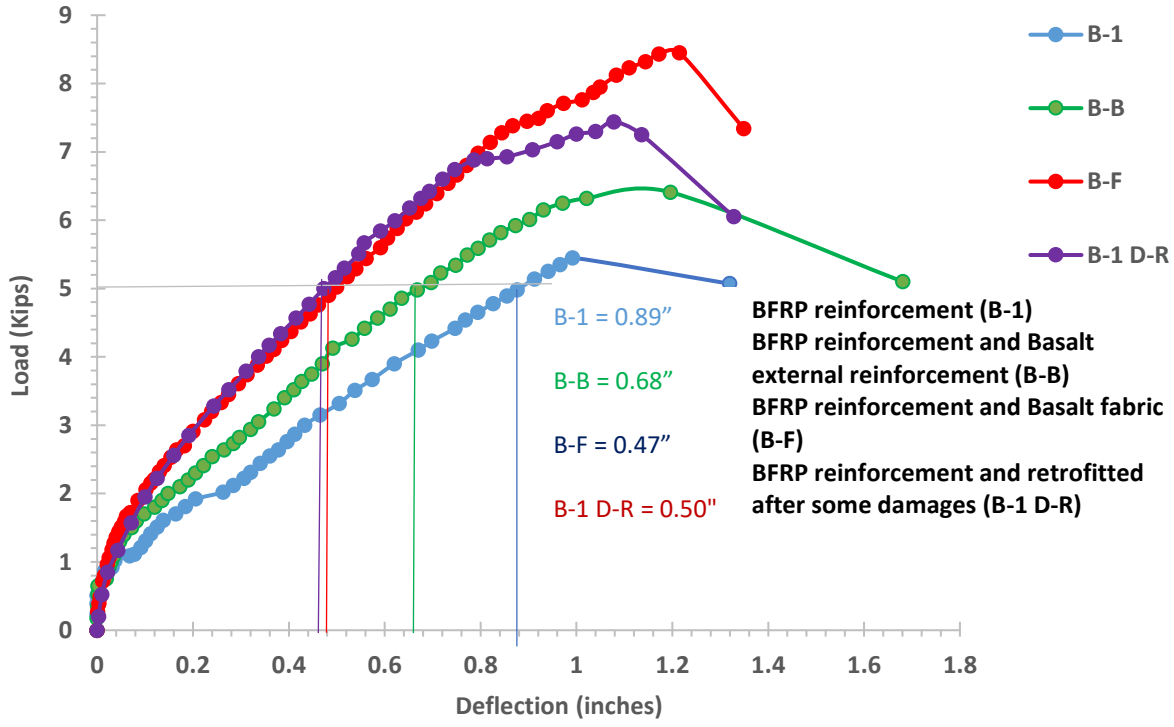

Figure 237. Experimental Comparation of Beam B-1, B-B, B-F, and B-1 D-R Deflection at Service Load of 5.0 kip

4.2 The Simply Supported Beam Under Impact Load

Table 12 represents the natural frequency, natural period and the impact velocity on the beam applied to each beam at 10-inch drop with impactor of 0.14 kips.

Table 12**.** Impact Force, Natural Frequency, Natural Period, and Impact Velocity at 10 inches Drop

Beam	ω (rad/sec)	Natural Frequency (Hz)	Natural Period (sec)
S-2	264.65	42.120	0.02365
S-B	264.18	42.045	0.02378
S-F	263.25	41.898	0.02386
B-B	266.06	42.345	0.02361
B-F	265.59	42.269	0.02357

Table 13 represents the force applied to each beam at 10 inches drop with impactor of 0.14 kips on all specimens.

Table 13. Impact Force at 10 inches Drop

Beam	Acceleration at 10” with 0.14-kip impactor (in/sec^2)	Impact Force at 10 inches (kips)
S-2	0.16	0.06
S-B	0.35	0.13
S-F	0.12	0.04
B-B	0.31	0.11
B-F	0.60	0.22

Table 14 represents the impact drop height, impact weight, acceleration at collapse and the impact force received by each beam at the collapse drop.

Table 14. Impact Force at Collapse

Beam	Impactor Drop Height (inches)	Impact weight (Kips)	Acceleration at Collapse (in/sec^2)	Impact Force at Collapse (kips)
S-2	21.0	0.14	1.50	0.54
S-B	7.0	0.40	4.50	4.66
S-F	21.0	0.14	4.47	1.62
B-B	25.0	0.14	3.84	1.39
B-F	17.0	0.40	8.36	8.65

Table 15 represents the impact drop height, impact weight, post-impact natural frequency at collapse and the post-impact natural frequency at 10-inch drop for each specimen.

Table 15. Post-impact Natural Frequency at Collapse and Post-impact Natural Frequency at 10 inches drop

Beam	Impactor Drop Height (inches)	Impact weight (Kips)	Post-Impact Natural frequency at collapse (Hz)	Post-Impact Natural frequency at 10 inches drop (Hz)
S-2	21.0	0.14	42.120	42.120
S-B	7.0	0.40	30.309	42.045
S-F	21.0	0.14	41.898	41.898
B-B	25.0	0.14	42.354	42.345
B-F	17.0	0.40	30.46	42.27

Table 16 represents the impact drop height, impact force at collapse/impact drop height ration, impact force at 10-inch drop/10-inch height ratio and the impact force at collapse/impact force inches drop ratio for each specimen.

Table 16. Impact Force at Collapse Normalized with Impact Force at 10 inches Drop

Beam	Impactor Drop Height (inches)	Impact Force at collapse / impact drop height	Impact force at 10 inches drop /10 inches height	Impact Force at collapse / Impact force at 10 inches drop
S-B	7.0	0.666	0.013	51.23
B-F	17.0	0.509	0.022	23.13
S-F	21.0	0.077	0.004	19.28
B-B	25.0	0.056	0.011	5.05
S-2	21.0	0.025	0.006	4.17

4.2.1 Acceleration Response for Each Simply Supported Beam

In this section, the acceleration results under three different load conditions are presented. The first is the acceleration of each the specimen tested under impact load using impactor 1 (0.60 drop) dropped at 10 inches. The second condition was at the beam collapse. The beam collapse is presented here; however, it was not compared with the theoretical beam acceleration, due to the beam vibration does not generate a uniform oscillation due to the amounts of cracks in the beam that can affect the support were the accelerometer was attached to the beam.

Figure 238 represents the acceleration of Specimen S-2 using the impactor 2 (0.14 kips) dropped at 10 inches high. The maximum positive acceleration for the beam was 0.16 g's at 0.0043 second and the maximum negative acceleration was 0.14 g's at 0.0195 second. A theoretical acceleration was developed for this test using an 8.75 percent damping to be in line with the experimental acceleration. Figure 239 represents the acceleration of Specimen S-2 using impactor 2 (0.14 kips) dropped at 21 inches high; during this test the specimen collapsed. The maximum positive acceleration for the beam was 1.5 g's at 0.0594 second and the maximum negative acceleration was 0.38 g's at 0.0738 second.

Figure 240 represents the acceleration of Specimen S-B using the impactor 2 (0.14 kips) dropped at 10 inches high. The maximum positive acceleration for the beam was 0.27 g's at 0.0287 second and the maximum negative acceleration was 0.35 g's at 0.0152 second. A

theoretical acceleration was developed for this test using a 5.5 percent damping to be in line with the experimental acceleration. Figure 241 represents the acceleration of Specimen S-B using impactor 3 (0.40 kips) dropped at 7 inches high; during this test the specimen collapsed. The maximum positive acceleration for the beam was 4.2 g's at 0.0117 second and the maximum negative acceleration was 4.5 g's at 0.0231 second.

Figure 242 represents the acceleration of Specimen S-F using the impactor 2 (0.14 kips) dropped at 10 inches high. The maximum positive acceleration for the beam was 0.12 g's at 0.0078 second and the maximum negative acceleration was 0.01 g's at 0.088 second. Figure 244 represents the acceleration of Specimen S-F using impactor 2 (0.14 kips) dropped at 21 inches high; during this test the specimen collapsed. The maximum positive acceleration for the beam was 9.72 g's at 0.0395 second and the maximum negative acceleration was 10.39 g's at 0.08192 second. A theoretical acceleration was developed for this test using a 5.0 percent damping to be in line with the experimental acceleration.

Figure 243 represents the acceleration of Specimen B-B using the impactor 2 (0.14 kips) dropped at 10 inches high. The maximum positive acceleration for the beam was 0.17 g's at 0.0015 second and the maximum negative acceleration was 0.15 g's at 0.0109 second. A theoretical acceleration was developed for this test using a 5.5 percent damping to be in line with the experimental acceleration. Figure 244 represents the acceleration of Specimen B-B using impactor 2 (0.14 kips) dropped at 25 inches high; during this test the specimen collapsed. The maximum positive acceleration for the beam was 0.38 g's at 0.0028 second and the maximum negative acceleration was 0.03 g's at 0.0032 second.

Figure 245 represents the acceleration of the Specimen B-F using the impactor 2 (0.14 kips) dropped at 10 inches high. The maximum positive acceleration for the beam was 0.26 g's at 0.1613 second and the maximum negative acceleration was 0.60 g's at 0.0903 second. Figure 248 represents the acceleration of the Specimen B-F using impactor 3 (0.40 kips) dropped at 17 inches high; during this test the specimen collapsed. The maximum positive acceleration for the beam was 8.36 g's at 0.0012 second and the maximum negative acceleration was 5.77 g's at 0.0115 second.

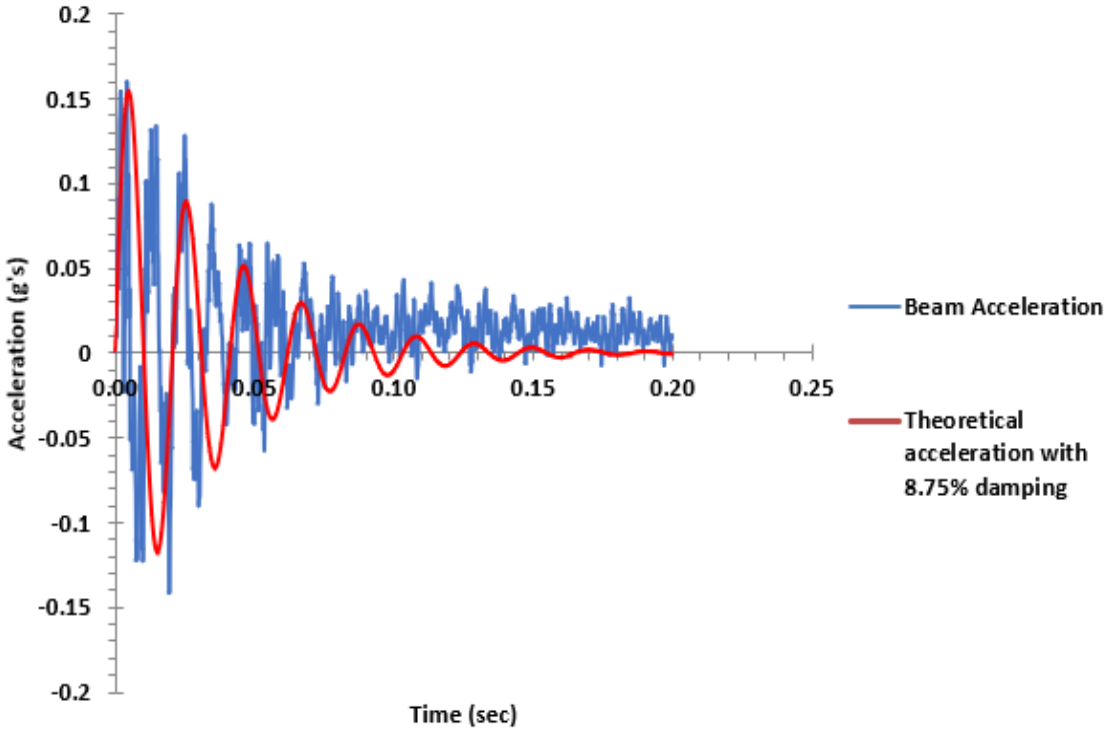

Figure 238. Experimental Beam Acceleration versus Theoretical Value for Specimen S-2 with Impactor 2 at 10 inches

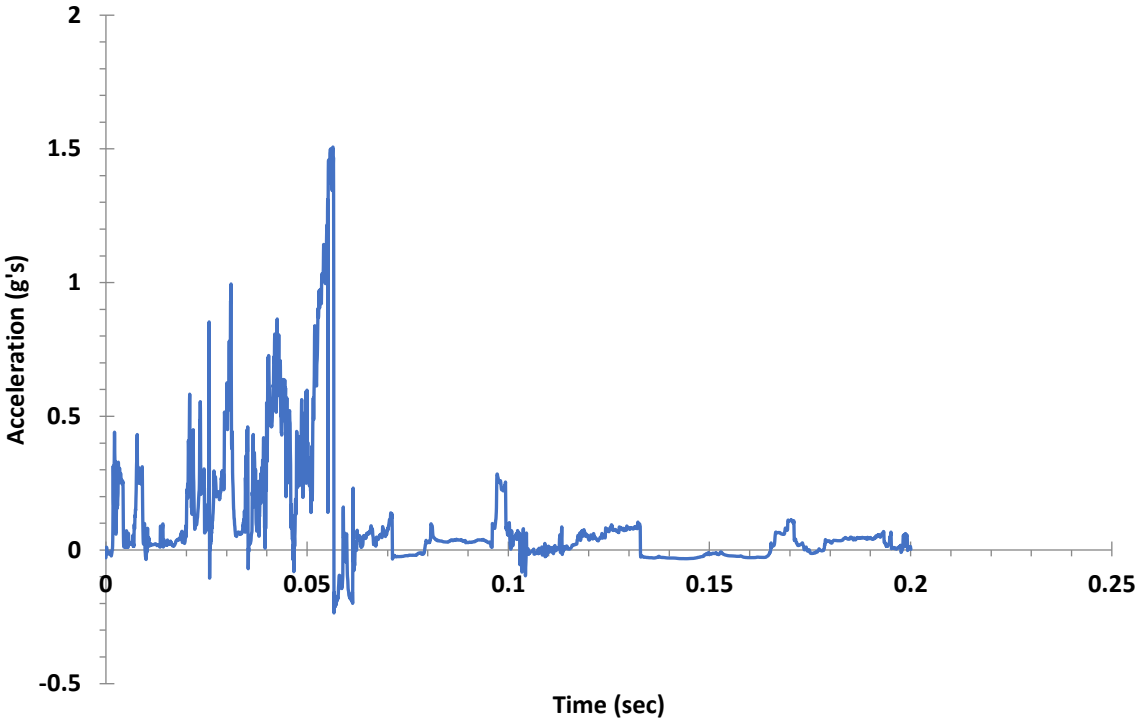

Figure 239. Experimental Beam Acceleration for Specimen S-2 with Impactor 2 at Collapsed Load

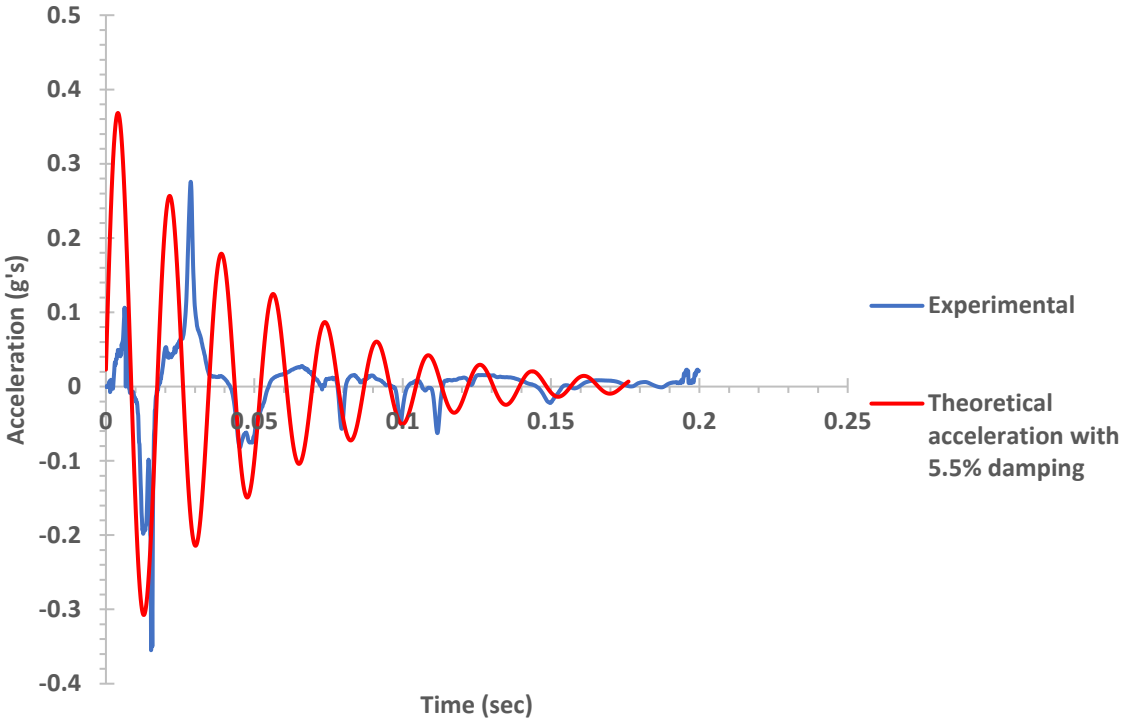

Figure 240. Experimental Beam Acceleration versus Theoretical Value for Specimen S-B with Impactor 2 at 10 inches

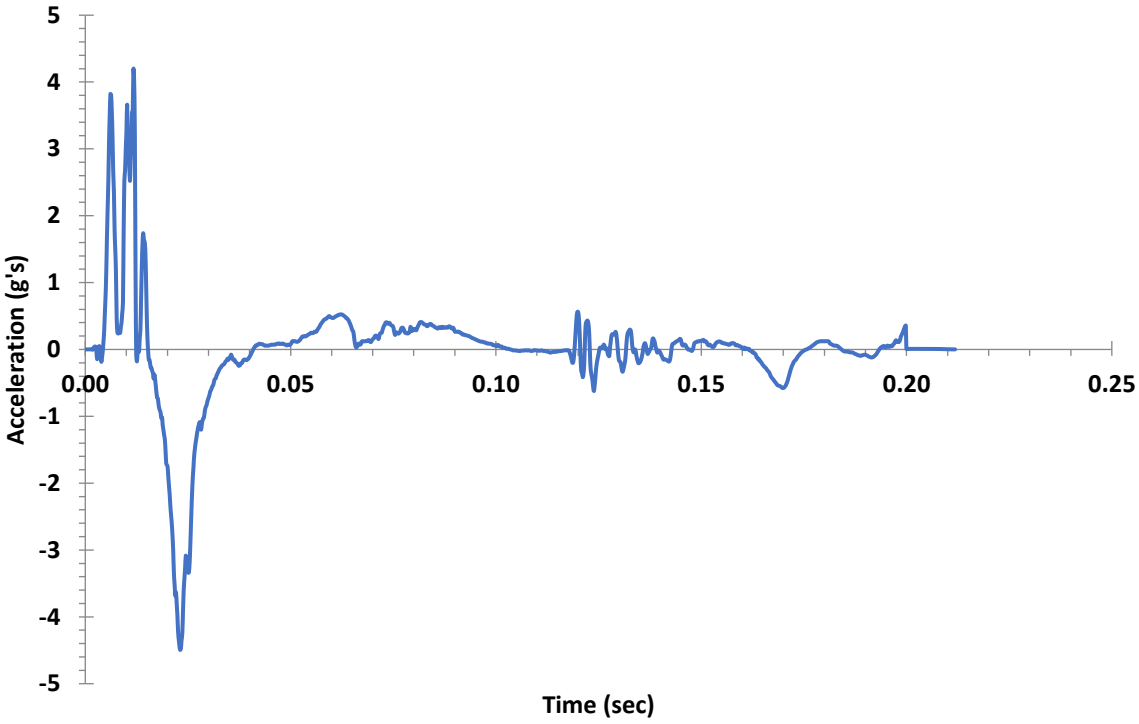

Figure 241. Experimental Beam Acceleration for Specimen S-B 2 with Impactor 2 at Collapsed Load

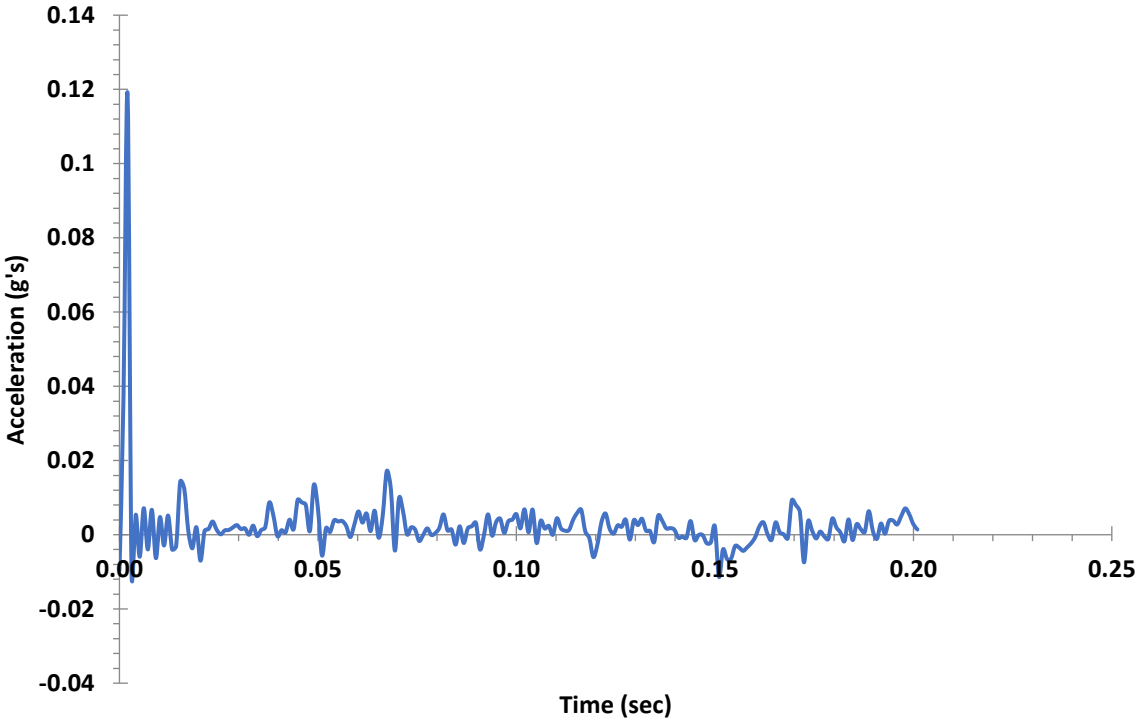

Figure 242. Experimental Beam Acceleration for Specimen S-F 2 with Impactor 2 at 10 inches

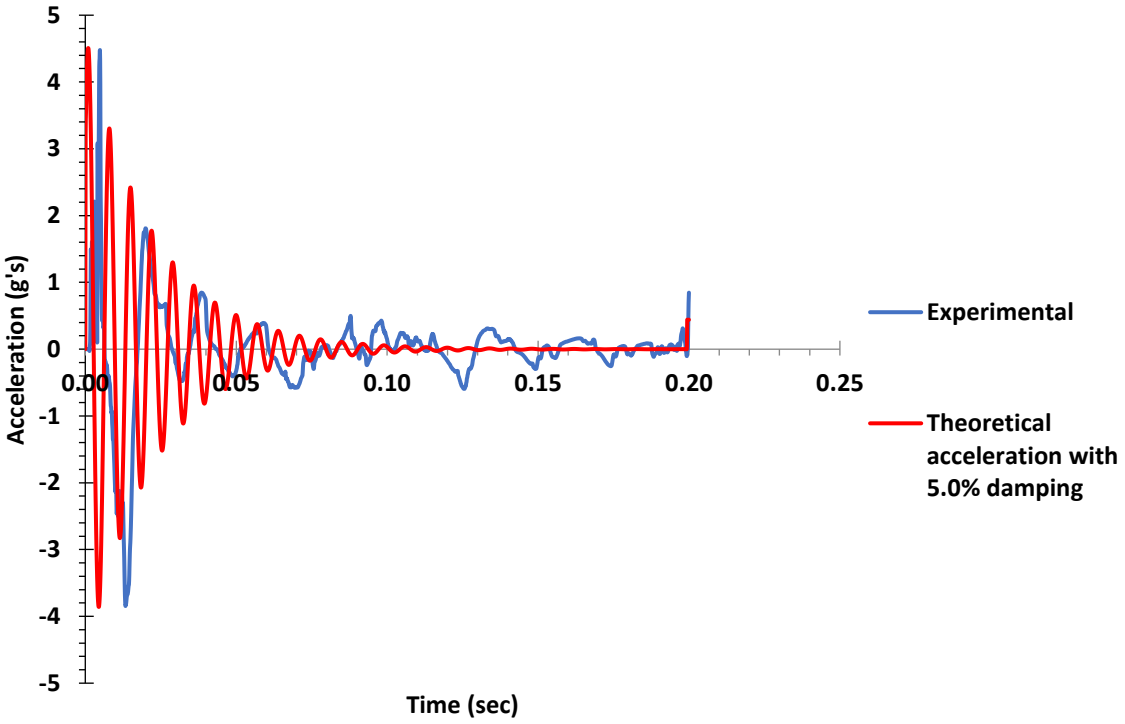

Figure 243. Experimental Beam Acceleration versus Theoretical Value for Specimen S-F 2 with Impactor 2 at Collapsed Load

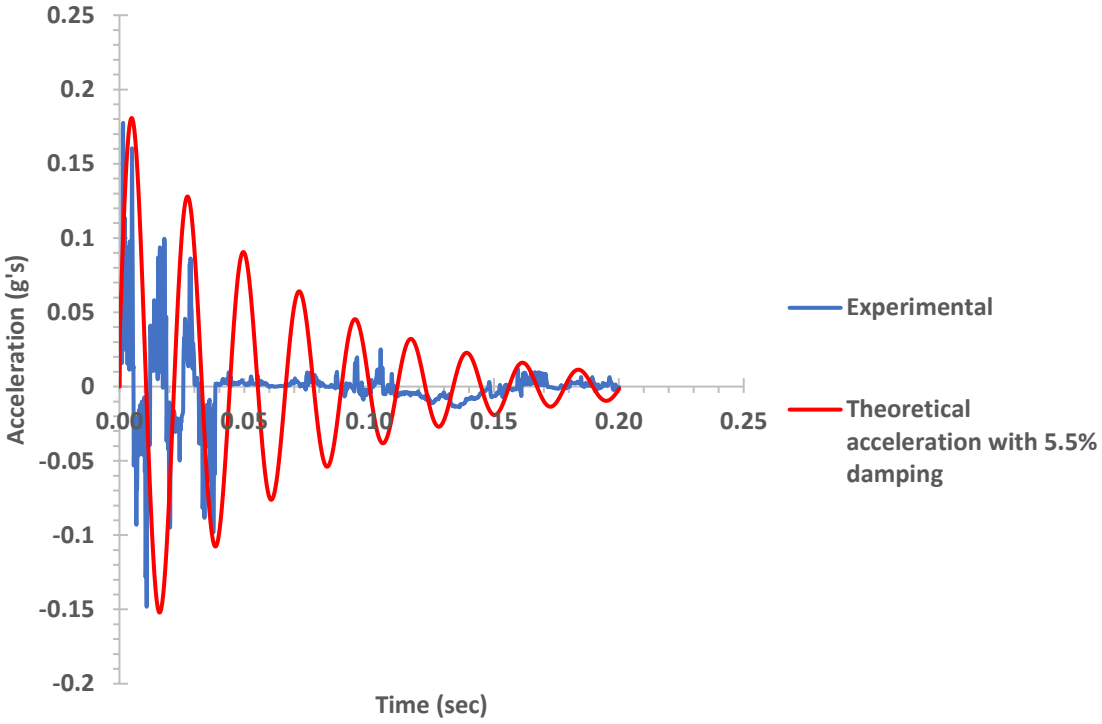

Figure 244. Experimental Beam Acceleration versus Theoretical Value for Specimen B-B with Impactor 2 at 10 inches

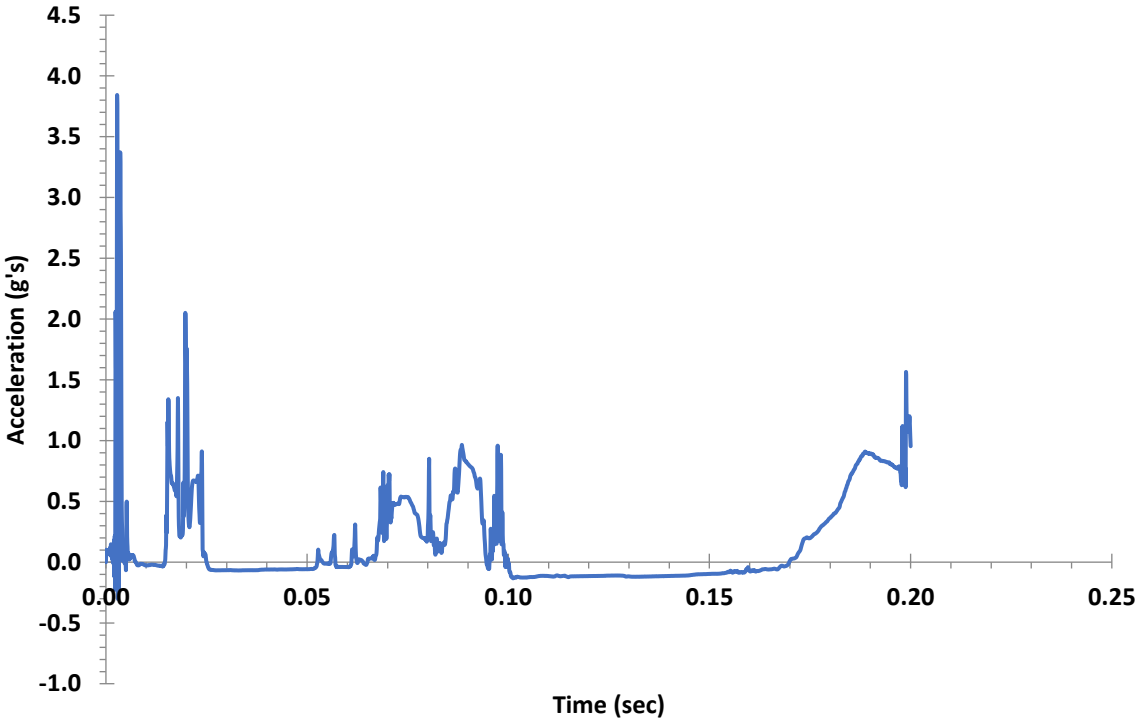

Figure 245. Experimental Beam Acceleration for Specimen B-B with Impactor 2 at Collapsed Load

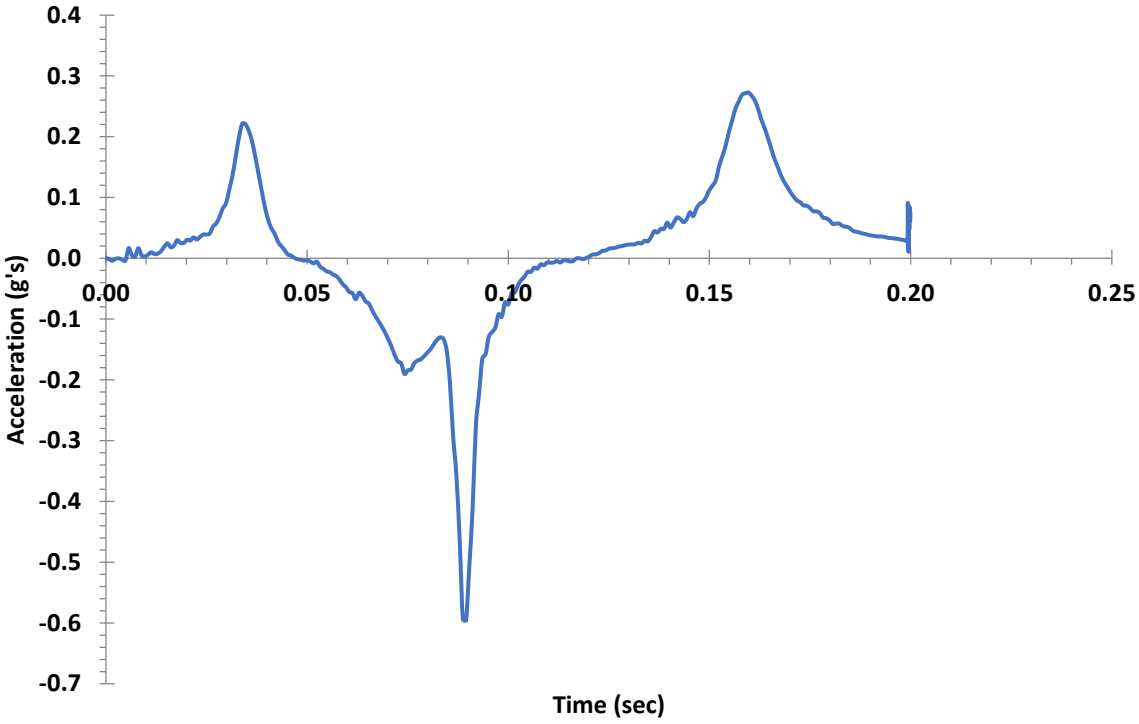

Figure 246. Experimental Beam Acceleration Value for Specimen B-F with Impactor 2 at 10 inches

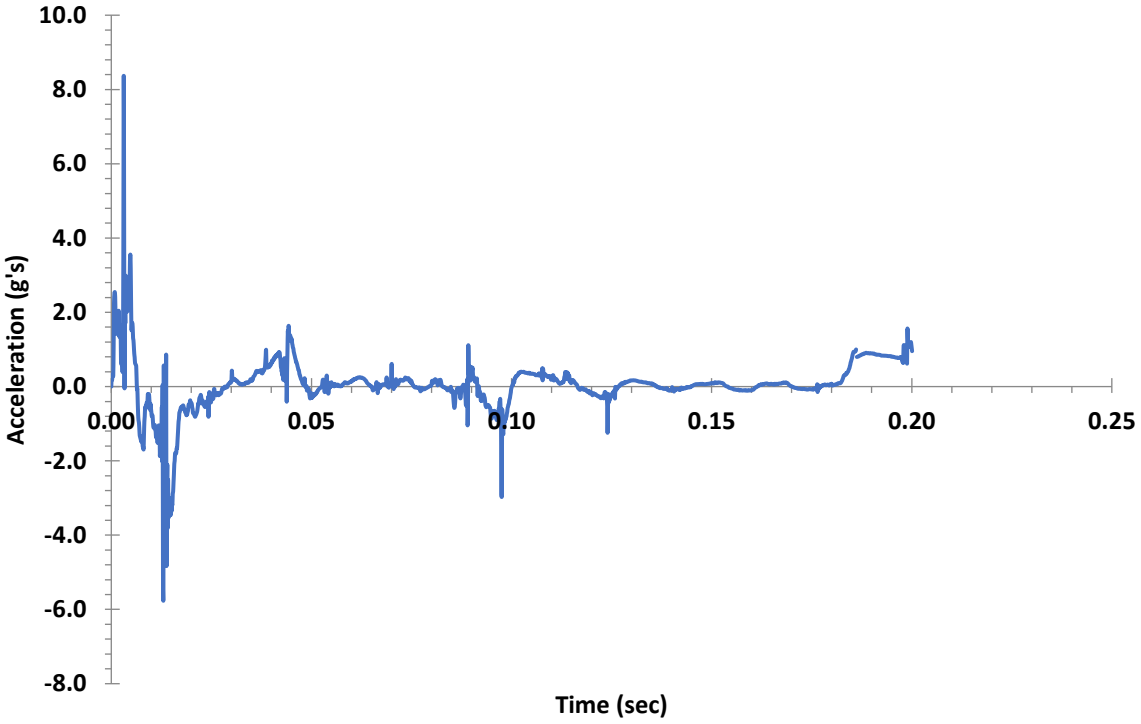

Figure 247. Experimental Beam Acceleration for Specimen B-F 2 with Impactor 3 at Collapsed Load

4.3 The Sub-assemblage Behavior Under Quasi-Static Load

Table 17 shows a comparison between the experimental maximum load and the theoretical maximum load for the four sub-assemblage specimens tested during this research. It was tested using moment-curvature and the finite difference techniques to obtain the load deflection for each of the beams. Table 18 indicates the experimental maximum moment and the theoretical maximum moment for each test during this research.

Table 17. Comparison between Experimental and Theoretical Maximum Load

Specimen	Experimental Load (kips)	Theoretical Load (kips)	Experimental / Theoretical
S2-1	5.80	6.07	0.96
S2-2	5.35	6.07	0.88
B2-1	4.85	7.06	0.69
B2-2	5.20	7.06	0.74

Table 18. Comparison between Experimental and Theoretical Maximum Moments at Missing Column

Test	Experimental	Theoretical	Experimental / Theoretical
	Max. Moment at Mid-point (kips-in)	Max. Moment at Mid-point (kips-in)	
S2-1	50.03	52.35	0.96
S2-2	46.14	52.35	0.88
B2-1	41.23	60.89	0.68
B2-2	44.20	60.89	0.73

For Specimen S2-1, the experimental load applied to the modified sub-assemblage was 5.80 kips. This beam was loaded up to the collapse load. The theoretical maximum load for the original sub-assemblage with 32 inches long was 6.07 kips and the experimental load was 5.80 kips. The load capability of this beam was decreased by 4.45 percent in comparison with the maximum theoretical load for the original sub-assemblage. The experimental moment in this specimen was 50.03 kips-in and the theoretical moment was 52.35 kips-in. This beam decreased the moment capability by 4.45 percent in comparison with the maximum theoretical moment capacity for the sub-assemblage. On Figure 156 was observed the amount of bending and shear cracks this sub-assemblage developed were not counted during the development of the moment-curvature, the only consideration was that the beam would fail for bending. These shear crack developed at the

fixed end supports and on both side of the missing column was the factor for the beam failure before reaching the collapse load of 6.07 kips.

All strain gauges recorded data during the entire test. At the collapse load four strain gauges exceeded the strain of the steel or the steel and concrete. Strain Gauge 3 had a reading of -0.0025 in/in, this strain value exceeded yield point of 0.0023 in/in for the steel reinforcement at this location. Strain Gauge four had a reading of -0.0044 in/in, this strain value exceeded yield point of 0.0023 in/in for the steel reinforcement and the concrete of 0.0031 in/in at this location. Strain Gauge twelve had a reading of -0.0046 in/in, this strain value exceeded yield point of 0.0023 in/in for the steel reinforcement and the concrete of 0.0031 in/in at this location. Strain Gauge thirteen had a reading of -0.0039 in/in, this strain gauge value exceeded yield point of 0.0023 in/in for the steel reinforcement and the concrete of 0.0031 in/in at this location.

The experimental maximum deflection at the failure column was recorded at 1.11 inches and the theoretical maximum deflection was 1.05 inches.

Compared the experimental deflection with the theoretical deflection, the experimental deflection was an increase by 5.41 percent. These sub-assemblages developed 11 flexural cracks. Figure 248 represents the comparison of the theoretical and experimental load-deflection curve. Figure 249 represents the comparison of the theoretical and experimental moment curvature.

For Specimen S2-2, the experimental load applied to the modified sub-assemblage was 5.35 kips. This beam was loaded up to the collapse load. The theoretical maximum load for the original sub-assemblage with 32 inches long was 6.07 kips and the experimental load was 5.35 kips. The load capability of this beam was decreased by 11.86 percent in comparison with the maximum theoretical load for the original sub-assemblage. The experimental moment in this specimen was 46.14 kips-in and the theoretical moment was 52.35 kips-in. This beam decreased the moment capability by 11.86 percent in comparison with the maximum theoretical moment capacity for the sub-assemblage. Figure 161 showed the amount of bending and shear cracks this sub-assemblage developed were not counted during the development of the moment-curvature, the only consideration was that the beam would fail for bending. These shear crack developed at the

fixed end supports and on both side of the missing column was the factor for the beam failure before reaching the collapse load of 6.07 kips.

Strain Gauge 4 does not record any additional data after a load of 2.15 kips was applied. At the collapse load four strain gauges exceeded the strain of the steel or the steel and concrete. Strain Gauge 3 had a reading of -0.0025 in/in, this strain value exceeded yield point of 0.0023 in/in for the steel reinforcement at this location. Strain Gauge 4 had a reading of -0.0044 in/in, this strain value exceeded yield point of 0.0023 in/in for the steel reinforcement and the concrete of 0.0031 in/in at this location. Strain Gauge 12 had a reading of -0.0046, this strain value exceeded yield point of 0.0023 in/in for the steel reinforcement and the concrete of 0.0031 in/in at this location. Strain Gauge 13 had a reading of -0.0039 in/in, this strain gauge value exceeded yield point of 0.0023 in/in for the steel reinforcement and the concrete of 0.0031 in/in at this location.

The experimental maximum deflection at the failure column was recorded at 1.68 inches and the theoretical maximum deflection was 1.05 inches. Compared the experimental deflection with the theoretical deflection, the experimental deflection increased by 37.5 percent. These sub-assemblages developed 21 flexural cracks. Figure 250 represents the comparison of the theoretical and experimental load-deflection curve. Figure 251 represents the comparison of the theoretical and experimental moment curvature.

For Specimen B2-1, the experimental load applied to the modified sub-assemblage was 4.85 kips. This beam was loaded up to the collapse load. The theoretical maximum load for the original sub-assemblage with 32 inches long was 7.06 kips and the experimental load was 4.85 kips. The load capability of this beam was decreased by 31.30 percent in comparison with the maximum theoretical load for the original sub-assemblage. The experimental moment in this specimen was 41.23 kips-in and the theoretical moment was 60.89 kips-in. This beam decreased the moment capability by 31.30 percent in comparison with the maximum theoretical moment capacity for the sub-assemblage. Figure 167 shows the amount of bending and shear cracks this sub-assemblage developed were not counted during the development of the moment-curvature, the only consideration was that the beam would fail for bending. These shear crack developed at

the fixed end supports and on both side of the missing column was the factor for the beam failure before reaching the collapse load of 7.06 kips.

All strain gauges recorded data during the entire test. At the collapse load four strain gauges exceeded the strain of the steel or the steel and concrete. Strain Gauge 3 had a reading of -0.0064 in/in, this strain value exceeded yield point of 0.0023 in/in for the steel reinforcement and the concrete of 0.0031 in/in at this location. Strain Gauge 5 had a reading of -0.0039, this strain value exceeded yield point of 0.0023 in/in for the steel reinforcement and the concrete of 0.0031 in/in at this location. Strain Gauge 8 had a reading of -0.0024 in/in, this strain value exceeded yield point of 0.0023 in/in for the steel reinforcement at this location. Strain Gauge 13 had a reading of -0.0038, this strain gauge value exceeded yield point of 0.0023 in/in for the steel reinforcement and the concrete of 0.003 in/in at this location. At the collapse load four strain gauges exceeded the strain of the concrete. Strain Gauge 3 had a reading of -0.0034 in/in, this strain value exceeded yield point of 0.0031 in/in for the concrete at this location. Strain Gauge 8 had a reading of -0.0048 in/in, this strain gauge value exceeded yield point of 0.0023 in/in for the steel reinforcement and the concrete of 0.0031 in/in for the concrete at this location. Strain Gauge 13 had a reading of -0.0042 in/in, this strain gauge value exceeded yield point of 0.0023 in/in for the steel reinforcement and the concrete of 0.0031 in/in for the concrete at this location. Strain Gauge 14 had a reading of -0.0082 in/in, this strain gauge value exceeded yield point of 0.0023 in/in for the steel reinforcement and the concrete of 0.0031 in/in for the concrete at this location.

The experimental maximum deflection at the failure column was recorded at 4.07 inches and the theoretical maximum deflection was 2.09 inches. Compared the experimental deflection with the theoretical deflection, the experimental deflection was an increase by 48.65 percent. These sub-assemblages developed 16 flexural cracks. Figure 252 represents the comparison of the theoretical and experimental load-deflection curve. Figure 253 represents the comparison of the theoretical and experimental moment curvature.

For Specimen B2-2, the experimental load applied to the modified sub-assemblage was 5.20 kips. This beam was loaded up to the collapse load. The theoretical maximum load for the

original sub-assemblage with 32 inches long was 7.06 kips and the experimental load was 5.20 kips. The load capability of this beam was decreased by 26.34 percent in comparison with the maximum theoretical load for the original sub-assemblage. The experimental moment in this specimen was 44.20 kips-in and the theoretical moment was 60.89 kips-in. This beam decreased the moment capability by 26.34 percent in comparison with the maximum theoretical moment capacity for the sub-assemblage. Figure 175 shows the amount of bending and shear cracks this sub-assemblage developed were not counted during the development of the moment-curvature, the only consideration was that the beam would fail for bending. These shear crack developed at the fixed end supports and on both side of the missing column was the factor for the beam failure before reaching the collapse load of 7.06 kips.

Strain Gauge 5 does not record any additional data after a load of 5.04 kips was applied. Strain Gauge 8 does not record any additional data after a load of 4.49 kips was applied. Strain Gauge 9 does not record any additional data after a load of 2.16 kips was applied. At the collapse load only one strain gauge exceeded the strain of the concrete. Strain Gauge 13 had a reading of -0.0033 in/in, this strain gauge value exceeded yield point of 0.0023 in/in for the steel reinforcement and the concrete of 0.0031 in/in for the concrete at this location.

The experimental maximum deflection at the failure column was recorded at 2.30 inches and the theoretical maximum deflection was 2.09 inches. Compared the experimental deflection with the theoretical deflection, the experimental deflection was an increase by 9.13 percent. These sub-assemblages developed 29 flexural cracks. Figure 254 represents the comparison of the theoretical and experimental load-deflection curve. Figure 254 represents the comparison of the theoretical and experimental moment curvature.

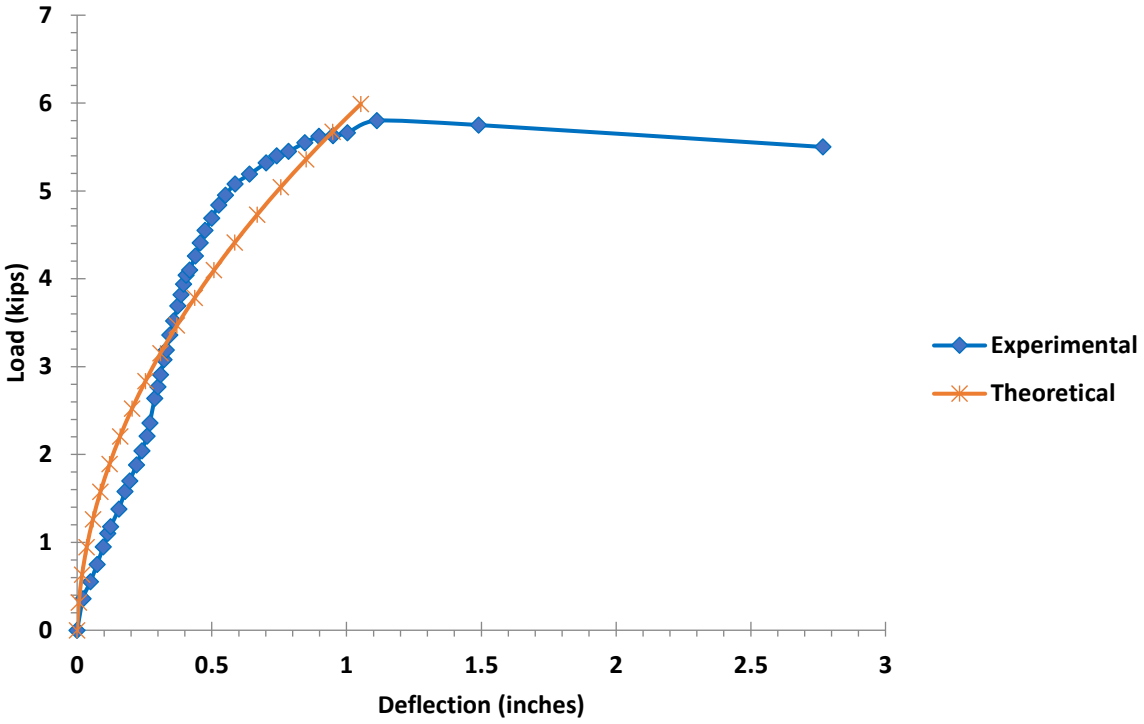

Figure 248. The Comparison of the Theoretical and Experimental Load-Deflection Curve for the Sub-assemblage S2-1

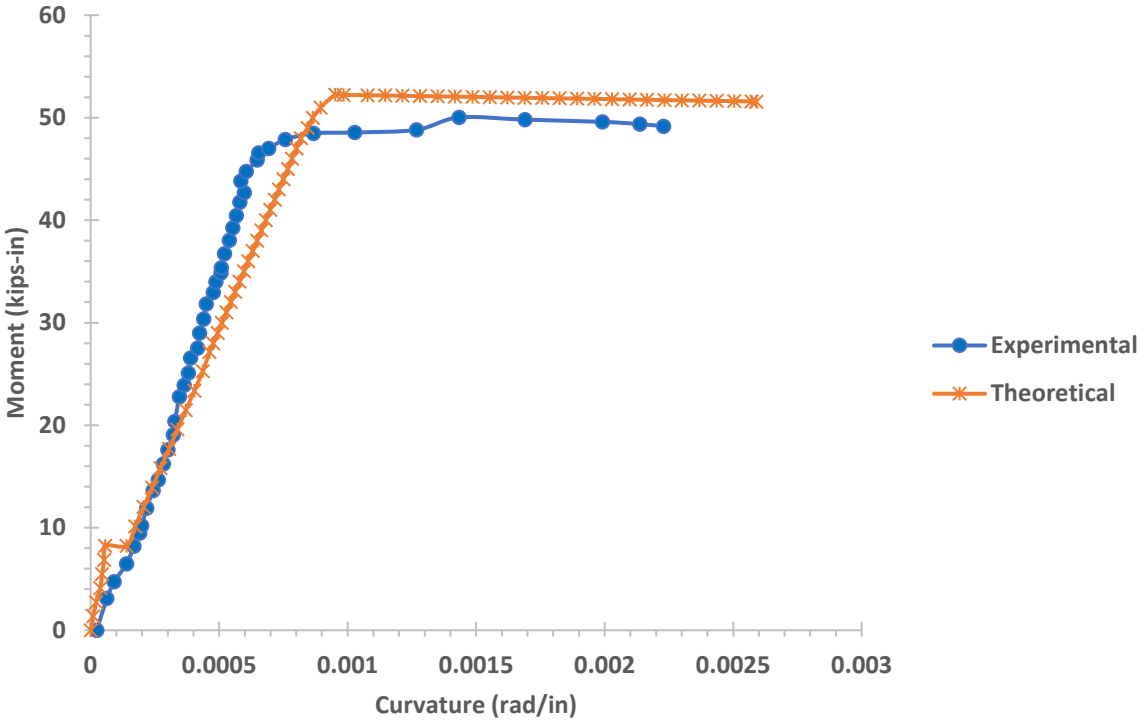

Figure 249. The Comparison of the Theoretical and Experimental Moment-Curvature for Sub-assemblage S2-1

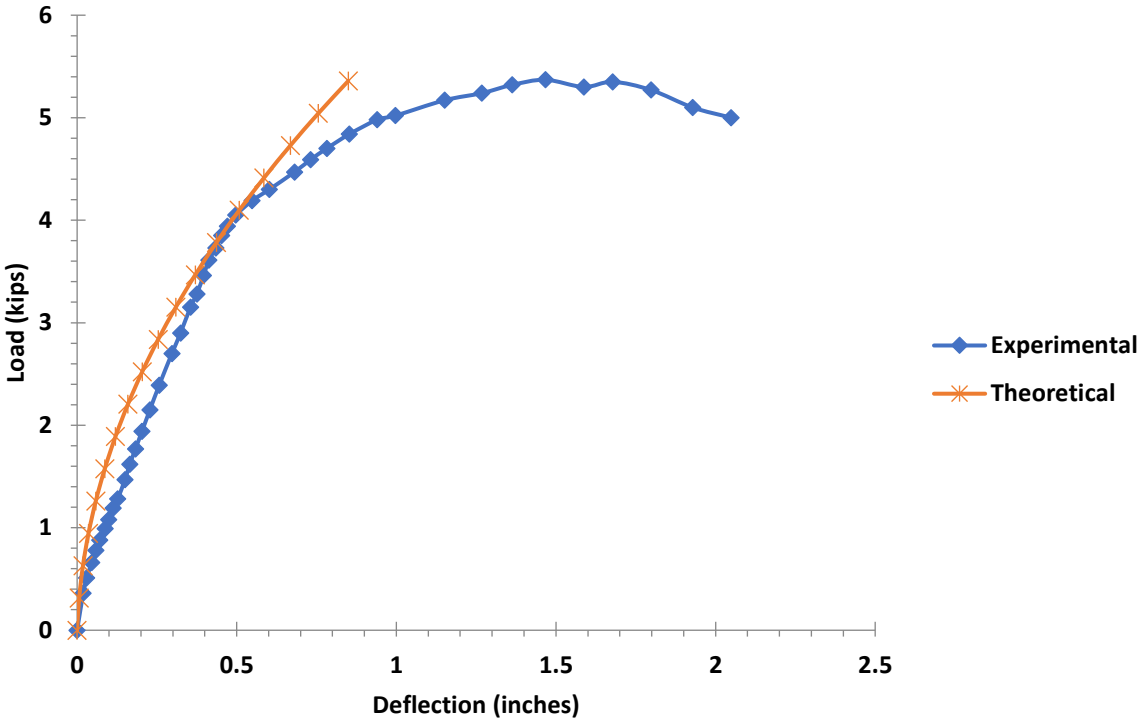

Figure 250. The Comparison of the Theoretical and Experimental Load-deflection Curve for Sub-assemblage S2-2

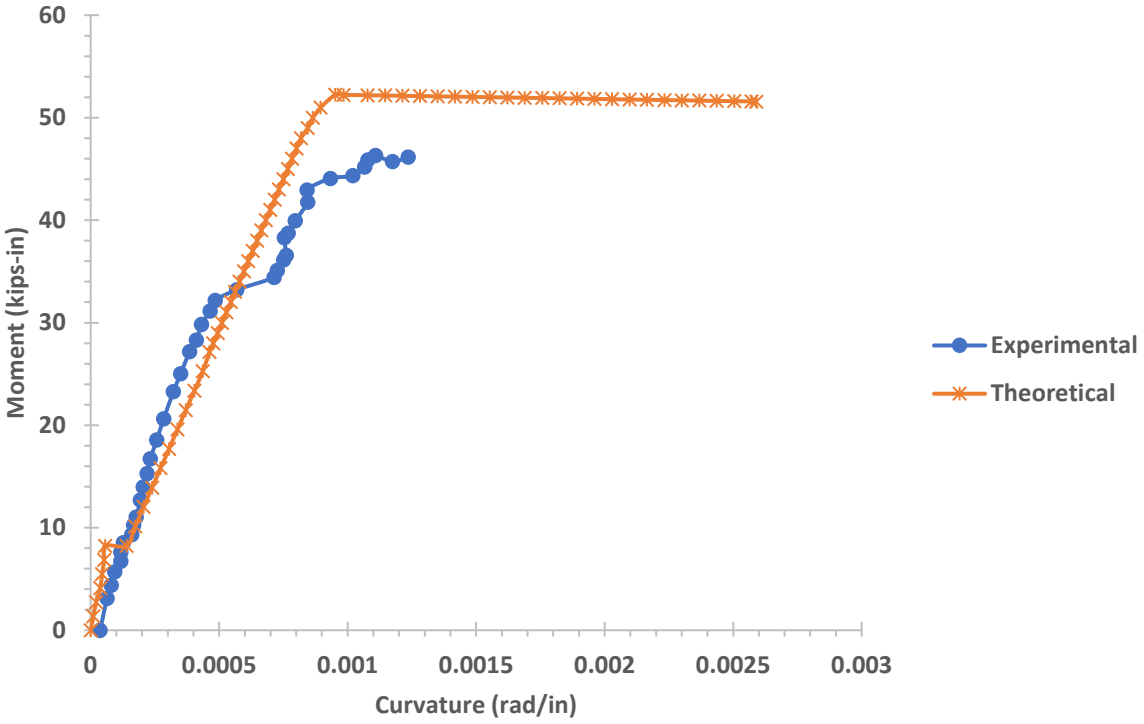

Figure 251. The Comparison of the Theoretical and Experimental Moment- curvature for Sub-assemblage S2-2

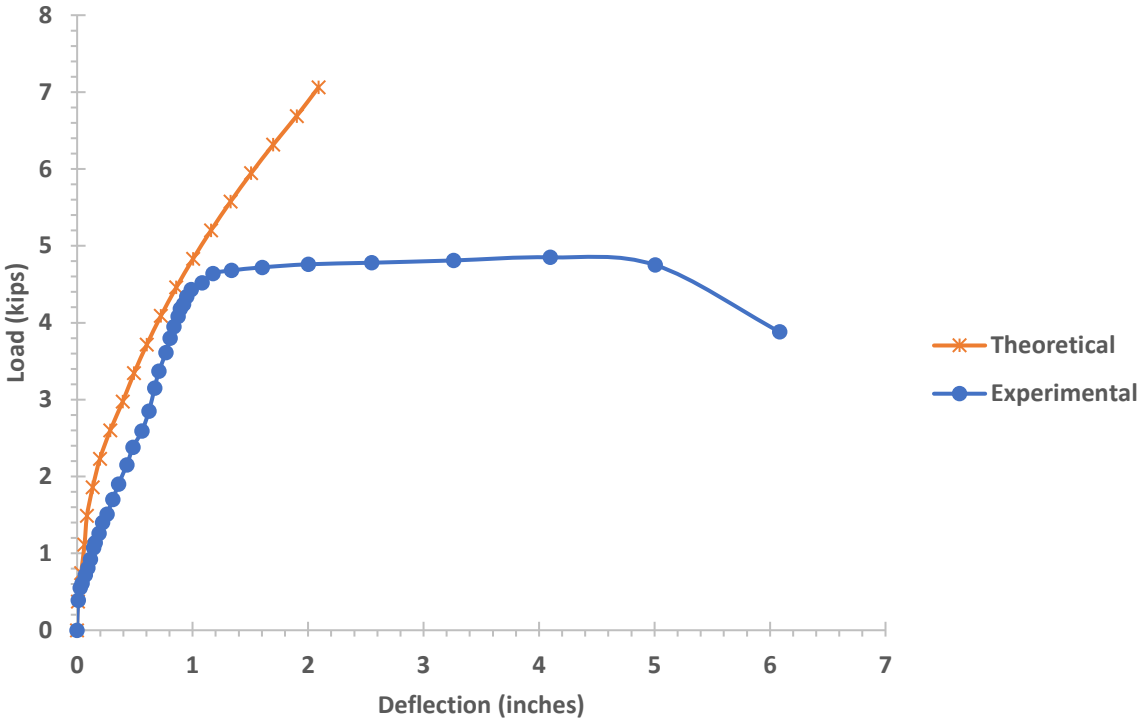

Figure 252. The Comparison of the Theoretical and Experimental Load-deflection Curve for Sub-assemblage B2-1

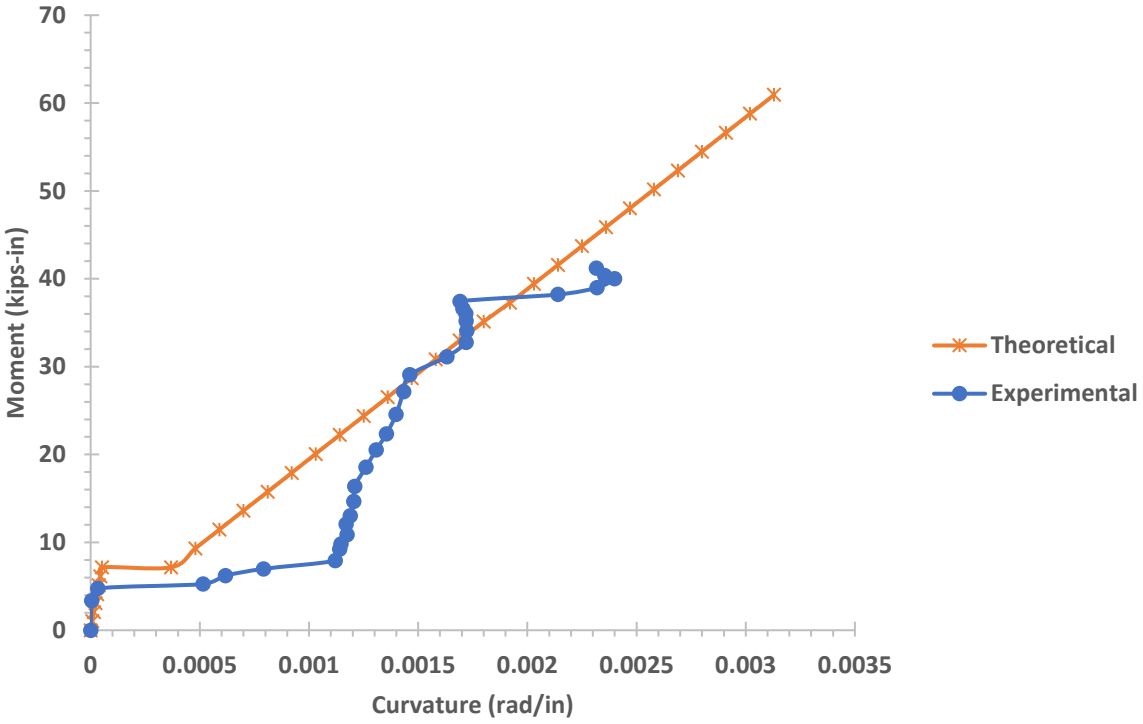

Figure 253. The Comparison of the Theoretical and Experimental Moment- curvature for Sub-assemblage B2-1

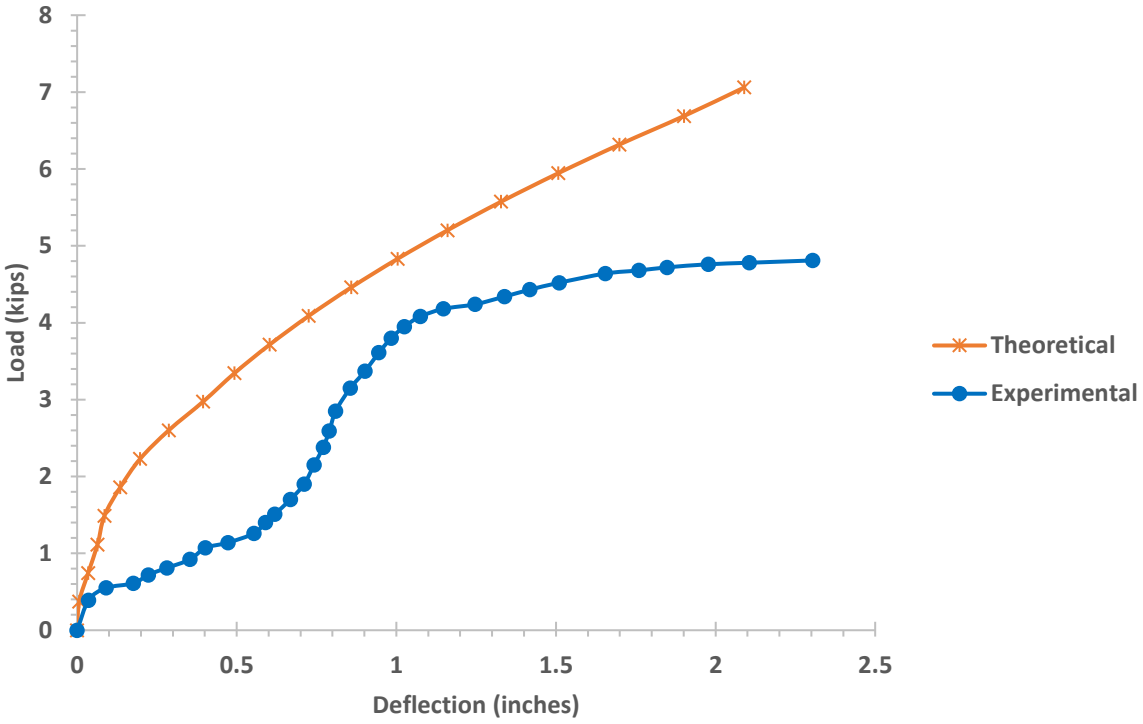

Figure 254. The Comparison of the Theoretical and Experimental Load-deflection Curve for Sub-assemblage B2-2

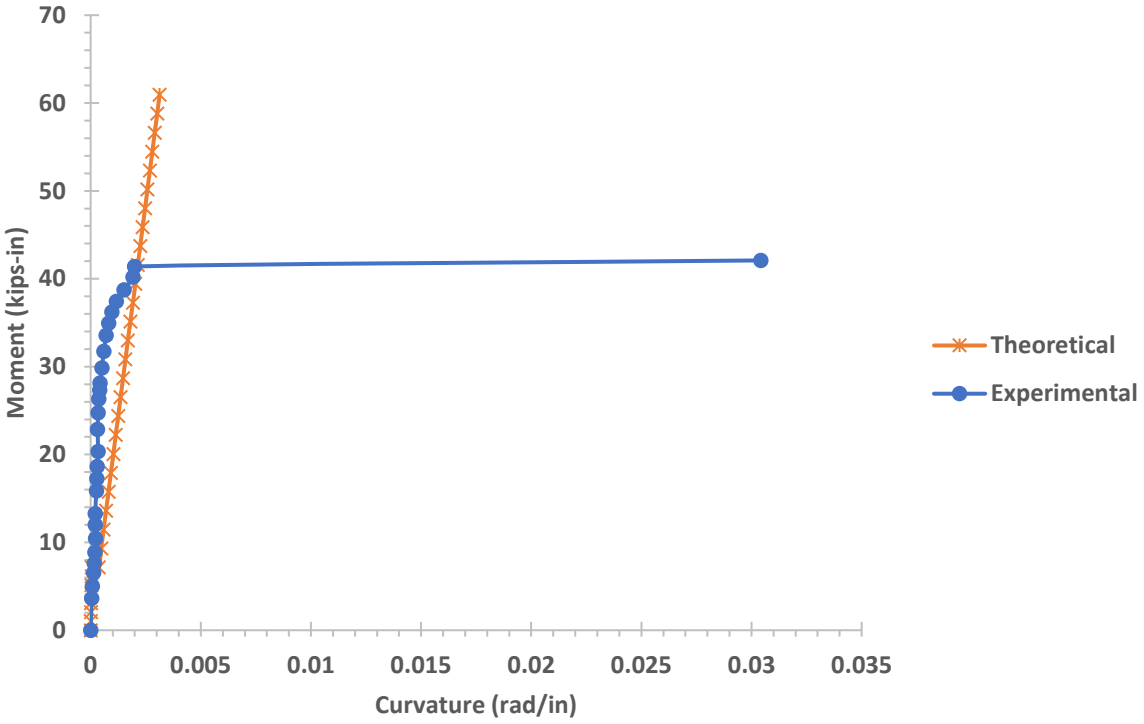

Figure 255. The Comparison of the Theoretical and Experimental Moment-curvature for Sub-assemblage B2-2

Figure 256 illustrates a comparison between sub-assemblage S2-1 and S2-2 at ultimate strength. Sub-assemblage S2-1 was loaded at 5.80 kips and sub-assemblage was loaded at 5.37 kips. Both sub-assemblages had the same amount of main reinforcement, the difference was in the shear detail, that sub-assemblage S2-2 had shear detail. The difference in load was due to the number of flexural cracks that developed the sub-assemblage S2-2 (21 cracks) in comparison with the number of cracks that developed the sub-assemblage S2-1 (11 cracks). Sub-assemblages S2-1 and S2-2 deflection at ultimate strength. Sub-assemblage S2-1 deflected 1.11 inches and sub-assemblage S2-2 deflected 1.47 inches.

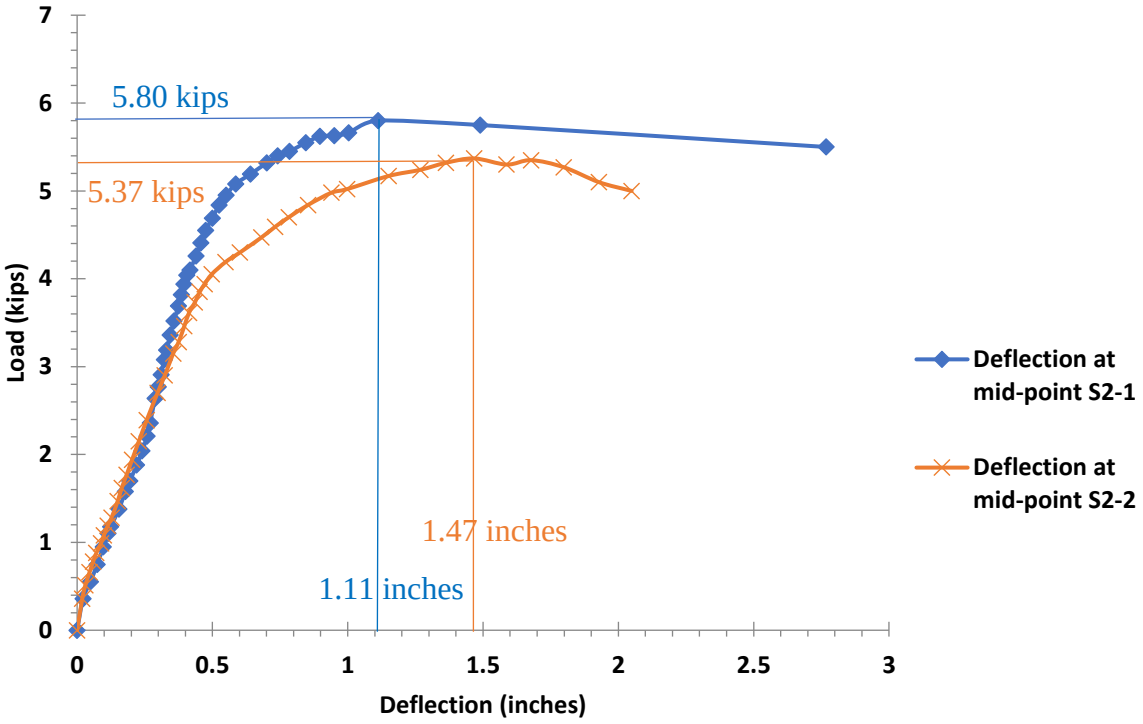

Figure 256. Experimental Comparison between Sub-assemblages S2-1 and S2-2 at Ultimate Strength

Figure 257 illustrates a comparison between sub-assemblage B2-1 and B2-2 at ultimate strength. Sub-assemblage B2-1 was loaded at 4.85 kips and sub-assemblage B2-2 was loaded at 5.20 kips. Both sub-assemblages had the same amount of main reinforcement, the difference was in the shear detail, that sub-assemblage B2-2 had shar detail. The difference in load was due to the number of flexural cracks that developed the B2-1 (16 cracks) in comparison with the number of cracks that developed the sub-assemblage B2-2 (29 cracks). Sub-assemblages B2-1 and B2-2 deflection at ultimate strength. Sub-assemblage B2-1 deflected 1.98 inches and sub-assemblage B2-2 deflected 4.10 inches.

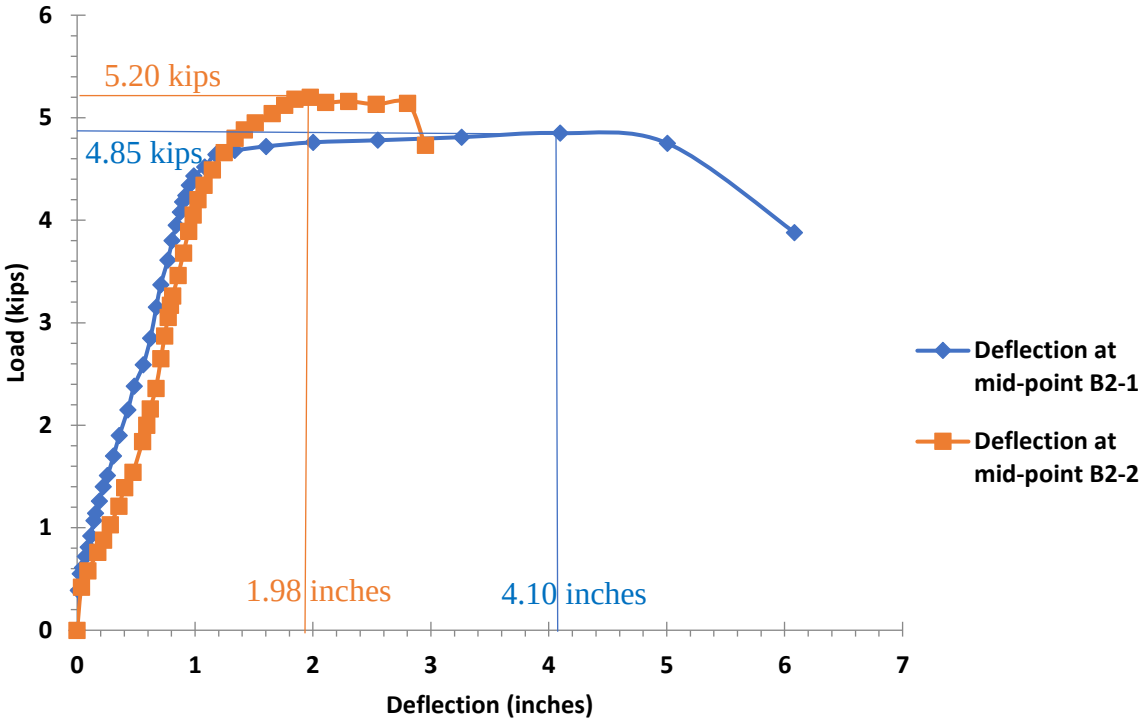

Figure 257. Experimental Comparison between Sub-assemblages B2-1 and B2-2 at Ultimate Strength

Figure 258 illustrates a comparison between sub-assemblage S2-1 and B2-1 at ultimate strength. Sub-assemblage S2-1 was loaded at 5.80 kips and sub-assemblage B2-1 was loaded at 4.85 kips. Both sub-assemblages had the same amount of main reinforcement, and the same shear details. Sub-assemblages S2-1 and B2-1 deflection at ultimate strength. Sub-assemblage S2-1 deflected 1.11 inches and sub-assemblage B2-1 deflected 4.10 inches.

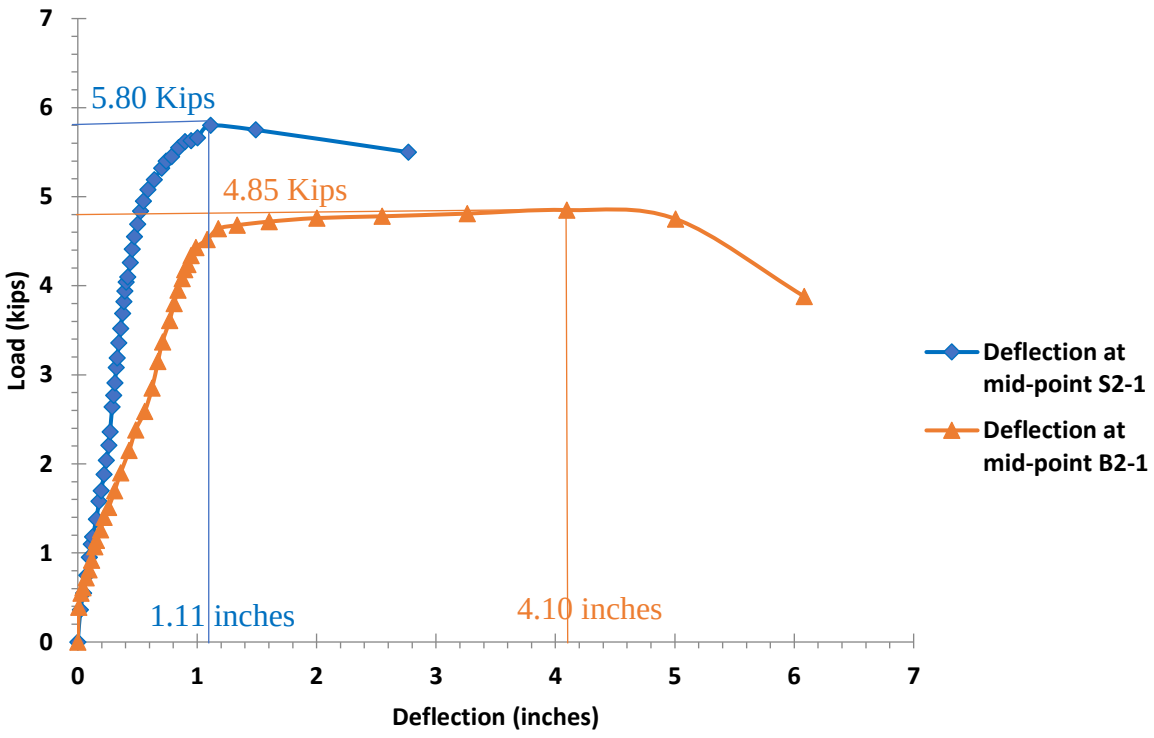

Figure 258. Experimental Comparison between Sub-assemblages S2-1 and B2-1 at Ultimate Strength

Figure 259 illustrates a comparison between sub-assemblage S2-2 and B2-2 at ultimate strength. Sub-assemblage S2-2 was loaded at 5.37 kips and sub-assemblage B2-2 was loaded at 5.20 kips. Both sub-assemblages had the same amount of main reinforcement and shear details. Sub-assemblages S2-1 and B2-2 deflection at ultimate strength. Sub-assemblage S2-2 deflected 1.47 inches and sub-assemblage B2-2 deflected 1.98 inches.

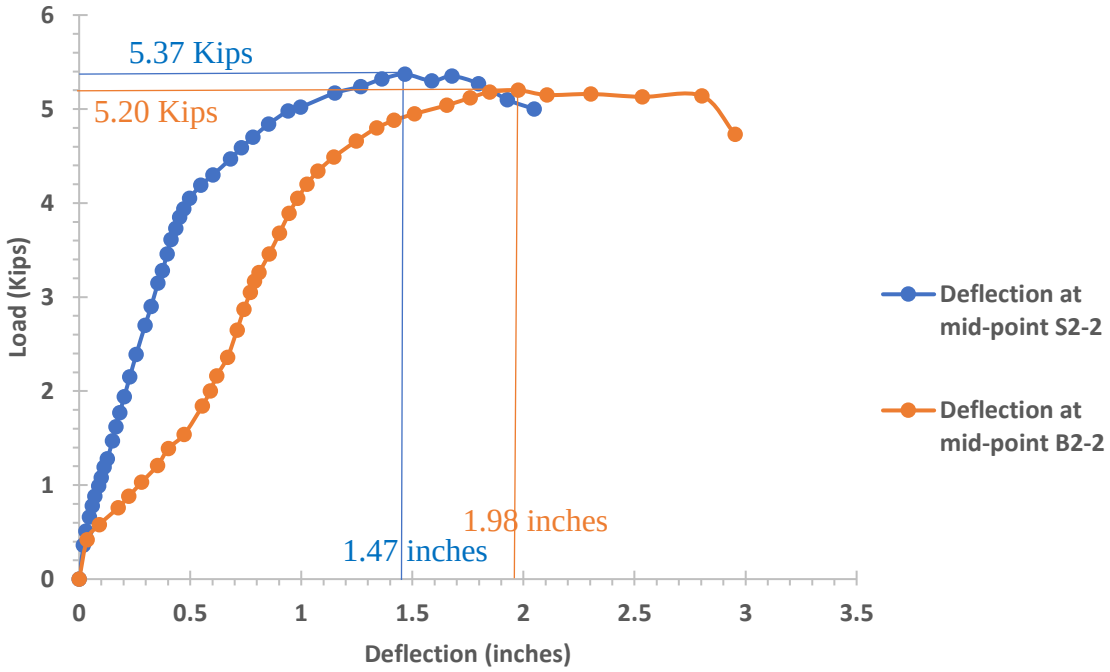

Figure 259. Experimental Comparison between Sub-assemblages S2-2 and B2-2 at Ultimate Strength

CHAPTER 5 CONCLUSION AND FUTURE RESEARCH

5.1 Conclusions

The following conclusions are drawn based on the investigation presented in this dissertation:

A. For beams subjected to quasi-static loading up to collapse:

1. The ultimate strength predictions based on the materially nonlinear analysis agreed well with those found experimentally and were within less than five percent of each other.
2. The beams with BFRP reinforcement showed higher deflection than that with steel reinforcement; however, the ultimate strength increased by up to 10 percent.
3. The beam with steel reinforcement and BFRP fabric wrap showed a 29 percent increase in the ultimate strength compared to that with no wrap.
4. The beam with steel reinforcement and retrofitted with two external 4mm BFRP reinforcing bars showed a 19 percent increase in the ultimate strength compared to that with no external retrofit.
5. The beam with BFRP reinforcement and BFRP wrap showed a 34 percent increase in the ultimate strength compared to that with no wrap.
6. The beam with BFRP reinforcement and retrofitted with two external 4mm BFRP reinforcing bars exhibited a 14 percent increase in the ultimate strength compared to that with no external retrofit.
7. At the maximum service load, the beam with BFRP reinforcement and BFRP fabric wrap reduced the deflection by nearly 56 percent compared to that with no wrap.
8. The beam with regular steel reinforcement and BFRP wrap resulted in an eight percent reduction in the service load deflection.
9. The sub-assemblage with steel reinforcement and without seismic details developed only 11 flexural cracks compared to 21 cracks developed when seismic details are included thereby resulting in an eight percent reduction in the load capacity as well as higher deflection.

10. The sub-assemblage with BFRP reinforcement and without seismic details developed only 16 flexural cracks compared to 29 cracks developed when seismic details are included thereby resulting in a six percent reduction in the load capacity as well as higher deflection.

B. For beams subjected to impact loading:

1. The post-impact single-degree-of-freedom based natural frequency analysis including vibration damping in the range from 5.0 to 8.75 percent of critical damping provided a fair agreement with only those experimental results that were not affected due to the impact load bouncing up and down causing multiple residual impacts after the first one.
2. The beam with the steel reinforcement and BFRP fabric showed a 25 percent reduction in the maximum beam response acceleration relative to that without the fabric.
3. The beam with the steel reinforcement retrofitted with a pair of external BFRP rebars showed a 54 percent increase in the maximum beam response acceleration relative to that without the external rebars.
4. The beam with the BFRP reinforcement and BFRP fabric showed a 48 percent increase in the maximum beam response acceleration relative to that without the fabric.
5. The post-impact damped natural frequency of the beam with only the steel reinforcement is nearly 42 Hz and remained practically unaltered for each of the four beams tested with various BFRP retrofitting schemes.
6. The ratio of the impact force at collapse to that with a 10 inches impactor drop height is found to be the largest for the beam with steel reinforcement and retrofitted with two external BFRP rebars, indicating a nearly twelve-fold increase in the strength of the beam at collapse relative to that for the beam with steel reinforcement only.

The study shows that the BFRP reinforcement used internally or externally as well as the BFRP wrap decreases the service-load deflections while increasing the strength of concrete beams. However, the beam with only the steel reinforcement has a natural frequency of 42 Hz and

remains practically unaltered regardless of whether only the BFRP rebars or any of the other BFRP retrofitting schemes are used. This means that the use of BFRP does not alter the beam stiffness. Nevertheless, the study reveals that a twelve-fold increase in the impact collapse resistance occurs when the primary steel reinforcement is combined with a pair of externally bonded BFRP rebars. Furthermore, the use of BFRP rebars and the wrap showed an increase in the impact resistance ranging from 1.21 to 5.55 times that of the baseline beam with the steel reinforcement only.

5.2 Future Research

Additional research can be conducted to control the 11.3-degree rotation permitted by the Unified Facilities Criteria (UFC) in order to effectively use BFRP as a tie force design component to create the so-called ‘cable action’ under progressive collapse. Research also needs to be conducted to determine the effectiveness of BFRP fabric in blast load and retrofitting applications.

REFERENCES

1) American Society of Civil Engineers (ASCE7-05), *Minimum Design Loads for Building and Other Structures*, ASCE, Virginia, 2005
2) Unified Facilities Criteria (UFC-4-023-03), *Design of Buildings to Resist Progressive Collapse*, Department of Defense, June 2013
3) American Concrete Institute (ACI-318-05), *Building Code Requirements for Structural Concrete and Commentary*, ACI, Michigan, 2008
4) American Concrete Institute, (ACI 440.1R-15) *Guide for the Design and Construction of Structural Concrete Reinforced with Fiber Reinforced Polymer (FRP) Bars*, ACI, Michigan, 2015
5) American Concrete Institute, (ACI 440.2R-08) Guide for the Design and Construction of externally Bonded FRP Systems for Strengthening Concrete Structures, Michigan, 2008
6) Yu, J., and Tan, K.A, *Structural Behavior of Reinforced Concrete Frames Subjected to Progressive Collapse*, ACI Structural Journal, Vol. 114, Issue 1, pp. 63-74, January 2010
7) Wang, H., Zhang, A., Li, Y., and Yan W., *Progressive Collapse of Building Structures*, The Open Civil Engineering Journal, Vol. 8, pp. 183-192, 2014
8) Mosalam, K.M., Talaat, M., and Park, S., *Modeling Progressive Collapse in Reinforced Concrete Framed Structures*, The 14th World Conference on Earthquake Engineering October 12-17, Beijing, China, 2008
9) Starossek, U., *Progressive Collapse of Structures*, Thomas Telford Publishing, 2009
10) Ovitigala, T., Ibrahim, M.A., and Isaa, M.A., *Serviceability and Ultimate Load Behavior of Concrete Beams Reinforced with Basalt Fiber-Reinforced Polymer Bars.* ACI Structural Journal Volume 113 # 4, pp. 757- 768, 2016
11) Elgabbas, F., Vicent, P., Ahmed, E.A., and Benmokrane, B., *Experimental Testing of Basalt FRP bar in Concrete Beams*, Elsevier Journal, Composites Part B 91, pp. 205-218, 2016
12) Maariappan, G., and Singaravadivelan, R., *Studies and Behavior of RCC Sub-assemblages Joint Retrofitted with Basalt Fiber Reinforced Polymer Sheet*, Global Journal of Research in Engineering Civil and Structural Engineering, Vol 13, Issue 5, version 1.0, 2013

13) Ghobarah, A., and Said, A., *Shear Strengthening of Sub-assemblages Joints*, Elsevier Journal Engineering Structures 24, pp. 881-888, 2002.

14) Singaravadivelan, R., *Strengthening of Concrete Elements using Basalt Fiber*, LAP Lambert Academy Publishing, 2013

15) Hall, R.L., Woodson, S.C., Baylot, J.T., Hayes, J.R., and Sohn, Y., *Development of Progressive Collapse Analysis Procedure and Condition Assessment for Structures,* US Army Engineer Research and Development Center and Defense Threat Reduction Agency, 2002

16) Baldridge, B., and Humay, F.K., *Preventing Progressive Collapse in Concrete Buildings, Concrete International*, 2003

17) Zhou, Y., Li, F., Wang, S., and Zhao, N., *Progressive Collapse Resistance of Reinforce Concrete Frame Structure*, Revista de la Facultad de Ingenieria U.C.V, Experimental, Vol 31 No 7, pp152-161, 2016.

18) American Society of Civil Engineer (ASCE7-16), *Minimum Design Loads for Building and Other Structures*, ASCE, Virginia 2016

19) Yu, J., and Tan, K.H., *Progressive Collapse Resistance of RC Sub-assemblages,* Design and Analysis of Protective Structures, 3rd conference, Singapore, 2010

20) Orton, S. L., *Development of a CFRP System to Provide Continuity in Existing Reinforced Concrete Building Vulnerable to Progressive Collapse,* Research report, The University of Texas at Austin, August 2007

21) Ramanna-Sanjeevaiah, N., S*tatic and Impact Load Response of Reinforced Concrete Beams and Slabs with NSM-CFRP Retrofitting,* Structures research report, Department of Civil and Environmental Engineering, Old Dominion University, May 2012.

22) Fujikake, K., Li, B., and Soeun, S. Impact Response of Reinforced Concrete Beam and its Analytical Evaluation, Journal of Structural Engineering, ASCE, August 2009.

APPENDICES

APPENDIX A

MatLab Program to Calculate the M-Phi Relation of Singly Reinforced Rectangular Beams by Layered Element Technique Unretroffited Beams

```
% Matlab Program to calculate the M-Phi relation of Singly Reinforced
% Rectangular Beams by Layered Element Technique
% Unretrofitted Beams
% Loading is taken as one-point loads acting at L/2
% Author - José Luis Carrasquillo & Nakul Ramanna & Dr. Razzaq
% Last Revision - 04/29/19
% Notes:
% Once concrete cracks, its tensile stress is accounted up to the last
% uncracked layer
% Consider pre-allocating arrays for faster processing.
clc
clear all
% Data Input
b=4.5; % Enter the width of the beam in inch
h=5.5; % Enter the total depth of the beam in inch
d=4.313; % Enter the effective depth of the beam in inch
dr=0.375; % Enter the diameter of tension reinforcement (rebar) in
% inch
nr=2; % Number of tensile rebars
c=3.0; % Enter an initial value for the depth of Neutral Axis (in inch)
n=100; % Enter the number of rectangular elements across the depth of
% the beam section (Layers)
fy=68.20; % Steel Yield Stress in ksi
Es=29380; % Mod of Elasticity of Steel in ksi
Fc=4.213; % Concrete Compression Strength in ksi
Fcu=3.91; % Fc unloading part in the stress strain curve for concrete
%(in Ksi)
fr=7.5*sqrt(Fc*1000); % Flexural Strength of Concrete
count=0;
%Moment Curvature Program Begins
%=========================================
for et=0:0.00005:0.0032 %Increments concrete strain value in the top
%fibre by 0.00005
while ~0
%Calculating Strain in each Concrete Layer
for i=1:n
e(i)=(et*(c-(h/n*(i-0.5))))/c;
end
% Determining Concrete Stress 'fc' (in ksi) from Stress-Strain
%Relationship
for i=1:n
if e(i)<=0.00163
fc(i)=e(i)*Fc* 666.667;
```

```
elseif e(i)>0.00163 && e(i)<=0.002175
fc(i)=Fc;
else
fc(i)=Fc+((Fc-Fcu)*(0.002175-e(i))/0.0005);
end
end
% Calculating Strain in Steel
es=(c-d)*et/c; %Accounting for tension strain as -ve, d-c
% becomes c-d
% Determining Steel Stress 'fs' (in ksi) from Stress-Strain
%Relationship
ey=fy/Es;
if abs(es)<ey
fs=Es*es;
else
fs=-fy;
end
C=0; %Total Compressive Force
T=0; %Total Tensile Force
% Computing Compressive and Tensile Force in Concrete
for i=1:n
if e(i)>=0
N1(i)=fc(i)*b*h/n; %Compressive force in concrete layer
C=C+N1(i);
else
if abs(fc(i)*1000)<fr % Check for concrete cracking in
% tension
N(i)=fc(i)*b*h/n; %Tensile force in concrete layer
T=T+N(i);
end
end
end
% Computing Total Tensile Force of section (including steel)
T=T+fs*nr*3.1428*(dr)^2/4;
% Equilibrium Check C==T ???
C1=round(C*100)/100; %2 decimal rounding
T1=round(T*100)/100;
if abs(C1-abs(T1))<=0.02
disp('=======================================================')
disp('Stress @ bottom of Concrete, fc (psi) =')
disp(fc(n)*1000)
disp('Depth of NA, c (in) =')
disp(c)
disp('Total Compressive Force, C (kips) =')
disp(C1)
disp('Total Tensile Force, T (kips) =')
disp(T1)
disp('C1-abs(T1) =')
disp(abs(C1-abs(T1)))
disp('=======================================================')
count=count+1;
break % Exits while loop
elseif C1<abs(T1)
```

```
c=c+0.0005;
else
c=c-0.0005;
end
end % while loop end
% Calculating Moment in Kip -in (m=T*jd)
if et<=0.00163
m=abs(T1)*(d-c/3);
elseif et>0.00163 && et<=0.002175
dk=0.00163*c/et;
A=(Fc*(c-dk)^2/2) + (0.5*Fc*dk*(c-2/3*dk));
B=(Fc*(c-dk))+(0.5*Fc*dk);
ybar=A/B;
m=abs(T1)*(d-ybar);
else
dk=0.00163*c/et;
dl=0.002175*c/et;
A=(0.5*Fc*dk*(c-2*dk/3))+(Fc*(dl-dk)*(c-dl/2-dk/2))+(Fcu*(c-dl)^2/2)+(0.3333*(Fc-
Fcu)*(c-dl)^2);
B=(0.5*dk*Fc)+(Fc*(dl-dk))+(Fcu*(c-dl))+(0.5*(Fc-Fcu)*(c-dl));
ybar=A/B;
m=abs(T1)*(d-ybar);
end
M(count)=m; % Moment in K-in
phi(count)=et/c; % Curvature in rads/in
% Plotting Moment-Curvature Relationship
plot(phi,M,'o')
hold on
plot(phi,M)
xlabel('Curvature (rads/inch)')
ylabel('Moment (K-in)')
title('Moment Curvature Plot')
end % for loop end
```

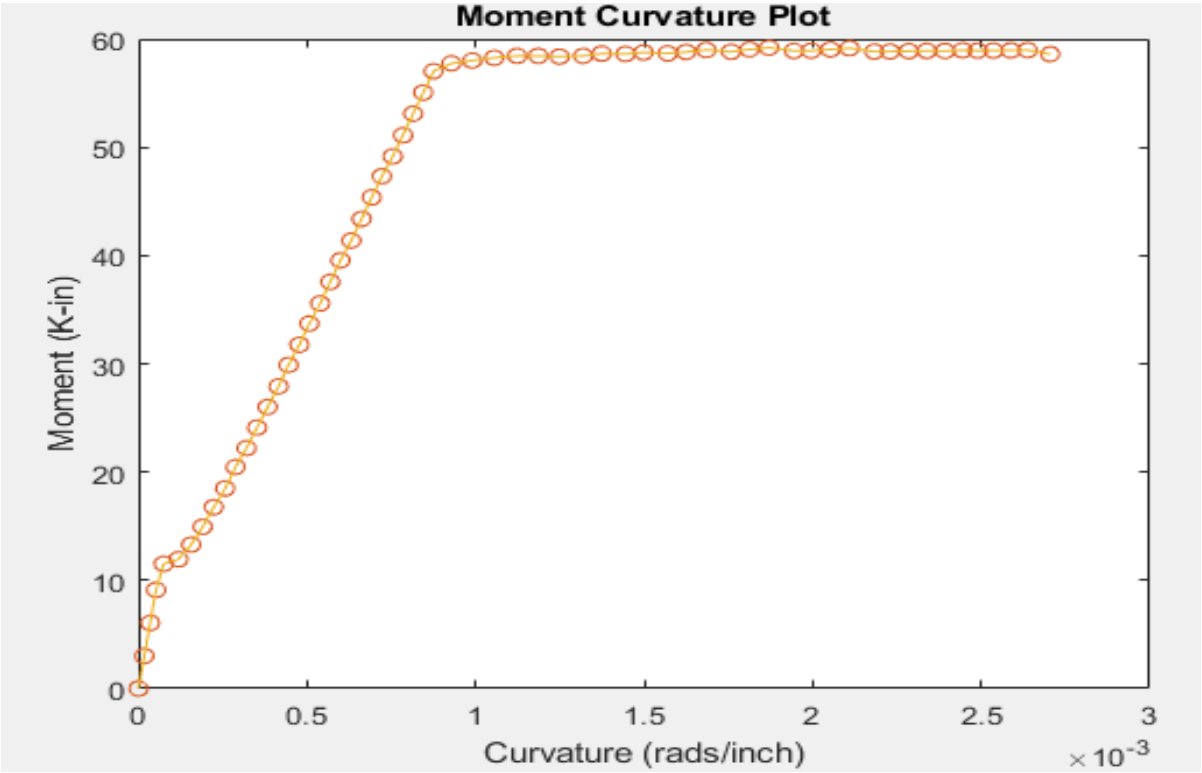
Moment Curvature Plot
Moment (K-in)
Curvature (rads/inch)
$\times 10^{-3}$
0
10
20
30
40
50
60
0
0.5
1
1.5
2
2.5
3

APPENDIX B

MatLab Program to Calculate the M-Phi Relation of Singly Reinforced Rectangular Beams by Layered Element Technique – Beam with Steal Reinforcement and Retroffitted in Tension Zone

```
% Matlab Program to calculate the M-Phi relation of Singly Reinforced
% Rectangular Beams by Layered Element Technique
% Beam with steel reinforcement and retrofitted in tension zone
% Loading is taken as single point loads acting at L/2
% Author - José Luis Carrasquillo & Nakul Ramanna & Dr. Razzaq
% Last Revised - 10/23/2023
% Notes:
% Once concrete cracks, its tensile stress is accounted up to the last
% uncracked layer.
% Program doesn't account for debonding of BFRP reinforcement
% Consider pre-allocating arrays for faster processing.
clc
clear all
% Data Input
%============================================================
b=4.5; % Enter the width of the beam in inch
h=5.5; % Enter the total depth of the beam in inch
d=4.313; % Enter the effective depth of the beam in inch
dr=0.375; % Enter the diameter of tension reinforcement (rebar) in
% inch
nr=2; % Number of tensile rebars
c=2.0; % Enter an initial value for the depth of Neutral Axis (in inch)
n=100; % Enter the number of rectangular elements across the depth of
% the beam section (Layers)
fy=68.2; % Steel Yield Stress in ksi
Es=29038; % Mod of Elasticity of Steel in ksi
Fc=4.2130; % Concrete Compression Strength in ksi
Fcu=3.581; % Fc unloading part in the stress strain curve for concrete
```

```
% (in Ksi)
nft=2; % no of BFRP reinforcement in tension zone
abasalt=0.019; % area of BFRP reinforcement in inch^2
Ef=6,228.8; % Mod of Elasticity of BFRP reinforcement in ksi
ffy=138.85; % BFRP Yield Stress in ksi
fr=7.5*sqrt(Fc*1000); % Flexural Strength of Concrete
count=0;
%Moment Curvature Program Begins
for et=0:0.00005:0.0031 % Increments concrete strain value in the top
% fiber by 0.00005
while ~0
%Calculating Strain in each Concrete Layer
for i=1:n
e(i) = (et*(c-(h/n*(i-0.5))))/c;
end
% Determining Concrete Stress 'fc' (in ksi) from Stress-Strain
% Relationship
for i=1:n
if e(i)<=0.00163
fc(i)=e(i)*Fc*666.667;
elseif e(i)>0.00163 && e(i)<=0.002175
fc(i)=Fc;
else
fc(i)=Fc+((Fc-Fcu)*(0.002175-e(i))/0.0005);
end
end
% Calculating tensile strain in Steel
es=(c-d)*et/c; %Accounting for tension strain as -ve, d-c
% becomes c-d
% Determining Steel Stress 'fs' (in ksi) from Stress-Strain
% Relationship
ey=fy/Es;
if abs(es)<ey
fs=Es*es;
else
```

```
fs=-fy;
end
% Calculating tensile strain in BFRP bar
ef=(c+0.5-h)*et/c; %Accounting for tension strain as -ve, h-
% 0.5-c becomes c+0.5-h
% Determining CFRP Stress 'ffs'(in ksi) from stress-strain Relationship
ffs=Ef*ef;
if abs(ffs)<ffy
ffs=ffs;
else
ffs=-ffy;
end
C=0; %Total Compressive Force
Tc=0; %Tensile Force of Concrete
% Computing Compressive and Tensile Force in Concrete
for i=1:n
if e(i)>=0
N1(i)=fc(i)*b*h/n; %Compressive force in concrete layer
C=C+N1(i);
else
if abs(fc(i)*1000)<fr % Check for concrete cracking in
% tension
N(i)=fc(i)*b*h/n; %Tensile force in concrete layer
Tc=Tc+N(i);
end
end
end
% Computing Total Tensile Force 'T' of section (including steel and
% CFRP)
T=Tc+fs*nr*3.1428*(dr)^2/4+ffs*nft*abasalt;
% Equilibrium Check C==T ???
C1=round(C*100)/100; %2 decimal rounding
T1=round(T*100)/100; %2 decimal rounding
if abs(C1-abs(T1))<=0.02
disp('=======================================================')
```

```
disp('Stress @ bottom of Concrete, fc (psi) =')
disp(fc(n)*1000)
disp('Depth of NA, c (in) =')
disp(c)
disp('Total Compressive Force, C (kips) =')
disp(C1)
disp('Total Tensile Force, T (kips) =')
disp(T1)
disp('C1-abs(T1) =')
disp(abs(C1-abs(T1)))
disp('=======================================================')
count=count+1;
break % Exits while loop
elseif C1<abs(T1)
c=c+0.0004;
else
c=c-0.0004;
end
end % while loop end
% Calculating Moment in Kip -in (m=T*jd)
if et<=0.00163
m=abs(T1)*(d-c/3);
elseif et>0.00163 && et<=0.002175
dk=0.00163*c/et;
A=(Fc*(c-dk)^2/2)+(0.5*Fc*dk*(c-2/3*dk));
B=(Fc*(c-dk))+(0.5*Fc*dk);
ybar=A/B;
m=abs(T1)*(d+1.29-ybar);
else
dk=0.00163*c/et;
dl=0.002175*c/et;
A=(0.5*Fc*dk*(c-2*dk/3))+(Fc*(dl-dk)*(c-dl/2-dk/2))+(Fcu*(c-dl)^2/2)+(0.3333*(Fc-
Fcu)*(c-dl)^2);
B=(0.5*dk*Fc)+(Fc*(dl-dk))+(Fcu*(c-dl))+(0.5*(Fc-Fcu) *(c-dl));
ybar=A/B;
m=abs(T1)*(d-ybar);
```

```
end
M(count)=m; % Moment in K-in
phi(count)=et/c; % Curvature in rads/in
% Plotting Moment-Curvature Relationship
plot(phi,M,'o')
hold on
plot(phi,M)
xlabel('Curvature (rads/inch)')
ylabel('Moment (K-in)')
title('Moment Curvature Plot')
end % for loop end
```

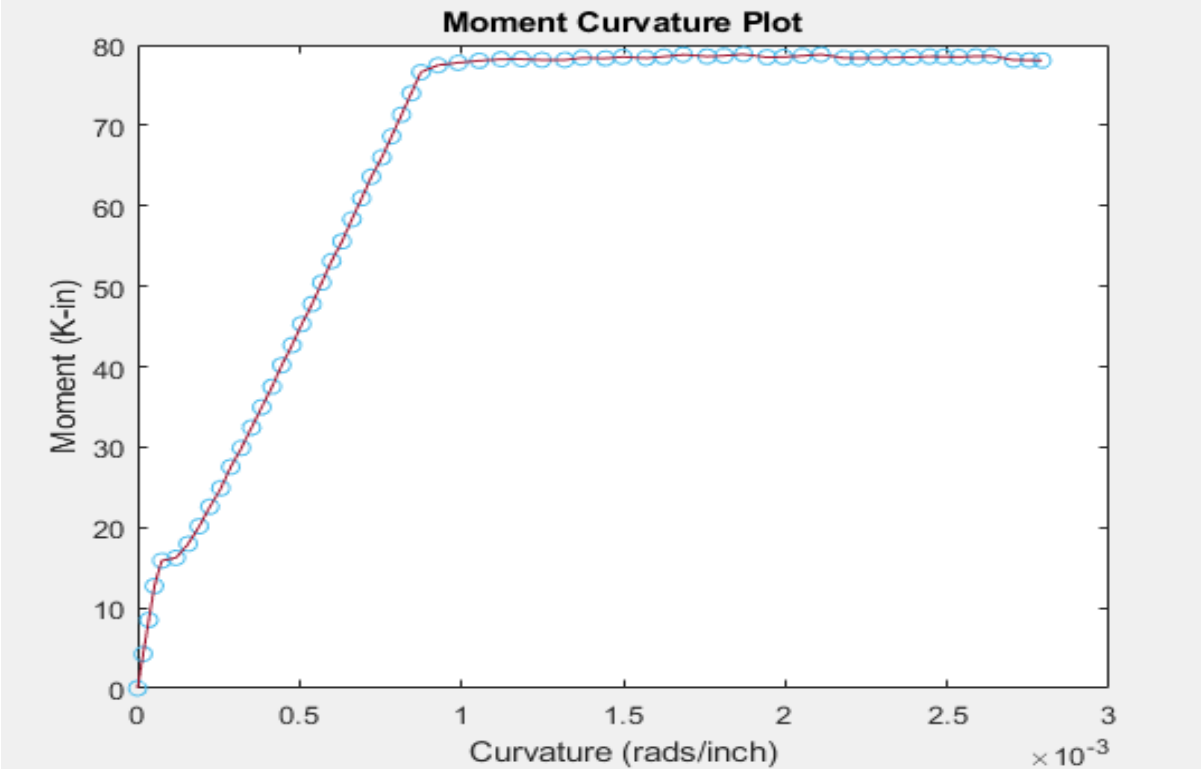

APPENDIX C

MatLab Program to Calculate the M-Phi Relation of Singly Reinforced Rectangular Beams by Layered Element Technique Un-retrofitted Basalt Beams

```
% Matlab Program to calculate the M-Phi relation of Singly Reinforced
% Rectangular Beams by Layered Element Technique
% Un-retrofitted Basalt Beams
% Loading is taken as single point loads acting at L/2
% Author - José Luis Carrasquillo & Nakul Ramanna & Dr. Razzaq
% Last Revision - 11/25/23
% Notes:
% Once concrete cracks, its tensile stress is accounted up to the last
% uncracked layer
% Consider pre-allocating arrays for faster processing.
clc
clear all
% Data Input
b=4.5; % Enter the width of the beam in inch
h=5.5; % Enter the total depth of the beam in inch
d=4.30; % Enter the effective depth of the beam in inch
dr=0.3937; % Enter the diameter of tension BFRP reinforcement (rebar) in
% inch
nr=2; % Number of tensile rebars
c=3.0; % Enter an initial value for the depth of Neutral Axis (in inch)
n=100; % Enter the number of rectangular elements across the depth of
% the beam section (Layers)
fb=71.56; % Basalt rupture point in ksi
Eb=5778; % Mod of Elasticity of Basalt in ksi
Fc=4.213; % Concrete Compression Strength in ksi
Fcu=3.581; % Fc unloading part in the stress strain curve for concrete
%(in Ksi)
fr=7.5*sqrt(Fc*1000); % Flexural Strength of Concrete
count=0;
%Moment Curvature Program Begins
%=========================================
for et=0:0.00005:0.0030 %Increments concrete strain value in the top
%fiber by 0.00005
while ~0
%Calculating Strain in each Concrete Layer
for i=1:n
e(i)=(et*(c-(h/n*(i-0.5))))/c;
end
% Determining Concrete Stress 'fc' (in ksi) from Stress-Strain
%Relationship
for i=1:n
if e(i)<=0.00163
fc(i)=e(i)*Fc* 666.667;
elseif e(i)>0.00163 && e(i)<=0.002175
fc(i)=Fc;
else
```

```
fc(i)=Fc+((Fc-Fcu)*(0.002175-e(i))/0.0005);
end
end
% Calculating Strain in Basalt
eb=(c-d)*et/c; %Accounting for tension strain as -ve, d-c
% becomes c-d
% Determining Basalt Stress 'fb' (in ksi) from Stress-Strain
%Relationship
er=fb/Eb;
if abs(eb)<er
fs=Eb*eb;
else
fs=-fb;
end
C=0; %Total Compressive Force
T=0; %Total Tensile Force
% Computing Compressive and Tensile Force in Concrete
for i=1:n
if e(i)>=0
N1(i)=fc(i)*b*h/n; %Compressive force in concrete layer
C=C+N1(i);
else
if abs(fc(i)*1000)<fr % Check for concrete cracking in
% tension
N(i)=fc(i)*b*h/n; %Tensile force in concrete layer
T=T+N(i);
end
end
end
% Computing Total Tensile Force of section (including steel)
T=T+fs*nr*3.1428*(dr)^2/4;
% Equilibrium Check C==T ???
C1=round(C*100)/100; %2 decimal rounding
T1=round(T*100)/100;
if abs(C1-abs(T1))<=0.02
disp('=====================================================')
disp('Stress @ bottom of Concrete, fc (psi) =')
disp(fc(n)*1000)
disp('Depth of NA, c (in) =')
disp(c)
disp('Total Compressive Force, C (kips) =')
disp(C1)
disp('Total Tensile Force, T (kips) =')
disp(T1)
disp('C1-abs(T1) =')
disp(abs(C1-abs(T1)))
disp('=====================================================')
count=count+1;
break % Exits while loop
elseif C1<abs(T1)
c=c+0.0004;
else
c=c-0.0004;
```

```
end
end % while loop end
% Calculating Moment in Kip -in (m=T*jd)
if et<=0.00163
m=abs(T1)*(d-c/3);
elseif et>0.00163 && et<=0.002175
dk=0.00163*c/et;
A=(Fc*(c-dk)^2/2) + (0.5*Fc*dk*(c-2/3*dk));
B=(Fc*(c-dk))+(0.5*Fc*dk);
ybar=A/B;
m=abs(T1)*(d+1.225-ybar);
else
dk=0.00163*c/et;
dl=0.002175*c/et;
A=(0.5*Fc*dk*(c-2*dk/3))+(Fc*(dl-dk)*(c-dl/2-dk/2))+(Fcu*(c-dl)^2/2)+(0.3333*(Fc-
Fcu)*(c-dl)^2);
B=(0.5*dk*Fc)+(Fc*(dl-dk))+(Fcu*(c-dl))+(0.5*(Fc-Fcu)*(c-dl));
ybar=A/B;
m=abs(T1)*(d-ybar);
end
M(count)=m; % Moment in K-in
phi(count)=et/c; % Curvature in rads/in
% Plotting Moment-Curvature Relationship
plot(phi,M,'o')
hold on
plot(phi,M)
xlabel('Curvature (rads/inch)')
ylabel('Moment (K-in)')
title('Moment Curvature Plot')
end % for loop end
```

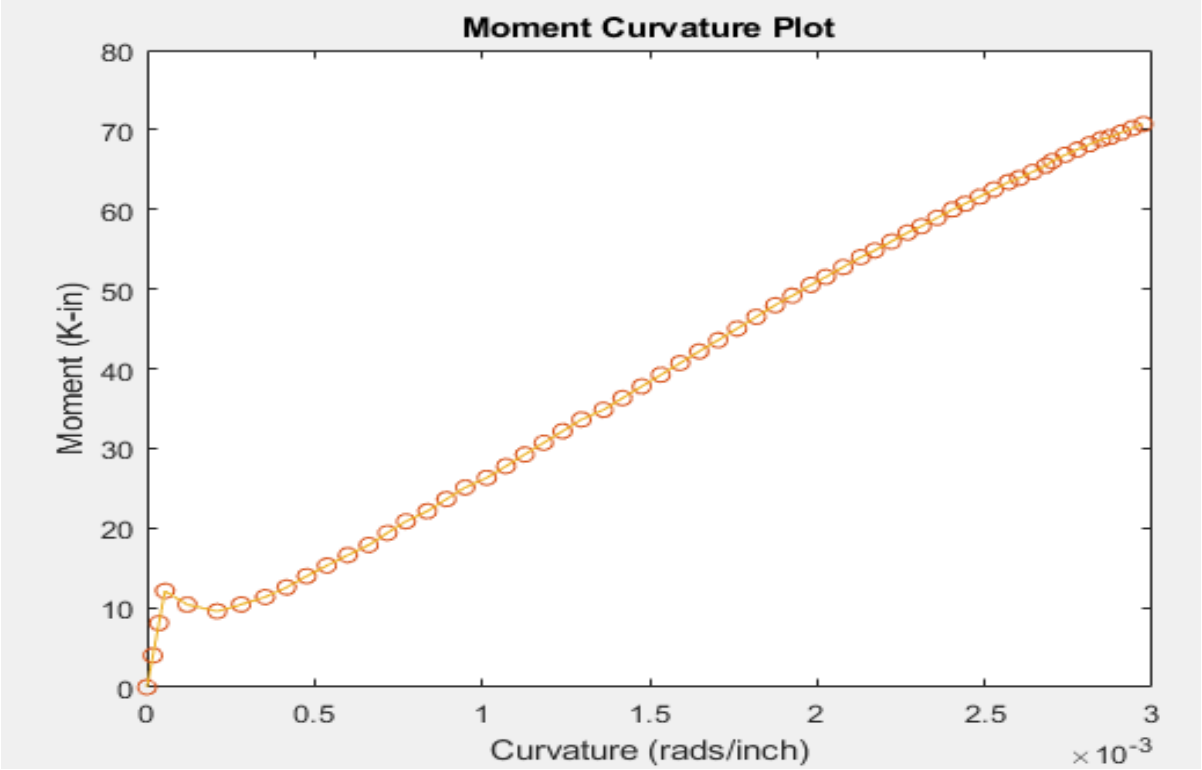
Moment Curvature Plot
Moment (K-in)
Curvature (rads/inch)
$\times 10^{-3}$
0
10
20
30
40
50
60
70
80
0
0.5
1
1.5
2
2.5
3

APPENDIX D

MatLab Program to Calculate the M-Phi Relation of Singly Reinforced Rectangular Beams by Layered Element Technique Basalt Reinforcement and Retrofitted in Tension Zone

```
% Matlab Program to calculate the M-Phi relation of Singly Reinforced
% Rectangular Beams by Layered Element Technique
% Basalt Reinforcement and Retrofitted in tension zone
% Loading is taken as single point loads acting at L/2
% Author - José Luis Carrasquillo & Nakul Ramanna & Dr. Razzaq
% Last Revised - 10/23/2023
% Notes:
% Once concrete cracks, its tensile stress is accounted up to the last
% uncracked layer.
% Program doesn't account for debonding of BFRP reinforcement
% Consider pre-allocating arrays for faster processing.
clc
clear all
% Data Input
%=============================================================
b=4.5; % Enter the width of the beam in inch
h=5.5; % Enter the total depth of the beam in inch
d=4.313; % Enter the effective depth of the beam in inch
dr=0.3937; % Enter the diameter of tension reinforcement (rebar) in
% inch
nr=2; % Number of tensile rebars
c=2.0; % Enter an initial value for the depth of Neutral Axis (in inch)
n=100; % Enter the number of rectangular elements across the depth of
% the beam section (Layers)
fy=71.56; % Steel Yield Stress in ksi
Es=5777.65; % Mod of Elasticity of Steel in ksi
Fc=4.2130; % Concrete Compression Strength in ksi
Fcu=3.581; % Fc unloading part in the stress strain curve for concrete
% (in Ksi)
nft=2; % no of BFRP reinforcement in tension zone
abasalt=0.012; % area of BFRP reinforcement in inch^2
Ef=6,228.8; % Mod of Elasticity of BFRP reinforcement in ksi
ffy=138.85; % BFRP rupture point in ksi
fr=7.5*sqrt(Fc*1000); % Flexural Strength of Concrete
count=0;
%Moment Curvature Program Begins
for et=0:0.00005:0.0031 % Increments concrete strain value in the top
% fiber by 0.00001
while ~0
%Calculating Strain in each Concrete Layer
for i=1:n
e(i) = (et*(c-(h/n*(i-0.5))))/c;
end
% Determining Concrete Stress 'fc' (in ksi) from Stress-Strain
% Relationship
for i=1:n
```

```
if e(i)<=0.00163
fc(i)=e(i)*Fc*666.667;
elseif e(i)>0.00163 && e(i)<=0.002175
fc(i)=Fc;
else
fc(i)=Fc+((Fc-Fcu)*(0.002175-e(i))/0.0005);
end
end
% Calculating tensile strain in Steel
es=(c-d)*et/c; %Accounting for tension strain as -ve, d-c
% becomes c-d
% Determining Steel Stress 'fs' (in ksi) from Stress-Strain
% Relationship
ey=fy/Es;
if abs(es)<ey
fs=Es*es;
else
fs=-fy;
end
% Calculating tensile strain in BFRP Bar
ef=(c+0.5-h)*et/c; %Accounting for tension strain as -ve, h-
% 0.5-c becomes c+0.5-h
% Determining BFRP Stress 'ffs'(in ksi) from stress-strain Relationship
ffs=Ef*ef;
if abs(ffs)<ffy
ffs=ffs;
else
ffs=-ffy;
end
C=0; %Total Compressive Force
Tc=0; %Tensile Force of Concrete
% Computing Compressive and Tensile Force in Concrete
for i=1:n
if e(i)>=0
N1(i)=fc(i)*b*h/n; %Compressive force in concrete layer
C=C+N1(i);
else
if abs(fc(i)*1000)<fr % Check for concrete cracking in
% tension
N(i)=fc(i)*b*h/n; %Tensile force in concrete layer
Tc=Tc+N(i);
end
end
end
% Computing Total Tensile Force 'T' of section (including steel and
% CFRP)
T=Tc+fs*nr*3.1428*(dr)^2/4+ffs*nft*abasalt;
% Equilibrium Check C==T ???
C1=round(C*100)/100; %2 decimal rounding
T1=round(T*100)/100; %2 decimal rounding
if abs(C1-abs(T1))<=0.02
disp('=====================================================')
disp('Stress @ bottom of Concrete, fc (psi) =')
```

```
disp(fc(n)*1000)
disp('Depth of NA, c (in) =')
disp(c)
disp('Total Compressive Force, C (kips) =')
disp(C1)
disp('Total Tensile Force, T (kips) =')
disp(T1)
disp('C1-abs(T1) =')
disp(abs(C1-abs(T1)))
disp('======================================================')
count=count+1;
break % Exits while loop
elseif C1<abs(T1)
c=c+0.0004;
else
c=c-0.0004;
end
end % while loop end
% Calculating Moment in Kip -in (m=T*jd)
if et<=0.00163
m=abs(T1)*(d+2.447-c/3);
elseif et>0.00163 && et<=0.002175
dk=0.00163*c/et;
A=(Fc*(c-dk)^2/2)+(0.5*Fc*dk*(c-2/3*dk));
B=(Fc*(c-dk))+(0.5*Fc*dk);
ybar=A/B;
m=abs(T1)*(d-ybar);
else
dk=0.00163*c/et;
dl=0.002175*c/et;
A=(0.5*Fc*dk*(c-2*dk/3))+(Fc*(dl-dk)*(c-dl/2-dk/2))+(Fcu*(c-dl)^2/2)+(0.3333*(Fc-
Fcu)*(c-dl)^2);
B=(0.5*dk*Fc)+(Fc*(dl-dk))+(Fcu*(c-dl))+(0.5*(Fc-Fcu) *(c-dl));
ybar=A/B;
m=abs(T1)*(d-ybar);
end
M(count)=m; % Moment in K-in
phi(count)=et/c; % Curvature in rads/in
% Plotting Moment-Curvature Relationship
plot(phi,M,'o')
hold on
plot(phi,M)
xlabel('Curvature (rads/inch)')
ylabel('Moment (K-in)')
title('Moment Curvature Plot')
end % for loop end
```

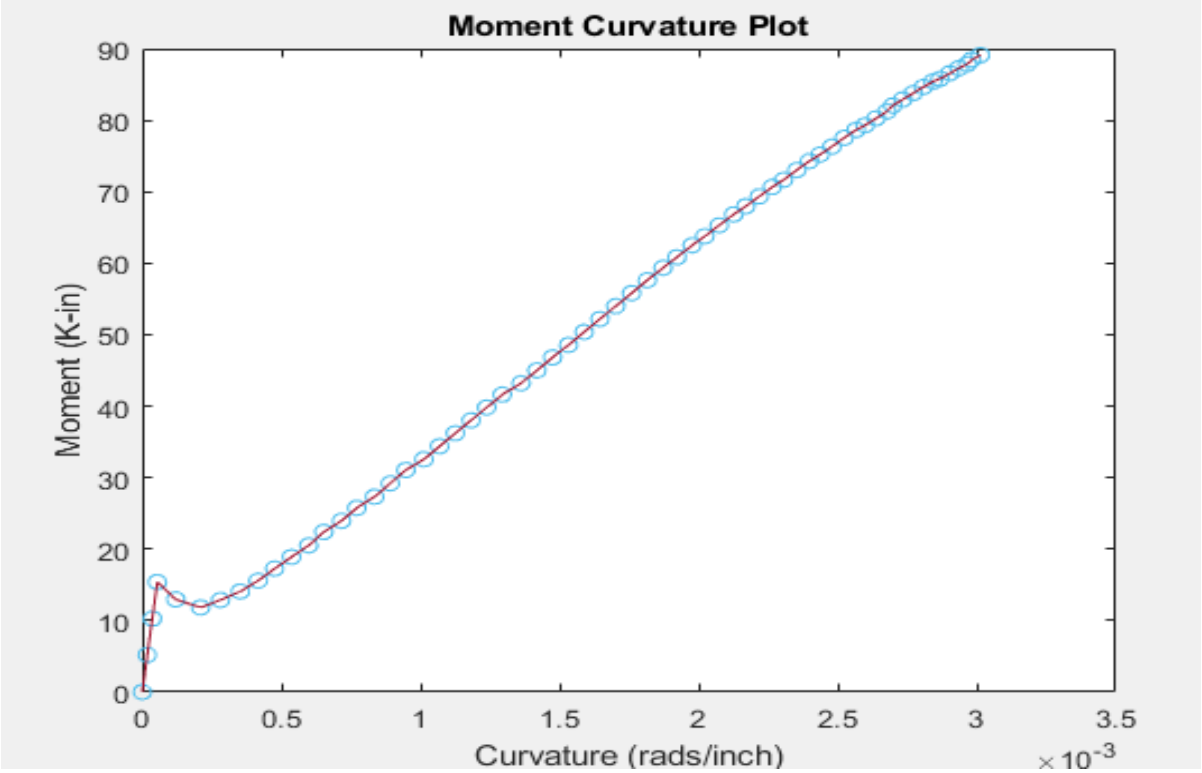
Moment Curvature Plot
Moment (K-in)
Curvature (rads/inch)
$\times 10^{-3}$
0
10
20
30
40
50
60
70
80
90
0
0.5
1
1.5
2
2.5
3
3.5

APPENDIX E

MatLab Program to Calculate Deflection at the Center of Reinforced Concrete Beam by Piecewise Linear Finite Difference Algorithm

```
% Matlab Program to calculate deflection at the center of reinforced
% concrete beam by Piecewise linear finite difference algorithm (PLFD
% algo.)
% Beam with Steel reinforcement
% Loading is taken as single point loads acting at L/2
% Author - José Luis Carrasquillo & Nakul Ramanna & Dr. Razzaq
% Last Revised - 11/21/2023
% Notes:
% Nonlinear polynomial regression equation obtained from curve fitting
% of Pseudo experimental moment curvature relationship is used to
% Calculate curvature in this program
% Deflection is calculated for a given w array (load array)
% C matrix = 13x13; found to be optimum
clc
clear all
% Data Input
% ================================================================
np=12;
%Enter no of parts/sections=; if this changes C (coefficient)
%matrix changes
h=27.5/np; %h = width of individual section, 27.5in is half the length of
%the beam
%Enter Load P in kips
w=[0 0.2284 0.4568 0.6852 0.9136
1.1420 1.3704 1.5988 1.8272 2.0556
2.2840 2.5124 2.7408 2.9692 3.1976
 3.4260 3.6544 3.8828 4.1112 4.33];
% ====================pr0gram Begins ==========================
for k=1:numel(w) %numel(w) = number of elements in array w
x=0;
for i=1:np+1
if x<=27.5 %27.5 is the length of triangular portion of BMD; also
%L/2 where L = length of beam (55 inch)
M(i)=w(k)*x/17;
x=x+h;
else
M(i)=w(k)*27.5/17;
x=x+h;
end
phi(i)=1.72682E-05*M(i)^2 + 1.0347E-05*M(i); %Beam 5 eqn, phi =
%curvature
end
%Coefficient : matrix, made for h = 3in or 12 sections
C= [1 1 0 0 0 0 0 0 0 0 0 0 0
0 -2 1 0 0 0 0 0 0 0 0 0 0
0 1 -2 1 0 0 0 0 0 0 0 0 0
```

```
0 0 1 -2 1 0 0 0 0 0 0 0 0
0 0 0 1 -2 1 0 0 0 0 0 0 0
0 0 0 0 1 -2 1 0 0 0 0 0 0
0 0 0 0 0 1 -2 1 0 0 0 0 0
0 0 0 0 0 0 1 -2 1 0 0 0 0
0 0 0 0 0 0 0 1 -2 1 0 0 0
0 0 0 0 0 0 0 0 1 -2 1 0 0
0 0 0 0 0 0 0 0 0 1 -2 1 0
0 0 0 0 0 0 0 0 0 0 1 -2 1
0 0 0 0 0 0 0 0 0 0 0 2 -2];
v=inv(C)*(-h^2*phi'); %v = deflection, 3 is the width of each section
%in inch
V(k)=v(end); %Capturing deflection at the center of the beam per load
%applied
disp('Max deflection in inch')
disp(v(end))
end %end of for loop
```

Load (kips)	Deflection (in)
0	0
0.2284	0.0018
0.4568	0.0048
0.6852	0.0091
0.9136	0.0147
1.1420	0.0215
1.3704	0.0295
1.5988	0.0389
1.8272	0.0495
2.0556	0.0613
2.2840	0.0744
2.5124	0.0888
2.7408	0.1044
2.9692	0.1213
3.1976	0.1394
3.4260	0.1588
3.6544	0.1795
3.8828	0.2014

4.1112	0.2246
4.34	0.2490

APPENDIX F

MatLab Program to Calculate Deflection at the Center of Reinforced Concrete Beam by Piecewise Linear Finite Algorithm Beam with Basalt FRP Reinforcement

```
% Matlab Program to calculate deflection at the center of reinforced
% concrete beam by Piecewise linear finite difference algorithm (PLFD
% algo.)
% beam with Basalt FRP Reinforcement
% Loading is taken as single point loads acting at L/2
% Author - José Luis Carrasquillo & Nakul Ramanna & Dr. Razzaq
% Last Revised - 11/21/2023
% Notes:
% Nonlinear polynomial regression equation obtained from curve fitting
% of Pseudo experimental moment curvature relationship is used to
% Calculate curvature in this program
% Deflection is calculated for a given w array (load array)
% C matrix = 13x13; found to be optimum
clc
clear all
% Data Input
% ================================================================
np=12;
%Enter no of parts/sections=; if this changes C (coefficient)
%matrix changes
h=27.5/np; %h = width of individual section, 27.5in is half the length of
%the beam
%Enter Load P in kips
w=[0 0.27052 0.54105 0.81157 1.08209
1.35261 1.62313 1.89365 2.16417 2.43469
2.70521 2.97573 3.24625 3.51677 3.78729
 4.0578 4.32833 4.59885 4.86937 5.14];
% ====================pr0gram Begins ==========================
for k=1:numel(w) %numel(w) = number of elements in array w
x=0;
for i=1:np+1
if x<=27.5 %27.5 is the length of triangular portion of BMD; also
%L/2 where L = length of beam (55 inch)
M(i)=w(k)*x/3;
x=x+h;
else
M(i)=w(k)*27.5/3
;
x=x+h;
end
phi(i)=1.9324E-06*M(i)^2 + 1.0547E-06*M(i); %Beam B-1 eqn, phi =
%curvature
end
%Coefficient : matrix, made for h = 3in or 12 sections
C= [1 1 0 0 0 0 0 0 0 0 0 0 0
0 -2 1 0 0 0 0 0 0 0 0 0 0
```

```
0 1 -2 1 0 0 0 0 0 0 0 0 0
0 0 1 -2 1 0 0 0 0 0 0 0 0
0 0 0 1 -2 1 0 0 0 0 0 0 0
0 0 0 0 1 -2 1 0 0 0 0 0 0
0 0 0 0 0 1 -2 1 0 0 0 0 0
0 0 0 0 0 0 1 -2 1 0 0 0 0
0 0 0 0 0 0 0 1 -2 1 0 0 0
0 0 0 0 0 0 0 0 1 -2 1 0 0
0 0 0 0 0 0 0 0 0 1 -2 1 0
0 0 0 0 0 0 0 0 0 0 1 -2 1
0 0 0 0 0 0 0 0 0 0 0 2 -2];
v=inv(C)*(-h^2*phi'); %v = deflection, 3 is the width of each section
%in inch
V(k)=v(end); %Capturing deflection at the center of the beam per load
%applied
disp('Max deflection in inch')
disp(v(end))
end %end of for loop
```

Load (kips)	Deflection (in)
0	0
0.2705	0.0045
0.5411	0.0136
0.8116	0.0274
1.0821	0.0459
1.3526	0.0690
1.6231	0.0968
1.8936	0.1292
2.1642	0.1662
2.4347	0.2080
2.7052	0.2543
2.9757	0.3054
3.2463	0.3611
3.5168	0.4214
3.7873	0.4464
4.0578	0.5560
4.3283	0.6303

4.5989	0.7093
4.8694	0.7793
5.14	0.8812

APPENDIX G

Code to Determine the Beam and Impactor Mass, Omega Impact Velocity of Each Test, Natural Frequency, and Natural Period

Beam properties:

$f_c := 4213 \quad psi$ $\quad B := 4.5 \quad in$ $\quad l := 60 \quad in$

$E := 57000 \cdot \sqrt{f_c}$ $\quad H := 5.5 \quad in$

$E = 3.7 \cdot 10^6 \quad psi$

$I := \frac{B \cdot H^3}{12}$ $\quad k := \frac{(48 \cdot E \cdot I)}{l^3}$

$I = 62.391 \quad in^4$ $\quad k = 5.13 \cdot 10^4 \quad \frac{lb}{in}$

$w_{beam} := 151 \quad lb$

$g := 386.4 \quad \frac{in}{sec^2}$

$w_{impactor} := 140 \quad lb$

$m_{beam} := \frac{w_{beam}}{g}$ $\quad m_{impactor} := \frac{w_{impactor}}{g}$

$m_{beam} = 0.391 \quad \frac{lb - sec^2}{in}$ $\quad m_{impactor} = 0.362 \quad \frac{lb - sec^2}{in}$

Heigh of the drop:

$H_{drop} := 7 \quad in$

$\omega := \sqrt{\frac{k}{m_{beam}}}$

$\omega = 362.3 \quad \frac{rad}{sec}$

Initial velocity of the impactor:

$v_i := 0 \quad \frac{in}{sec}$

Impactor final velocity:

$v_f := \sqrt{2 \cdot g \cdot H_{drop}}$

$v_f = 73.55 \quad \frac{in}{sec}$

Natural Frequency:

$f := \frac{\omega}{2 \cdot \pi}$

$f = 57.662 \quad Hz$

Natural Period:

$T := \frac{1}{f}$

$T = 0.017 \quad sec$

VITA

José Luis Carrasquillo

Department of Civil and Environmental Engineering

135 Kaufman Hall Old Dominion University Norfolk, VA 23529

José Luis was born in Fajardo, Puerto Rico. He received his bachelor's degree in civil engineering from the Polytechnic University of Puerto Rico in 1997. During his time in college, he worked with Emali Corp as a construction supervisor, with Las Piedras Construction in the role of highway land surveyor team lead, and with Miguel P. Velez and assisted as a highway construction inspector in Puerto Rico before he started his carrier in the Federal Government. José has thirty years in the Federal service where he first served as a Manager of the Administrative Office where he was in charge of repair and alteration project and procurement for the Caribbean District. In 2002 he moved to Virginia as a contract manager for multi-million dollars construction projects. In 2006, Jose received a master's degree in civil engineering from the University of Virginia and began his PhD program in Civil Engineering at ODU. In 2009, José moved to General Service Administration as a project manager in the design division where he managed a regular design and alteration project and a multimillion emergency project. In 2011, he managed a multimillion project to repair damage from an earthquake in the Virginia area. In 2013, José moved to the Department of Defense as a structural engineer where he conducted structural assessments, blast mitigations, and taught a security engineering class during assessments. José is member of different organizations, such as the Puerto Rico College of Engineer and Land Surveyors of Puerto Rico, the American Society of Civil Engineering, the American Concrete Institute, and the American Society of Military Engineers.